STRATHCLYDE INSTITUTE OF PHARMACY & BIOMEDICAL SCIENCES

Application of high-resolution mass spectrometry with MS^n fragmentation in the elucidation of double bond positions in fatty acids following formation of hydroperoxides and hydroxides, and application of derivatisation for improved sensitivity in fatty acid analysis.

By

Adnan Faysal AlKhalil

201360397

Supervisor

Dr. David G. Watson

A Thesis Submitted in Partial Fulfilment of the Requirement for the Award of a Degree of Doctor of Philosophy in the Strathclyde Institute of Pharmacy and Biomedical Sciences at the University of Strathclyde.

Author's Declaration:

I declare that this thesis is the result of the author's original research. It has been composed by the author and has not been previously submitted for examination which has led to the award of a degree.

Signed: ----------

Date: ----------

Acknowledgments

I start this thesis with the name of Allah, the most beneficent, the most merciful. First and most important I thank Allah for giving me the health, power, will, persistence and resilience to proceed with the work in this thesis despite all of the difficulties we, I and my family, went through.

I acknowledge with deep gratitude the continuous guidance, support, and encouragement I received from my supervisor, Dr David Watson, throughout the course of my studies. Not only that, but also the profound effect he had on me when he listened to me while I was going through the most difficult phases of my life and helped me stay focused on the most important things.

I will never forget the support from my second supervisor Prof A. I. Gray, who, although the circumstances of his retirement did not allow him to contribute to the content of this work, his support and assistance on a personal level were a factor in helping me to persevere.

I am thankful to all my colleagues, past and present, for their support, funny moment and useful sharing information and experiences.

I extend my heartfelt gratitude to my parents, Prof Faysal AlKhalil and Mrs Wafaa AlKhalil for their love, faithful support, prayerful concern, continuous encouragement and understanding all this time while they have been facing the harshest circumstances.

I want to express my gratitude to my dear brothers Abdul Hameed, Alaa, Imran and Aubai, who, despite all they have been going through, have been a source of support and solace during the period of this study. I would like to give special thanks to Abdul Hameed, who was and is the rock that I know I can bank on when injustices engulf me, and without whom I would not have been able to accomplish this work.

My thanks won't be sufficient to my wife Hazar for giving me Faris and Jana and for being as patient as she could be through the unbelievably hard years we went through together.

There is nothing can express the magnitude of the reason that the lights of my soul, my children, Faris and Jana, has given me to keep going. And for that, I will remain grateful for the rest of my life.

Finally, I am more than grateful for the award of scholarship by Damascus University, Syria, which, despite its cessation during the harsh conditions of the ferocious war and the unjust sanctions on the Syrian people, this work would not have seen the light and I would not have been here in the first place.

Abstract

Fatty acids (FAs) are the constitutional component of all lipid classes and the main source of structural diversity of lipids that have a myriad of biochemical functions. These include roles as the fundamental building blocks of complex cell membranes bilayer structures (*e.g.*, glycerophosholipids (GPs)); energy sources (*e.g.*, in triacylglycerols (TAGs)); and cellular signalling (*e.g.*, adipokines and DAG). All these functions are vital to cellular metabolism in living systems. In all these contexts, cellular biochemistry can be profoundly impacted by small differences in FAs molecular structure. Therefore, the identification and quantitation of FAs is a critical and challenging task in bioanalytical chemistry. Many FAs can be found in nature as mixtures of isomeric forms that might differ only in the site(s) of unsaturation. Gas chromatography – mass spectrometry (GC-MS) of fatty acid methyl ester derivatives has been the conventional method of choice for fatty acid analysis. Despite attaining generally effective chromatographic separations of the positional isomeric lipids, disambiguation in assigning the identity of these lipids could not be accomplished because their resulting electron ionisation mass spectra were most often indistinguishable. On the other hand, a relatively novel approach is being increasingly used for FA analysis that makes use of liquid chromatography coupled with electrospray ionisation mass spectrometry (LC-ESI-MS). Derivatisation strategies can further enhance this approach through improving the ionisation efficiency of FAs and/or generating distinct product ions useful for structural elucidation, upon application of collision-induced dissociation (CID).

In this project, a novel derivatisation strategy was designed and assessed based on combining LC-MS^2 and MRM for several isomers of specific fatty acid oxidation products with the well-established knowledge of chemically induced free radical oxidation that leads to the formation of these isomers which mechanism is not only determined by the number of double bonds and their locations but also on their relative positions to each other. Even though the study of fatty acids hydroperoxides has been proved to generate diagnostic product ions that can be used for pinpointing the position of double bonds, the reduced sensitivity, and the complexity of tandem MS spectra of

the hydroperoxides can be limiting factors for the application of this method, especially in complex samples. In contrast, the hydroxides obtained by the reduction of those hydroperoxides exhibited specificity for producing two different types of diagnostic fragment ion species for each isomeric fatty acid hydroxide upon CID via cleavages at the positions allylic to the hydroxyl group. The distinctive mass spectral features, arising from CID, enabled unambiguous assignment of site(s) of unsaturation within FAs. This analytical method offers specific, easily interpreted mass spectrometry data while applying simple low-cost experimental setup without the requirement of any modification of the mass spectrometry instrument. Additionally, this method demonstrated efficiency in the differentiation of regioisomers of MUFAs and PUFAs in a group of natural fixed oils.

In chapter two, the suitability of three tagging agents, DPD, DMEE and 1MP in the presence of EDC as an activating agent, for the analysis of long chain fatty acids was investigated. The detection of the FAs reversed-phase liquid chromatography (RPLC) in combination with mass spectrometry (MS) was greatly improved along with chromatographic resolution allowing for easy identification of FAs. Moreover, the possibility of applying EDC independently as a derivatising agent was assessed in principle for the same purpose of improving sensitivity of LC-MS analysis of FAs. The results of the study on EDC as a tagging agent confirmed that this method can offer a one-step highly sensitive and thus very useful derivatisation strategy of FAs that greatly improves their detection identification and quantification by LCMS. Thus, EDC shows potential for the sensitive analysis of bioactive oxidised fatty acids which are found in trace amounts in biological systems.

This new toolbox of methods will assist researchers in investigating the composition of the lipidome providing unparalleled fidelity in isomer discrimination.

Table of contents

List of Schemes

List of figures

List of tables

List of abbreviations

1MP	1-methylpiperazine
2DLC	Two-dimensional Liquid Chromatography
6-HO7,9,12TE	6-hydroxyoctadeca-7, 9, 12-trienoic acid
8-HO9ME	8-hydroxy-9-octadecenoic acid
8-HpO9ME	8-hydroperoxy-9-octadecenoic acid
9-HO6,10,12TE	9-hydroxyoctadeca-6, 10, 12-trienoic acid
9-HO10,12DE	9-hydroxyoctadeca-10, 12-dienoic acid
9-HO10ME	9-hydroxy-10-octadecenoic acid
9-HO10,12,15TE	9-hydroxyoctadeca-10, 12, 15-trienoic acid
9-HpO10,12DE	9-hydroperoxyoctadeca-10, 12-dienoic acid
9-HpO10ME	9-hydroperoxy-10-octadecenoic acid
9-HpO10,12,15TE	9-hydroperoxyoctadeca-10, 12, 15-trienoic acid
10-HO6,8,12TE	10-hydroxyoctadeca-6, 8, 12-trienoic acid
10-HO8ME	10-hydroxy-8-octadecenoic acid
10-HO11ME	10-hydroxy-11-octadecenoic acid
10-HpO8ME	10-hydroperoxy-8-octadecenoic acid
10-HpO11ME	10-hydroperoxy-11-octadecenoic acid
11-HO9ME	11-hydroxy-9-octadecenoic acid
11-HO12ME	11-hydroxy-12-octadecenoic acid
11-HpO9ME	11-hydroperoxy-9-octadecenoic acid

11-HpO12ME	11-hydroperoxy-12-octadecenoic acid
12-HO9,13,15TE	12-hydroxyoctadeca-9, 13, 15-trienoic acid
12-HO10ME	12-hydroxy-10-octadecenoic acid
12-HpO9,13,15TE	12-hydroperoxy-9, 13, 15-octadecatrienoic acid
12-HpO10ME	12-hydroperoxy-10-octadecenoic acid
13-HO6,9,11TE	13-hydroxyoctadeca-6, 9, 11-trienoic acid
13-HO9,11DE	13-hydroxyoctadeca-9, 11-dienoic acid
13-HO9,11,15TE	13-hydroxyoctadeca-9, 11, 15-trienoic acid
13-HO11ME	13-hydroxy-11-octadecenoic acid
13-HpO9,11DE	13-hydroperoxyoctadeca-9, 11-dienoic acid
13-HpO9,11,15TE	13-hydroperoxy-9, 11, 15-octadecatrienoic acid
13-HpO11ME	13-hydroperoxy-11-octadecenoic acid
16-HO9,12,14TE	16-hydroxyoctadeca-9, 12, 14-trienoic acid
16-HpO9,12,14TE	16-hydroperoxyoctadeca-9, 12, 14-trienoic acid
ABAP	2,2′-azobis-(2-amidinopropane)- dihydrochloride
ACN	Acetonitrile
AChR	Acetylcholine Receptor
Ag-LC	Silver ion Liquid Chromatography
AMPP	*N*-(4- aminomethylphenyl) pyridinium
APCACI	Atmospheric Pressure Covalent Adduct Chemical Ionisation
APCI	Atmospheric Pressure Chemical Ionisation
CACI	Covalent Adduct Chemical Ionisation
CE	Capillary Electrophoresis

CID	Collision-induced dissociation
DAG	Diacylglycerol
DESI	Desorption electrospray ionization
DMDS	Dimethyl disulphide
DMEE	*N*,*N*-Dimethyl-N'-ethylethylenediamine
DMS	Differential ion mobility spectrometry
DPD	*N*,*N*-Dimethyl-P-phenylenediamine
DTIM	Drift-time ion mobility
ECD	Electron Capture Dissociation
EDC	1-ethyl-3-(3-dimethylaminopropyl) carbodiimide hydrochloride
EI	Electron Impact
EID	Electron-induced dissociation
EIEIO	Electron Impact Excitation of Ions from Organics
Erk	Extracellular signal-regulated kinases
ESI	Electrospray ionisation
FA	Fatty Acid
FAB	Fast Atom Bombardment
FAIMS	Field Asymmetric Ion Mobility Spectrometry
FAMEs	Fatty Acid Methyl Esters
FAs	Fatty acids
FFAs	Free fatty acids
FTICR	Fourier Transform Ion Cyclotron Resonance
GC	Gas Chromatography

GM2	Ganglioside GM2
GPs	Glycerophosholipids
HILIC	Hydrophilic Interaction Liquid chromatography
HPLC	High Performance Liquid Chromatography
HRMS	High-resolution mass spectrometry
HPTLC	High-performance thin layer chromatography
ICR	Ion Cyclotron Resonance
IM	Ion Mobility
ISs	Internal standards
IUB	International Union of Biochemistry
IUPAC	International Union of Pure and Applied Chemistry
K-Ras	Kirsten rat sarcoma protein
LC	Liquid Chromatography
LDs	Lipid droplets
LPS	Lipopolysaccharide
LTP	Low Temperature Plasma
MALDI	Matrix Assisted Laser Desorption/Ionization
MAPK	Mitogen-activated protein kinases
MRM	Multiple Reaction Monitoring
MS	Mass Spectrometry
MSI	Mass Spectrometry Imaging
MUFAs	Monounsaturated fatty acids
NFkB	Nuclear factor kappa B

OzESI	Ozone electrospray ionisation
OzID	Ozone-induced dissociation
PB	Paternò–Büchi
PIP2	Phosphatidylinositol 4,5-biophosphate
PUFAs	Poly-unsaturated fatty acids
Q-TOF	Quadrupole time-of-flight
RPLC	Reversed-phase Liquid Chromatography
Rt	Retention time
SFC	Supercritical Fluid Chromatography
SH2	Src homology 2 domains
TAG	Triacylglycerol
THF	Tetrahydrofuran
TIC	Total Ion Chromatogram
TIMS	Trapped Ion Mobility Spectrometry
TLC	Thin Layer Chromatography
TLR4	Toll-like receptor 4
TWIM	Travelling-wave ion mobility
UHPLC	Ultrahigh performance Liquid chromatography
UV–vis	Ultraviolet-visual

Chapter One:
Study of unsaturated fatty acid oxidation products as a tool for determination of double bond positions

1 Chapter one introduction

1.1 Principles of Chromatography

The separation of molecules due to differences in their structure and/or composition is the basic concept of chromatography as an analytical technique. The notion to use the term chromatography to describe the separation technique based on the relative interaction of a solute with two phases began in the early 1900s (Alpert, 1990). These two phases forming a chromatographic system are: the stationary phase which is immobilised on the support particles and the mobilised phase percolates through or along the stationary bed, in a definite direction. The mobile phase may be a liquid (Liquid Chromatography) comprising an organic solvent or a mixture of two or more solvents that can dissolve the solute or mixture and carry it through or over the stationary phase, a gas (Gas Chromatography), or a supercritical fluid (Supercritical-Fluid Chromatography) (Meyer, 2010). The molecules in the sample will have different affinities and interactions with the stationary phase, leading to separation of molecules. The stronger these interactions the more slowly the sample components move through the column. Accordingly, different compounds can be separated from each other as they move through the column. The affinity of a component towards the column can be described by retention factor (k, defined in equation 1) which is characteristic of a given compound at a given mobile phase composition, temperature, and column type. Most commonly used Separation techniques are partition chromatography, adsorption chromatography, ion-exchange chromatography and size exclusion chromatography. Chromatographic separations can be performed using a variety of stationary phases and this choice of separation method is taken depending on the analyte's nature, for example volatile compounds and gases employ gas chromatography while liquid chromatography is ideal for non-volatile compounds, ionic compounds employ ion exchange chromatography and in the case of separation of compounds according to their molecular weight (size exclusion chromatography) can be operated (Watson, 2012).

1.1.1 High performance liquid chromatography (HPLC)

The acronym HPLC originally denoted high-pressure liquid chromatography, demonstrating the significance of the use of pressurised pumping systems to pump of mobile phase through a packed column instead of relying on atmospheric pressure and gravity flow in traditional column chromatography. Conventional HPLC instruments operate at high back-pressures (approximately 3000 psi). The behaviour of individual component of interest present in mixture and/or sample solution determines the rate at which it is passed through when the sample is injected into the column (Akash & Rehman, 2019).

A schematic representation of modern High Performance Liquid Chromatography (HPLC) system has been described in figure 1-1 It includes an eluent or a mixture of eluents and a high-pressure pump that drives the eluent through the system. The sample to be separated is introduced by an injector where a pre-filled sample loop is brought online by turning the injector from the load to the inject position. The column where the separation is achieved is positioned downstream the injector. Finally, the analytes, the different substances that emerge from the column, need to be recorded by a suitable detector since HPLC is merely a separation technique. There is a wide variety of detectors available on the market for use in liquid chromatography, from simple absorbance detectors to tandem mass spectrometers and the nature of samples determine the choice of the detector.

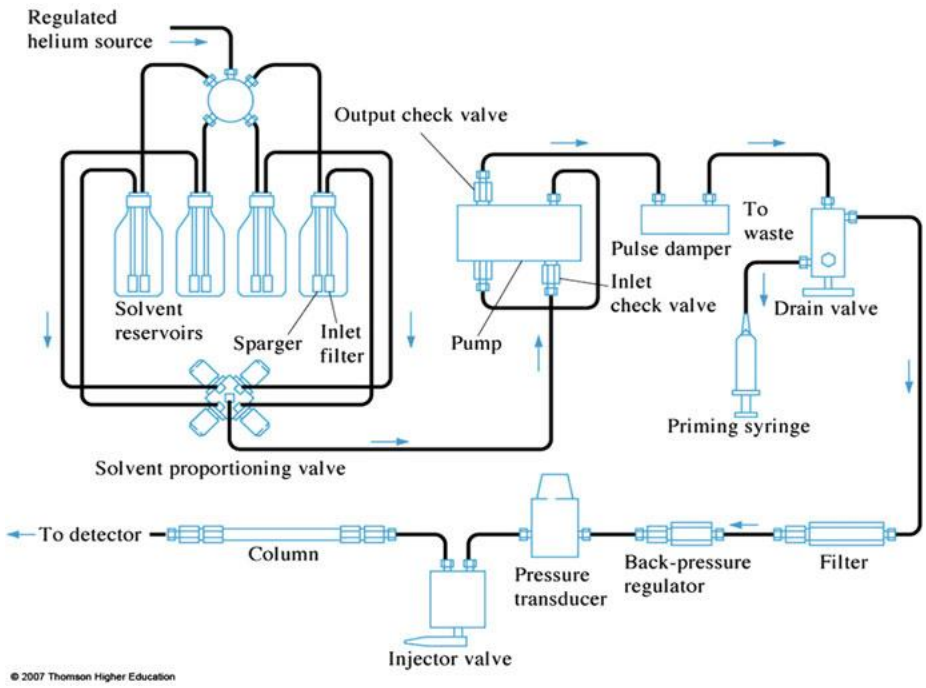

Figure 1-1 Schematic representation of a HPLC set-up (Akash & Rehman, 2019)

1.1.2 Chromatographic Performance

Having perception of how separation is affected by experimental conditions ensures successful use of chromatography. The efficiency of separation of any two compounds in liquid chromatography is determined by the difference in retention on the stationary phase in the HPLC column. Retention mechanism can be caused by one of two different modes in chromatography; partitioning and/or adsorption whereas in size exclusion chromatography ideally there is no interaction between the analytes and the stationary phase, however the separation occurs depending on the accessible pores to a molecule *i.e.*, the smaller the molecule, the longer time it will take to elute from the column.

The time between the injection of a compound and its appearance at the detector is called its retention time (t_R). Figure 1-2 shows the time the compound spends on the stationary phase (t_R) and the time spent by an un-retained compound which has no affinity for stationary phase which elutes in solvent front called t_0 or t_M. For the chromatographer, the substantial time variable is the relative retention factor (Snyder et al., 2010), this has to be calculated from equation 1

Equation 1

$$K = \frac{t_R - t_0}{t_0}$$

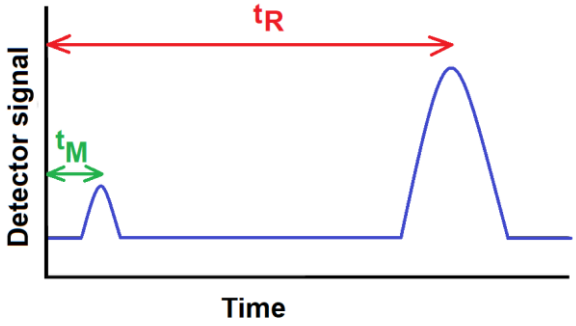

Figure 1-2 The retention time (t_R) of analyte and the retention of un-retained compound (t_M)

The retention factor and the number of theoretical plates of a column are used to assess column efficiency to compare columns and analytes in different HPLC set-ups. A higher N number of theoretical plates of specific column will enable it to produce a

narrower peak at a given retention time when weighed against a column with a lower N number and it can be calculated from **Equation 2**:

Equation 2

$$N = a\left[\left(\frac{t_R}{W}\right)\right]^2$$

Where W is the peak width (in the same units as t_R) at either the baseline (a=16) or at half peak height (a=5.54). The more plates per meter, the more efficient the column; in other words, it is determined by how narrow the peaks are in proportion to their retention time. The term N is an indirect measure of peak width for a peak at a specific retention time. According to the plate model, the process of separation within a column is hypothetically conceived as a course of successive separate equilibrations of the sample between the stationary and mobile phases that take place in a large number of separate layers, called *theoretical plates*, contained in the chromatographic column. The analyte moves down the column by transfer of equilibrated mobile phase from one plate to the next. The number of theoretical plates per meter (N/m) is often used as a comparison parameter of columns efficiencies.

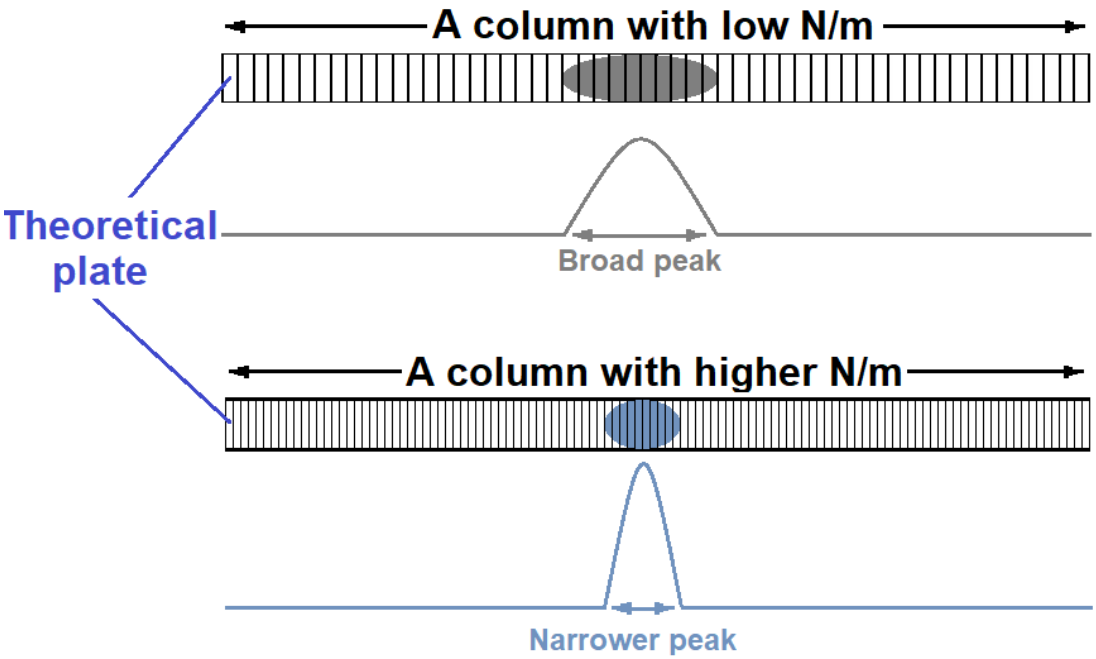

Figure 1-3 Theoretical plates model

An accurate determination of theoretical descriptions and retention factor requires accurate estimation of the void volume (V_0) which can be estimated for a well packed

column as either to be equal to approximately 60% of the total column volume or by calculation via **Equation 3** (Meyer, 2010):

Equation 3

$$V_0 = t_0 \times f$$

Where;

t_0 is the un-retained peak time

f is the column flow rate

Ideally, all chromatographic peaks would be symmetrical or Gaussian, however, they may show tailing behaviour due to the effect of instrument dead volume, adsorptive effects of the stationary phase and the quality of the column packing. Figure 1-4 illustrates the concept of tailing where a peak whose tail portion distance (B) in the diagram is wider than distance (A). The ratio of B/A can be used to measure the asymmetry of the peak, the best peak shape is attained when this value is 1 or close to 1 (Meyer, 2010). In RP-HPLC, peak tailing is normally observed in the analysis of bases due to interaction with residual silanol activity in bonded C8 or C18 phases. This can be minimised by using base deactivated silica which is acid treated to remove metallic impurities that activate silanol activity or by secondary methylation, a process known as end-capping. On the other hand, peak fronting is observed in cases where the injection solvent is stronger than the mobile phase composition (or the initial mobile phase composition in gradient elution) – a situation that leads to poor analyte focusing. In general, however, As values in the range of 0.9—1.5 are considered adequate for most chromatographic work (D C Harris & Lucy, 2020).

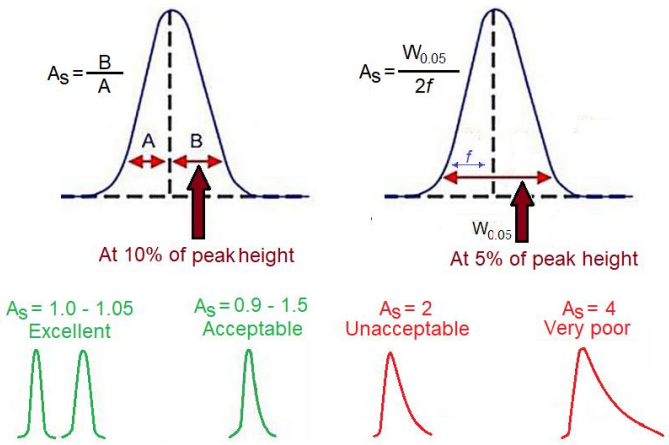

Figure 1-4 The asymmetry (As) of peak shape

1.1.3 Band Broadening and Column Efficiency

Since the competence of a separating system is best demonstrated by the resolution of its peaks, to chromatographer who aims to resolve the peaks of two compounds 1 and 2 in a mixture, the most important equation is the resolution (**Equation 4**) between their peaks. The higher this resolution is the less the overlap between these two peaks. Band broadening that occurs as the sample passes through the column compromises column efficiency. If the velocity of the mobile phase is too high for the time required for the equilibration of an analyte between the stationary and mobile phase, the analyte in the mobile phase will move ahead of the analyte in the stationary phase, especially if the analyte has a strong affinity for the stationary phase. The result of this effect is band broadening which will produce a poor separation.

Equation 4

$$R = 1.18\left(\frac{t_{R2} - t_{R2}}{W_{h1} + W_{h2}}\right) = \frac{\sqrt{N}}{4}\left(\frac{\alpha - 1}{\alpha}\right)\left(\frac{K_2}{1 + \bar{K}}\right)$$

$$\bar{K} = \frac{K_1 - K_2}{2}$$

Where;

t_{R1} and t_{R2} are the retention times of the first peak and the second peak, respectively. W_{h1} the peak width at half height of peak 1 and W_{h2} is the width of the second peak at half height (both widths in unit of time).

α is the separation factor

K_1 and K_2 are the retention factors of the first peak and the second peak, respectively.

N the number of theoretical plates.

The factor that has the most effective and direct effect on resolution is the selectivity or separation factor (α), which represents the difference in levels of intensity of which the components in question interact with the mobile and/or stationary phase. This might be governed by the type of interaction forces engendered with the column and mobile phase (Snyder et al., 2010). Selectivity can be expressed as in **Equation 5**:

Equation 5

$$\alpha = \frac{K_1}{K_2}$$

Where;

K_1 and K_2 are the retention factors of the first peak and the second peak, respectively.

The efficiency of the column can be affected by the number of theoretical plates in the column that depends on the plate height (H) which can be improved through optimum mobile phase flow and better packing as shown in **Equation 7**. Moreover, increasing column length can lead to higher number of theoretical plates as shown in **Equation 6** when L is the length of the column:

Equation 6

$$N = \frac{L}{H}$$

The plate height, H, describes the extent of peak dispersion, caused by mixing the analyte with the mobile phase. According to **Equation 6**, the smaller the value of H the higher the efficiency of the separation system will be.

1.1.4 The Van Deemter Equation

The Van Deemter equation is as follows:

Equation 7

$$HETP = A + {}^{B}/_{\mu} + C.\mu$$

Where;

HETP = height equivalent to a theoretical plate, a measure of the resolving power of the column [m].

A is Eddy-diffusion parameter caused by un-ideal packing [m], particle size and particle size distribution.

B is diffusion coefficient of the eluting particles in the longitudinal direction, resulting in dispersion [$m^2\ s^{-1}$].

C is mass transfer coefficient of the analyte between mobile and stationary phase.

μ is Linear velocity [$m\ s^{-1}$].

As can be seen from (**Equation 4)**, resolution can be described as a function of the number of theoretical plates of a particular column for a specific analyte (*N*) which represents the column efficiency. In the Van Deemter equation, column efficiency, which is represented by the theoretical plate height (*HETP*), is described as a function of linear velocity (μ) or flow rate. Accordingly enhancing the number of theoretical plates via reducing the height of theoretical plate could lead to a higher resolution and a better separation. A resolution between two peaks that is ≥1.5 leads to an ideal separation. The interference of poor peak shape will reduce this value, and therefore, the three terms A, B and C of the van Deemter equation (**Equation 7**) can be viewed as factors that contribute to band broadening. Thus, minimisation the van Deemter parameters will help controlling the band broadening effects (Alvarez-Segura et al., 2019).

The A term, figure 1-5, is determined by a phenomenon called Eddy Diffusion. It describes the randomness of the paths of diffusion taken by molecules of analytes through column's stationary phase particles and the variations in length of these paths which leads to the broadening of the band. The flow rate of the mobile phase has a negligible effect on the A term but the column packing, particle size and particle size distribution could affect the diffusion as it determines the movement of the solute. The use of smaller particles has a direct impact on the A term according to **Equation 8**:

Equation 8

$$\boldsymbol{A = 2\lambda\, d_p}$$

Where;

A is Eddy-diffusion parameter

d_p is the average particle diameter

$\boldsymbol{\lambda}$ l is a coefficient that defines the granulometry of the particles.

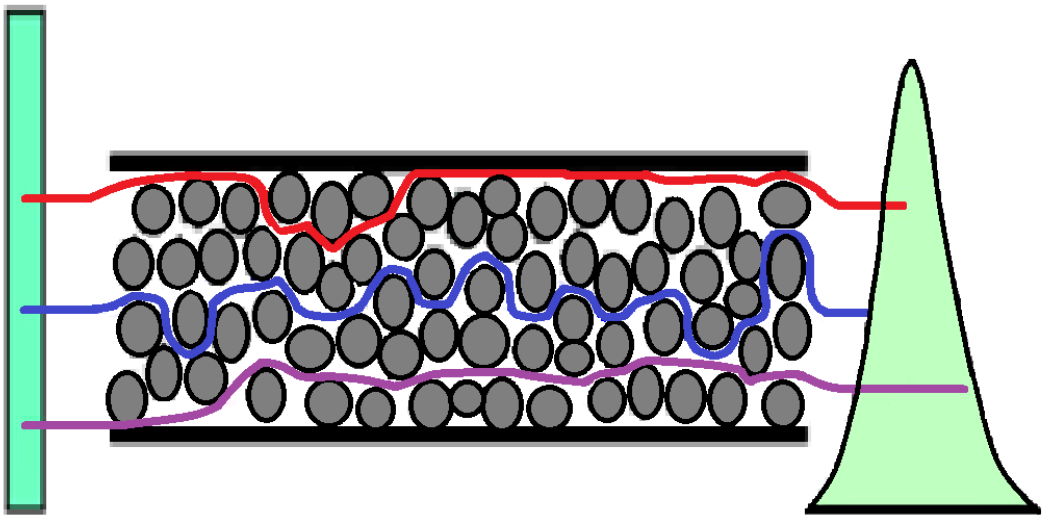

Figure 1-5 Different pathways by analyte's molecules cause term A.

The B term in figure 1-6 is called the longitudinal diffusion and relates to the movement of an analyte molecule by spreading out from the centre of its band to the edges in the solvent without any external influence. When mobile phase velocity is very low in relation to the particle diameter, the normal diffusion rates in the mobile phase become considerable and entails a disadvantageous effect on plate height. As the solute passes through the column, the random diffusion is superimposed upon its normal movement, which results in band broadening. The term B has a much larger effect at low mobile phase velocity (flow), thus higher mobile phase flow velocity will limit this distribution that longitudinal diffusion has no adverse effect. This applies when

Equation 9

$$\mu > \frac{2\,D_m}{d_p}$$

Where;

μ is the linear flow velocity of the mobile phase,

D_m is the diffusion coefficient of the sample in the mobile phase

d_p is the average particle diameter.

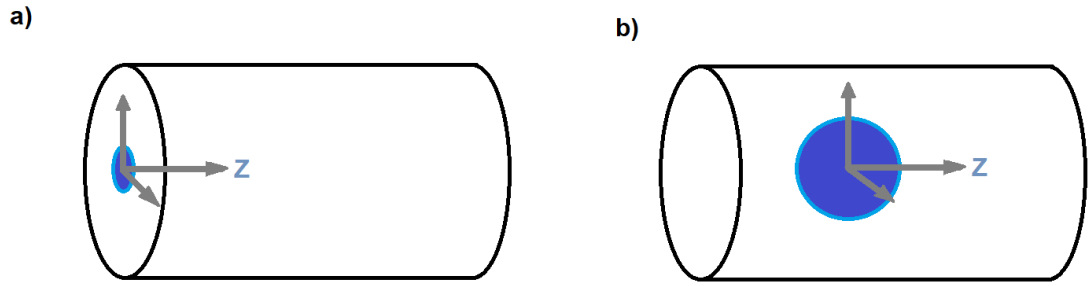

Figure 1-6 Band broadening by longitudinal diffusion. a) Sample zone immediately after injection It will spread out in all three axes of space (arrow directions). b) Sample zone at a later moment. It is larger now due to diffusion and it has also been transported

The packing material of a stationary phase is porous to allow a very large surface area for separation to occur. However, as those channels can be wide or narrow, some analyte molecules pass right through the whole particle in the bulk mobile phase and others are closed off in the pores that are filled with mobile phase which does not move (it stagnates) in relation to the normal flow through the column. This will give arise to term C, figure 1-7, also referred to as the resistance to mass transfer. This is because it describes the band broadening resulting from the hinderance instigated by the time needed by the analyte molecules trapped in the pores to diffuse back to the mobile flux phase. The hindered molecules have to travel through the stagnant mobile phase contained in pores only by means of diffusion, as they cease to be transported by the solvent flux, before they can interact with the surface to partition into the stationary phase and back out, consuming additional amount of time all the while the mobile phase is moving. If the velocity of the mobile phase is high, and the analyte has a strong affinity for the stationary phase, then the sample molecules remaining in the moving solvent become further distant from the stagnant molecules, accordingly, band broadening increases with increasing mobile phase flow velocity. Therefore, it is necessary to minimise equilibration time for the analyte molecules between the phases. This can be achieved by reducing the particle size (diameter) of the packing material to make the pores as shallow as possible. In addition, using less viscous mobile phase will cause the trapped molecules to diffuse faster in and out of the pores.

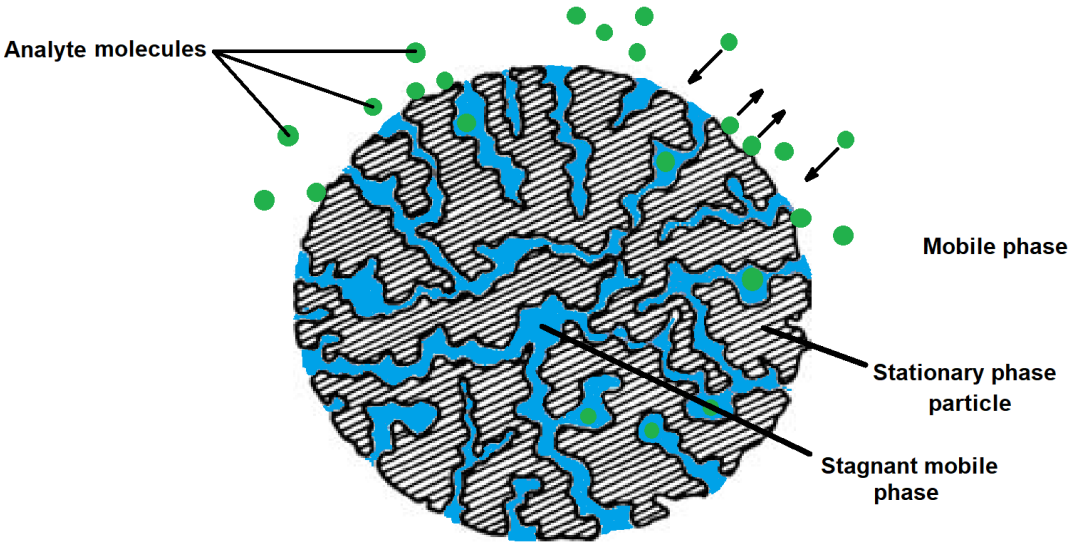

Figure 1-7 Term "C "the diffusion of analyte into and out of the stagnant mobile phase in the silica pore.

As the efficiency of the column is evaluated as a function of linear velocity in the Van Deemter equation, the assessment of the performance of different columns is often carried out by plotting Van Deemter curves that can additionally help to understand the optimum linear velocity for a specific method.

Figure 1-8 displays the first plot by van Deemter; it shows that at high and low flow rates the efficiency will be poor, however in between an optimum flow corresponds to a maximum efficiency. At low flow rates, the diffusion rate of the solute becomes considerable proportionate to the flow velocity, which results in poor efficiency. Whilst at higher flow rates the contributions from the other factors of band broadening become significant (Meyer, 2010).

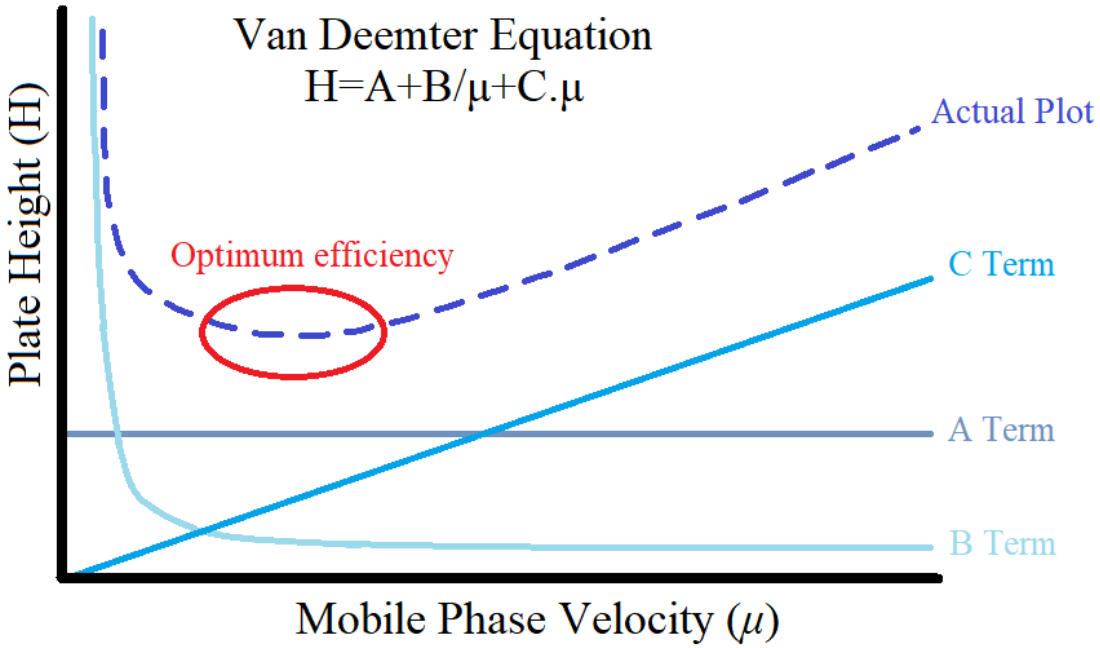

Figure 1-8 A plot of the van Deemter Equation describes the relationship between column flow rate and peak efficiency, referred to band broadening.

Fortunately, as the Van Deemter curve (Figure 1-8) shows, most of the broadening because of the term B can be eliminated if separations were basically sped up. Consequently, the decreasing of term A decreases the minimum value of van Deemter`s height of a theoretical plate, and the decreasing of term C shifts this minimum toward higher linear velocities. In practice, the use of particles with lower average particle diameter permits attaining higher efficiencies at higher flows.

1.1.5 Chromatographic elution profiles

Subject to the composition of mobile phase, chromatographic separations use three main forms of elution. These are: isocratic, gradient and stepwise profiles. In isocratic elution, the composition of the mobile phase remains unvarying throughout the entire run. In contrast, in gradient elution, mobile phase strength increases with time during the run by a constant rate. Stepwise profile is when elution is carried out in several successive isocratic intervals of gradually increasing solvent strength (e.g. by increasing the proportion of organic solvent in reversed phase HPLC) (Daniel C. Harris & Lucy, 2016; Watson, 2012).

Most chromatographic analyses employ either isocratic or gradient elution. The results of a *scouting* run can be used to decide whether to use isocratic or gradient profiles during chromatography (Dolan, 2013). A broad scouting gradient (e.g. 5-95% acetonitrile in 40 min in reversed phase) is first performed so that the compounds in a sample mixture have all eluted. The retention time difference, Δt, between the most and least retained compounds, and the gradient time, t_G, are then noted. The criterion is that:

if $\Delta t/t_G \leq 0.25$ then isocratic elution should be used; and if $\Delta t/t_G \geq 0.40$, gradient elution should be used. For $\Delta t/t_G$ values between 0.25 and 0.4, isocratic or gradient methods can be used but gradient elution is usually preferred (Haidar Ahmad, 2017; Silver, 2019).

Where;

Δt is the retention time difference between the first and last peaks

t_G is the gradient time (time over which the solvent composition changes).

This entails that isocratic elution is possible, when all the analytes in a sample can be eluted over a narrow solvent range (i.e. small Δt), and it thus recommended. On the other hand, gradient elution is more appropriate if a wide solvent range is required for the elution, as an isocratic profile would mean longer analysis times. During analysis with isocratic elution, the retention of analytes is governed by the following empirically derived equation, relating the retention factor (k) and solvent strength ($\emptyset$):

Equation 10

$$\log k \approx \log k_w - S\emptyset$$

Where;

k is retention factor of the analyte

k_w is the extrapolated retention factor for 100% aqueous eluent (in a plot of $\log k$ vs. $\emptyset$)

$\emptyset$ is the fraction of the organic solvent

S is a constant for a given compound, typically 4 for small molecules.

In gradient elution, as the composition of the mobile phase is changing at any given point in time, analyte retention can be considered in terms of the average retention factor, k^*, which is the value of k when the analyte has travelled half-way through the column. The equation for calculating k^* is as follows:

Equation 11

$$k^* = \frac{t_G\, F}{\Delta\emptyset\, V_m S}$$

Where;

t_G is the gradient time (min)

F is the flow rate (mL/min)

$\Delta\emptyset$ is the change in solvent composition during the gradient

V_m is the volume of mobile phase in the column (mL)

S is the slope in the linear solvent-strength model.

A convenient starting point in method development for both isocratic and gradient elution profiles is a k (or k^*) of ~5. In addition, a good starting mobile phase composition during isocratic method development is the solvent strength halfway through the interval, Δt, of the scouting gradient run. The developed method can then be optimised so that all the peaks are fully resolved ($Rs \geq 1.5$) from each other, with k values in the range of $2 \leq k \leq 10$ at reasonable back pressures of the pump because the resolution diminishes at a low k value and does not significantly improve at a value above 10. Moreover, setting a minimum retention factor of 2 helps minimise the interference from the solvent front peak with the peaks of interest and enhance quantitation of early eluting peaks, and decreases the effect of small deviations in % organic on retention time (Haidar Ahmad, 2017; Daniel C. Harris & Lucy, 2016).

1.2 Mass Spectrometry (MS)

Mass spectrometry is a technique for measuring molecular weights of compounds by calculating their gas-phase ionic trajectories after being accelerated through electric and magnetic fields in vacuum (Schuberth, 2000). Given that mass spectrometry is both selective and sensitive method of analyte detection in LC-MS systems, its use

helps minimising the need for laborious sample preparation and complete chromatographic resolution of components as pre-requisites for analysis of complex samples.

The contradiction between the high solvent pressures in the chromatographic system and the low-pressure requirement of the MS system, for molecular collisions prevention, initially frustrated the deployment of mass spectrometry as an online detector for HPLC. The liquid mobile-phase evaporation generates extremely high gas volumes [e.g. 18g of water (1 mole) generates 22.4L of gas phase at standard conditions of temperature and pressure], with their accompanying pressures. In this case, the LC eluate would most likely overwhelm the pumping capabilities of the MS system, making vacuum stabilisation, and hence reactions, during ion mass analysis difficult to maintain. Certain procedures were required to overcome this challenge, such as the reduction of the huge excess of matter in the interface between the LC and MS systems and the avoidance of mobile phase additives that are difficult to volatilise such as phosphate-containing buffers. Even with these measures, the MS could only be employed for relatively small, nonpolar, compounds that could be easily volatilised. Large biological molecules (with molecular weights $\geq$ 1000Da), such as large peptides and proteins, were impossible to be transformed into gas-phase ions without extensive molecular deformation (D C Harris & Lucy, 2020).

The development of two new ionisation techniques in the past two decades: (1) electrospray ionisation (ESI) and (2) matrix-assisted laser desorption/ionization (MALDI) made it possible to overcome these major difficulties and allowed the conversion of almost any large, non-volatile and thermally labile compound into a gas-phase ion. Additionally, ESI has led to a revival of the technique of atmospheric-pressure chemical ionization (APCI). With ESI and APCI techniques, it was possible to generate a charged mist of the LC eluate from which the solvents could be extinguished, and gas-phase ions formed before they were introduced into the mass analyser compartment of the MS. This made it possible to conjugate HPLC systems to the mass spectrometer.

Basically, the main components of a MS system are an ionisation source, a mass analyser and a detector (Figure 1-9). Analytes elute from the LC column to enter the

ion source chamber and become converted into gas-phase ions (positive, negative, or both) (Becker, 2008). Following the ionisation, ions are transferred to the mass analyser maintained under a high vacuum. The ions are separated within the mass analyser based on their mass to charge (*m/z*) ratios (Schuberth, 2000) and a mass spectrum is produced when ion current is detected. On the subject of mass analyser, a variety of technological instruments are currently available commercially and include: magnetic sector instruments, single and triple quadrupoles (Becker, 2008; de Hoffmann & Stroobant, 2007), time-of-flight (ToF) instruments (Watson, 2012), ion traps, Fourier transform ion cyclotron resonance (FT-ICR) spec-trometers (Scigelova et al., 2011) and Orbitraps (Zubarev & Makarov, 2013). The latter is one of the latest technologies with the advantages of high mass resolution, mass accuracy and dynamic range (Eliuk & Makarov, 2015).

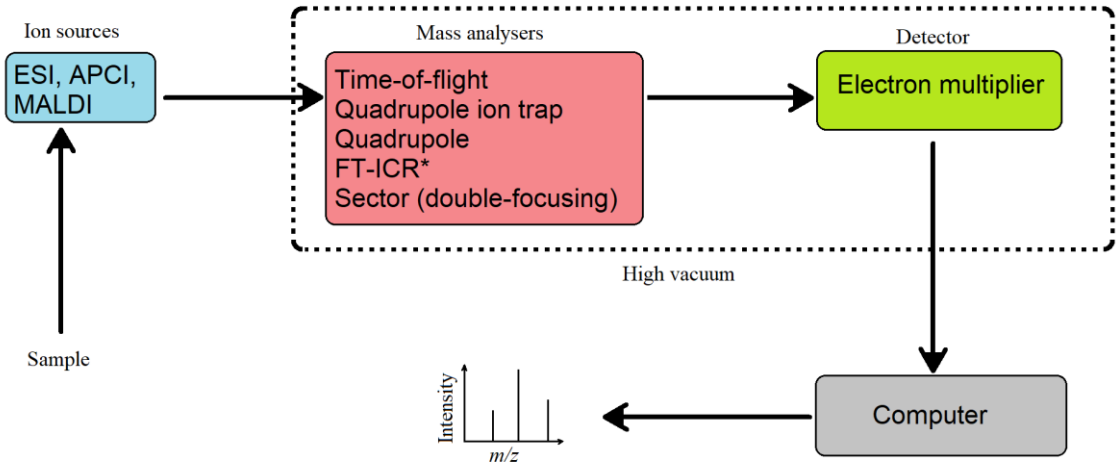

Figure 1-9 Basic components of a typical mass spectrometer used in drug discovery. *FT-ICR does not use an electron multiplier.

Several factors can affect the ionisation process in the mass spectrometer, including type of analyte, nature and strength of buffer used, mobile phase composition, and mode of ion formation. The main mechanisms of ion formation in MS are electrospray ionisation (ESI) (B. Hu & Yao, 2022), atmospheric pressure chemical ionisation (APCI), chemical ionisation (CI), matrix assisted laser desorption/ionisation (MALDI) (Awad et al., 2015) and electron impact (EI) (Watson, 2012). While EI is considered to be a "hard" ionisation technique because of the high-energy collisions of electrons with molecules that produce fragmentations, the rest are considered to be "soft"

ionisation techniques given that ionisation is not associated with significant fragmentation which gives rise to the formation of molecular ions such as $[M+H^+]^+$ or $[M-H^+]^-$. Because of its simplicity and applicability to a wide range of analytes, ESI is the most used soft ionisation techniques for the majority of analytical assays.

1.2.1 The ESI technique

During electrospray ionization (ESI), ions are generated at atmospheric pressure by introducing solution-based sample into the ionisation chamber via a fine, capillary needle (spray needle) that is at a potential difference relative to a counter electrode surrounded by a flowing sheath gas of nitrogen (Awad et al., 2015). As the analytes flow into the chamber, they are ionised by the potential difference between the inner surface of the spray needle and the counter electrode.

The solvents that make up the solution and the inner diameter of the needle determine the actual voltage required. Usually, solvents with higher boiling points and capillaries with larger inner diameters require higher voltages.

The charged ions first form a Taylor cone at the tip of the needle which then gives rise to a charged aerosol—a process that is assisted by the sheath gas flow consisting of dry nitrogen gas (Figure 1-10).

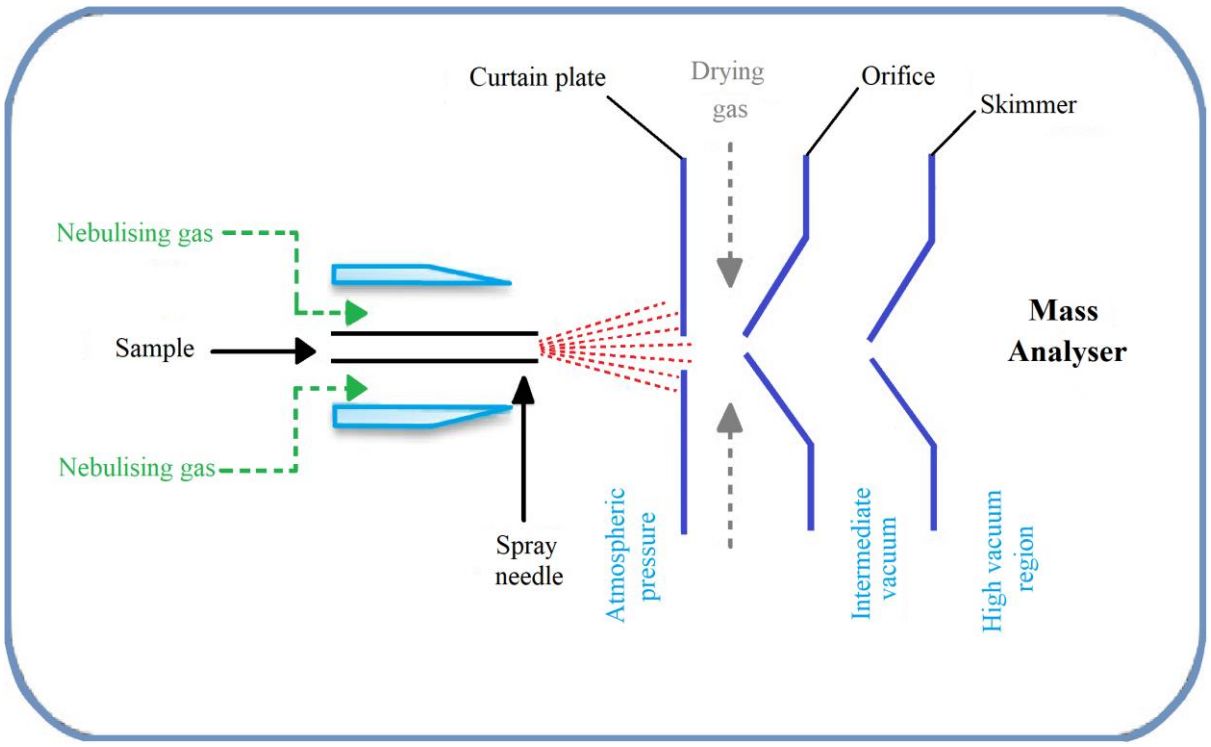

Figure 1-10 Schematic diagram of an ESI source.

Ions with a similar charge to that on the spray needle are repelled into the centre of the Taylor cone while those possessing opposite charge remain stuck on the needle. Ions in ESI is proposed to be generated by one of two different mechanisms, figure 1-11. The ion evaporation mechanism involves solvent evaporation and Coulombic fissions of the charged droplets so, they become smaller in size. The gas-phase ions are directly released/desorbed from the surface of the small droplets when the Columbic repulsion increases as similar charges in the drop are brought closer to each other to reach a certain point, known as Rayleigh limit (Fenn et al., 1989) where the magnitude of these repulsive forces overcomes the cohesive force of the surface tension which causes the drop to break up, ejecting tiny droplets with diameters of ~10 nm. In the charge residual model, the molecule will be freed by complete evaporation of the solvent without getting desorbed from the charged droplet, and this is more likely to happen with large molecules (Awad et al., 2015).

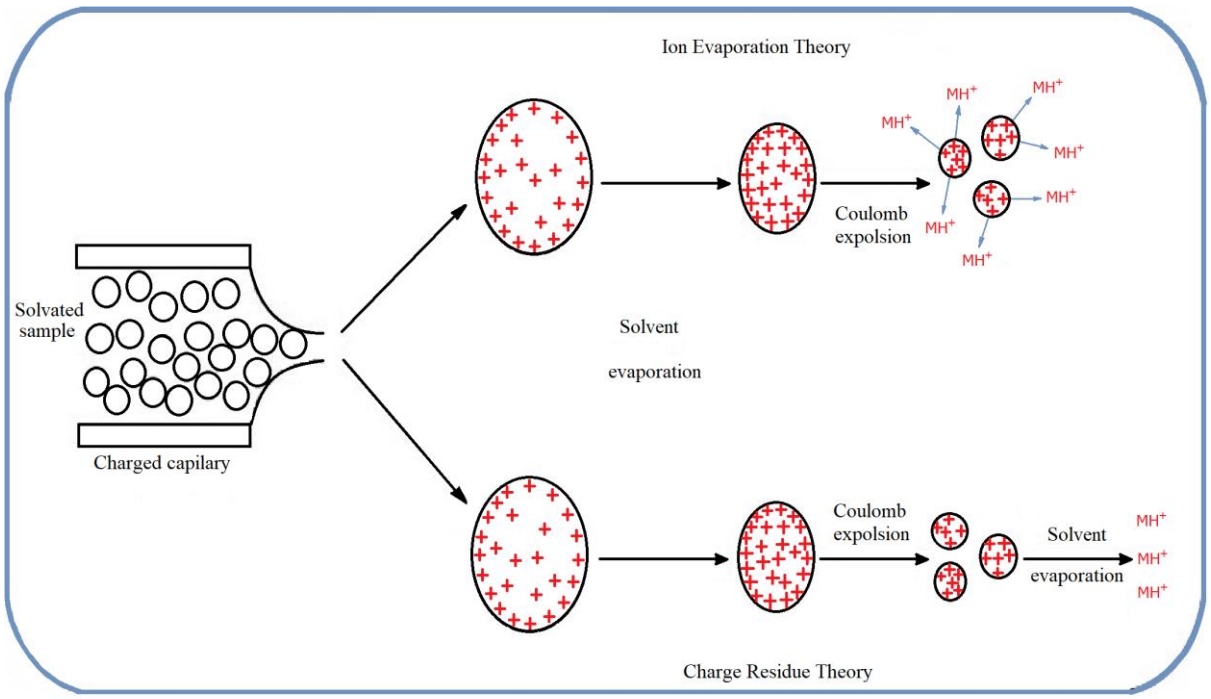

Figure 1-11 Proposed mechanisms of ion formation during electrospray ionization.

The flow of the nitrogen gas and heating enhance this process by causing evaporation of solvent until naked charged molecules are formed**.** It should be noted that the efficiency of the ESI process can be enhanced by using mobile phases that contain a high proportion of organic solvents, and therefore lower surface tension, and mobile phase additives such as formic acid. The charged gas molecules are then sucked into a high vacuum analyser region for mass measurement. Labelling of ESI a "soft" ionisation technique comes from the fact that the ion generation process occurs at low energies and the desolvation process efficiently lowers internal energies of analyte ions which leaves them free from fragmentation as they enter the mass analyser (Banerjee & Mazumdar, 2012).

1.2.2 The LTQ-Orbitrap MS

The LTQ-Orbitrap is a hybrid system introduced by Thermo Electron (now Thermo Fisher Scientific) in 2005, the LTQ Orbitrap mass spectrometer, which was the first commercial instrument to incorporate an Orbitrap mass analyzer (Q. Hu et al., 2005). The original design of the LTQ Orbitrap instrument, with the ion trap coupled to an Orbitrap mass analyser provided researchers with the flexibility for which they yearned. The LTQ—which stands for linear trap quadrupole—is a mass spectrometer

in its own right (e.g. as LTQ-FT-MS, supplied by Thermo Electron Corporation). On its own, the LTQ has the capability to detect both MS and MS^n spectra with high speed and sensitivity but with poor resolution and mass accuracy (Eliuk & Makarov, 2015). However, far more superior mass detection occurs with higher resolution when it is coupled to the Orbitrap along with increased mass accuracy and higher sensitivity. The design comprised a curved, resonant frequency (rf)-only, voltage-gated trap known as C-trap that links the LTQ and the Orbitrap components—consequently completing a triad of traps within the instrument (Figure 1-12).

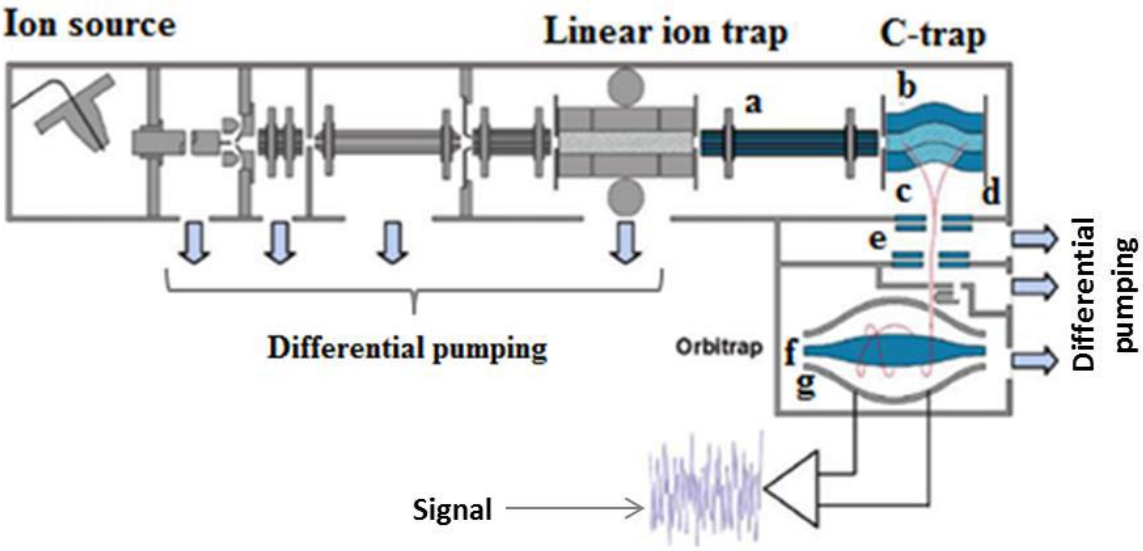

Figure 1-12 A schematic layout of the Orbitrap mass spectrometer. The main parts are: (a) Transfer octapole; (b) C-trap; (c) gate electrode; (d) trap electrode; (e) ion optics; (f) inner Orbitrap electrode;(g) outer Orbitrap electrodes.

After leaving the electrospray source, ions are let into the linear trap of the LTQ via rf-only octapoles, wherein they are analysed and radially ejected to a pair of secondary electron multipliers. A short prescan is made in the ion trap to determine the ion current within the range of interest by means of a procedure known as automatic gain control (AGC) that ensure quantitative accuracy and dynamic range. This enables storage of a defined number of ions (known as AGC target value) for the subsequent analytical scan (Belov et al., 2003; Eliuk & Makarov, 2015). This circumvents the problem of space charging which would occur if more ions than required were stored in the quadrupole that has limited storage capacity. By using the AGC procedure, both sensitivity and resolution are maximised by specifying the exact fill time of the trap

because space charging would compromise sensitivity and resolution (Eliuk & Makarov, 2015).

The C-trap allows further accumulation and transient storage of a significant ion population when they are being transferred from the linear ion trap prior to injection into the Orbitrap analyser (Makarov & Scigelova, 2010; Nolting et al., 2019). This additional temporary ion storage brings about enhancements to the analytical capabilities of the instrument and permits additional high energy collision induced dissociations (CIDs) to be carried out in the C-trap for MS^n spectra. From the C-trap, ions are injected into the Orbitrap mass analyser as short, pulsed ion beams, allowing each mass/charge ratio subpopulation to form sub-microsecond pulses (Eliuk & Makarov, 2015; Zubarev & Makarov, 2013). For MS/MS, the C-trap could be used as a collision chamber to enable triple quadrupole–like fragmentation in the LTQ Orbitrap. Precursor ions would be accumulated and isolated in the linear ion trap (LTQ) before they are allowed to accelerate into the C-trap passing through the transport octapole. After several oscillations in the C-trap which is maintained at a nitrogen pressure of B1mTorr, most of the precursor ions would undergo dissociating fragmentation, and most fragment ions would be retained in the middle of the C-trap being confined by voltages on the gate aperture and trapping plate before they are injected into the orbitrap for mass spectrometric detection with high resolution and mass accuracy (Olsen et al., 2007). Once injected, these ion beams enter the Orbitrap mass analyser in the region between two electrodes: an inner (central) spindle-shaped electrode and outer barrel-shaped electrode coaxial with the first (Q. Hu et al., 2005; Zubarev & Makarov, 2013). This region contains a rapidly changing electric field arising from a quadro-logarithmic electrostatic potential (equation 9) created by specially designed, axially symmetric electrodes (eq) (Scigelova et al., 2011) .

Equation 12

$$U_{(r,z)} = \frac{k}{2}\left\{z^2 - \frac{r^2}{2} + \frac{k}{2} R_m^2 \, ln\left[\frac{r}{R_m}\right]\right\}$$

Where;

r and z are cylindrical coordinates

k is the field curvature (a constant that is proportional to the potential difference between the central and the outer electrodes)

Rm is the characteristic radius

In the Orbitrap analyser, an electric field that is inhomogeneous in two directions, radial and axial, is created by the two coaxial electrodes of the mass spectrometer. The radial field is stronger near the central electrode, and it attracts ions toward the central electrode. Therefore, in order to provide a circular trajectory, the ions from the C-trap must be injected with such a tangential velocity as to that the centrifugal force compensates the force created by the radial field that they avoid collision with the inner electrode. Stable trajectories formed by these ions in the Orbitrap have a shape of a complicated spiral that combine rotation around the central electrode, discussed above, with oscillations along the axis. These trajectories are caused by the harmonious acts of the velocity of the ions and the electric field intensity. (Figure 1-13)

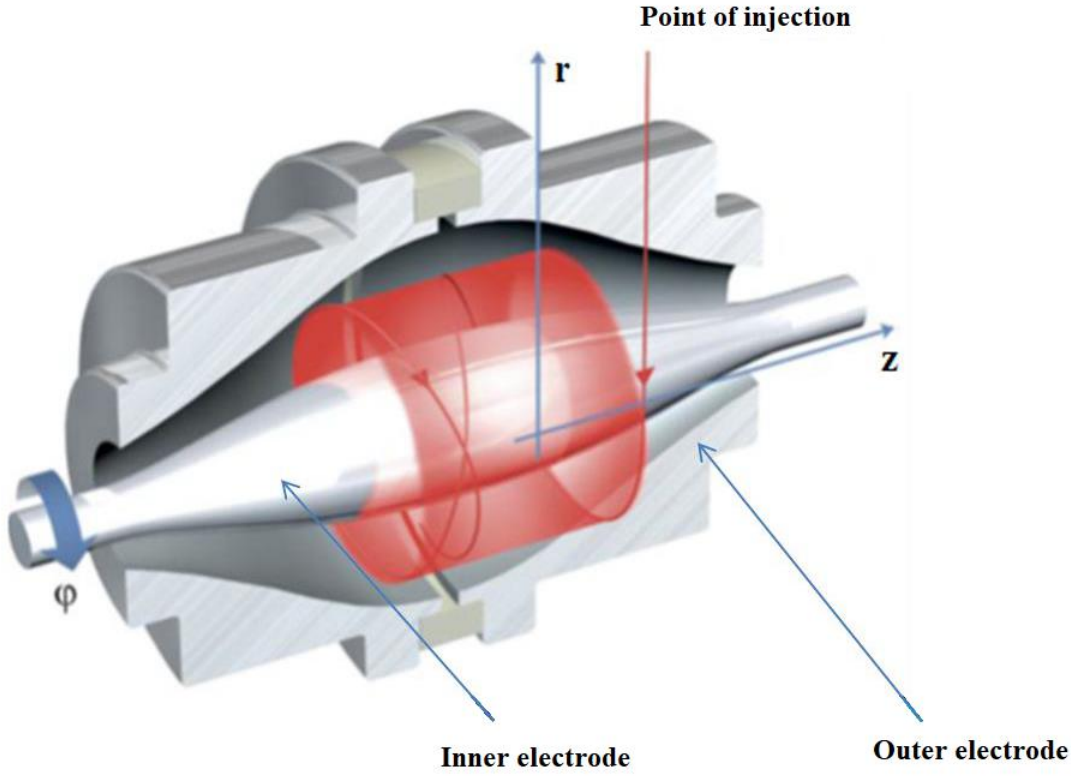

Figure 1-13 A section through the Orbitrap mass analyser. Ions enter the Orbitrap as shown by the red arrow perpendicular to the axis of the spindle-shaped electrode (z-axis). The point of injection is slightly offset from Z = 0 in order to give the ions axial potential energy, thus initiating harmonic axial oscillations, a term known as "excitation by injection". The quadro-logarithmic field inside the analyser stabilises the axial oscillations through rotations around the central electrode.

In the harmonically concurrent axially-oscillating component of this motion, the axial electrostatic field directs the ions toward the equator of the trap with a force proportional to the distance from the equator. The ions are accelerated toward the equator plane of the Orbitrap analyser along the z axis and continue to travel through the equator plane, where the electrostatic field strength is at zero. As they continue toward the opposite end of the Orbitrap, these ions expend the axial velocity previously gained in traversing the electric field gradient from the starting point to the equator. They decelerate as they go through the adverse force generated by the electrostatic field before they are accelerated back toward the equator of the trap by the symmetric electric field that increases evenly in opposing directions along the z axis as the two coaxial electrodes become increasingly closer.

Whereas rotational and radial frequencies of the ions in the beams are strongly dependent on their initial energies, positions or angles, which in turn results in the spread of the ion packet over the angular coordinate to form a thin ring (Makarov & Scigelova, 2010), the frequency of harmonic oscillations along the axis of the central electrode is completely independent of these initial parameters, but depends solely on the mass-to-charge ratio (*m/z*) of the ions and the field curvature, *k*, as follows:

Equation 13

$$\omega = \sqrt{\frac{e}{(m/z)}. k}$$

Where;

e is the elementary charge

ω is the frequency

z is the charge on the ion

m is the mass of the ion

k is the field curvature (Grinfeld et al., 2019; Makarov et al., 2009).

Therefore, the *m/z* values of the ions can only be determined by measuring the frequencies of the axial oscillations using fast Fourier transform mathematical algorithm of the broadband image current signal produced by the ions and detected on two split halves of the outer electrode of the trap. The technique gives high resolution (~ 150,000 fwhm) spectra of the ions being measured along with good sensitivity, high mass accuracy (2-5ppm) and up to 8-fold relative mass range (Eliuk & Makarov, 2015; Q. Hu et al., 2005).

Because of its high resolution, selectivity, and sensitivity, the LTQ-Orbitrap mass spectrometer can be used for detecting analytes in biological samples. Moreover, it has the potential for performing reaction monitoring in both selective ion monitoring (SIM) and selective reaction monitoring (SRM) functions as well. It is because of these strengths that the Orbitrap has seen increased applications, and led to significant

advances, in proteomics (Orsburn, 2021), metabolomics (López-Yerena et al., 2021), lipidomics (Züllig & Köfeler, 2021), food safety and environmental analysis, in addition to phytochemistry, natural products (Alvarez-Rivera et al., 2019) and quality control analysis of pharmaceuticals (Eliuk & Makarov, 2015; Makarov & Scigelova, 2010).

1.2.3 Isobaric Interferences

The accurate mass of a target ion is valuable information for its unequivocal identification. However, mass accuracy can be affected by different factors. Presence of coeluting interferences can alter accurate mass measurements, resulting in false negative and positive results. the most common interferences are the spectral interferences, also called isobaric interferences (Romero-González & Frenich, 2017). They are due to overlapping peaks which can mask the analyte of interest and can give erroneous results. Such interferences may occur from ions of other elements within the sample matrix, elemental combination, oxide formation, doubly charged ions, and so on. Isobaric interference occurs between species with the same mass-to-charge (*m/z*) ratio and isobaric compounds could be either structural isomers of the target analyte that share its elemental formula or structurally unrelated compounds that have the same nominal molecular mass as the target analyte. Another apparent isobaric effect may actually also be attributable to the presence of a multiply charged ion of an unrelated molecule with a several-fold mass of the target analyte. In single stag MS (i.e., GC-MS or LC-MS with low-resolution single-quadrupole or ion-trap detectors), for which the analyte detection is based solely on its molecular weight, the overlapping isobaric or nearly isobaric species will skew the mass reading and cause a serious risk of obtaining a false- positive result if the user sets an extraction window that is too wide due to the interferences. In effect, they will be unable to achieve a very accurate mass reading since unobserved interferences will contribute to the peak area detected for the compound of interest. On the other hand, a risk of obtaining a false-negative result can arise if the user sets an extraction window too narrow. In this case the compound showing a higher mass deviation than expected due to the presence of an unresolved interference could go completely undetected (Vogeser & Seger, 2010).

A solution to the overlapping peaks problem consists of identifying the interfering species and applying corrections for their contribution to the signal from the analyte.

Corrections are based on identifying an isotope of the suspected interfering element that does not itself suffer from spectral interference and that can be measured with a sufficiently accurate signal. Then, knowing the relative natural abundance of the isotopes, the contribution of this interfering element to the signal at the mass of interest can be calculated. If the interfering compound is

present in much higher concentrations than the target analyte, this correction would not be appropriate because the error on the measurement can be too large (Romero-González & Frenich, 2017; Vogeser & Seger, 2010).

Mass spectrometry analysers that comprise a collision cell could offer another solution to eliminate some of these interferences by dissociating an interfering species because of the fact that an isobaric interference will not likely produce both the protonated/deprotonated molecular ion and the fragment ions in the same proportions as the target compound. However, quantitative fragmentation patterns, which determine branching ratios, are a result of complex individual instrument characteristics and they usually differ between instruments and even can show distinct matrix effects. Consequently, accepted branching ratios must regularly be assessed with matrix-matched solutions of the target compound.

High-resolution mass spectrometers have the ability to resolve many isobaric interferences from the analyte as they can potentially distinguish compounds with identical nominal masses but different elemental formulas and thus allow unambiguous quantitative analysis to be carried out. Such platforms rely on sophisticated software algorithms and can be used to predict the elemental formula of unknown compounds based on a single accurate mass measurement (Daniel C. Harris & Lucy, 2016).

Electrospray ionization (ESI) or nano-ESI coupled with high resolution accurate mass spectrometry such as Orbitrap mass analysers, which can reach a resolving power of 140 000–480 000 FWHM at *m/z* 100 and *m/z* accuracy of 1–5 ppm with external calibration, are increasingly used, especially when they are combined with online or offline chromatographic

separation techniques, for lipidome analysis to overcome limitations associated with isobaric mass overlap that is inherent to low resolution MS analysis methods (Daniel C. Harris & Lucy, 2016; Hofferek et al., 2021).

1.3 Lipids

1.3.1 Lipids Definition and Classification

The denotation of the term "**lipid**" enjoys a common understanding amongst most of researchers who work with these molecules. However, the definition of "**lipids**" is disputed in the lipid community. (CHRISTIE & HAN, 2010) used the historical perspective of the term offered by (Gidez, 1984) in an approach to assist with a definition. It has evolved via a few terms such as ‘lipoid’ meaning resembling fat which was first used in 1876, ‘lipine’ in 1910 that was used to represent compounds of fatty acids containing nitrogen but no phosphorus or carbohydrate group, ‘lipin’ suggested as a generic name for fats and fat-like substances (lipoids) in 1912, and ‘lipide’ in 1923 before the introduction of the term "**lipid**".

Typical biochemistry dictionary like (Cammack et al., 2006) and university biochemistry textbooks such as (Voet et al., 2016) and (T.S. Work and E. Work, 1972) opt to give an imprecise description for lipids as a broadly defined group of naturally occurring organic compounds, with the common characteristics of oily texture and facile solubility in organic solvents such as chloroform, hydrocarbons, benzene, alcohols and ethers, in addition to the fact that they constitute a principal structural material of living cells together with carbohydrates and proteins. Lipids comprise a diverse range of compounds that can encompass fatty acids and their derivatives, carotenoids, terpenes, steroids and bile acids. Evidently, those compounds are structurally diverse despite the fact that specific functions may be common amongst them. In fact, there are many examples of the substances that are now widely considered as lipids that do not adhere to this loose definition such as bile acids and gangliosides that have good aqueous solubility (CHRISTIE & HAN, 2010).

The lack of a recognised definition of a "**lipid**" that has been accepted by any international body that recommends standards or comments on nomenclature issues has led some in the scientific community to define this widely diverse group of

molecules on the basis of their biosynthetic origin. The LIPID MAPS Consortium (Fahy et al., 2009) has defined lipids as 'hydrophobic or amphipathic small molecules that may originate entirely or in part by carbanion-based condensation of thioesters (fatty acids, polyketides, etc.) and/or by carbocation-based condensation of isoprene units (prenols, sterols, etc.)'

An alternative definition that is more appealing for chemists was suggested by (CHRISTIE & HAN, 2010) and it substantiates the significance of fatty acids as the building blocks of lipids. This definition is-

'Lipids are fatty acids and their derivatives, and substances related biosynthetically or functionally to these compounds.'

According to (Gidez, 1984), first effort to classify lipids was done by Bloor in 1920 who outlined "lipoids" classification into three groups, simple lipoids (fats and waxes), compound lipoids (phospholipoids and glycolipoids) and derived lipoids (fatty acids, alcohols and sterols).

The LIPID MAPS classification system is based on their aforementioned definition of lipids in terms of biosynthetic mechanisms and in conjunction with the International Committee for the Classification and Nomenclature of Lipids. Therefore, (Fahy et al., 2012) have defined eight categories of lipids based on their chemically functional backbone - fatty acyls, glycerolipids, glycerophospholipids, sphingolipids, sterol lipids, prenol lipids, saccharolipids, and polyketides, in addition to several classes and subclasses to allow one to describe all lipid molecular species.

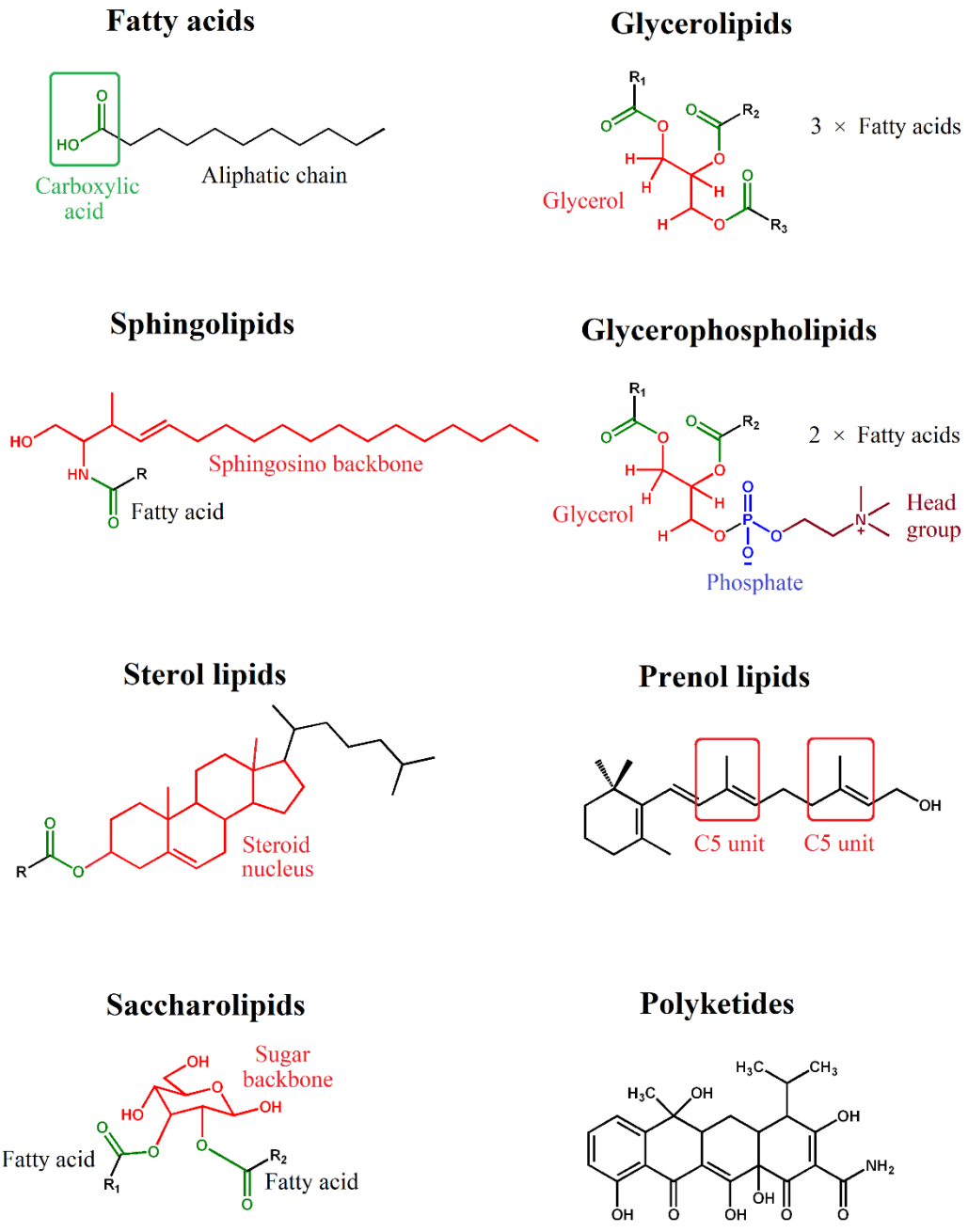

Figure 1-14 Categories of lipids based on their chemically functional backbone.

1.3.2 The roles of lipids in Biology

1.3.2.1 Lipids in cellular structure

Semi-permeability of plasma membranes allows cells to separate themselves from their external surroundings, notwithstanding it offers selectivity of importing, maintaining and exporting various types of molecules. One of the most important roles

of lipids in biological organisms is the formation of this semi-permeability by means of providing the fundamental building blocks of cell membranes bilayer structures. Therefore, necessary substances such as nutrients may be imported into cells, while unwanted molecules such as toxins can be excluded from entry. In the same way, certain products of cells metabolism, such as waste products or actively secreted compounds can be selectively exported by the means of the plasma membrane (Vance & Vance, 2002). In addition to forming the cellular membrane, lipids play essential roles in the construction and maintenance of membranes that surround the diverse specialised sub-compartments, or organelles within eukaryotic cells. The development of this endomembrane system was a vital landmark in the prokaryote-to-eukaryote evolutionary transition that introduced compartmentalisation that enables each cell to carry out a wide range of metabolic functions in an efficient and well-regulated manner (Dacks & Field, 2007; Hurley et al., 2010).

The composition of lipids and their physical properties can act as the fundamental model for important properties of membrane such as curvature, thickness, and tension. Moreover, asymmetry is largely a product of enriched varieties of lipids within distinct membrane leaflets. In mammalian cells, the membrane's cytoplasmic leaflet usually contains more phosphatidylserine as in the inner side of human red blood cell membranes when compared with the outer monolayer rich in phosphatidylcholine (Goñi, 2014). In addition, lipids can have different overall intrinsic geometric shapes depending on inherent properties, such as head group size and the length and/or saturation of their acyl chain tails (Goñi, 2014; McMahon & Boucrot, 2015). Interference of integrated sterols with acyl chain packing promotes maintenance of membrane fluidity, despite the presence of saturated lipids. On the other hand, membrane rigidity can be increased when sterols are associated with flexible unsaturated lipid bilayer because of their poor flexibility (Goñi, 2014; Mondal et al., 2009).

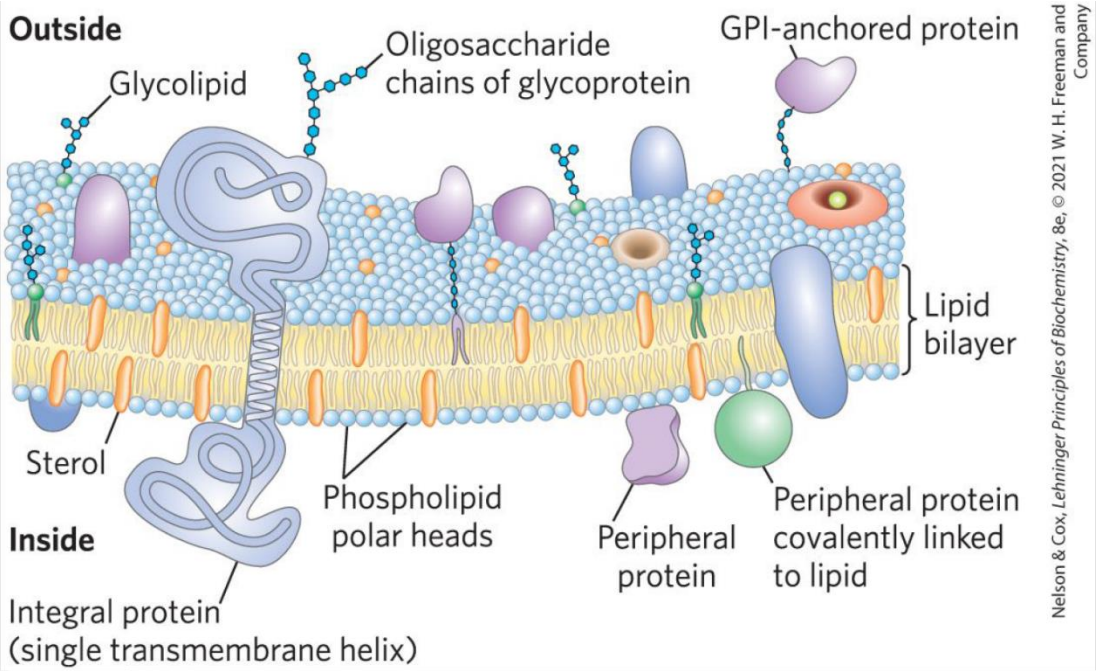

Figure 1-15 Fluid mosaic model for membrane structure (Nelson & Cox, 2021).

At the cellular level, lipids are synthesised by complex molecular pathways so they can provide essential building blocks in membrane biogenesis to support organelle or cell growth. The synthesis of lipids necessitates storing of excess fatty acids as neutral lipids, such as triacylglycerol or sterol esters. This storage takes place in specialized organelles called lipid droplets (LDs) (Henne et al., 2019; Ueno et al., 2016) .

1.3.2.2 Lipids as reservoirs for energy storage

The housing of different classes of lipids by Lipid droplets (LDs) does not only serve as a storage process for key building blocks for formation of the cellular membrane system, but it also mainly provides energy reservoirs at the cellular level (Henne et al., 2019).

Amid conditions with strained availability of energy sources, the universal need of eukaryotic organisms for the lipid droplets (LDs) specialisation in synthesising, storing, and then supplying excess energy from nutrients in the form of non-polar or "neutral" lipids is essential for their survival (Onal et al., 2017; Pol et al., 2014). To that end, higher organisms adapt to excess energy by the evolution of adipose tissue in which white adipocytes perform optimisation of energy storage efficiency and lipid

uptake, metabolism, trafficking, and signalling via their huge unilocular LDs (Jarc & Petan, 2019; Robbins & Savage, 2015).

White adipose tissue not only serves as the main storage site for almost all triglycerides in healthy adult humans, but also plays a central role in regulation of the uptake of substrates (e.g., glucose and non-esterified fatty acids), assembly of non-polar or "neutral" lipid for storage, and lipolysis process, through which the stored triglycerides is released. These processes enable homeostatic energy balance and they are influenced by nervous, hormonal, and nutritional factors (Mann & Savage, 2019). Secretion of the adipose-derived hormone leptin by adipocytes serves as an indicator of the status of their energy reserves, as well as being a mediator that acts centrally on the interaction between peripheral signals and brain targets to influence feeding, energy balance and reproductive capacity (Ahima & Flier, 2000; Mann & Savage, 2019).

The presence of another distinct type of multilocular LDs that promote energy expenditure is considered characteristic of brown adipocytes that develop in distinctive developmental depots of brown adipose tissue. Their main function is to dissipate chemical energy to generate heat in response to various stimuli, including catecholamines that are secreted by sympathetic nerves in BAT on cold exposure by oxidizing glucose and lipids via a mechanism mediated by a protein called the uncoupling protein-1 (UCP-1), present in the inner membrane of mitochondria(Jarc & Petan, 2019; W. Wang & Seale, 2016).

A third type of adipocyte with an intermediate morphology between that of white and brown adipocytes, also referred to as beige, "brite" (brown-like-in-white) or "inducible brown" adipocytes, that form in white adipose tissue (WAT) depots in response to various stimuli, including cold exposure or β3-adrenergic agonists. Despite similarities to brown adipocytes, such as the expression of uncoupling protein 1 (UCP1)- and thermogenical competence, beige adipocytes can undergo a thermogenic or storage phenotype depending on environmental conditions (Mulya & Kirwan, 2016; W. Wang & Seale, 2016).

Nutrient storage in the form of triacylglycerol (TAG) has two advantages over carbohydrate (glycogen)-based forms of energy: the more highly reduced carbons of

fatty acids yield more energy per gram than carbohydrates (9kcal/g for fatty acids versus 4kcal/g for carbohydrates) and the hydrophobicity of lipids allows anhydrous 'lighter' storage. For the same mass of carbohydrates, triacylglycerol yields more than sixfold the amount of energy (Robbins & Savage, 2015).

Although protein, carbohydrates, and fat can all be catabolised to provide energy, living organisms can only store surplus energy in the form of carbohydrates (as glycogen) or as fat (mainly triacylglycerol). As mentioned previously, fat is a far more efficient way to store energy in terms of its relative weight and space requirements. It is therefore not surprising that estimates of the total amount of energy that can be stored as glycogen or fat in a lean adult human differ by 100-fold (fat: 600– 800MJ; glycogen: 6–8MJ) (Mann & Savage, 2019; Robbins & Savage, 2015).

1.3.2.3 Lipids in cellular signalling processes

As discussed above, Lipid droplets (LDs) are no longer considered passive cytosolic inclusions or merely storage sites for triglyceride energy as it was the case for decades. LDs are now highly appreciated as important metabolic hubs of cells. LDs are intricate and dynamic organelles that play key role in the regulation of lipid homeostasis. LDs and adipocytes provide substrates for energy metabolism and membrane synthesis, and they also secrete a multitude of other of essential lipid-derived molecules such as leptin and lipoproteins (collectively known as adipokines) with a range of purported signalling functions (Mann & Savage, 2019; Pol et al., 2014).

Lipids, on their part, have more recently surfaced as crucial regulatory compounds of cellular signalling processes amongst their multiple roles in providing unique and fundamental model for physical and chemical properties of cellular membranes. They perform their regulatory roles either by directly combining with receptors and second messengers, or by mediating in complex signalling networks (Hannah Sunshine and M. Luisa Iruela-Arisp, 2017).

Several lipids are known to act as direct ligands to receptors and secondary messengers during cell signalling. For instance, sphingosine, the membrane lipid, has been shown to modulate protein kinase C. Moreover, diacylglycerol (DAG) produced by the hydrolysis of phosphatidylinositol 4,5-biophosphate (PIP2) by phospholipase C as a

part of the phosphatidylinositol signalling pathway activates protein kinase C (Hannun & Bell, 1989; Mérida et al., 2019), while the other product of hydrolysis, inositol 1,4,5-triphosphate (IP3), plays a crucial role in the control of calcium levels promoting a multitude of cellular responses including core metabolic pathways, transcription, cell growth, apoptosis sensitivity and immune responses (Hannun & Bell, 1989; Kania et al., 2017).

An additional direct lipid-dependent receptor signalling process was recently revealed. The correlation between tumour progression, including transition process by which epithelial cells become mesenchymal stem cells and gain migratory and invasive properties, and the overexpression of ganglioside GM2 in the cell surface of cancer cells has been previously detected (Mahata et al., 2015). Furthermore, a new mechanism of promoting tumour cell migration by ganglioside GM2 was indicated by the work of (Kundu et al., 2016) in vitro. The indicated mechanism involved the direct biophysical interaction of GM2 with beta1 integrins leading to promoting integrin activation along with downstream signalling including consequent phosphorylation of Erk-MAPK resulting in cytoskeletal changes and increased migration. Activated integrins might be located on the same cell (in *cis* activation) or on different cells (in *trans* activation) or both simultaneously.

Lipids regulatory effects on the assembly of complex signalling networks can be demonstrated by the impact of lipid phases on macrodomain heterogeneity. Segregation and crowding promoted by macrodomain heterogeneity in cellular membrane constrains lateral diffusion resulting in either facilitating or hindering protein-protein interactions with implications on cell signalling (Goñi, 2014). In addition, cell signalling has been recently shown to be affected by modulating the exposure of specific protein domains to the cytosol or the type of protein anchorage to plasma membrane. Local lipid composition regulates how signalling proteins attach to the plasma membrane, for instance, the association of the enzyme K-Ras, that regulates multiple signalling pathways and is known to be linked to several cancers, with distinct phospholipids dictating its orientation and hence its function. Thus, how the protein is anchored in the membrane and how its catalytic domain is oriented can be significantly affected by the composition of phospholipids in the membrane because of their

versatile affinities for this protein (Z. L. Li & Buck, 2017). One more example of the role of lipids composition in modulating protein-protein interactions and downstream signalling processes are Src homology 2 domains (SH2) that are essential to downstream signalling in multiple phosphotyrosine receptor pathways (Park et al., 2016).

The degree of saturation in the phospholipid fatty acid chains might also be able to modify Cell signalling processes. In addition to their significance in determining stiffness and elasticity of cellular membranes, changes in fatty acid saturation can impair lipopolysaccharide (LPS)-mediated activation of TLR4 which eventually promotes the activation of the nuclear factor kappa B (NFkB). Moreover, (Schoeniger et al., 2016) suggest that modulation of the physical-chemical properties of membrane microdomains caused by poly-unsaturated fatty acids (PUFAs) enrichment can substantially impair stimulation of TLR4 through the disruption of membrane microdomains.

Table 1-1 Classification of lipid mediators (Shimizu, 2009)

Lipid class	Lipid mediators (abbreviated names)	Biological effects
Fatty acids	Prostaglandins (PG)	fever, pain, inflammation
	Thromoboxane (TX)	platelet aggregation, vasoconstriction
	Leukotrienes (LT) lipoxins (LX)	Inflammation
	Resolvins (Res)	Anti-inflammation
	12-Hydroxy-heptadecatrienoic acid (12-HHT)	Chemotaxis
	Isoprostanes	Contraction of smooth muscle
	Short-chain fatty acids	Insulin secretion
Glycerophospholipids	Phosphatidylinositol 4,5-bisphosphate (PIP2)	Precursor of DAG and IP3
	Diacylglycerol (DAG)	Protein kinase C activation
	Inositol 1,4,5-triphosphate (IP3)	Increase of intracellular calcium and promotion of transcription, cell growth and immune responses.
	Platelet-activating factor (PAF)	Inflammation, bone resorption
	Oxidized phospholipids (Ox-PL)	Vasoconstriction, chemotaxis
	Ceramide	Apoptosis, autophagy, mitophagy, cell cycle arrest and senescence

Sphingolipids	Ceramide-1-phosphate	Cell proliferation and migration
	Sphingosine	Apoptosis, protein kinase C modulation
	Sphingosine 1-phosphate (S1P)	Cell-survival, differentiation, inflammation, and angiogenesis
	Psychosine (Psy)	Widespread demyelination and subsequent neuropathological events
	Lysophosphatidic acid (LPA)	Cell proliferation and development
Lysophospholipids	Arachidonoylethanolamide	Endogenous agonist of cannabinoid receptors
N-acylethanolamines	Palmitoylethanolamide	Anti-inflammatory and analgesic
	Oleoylethanolamide	Appetite-suppressing and anti-obesity effects

1.4 Fatty acids

Fatty acids are the main constitutional component of lipid classes according to the definition lipids by (Christie & Han, 2012a), and they encompass carboxylic acids with even numbers of carbon atoms either saturated in straight chains or unsaturated, with double bonds in specific positions in relation to the carboxyl group at one end of the carbon chain. The length of carbon chains and composition of fatty acids vary according to species and tissue. Fatty acids in animal tissues reach a chain length of between 2 and 36 carbon atoms or even more. Nevertheless, fatty acids with chain lengths longer than 22 and shorter than 14 carbon atoms exist only in minor concentrations. On the other hand, specific groups of microorganisms can contain fatty acids with 80 or more carbon atoms, but chain length ranges in higher plants usually are more restricted. Unsaturated fatty acids in algae, plants and animal tissues may have one to six double bonds, although, those in the higher plants rarely have more than three while microbial fatty acids only occasionally have more than one (Christie & Han, 2012b; Tvrzicka et al., 2011).

1.4.1 Fatty acid nomenclature and numbering

Common names of fatty acids that are usually derived from the origin of these compounds such as palmitic acid of palm oil, oleic of olive oil (coming from the Latin

oleum, oil) do not provide any information about their chemistry. Therefore, a need has arisen for more systematic nomenclature that conveys structural characterisation of fatty acids. These characteristics include chain length, degree of unsaturation, position and geometry '*cis*' or '*trans*' of double bonds and presence of other substituents. The International Union of Pure and Applied Chemistry (IUPAC) and the International Union of Biochemistry (IUB) have laid down a naming system where fatty acid nomenclature can be expressed as a schematic formula (shorthand notation) as in x-C:n where x represents position of the first double bond if any, C- total number of carbon atoms and n- number of double bonds.

There are two systems for carbon atoms numbering in fatty acids, each one of them indicates carbon atoms positions relative to one end of the carbon chain. The standard system adopted by the IUB/IUPAC numbers carbon atoms from the carboxyl end while the other system counts from the noncarboxyl (methyl) end. Depending on the numbering system used, the aforementioned schematic formula can be preceded by position of substitution in addition to '*c*' or '*t*' for '*cis*' or '*trans*' to express 'double bonds geometry (Gurr et al., 2016).

Fatty acids (FAs) are classified structurally and stereo-chemically mostly according to the presence or absence of double bonds as saturated (SFAs—without double bonds), monounsaturated (MUFAs—with one double bond) and polyunsaturated fatty acids (PUFAs—with two or up to six double bonds); further, as *cis* or *trans* based on the configuration of the double bonds and as n-3 or n-6 PUFAs depending on the position of the first double bond from the fatty acid methyl-end. This classification accentuates the impact of the stereochemistry of fatty acids on their biological roles and nutritional significance. It is important to underscore that, although several fatty acids can be synthesised in the human body even with a double bond on C9 from the methyl end, the synthesis of PUFAs with the first double bond on C3 and C6 from the methyl end is not possible because of the absence of appropriate enzymes. Consequently, these fatty acids, linoleic and alpha-linolenic acids, are termed "essential" as they need to be ingested with the diet (Davis et al., 2022; Orsavova et al., 2015).

Linoleic acid (18:2n-6) and α-linolenic acid (18:3n-3) are the principal essential unsaturated fatty acids. These fatty acids can be elongated and desaturated into their

longer-chain derivatives. The most prevalent n-6 in animal and human diets, linoleic acid, is metabolised to the long-chain FA arachidonic acid (AA) arachidonic acid (20:4n-6) that has an important role in brain development and function and synthesis of eicosanoids, while α-linolenic acid, the main omega-3 PUFA, is metabolised to the long-chain FAs (DHA, C22:6) eicosapentaenoic acid (EPA; 20:5n-3) and docosahexaenoic acid (DHA; 22:6n-3) that comprise important parts of all cell and organelle membranes and is found in the brain and retina.

From a nutritional viewpoint, some theories suggest a competitive relationship between n-3 and n-6 fatty acids where both groups compete for the same enzymatic activities of elongation and desaturation in the course of their metabolic pathways. Since high linoleic acid intakes dominate the shared enzymes responsible for n-3 LCFA synthesis, the ratio of n-6:n-3 (and specifically LA:ALA) has risen to be an important aspect of animal and human nutrition and health (Baker et al., 2016; Davis et al., 2022; Zárate et al., 2017).

Unsaturated fatty acids can exist in a *cis*- or *trans*-configuration. The former configuration is found in most naturally occurring unsaturated fatty acids, the latter configuration although its presence in the human diet as well is generally considered as a result of technology processing, such as hydrogenation. *Trans* configuration in the structure of fatty acid results in a straighter molecular shape than those with a double bond in a *cis* configuration (J. Chen & Liu, 2020; Orsavova et al., 2015).

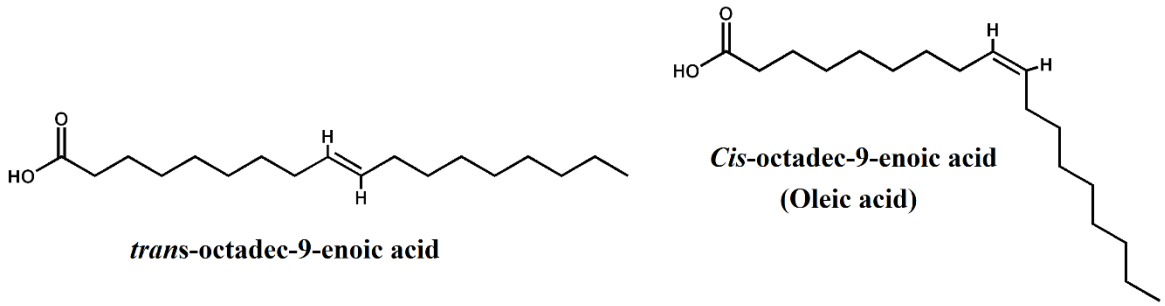

Figure 1-16 Geometric isomerism in unsaturated fatty acids

Cis-unsaturated fatty acids, whether mono or poly unsaturated, are promoted by international guidelines to replace saturated fatty acids in diets because of their

attributed healthful properties. They are potent inducers of lipid droplets (adiposomes), which have important roles in cell signalling, regulation of lipid metabolism and control of the synthesis and secretion of inflammatory mediators as we discuss later. On the other hand, *trans*- unsaturated fatty acids, which are unsaturated fatty acids with at least one double bond in the *trans* configuration that is not part of a conjugated system, are not essential, and they do not serve any vital functions (Brouwer et al., 2013). Conversely, the consumption of trans fatty acids (usually identified on food labels as "partially hydrogenated vegetable fats") has adverse effects on lipid and lipoprotein metabolism, i.e., increase in LDL cholesterol, reduction of HDL cholesterol, and deterioration of endothelial function, perhaps due to their pro inflammatory actions. There is a clear direct association between consumption of trans fatty acids with food and coronary risk (De Souza et al., 2015; Visioli & Poli, 2020).

Variability in oil content of fatty acid, has been shown to be affected by environmental conditions prevalent during the growing season, location, climate, harvest time, and the degree of maturity of the part of plant from which they are extracted (Nasri et al., 2021; Ouzir et al., 2021). In avocado fruits, the climate and country of origin in addition to other factors like their variety and soil type can affect the fruit quality and hence, the fatty acid profile of the oil (Flores et al., 2019; Green & Wang, 2020). Comparable observations were reported in pistachio regarding the impact of climate conditions during the growing season, in particular during the summer months (Bacchetta et al., 2013).

Fatty acid profile of olive oil is one of the main factors that contributed to the positive health benefits of the diet of the countries surrounding the Mediterranean Sea like low incidence of chronic degenerative diseases. Studies results has demonstrated the effect of climate and latitude of cultivation on the degree of fatty acid unsaturation and the oil content in olive (Bacchetta et al., 2013).

1.4.2 Significance of double bond position in unsaturated fatty acids

It is already profoundly established that small modifications in chemical structure of lipids can modify their physical and biochemical properties. The diversity of fatty acyl

chains in numbers and lengths, head groups, degrees of unsaturation and double bond position is the main source of the structural variability among lipid categories (Ying Zhou et al., 2014).

In 1981, (Stubbs et al., 1981) observed the changes in motional parameters of membranes caused by the variability in the precise position of the unsaturated acyl chain(s) and the number and position of the bonds within the acyl chains. Thereafter, thermodynamic, dynamic and structural properties of the lipid bilayer membrane in the fluid state have been elucidated to be affected by the variation of double bond position along the acyl chain. In some studies of (C. Huang et al., 1997; Marsh, 1999), the workers presented a demonstration of how the position of a double bond near the geometric centre of an acyl chain can cause a reduction in the temperature and enthalpy of the main phase transition more than the case where a double bond is located closer to either end of the chain. These changes in the main phase transition temperature and associated dynamic and structural properties, specifically, membrane fluidity (disorder in the acyl chain region) has been noticed to be compatible with atomic-scale molecular dynamics simulations studies by (Martinez-Seara et al., 2007). In these simulations, the presence of double bond in the middle of an acyl chain was found to minimise membrane order and packing in the membrane hydrocarbon region, increase area per lipid, decrease membrane thickness, density and dehydration. Furthermore, the subsequent impact on membrane fluidity was shown to fluctuate with variation of the double bond position. Moreover, all of these changes were found to get amplified when the double bond is in the vicinity of cholesterol molecules in the membranes (Martinez-Seara et al., 2008).

Free fatty acids (FFAs) behave as low affinity non-competitive antagonists of the nicotinic acetylcholine receptor (AChR). The purposed site of this inhibitory behaviour is at the lipid-protein interface. Furthermore, structural characteristics of FFAs, namely the presence, position and isomerism of the double bond play an important role in controlling their effects on the AChR conformational state. Although that the AChR detects all FFAs effectively localised in the environment of the protein which results in the conformational changes, the inhibition activity is only observed

with those FFAs having the double bond at a superficial position relative to the lipid (Perillo et al., 2012).

The degree of desaturation and the position of double bonds along the fatty acid chains are closely connected to the activity of desaturase enzyme family that forms an important step in the synthesis of other fatty acids and lipids (Antonny et al., 2015; Rioux et al., 2015). Additionally, as the main site for the lipid peroxidation process, double bond positions contribute to determining the structure of primary and secondary products of lipid peroxidation (Ayala et al., 2014).

1.5 MS-Based techniques in lipid analysis

1.5.1 Mass Spectrometry imaging

As the term might suggest, MSI is an imaging method that provides visual illustration and disposition of individual lipid molecules in tissue samples by direct ionisation and MS detection methods. Diverse biological processes that are related to lipid species of interest and their interactions and dynamic spatial distributions can be examined via MSI-created images of a biological sample, such as complex tissues since they provide the visualisation and distribution information of these molecules. Compared with other existing imaging methods like fluorescence imaging, MSI is not as highly sensitive. Nevertheless, it is relatively new method that is still witnessing advances in ionisation techniques that can improve sensitivity and spatial resolution. The main ionisation techniques that are used in MSI are MALDI, desorption electrospray ionization (DESI), and secondary ion mass spectrometry (SIMS) (M. Li et al., 2014; K. Yang & Han, 2016).

1.5.2 Chromatography-coupled Mass Spectrometry

In the extensive analysis of complex biological lipid samples, it is a necessity to employ the chromatographic methods with high separation capacity prior to MS in an aim to separate lipid isomers, decrease matrix effects and augment low-abundance lipid molecules. Chromatographic methods coupled with MS platforms provide data that comprise both chromatograms (total ion current, extracted ion current) and mass spectra. The identification of lipid compounds is accomplished making use of both the retention time in their chromatograms and the characteristic fragment ion information in their mass spectra. Several separation technologies have been explored in combination with MS. Despite of its ability to quickly and inexpensively separate lipid mixtures into individual categories of lipids, Thin Layer Chromatography (TLC) has problems of low separation efficiency and inadequate sensitivity that lead to poor resolution, larger sample size requirement and difficulties in coupling with MS to improve sensitivity. Improvement to resolution and peak capacity in TLC was achieved either by using smaller particle size and thinner stationary phase layer, as in high-performance thin layer chromatography (HPTLC), or by implementing two-

dimensional TLC that can separate samples in two orthogonal directions. Generally, TLC can be used as an off-line separation method in combination with MALDI-MS (Griesinger et al., 2014; L. Li et al., 2014). The high separation efficiency of Gas Chromatography (GC) and its ability to separate isomers and high sensitivity for quantitation permit its use as a powerful chromatographic separation method for lipid analysis, specifically for the separation of volatile compounds. The combination of GC and MS is currently the principal method for the profiling and quantitation of some lipid classes like FAs and cholesterol and its esters. However, because it is restricted to volatile lipids, samples require the derivatisation of non-volatile lipids before detection which may compromise structural information of lipid molecular species thus indicating the principal limitation of the use of GC in lipidomics (L. Li et al., 2014; Son et al., 2014; Zanfini et al., 2014). On the other hand, liquid Chromatography (LC) is suitable for the separation of both volatile and non-volatile lipids and can be readily coupled with MS. High Performance Liquid Chromatography (HPLC) displays high separation efficiency, selectivity and visibility, and because of this it is the most popular and widely used separation method in lipidomics, especially when coupled with electrospray ionisation (ESI)-MS. Usually, hydrophilic head group in lipid classes is the determinant structural feature in normal-phase HPLC and HILIC separation; those lipids with identical head groups will elute together in these separation techniques. To the contrary, the hydrophobicity of FA chains in lipids dictates their separation in reversed phase HPLC, and the length of the FA chain and number of double bonds plays a major role in their elution order. In reversed-phase HPLC, C8, C18 and C30 columns are the most commonly used in lipid analyses. An integration of the potently designative capabilities of NPLC or HILIC towards different classes of lipids with the high resolution-separation that RPLC can provide separation for molecular species within each specific lipid class according to their different fatty acid chains. This is available via two-dimensional LC (2D LC) which can offer comprehensive chromatographic information for lipid samples before MS detection (Rustam & Reid, 2018). The main drawbacks that 2D LC has to overcome are the immiscibility of the mobile phase between NPLC and RPLC and the need for customised instrumentation, a manual off-line 2D LC/MS approach on lipid profiling was established without much device modification in the work of (Fauland et al., 2011)

where the fractions were collected manually after the first dimensional separation before they were injected to the second dimensional column. Thereafter, less labour-intensive and time-consuming methods to achieve 2D LC/MS have been introduced, where on-line pre-fractionation and column-switching were employed (Ling et al., 2014; S. Wang et al., 2017). The recent developments of LC-MS methods allow high-throughput sensitivity and resolution of lipidomics analysis. A dramatic increase in peak capacity, resolution, analytical speed, and sensitivity and an aligned decrease in matrix effects were achieved using ultrahigh performance LC (UHPLC) columns that have smaller stationary phase particles size, sub-2 μm sized particles compared to 5 μm sized particles in conventional HPLC, and function at high pressures (6000–15000 psi) (Rustam & Reid, 2018). Higher separation efficiency was also provided through reduced inner diameter of the column, accompanied with a reduction in the flow rate of the mobile phase, as in nano LC (Danne-Rasche et al., 2018). A less commonly used separation mode is silver ion chromatography (Ag-LC), which is mainly used for the separation of FAs and triacylglycerols. Ag-LC separates lipid compounds based on the length of FA chains and number and configuration of double bonds because its main retention mechanism relies on the formation of polar complexes between silver ions and double bounds in unsaturated FA chains. FAs and triacylglycerol isomers differing in the position or/and configuration of double bond can be separated on Ag-LC (Lange et al., 2019). A few other separation technologies such as supercritical fluid chromatography (SFC) and Capillary Electrophoresis (CE), which are more environmentally friendly because they use much lower amounts of organic solvents, can be applied in combination with MS to separate lipids. Regarding the employment of SFC devices, SFC–MS demonstrated the maximum efficiency in the target analysis of lipids in complex biological samples due to the advantages of the use of supercritical fluid as the mobile phase. Moreover, because of the physical characteristics of the mobile phase, a vacuum solvent evaporation interface was developed to realise the use of SFC as the first-dimension separation technique in a nonstop-flow 2D LC/MS based method for lipid profiling (Bamba et al., 2012; L. Yang et al., 2020). To tackle the complication that comes with the poor solubility of most lipids in aqueous solutions that is commonly used in CE, (F. Gao et al., 2007) reported a nonaqueous CE method that can separate phospholipids.

1.5.3 Shotgun Mass Spectrometry

Shotgun MS in lipid analysis was originally determined as a strategy for the analysis of the cellular lipidome directly from a biological sample in a high throughput format. Currently, the term is generally used with regards to the lipid analysis methods based on direct infusion into the MS instrument without previous chromatographic separation (X. Han & Gross, 2005). Shotgun analysis has various analytical advantages over other methods such as its promptness, convenience and reproducibility. Shotgun lipid analysis involves few platforms like qualitative tandem MS technologies, high resolution MS technologies, multidimensional MS technologies and ion mobility mass spectrometry (IM- MS) (K. Yang & Han, 2016). Regarding ionisation techniques used in shotgun analysis, electrospray ionisation (ESI) has grown to be the most prominent approach and has enjoyed the most success (K. Yang & Han, 2011).

Notwithstanding all the advantages offered by shotgun lipidomics, it has its limitations including the matrix-induced severe suppression of ionisation that renders the detection of lipid molecules with relative lower abundances difficult if not impossible. Moreover, the incapability to distinguish lipid isomers without a preliminary separation (Gross et al., 2005).

In order to identify the specific lipid class of the sample, a tandem MS shotgun method can apply various types of scans such as precursor ions scan, product ions scan and neutral loss scan. Non-endogenous analogues or isotopic internal standards (ISs) are essential to compare with samples when direct infusion tandem MS is implemented for quantification analysis. MS methods that provide increased accuracy for mass values of lipid molecules and their product ions, such as Fourier transform ion cyclotron resonance MS (FTICR-MS), Q-TOF-MS and orbitrap MS, can assist in eliminating matrix interference and in differentiating lipid isobaric ions. Therefore, they are the most commonly used methods in shotgun lipidomics (K. Yang & Han, 2016). In recent years, multidimensional MS and IM-MS have become available for lipidomics analyses. Joining separational capabilities of ion mobility spectrometry and high-resolution MS techniques enables IM-MS methods to achieve the separation of ionised lipid molecules not only by their charge and mass but also by their size and shape that vary with their structural diversities, such as different backbone and head

group, depending on the variations in mobilities of their ions in low or high electric fields. At present, commercially available IM-MS instruments could be classified to three types, including time-dispersive, counting the travelling-wave IM (TWIM), drift-time IM (DTIM), spatially-dispersive and confinement and selective release instruments (Tu et al., 2019). In the time-dispersive approaches, all the ions are allowed to pass within the mobility cell through the buffer gas either in propelled motion driven by a 'traveling wave', generated by a sequence of applied voltages, like in TWIM or drifting in the presence of an axial, linear electric-field gradient like in DTIM. One of the most used IMS-based techniques is field asymmetric IM (FAIMS), that also known as differential ion mobility spectrometry (DMS). In this approach, selected ions are filtered in a space-dispersive fashion by varying the compensation voltage to differentiate ions based on their mobility differences. While in trapped IMS (TIMS), ions separation is performed in confinement and selective release manner by trapping ions and selectively ejecting them (Paglia et al., 2015; Tu et al., 2019; X. Zhang et al., 2018).

The use of IM-MS in shotgun lipidomics has a massive potential as it can enhance post-ionisation separation and hence increases peak capacity and signal-to-noise ratio and generate cleaner mass spectra for complex shotgun MS lipidomics samples (Paglia & Astarita, 2017).

1.6 Mass Spectrometry technologies to identify lipid double bond locations

On account of its high sensitivity, selectivity and efficiency for delivering comprehensive structural information, high-resolution mass spectrometry (HRMS) has come to be the method of choice for lipid analysis (X. Han et al., 2012). However, applying the widely used low-energy collision-induced dissociation (CID) processes would not be effective to generate the ion fragments that indicate the double bond positions which makes it a real challenge to determine the positions of double bonds by conventional high-resolution MS alone (Thomas et al., 2007). To conquer this problem, the lipidomics community explored a variety of methods to identify double bond positions along fatty acyl chains in lipid molecules. These methods included direct MS methods (on-line MS methods) and other methods that contained derivatisation preceding MS analysis (off-line methods).

1.6.1 On-line mass spectrometry methods

Different ionisation technologies in MS were exploited for identification of double bond locations in underivatised lipids, although some of these methods involved some forms of *in situ* derivatisation.

1.6.1.1 Fast Atom Bombardment (FAB)

The pioneering efforts of (Tomer et al., 1983) on charge remote fragmentation by high energy collisional-induced dissociation (CID) of intact lipids using fast atom bombardment (FAB) produced mass spectra in the negative ion mode that showed abundant molecular FA carboxylate ions in addition to product ions that arise from the cleavage of allylic carbon–carbon bonds on both sides of the double bond. Nevertheless, when attempts were made to locate the double bonds in polyunsaturated fatty acyls using this method, mass spectral data was not as readily interpreted as that for monounsaturated acids.

At the time, this innovative approach was further investigated by the attempts of (Bryant et al., 1991) to obtain FAB-MS^3 fragmentation data to locate double bonds as part of the analysis of phosphatidylcholines present in a human immunodeficiency virus using a four sector MS instrument. Even with the use of this instrument arrangement, the obtained sensitivity was relatively low compared with that of the mass spectrometers currently available.

1.6.1.2 Electrospray Ionization (ESI)

Electrospray ionisation (ESI) is the ionisation method of choice in MS for lipid analysis in biological samples, and this has been the case since the recent developments of MS, specifically the introduction of soft ionisation techniques (X. Han & Gross, 2003).

ESI was used for direct identification of double bond position by exploring the capabilities of alkali metal adducts produced in an ESI source, namely Lithium adducts, to generate ion fragments of fatty acid chains (F.-F. Hsu & Turk, 1999, 2008, 2010). Although the quality of obtained data via low-energy CID of dilithiated lipid adduct ions produced in the ESI source was an improvement from older techniques

and hydrocarbon fragment ions were actually generated from the fatty acyl chains, forming allylic and vinylic fragment ions, However, it was not facile to resolve MS data using this kind of method. Two main challenges were faced with this method, first one was the complexity of detecting and locating double bonds that was caused by the multi-stage fragmentation required to obtain double bond information, up to MS^5. Second one was the low intensity of the MS^n data resulting in very low ion abundances of fragment ions that belong to the fatty acyl moieties (Castro-Perez et al., 2011; F.-F. Hsu & Turk, 2008).

An alternative technique involving ESI and tandem mass spectrometry to determine double bonds position has emerged by developing an off-line ozonolysis method, discussed below in off-line mass spectrometry methods, to provide on-line approaches. In Ozone Electrospray Ionisation Mass Spectrometry (OzESI-MS), ozone gas reacted with double bonds in the source gas as part of electrospray process instead of being applied to samples prior to MS analysis as in the off-line experiment (Ellis et al., 2012; Thomas et al., 2007).

In order to produce ozone within gas source, (Thomas et al., 2006) used oxygen as nebulising gas and increased the capillary voltage in negative mode to generate corona discharge. This helped to perform the on-line ozonolysis of lipid double bonds without any prior sample preparation nor modification requirements on commercial ESI-MS instruments. However, the analysis of anionic lipids via this method was significantly more achievable than that of cationic ones because of the much weaker corona effect in positive mode, hence the much lower ozone production, in addition to the fact that ion abundance would be distinctly decreased because of elevated ESI capillary voltage and accordingly overall sensitivity would be reduced to add to the complication and difficulty of resolving the resulting mass spectrum in the case of analysing complex lipid mixtures with multiple double bonds (Brown et al., 2011; Thomas et al., 2007). In place of oxygen gas and corona discharge produced by elevated capillary voltage, (J. I. Zhang et al., 2011) used ambient air as the oxidising agent with low temperature plasma (LTP) probe in order to generate ozone gas for ozonolysis. Both negative and positive analyses were performed efficiently on ozone-oxidation products with similar types of indicative fragment ions and with results comparable to other OzESI-MS

methods. A different method to achieve in-source ozonolysis of double bond-containing ions includes an instrument-modification that is dedicating an ozone generator to supply ozone gas externally into the ESI source. The higher concentrations of ozone gas provided by the ozone generator do not only resolve the issues encountered in analysing cationic lipids but also restore the ability to optimise capillary voltages for maximum ion abundance rather than ozone concentration, thus improving overall sensitivity. Moreover, the increase in ozone concentrations offers a more efficient cleavage of targeted double bonds (Brown et al., 2011).

Following on the same path of capitalising on the advantages of using ozone generator and in order to overcome the complexity that arises in complex lipid mixtures, a more advanced method of on-line ozonolysis has been developed in which ozone gas can be applied to isolated lipid ions within an ion-trap mass spectrometer. This method is known now as Ozone-Induced Dissociation (OzID) and it enables the possibility of mass-selecting each lipid of interest within the ion-trap before getting it subjected to ozonolysis, permitting the assignment of fragments to their respective precursors in complex mixtures (Thomas et al., 2008).

1.6.1.3 Electron-induced dissociation (EID)

Determination of double bond position in lipids has been demonstrated through an alternative ionisation mode, in which the induction of the dissociation of the lipid ion of interest could be achieved via the chemistry between the ion and electrons in the gas phase. The technique that had been used before in the structural elucidation of diverse biological molecules was examined (Jones et al., 2015) and ion dissociation, excitation and detection were performed inside a Fourier transform ion cyclotron resonance (FT-ICR) cell in order to localise double bonds in mass-selected Phosphatidylcholine ions produced via matrix-assisted laser desorption ionisation (MALDI) and the technique was referred to as Electron-induced dissociation (EID).

This technique wherein the impact of a beam of energetic electrons (~10eV) is used to fragment isolated ions and obtain highly informative fragment ions was also referred to as Electron Impact Excitation of Ions from Organics (EIEIO) by (Campbell & Baba, 2015). Using a newly developed high throughput Electron Capture Dissociation (ECD) device (Baba et al., 2015) precursor ions generated by electrospray ionization (ESI)

were analysed and in-depth molecular structure identification of Phosphatidylcholines (Campbell & Baba, 2015), Sphingomyelin (Baba, Campbell, Blanc, et al., 2016) and triacylglycerols (TAGs) (Baba, Campbell, Le Blanc, et al., 2016) was achieved by operating on a quadrupole time-of flight Q-TOF mass spectrometer.

1.6.1.4 On-line gas-phase reactions with tandem mass spectrometry

In order to achieve positional demonstration of double bonds in lipids, on-line chemical reactions in gas phase have been deployed as well to generate adduct or derivative ions within mass spectrometer instruments to serve as precursor ions preceding further fragmentation with tandem mass spectrometry. Creation of covalent adduct through gas-phase reaction or chemical ionisation in the presence of acetonitrile leads to the production of (1-methyleneimino)-1-ethylium ions, $CH_2=C=N^+=CH_2$, that in turn react with carbon-carbon double bond to form adduct ions (Van Pelt & Brenna, 1999). After being subjected to collision-induced dissociation in ion-trap mass spectrometer coupled with a Gas Chromatograph (GC), these adduct ions have been used to generate diagnostic and informative fragment ions that facilitate elucidation of the position and stereochemistry, to some extent, of the double bonds in unsaturated Fatty Acid Methyl Esters (FAMEs) (Lawrence & Brenna, 2006; Michaud et al., 2002, 2003; Van Pelt & Brenna, 1999). Additionally, a variation of Covalent Adduct Chemical Ionisation (CACI) was performed under conditions of Atmospheric Pressure (APCACI) to localise double bonds in triacylglycerols that contain mono- and di-unsaturated fatty acyl chains (Xu & Brenna, 2007).

The very same approach was used by Vrkoslav and co-workers with the variation of coupling the APCI-MS instrument with High Performance Liquid Chromatograph (HPLC) instead of GC for separation to overcome the limitations connected with the need for adequate degree of volatility and thermal stability of the analysed lipids and to avoid the additional step of hydrolysing GC-intractable lipid analytes (Vrkoslav et al., 2011; Vrkoslav & Cvaˇ, 2012).

In the work of Ma *et al.*, a comparable approach was followed to obtain derivatised ions with carbon-carbon double bond position information using the decomposition of on-line induced Paternò–Büchi (PB) reaction products. A photochemical

cycloaddition reaction was achieved on-line between acetone as the PB reagent and unsaturated lipids by placing a low-pressure mercury lamp with ultraviolet emission band of 254 nm in close proximity to a nano electrospray ionisation source resulting in a fast and highly specific modification of the C=C bonds in lipids and formation of two position isomers of derivatives containing four-membered oxetane ring. Informative ions were generated through thermal dissociation of PB-formed oxetanes or what was described by (Ma & Xia, 2014) as retro PB reaction. Low-energy CID MS for each oxetane ring produced two diagnostic families of ions, one with an aldehyde group and one with newly derived olefin structures (Ma et al., 2016; Ma & Xia, 2014; Xie & Xia, 2019).

1.6.2 Off-line mass spectrometry methods

The combination of off-line chemical derivatisation of lipids and tandem mass spectrometry has been used to improve detection sensitivity, specificity and structure resolution in general lipid analysis. The application of this approach in the field of identifying double bond positions has been proved important (Kwon et al., 2011). Trials to employ chemical derivatisation in this area have gone into two directions:

1.6.2.1 Off-line derivatisation of the carboxyl group of fatty acids

In this approach, the application of Electron Impact (EI) ionisation in GC-MS or CID in LC-MS to identify double bond locations benefits from charge-remote fragmentation in the mass spectrometer. Fragment ions that are indicative of double bond locations can be generated via derivatisation of carboxyl groups in unsaturated fatty acyl chains by means of using a suitable derivatisation reagent.

Nitrogen containing compounds have been used to form fatty acid derivatives by reacting with carboxyl group in what is called ‘remote-site’ derivatisation (Spitzer, 1996). The ionisation of the hydrocarbon chain in derivatised fatty acids is suppressed because of ionisation preference at nitrogen functional groups. However, the formation of radical sites at any position on the hydrocarbon chain is possible as a result of potential hydrogen atoms migration from any site on the chain to the charge site. This can lead to the induction of radical site fragmentation processes that produce ion

fragments that can be informative about double bond positions. According to (Christie, 1998; Spitzer, 1996) many fatty acid derivatives have been investigated in GC-MS methods including pyrrolidides, triazolopyridines and 2-alkenylbenzoxazoles and piperidyl, picolinyl and morpholinyl esters. Among these derivatives, the picolinyl esters and pyrrolidide derivatives are the most frequently used in spite of the poorer GC resolution, when compared to that of the FA methyl esters, which cause a relative decrease in detection sensitivity and separation efficiency.

A comparable concept was used by (K. Yang et al., 2013) to localise double bonds using a direct infusion method that was based on the derivatisation method reported by (Bollinger et al., 2010) in which they tried to improve the sensitivity of LC-MS/MS detection of eicosanoids via employing N-(4- aminomethylphenyl) pyridinium (AMPP) as a derivatisation agent. Through derivatising carboxylic group in FAs with AMPP, fragmentation processes were induced by a series of 1,4-hydrogen eliminations that generated a diagnostic fragmentation ion which could be inducive to localisation of proximal double bonds in PUFAs in addition to other allylic cleavage-induced fragmentation patterns that could help substantiate the assignment of the multiple bond positions.

1.6.2.2 Off-line derivatisation of the double bonds in fatty acids

Over the decades, many authors adopted the approach of off-line preparation of suitable chemical derivatives in an aim to obtain, when followed by the appropriate mass spectrometry method, fragment ions labelled at the original position of the double bond. Further MS analysis of these labelled ions produces characteristic fragment ions that can be linked more readily to double bond positions. One commonly used method for double bond chemical derivatisation in association with MS analysis is employing dimethyl disulphide (DMDS) to label double bonds by reacting with them in unsaturated lipids to produce vicinal bis-methyl thiol ethers. Capillary GC-MS-EI analysis of DMDS-derivatives of fatty acid methyl esters generated diagnostic

fragment ions that result from a cleavage between adjacent carbons bearing methylthio groups in the original location of the double bond that, in addition to the molecular ion, helped in determination of double bond position in monounsaturated fatty acids (MUFAs) (Dunkelblum et al., 1985; P. Gao et al., 2012).

In order to achieve double bond localisation as a part of diacylglycerols (DAGs) structural characterisation, DMDS-derivatisation was used as well by (Deng et al., 2016) collectively with an analytical strategy that included ultra-performance liquid chromatography and hybrid quadrupole time-of-flight mass spectrometry (UPLC/Q-TOF MS). However, tandem MS analysis of DMDS-derivatives in the work of (Deng et al., 2016) showed the formation of mono-methylthio adducts instead of the previously reported bis-methylthio ones. The formation of these derivatives, although was beneficial in double bond localisation in DAGs with MUFAs but caused a limitation to the application of this method for overall double bond location determination in DAGs with polyunsaturated double bonds for the reason that the mono-methylthio derivatives was only formed at the first double bond farthest from the ester terminus.

The use of oxidative reactions in order to yield derivatives that are labelled at the initial locations of double bonds has achieved promising results. Pre-treatment of fatty acid esters with osmium tetroxide OsO_4 produced vicinal dihydroxylation of double bonds that resulted in the formation of di-hydroxy and *O*-isopropylidene derivatives that were helpful in determining unsaturation sites by the use of GC/EI-MS (McCloskey & McClell, 1965). Employing the same method of derivatisation in combination with negative-ion ESI low-energy CAD MS/MS has given rise to fragment ions of diagnostic value in tandem MS spectra of derivatised unsaturated FAs (Moe & Jensen, 2004). The ESI-MS/MS analyses of various di-hydroxylated phospholipids resulting from osmium tetroxide-catalysed derivatisation have shown characteristic cleavage upon CID. Accordingly original positions of double bonds were identified (Moe et al., 2004, 2005).

Additional derivatising oxidative reaction that has been widely used recently is referred to as ‘Ozonolysis’. Ozonolysis depends on the use of ozone gas to cause oxidative cleavage in double bonds forming ozonide adducts that can be analysed

using various techniques. This reaction has been observed and studied since the turn of the past century and the investigation of its underlying mechanism goes back to earlier work (Criegee, 1975). The application of this derivatisation method for the identification of double bonds positions in unsaturated lipid molecules has been attempted for over fifty years (Privett et al., 1963) where it was combined with chromatographic techniques. several mass-spectrometric analytical methods have been employed as well to analyse the structure of the unsaturated lipids ozonolysis products such as chemical ionisation (M. Wu et al., 1992) and FAB (Santrock et al., 1992) while the introduction of ESI-MS as the analytical tool associated with off-line ozonolysis of unsaturated lipids was previously undertaken (Harrison & Murphy, 1996) and that included exposing a dry thin layer of phospholipids to ozone gas generated by a commercial ozone generating instrument. Almost complete derivatisation of double bonds into their ozonide adducts resulted from this approach. When the ozonide derivatives were ionised, either in negative or positive mode, and subjected to CID fragmentation via ESI-MS/MS, the ozone moieties were disassembled and gave rise to characteristic pairs of product ions that indicated the initial double bond locations.

Triatomic oxygen (ozone) has not been the only form of oxygen that was applied as an oxidising reagent to derivatise unsaturated lipids. In the work of (Ying Zhou et al., 2014), monoatomic oxygen was attributed to be a parallel, even more efficient, reactive source of double bond surface oxidation in unsaturated lipids when they were subjected exposure to ambient air.

1.7 Aims and Objectives

The aim of this work is to gain better insights into the fragmentation mechanisms of the products of unsaturated fatty acid autooxidation, with a special focus on the effects of double bonds on the fragmentation patterns. This could make an addition to the methods suggested to address the challenge of determining the positions of double bonds along fatty acyl chains in lipid molecules by conventional high-resolution MS. The method proposes to use the simple auto-oxidative reaction as an off-line derivatisation strategy to yield derivatives that are labelled at the initial locations of double bonds that can give rise to fragment ions of diagnostic value in tandem MS spectra upon subjected to negative-ion ESI low-energy CAD MS^2. The method needs to work with complex samples, such as fixed oils fats, where the differentiation of double bond positional isomers have been quite challenging for researchers. Based on the aims detailed above, the following objectives were formulated:

▪ To study the behaviour of different monounsaturated and polyunsaturated hydroperoxy fatty acids in LC-MS and LC-MS^n performed on the molecular ions $[M - H^+]^-$ and the factors that determine these behaviours.

▪ To assess the feasibility of obtaining diagnostic fragment ions that can help with the identification of the molecular ions of these hydroperoxides and thus, via the understanding of the chemistry of fatty acid peroxidation reaction, developing a method to determine the original double bond position/s.

▪ To study the behaviour of different hydroxides formed by the secondary-reduction of the studied hydroperoxy fatty acids in LC-MS and LC-MS^n performed on the molecular ions $[M - H^+]^-$ and the factors that determine these behaviours.

▪ Using our findings on their fragmentation patterns in LC-MS and LC-MS^n, to assess the feasibility of applying the same approach to develop a method for pinpointing the double bond position/s in fatty acids derived from various fixed oils.

2 Chapter one materials and methods

2.1 Chemicals and Materials

Oleic acid, vaccenic acid, linoleic acid, α-linolenic acid, γ-linolenic acid, sodium borohydride and 2,2′-azobis-(2-amidinopropane)- dihydrochloride (ABAP) were obtained from Sigma Aldrich Co. (Dorset UK). HPLC grade acetonitrile and methanol were obtained from Fisher Scientific (Leicestershire, UK). HPLC grade water was prepared in house using a Whatman Milli Q system.

The oils used for the study are almond oil, avocado oil, borage seed oil, grape seed oil, hazelnut oil, macadamia oil, and wheat germ oil. All natural oils were bought from the market as branded products. Prior to analysis, all oil samples were stored in dark amber glass bottles, under the same ambient temperature conditions for not more than 72 h.

2.2 LC-MS Analysis

Preliminary identification of the chemical structure of the oxidation products was performed by using a Dionex HPLC instrument connected to an Exactive Orbitrap (Thermo Fisher Scientific, UK). The HPLC was fitted with an ACE 5 C18-AR column (5 µm, 150mm x 4.6mm, HiChrom, Reading UK). The mobile phases consisted of 0.1% formic acid in water (A) and 0.1% formic acid in acetonitrile (B). The gradient system was 10% B, (0 min.); 90% B, (20-34 min.); 10% B, (35-40 min.). The flow rate of the mobile phase was 0.3 ml/min. The gradient used is illustrated in in the table below (Table 2-1). Blanks containing reagent alone were run before and after each sequence.

Table 2-1 Illustration of mobile phase gradient program used in LC-MS analysis.

Time	A%	B%	Flow Rate (µL/min)
0	90	10	300
20	10	90	300

34	10	90	300
35	90	10	300
40	90	10	300

Mass spectra were recorded using electrospray ionization (ESI) in negative and positive modes. Samples were run in negative mode using a needle voltage of - 4.0 kV and source temperature of 320°C. Optimum nebulization was achieved using nitrogen at sheath gas flow rate 50 and auxiliary gas flow rate 17 (units not specified by the manufacturer). The scanning of the total ion chromatograms (TIC) range was *m/z* 75-1000. For confirmation of the structure of the metabolites MS^2 was carried out by using an LTQ Orbitrap with a collision voltage of 35 V (Thermo Fisher Scientific, UK) and with the same chromatographic conditions as were used with the Exactive. Finally, the data were collected and processed using Xcalibur software Ver. 2.0, Thermo- Fisher Corporation, UK and SIEVE software Ver. 1.2.1, Thermo- Fisher Corporation, UK and Metworks Software Ver. 1.3, Thermo- Fisher Corporation, UK. The duty cycle was 200 milliseconds for full scan, 200 milliseconds selected ion for MS^2 and 200 milliseconds selected ion for MS^3.

2.3 Sample Preparation of fatty acid hydroperoxides and hydroxides

Fatty acid solutions (0.01 M) were dissolved in tert-butyl alcohol–water (3: 2 v/v) mixed solvent and incubated at room temperature with water-soluble azo initiator 2,2′-azobis-(2-amidinopropane)- dihydrochloride (ABAP) (50 mM) to initiate the peroxidation.

Aliquots of the reaction mixtures were taken out after 120 minutes. The solutions were adjusted to about pH 3.0 with formic acid and subjected to LC-MS. The secondary decomposition of peroxides to form hydroxyl derivatives of fatty acids was achieved by the same method followed by treating the mixture with an excess of sodium borohydride ($NaBH_4$). Fresh 100 mM sodium borohydride solution was prepared immediately before reaction by dissolving 37.8 mg NaBH4 in 10 mL distilled water. Reduction reaction was carried out by injecting 100 µl $NaBH_4$ solution in a single shot

into the reaction vials under vacuum. 600 µl of water was then added and solution transferred into HPLC vials for LCMS analysis.

2.4 Natural fixed oils samples preparation and formation of hydroperoxides and hydroxides from the fatty acids liberated from the fixed oil samples.

Firstly, the triglycerides from the selected oils had to be hydrolysed to give fatty acids. A stock solution of 0.5 M KOH in ethanol was prepared to achieve fatty acids saponification. Samples of 200 mg of the oil were taken and dissolved in 2ml of ethanolic potassium hydroxide and heated in a sealed tube at 60°C for 30 minutes. The produced potassium fatty acid potassium salts were neutralised by addition of 2 ml of 1 M HCl to liberate fatty acids before they were extracted with 4 ml of hexane. The hexane layer was removed and blown to dryness (Horwitz, 1982). An estimate of 80 mg of the fatty acids was obtained and the solution was then diluted and put through the peroxidation process described above.

3 Chapter one results and discussion

3.1 Analysis of hydroperoxy mono-unsaturated fatty acids

3.1.1 Analysis of Oleic acid hydroperoxides

3.1.1.1 Hydroperoxide formation

Hydroperoxides formation from octadec-9-enoic acid (Oleic acid, FA 18:1 (n−9)) followed the classical mechanism for free radical oxidation that involves the abstraction of hydrogen at the allylic carbon-8 and carbon-11 to produce two intermediate delocalised three-carbon allylic radicals (Frankel et al., 1984; Porter et al., 1995; Pratt et al., 2011). Hydrogen abstraction is induced by the chemical initiator, 2,2´- Azobis (2-amidinopropane) dihydrochloride (AAPH, AAP, ABAP, and ABA) that is commonly used for initiation of free radical oxidations mechanism at (Scheme 3-1) (Niki, 1990; Werber et al., 2011). As a result, the end-carbon positions of these intermediates become preferably prone to oxygen attack to produce a mixture of four allylic hydroperoxides containing OOH groups on carbons 8, 9, 10 and 11:

9-hydroperoxy-10-octadecenoic acid (9-HpO10ME)

11-hydroperoxy-9-octadecenoic acid (11-HpO9ME)

10-hydroperoxy-8-octadecenoic acid (10-HpO8ME)

8-hydroperoxy-9-octadecenoic acid (8-HpO9ME)

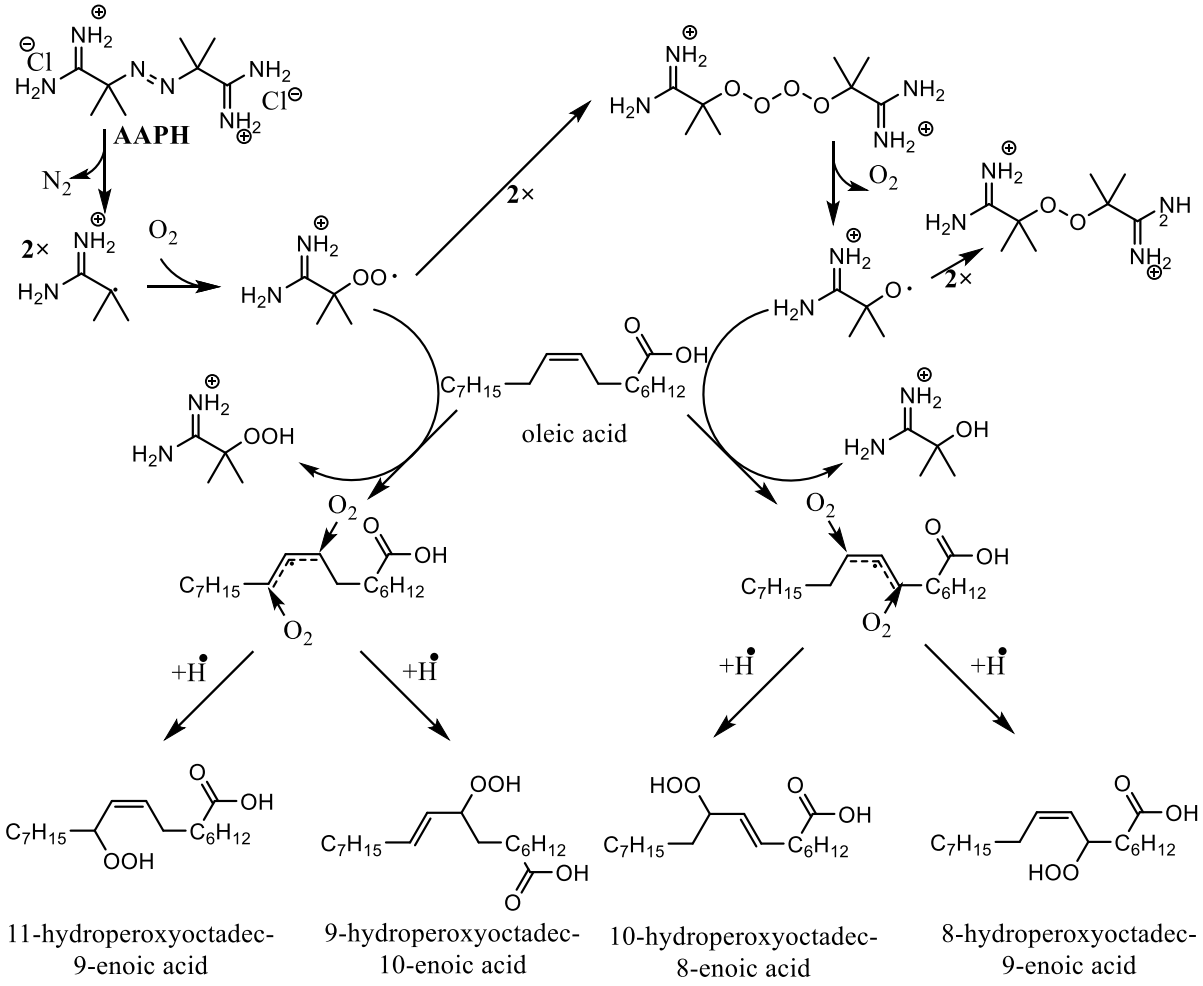

Scheme 3-1 Overall reaction scheme for Oleic acid hydroperoxides formation via AAPH-induced oxidation using simplified versions of the reaction schemes published by (Porter et al., 1995; Pratt et al., 2011; Werber et al., 2011).

3.1.1.2 LC-MS analysis of oleic acid hydroperoxides

Mass range chromatograms of hydroperoxides (HpOMEs) generated by oxidation of octadec-9-enoic acid (Oleic acid, FA 18:1 (n−9)) samples showed four isomers corresponding to predicted hydroperoxide derivatives of octadec-9-enoic acid in agreement with preferred location of hydrogen abstraction determined by electron resonance distribution over double bond and neighbouring carbons. The MS spectra of isomers did not contain any unique structural information that could be used for structure elucidation. Loss of water $[M - (H^+ + H_2O)]^-$ at *m/z* 295 was the only major fragment ion peak observed in all spectra of hydroperoxides species in mass range chromatogram of $[M - H^+]^-$ (Figure 3-1).

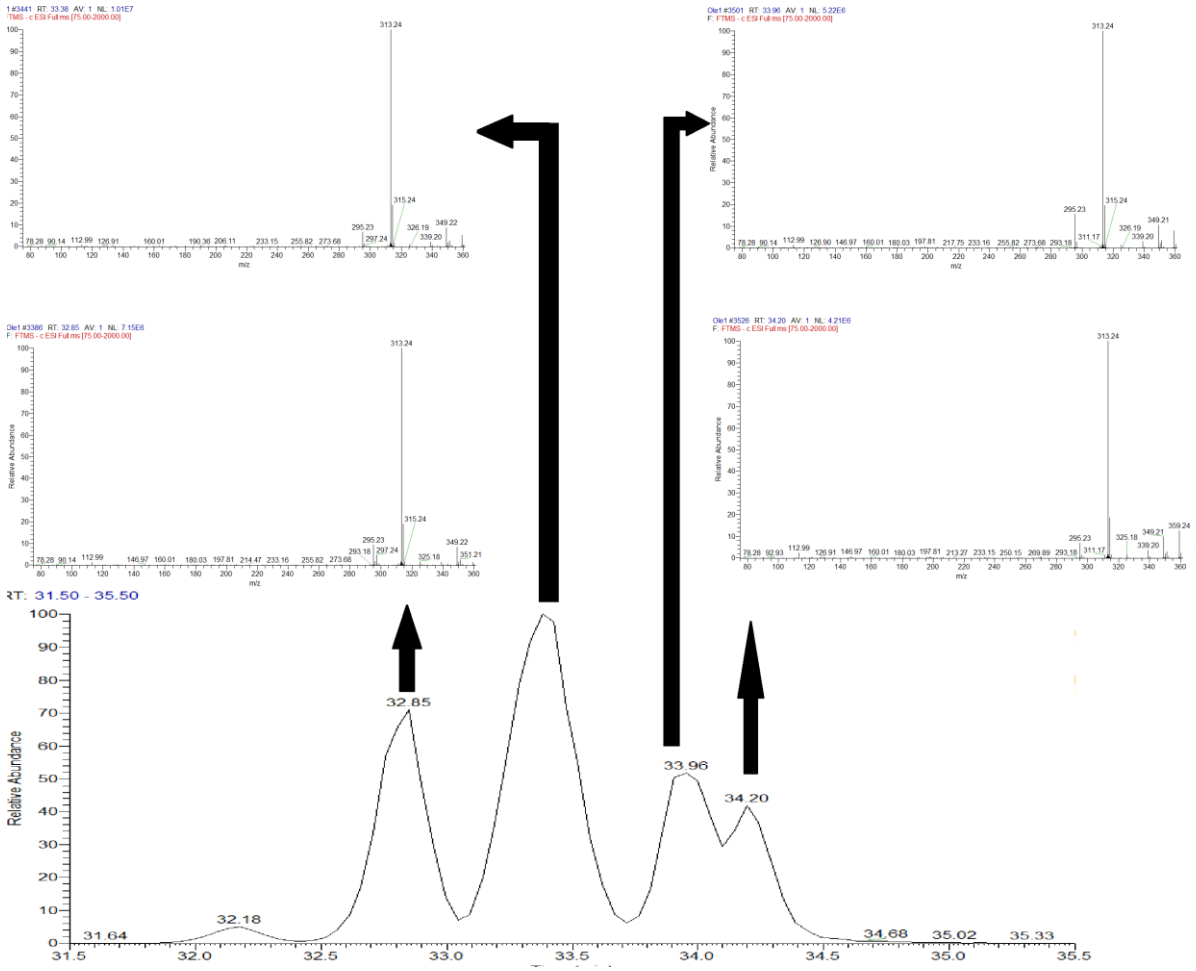

Figure 3-1 Mass range chromatogram & mass spectra of ions of m/z 313 in liquid chromatography- mass spectrometry (LC-MS) analysis of oxidised octadec-9-enoic acid sample.

The elucidation of hydroperoxide isomers required further investigations using MS^2 spectrometry. Nonetheless, product ion spectra obtained for $[M - H^+]^-$ precursor ions derived from oleic acid hydroperoxides in all the regioisomer peaks (Figure 3-2) only confirmed the previous observation regarding the main fragmentation pathway via neutral loss of water with no information about isomer identification and no characteristic fragmentation patterns. The sole abundant product ion in all observed peaks resulted from loss of water $[M - (H^+ + H_2O)]^-$ at *m/z* 295 (Figure 3-2).

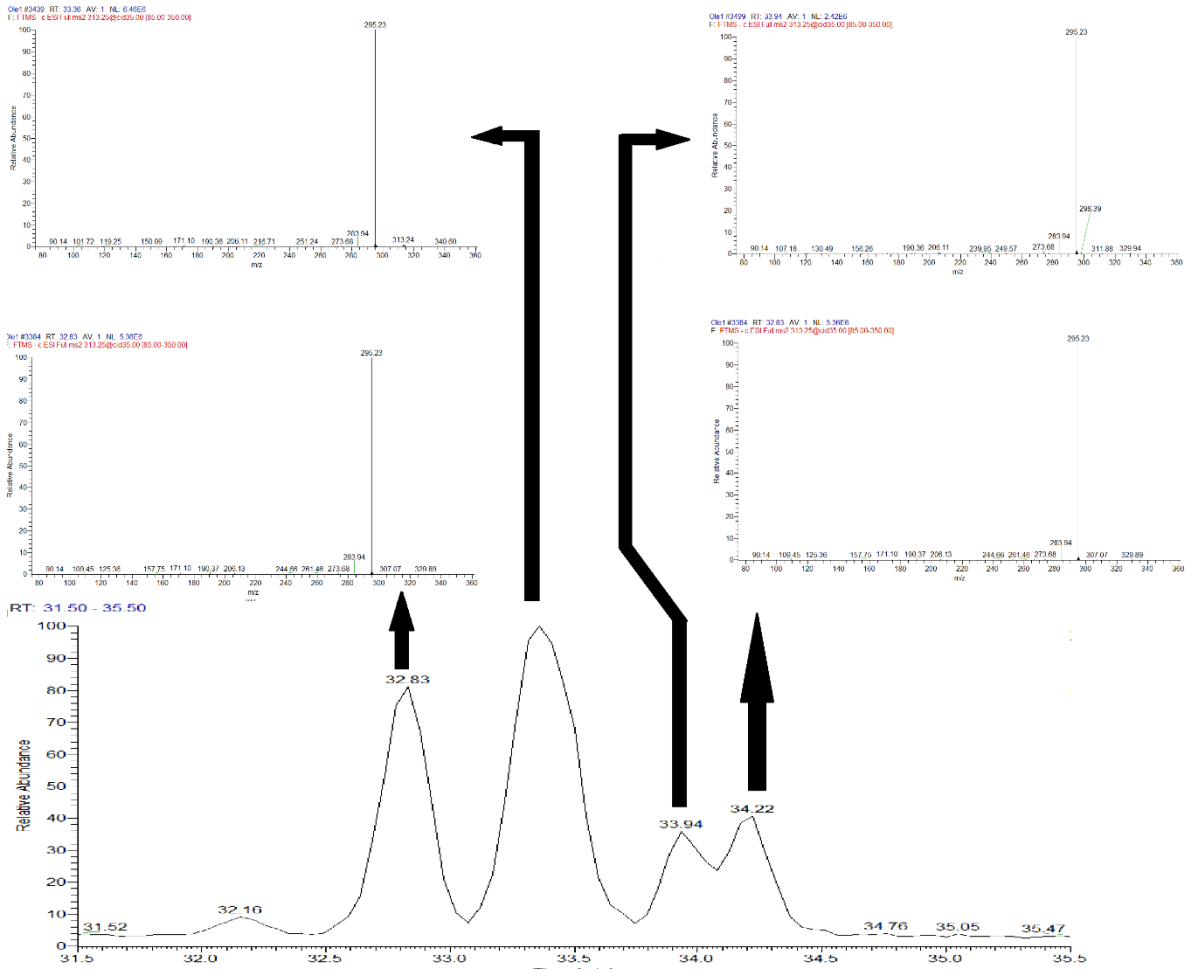

Figure 3-2 Total ion chromatogram & MS^2 spectrometry (LC- MS^2) following collision-induced decomposition of the molecular anion $[M - H]^-$ of octadec-9-enoic acid hydroperoxides at *m/z* 313.

MS^3 on these major fragments, $[M-(H^+ + H_2O)]^-$ was carried out in order to attain more specific structural information. The resulting spectra revealed different fragmentation patterns for the four peaks recognised in parent ion chromatogram in figure 3-2. Alongside precursor ion $[M-(H^+ + H_2O)]^-$ *m/z* 295, which showed high stability in some of the regioisomers, another recurring product ion resulted from further loss of water $[M-(H^+ + 2H_2O)]^-$ *m/z* 277 could be found in all observed isomer peaks. An additional commonly observed product ion in all isomer peaks is *m/z* 251 (Figure 3-2) which is proposed to be $[C_{17}H_{32}O- H^+]^-$ and to be formed by loss of CO_2 $[M-(H^+ + H_2O + CO_2)]^-$ (Figure 3-3).

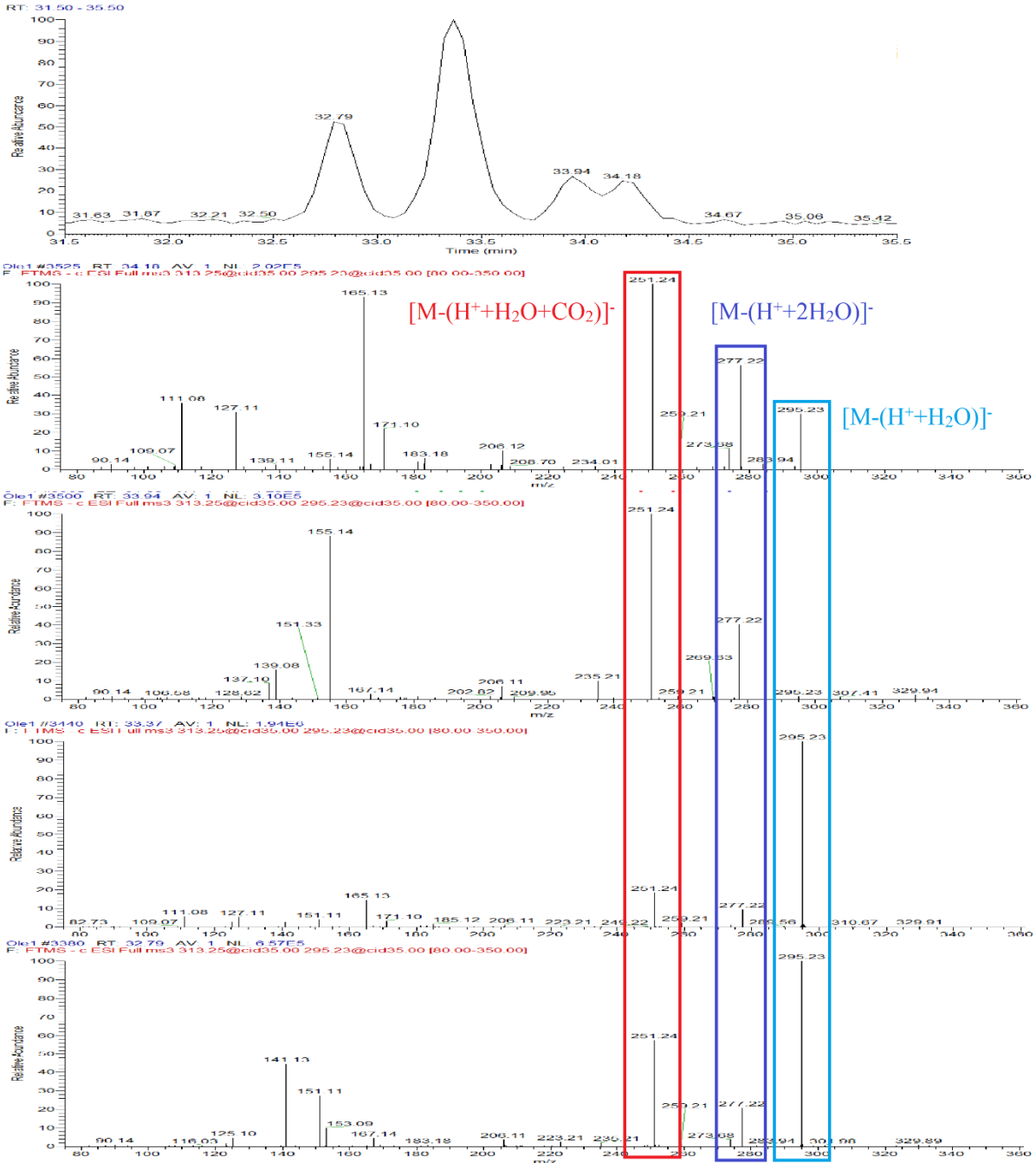

Figure 3-3 Chromatogram & MS^3 spectrometry (LC-MS^3) following collision-induced decomposition of MS^2-generated product ion [M - (H+ + H_2O)]- at *m/z* 295 derived from octadec-9-enoic acid hydroperoxides.

Peak at Rt 32.79 min. (Figure 3-4) in the TIC LC-MS^3 chromatogram that corresponds to parent ion LC-MS chromatogram peaks of Rt 32.85 min. showed the common peaks mentioned above (*m/z* 295, *m/z* 277 and *m/z* 251) in addition to some of the product ions that can be considered characteristic and could be linked to the 11-regioisomer.

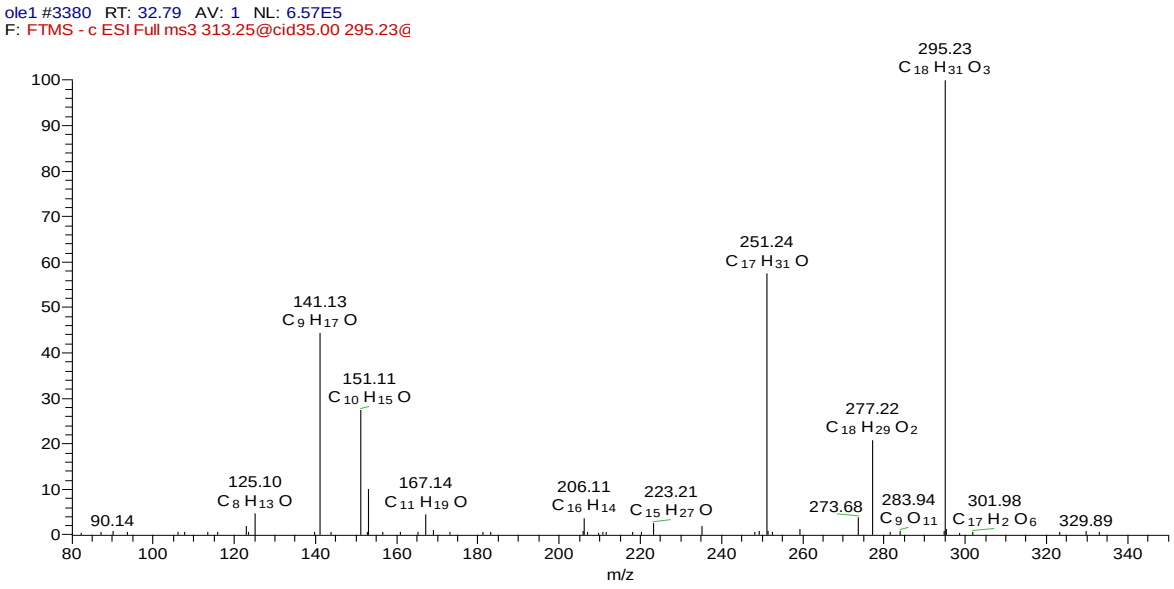

Figure 3-4 (MS^3) spectrum of MS^2-generated product ion of *m/z* 295.23 from octadec-9-enoic acid oxidation sample at Rt 32.79 min.

Table 3-1 The most abundant MS^3 spectrum ions at Rt 32.79 min. in the TIC LC-MS^3 chromatogram of the MS^2-generated product ion of *m/z* 295.23 from octadec-9-enoic acid oxidation sample.

Rt: 32.79		
m/z	**Relative abundance**	**Composition**
295.23	100.00	$C_{18}H_{31}O_3$
141.13	44.34	$C_9H_{17}O$
151.11	27.26	$C_{10}H_{15}O$
153.09	9.89	$C_9H_{13}O_2$
125.10	4.61	$C_8H_{13}O$
167.14	4.34	$C_{11}H_{19}O$

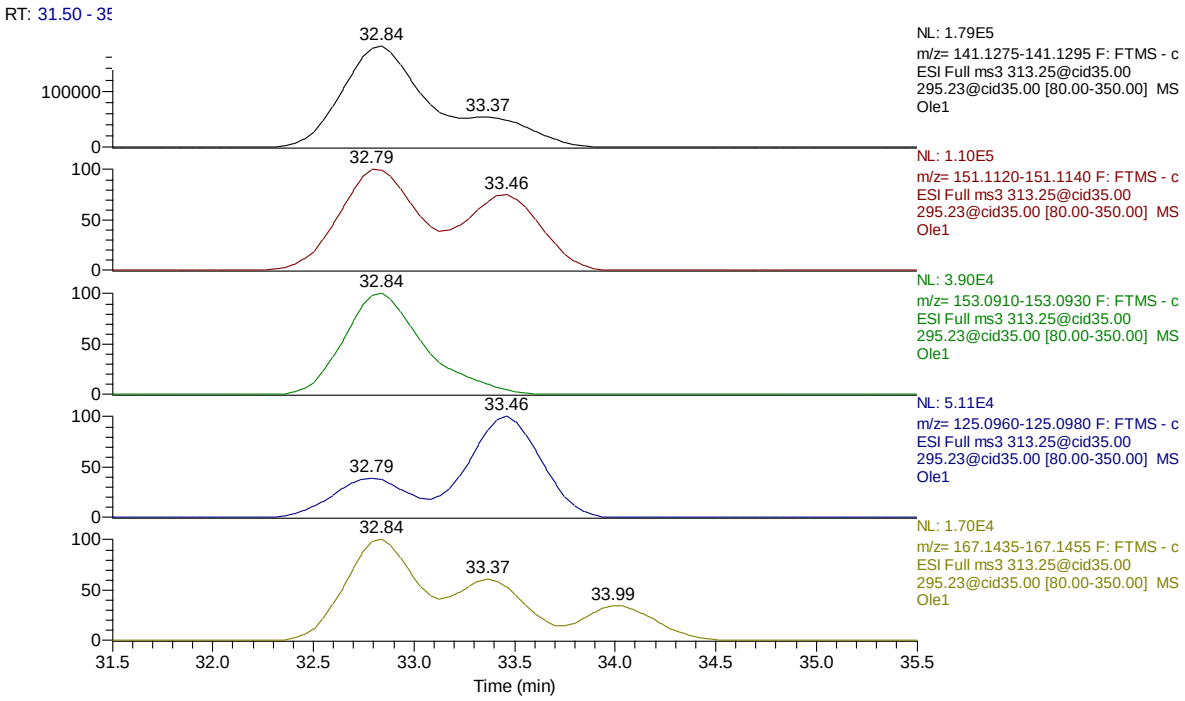

Figure 3-5 Selective mass range-chromatograms of the most relatively abundant MS^3-generated product ions at Rt 32.79 min. that were detected from the octadec-9-enoic acid oxidation sample.

The most abundant product ion observed in the MS^3 spectrum of the peak at Rt 32.79 min. that have was the product ion *m/z* at 141 which can be proposed to be $[C_9H_{18}O-H^+]^-$ and could be linked to 11-regioisomers by a fragmentation process that involves double bond shift towards the carboxyl end to facilitate scission in the C9–C10 bond (see Scheme 3-2). The product ion *m/z* 151 which can be proposed to be $[C_{10}H_{16}O-H^+]^-$ could be linked to 11-regioisomers by the same pathway except that in this case enolisation of the carbonyl group forms double bond in the same direction of double bond shift and creates a transient conjugated diene ion that goes through a loss of neutral CO_2 to form an alkoxide ion that suffers from a cleavage in the C11–C12 bond losing H_2 in the process.

Scheme 3-2 suggests putative fragmentation pathways for product ions with low relative abundance *m/z* 125, *m/z* 153 and *m/z* 167 that are proposed to be $[C_8H_{14}O-H^+]^-$, $[C_9H_{14}O_2-H^+]^-$ and $[C_{11}H_{20}O-H^+]^-$, respectively. For product ion *m/z* 125, fragmentation pathway would involve double bond shift towards the carboxyl end preceding enolisation of carbonyl group to form double bond in the opposite direction associated with extraction of C14 proton forming a transient conjugated diene ion that

undergoes scission in the C10-C11 bond. The presented pathway for formation of the product ion at *m/z* 153 from 11-regioisomers requires a double bond shift towards the carboxyl group end to facilitate enolisation of carbonyl group in the same direction forming a transient conjugated diene ion that undergoes two consecutive 1, 5 sigmatropic rearrangement to guide collision-induced scission to C9-C10 bond.

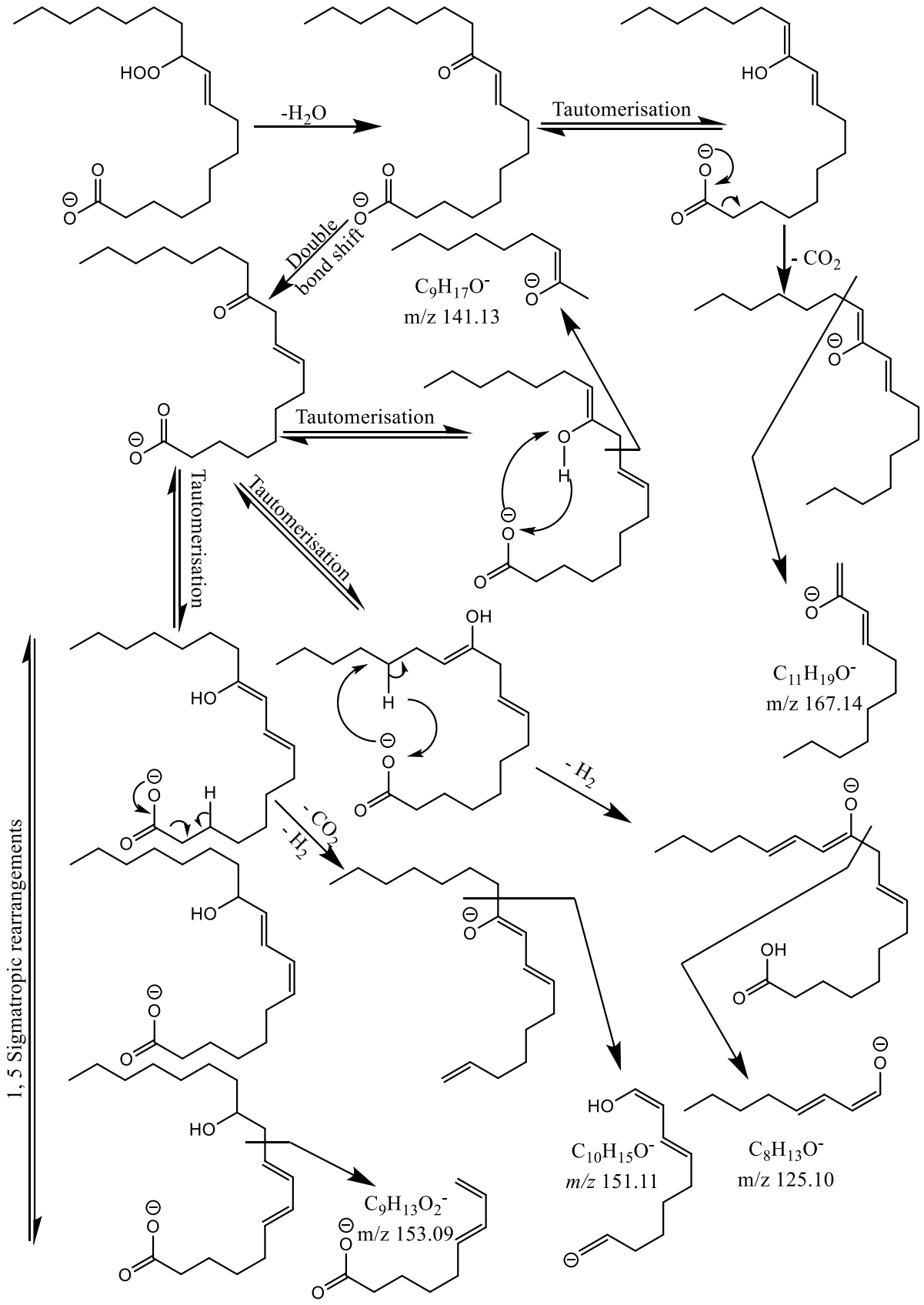

Scheme 3-2 Putative sources of product ions with characteristic significance from 11-HpO9ME molecular ion in (MS^3)-chromatographic peak at Rt 32.79 min.

The product ion at *m/z* 167 could be generated from the fragment ion [M-(H^++H_2O+CO_2)]$^-$ by undergoing ketone/enol tautomerisation and forming a double bond away from the carboxyl end to facilitate cleavage in the C12–C13 bond (Scheme 3-2).

The peak at Rt 33.37 min. in the TIC LC-MS^3 chromatogram that corresponds to parent ion LC-MS chromatogram peaks of Rt 33.38 min. (Figure 3-6) showed high stability of the parent peak at *m/z* 295 and accordingly, all fragment product ions including the common peaks mentioned above (*m/z* 277 and *m/z* 251) became less abundant. The most abundant product ion that can be considered characteristic was *m/z* 165 which is proposed to be [$C_{11}H_{18}O-H^+$]$^-$. Formation of *m/z* 165 fragment ion could be linked to the 8-regioisomer via a proposed pathway that required double bond shift away from the carbonyl group towards the methyl end to facilitate enolisation of carbonyl group in the same direction forming a transient conjugated diene ion that undergoes a further double bond shift, 1, 5 sigmatropic rearrangement. Consequently, the alkoxide ion generated by the loss of neutral CO_2 goes through a cleavage in C7–C8 bond losing H_2 in the process (see Scheme 3-3).

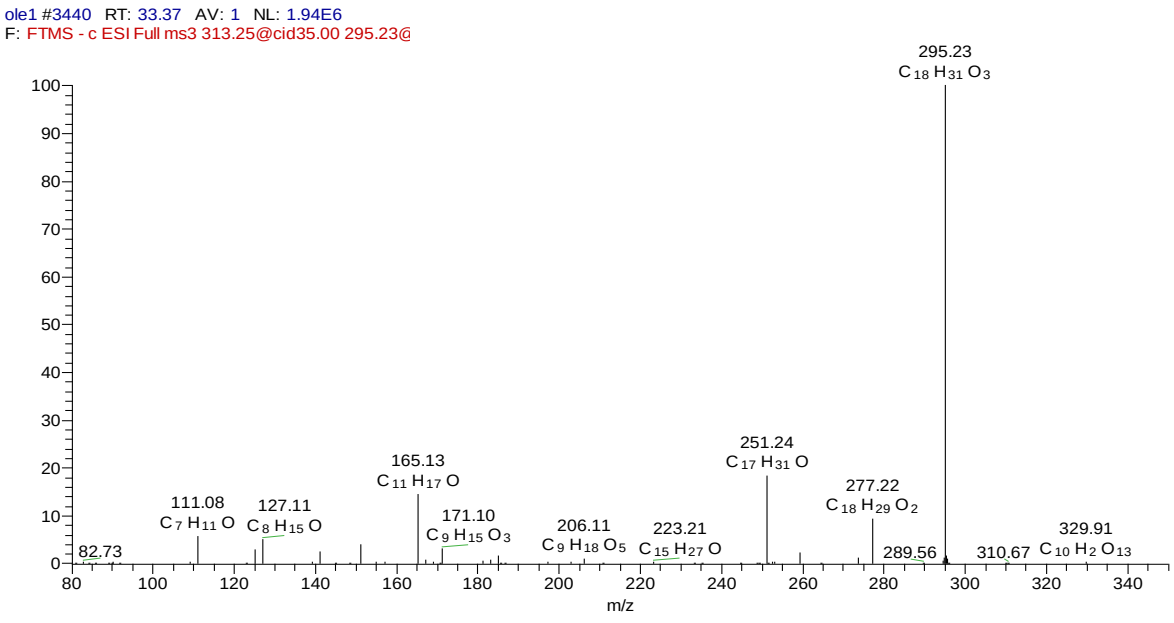

Figure 3-6 (MS^3) spectrum of the MS^2-generated product ion of *m/z* 295.23 from the octadec-9-enoic acid oxidation sample at Rt 33.37 min.

Table 3-2 The most abundant MS^3 spectrum peaks at Rt 33.37 min. in the TIC LC-MS^3 chromatogram of the MS^2-generated product ion of *m/z* 295.23 from octadec-9-enoic acid oxidation sample.

Rt: 33.37		
m/z	**Relative abundance**	**Composition**
295.23	100.00	$C_{18}H_{31}O_3$
165.13	14.51	$C_{11}H_{17}O$
111.08	5.7	$C_7H_{11}O$
127.11	5.13	$C_8H_{15}O$
151.11	3.96	$C_{10}H_{15}O$
171.10	3.19	$C_9H_{15}O_3$
125.10	2.86	$C_8H_{13}O$

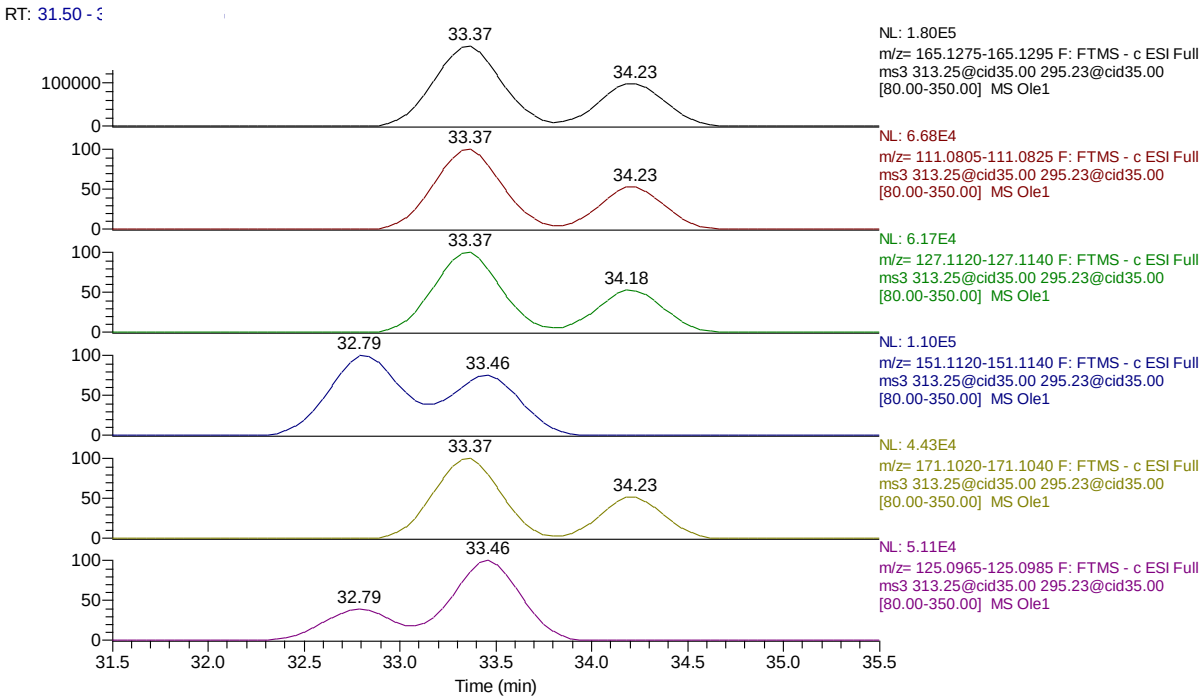

Figure 3-7 Selective mass range- chromatograms of the most relatively abundant MS^3-generated product ions at Rt 33.37 min. that were detected from octadec-9-enoic acid oxidation sample.

Formation of a double bond in the opposite direction during enolisation of carbonyl group, towards the carboxyl end, would initiate a different fragmentation pathway. Formation of product ions *m/z* 171 and *m/z* 127, proposed to be $[C_9H_{16}O_3 - H^+]^-$ and $[C_8H_{16}O - H^+]^-$, respectively, via this fragmentation process suggests a double bond shift away from carboxylic group to guide collision-induced scission towards the C9-C10 bond, taking into account that the fragmentation pathway of product ion *m/z* 127

involves neutral loss of CO_2 before or after scission in the C9-C10 bond (Scheme 3-3).

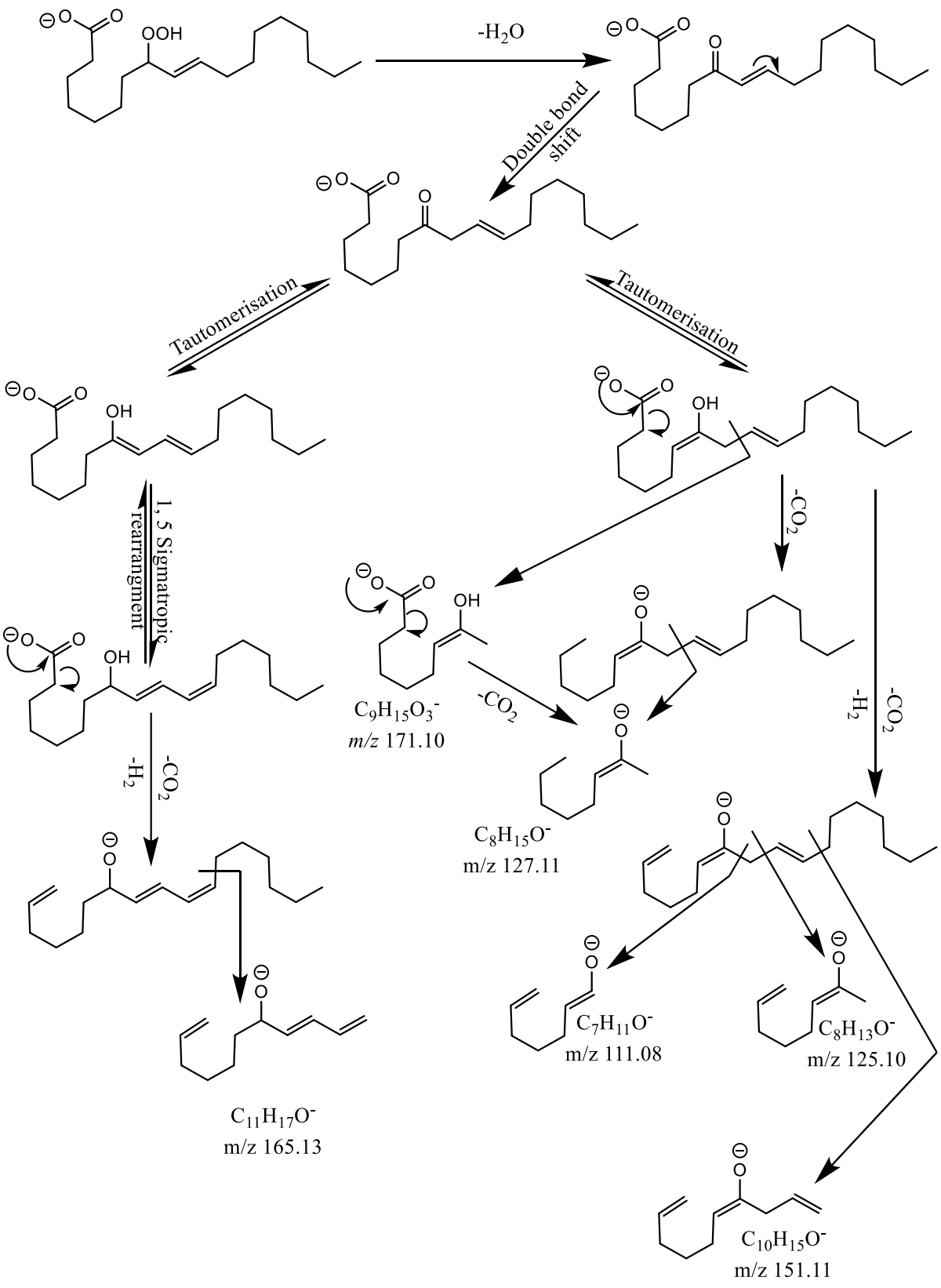

Scheme 3-3 Putative sources of product ions with characteristic significance from 8-HpO9ME molecular ion in (MS^3)-chromatographic peak at Rt 33.37 min.

The alkoxide ion generated by the loss of neutral CO_2 accompanied by loss of H_2 could be the source of three additional fragment ions via collision-induced scission guided by double bond positions (Scheme 3-3). A cleavage in the C8–C9 bond would result in formation of product ion at *m/z* 111 which is proposed to be $[C_7H_{12}O- H^+]^-$, a cleavage in the C9–C10 bond would result in formation of a product ion at *m/z* 125 which is proposed to be $[C_8H_{14}O- H^+]^-$ and a cleavage in C8–C9 bond would result in formation of a product ion at *m/z* 151 which is proposed to be $[C_{10}H_{16}O- H^+]^-$.

The peak at Rt 33.94 min. in the TIC LC-MS^3 chromatogram that corresponds to the parent ion LC-MS chromatogram peaks of Rt 33.96 min. (Figure 3-8) showed the common peaks mentioned above (*m/z* 295, *m/z* 277 and *m/z* 251) in addition to some of the product ions that can be considered characteristic and could be linked to the 10-regioisomer (Table 3-3) such as *m/z* 155 which is proposed to be $[C_{10}H_{20}O- H^+]^-$ and could be linked to the 10-regioisomer by a fragmentation process that involves a double bond shift towards the carboxyl end to direct collision-induced decomposition to the C8–C9 bond (see Scheme 3-4). This double bond shift could facilitate enolisation of the carbonyl group to form double bond in the same direction and to create a transient conjugated diene ion that undergoes two consecutive 1, 5 sigmatropic rearrangements to guide collision-induced scission to the C8-C9 bond resulting in formation of a product ion at *m/z* 139.08 which is proposed to be $[C_8H_{12}O_2- H^+]^-$ and observed in spectrum of the same chromatographic peak.

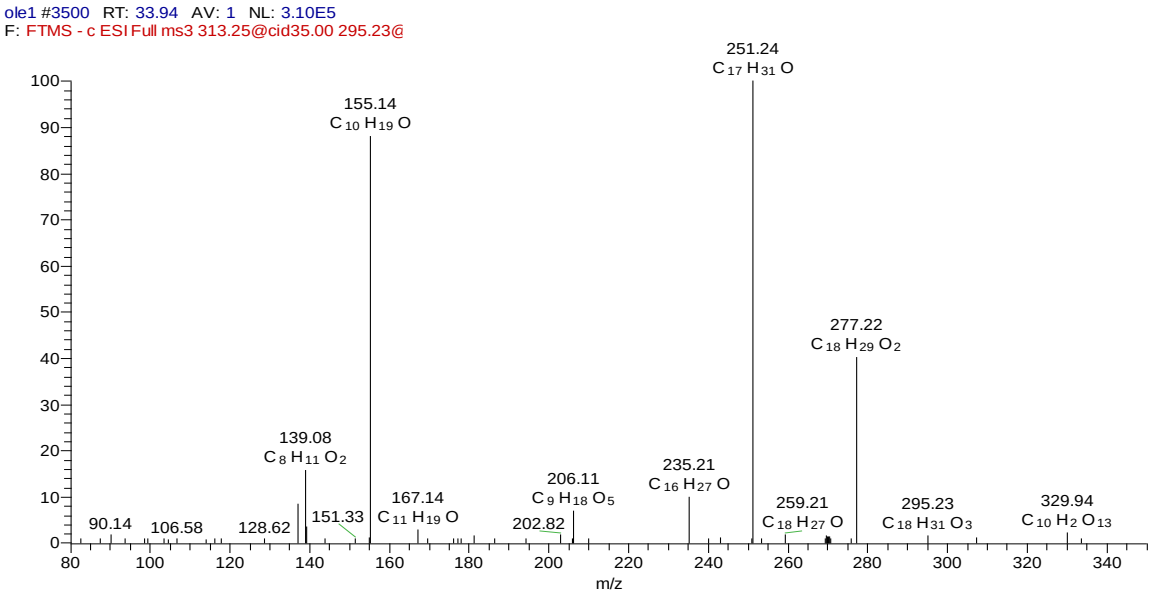

Figure 3-8 (MS^3) spectrum of the MS^2-generated product ion of *m/z* 295.23 from the octadic-9-enoic acid oxidation sample at Rt 33.94 min.

Table 3-3 The most abundant MS^3 spectrum ions at Rt 33.94 min. in the TIC LC-MS^3 chromatogram of the MS^2-generated product ion of *m/z* 295.23 from octadec-9-enoic acid oxidation sample.

Rt: 33.94		
m/z	**Relative abundance**	**Composition**
251.24	100.00	$C_{17}H_{31}O$
155.14	88.12	$C_{10}H_{19}O$
139.08	15.87	$C_8H_{11}O_2$
137.10	8.52	$C_9H_{13}O$
139.11	3.56	$C_9H_{15}O$
167.14	2.85	$C_{11}H_{19}O$

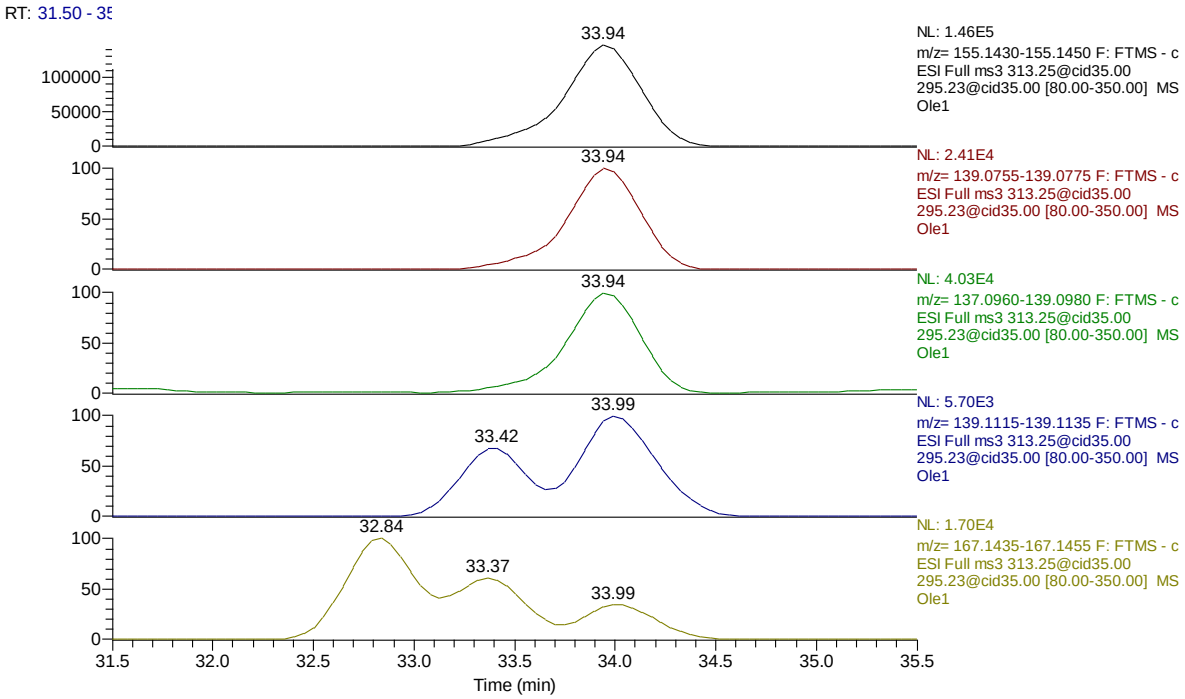

Figure 3-9 Selective mass range-chromatograms of the most relatively abundant MS^3-generated product ions at Rt 33.99 min. that were detected from octadec-9-enoic acid oxidation sample.

An additional low abundance fragment ion observed in spectrum of MS^3 chromatographic peak at Rt 33.94 min. is at *m/z* 137 which is proposed to be $[C_9H_{14}O–H^+]^-$ and it could also originate from the same transient conjugated diene ion that goes through a loss of neutral CO_2 to form an alkoxide ion that suffers from a cleavage in the C10–C11 bond losing H_2 in the process (Scheme 3-4).

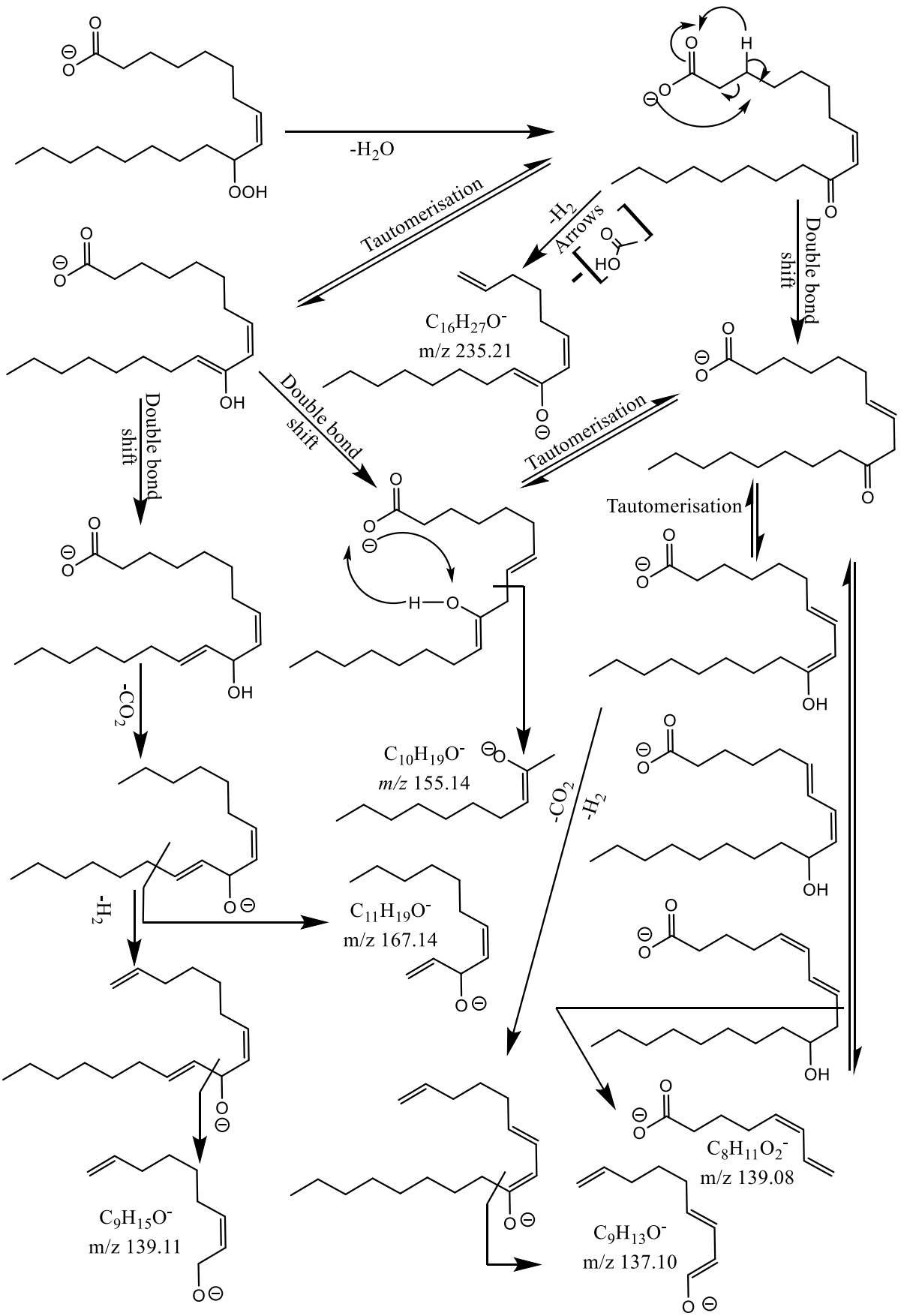
-H2O
Tautomerisation
-H2
Arrows
Double bond shift
C16H27O-
m/z 235.21
Double bond shift
Double bond shift
Tautomerisation
Tautomerisation
-CO2
C10H19O-
m/z 155.14
-CO2
-H2
-H2
C11H19O-
m/z 167.14
C8H11O2-
m/z 139.08
C9H15O-
m/z 139.11
C9H13O-
m/z 137.10

Scheme 3-4 Putative sources of product ions with characteristic significance from 10-HpO8ME molecular ion in (MS^3) spectrum of the chromatographic peak at Rt 33.94 min.

Scheme 3-4 illustrates additional pathways initiated by forming a double bond in the opposite direction during enolisation of the carbonyl group, away from the carboxyl group, followed by a double bond shift in the same direction. This fragmentation process is associated with generating a fragment ion *m/z* 251, $[M-(H^+ + H_2O + CO_2)]^-$, by going through a neutral loss of CO_2, which in turn, could be the source of two additional fragment ions via collision-induced scission guided by double bond positions. Accordingly, product ion *m/z* 167 which is proposed to be $[C_{11}H_{20}O- H^+]^-$ could be formed by cleavage in the C12–C13 bond, and the product ion at *m/z* 139.11 which is proposed to be $[C_9H_{16}O- H^+]^-$ could be formed by cleavage in the C10–C11 bond losing H_2 in the process.

Peak at Rt 34.18 min. in the TIC LC-MS^3 chromatogram that corresponds to parent ion LC-MS chromatogram peaks of Rt 34.20 min. (Figure 3-10) showed the common peaks mentioned above (*m/z* 295, *m/z* 277 and *m/z* 251) in addition to product ions *m/z* 171 and *m/z* 127 which are proposed to be $[C_9H_{16}O_3- H^+]^-$ and $[C_8H_{16}O- H^+]^-$, respectively. Both fragment ions can be considered highly characteristic for 9-regioisomers as they could be generated via simple α cleavage (scission in C9-C10 bond) preceded by double bond shift away from carboxylic end, taking into account that the fragmentation pathway producing the product ion *m/z* 127 involves neutral loss of CO_2 before or after scission in C9-C10 bond as explained in scheme 3-5.

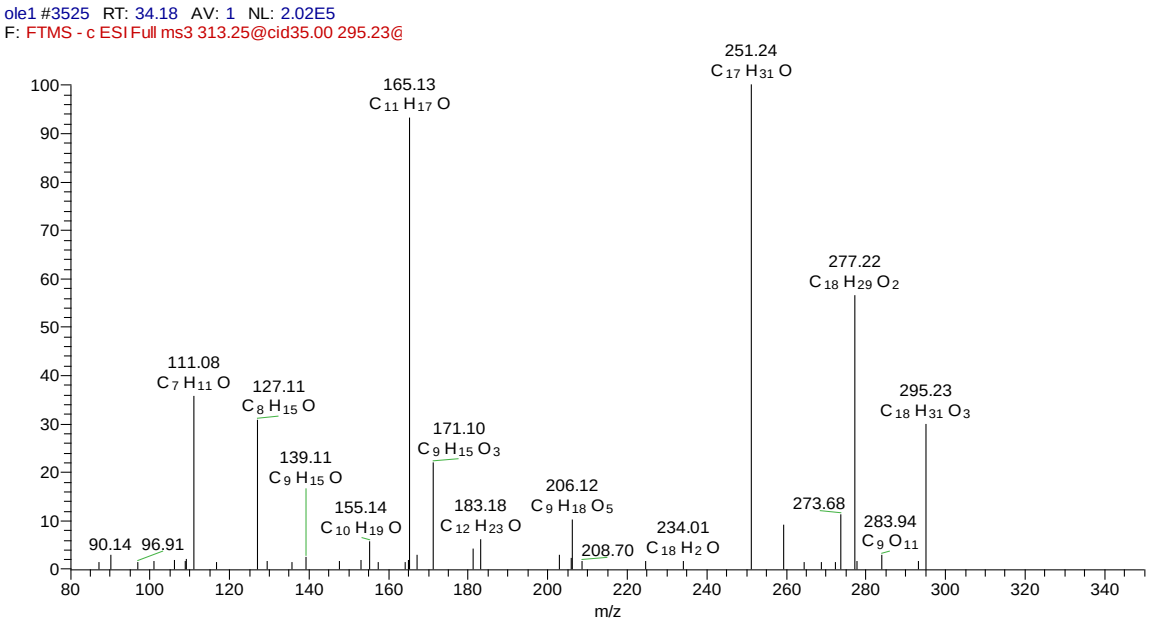

Figure 3-10 (MS^3) spectrum of MS^2-generated product ion of m/z 295.23 from octadec-9-enoic acid oxidation sample at Rt 34.18 min.

Table 3-4 The most abundant MS^3 spectrum ions at Rt 33.94 min. in the TIC LC-MS^3 chromatogram of the MS^2-generated product ion of *m/z* 295.23 from octadec-9-enoic acid oxidation sample.

Rt: 34.18		
m/z	**Relative abundance**	**Composition**
251.24	100.00	$C_{17}H_{31}O$
165.13	93.22	$C_{11}H_{17}O$
111.08	35.70	$C_7H_{11}O$
127.11	30.79	$C_8H_{15}O$
171.10	21.90	$C_9H_{15}O_3$

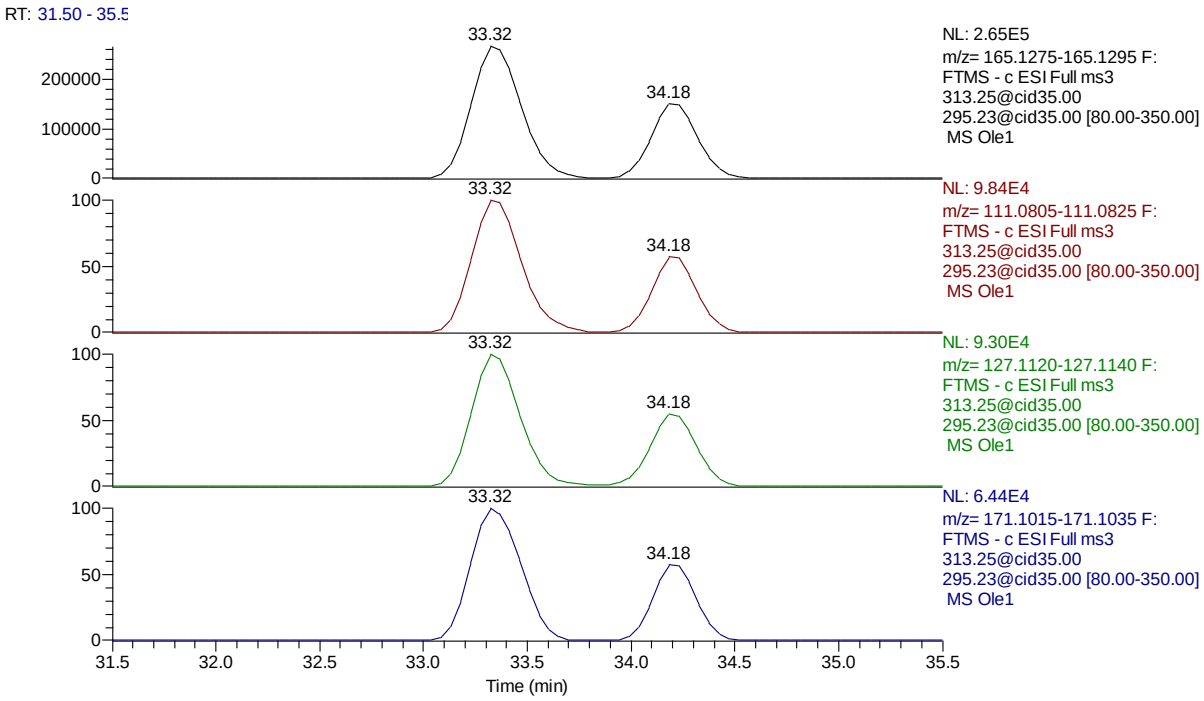

Figure 3-11 Selective mass range-chromatograms of the most relatively abundant MS^3-generated product ions at Rt 34.18min. that were detected from octadec-9-enoic acid oxidation sample.

The fragment ions with higher intensity in the MS^3 spectrum of the chromatographic peak at Rt 34.18 min. (Figure 3-10) can be linked to the 9-regioisomer likewise, for instance the most abundant fragment ion *m/z* 165 which is proposed to be $[C_{11}H_{18}O-H^+]^-$ shown in scheme 3-5 and can be formed by similar fragmentation process initiated by the same double bond shift, away from carboxylic end, to direct collision-induced scission towards the C12–C13 bond of fragment ion $[M-(H^+ + H_2O + CO_2)]^-$ losing H_2 in the process.

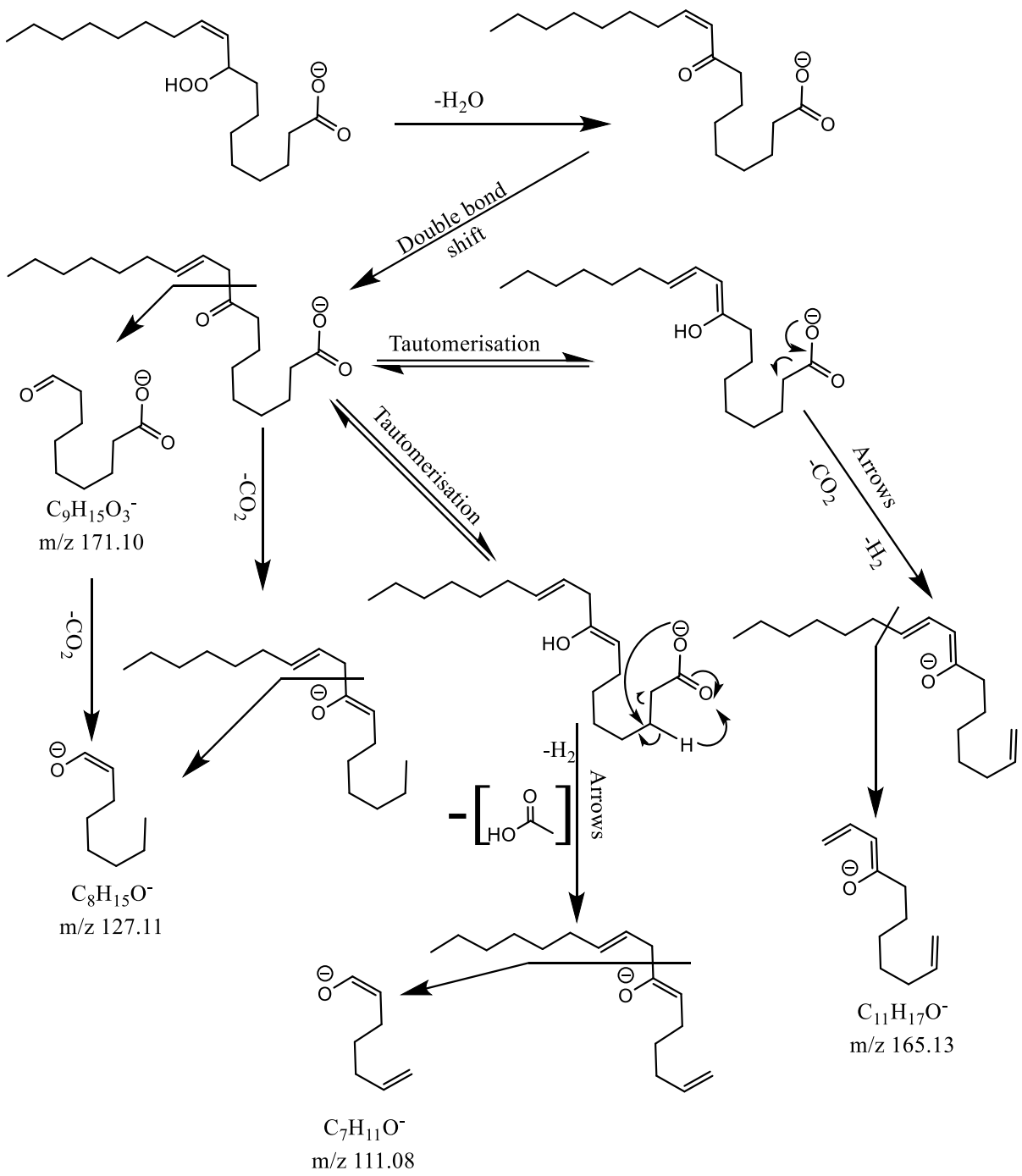

Scheme 3-5 Putative sources of product ions with characteristic significance from 9-HpO10ME molecular ion in (MS^3)-chromatographic peak at Rt 34.18 min.

Proton rearrangement involving extraction of a proton on C3, consequently causing loss of neutral acetic acid ($C_2H_4O_2$) from the same transient ion, with double bond shift, can be suggested as fragmentation pathway to link the product ion at *m/z* 111 observed in spectrum of MS^3 chromatographic peak at Rt 34.18 min. which can be

proposed to be $[C_7H_{12}O- H^+]^-$ to the 9-regioisomer via cleavage in C9–C10 bond associated with neutral loss of H_2 (Scheme 3-5).

3.1.1.3 LC-MS chromatographic peaks identification

The MS^3 fragment ion *m/z* 167 proposed to be $[C_{11}H_{20}O- H^+]^-$ was encountered in the spectra of the peaks at Rt 32.79, 33.37 and 33.94 min. in the TIC of LC-MS^3 chromatogram that correspond to parent ion LC-MS chromatogram peaks at Rt 32.85, 33.38 and 33.96 min, respectively. This fragment ion could be linked to 11-HpO9ME, 8-HpO9ME and 10-HpO8ME via fragmentation pathways proposed in schemes 3-2, 3-3 and 3-4, respectively. This recurrence diminished the significance of this fragment ion for structural elucidation.

Fragment ions at *m/z* 125 and *m/z* 151, proposed to be due to $[C_8H_{14}O- H^+]^-$ and $[C_{10}H_{16}O- H^+]^-$, respectively, that are presented in LC-MS^3 chromatogram peaks corresponding to the parent ion LC-MS chromatogram peaks at Rt 32.85 and Rt 33.38 min. could be linked to 11 regioisomer and 8 regioisomer via fragmentation pathways proposed in schemes 3-1 and 3-2. Moreover, although presented in both LC-MS^3 chromatographic peaks, MS^3 fragment ions at *m/z* 141, proposed to be $[C_9H_{18}O- H^+]^-$, could be linked to the 11-regioisomer rather than the 8-regioisomer via the fragmentation pathway proposed in scheme 3-2.

From the above discussion, the parent ion LC-MS chromatogram peaks at Rt 32.85 and Rt 33.38 min. were limited to be 11-HpO9ME and 8-HpO9ME. Furthermore, the MS^3 fragment ion at *m/z* 153, proposed to be due to $[C_9H_{14}O_2- H^+]^-$, which was encountered exclusively in the chromatographic peak at Rt 32.85 min. could not be generated by CID activation of the dehydrated 8-regioisomer because of the presence of two oxygens and could only be a result of the fragmentation pathway of the 11-regioisomer proposed in scheme 3-2. In consequence, the parent ion in LC-MS chromatographic peak at Rt 32.85 was elucidated as 11-HpO9ME.

Correlative fragment ion-pair at *m/z* 127 and *m/z* 171, proposed to be $[C_8H_{16}O- H^+]^-$ and $[C_9H_{16}O_3- H^+]^-$, in the peaks at Rt 33.38 and Rt 34.20 min. could be only linked to the 8-regioisomer and 9- regioisomer via fragmentation pathways proposed in schemes 3-3 and 3-5, and have no possibility to be originated from the 10-regioisomer or 11 regioisomer, especially because of the presence of three oxygens in the elemental

composition of the later. The MS^3 fragment ion *m/z* 111, proposed to be $[C_7H_{11}O- H^+]^-$, played decisive role in proposing parent ion LC-MS chromatographic peak at Rt 33.38 min. being due to 8-HpO9ME as a result of the fragmentation pathway proposed in scheme 3-3 which is directed by the position of dehydrated hydroperoxy moiety on C8.

Elucidation of LC-MS chromatographic peak at Rt 33.38 min. as 8-HpO9ME produced the conclusion that the LC-MS chromatographic peak at Rt 34.20 min. was 9-HpO10ME in light of the presence of correlative fragment ion-pair *m/z* 127 and *m/z* 171 in the corresponding LC-MS^3 spectrum of chromatographic peak that could be generated by fragmentation pathways suggested in scheme 3-5 by a simple cleavage in the bond at α position to dehydrated hydroperoxy moiety on C9 (C9-C10 bond)

MS^3 fragment ions *m/z* 137, *m/z* 139.08 and *m/z* 155, proposed to be $[C_9H_{14}O- H^+]^-$, $[C_8H_{12}O_2- H^+]^-$ and $[C_{10}H_{20}O- H^+]^-$, respectively, that were only detected in chromatographic peak at Rt 33.94 min. and could be linked to 10-regioisomer via fragmentation pathways proposed in scheme 3-4 that were directed by the position of dehydrated hydroperoxy moiety on C10. Therefore, parent ion LC-MS chromatographic peak at Rt 33.94 min. was elucidated as 10-HpO8ME.

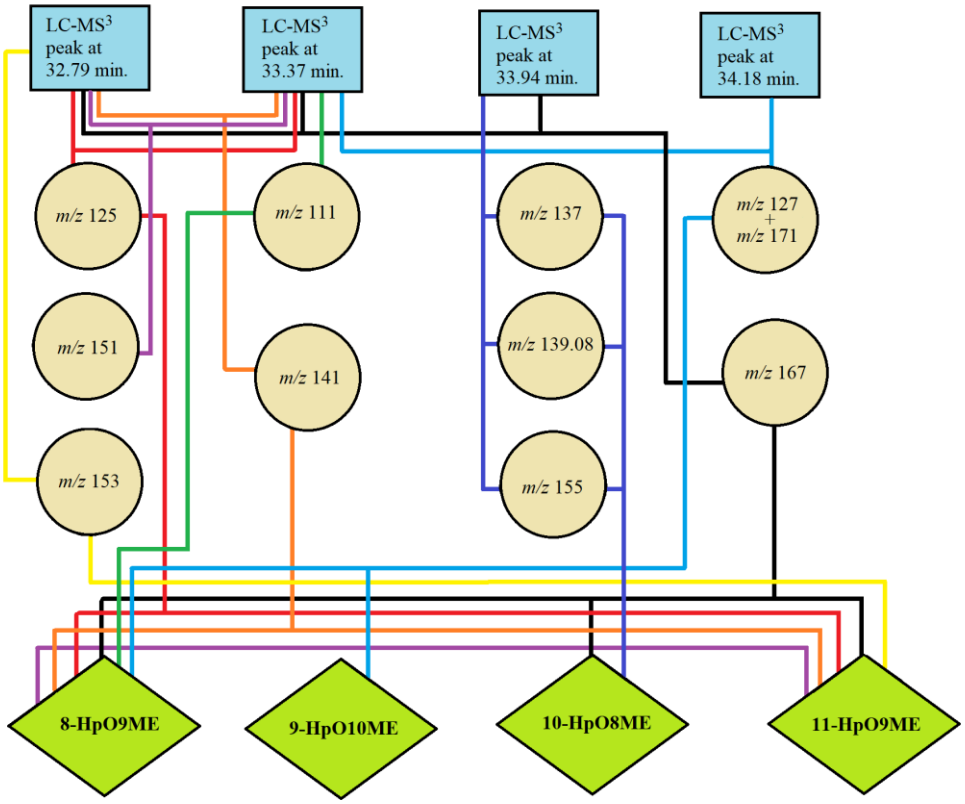

Figure 3-12 A flow chart showing the method used to select characteristic ions for each isomer with the purpose of identifying (MS^3)-chromatographic peaks from octadec-9-enoic acid oxidation sample.

3.1.2 Analysis of Vaccenic acid hydroperoxides

3.1.2.1 Hydroperoxide formation

Vaccenic acid is a positional isomer of oleic acid with the double bond on C11 (n-7). Therefore, when subjected to hydrogen abstraction by the chemical initiator (ABAP), the peroxidation process proceeds in the same mechanism of MUFAs oxidation explained by (Frankel et al., 1984; Porter et al., 1995; Pratt et al., 2011). Hydrogens at the allylic carbon-10 and carbon-13 are the ones that get abstracted to produce a mixture of four allylic hydroperoxides (Scheme 3-6) containing OOH groups on carbons 10, 11, 12 and 13:

11-hydroperoxy-12-octadecenoic acid (11-HpO12ME)

13-hydroperoxy-11-octadecenoic acid (13-HpO11ME)

12-hydroperoxy-10-octadecenoic acid (12-HpO10ME)

10-hydroperoxy-11-octadecenoic acid (10-HpO11ME)

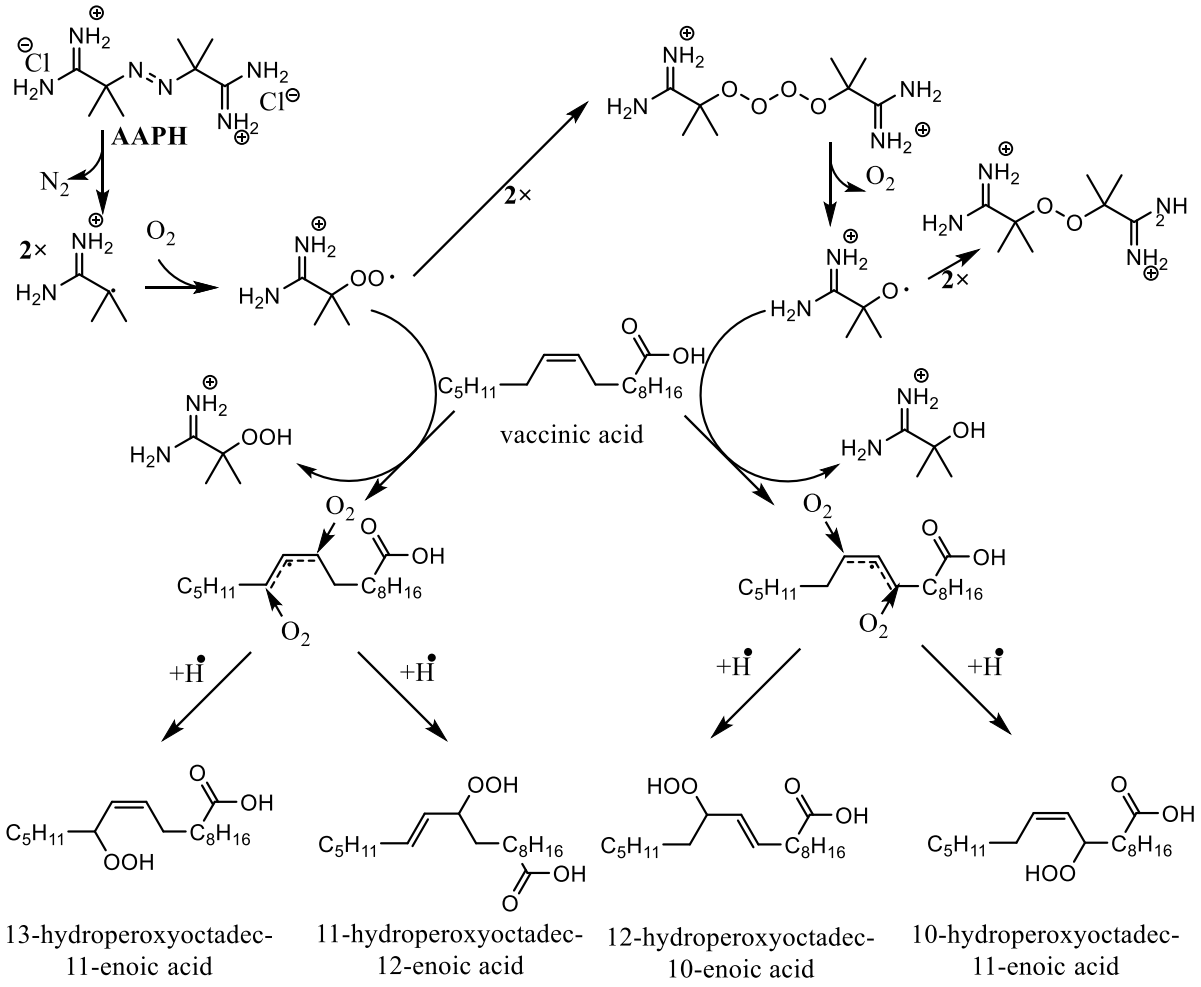

Scheme 3-6 Overall reaction scheme for Vaccenic acid hydroperoxides formation via AAPH-induced oxidation using simplified versions of the reaction schemes published by (Porter et al., 1995; Pratt et al., 2011; Werber et al., 2011).

3.1.2.2 LC-MS analysis of Vaccenic acid hydroperoxides

Mass range chromatograms for the hydroperoxides generated by oxidation of octadec-11-enoic acid (Vaccenic acid, FA 18:1 (n−7)) samples (HpO11ME) showed four isomer peaks, with partial co-elution of first two peaks, corresponding to hydroperoxide derivatives of vaccenic acid in agreement with predicted sites of hydrogen abstraction determined by electron resonance distribution over the double bond and neighbouring carbons. The isomer peaks spectra did not contain any unique structural information which could be used for structure elucidation. Loss of water [M - (H^+ + H_2O)]$^-$ at *m/z* 295 was the only major fragment ion peak observed in all spectra

of the hydroperoxide species in the mass range chromatogram of $[M - H^+]^-$ (Figure 3-13).

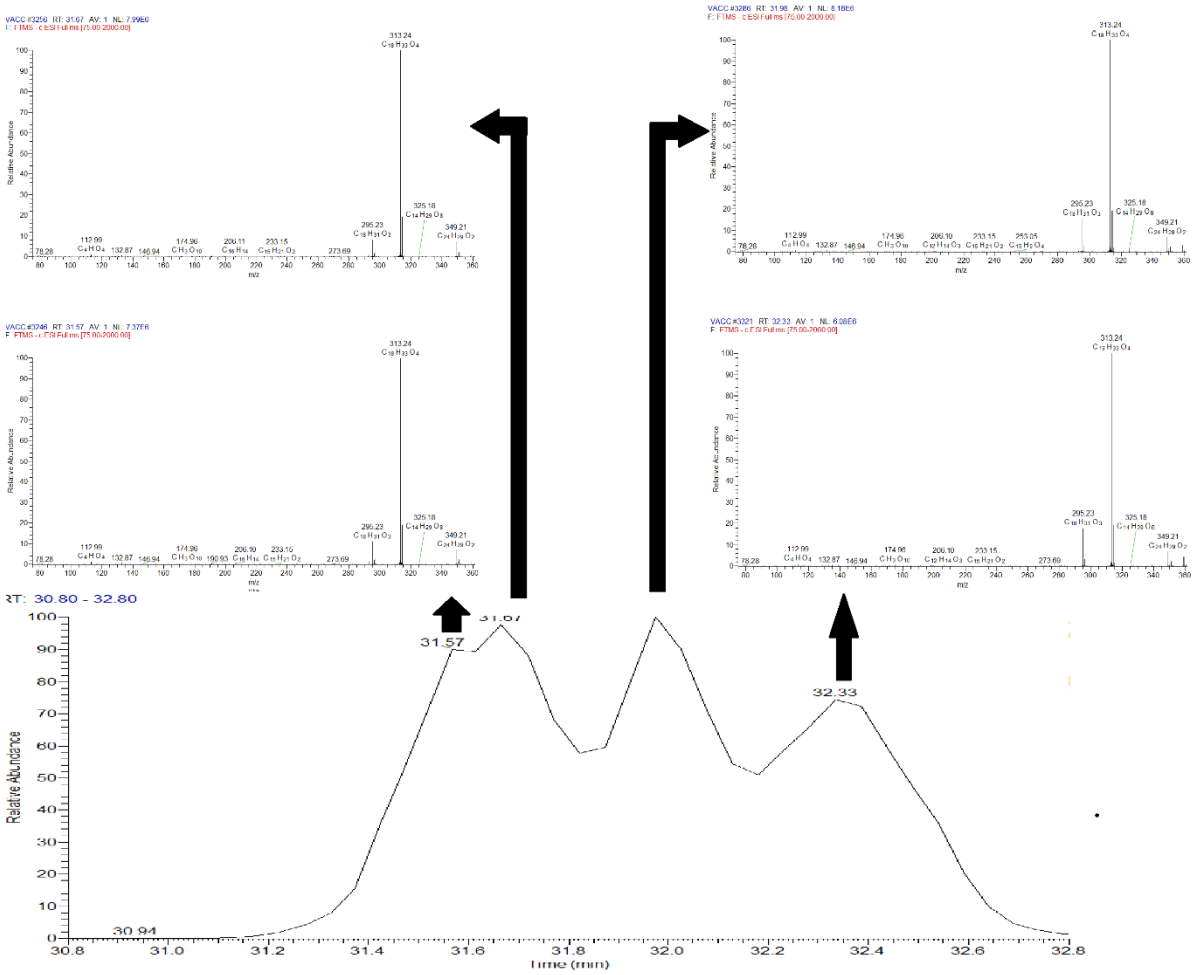

Figure 3-13 Mass range chromatogram & mass spectra of ions of *m/z* 313 in liquid chromatography- mass spectrometry (LC-MS) analysis of oxidised octadec-11-enoic acid sample.

The elucidation of hydroperoxide isomers required further investigations using MS^2 spectrometry. Nonetheless, product ion spectra obtained for $[M - H^+]^-$ precursor ions derived from octadec-11-enoic acid hydroperoxides in all regioisomer peaks (Figure 3-14) barely confirmed the previous observation regarding the main fragmentation pathway via neutral loss of water with no information about isomer identification and no characteristic fragmentation patterns. In the same manner with oleic acid, the sole abundant product ion in all observed peaks resulted from loss of water $[M - (H^+ + H_2O)]^-$ at *m/z* 295 (Figure 3-14).

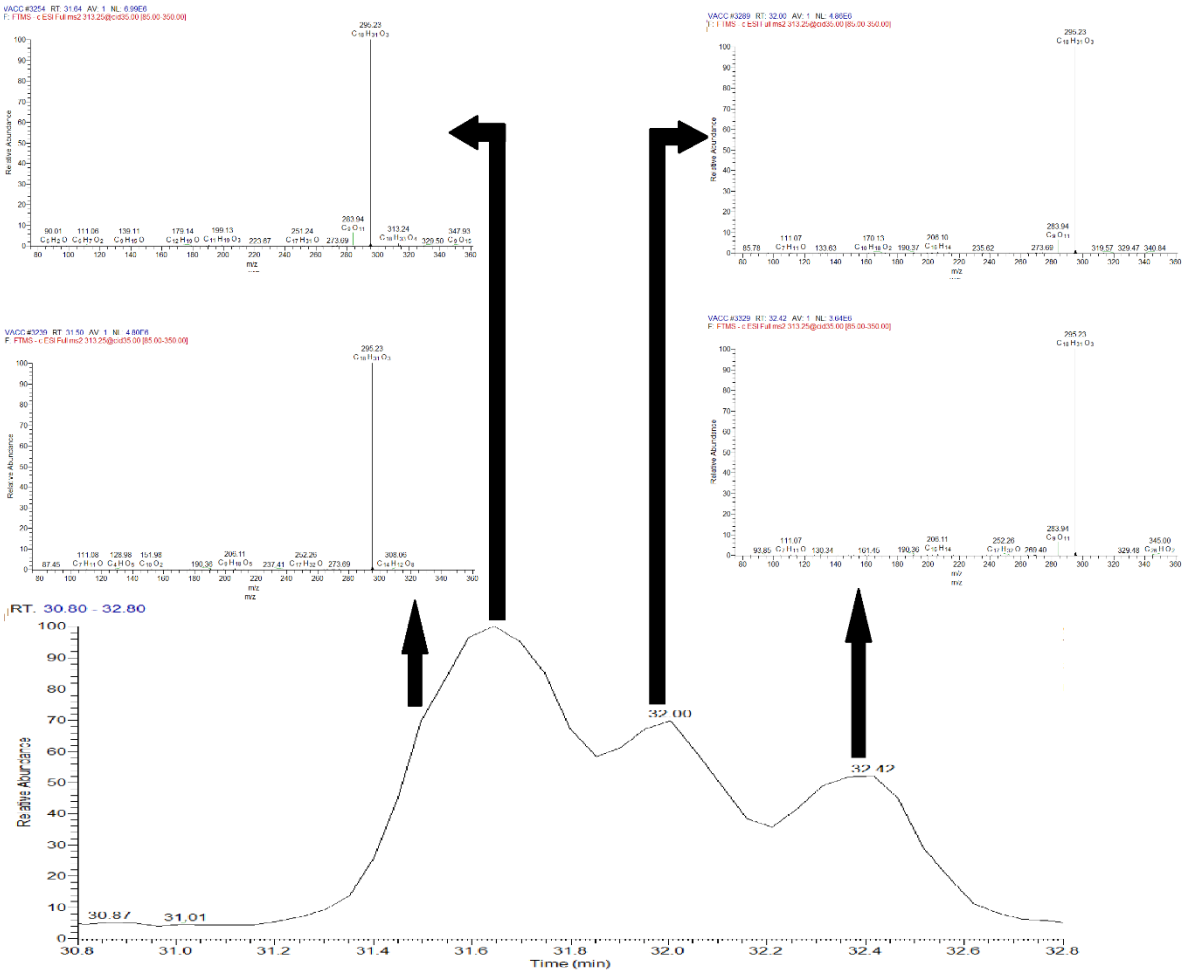

Figure 3-14 Total ion chromatogram & MS^2 spectrometry (LC- MS^2) following collision induced decomposition of the molecular anion [M – H]- at *m/z* 313 derived from HpO11ME.

In order to reach more specific structural information, MS^3 was carried out on these major fragments, $[M-(H^+ + H_2O)]^-$. The resulting spectra revealed different fragmentation patterns for the four peaks recognised in parent ion chromatogram in figure 3-14. Similarly to the case of octadec-9-enoic acid, parent molecular ion $[M-(H^+ + H_2O)]^-$ *m/z* 295, fragment product ion resulted from successive loss of water $[M-(H^+ + 2H_2O)]^-$ *m/z* 277 and product ion *m/z* 251 which is proposed to be formed by loss of CO_2 $[M-(H^+ + H_2O + CO_2)]^-$ could be found in all observed isomer peaks (Figure 3-15).

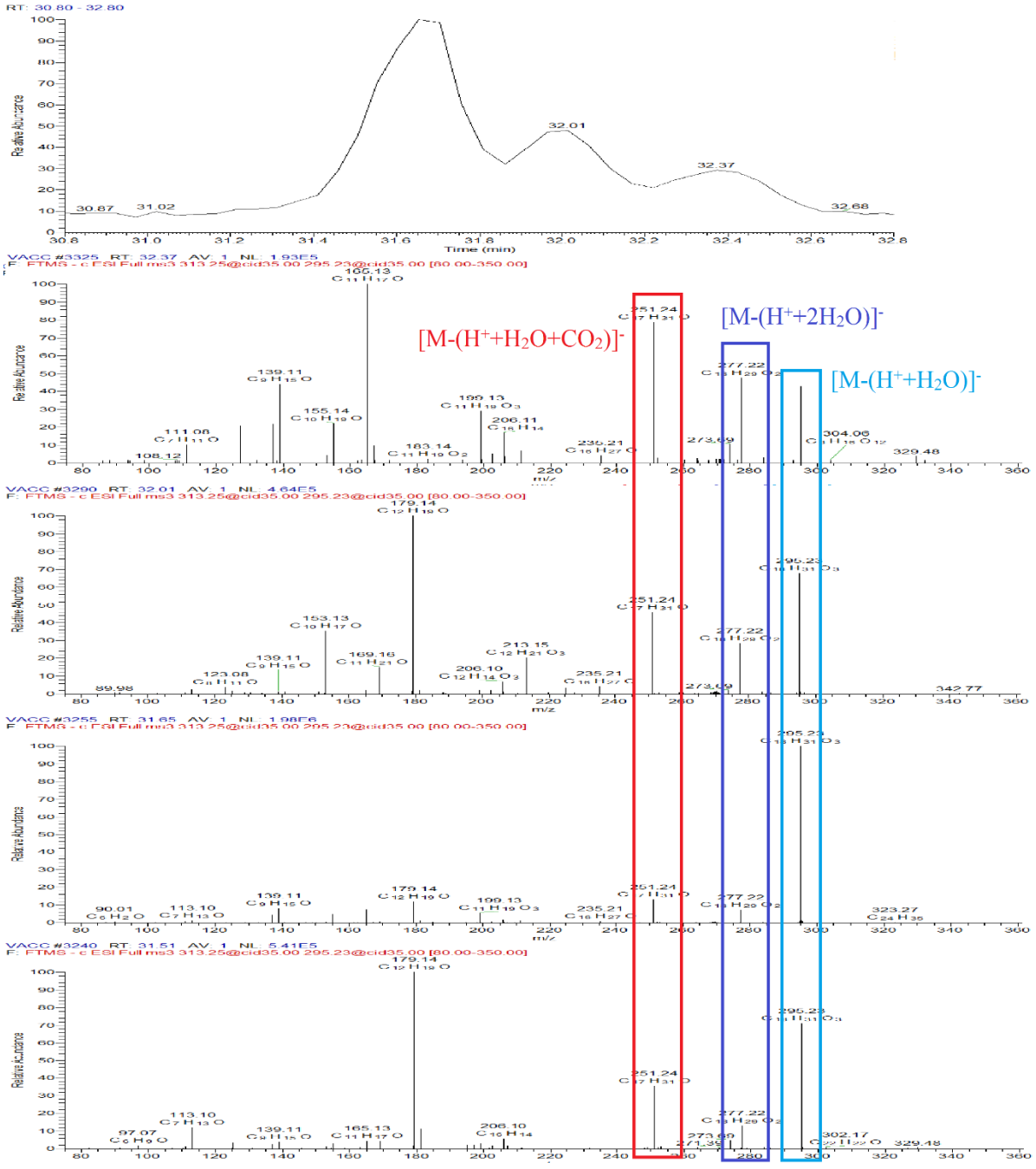

Figure 3-15 (LC-MS^3 chromatogram) following collision induced decomposition of MS^2-generated product ion [M - (H+ + H_2O)]- at *m/z* 295 derived from HpO11ME.

In addition to the common peaks shown in figure 3-15 (*m/z* 295, *m/z* 277 and *m/z* 251), peak at Rt 31.51 min. (Figure 3-16) showed some of the product ions that have characteristic significance (Table 3-5) and could be linked to 13-regioisomers. The proposed formation pathway of the most abundant product ion, *m/z* 179 which is

proposed to be $[C_{12}H_{20}O- H^+]^-$, required a double bond shift towards the carboxyl end and enolisation of the carbonyl group to form a double bond in the same direction and to create a transient conjugated diene ion that goes through a cleavage in C13–C14 bond preceded by a loss of neutral CO_2 and H_2 (Scheme 3-7).

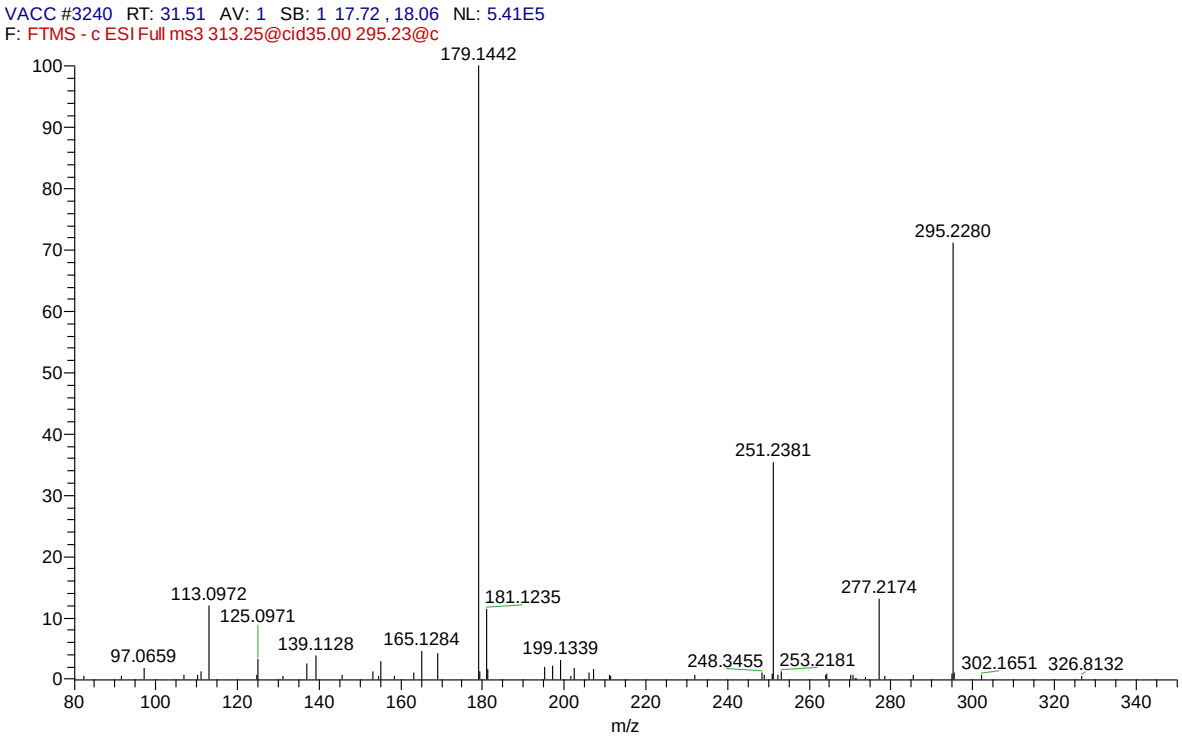

Figure 3-16 (MS^3) spectrum of the MS^2-generated product ion of *m/z* 295.23 from octadec-11-enoic acid oxidation sample at Rt 31.76 min.

Table 3-5 The most abundant MS^3 spectrum ions at Rt 31.51 min. in the TIC LC-MS^3 chromatogram of the MS^2-generated product ion of *m/z* 295.23 from octadec-11-enoic acid oxidation sample.

Rt: 31.51		
m/z	**Relative abundance**	**Composition**
179.14	100.00	$C_{12}H_{19}O$
113.10	11.98	$C_7H_{13}O$
181.12	11.33	$C_{11}H_{17}O_2$
165.13	4.50	$C_{11}H_{17}O$
169.12	4.17	$C_{10}H_{17}O2$

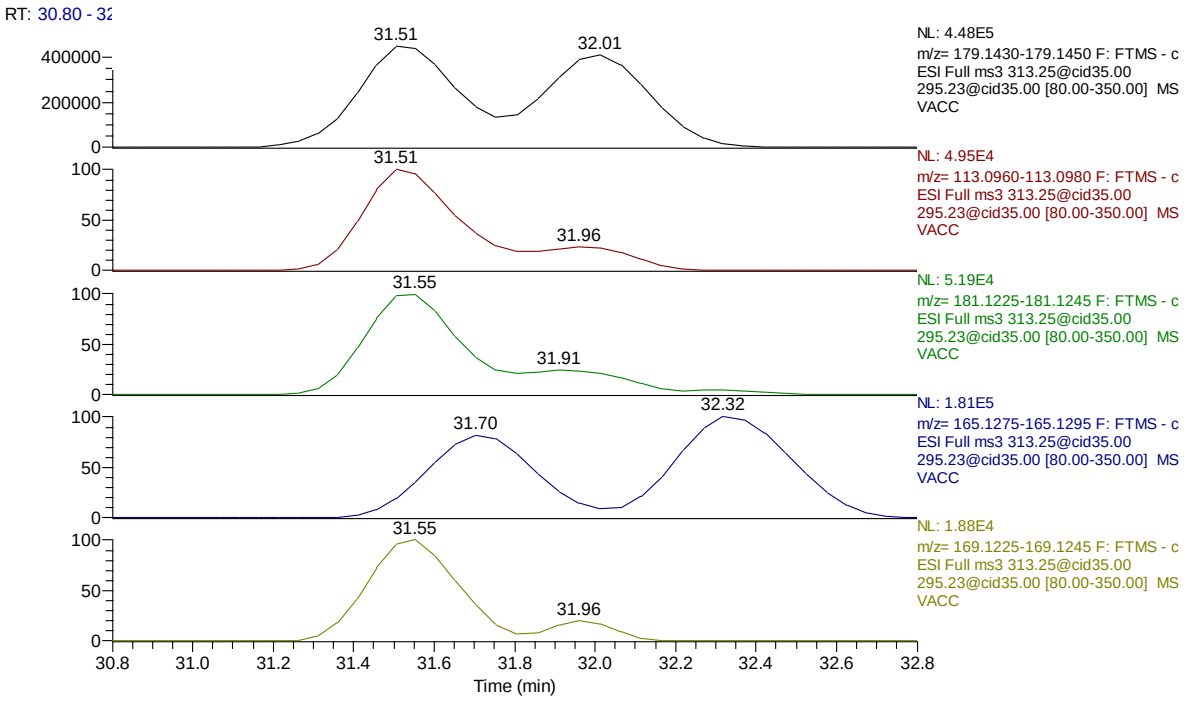

Figure 3-17 Selective mass range-chromatograms of the most relatively abundant MS^3-generated product ions at Rt 31.51 min. that were detected from octadec-11-enoic acid oxidation sample.

The rest of fragment ions that can be considered characteristic in spectrum of (MS^3)-chromatographic peak at Rt 31.51 min. had low relative abundance of 4- 12%. Product ion *m/z* 113 which is proposed to be $[C_7H_{14}O- H^+]^-$ could be linked to 13-regioisomers by a fragmentation process that involves double bond shift towards the carboxyl end to facilitate scission in C11–C12 bond (Scheme 3-7).

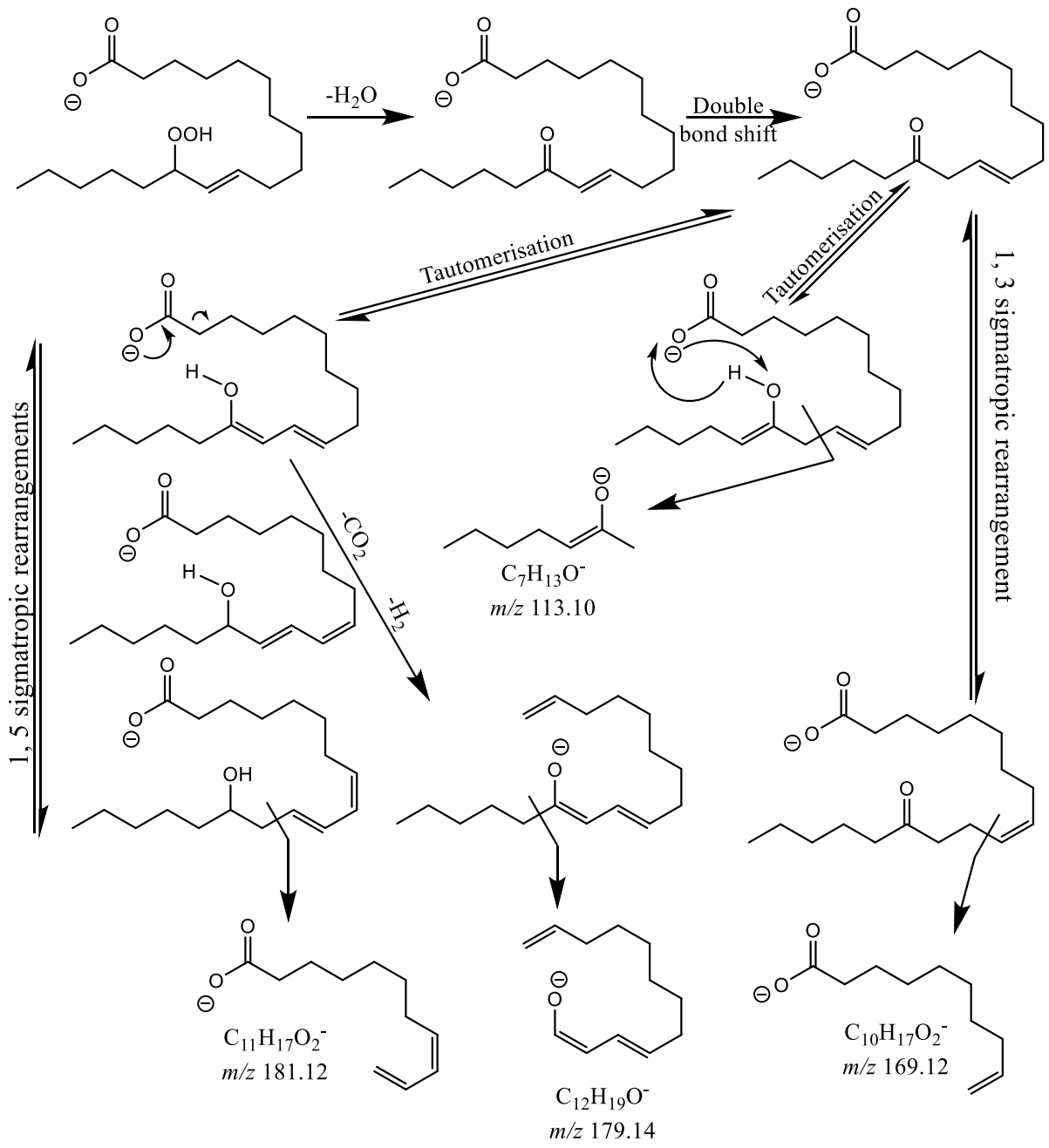

Scheme 3-7 Putative sources of product ions with characteristic significance from 13-HpO11ME molecular ion in (MS^3)-chromatographic peak at Rt 31.51 min.

Scheme 3-7 suggests putative fragmentation pathways for the formation of the product ions at *m/z* 169 and *m/z* 181 that are proposed to be $[C_{10}H_{18}O_2 - H^+]^-$ and $[C_{11}H_{18}O_2 - H^+]^-$, respectively. The presented pathway for product ion *m/z* 169 involves two consecutive 1, 3 sigmatropic rearrangements (double bond shifts) towards the carboxyl end moving the double bond to C9 hence directing collision-induced scission to C10-

C11 bond. Likewise, the product ion at *m/z* 181 formation from the 13-regioisomer required a double bond shift towards the carboxyl group end to facilitate enolisation of carbonyl group in the same direction forming a transient conjugated diene ion that undergoes two consecutive 1, 5 sigmatropic rearrangement to guide collision-induced scission to C11-C12 bond.

The product ion at *m/z* 165 observed in spectrum of MS^3-chromatographic peak at Rt 31.51 min. with low relative abundance of 4.5%, is proposed to be $[C_{11}H_{18}O- H^+]^-$ and appears to be a result of co-elution with MS^3-chromatographic peak at Rt 31.76 min.

The peak at Rt 31.76 min. (Figure 3-18) showed high stability of the parent peak *m/z* 295, accordingly, all fragment product ions including the common peaks mentioned above (*m/z* 277 and *m/z* 251) became less abundant. All product ions that could have characteristic significance had a relative abundance between 10- 22% (Table 3-6). The most abundant product ion that can be considered characteristic was *m/z* 139 which is proposed to be $[C_9H_{16}O- H^+]^-$ and could be linked to the 10-regioisomer via a fragmentation process that requires a 1,3 sigmatropic rearrangement, away from the carboxyl end preceding ketone/enol tautomerisation creating a double bond in the same direction and forming a conjugated diene transient ion that suffers a scission in C9–C10 bond (Scheme 3-8).

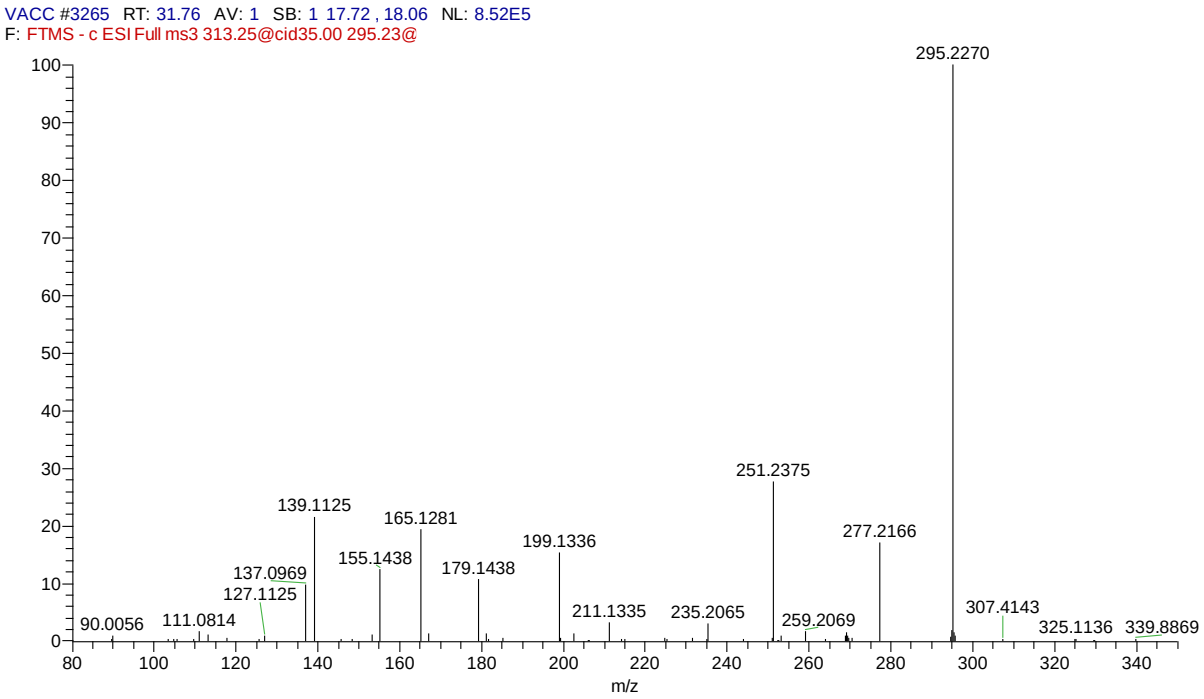

Figure 3-18 (MS^3) spectrum of MS^2-generated product ion of *m/z* 295.23 from octadec-11-enoic acid oxidation sample at Rt 31.76 min.

Table 3-6 The most abundant MS^3 spectrum ions at Rt 31.76 min. in the TIC LC-MS^3 chromatogram of the MS^2-generated product ion of *m/z* 295.23 from octadec-11-enoic acid oxidation sample.

Rt: 31.76		
m/z	**Relative abundance**	**Composition**
295.23	100.00	$C_{18}H_{31}O_3$
139.11	21.58	$C_9H_{15}O$
165.13	19.50	$C_{11}H_{17}O$
199.13	15.45	$C_{11}H_{19}O_3$
155.14	12.57	$C_{10}H_{19}O$
179.14	10.87	$C_{12}H_{19}O$

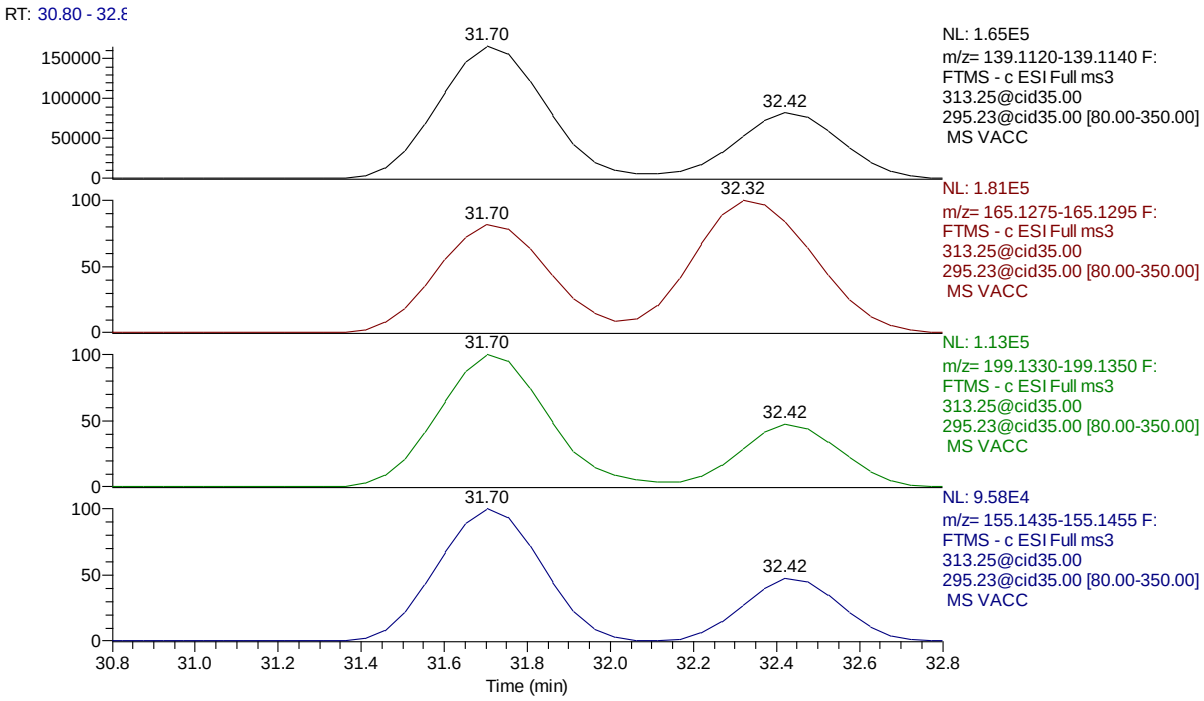

Figure 3-19 Selective mass range-chromatograms of the most relatively abundant MS^3-generated product ions at Rt 31.76 min. that were detected from octadec-11-enoic acid oxidation sample.

Formation of a double bond in the opposite direction during enolisation of carbonyl group, towards the carboxyl end, preceding any double bond shift offers conceivable illustration of a substitute fragmentation pathway that gives rise to a different conjugated diene transient ion. Product ion *m/z* 165 which is proposed to be $[C_9H_{16}O-H^+]^-$ and could result from this transient ion by going through neutral losses of CO_2 and H_2 and a scission in the C12–C13 bond (Scheme 3-8). Formation of product ions *m/z* 199 and *m/z* 155, proposed to be $[C_{11}H_{20}O_3- H^+]^-$ and $[C_{10}H_{20}O- H^+]^-$, respectively, from the same transient ion suggests a double bond shift away from carboxylic group to guide collision-induced scission towards the C11-C12 bond, taking into account the fragmentation pathway of the product ion *m/z* 155 involves neutral loss of CO_2 before or after scission in C11-C12 bond (Scheme 3-8).

Product ion *m/z* 179 that has low relative abundance in the MS^3-chromatographic peak at Rt 31.76 min. and is proposed to be $[C_{12}H_{20}O- H^+]^-$ and can be a result of co-elution with the MS^3-chromatographic peak at Rt 31.51 min. Nevertheless, product ion *m/z* 179 can be theoretically linked to the 10-regioisomer via the same fragmentation

pathway producing *m/z* 139 where the conjugated diene transient ion could go through neutral losses of CO_2 and H_2 and a scission in C13–C14 bond (Scheme 3-8).

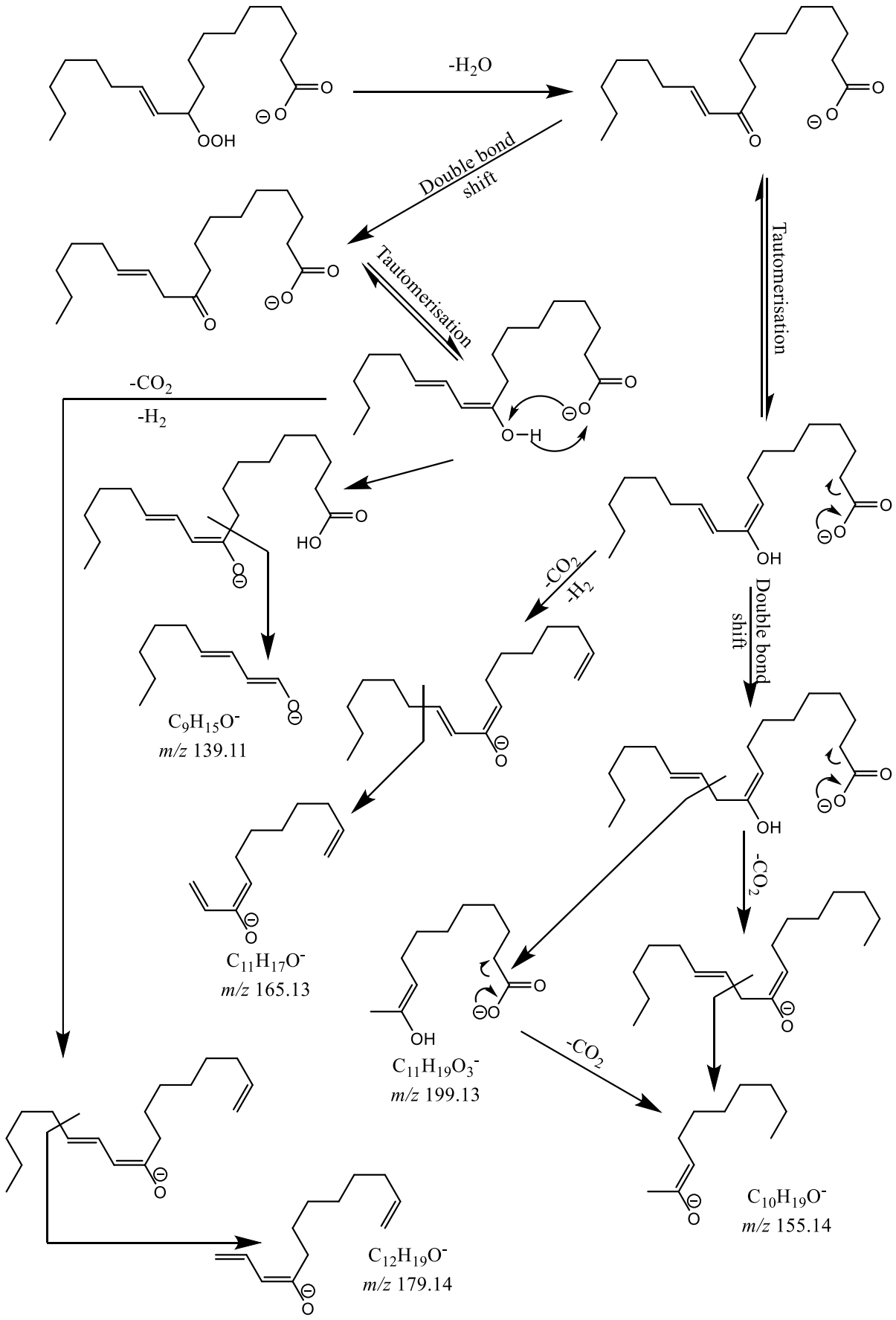
-H2O
Double bond shift
Tautomerisation
Tautomerisation
-CO2
-H2
-CO2
-H2
Double bond shift
-CO2
-CO2
C9H15O-
m/z 139.11
C11H17O-
m/z 165.13
C11H19O3-
m/z 199.13
C10H19O-
m/z 155.14
C12H19O-
m/z 179.14

Scheme 3-8 Putative sources of product ions with characteristic significance from 10-HpO11ME molecular ion in (MS^3)-chromatographic peak at Rt 31.76 min.

Peak at Rt 32.01 min. (Figure 3-20) showed the common peaks mentioned above (*m/z* 295, *m/z* 277 and *m/z* 251) in addition to some of the product ions that can be considered characteristic (Table 3-7) and could be linked to the 12-regioisomer. The proposed formation pathway of the most abundant product ion, *m/z* 179 which is proposed to be $[C_{12}H_{20}O- H^+]^-$, required enolisation of carbonyl group creating a double bond towards the methyl end to facilitate a cleavage in C13–C14 bond preceded by a loss of neutral CO_2 and H_2 (see Scheme 3-9).

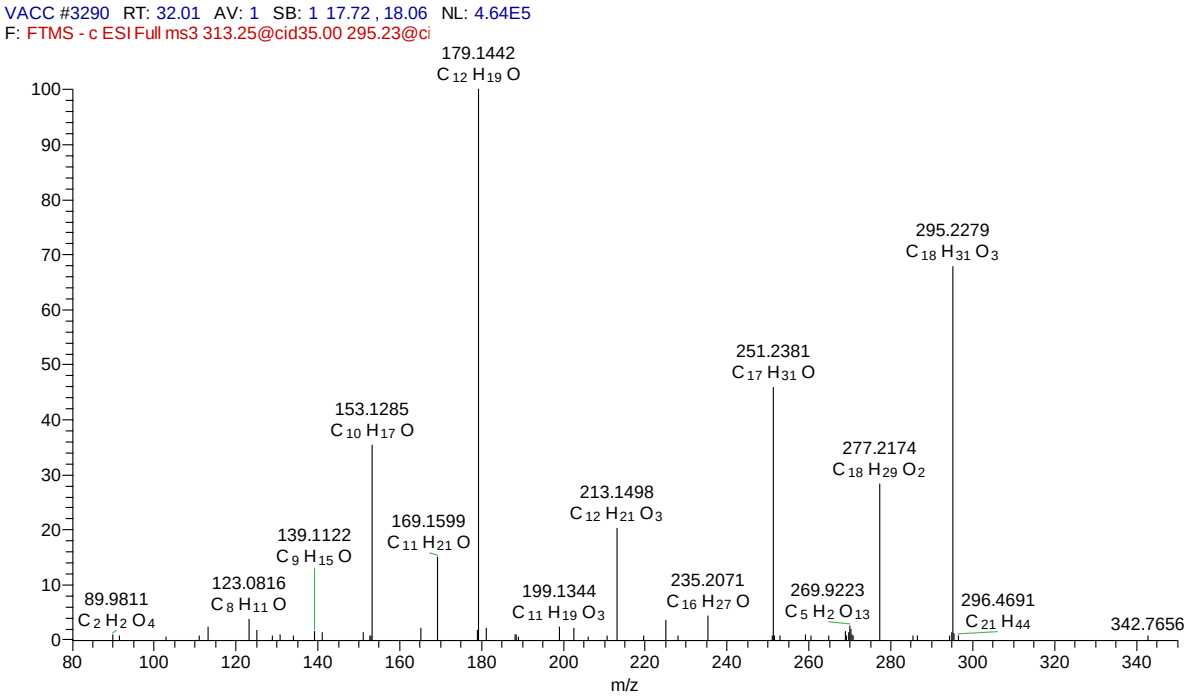

Figure 3-20 (MS^3) spectrum of MS^2-generated product ion of *m/z* 295.23 from octadec-11-enoic acid oxidation sample at Rt 32.01 min.

Table 3-7 The most abundant MS^3 spectrum ions at Rt 32.01 min. in the TIC LC-MS^3 chromatogram of the MS^2-generated product ion of *m/z* 295.23 from octadec-11-enoic acid oxidation sample.

Rt: 32.01		
m/z	**Relative abundance**	**Composition**
179.14	100.00	$C_{12}H_{19}O$
153.13	35.39	$C_{10}H_{17}O$
213.15	20.31	$C_{12}H_{21}O_3$
169.16	14.94	$C_{11}H_{21}O$
235.21	4.25	$C_{16}H_{27}O$

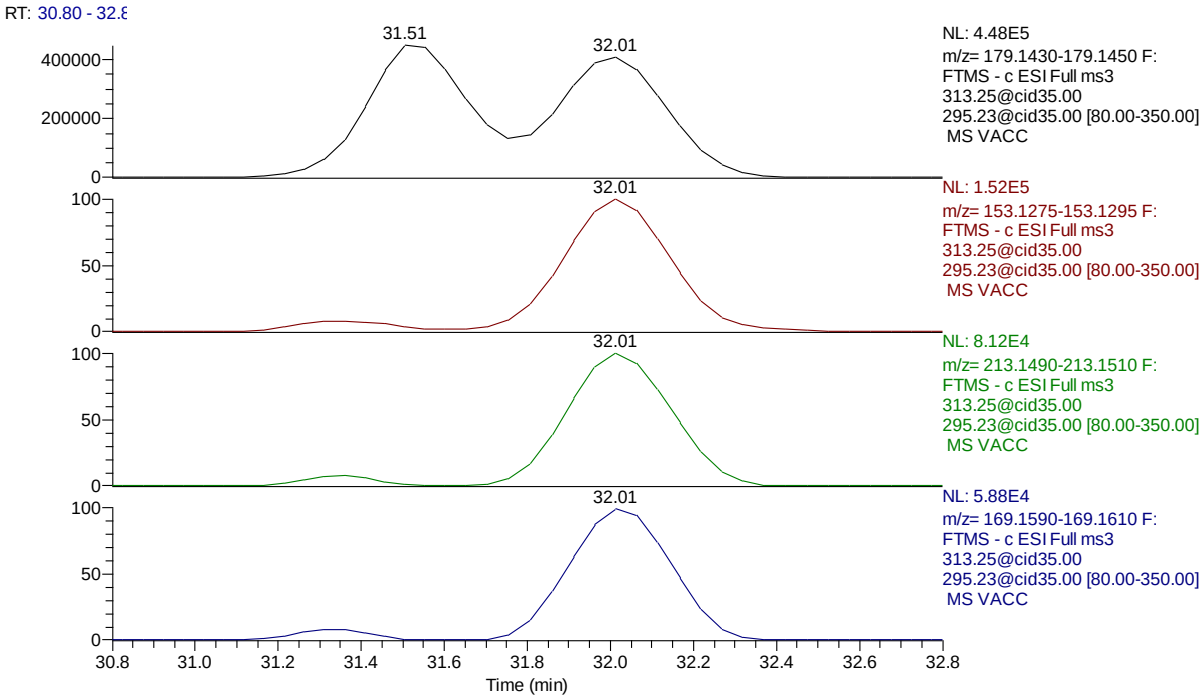

Figure 3-21 Selective mass range-chromatograms of the most relatively abundant MS^3-generated product ions at Rt 32.01 min. that were detected from octadec-11-enoic acid oxidation sample.

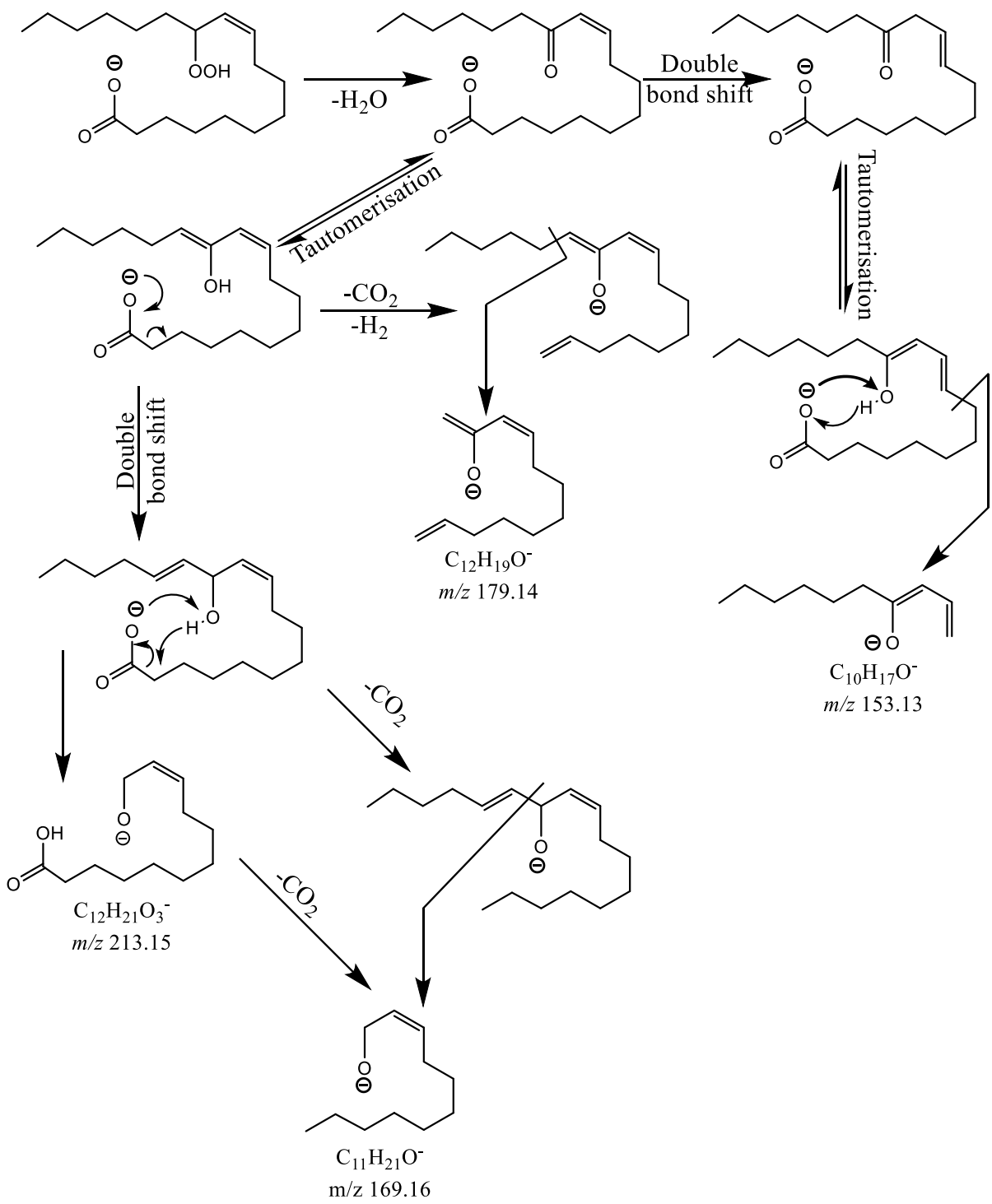

Scheme 3-9 Putative sources of product ions with characteristic significance from 12-HpO11ME molecular ion in (MS^3)-chromatographic peak at Rt 32.01 min.

In addition to formation of *m/z* 179 product ion, scheme 3-9 shows the fragmentation pathway for the two less abundant product ions observed in spectrum of peak at Rt

32.01 min., *m/z* 169 and *m/z* 213, that can be proposed to be $[C_{11}H_{22}O- H^+]^-$ and $[C_{12}H_{22}O_3- H^+]^-$, respectively, and can be linked to the 12-regioisomer via a similar fragmentation process, except that in those cases, the transient conjugated diene ion resulting from tautomerisation undergoes further double bond shift, 1, 3 sigmatropic rearrangement, away from the carboxyl end to direct collision-induced scission towards C12–C13 bond forming product ion *m/z* 213. While product ion *m/z* 169 needs loss of neutral CO_2 before or after C12–C13 cleavage to be formed.

The second most abundant product ion that can be considered characteristic in the (MS^3) spectrum of the peak at Rt 32.01 min. was *m/z* 153 which is proposed to be $[C_{10}H_{18}O- H^+]^-$ and to be formed by a fragmentation process that involves a double bond shift towards the carboxyl end to facilitate enolisation of carbonyl group and formation of a double bond in the same direction creating a transient conjugated diene ion that suffers a scission in the C8–C9 bond (see Scheme 3-9).

The peak at Rt 32.37 min. (Figure 3-22) showed the common peaks mentioned above (*m/z* 295, *m/z* 277 and *m/z* 251) in addition to some of the product ions that can be considered characteristic (Table 3-8) and could be linked to the 11-regioisomer such as *m/z* 165 which is proposed to be $[C_{11}H_{18}O- H^+]^-$ and to be generated by undergoing ketone/enol tautomerisation and 1, 3 sigmatropic proton shift. The pathway involves formation of fragment ion $[M-(H^+ + H_2O + CO_2)]^-$ before it goes through a loss of H_2 and cleavage in C12–C13 bond (Scheme 3-10).

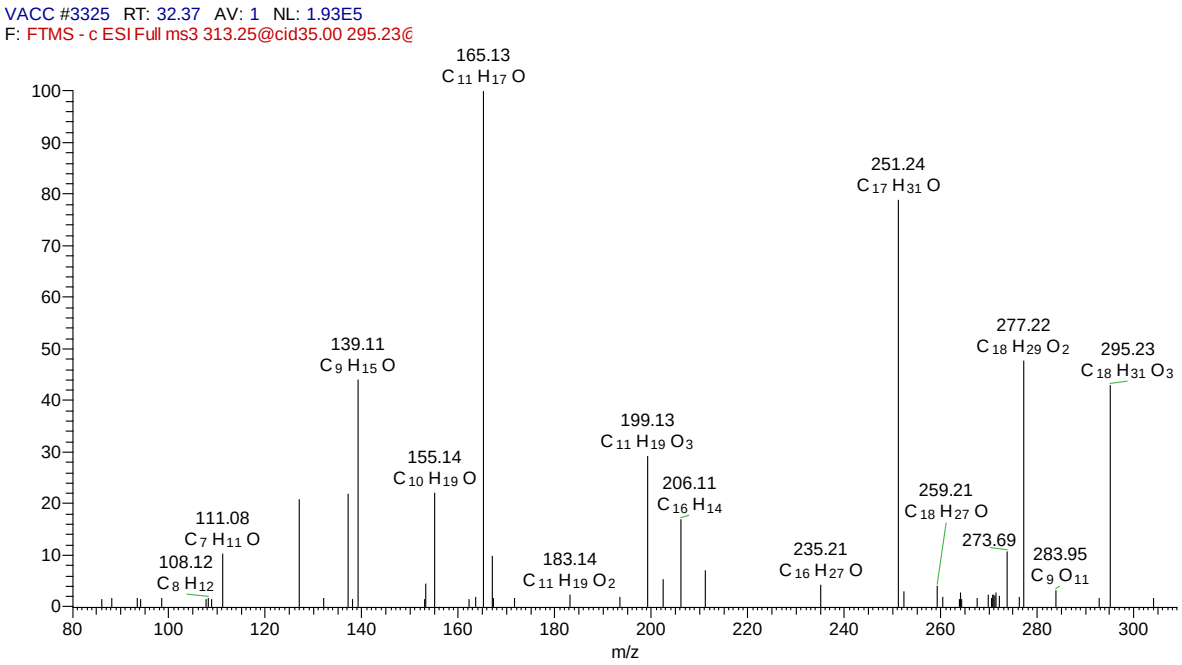

Figure 3-22 (MS^3) spectrum of MS^2-generated product ion of *m/z* 295.23 from octadec-11-enoic acid oxidation sample at Rt 32.37 min.

Table 3-8 The most abundant MS^3 spectrum ions at Rt 32.37 min. in the TIC LC-MS^3 chromatogram of the MS^2-generated product ion of *m/z* 295.23 from octadec-11-enoic acid oxidation sample.

Rt: 32.37		
m/z	**Relative abundance**	**Composition**
165.13	100.00	$C_{11}H_{17}O$
139.11	43.96	$C_9H_{15}O$
199.13	29.19	$C_{11}H_{19}O_3$
155.14	22.06	$C_{10}H_{19}O$
137.10	21.88	$C_9H_{13}O$
127.11	20.70	$C_8H_{15}O$

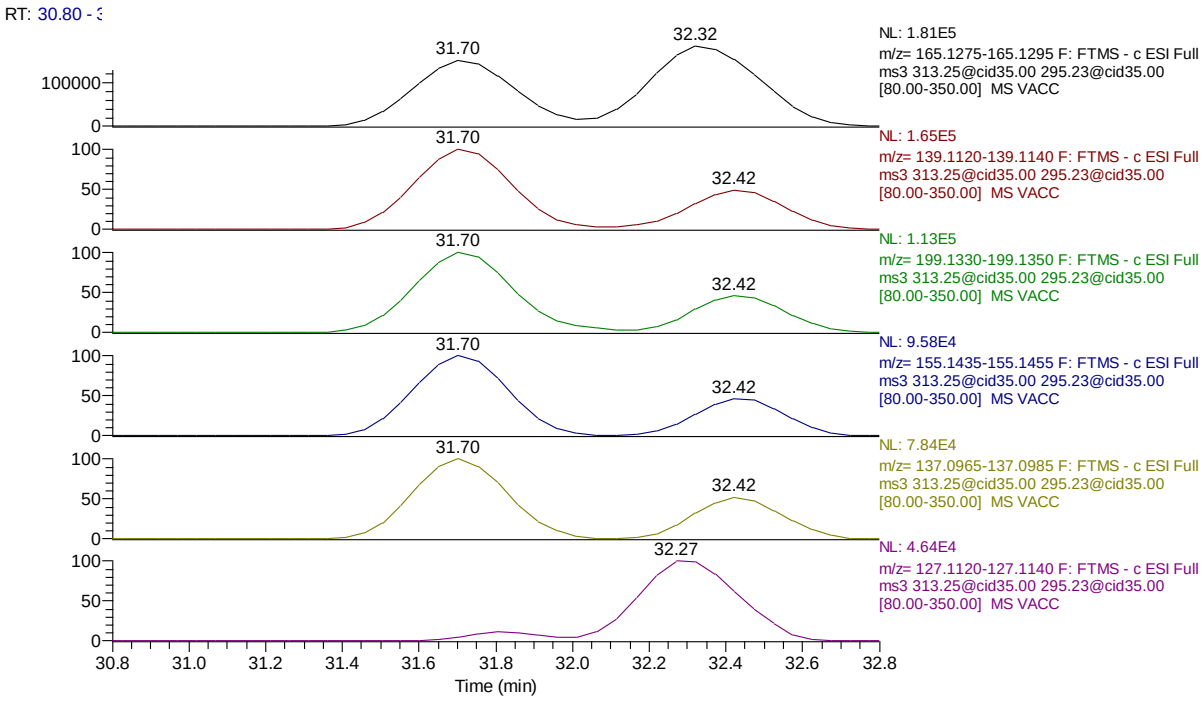

Figure 3-23 Selective mass ranges chromatograms of the most relatively abundant MS^3-generated product ions at Rt 32.37 min. that were detected from octadec-11-enoic acid oxidation sample.

The product ion at *m/z* 139 observed in spectrum of peak at Rt 32.37 min. which can be proposed to be $[C_9H_{16}O- H^+]^-$ can be a result of fragmentation process that involves enolisation of the carbonyl group leading to formation of a double bond towards carboxyl end to facilitate a scission in the C9–C10 bond (see Scheme 3-10).

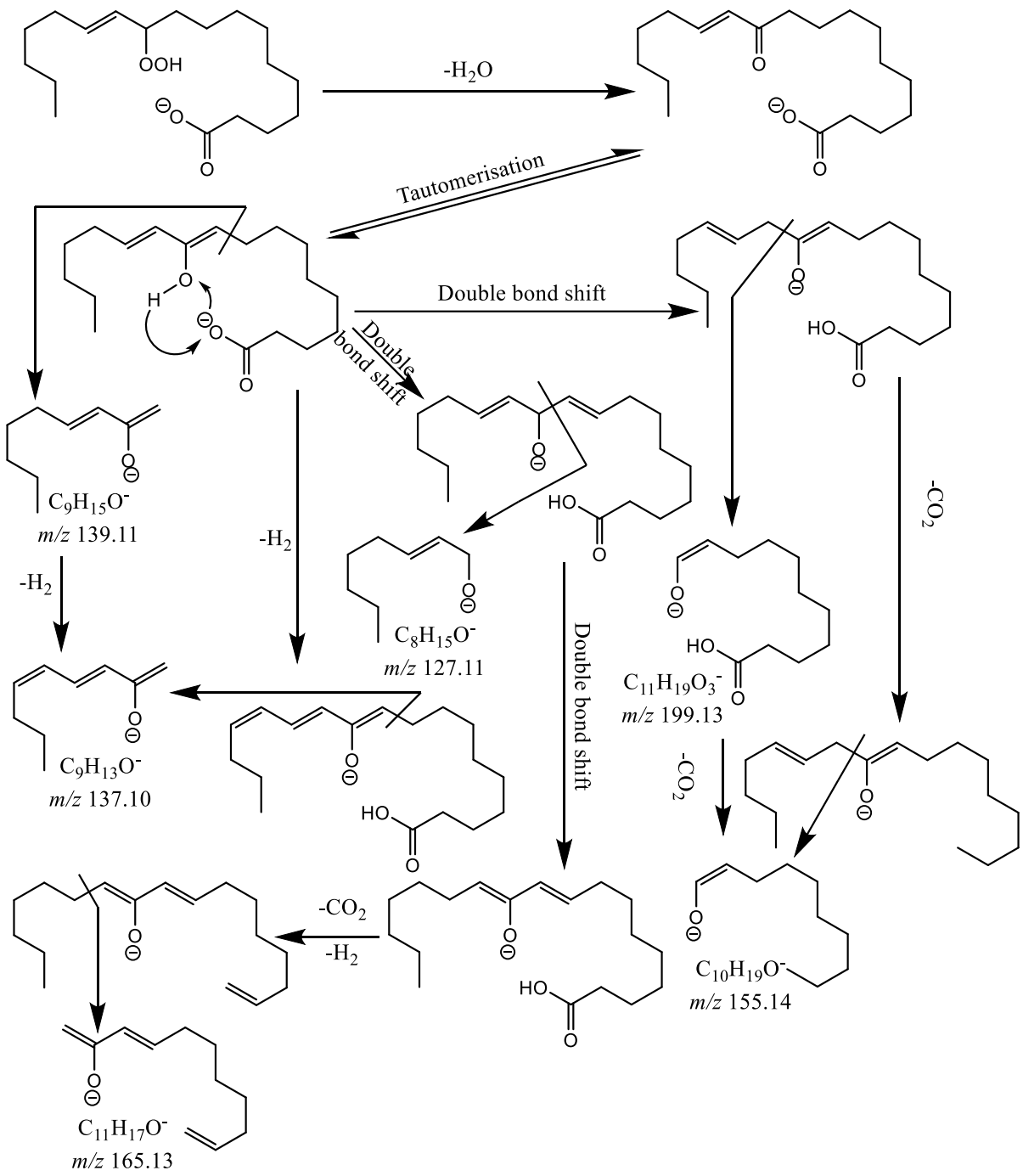

Scheme 3-10 Putative sources of product ions with characteristic significance from 11-HpO11ME molecular ion in (MS^3)-chromatographic peak at Rt 32.37 min.

Formation of the MS^3 product ion at *m/z* 137 , proposed to be $[C_9H_{14}O- H^+]^-$, from 11-hydroperoxy vaccenic acid in spectrum of the same peak is anticipated to be via a fragmentation process similar to the formation of product ion *m/z* 139 see (Scheme 3-10) that involves proton abstraction from the saturated carbon C14 coinciding with a

further loss of H_2 to create a conjugated triene transient ion that suffers a scission in same position (C9–C10 bond) or could be simply formed from product ion *m/z* 139 by neutral loss of H_2.

Scheme 3-10 additionally elucidates formation of comparatively low abundance product ion *m/z* 127 which can be proposed to be $[C_8H_{16}O- H^+]^-$ that has a highly characteristic significance and can confirm identification of peak at Rt 32.37 min. as 11-hydroperoxy vaccenic acid. The pathway would include ketone/enol tautomerisation creating a double bond towards the carboxyl end in the same manner of the formation of product ion *m/z* 139 added to going through double bond shift in the same direction to guide collision-induced scission towards C10-C11 bond.

Product ions *m/z* 199 and *m/z* 155 observed in spectrum of peak at Rt 32.37 min. that can be proposed to be $[C_{11}H_{20}O_3- H^+]^-$ and $[C_{10}H_{20}O- H^+]^-$, respectively, can be simply a result of cleavage in C11–C12 bond, taking into account that the fragmentation pathway of product ion *m/z* 155 involves formation of fragment ion $[M-(H^++H_2O+CO_2)]^-$ before it goes through cleavage in C11–C12 bond or neutral loss of CO_2 from product ion *m/z* 199 (Scheme 3-10).

3.1.2.3 LC-MS chromatographic peaks identification

The MS^3 fragment ion *m/z* 179 proposed to be $[C_{12}H_{20}O- H^+]^-$ was encountered in the peaks at Rt 31.51 and 32.01 min. in the TIC LC-MS^3 chromatogram that correspond to parent ion LC-MS chromatogram peaks of Rt 31.57 and 31.98 min., respectively, besides occurring at Rt 31.76 min. in LC-MS^3 chromatogram as result of co-elution with the MS^3-chromatographic peak at Rt 31.51 min. This fragment ion could be linked to 13-HpO11ME and 12-HpO11ME and theoretically to 10-HpO11ME via fragmentation pathways proposed in schemes 3-7, 3-9 and 3-8, respectively. This recurrence reduced the usefulness of this fragment ion for structural elucidation.

The MS^3 fragment ions at *m/z* 113, *m/z* 169 and *m/z* 181, proposed to be $[C_7H_{14}O- H^+]^-$, $[C_{10}H_{18}O_2- H^+]^-$ and $[C_{11}H_{18}O_2- H^+]^-$, respectively, that were only detected in chromatographic peak Rt 31.57 min. could be linked to the 13 regioisomer via fragmentation pathways proposed in scheme 3-7 that were directed by the position of dehydrated hydroperoxy moiety on C13. Therefore, parent ion LC-MS chromatographic peak at Rt 31.57 min. was elucidated as being due to 13-HpO11ME.

The fragment ions at *m/z* 139 and *m/z* 165, were proposed to be due to $[C_9H_{16}O- H^+]^-$ and $[C_{11}H_{18}O- H^+]^-$, respectively, that are presented at LC-MS^3 chromatogram peaks corresponding to parent ion LC-MS chromatogram peaks of Rt 31.67 and Rt 32.33 min. could be linked to the 10-regioisomer and 11-regioisomer via fragmentation pathways proposed in schemes 3-8 and 3-10. Moreover, correlative fragment ion-pair *m/z* 155 and *m/z* 199, proposed to be $[C_{10}H_{20}O- H^+]^-$ and $[C_{11}H_{20}O_3- H^+]^-$, respectively, in both peaks at Rt 31.67 and Rt 32.33 min. could be only linked to the 10-regioisomer and 11-regioisomers via fragmentation pathways proposed in schemes 3-8 and 3-10, and have no possibility to be originated from the 12-regioisomers or 13-regioisomer, especially because of the presence of three oxygens in the elemental composition of the later.

From the above discussion, parent ion LC-MS chromatogram peaks at Rt 31.67 and Rt 32.33 min. were limited to be either 10-HpO11ME and 11-HpO11ME. The distinctive MS^3 fragment ion at *m/z* 127, proposed to be $[C_8H_{16}O- H^+]^-$, which could not be generated by CID activation of dehydrated 10-regioisomer and could only be a result of the fragmentation pathway of the 11-regioisomer proposed in scheme 3-10 was exclusively encountered in chromatographic peak at Rt 32.33 min. Accordingly, the parent ion LC-MS chromatographic peak at Rt 32.33 min. was elucidated as 11-HpO11ME and parent ion LC-MS chromatographic peak at Rt 31.67 min. was elucidated as 10-HpO11ME.

The presence of MS^3 fragment ion *m/z* 153 and correlative fragment ion-pair *m/z* 169 and *m/z* 213, proposed to be $[C_{10}H_{18}O- H^+]^-$, $[C_{11}H_{22}O- H^+]^-$ and $[C_{12}H_{22}O_3- H^+]^-$, respectively, in corresponding LC-MS^3 spectrum of the chromatographic peak at Rt 31.98 min. indicted that this peak was 12-HpO11ME in the light of the proposed fragmentation pathways in scheme 3-9 that were directed by position of dehydrated hydroperoxy moiety on C12.

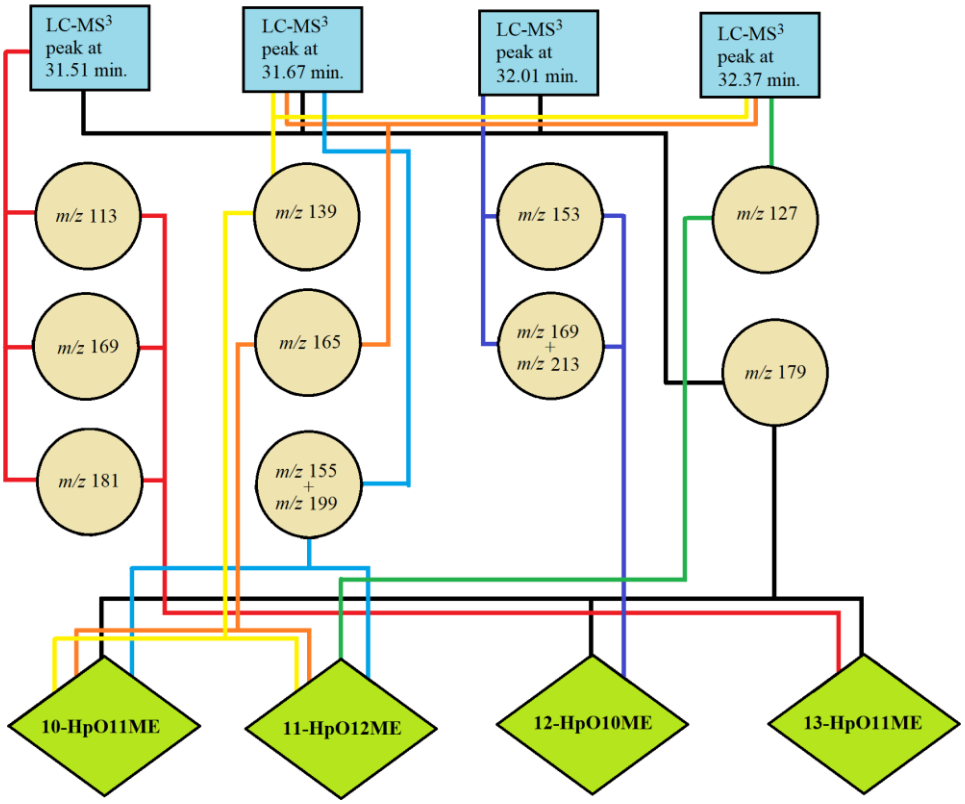

Figure 3-24 A flow chart showing the method used to select characteristic ions for each isomer with the purpose of identifying (MS3)-chromatographic peaks from octadec-11-enoic acid oxidation sample.

3.2 Discussion of hydroperoxy mono-unsaturated fatty acids analysis as a tool for double bond position determination

The behaviour of different monounsaturated (18:1 FA) hydroperoxy fatty acids in LC-MS and LC-MS^n performed on the molecular ions $[M - H^+]^-$ was comparable. Figures (3-2 and 3-14) show that collisional activation of the $[M - H^+]^-$ from monounsaturated hydroperoxy fatty acids led to facile neutral loss of H_2O, that was observed in mass range chromatograms even before collisional activation, as a dominant reaction and all MS^3 fragment ions resulting from subsequent collisional activation of $[M-(H^+ + H_2O)]^-$ advocate that this dehydration step involves the loss of the oxygen of hydroperoxy group and the hydrogen atom on the same carbon atom bearing the hydroperoxy moiety which would cause generation of fragment ion of the corresponding keto fatty acid. These findings are consistent with the

results of (Schneider *et al.*, 1997) and isotope labelling studies carried out by (Macmillan & Murphy, 1995). Besides those formed by loss of water at *m/z* 295, precursor ions, and product ions observed from all studied species of $[M-(H^+ + H_2O)]^-$ included loss of CO_2 and H_2O from the carboxylate anion *m/z* 251. Loss of two water molecules from the carboxylate anion was also common to all the species studied and yielded *m/z* 277.

Feasibility of the decomposition of the dehydrated carboxylate anions $[M-(H^+ + H_2O)]^-$ in the MS^3 spectrometery and the complexity of this process were substantially determined by the positions of double bond and the hydroperoxy moiety in the fatty acid chain, taking into consideration that the position of the latter depends on the initial double bond position in the first place. The course of decomposition was mainly driven by the electron withdrawing properties of the p-orbital of the double bond to cause the breaking of the bond allylic to it and/or by the electronegativity of the oxygen atom at carbonyl and hydroxyl groups (resulting from tautomerisation) to cause the cleavage of the vinylic bond of these moieties.

The effect of charge position on proposed fragmentation patterns was imperceptible in most cases and the reactions occurring around the double bond and the functional group were mainly charge remote and were directed by the chemical reactivity of double bond and the functional group but not the charge. This gives the structural information coming from ESI-LC-tandem MS higher significance in double bond position elucidation.

Variable decomposition pathways resulted from subsequent MS^3-collisional activation of $[M-(H^+ + H_2O)]^-$ differentiated by the existence of the following main steps and the order of their occurrence.

- Tautomerisation of the resultant carbonyl group.
- Sigmatropic hydrogen rearrangements that precede and/or succeed keto-enol tautomerisation causing freedom of double bond migration.
- Carboxylate anion abstraction of the proton of the alcohol functional group (resulting from tautomerisation), leaving an alkoxide anion at that position.

- A parallel tendency for CO_2 loss.
- Loss of hydrogen gas (H_2).

A considerable amount of literature has been published on the chemistry of monounsaturated fatty acid peroxidation (Murphy et al., 2001; Wong, 2018) which made it a well-understood reaction that the molecular ions of hydroperoxides could be reliably predicted and thus identification of the molecular ions of these hydroperoxides would unequivocally determine the original double bond position in fatty acyl chain without the need for comparison to standard compounds. Nonetheless, the fact that every double bond positional isomer would produce four hydroperoxy derivatives besides the spectral complexity of each regioisomer that arises from factors mentioned above make the resulting spectrum difficult to interpret especially in the cases of complex mixtures of natural or biological origins. While it can be attempted to get some of the spectral complexity reduced by performing neutral loss or precursor ion scans, the instability of hydroperoxide derivatives would add another limitation of decreased sensitivity.

3.3 Analysis of hydroperoxy Poly-unsaturated fatty acids

3.3.1 Analysis of Linoleic acid hydroperoxides

3.3.1.1 Hydroperoxide formation

The introduction of second double bond into the 18-membered carbon unsaturated fatty acyl chain leads to a major increase in reactivity (Cosgrove et al., 1987; Trades & Chem, 1947). Linoleic acid has an active bis-allylic methylene group on carbon-11 between two double bonds that has higher proneness to lose a hydrogen atom to produce a hybrid pentadienyl radical, which reacts with oxygen at the end carbon-9 and carbon-13 positions to produce a mixture of two conjugated diene 9- and 13-hydroperoxides (Scheme 3-11) (Porter et al., 1995; Pratt et al., 2011). Resonance is a stabilising factor for the pentadienyl radical intermediate and the resulting dienoic hydroperoxides produced are stabilised by conjugation. These isomeric conjugated dienoic hydroperoxides are:

9-hydroperoxyoctadeca-10, 12-dienoic acid (9-HpO10,12DE)

13-hydroperoxyoctadeca-9, 11-dienoic acid (13-HpO9,11DE)

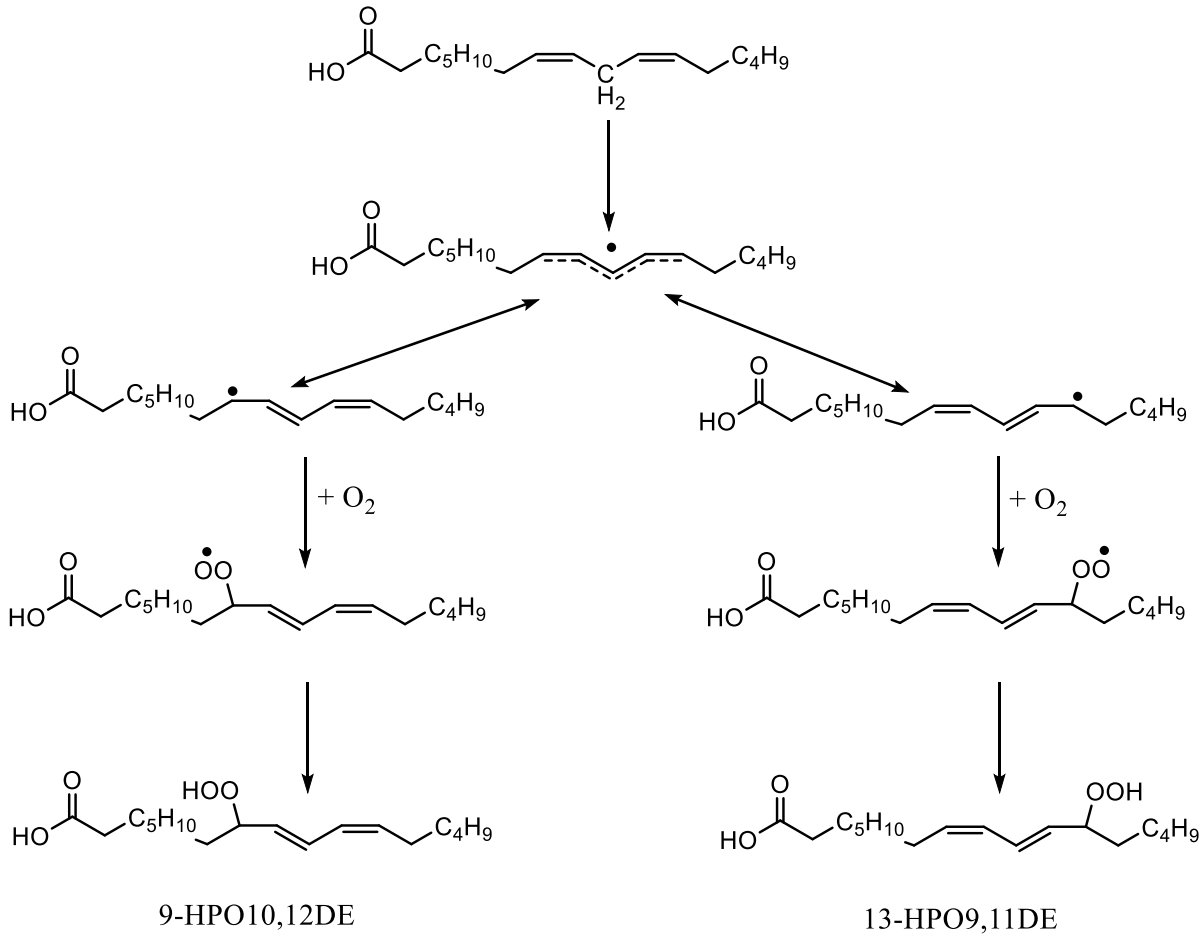

Scheme 3-11 Overall reaction scheme for linoleic acid hydroperoxides formation using simplified versions of the reaction schemes published by (Porter et al., 1995; Pratt et al., 2011).

3.3.1.2 LC-MS analysis of Linoleic acid hydroperoxides

In the course of initial LC-MS analyses of chemically oxidised octadeca-9,12-dienoic acid (Linoleic acid, FA 18:2 (n−6)) samples (OD9,12D), four isomeric peaks were found in the parent ion Mass range chromatogram, corresponding to two expected regioisomeric hydroperoxide derivatives of linoleic acid, as two stereoisomers can be expected for each hydroperoxide regioisomer. For all studied species, little or no characteristic fragmentation was observed in the MS^1 spectra. Loss of water [M - (H^+ + H_2O)]$^-$ at *m/z* 293 was the only major fragment ion peak observed in all spectra of hydroperoxides species in mass range chromatogram of [M – H^+]$^-$ (Figure 3-25).

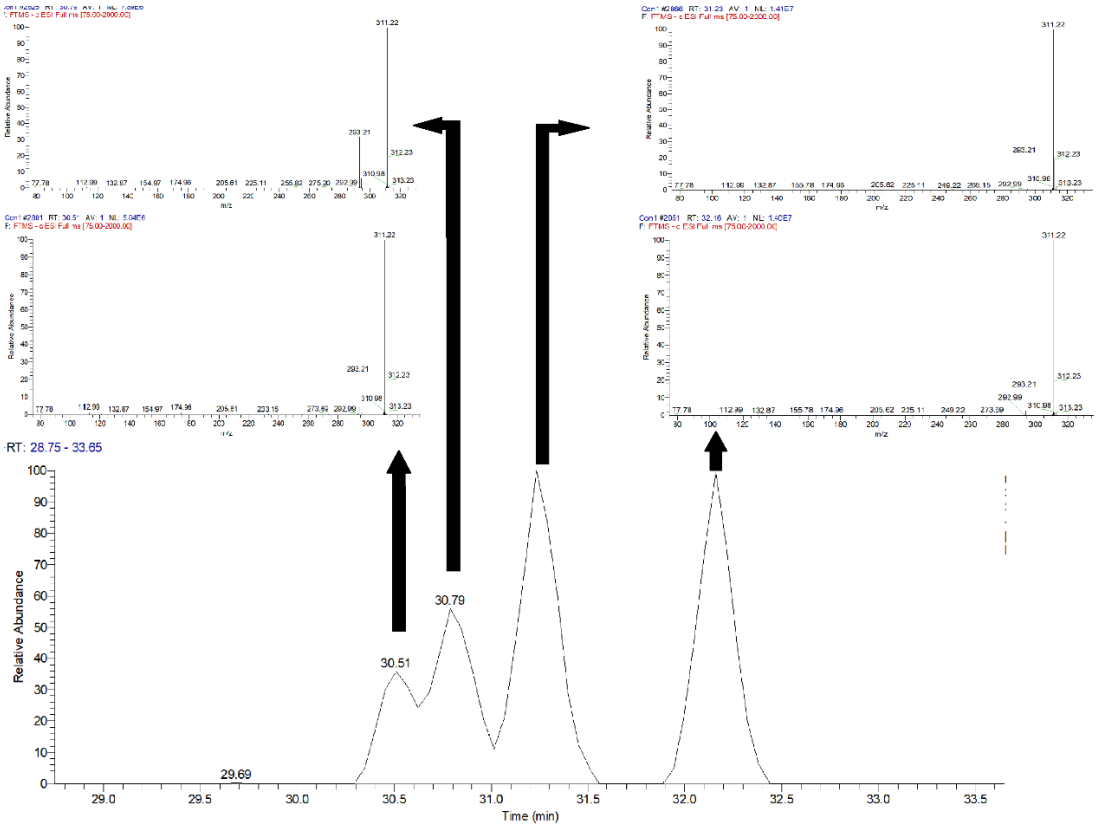

Figure 3-25 Mass range chromatogram & mass spectra of ions of *m/z* 311 in liquid chromatography- mass spectrometry (LC-MS) analysis of oxidised octadeca-9,12-dienoic acid sample.

MS^2 spectra obtained of $[M - H^+]^-$ precursor ions derived from linoleic acid hydroperoxides confirmed the previous observation with little information about isomer identification and no characteristic fragmentation patterns. The most abundant product ion in all observed peaks resulted from loss of water $[M - (H^+ + H_2O)]^-$ at *m/z* 293 (Figure 3-26)

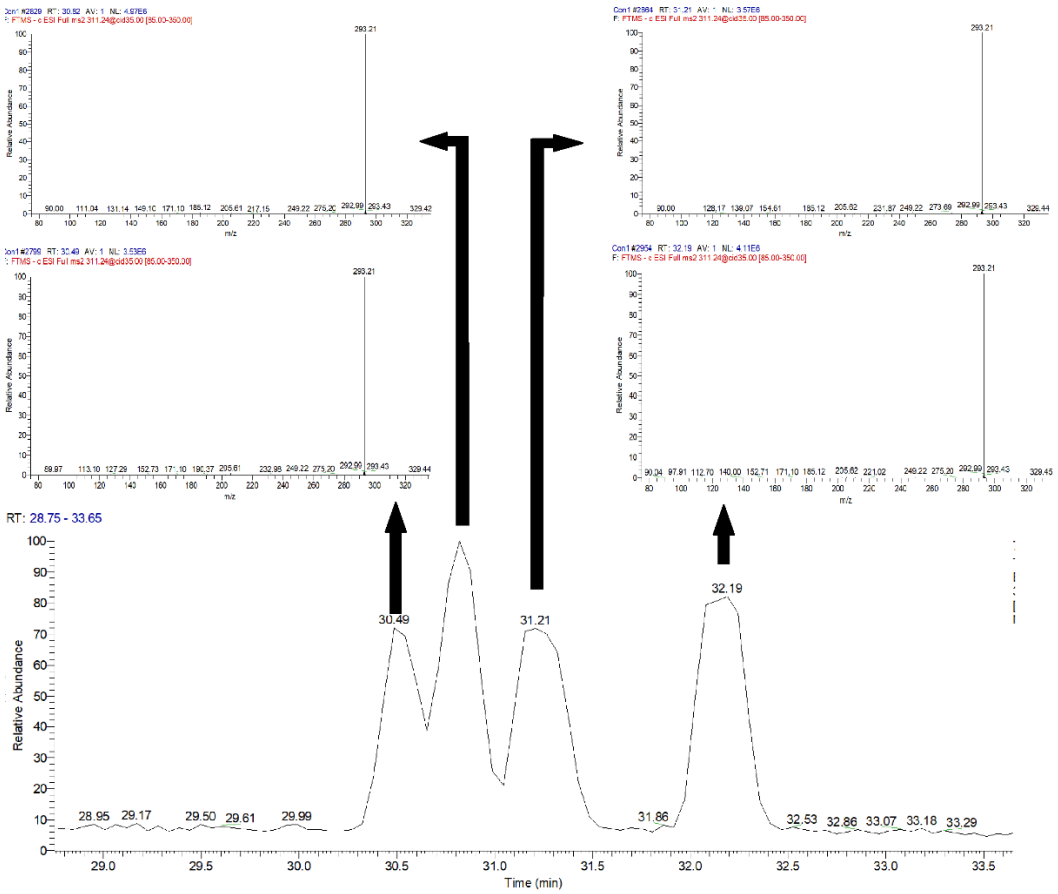

Figure 3-26 MS^2 chromatogram following collision-induced decomposition of the molecular anion [M – H]$^-$ at *m/z* 311 derived from HpOD9,12D.

MS^3 spectra of the ions generated by loss of water following MS^2 of linoleic acid hydroperoxides *m/z* 293 (Figure 3-27) revealed two main different fragmentation patterns for the four peaks recognised in parent ion chromatogram with indications of coelution of two of the positional isomers in the peaks at Rt 30.49 and 30.83 min. in the LC-MS^3 chromatogram that correspond to peaks of Rt 30.51 and 30.79 min., respectively, in the reconstructed parent ion LC-MS chromatogram (Figure 3-25). Product ion resulted from further loss of water [M - (H^+ + 2H_2O)]$^-$ at *m/z* 275 that can be found in all the observed isomer peaks. An additional commonly observed product ion in all isomer peaks was at *m/z* 249 (Figure 3-27) which is proposed to be ([$C_{17}H_{30}O$– H^+]$^-$) and to be formed by further loss of CO_2 [M - (H^+ + H_2O + CO_2)]$^-$.

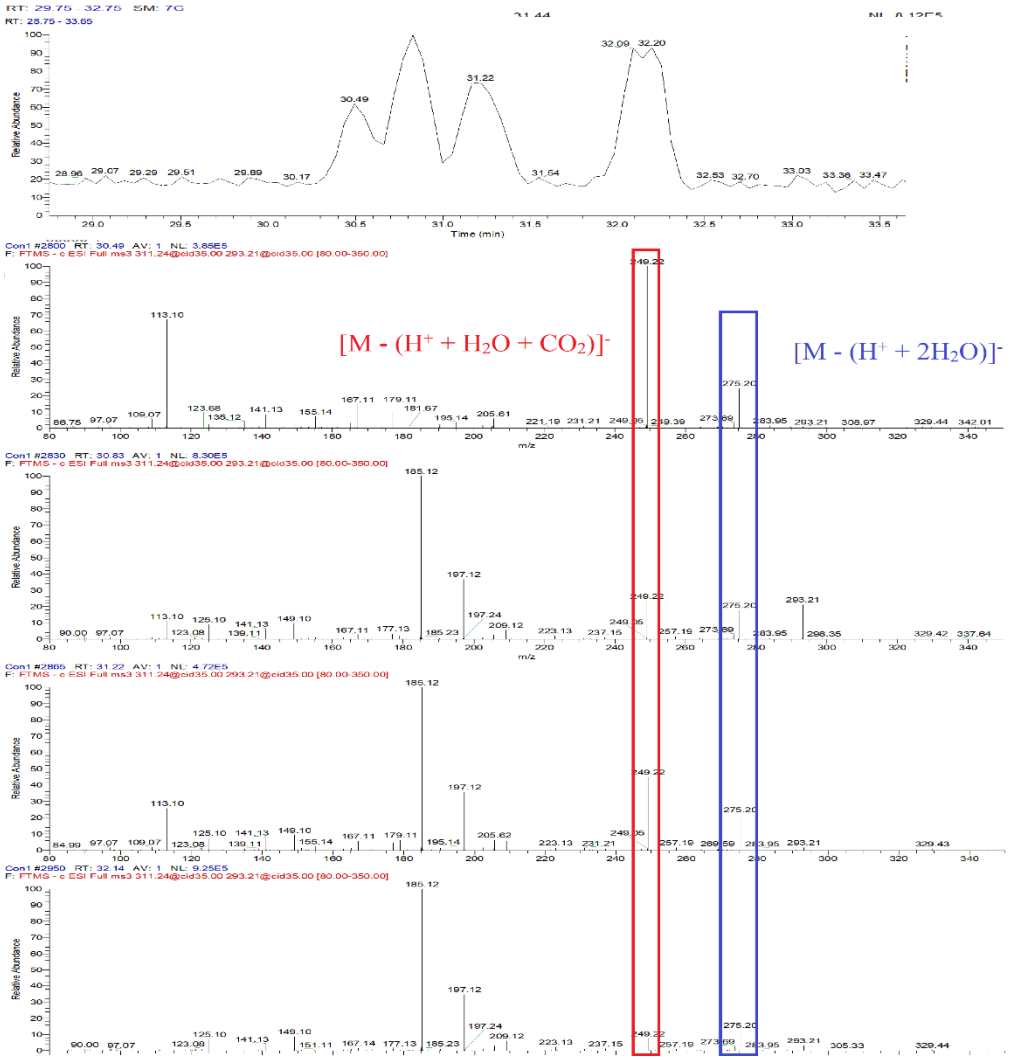

Figure 3-27 Chromatogram & MS^3 spectrometry (LC-MS^3) following collision induced decomposition of MS^2-generated product ion [M - (H+ + H2O)]$^-$ at *m/z* 293 derived from hydroperoxy octadeca-9,12-dienoic acid.

MS^3 spectrum of the peak at Rt 30.49 min. (Figure 3-28) showed the common ions mentioned above (*m/z* 275 and *m/z* 249) (Figure 3-27) in addition to other fragment ions that could be linked to 13-hydroperoxy-octadeca 9,11-dienoic acid (13-HpO9,11DE) by a fragmentation pathway that are directed by a number of 1, 5 sigmatropic rearrangements towards the carboxyl end to facilitate different types of scissions. Following the first proton shift, the conjugated di-ene system would become out of conjugation with carbonyl group and a scission in C12-C13 bond, at vicinal position to carbonyl group (see Scheme 3-12), would become rather attainable to generate relatively low-abundant but characteristic fragment ion at *m/z* 195 which is proposed to be $[C_{12}H_{20}O_2 - H^+]^-$. The most abundant structurally significant product

ion *m/z* 113 which is proposed to be $[C_7H_{14}O- H^+]^-$ that can be considered characteristic and a scission in C11–C12 double bond allylic to the hydroperoxy group. Because it involves cleavage at double bond location, this formation, at first sight, would not appear reasonably probable.

The suggested fragmentation process involves two further 1 ,5 sigmatropic shifts. The rearrangement of the di-ene system into position between C6 and C9 would facilitate extraction of hydrogen at C10 and the formation of alkoxide anion at *m/z* 113 as a result of charge driven cleavage of C11–C12 bond (Scheme 3-12).

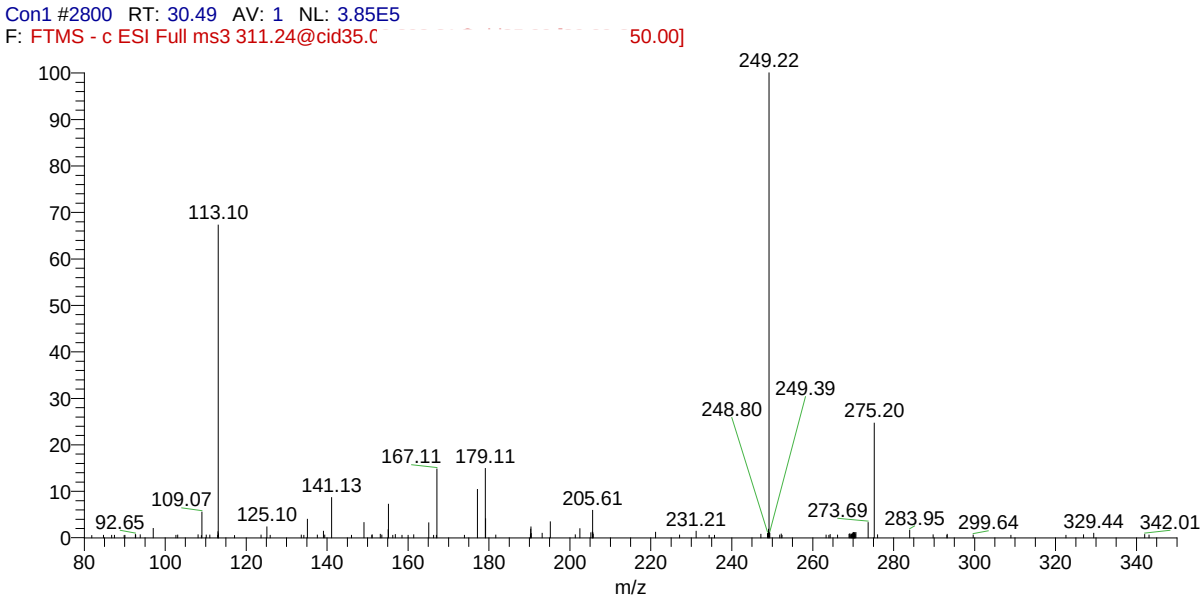

Figure 3-28 (MS^3) spectrum of MS^2-generated product ion of *m/z* 293.21 from octadeca-9,12-dienoic acid oxidation sample at Rt 30.49 min.

A scission in the same location, C11–C12, of the intermediate rearranged ion discussed above could be caused by ene reaction (γ-proton transfer) and could be the source of the fragment ion observed at *m/z* 179 that is proposed to be $[C_{11}H_{16}O_2- H^+]^-$ and to contain a conjugated triene (Scheme 3-12). Whereas a scission in C10–C11 bond that was rendered allylic to double bond in the same transient fragment ion could lead to the formation of observed *m/z* 167 fragment ion that is proposed to be $[C_{10}H_{16}O_2- H^+]^-$ (Scheme 3-12).

Two fragment ions at *m/z* 155.11 $[C_9H_{16}O_2- H^+]^-$ and *m/z* 155.14 $[C_{10}H_{20}O- H^+]^-$ were observed as well and linked to the 13-regioisomer. The suggested fragmentation pathway requires further 1 ,5 sigmatropic shift to form a transient anion that could

undergo either a scission in C9–C10 losing H_2 in the process to form the *m/z* 155.11 fragment ion or a charge driven scission in C10–C11 to form the *m/z* 155.14 fragment ion.

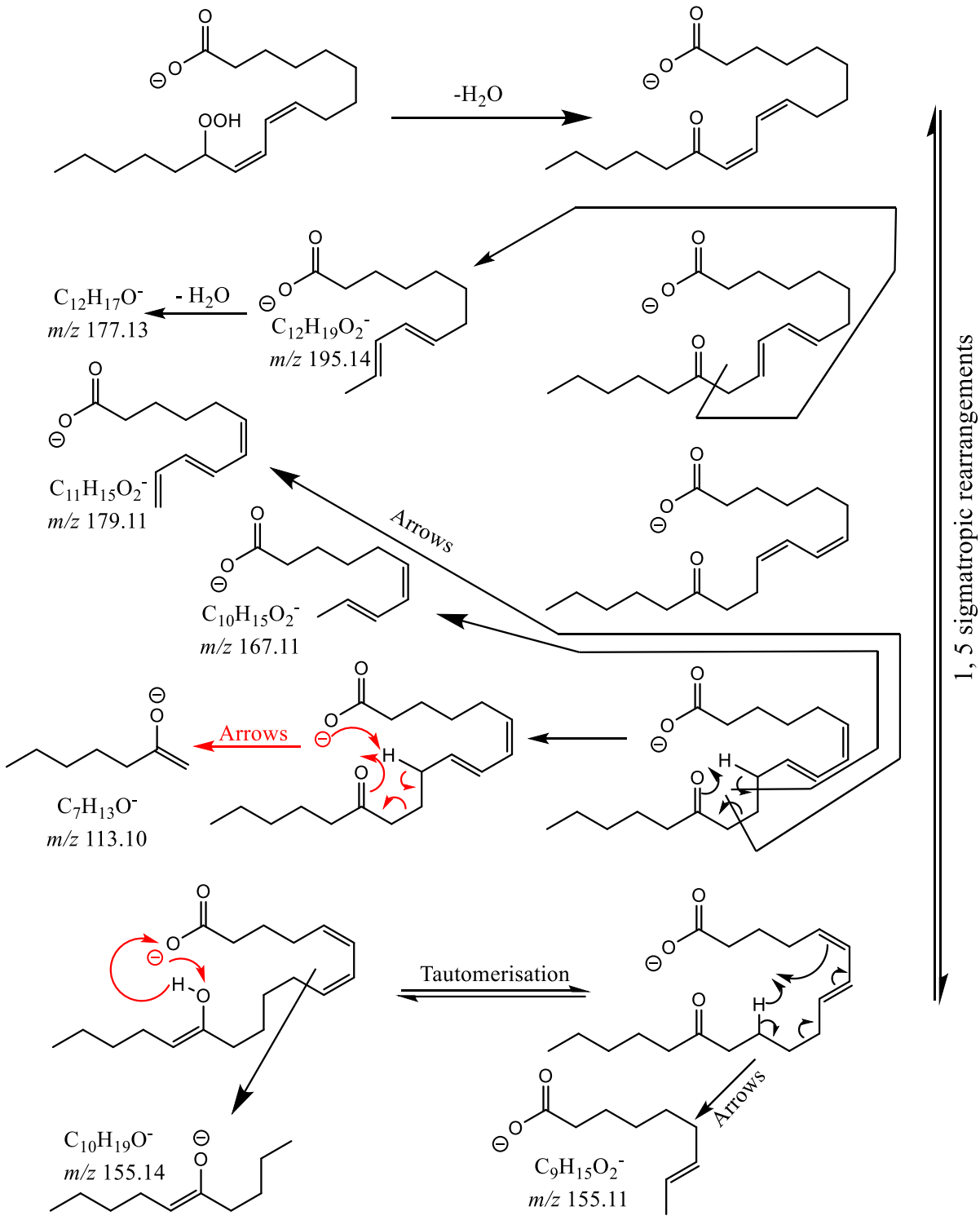

Scheme 3-12 Putative sources of product ions with characteristic significance from 13-HpO9,11DE molecular ion in (MS^3)-chromatographic peak at Rt 30.49 min.

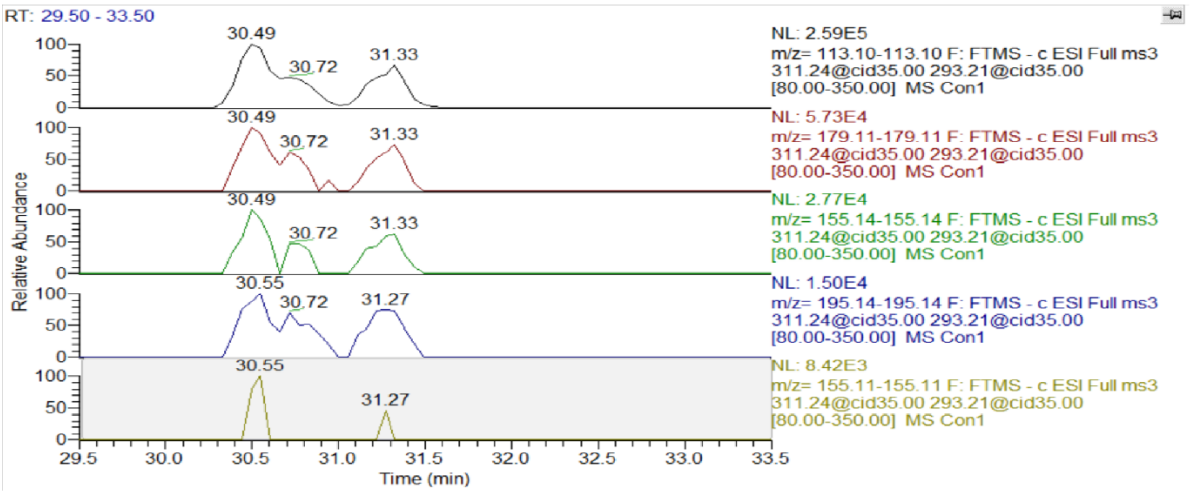

Figure 3-29 Selective mass range-chromatograms of characteristically significant MS^3-generated product ions from 13-HpO9,11DE molecular ion.

These same mechanisms appear to be operating to some extent for the the 9-regioisomer in the MS^3 spectrum of the peak at Rt 32.20 min. (Figure 3-30) which showed the common ions mentioned above (*m/z* 275 and *m/z* 249) in addition to a group of characteristic fragment ions originating from transient ions that are rearranged by a series of proton shifts. The product ion is *m/z* 125 which is proposed to be $[C_8H_{14}O- H^+]^-$ could be the dehydration product of product ion *m/z* 143 which is proposed to be $[C_8H_{16}O_2- H^+]^-$. This fragment ion could be a result of vicinal bond cleavage at C8-C9 following the first proton shift.

Further two 1, 5 sigmatropic rearrangements could enable the generation of two relatively abundant product ions that can be considered characteristic and could be linked to 9-hydroperoxy-octadeca 10,12-dienoic acid (9-HpO10,12DE) via fragmentation pathways that appear to be quite unlikely as it was the case for the formation of product ions *m/z* 113 and *m/z* 179 from 13-HpO9,11DE. These characteristic product ions are the most abundant product ion (base peak), *m/z* 185 which can be proposed to be $[C_{10}H_{18}O_3- H^+]^-$ and can be a result a cleavage in the C10–C11 (at double bond location), and the second most abundant product ion, *m/z*

197 which is proposed to be $[C_{11}H_{18}O_3 - H^+]^-$ that can be formed by a cleavage in the C11–C12 bond (in between the conjugated diene).

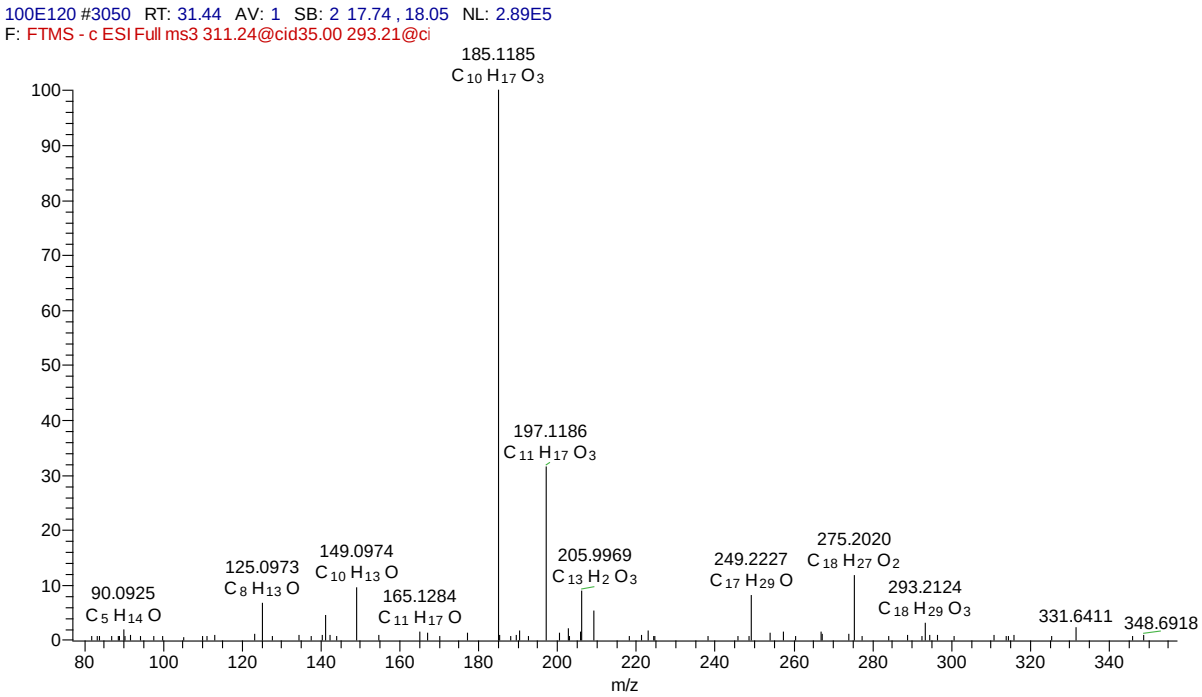

Figure 3-30 (MS^3) spectrum of MS^2-generated product ion of *m/z* 293.21 from octadeca-9,12-dienoic acid oxidation sample at Rt 31.44 min.

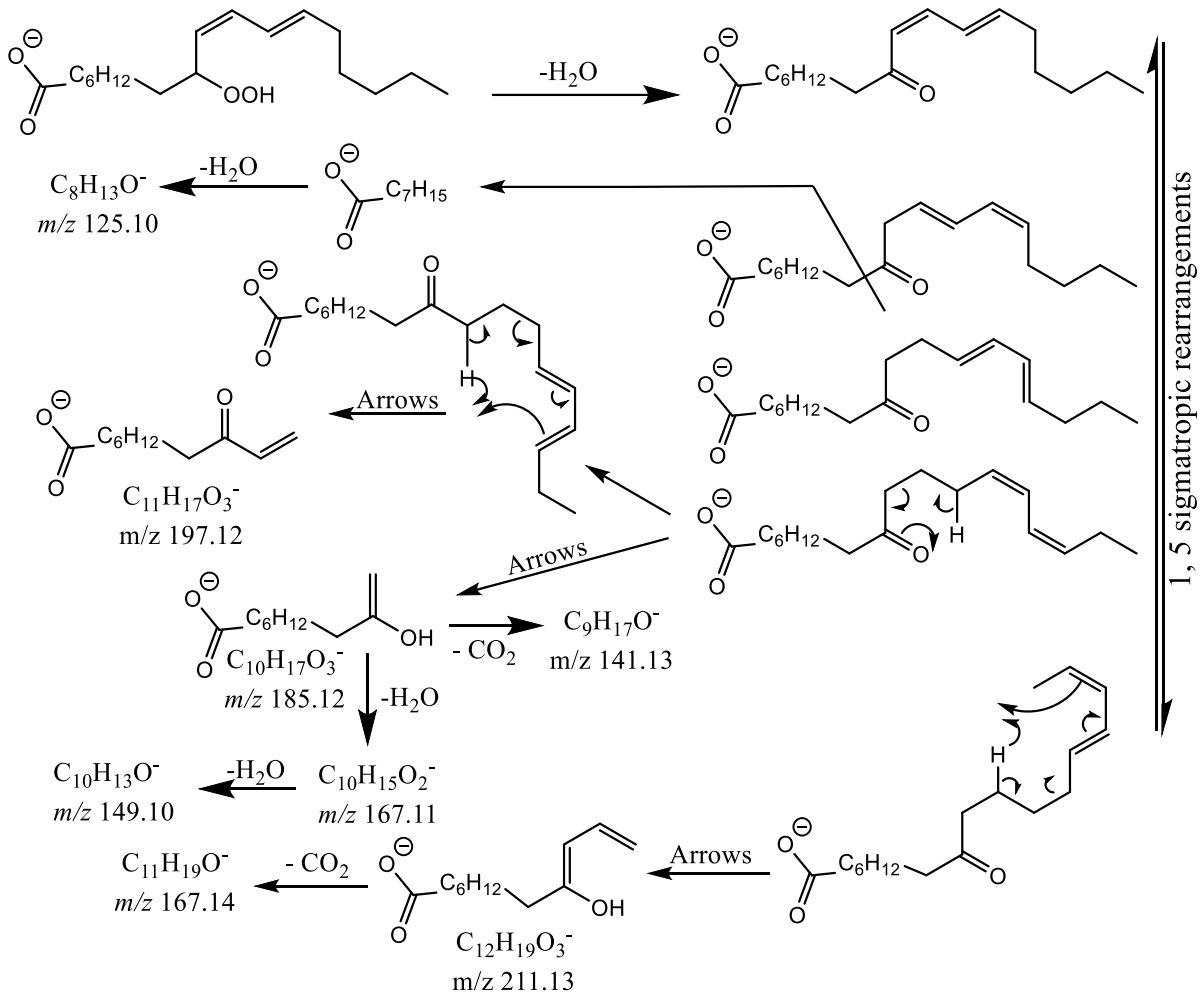

Scheme 3-13 Putative sources of product ions with characteristic significance from 9-HpO10,12DE molecular ion in the (MS^3)-chromatographic peak at Rt 31.44 min.

(Scheme 3-13) illustrates the proposed fragmentation pathways for those product ions that include ene reaction (γ-proton transfer) to cause a scission in the C10–C11 bond to form the product ion at *m/z* 185. Additional less abundant observed product ions in the same fragmentation pathway can also be linked to 9-regioisomers via the same pathway as product ion *m/z* 185, such as the ion at *m/z* 141 proposed to be $[C_9H_{18}O–H^+]^-$ and could originate from the product ion at *m/z* 185 by neutral loss of CO_2 and *m/z* 167 proposed to be $[C_{10}H_{16}O_2– H^+]^-$, also observed in the 13-regioisomer-linked fragmentation pathway (Scheme 3-12), and could originate from the same product ion, *m/z* 185, by neutral loss of water before it could suffer, in turn, additional neutral loss of water to generate fragment product ion *m/z* 149.10 that is proposed to be $[C_{10}H_{14}O–$

$H^+]^-$. Moreover, the second product ion at *m/z* 197 would result from the same transient anion that could undergo scission in C11–C12 losing H_2 in the process.

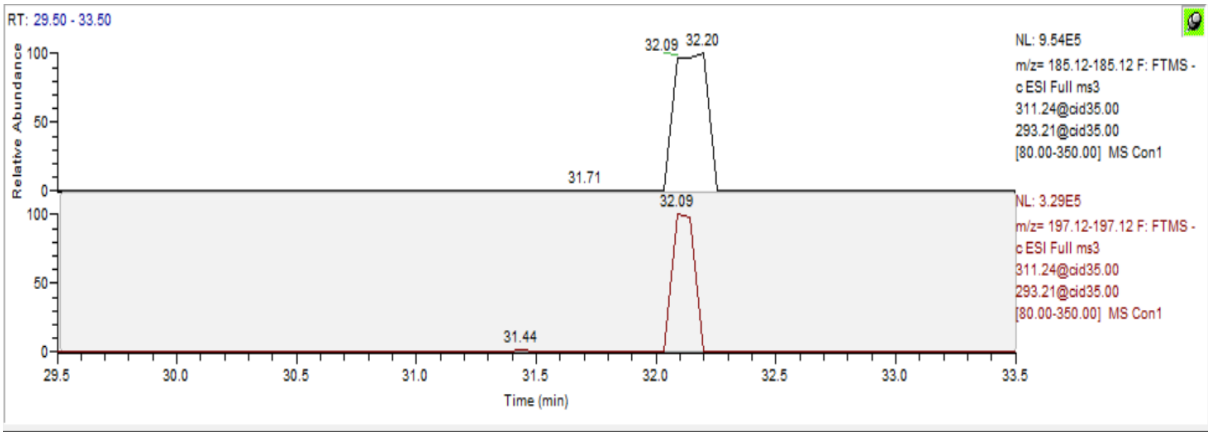

Figure 3-31 Selective mass range-chromatograms of characteristically significant MS^3-generated product ions from 9-HpO9,11DE molecular ion

Product ion, *m/z* 167 that is proposed to be $[C_{11}H_{20}O- H^+]^-$, was observed as part of both fragmentation patterns and could be linked to the 9-regioisomer via a fragmentation pathway explained in (Scheme 3-13) as result of a neutral loss of CO_2 from product ion at *m/z* 211.13 that is proposed to be $[C_{11}H_{22}O_2- H^+]^-$ and to be generated by a scission in the C12–C13 bond and accompanied by loss of H_2 from a transient anion formed by a further 1 ,5 sigmatropic shift towards the methyl end.

3.3.2 Analysis of α-Linolenic acid hydroperoxides

3.3.2.1 Hydroperoxide formation

The introduction of third double bond, as in linolenic acid, into the di-unsaturated carbon-chain of linoleic acid leads to a doubling of reactivity (Cosgrove et al., 1987; Trades & Chem, 1947). This is a result of creating second bis-allylic methylene group which reacts twice as fast with oxygen as linoleic acid. Therefore, by the same mechanism as linoleic acid, two pentadienyl radicals are formed. One between carbon-9 and carbon-13 by the abstraction of hydrogen on carbon-11 and the other between carbon-12 and carbon-16 by the abstraction of hydrogen on carbon-14 (Scheme 3-14).

Four hydroperoxide containing OOH groups on carbons 9, 12, 13 and 16 can be formed by the reaction with oxygen at the end-carbon positions of each pentadienyl radical. These hydroperoxides contain a conjugated diene system with a third isolated double bond (Frankel, 1991).

9-hydroperoxyoctadeca-10, 12, 15-trienoic acid (9-HpO10,12,15TE)

12-hydroperoxyoctadeca-9, 13, 15-trienoic acid (12-HpO9,13,15TE)

13-hydroperoxyoctadeca-9, 11, 15-trienoic acid (13-HpO9,11,15TE)

16-hydroperoxyctadeca-9, 12, 14-otrienoic acid (16-HpO9,12,14TE)

Two of these hydroperoxide isomers, 12- and 13- regioisomers, have the hydroperoxyl group located on an allylic position relative to the newly formed conjugated diene system and on homoallylic position to the isolated double bond. Because of the presence of a homoallylic double bond, these hydroperoxide isomers can undergo facile 1,3 cyclisation by intramolecular radical addition to the double bond and to form five-membered epidioxides (Frankel, 1991). These cyclised isomeric hydroperoxides of linolenic acid tend to react with oxygen and undergo further oxidation hence reducing the observed concentrations of the 12- and 13- hydroperoxides and forming additional secondary oxidation products that can interfere with analysis (Wong, 2018) (Scheme 3-15).

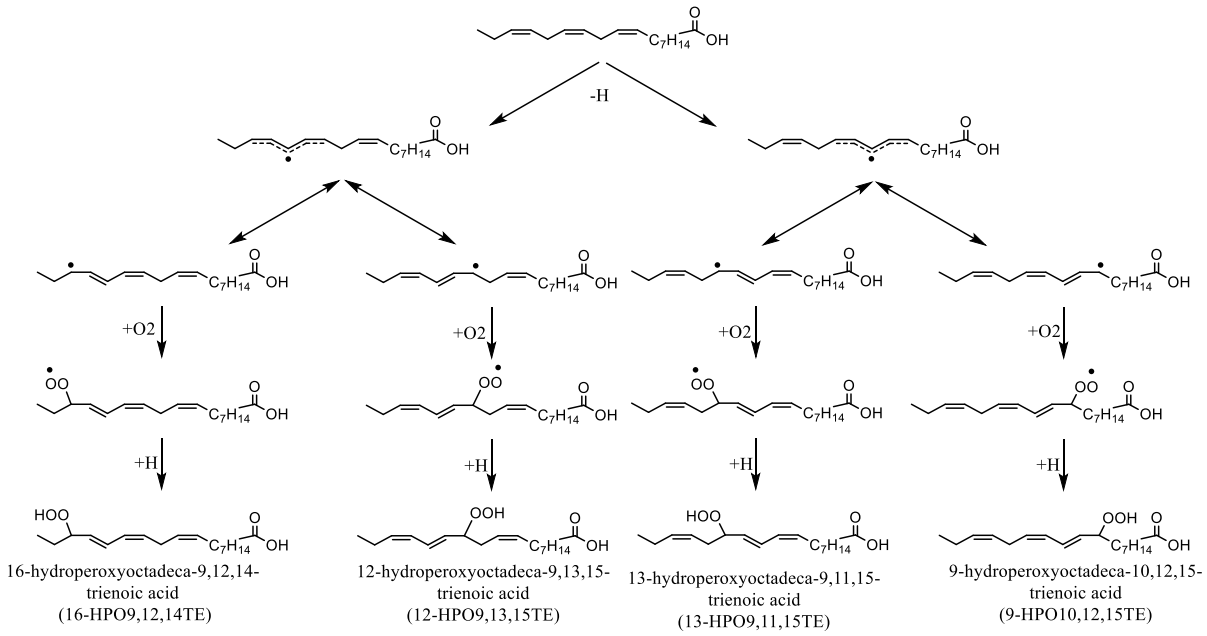

Scheme 3-14 Overall reaction scheme for linoleic acid hydroperoxides formation using version of the reaction scheme published by (Frankel, 1991) and data from (Wong, 2018).

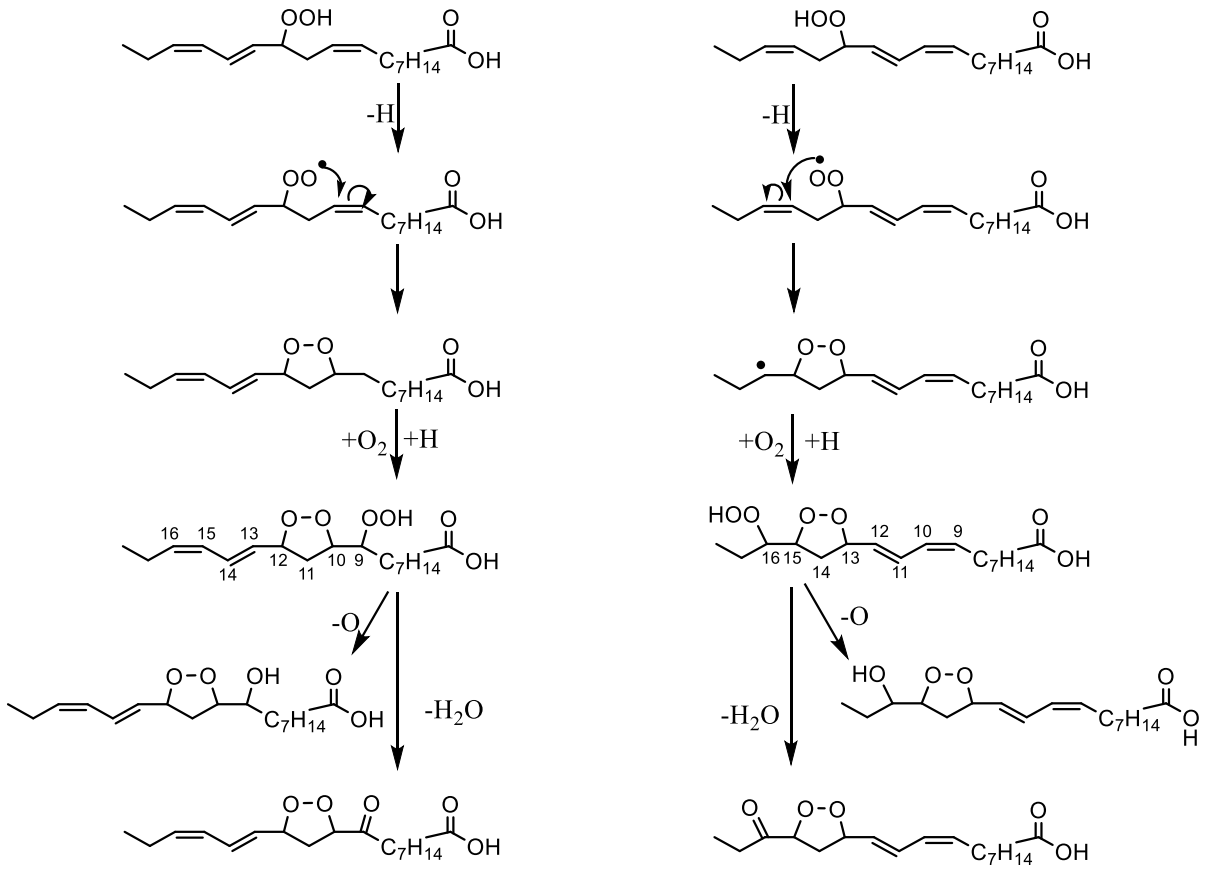

Scheme 3-15 Mechanism of cyclisation of 12- and 13-hydroperoxides of α-linolenic acid and subsequent formation of secondary oxidation products using version of the scheme published by (Wong, 2018)

3.3.2.2 LC-MS analysis of α-Linolenic acid hydroperoxides

Preliminary LC-MS analyses of chemically oxidised octadeca-9,12,15-trienoic acid (α-Linolenic acid, FA 18:3 (n-3)) samples (O9,12,15TA) showed chromatographic peaks for the four isomeric hydroperoxide derivatives of linolenic acid $[C_{18}H_{30}O_4\text{-}H^+]^-$ in mass range chromatogram of ions of *m/z* 309 at Rt 17.3-23.8 min. Additional oxidation products that could have molar ions that may include hydroperoxy linolenate as a part of their fragments were also observed within the same range of retention times in these samples. Main source of these oxidation products is the hydroperoxy epidioxides *m/z* 341 with chemical formula $[C_{18}H_{30}O_6\text{-}H^+]^-$ resulting from the cyclisation of 12- and 13- hydroperoxide isomers that were observed at Rt 19.00-20.12 min. (Figure 3-32). Keto epidioxides *m/z* 323 that result from hydroperoxy epidioxides loss of water with chemical formula $[C_{18}H_{28}O_5\text{-}H^+]^-$ were also observed within the same range of retention times of detected hydroperoxide isomers (Figure 3-33). Since these samples were subjected to reduction, hydroperoxy epidioxides suffered decomposition to produce hydroxy epidioxides with chemical formula $[C_{18}H_{30}O_5\text{-}H^+]^-$ that were likewise detectable within same range (Figure 3-34).

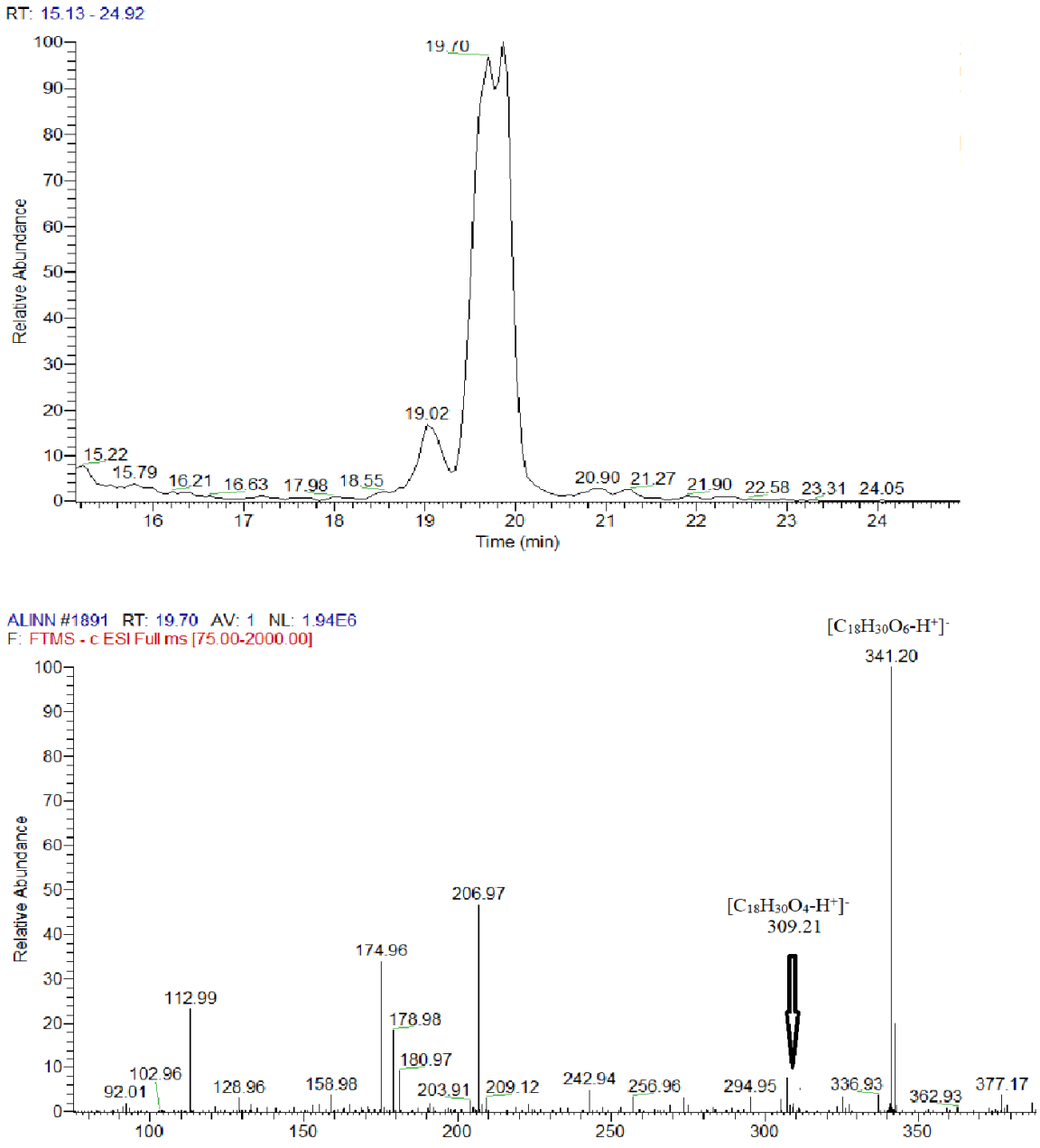

Figure 3-32 Mass range chromatogram & mass spectrum of ions of *m/z* 341 proposed to be for hydroperoxy epidioxides formed by cyclisation of 12- and 13- hydroperoxide isomers in liquid chromatography- mass spectrometry (LC-MS) analysis of oxidised octadeca-9,12,15-trienoic acid sample.

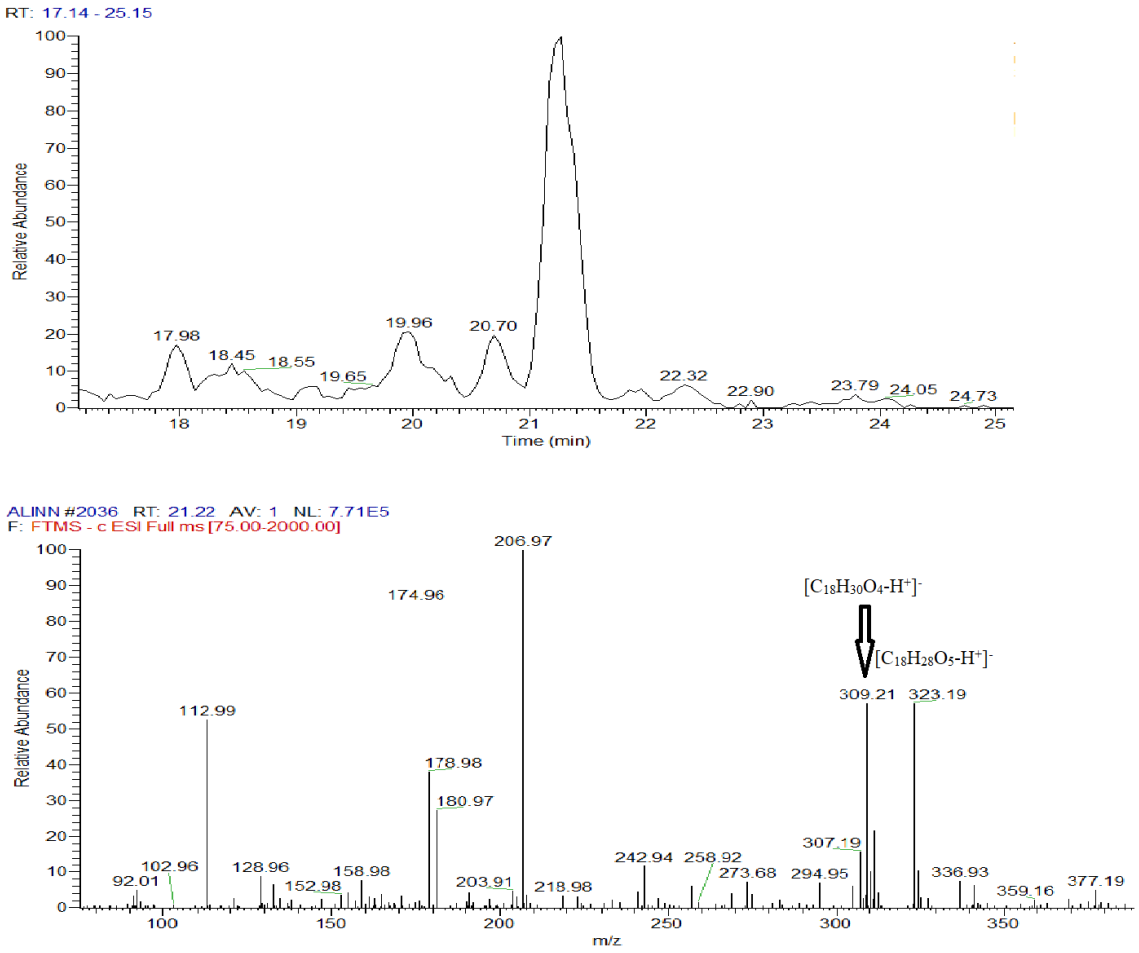

Figure 3-33 Mass range chromatogram & mass spectrum of ions of *m/z* 323 proposed to be for dehydrated hydroperoxy epidioxides formed by cyclisation of 12- and 13- hydroperoxide isomers (Keto epidioxides) in liquid chromatography- mass spectrometry (LC-MS) analysis of oxidised octadeca-9,12,15-trienoic acid sample.

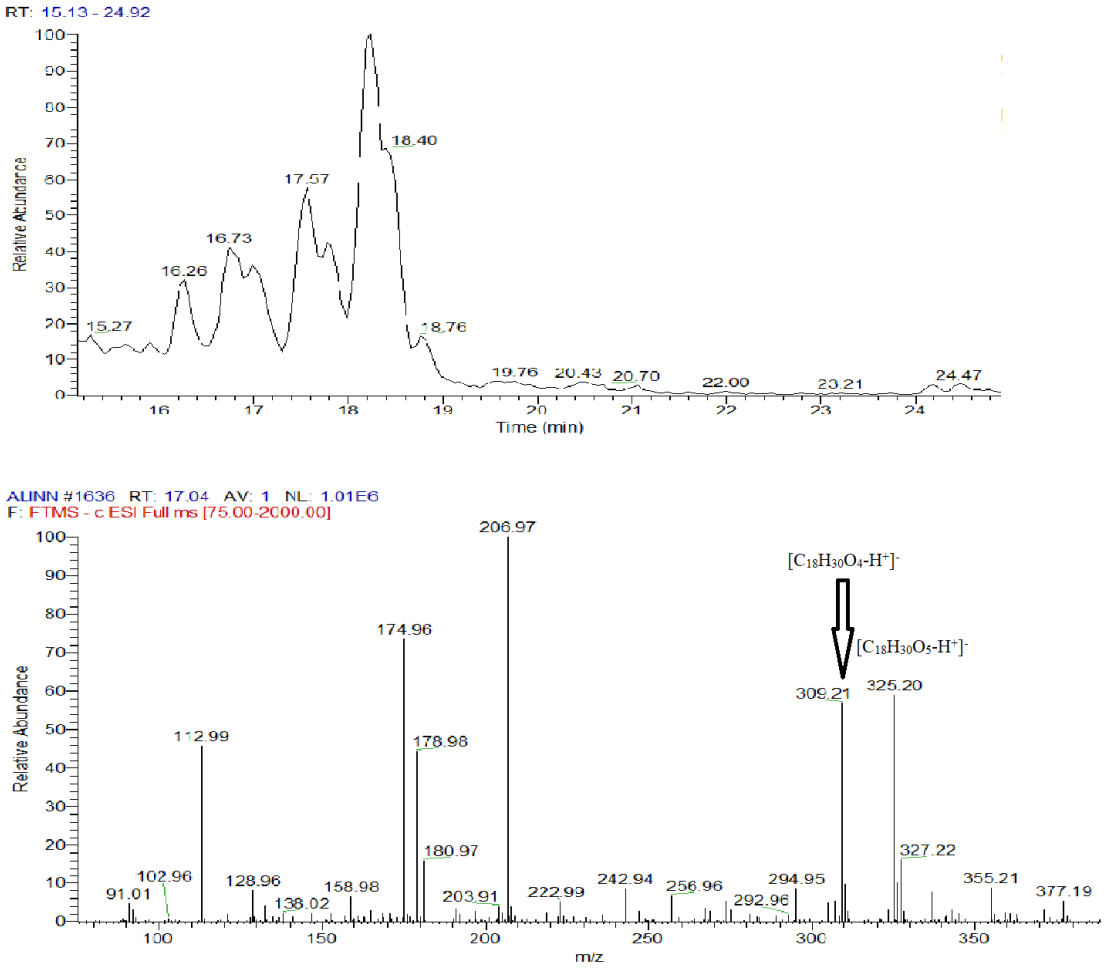

Figure 3-34 Mass range chromatogram & mass spectrum of ions of *m/z* 325 proposed to be for hydroxy epidioxides formed by decomposition of hydroperoxy epidioxides in liquid chromatography- mass spectrometry (LC-MS) analysis of oxidised octadeca-9,12,15- trienoic acid sample.

Linolenic acid hydroperoxy derivatives peaks however provided little or no characteristic information useful for the identification of positional isomers as the hydroperoxides and yielded the quasi-molecular ion in addition to few non-informative fragments. Furthermore, the dehydration product $[M - (H^+ + H_2O)]^-$ ions observed with previously studied hydroperoxy fatty acids were undetectable for all studied species in mass range chromatogram of $[M - H^+]^-$ (Figure 3-35).

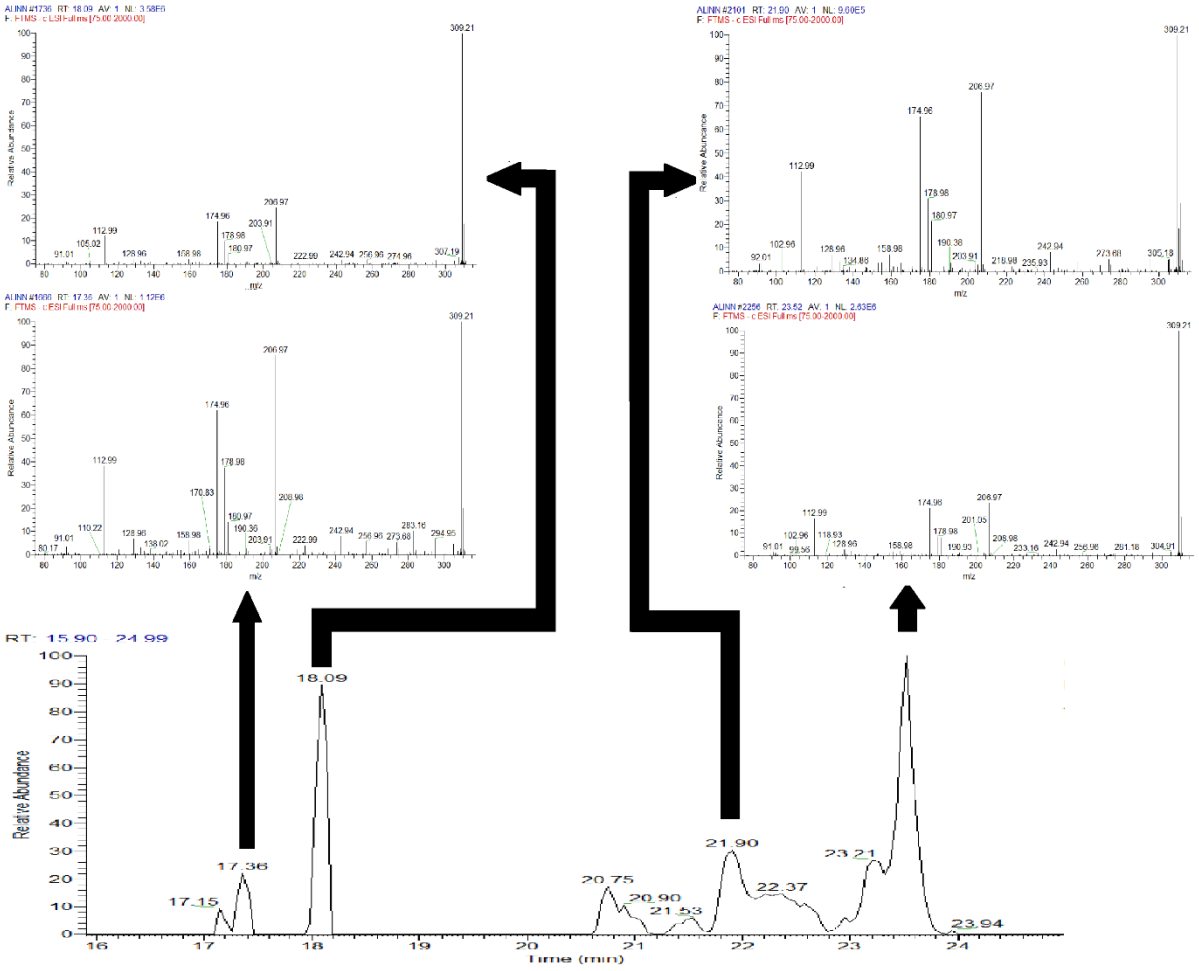

Figure 3-35 Mass range chromatogram & mass spectra of ions of *m/z* 309 in liquid chromatography- mass spectrometry (LC-MS) analysis of oxidised octadeca-9,12,15-trienoic acid sample.

The elucidation of hydroperoxide isomers required further investigations on MS^2 spectrometry. The MS^2 spectra for $[M - H^+]^-$ revealed, aside from the highly stable fragment ion of dehydrated hydroperoxides $[M-(H^+ + H_2O)]^-$ *m/z* 291 shown in all regioisomer spectra, different fragmentation patterns for the four peaks recognised in parent ion chromatogram in figure 3-35.

Peak at Rt 17.38 min. in LC- MS^2 total ion current chromatogram that corresponds to parent ion LC-MS chromatogram peaks of Rt 17.38 min. (Figure 3-36) showed the common peak $[M-(H^+ + H_2O)]^-$ mentioned above (*m/z* 291) in addition to some product ions that can be considered characteristic and could be linked to the 12-regioisomer such as the ion at *m/z* 183 which is proposed to be $[C_{11}H_{20}O_2 - H^+]^-$ and to be generated

by a vinylic cleavage of the bond adjacent to the hydroperoxide group and *m/z* 211 which is proposed to be $[C_{12}H_{20}O_3 - H^+]^-$ that can be produced from the dehydrated fragment ion $[M-(H^+ + H_2O)]^-$ by another vinylic cleavage on the other side of the newly formed carbonyl group preceded by 1, 5 sigmatropic proton shift towards the methyl end (Scheme 3-16).

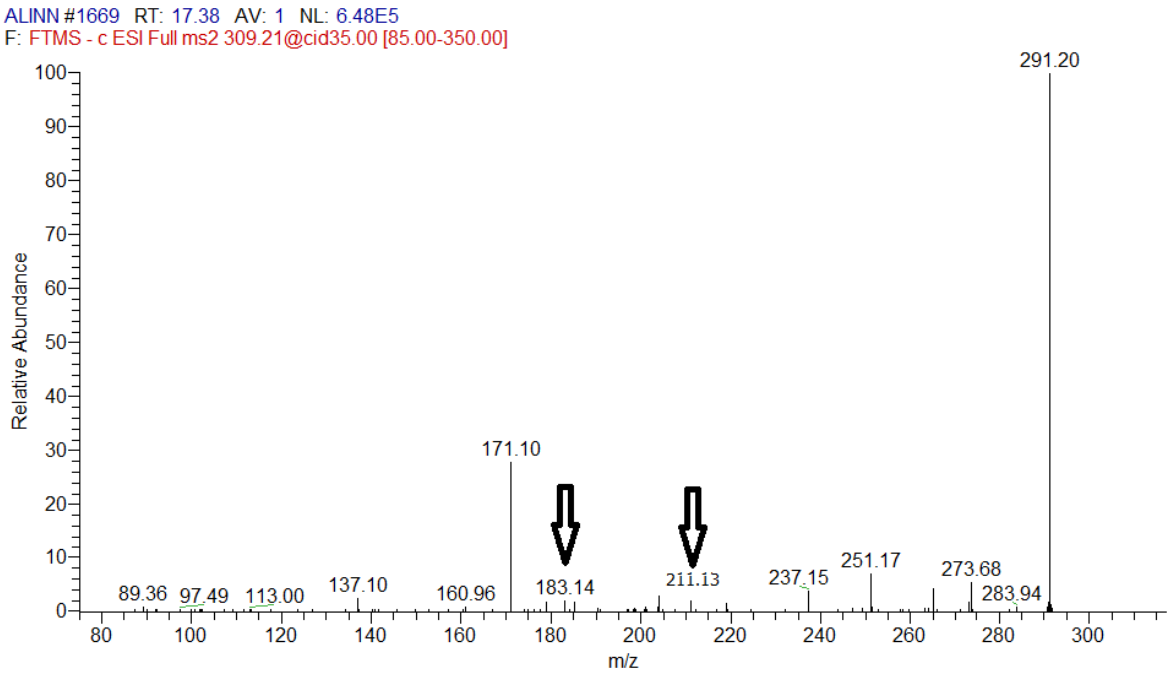

Figure 3-36 (MS^2) spectrum of linolenic acid hydroperoxide molecular ion of *m/z* 309.21 from linolenic acid oxidation sample at Rt 17.38 min.

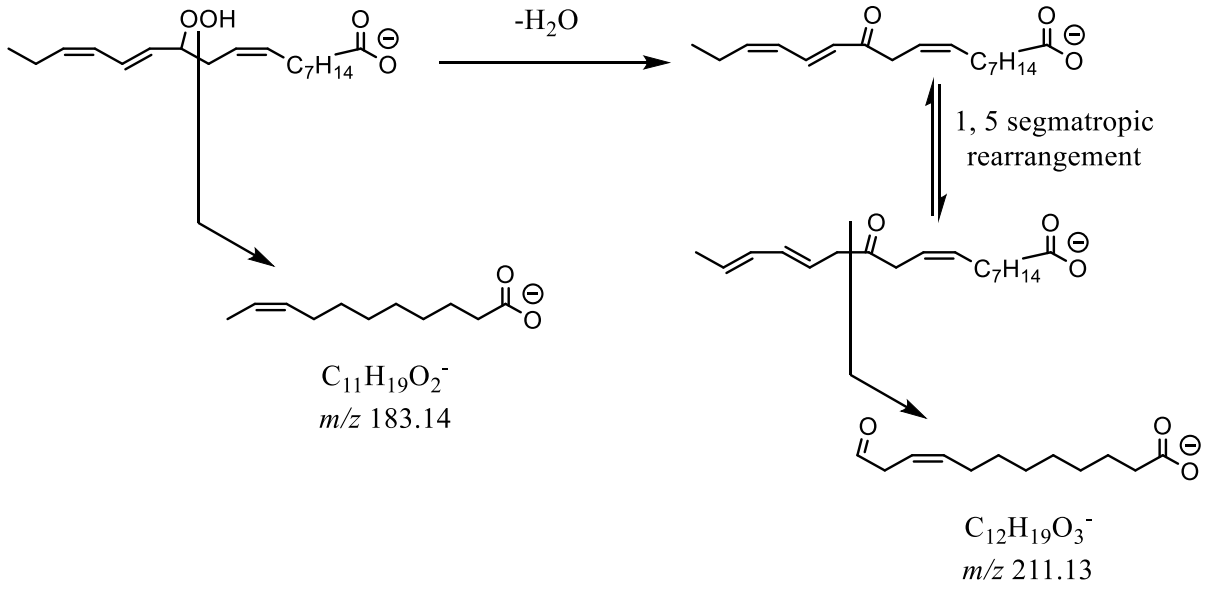

Scheme 3-16 Putative sources of characteristic MS^2-generated product ions (*m/z* 183 and *m/z* 211) linked to 12-HpO9,13,15TE molecular ion in (MS^2)-chromatographic peak of octadeca-9,12,15-trienoic acid oxidation sample at Rt 17.38 min.

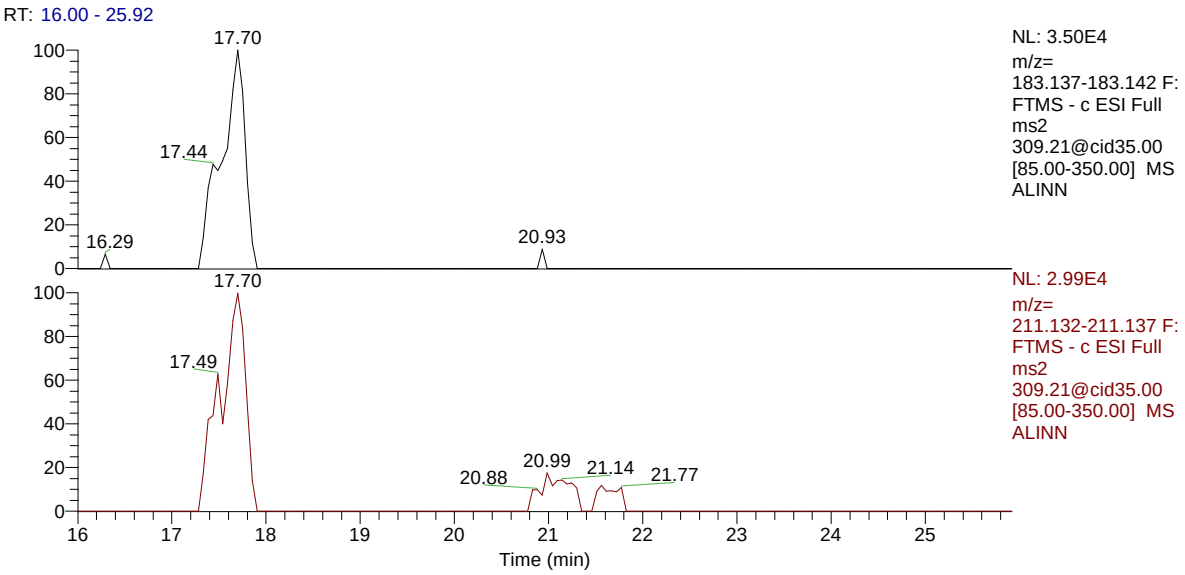

Figure 3-37 Selective mass range- chromatograms of characteristic MS^2-generated product ions (*m/z* 183 and *m/z* 211) linked to 12-HpO9,13,15TE from octadeca-9,12,15-trienoic acid oxidation sample.

The MS^2 fragmentation pattern of peak at Rt 18.11 min. in LC- MS^2 total ion chromatogram that corresponds to parent ion LC-MS chromatogram peaks of Rt 18.09 min. (Figure 3-38) showed common base peak mentioned above (*m/z* 291) in addition to few product ions that can be generated by the fragmentation of dehydrated ion [M-(H^++H_2O)]$^-$including two ions that can be considered characteristic and could be linked to 9-hydroperoxy-octadeca-10,12, 15-octadecatrienoic acid. First ion is at *m/z*

185 which is proposed to be $[C_{10}H_{18}O_3 - H^+]^-$ that can be the outcome of cleavage of the bond allylic to the carbonyl group (dehydrated hydroperoxyl group) that requires a preceding double bond shift towards the methyl end (Scheme 3-17). Second ion is *m/z* 171 proposed to be $[C_9H_{16}O_3 - H^+]^-$ generated by a vinylic cleavage of the bond adjacent to the same functional group that is facilitated by the same double bond shift (Scheme 3-17).

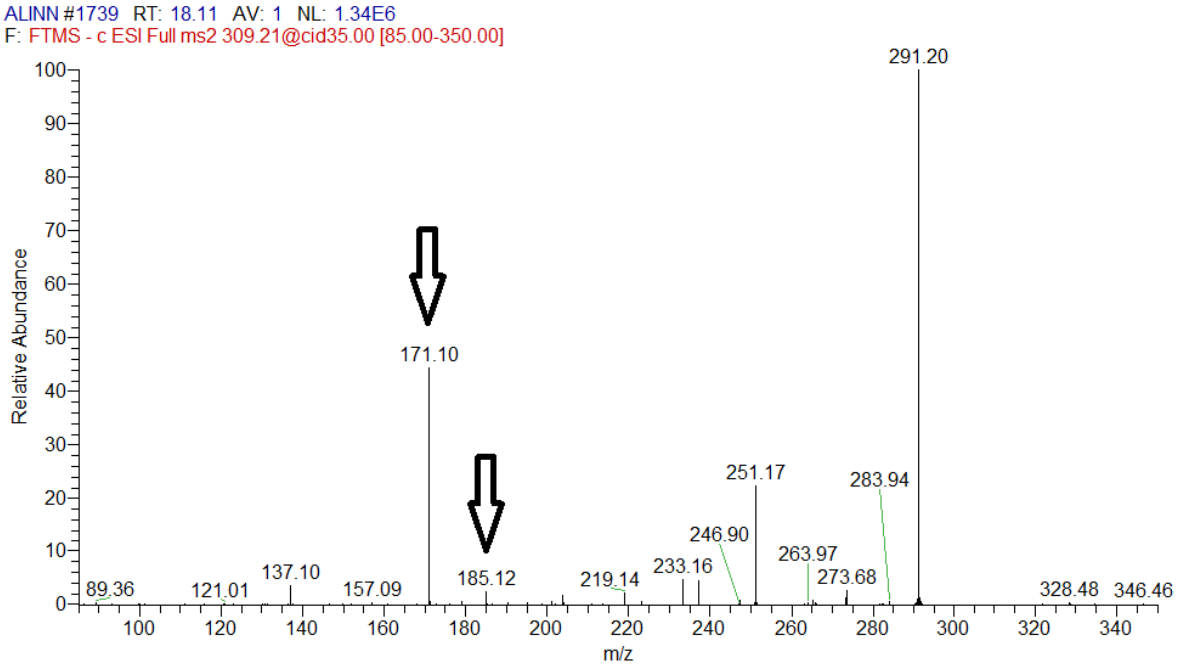

Figure 3-38 (MS^2) spectrum of linolenic acid hydroperoxide molecular ion of *m/z* 309.21 from linolenic acid oxidation sample at Rt 18.11 min.

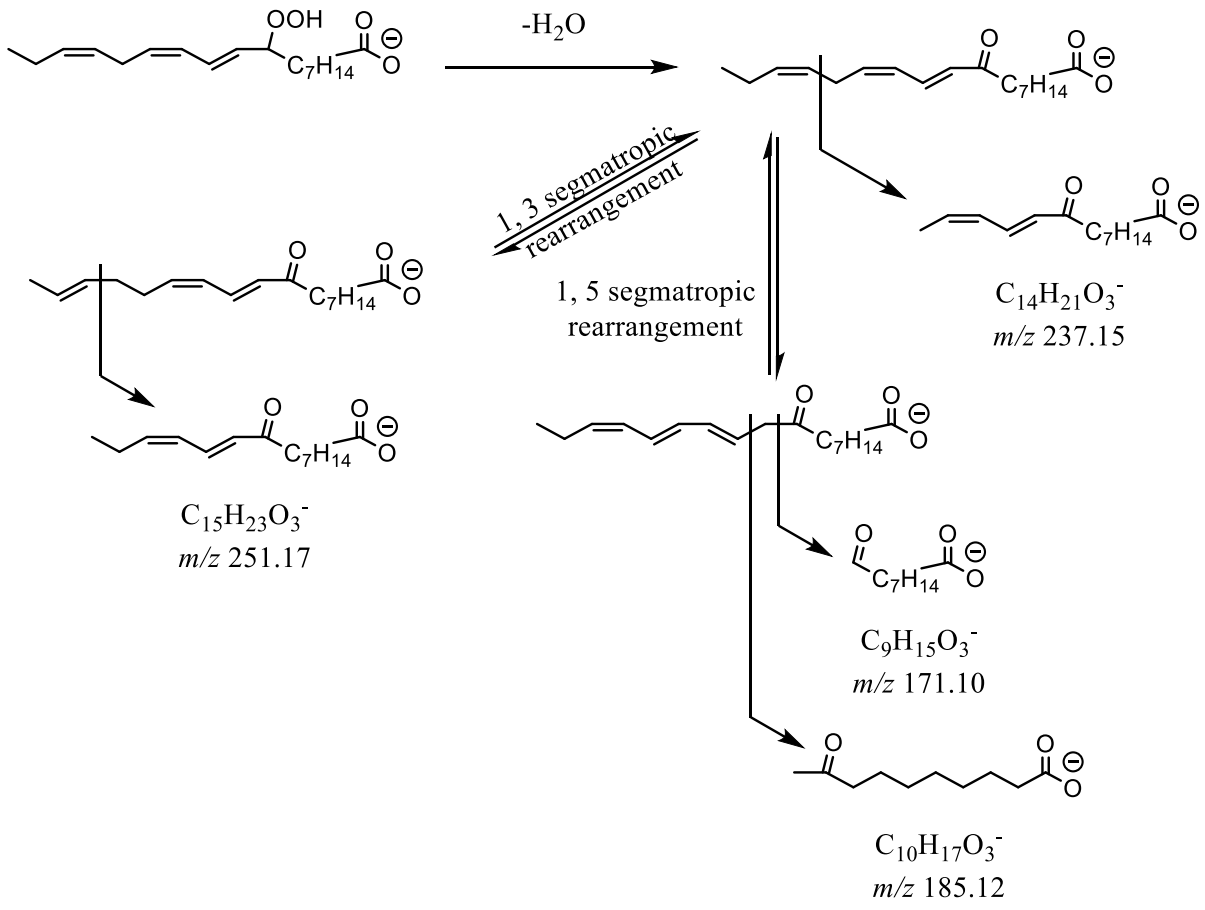

Scheme 3-17 Putative sources of characteristic MS^2-generated product ions (*m/z* 171 and *m/z* 185) linked to 9-HpO10,12,15TE molecular ion in (MS^2)-chromatographic peak of octadeca-9,12,15-trienoic acid oxidation sample at Rt 18.11 min.

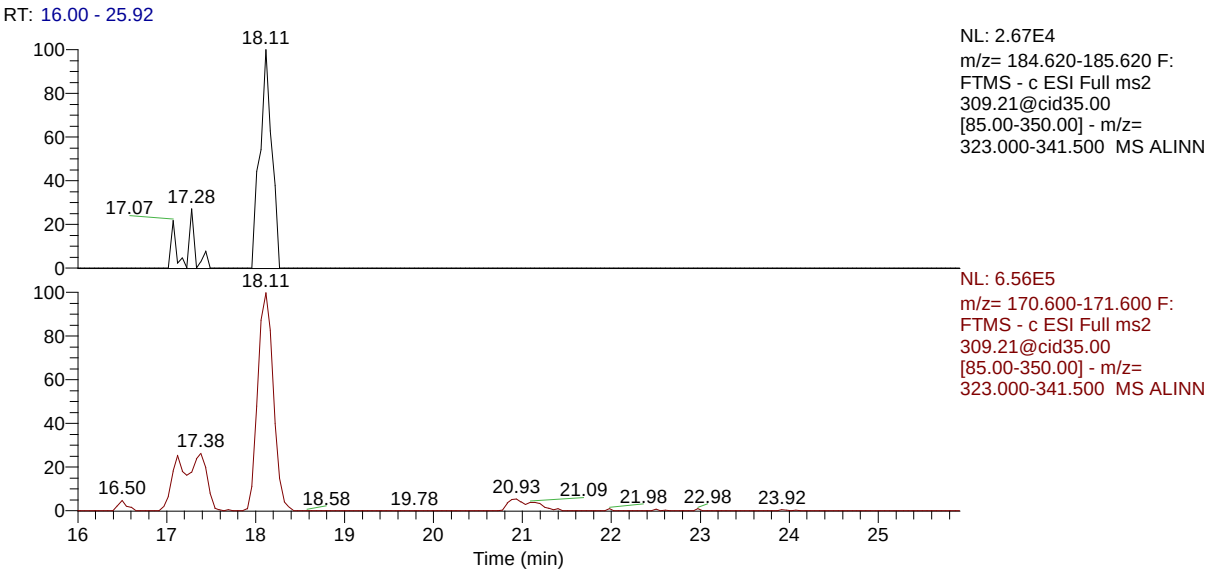

Figure 3-39 Selective mass range- chromatograms of characteristic MS^2-generated product ions (*m/z* 185 and *m/z* 171) linked to 9-HpO10,12,15TE from octadeca-9,12,15-trienoic acid oxidation sample.

Along with common base peak mentioned above (*m/z* 291), $[M\text{-}H^+]^-$ MS^2 spectrum for chromatographic peak at Rt 21.88 min. that corresponds to parent ion LC-MS chromatogram peaks of Rt 21.90 min. showed a fragment ion *m/z* 195 that is proposed to be $[C_{12}H_{20}O_2 - H^+]^-$ that indicates vinylic cleavage of the bond adjacent to the hydroperoxide group in 13-hydroperoxy-9, 11, 15-octadecatrienoic acid. A fragment ion at *m/z* 239 that was found in the same chromatographic peak (Figure 3-40) and is proposed to be $[C_{14}H_{24}O_3 - H^+]^-$ could only be linked to the cyclised form of the 13-regioisomer by a fragmentation pathway that includes rearrangement of the 1,2-dioxolane ring to form beta hydroxy ketone that goes through C13-C14 scission (Scheme 3-18). On the other hand, the fragment ion at *m/z* 223 that was only observed as a minor chromatographic peak at Rt 18.58 min. (Figure 3-41) and is proposed to be $[C_{13}H_{20}O_3 - H^+]^-$ can be linked exclusively to un-cyclised form of 13-regioisomers through simple cleavage of the bond vinylic to the carbonyl group (dehydrated hydroperoxyl group) and allylic to the isolated double bond accompanied by fragment ion at *m/z* 195 that can be linked to both forms of 13-regioisomer by the same scission at C12-C13. These observations can demonstrate the ability of differentiation between cyclised and un-cyclised forms of 13-hydroperoxy-9, 11, 15-octadecatrienoic acid (Scheme 3-18).

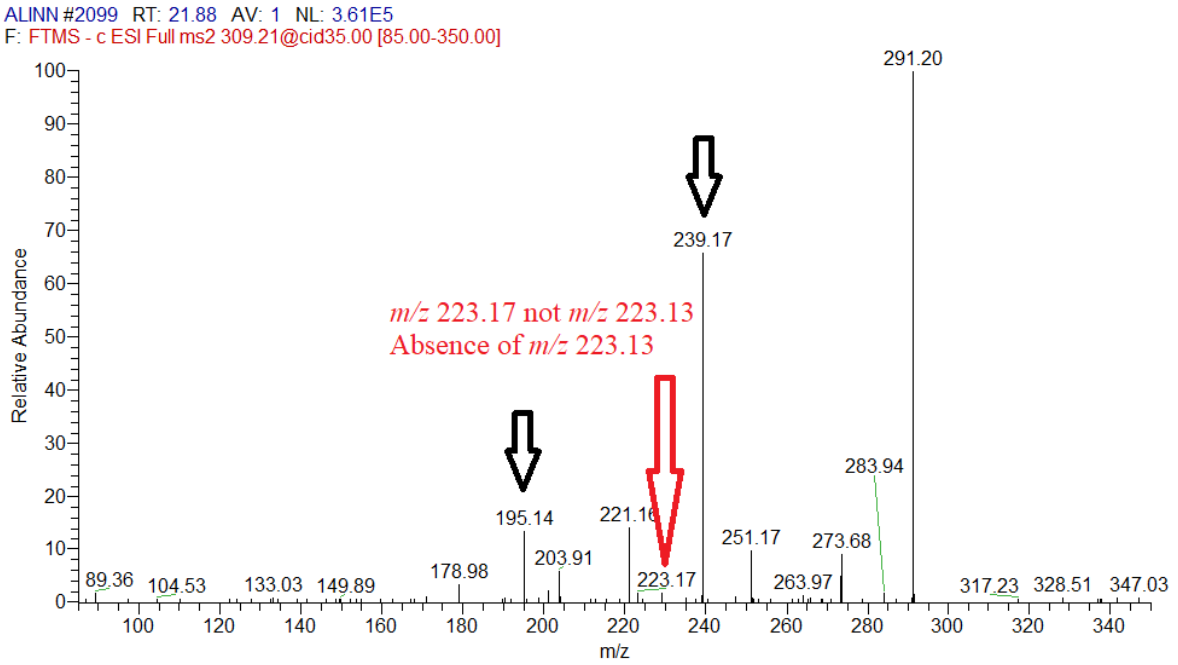

Figure 3-40 (MS^2) spectrum of linolenic acid hydroperoxide molecular ion of *m/z* 309.21 from linolenic acid oxidation sample at Rt 21.88 min.

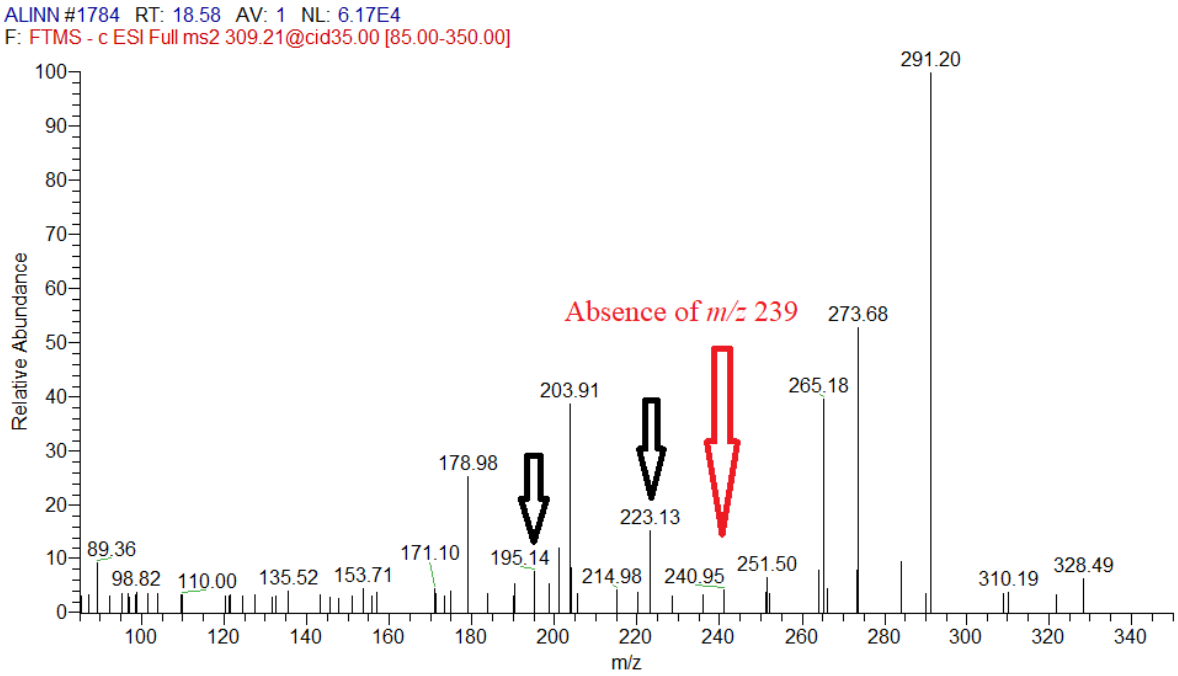

Figure 3-41 (MS^2) spectrum of linolenic acid hydroperoxide molecular ion of *m/z* 309.21 from linolenic acid oxidation sample at Rt 18.58 min.

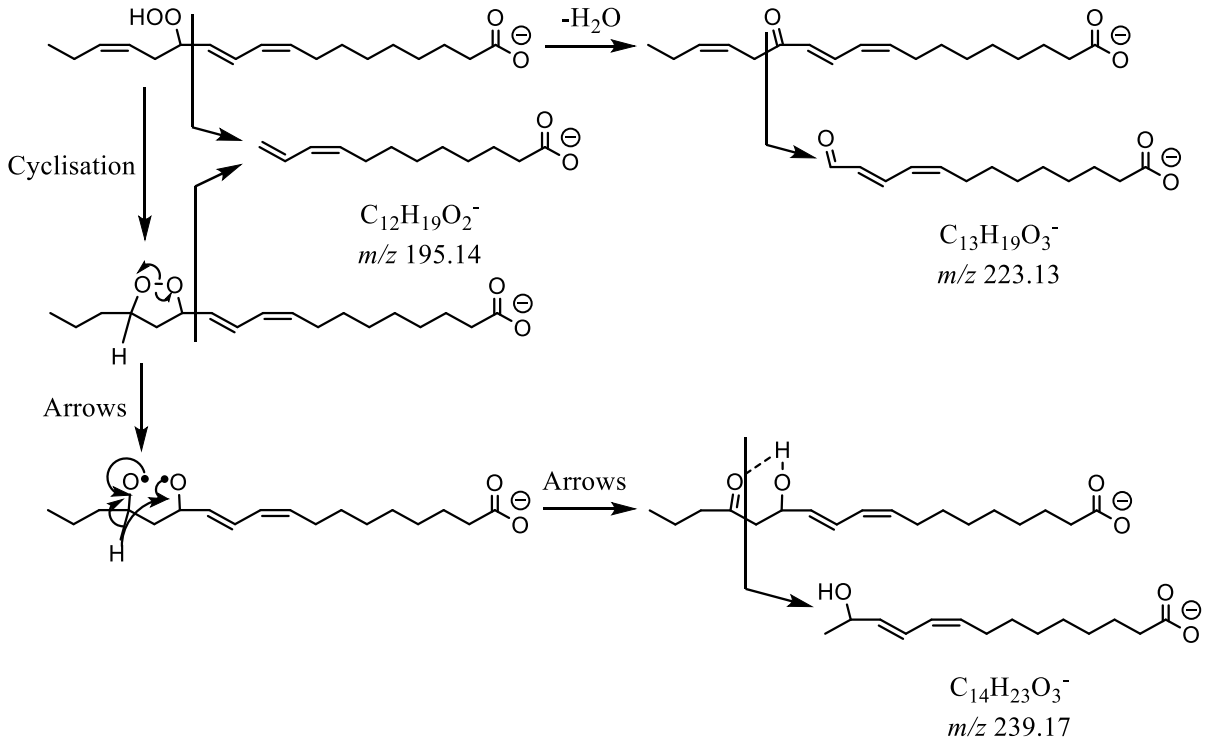

Scheme 3-18 Putative sources of characteristic MS^2-generated product ions (*m/z* 195, *m/z* 239 and *m/z* 223.13) linked to 13-HpO9,11,15TE molecular ion in (MS^2)-chromatographic peaks of octadeca-9,12,15-trienoic acid oxidation sample at Rt 18.58 and Rt 21.88 min.

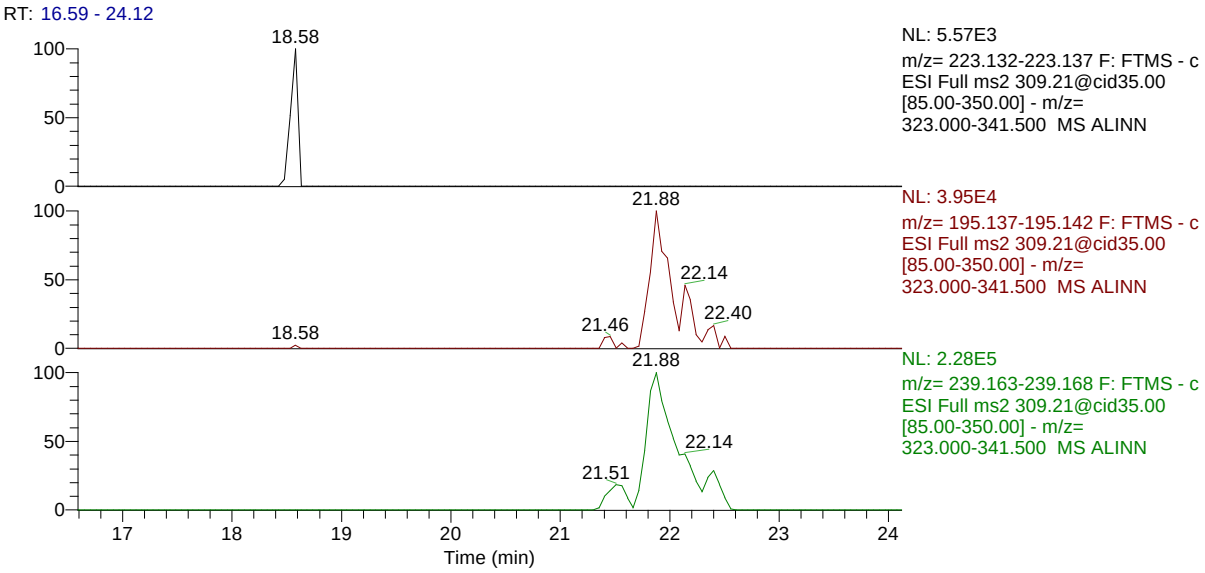

Figure 3-42 Selective mass range- chromatograms of characteristic MS^2-generated product ions (*m/z* 223.13, *m/z* 195 and *m/z* 239) linked to 13-HpO9,11,15TE from octadeca-9,12,15-trienoic acid oxidation sample.

The characteristic fragment ions in chromatographic peak at Rt 23.50 min. (Figure 3-43) that link the chromatographic peak to 16-regioisomers were proposed to be originated from the common base peak of the dehydrated hydroxide (*m/z* 291). The suggested fragmentation pathway for these ions includes keto-enol tautomerization to form double bond in the direction of the methyl end creating a new conjugated diene system that goes through a 1, 5 sigmatropic proton shift towards the methyl end. The resultant intermediate goes through cleavage of C13-C14 to generate a fragment ion at *m/z* 209 that is proposed to be $[C_{13}H_{22}O_2 - H^+]^-$ while the fragment ion at *m/z* 223 that is proposed to be $[C_{14}H_{24}O_2 - H^+]^-$ is proposed to be a result of C14-C15 scission (Scheme 3-19).

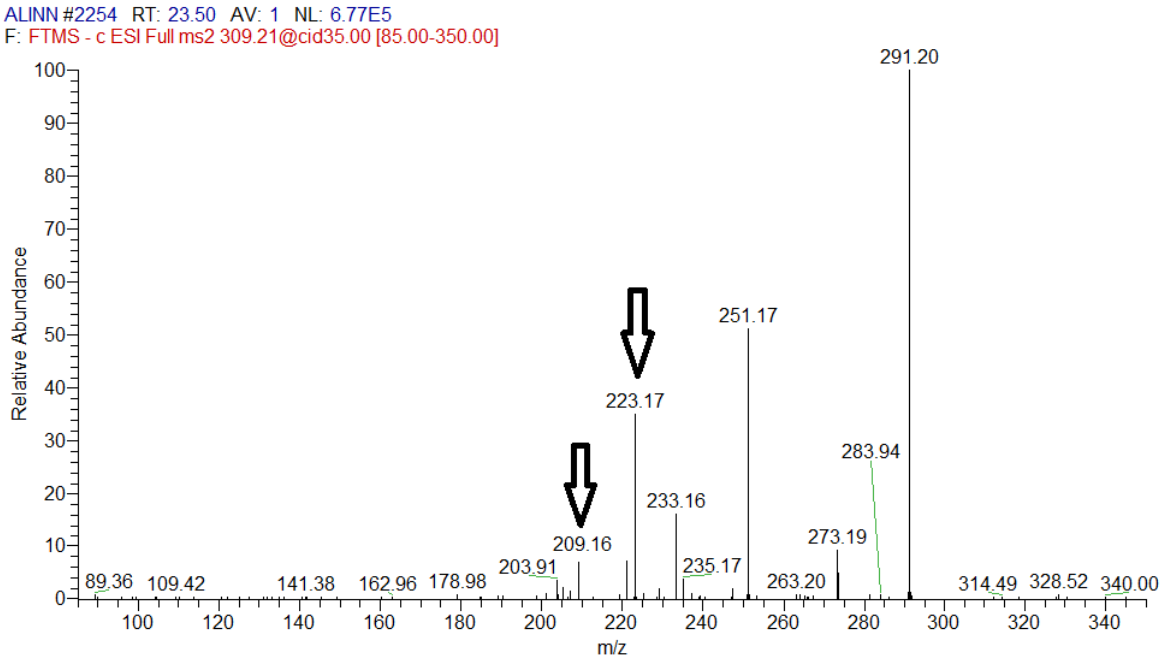

Figure 3-43 (MS^2) spectrum of linolenic acid hydroperoxide molecular ion of *m/z* 309.21 from linolenic acid oxidation sample at Rt 23.50 min.

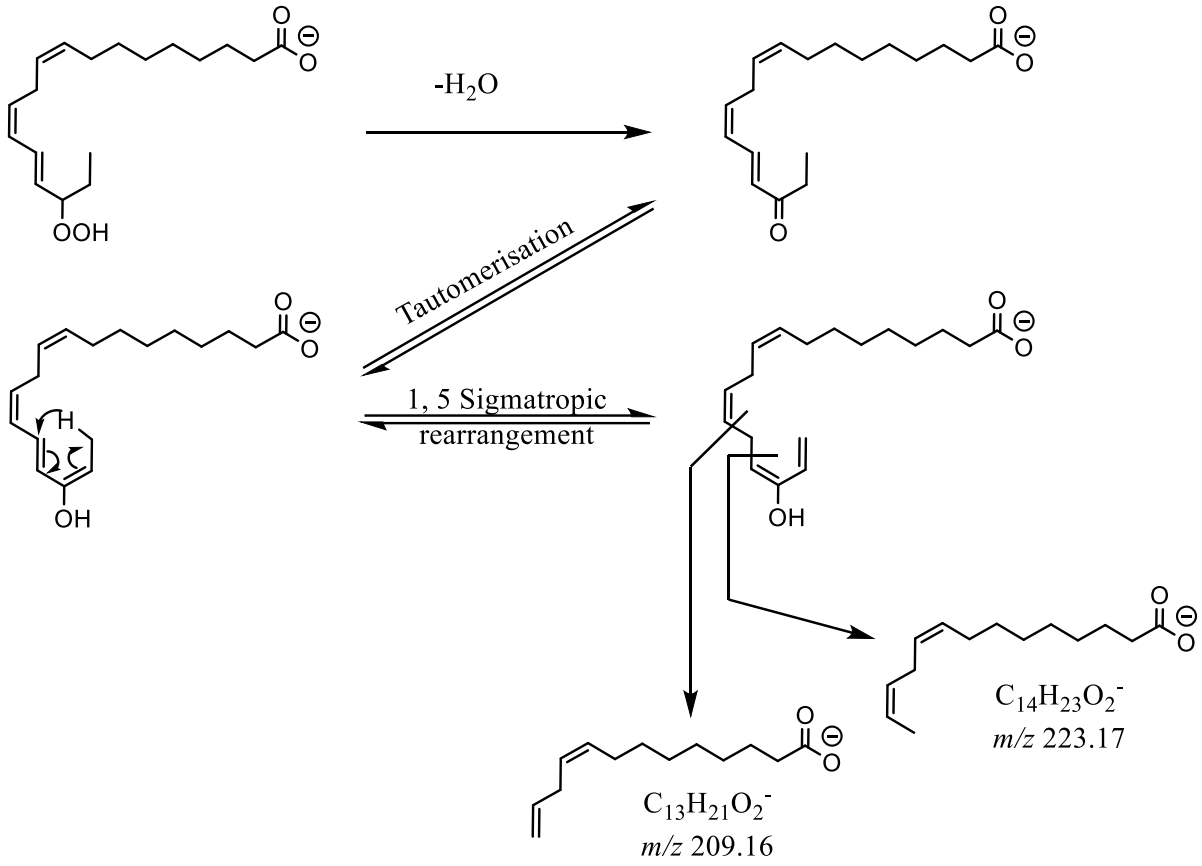

Scheme 3-19 Putative sources of characteristic MS^2-generated product ions (*m/z* 209 and *m/z* 223.17) linked to 16-HpO9,12,14TE molecular ion in (MS^2)-chromatographic peak of octadeca-9,12,15-trienoic acid oxidation sample at Rt 23.50 min.

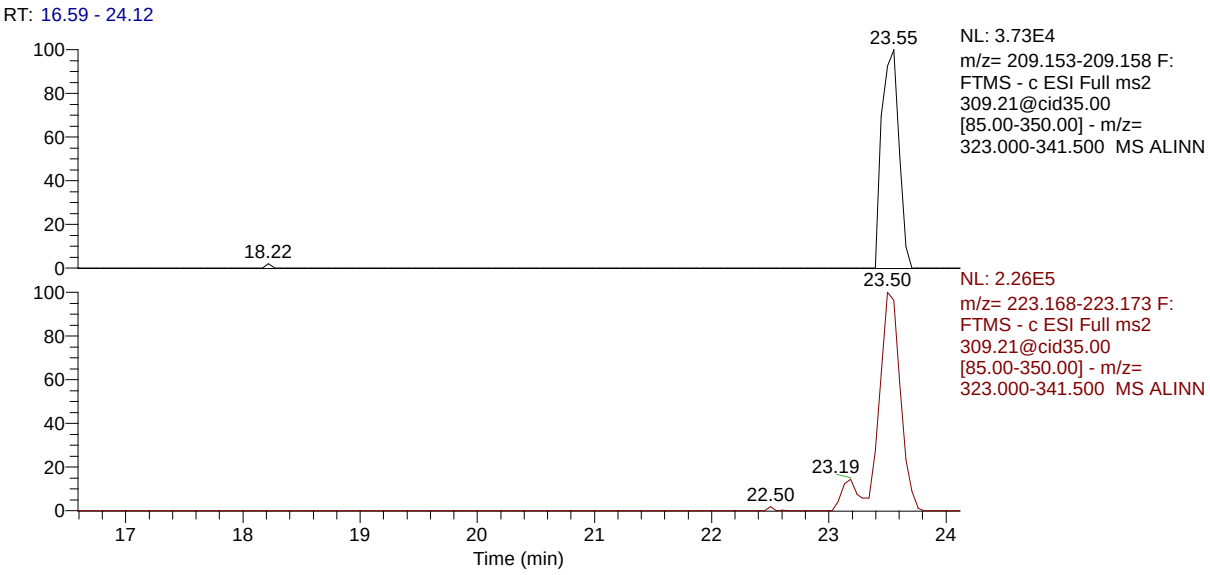

Figure 3-44 Selective mass range- chromatograms of characteristic MS^2-generated product ions (*m/z* 209 and *m/z* 223.17) linked to 16-HpO9,12,14TE from octadeca-9,12,15-trienoic acid oxidation sample.

MS^3 was carried out on the fragment ion at *m/z* 291 fragment ions, $[M-(H^+ + H_2O)]^-$, in order to explore the possibility of attaining more specific structural information. The resultant spectra showed many common fragment ions that could be found in all observed isomer peaks such as *m/z* 273 resulting from further loss of water $[M-(H^+ + 2H_2O)]^-$, *m/z* 247 product ions formed by loss of CO_2, $[M-(H^+ + H_2O + CO_2)]^-$, and even *m/z* 229 product ions that can be proposed to be formed by the combination of all of the above mentioned neutral losses , $[M-(H^+ + 2H_2O + CO_2)]^-$. Moreover, all observed isomer peaks showed a similar list of fragment ions with no additional discriminative product ions could be observed as a sign of excessive fragmentation.

3.4 Discussion of hydroperoxy poly-unsaturated fatty acids analysis as a tool for double bond position determination

When subjected to collisional induced dissociation in LC-MS^2 analysis, molar ions of hydroperoxy linoleic acid exhibited the same fragmentation tendency observed in monounsaturated hydroperoxy fatty acids to lose neutral water and produce keto linoleic acid ions as a dominant reaction that did not offer any structural information, while linolenic acid hydroperoxides showed additional fragment ions along with the dehydrated ion.

On the other hand, LC-MS^3 analysis conducted on the dehydrated ions of linoleic acid hydroperoxides yielded clear product ion spectra for all regioisomers. While similar analysis has only showed signs of excessive fragmentation when performed on dehydrated Linolenic acid hydroperoxides ions.

In general observations, $[M-(H^+ + H_2O + CO_2)]^-$ and $[M-(H^+ + 2H_2O)]^-$ were encountered commonly in the MS^3 spectra of all tested PUFA hydroperoxides.

Previous studies presented the possibility of characterisation of PUFA hydroperoxides positional isomers by means of monitoring structurally

significant fragment ions (Haefliger & Sulzer, 2007; Macmillan & Murphy, 1995; Oliw et al., 2006; Schneider et al., 1997).

Overall, the suggested fragmentation pathways and characteristic fragment ions are in accordance with the characterisation of linoleic acid hydroperoxides by (Macmillan & Murphy, 1995). An abundance of dehydrated ions and lack of structural information about location of hydroperoxyl group in negative ion full scan ESI-MS, hence, the need for further cleavage of precursor ion by collisional induced dissociation (CID) in MS^3 analysis were all in line with our observations. Characteristic fragment ions reported by (Macmillan & Murphy, 1995) such as *m/z* 185 and *m/z* 125 for 9-HpO10,12DE and *m/z* 113 and *m/z* 195 for 13-HpO9,11DE represent an essential part of the fragmentation pathways proposed in this work. Moreover, Macmillan & Murphy similarly suggested the need for proton shifts to facilitate cleavages that produce the most abundant fragment ions that otherwise would be reasonably unlikely.

Nevertheless, Macmillan & Murphy suggested a different mechanism for the decomposition pathways that lead to most abundant characteristic MS^3 product ions of *m/z* 185 from 9-HpODE and *m/z* 113 from 13-HpODE. This mechanism starts with a double bond shift away from the ketone site in the dehydration product of the HpODEs before cyclisation of the conjugated diene forming an intermediate species with four-membered ring on the position beta to the carbonyl group directing fragmentation to the bond between carbon alpha and carbon beta to the carbonyl group. As shown in scheme 3-20, dehydrated 9-HpODE would go through a double bond shift of conjugated diene from C10-C13 to C11-C14. A bond would join C11 and C14 causing the formation of a cyclobutadiene ring on C11 preceding the collapse of C10-C11 bond to give *m/z* 185, an enolate anion.

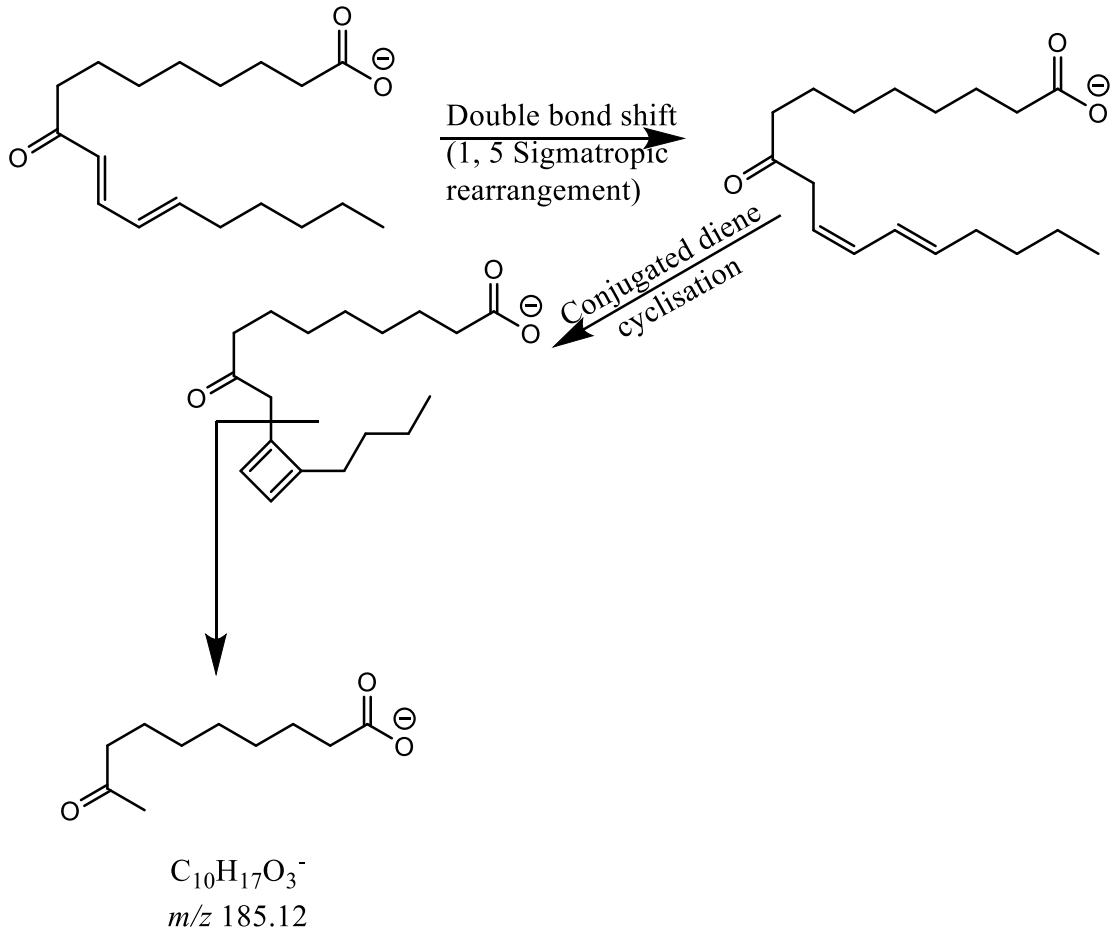

Scheme 3-20 Putative fragmentation pathway suggested by (Macmillan & Murphy, 1995) of product ion *m/z* 185 from dehydrated 9-hydroperoxy linoleic acid product ion.

The analogous pathway for 13-HpODE, explained in scheme 3-21, could be suggested to be the source for product ions of *m/z* 113 and *m/z* 179. In this case, double bond shift would take place from C9-C12 to C8-C11forming the four-membered ring between C8 and C11. Hence, the cleavage would take place between C11 and C12 to give two ionisable fragments (enolate anions) of *m/z* 113 and *m/z* 179.

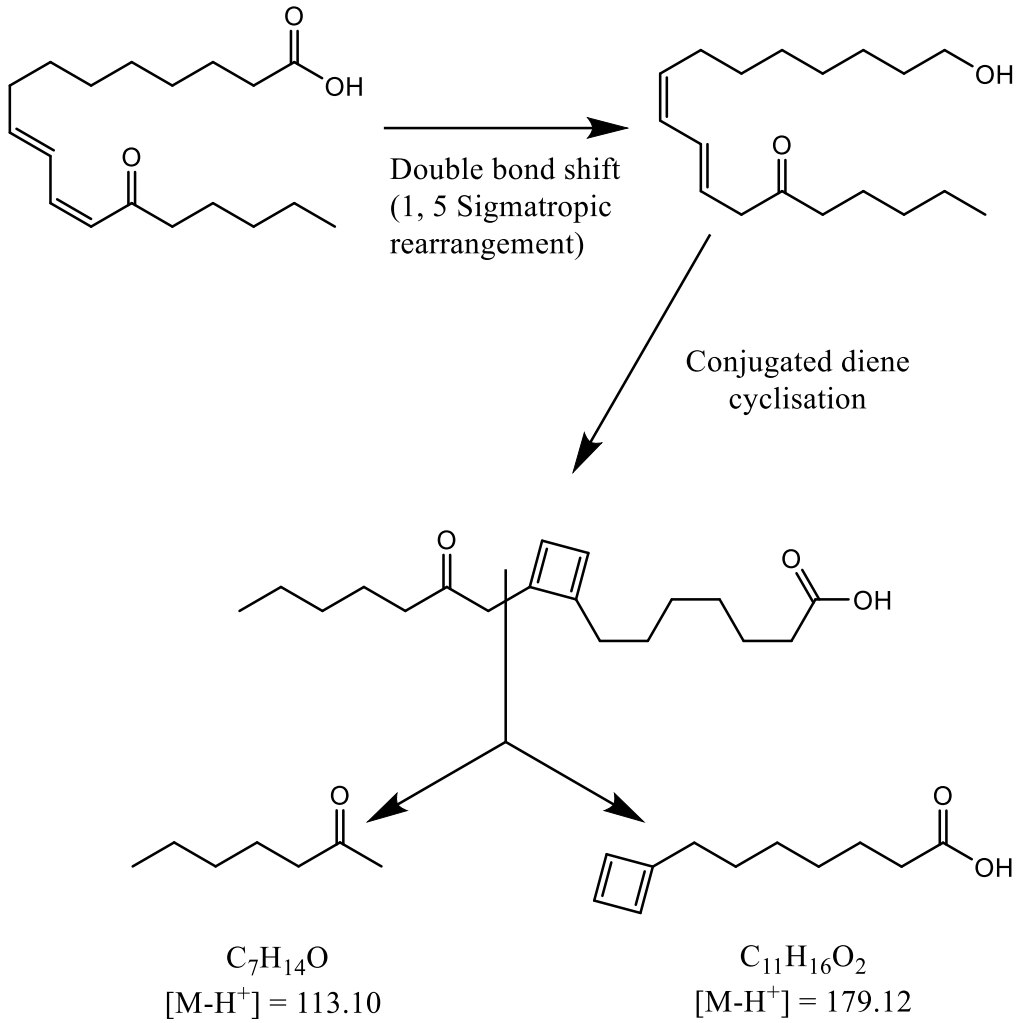

Scheme 3-21 Putative fragmentation pathway suggested by (Macmillan & Murphy, 1995) of product ions *m/z* 113 and *m/z* 179 from dehydrated 9-hydroperoxy linoleic acid product ion

However, it must be pointed that Macmillan & Murphy obtained those fragment ions by resorting to increased orifice voltages while we opted the option of further fragmentation of the dehydrated MS-MS product ion.

Similar patterns of fragmentation were obtained by (Oliw et al., 2006) by studying the MS-MS spectra of keto fatty acids transformed from 9-HpO10,12DE, 9-HpO10,12,15TE, 13-HpO9,11DE and 13-HpO9,11,15TE via treatment with hematin alongside their isotope labelled analogues. (Oliw et al., 2006) suggested enolisation of carbonyl group to form a vinyl alcohol as a step in the mechanism of formation of characteristic fragment ions mentioned above. In accordance with the present findings, Garscha et al. have demonstrated that in order to get structural information about the

position of the hydroperoxide moiety from ESI-MS spectra, the carboxylate anion was subjected to CID fragmentation and the full scan spectrum of the fragments was acquired (MS/MS or MS2) before a MS/MS/MS (MS^3) analysis was performed by selecting the dehydrated molar fragment ion and submitting it to CID fragmentation. In the same vein of our findings, the MS-MS (311 → full-scan) for both HpODEs studied by Garscha et al. 11-HpODE and 13-HpODE, showed mainly the loss of water, while the MS^3 (311 → 293 → full-scan) analysis yielded several fragments that were used to identify the hydroperoxide group position.

The effect of double bond positions was the determining factor in the fragmentation pathways suggested in this work and previous work discussed above. Fragmentation processes were controlled either by the electron withdrawing properties of the conjugated double bond systems and electronegativity of oxygen atoms at peroxyl moiety in charge remote fragmentation mechanisms or by reactivity of newly formed anion at the position of the in situ-generated carbonyl/hydroxy group in charge driven fragmentation mechanisms. Even though some of the product ions that were considered characteristic in LC- MS^2 of HpODTs and LC-MS^3 of HpODEs were proposedly formed by charge driven pathways, they could still provide essential structural information their precursor molecular ions since that the site of charge, site of peroxidation, is basically governed by double bonds locations.

Main steps that were apparently involved in diverse decomposition pathways during MS^3-collisional activation of dehydrated ions of HpODEs and MS^2 collisional activation of molar ions of HpODTs were similar to those encountered in LC-MS^3 of MUFAs hydroperoxides such as tautomerisation of the resulted carbonyl group, sigmatropic hydrogen rearrangements that precede and/or succeed keto-enol tautomerisation and formation of an alkoxide anion at the position of carbonyl/hydroxy group.

With regards to the purpose of developing a method for double bonds pinpointing using hydroperoxides, reduced sensitivity can be caused by instability of hydroperoxides and low relative abundance of some of the designated characteristic fragment ions as in case in some of those of Linolenic acid hydroperoxides. Another limitation can arise from the

complexity of tandem MS spectra of the hydroperoxides caused by the versatility in fragmentation pathways and the reality that an increase in number of double bonds in fatty acids carbon chain (n) means a concomitant increase in number of hydroperoxides positional isomers (2n-2) (Derogis et al., 2019; Esterbauer, 1993) and more complicated peroxidation mechanisms (Yin et al., 2007).

On the other hand, chemistry and mechanism of peroxidation of PUFAs are well established. Thus, structure and isomeration of their hydroperoxides can be predicted in confidence. From the forgoing, in theory, some selective fragment ions that were considered of characteristic significance in this work or in previous similar work could be used to identify PUFAs hydroperoxides, hence locating double bond positions in their precursor PUFAs.

For the purpose of monitoring the progress of the C6 flavour compounds production reaction from polyunsaturated C18 fatty acids through the 13-lipoxygenase/13-hydroperoxide lyase in soybean flour, (Haefliger & Sulzer, 2007) required accurate characterisation and quantification of reaction mixtures which included identification of 9-hydroperoxides and 13-hydroperoxides of Linoleic acid and Linolenic acid. Characteristic fragment ions generated by increased orifice voltage in ESI-MS source were used to determine positional isomers in a comparable approach to the work of (Macmillan & Murphy, 1995) with similar outcome as fragments *m/z* 185 was observed in 9-HpO10,12DE and 9-HpO10,12,15TE spectra and *m/z* 195 was observed in 13-HpO9,11DE and 13-HpO9,11,15TE.

Development of a MRM method using these fragment ions to quantify Linoleic acid hydroperoxides was attempted by (Reverberi et al., 2010) in their work to assess the effects of lipid peroxidation on ochratoxin A biosynthesis in *Aspergillus ochraceus*. The transitions monitored for Linoleic acid hydroperoxides, *m/z* 311 to *m/z* 185 for 9-HpO10,12DE and *m/z* 311 to *m/z* 195 for 13-HpO9,11DE, were built on the method and results described (Garscha et al., 2008; Hamberg et al., 1998; Oliw et al., 2006).

3.5 Analysis of hydroxy mono-unsaturated fatty acids

3.5.1 Analysis of oleic acid hydroxides

3.5.1.1 Hydroxide formation

Oleic acid hydroperoxides formed by chemically induced free radical oxidation of Oleic acid can be subjected to reductive cleavage of the O-O bond that is very susceptible to reduction. The reduction of hydroperoxides to alcohols can be achieved by many reagents, however, it is advisable to employ more selective catalytic reduction method using a mild reducing agent where carboxylic functional group is expected to survive. The most often suggested mechanism for these reductions is nucleophilic attack on oxygen (Gilchrist, 1991). Accordingly, applying $NaBH_4$ to reduce Oleic acid hydroperoxides represents a useful method for the synthesis of a mixture of four hydroxides where the positions of OH groups are determined by initial location of the double bond on C9 of the acyl chain (Scheme 3-22).

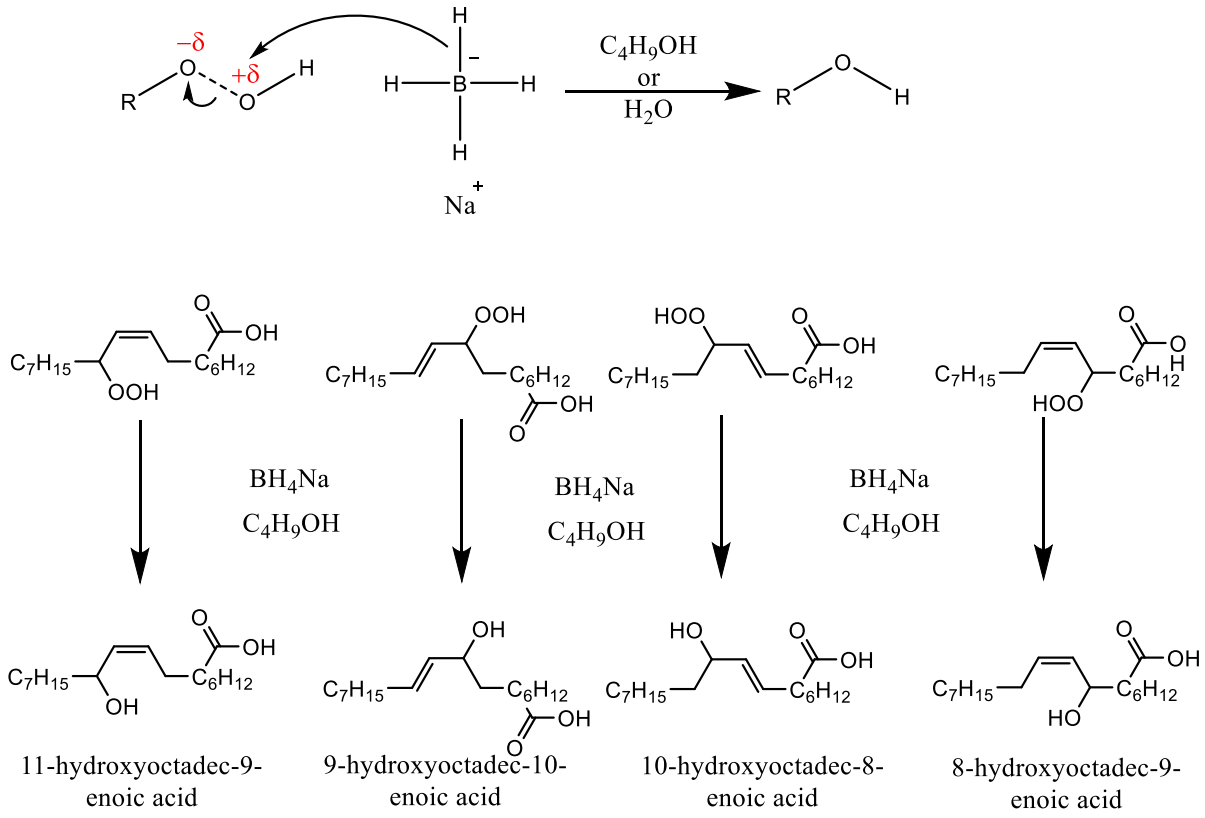

Scheme 3-22 Purposed reaction scheme for reduction of Oleic acid hydroperoxides to hydroxides via $NaBH_4$ nucleophilic attack

3.5.1.2 LC-MS analysis of oleic acid hydroxides

Mass range chromatograms of hydroxyl derivatives of octadec-9-enoic acid (Oleic acid, FA 18:1 (n−9)) (HO9MEs) generated by secondary decomposition of HpO9ME isomers showed four isomer peaks resulting from previously determined hydroperoxide derivatives of octadec-9-enoic acid. The isomer peaks spectra did not contain any unique structural information which could be used for structure elucidation. In contrast to the hydroperoxide cases, loss of water $[M - (H^+ + H_2O)]^-$ was not observed in any of the spectra of hydroxides species in mass range chromatogram of $[M - H^+]^-$ (Figure 3-45).

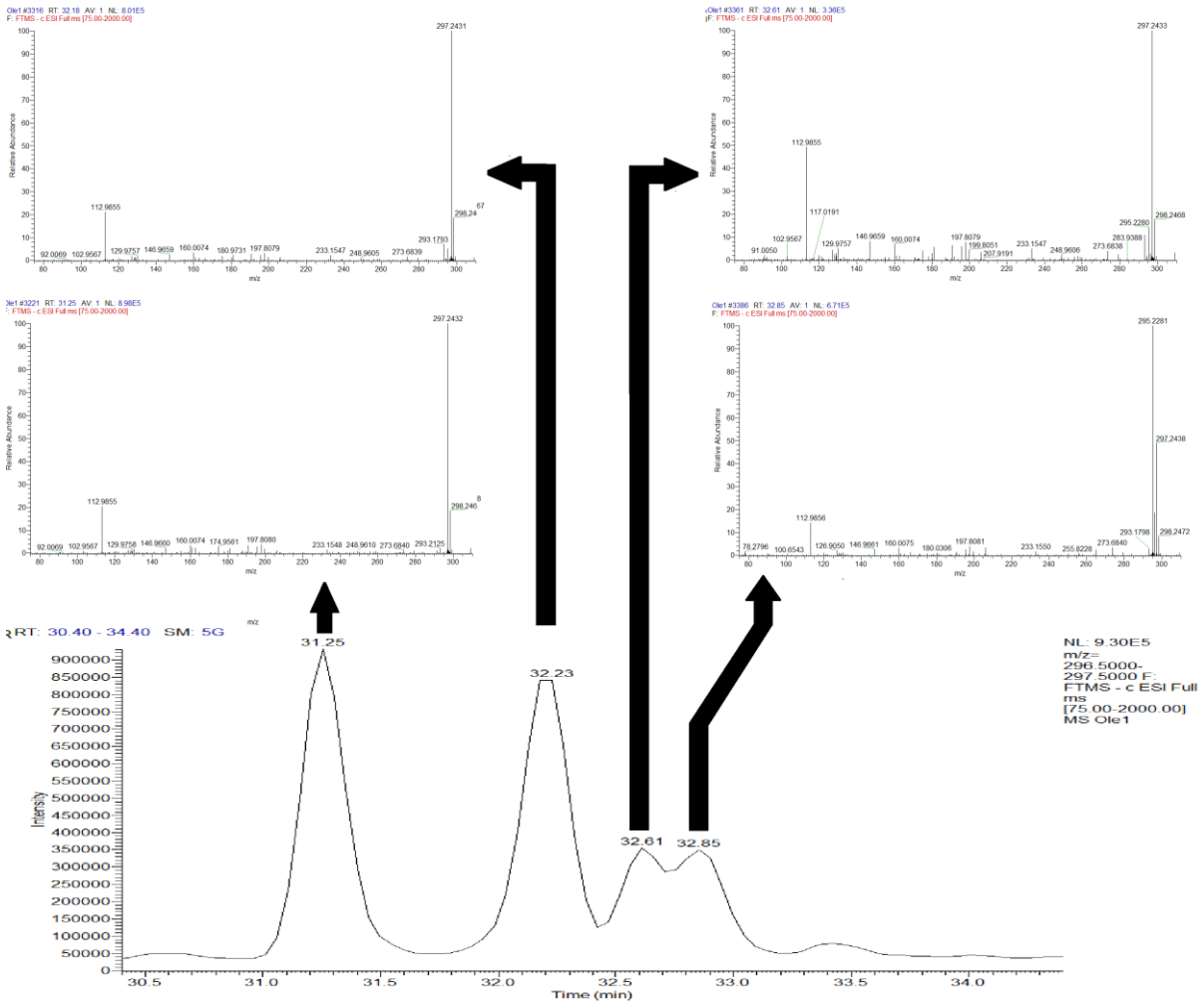

Figure 3-45 Mass range chromatogram & mass spectra of ions of *m/z* 297 in liquid chromatography- mass spectrometry (LC-MS) analysis of reduced octadec-9-enoic acid hydroperoxides sample.

The interpretation of hydroxide isomers required further investigations by MS^2 spectrometry. Besides neutral loss of water, $[M - (H^+ + H_2O)]^-$, that showed the highest abundance peaks in all octadec-9-enoic acid hydroxyl isomers (HO9MEs) MS^2 spectra, each isomeric peak showed a distinctive fragmentation pattern (Figure 3-46).

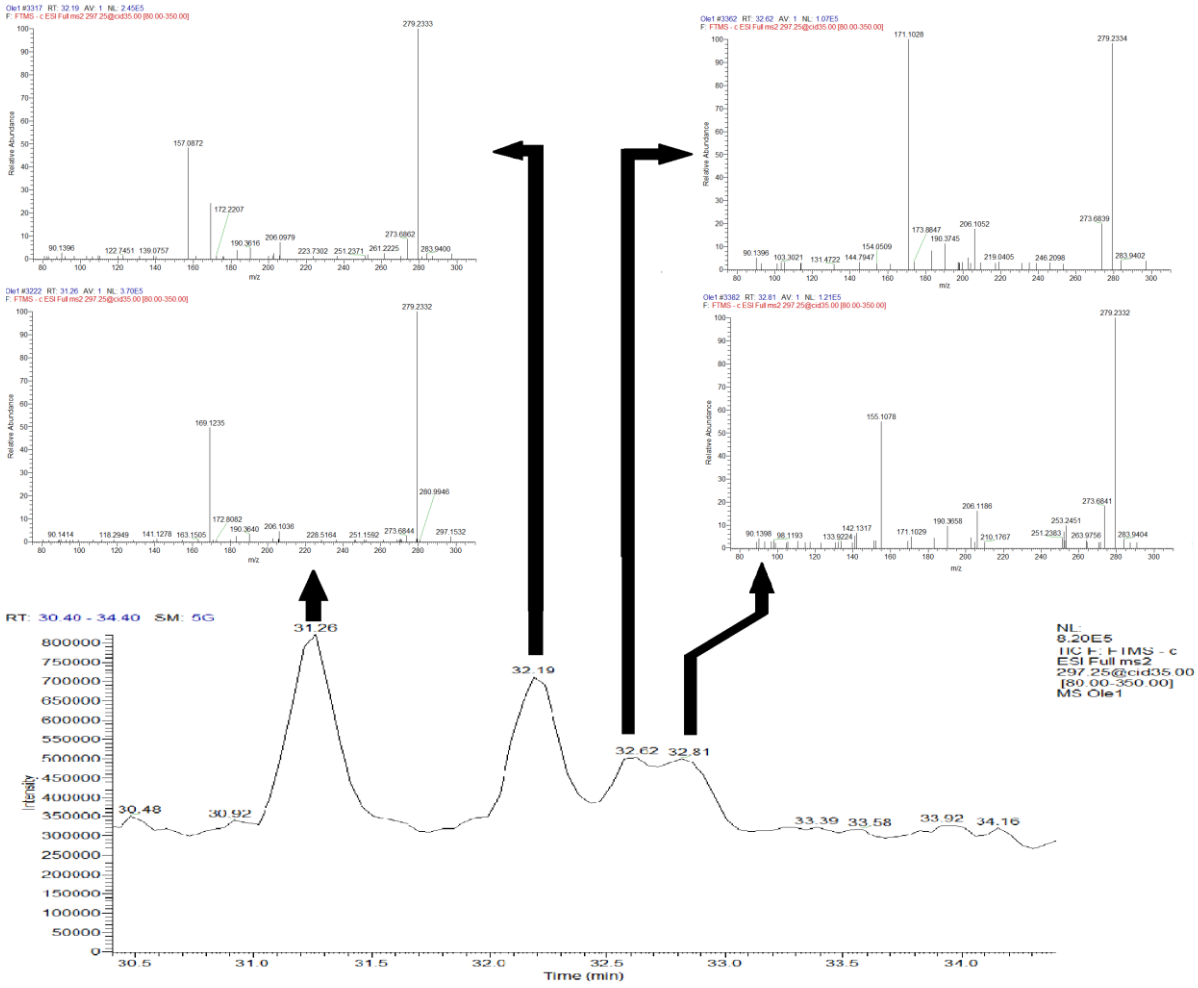

Figure 3-46 Total ion chromatogram & MS^2 spectrometry (LC- MS^2) following collision-induced decomposition of the molecular anion $[M - H^+]^-$ at *m/z* 297 of HO9ME.

The peak at Rt 31.26 min. in LC- MS^2 total ion current chromatogram that corresponds to precursor ion LC-MS chromatogram peak at Rt 31.25 min. (Figure 3-47) showed a product ion that can be considered characteristic and could be linked to 11-Hydroxy octadec-9-enoic acid (11-HO9ME) with *m/z* 169 which is proposed to be $[C_{10}H_{18}O_2 - H^+]^-$ and to be formed by a fragmentation pathway that involves a retro-ene reaction (Scheme 3-23). Preceded by double bond migration towards the carboxyl end to bring

the double bond to become homoallylic to the hydroxy functional group, the ensuing species can easily undergo cleavage in the C10–C11 bond forming a product ion at *m/z* 169 and leaving an aldehyde (neutral species) on the other side of the cleavage.

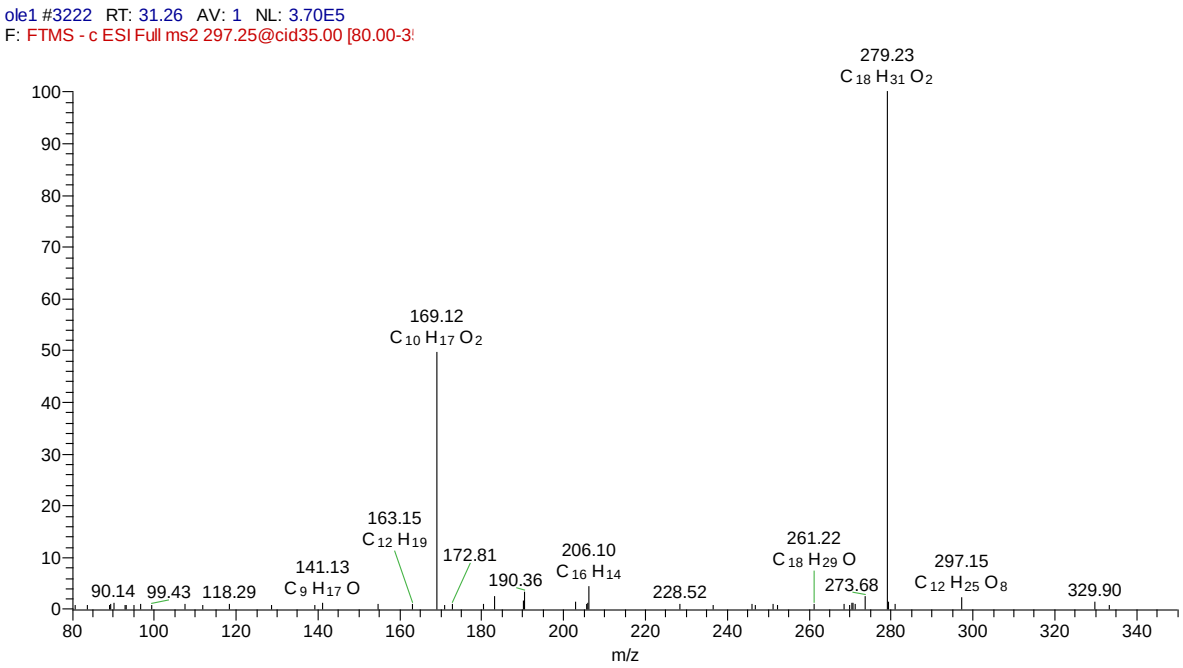

Figure 3-47 MS^2 spectrum of *m/z* 297.25 ion from octadec-9-enoic acid oxidation sample at Rt 31.26 min.

Table 3-9 The most abundant MS^2 spectrum ions at Rt 31.26 min. in the TIC LC-MS^2 chromatogram of the MS-trapped precursor ion of *m/z* 297.25 from reduced octadec-9-enoic acid hydroperoxides sample.

Rt: 31.26		
m/z	**Relative abundance**	**Composition**
279.23	100.00	$C_{18}H_{31}O_2$
169.12	49.63	$C_{10}H_{17}O_2$
206.10	4.48	$C_{16}H_{14}$
183.01	2.49	$C_4H_7O_8$
297.15	2.10	$C_{12}H_{25}O_8$
190.32	1.58	$C_{11}H_{26}O_2$

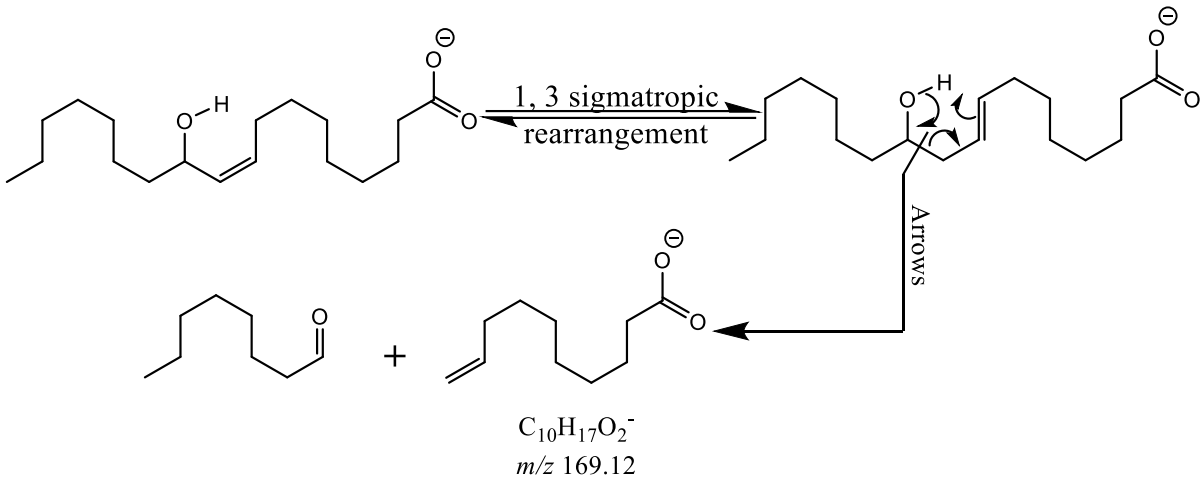

Scheme 3-23 Putative source of product ion *m/z* 169 from 11-HO9ME molecular ion in the MS^2 chromatographic peak at Rt 31.26 min.

Peak at Rt 32.19 min. in the TIC LC- MS^2 chromatogram that corresponds to the precursor ion LC-MS chromatogram peak at Rt 32.23 min. (Figure 3-48) showed a product ion *m/z* 157 which is proposed to be $[C_8H_{14}O_3 - H^+]^-$ and could be originated from 8-Hydroxy octadec-9-enoic acid (8-HO9ME) (Scheme 3-24) via a charge remote allylic fragmentation pathway similar to the fragmentation mechanism suggested to link product ion *m/z* 169 to 11-Hydroxy octadec-9-enoic acid (11-HO9ME) that includes double bond shift on the opposite direction, towards the methyl end, to render it homoallylic to the alcohol functional group followed by a retro-ene reaction that causes a cleavage in C8–C9 bond. Thus, acid-containing the aldehyde product ion at *m/z* 157 is produced (Scheme 3-24).

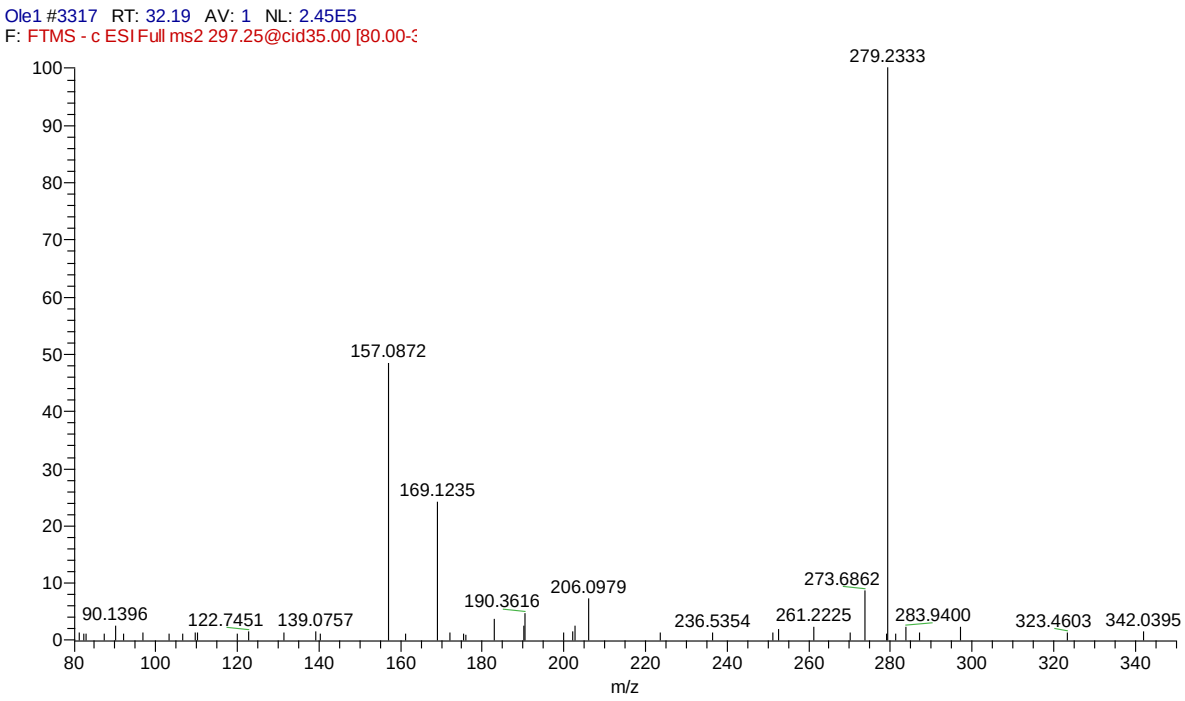

Figure 3-48 MS^2 spectrum of m/z 297.25 ion from octadec-9-enoic acid oxidation sample at Rt32.19 min.

Table 3-10 The most abundant MS^2 spectrum ions at Rt 32.19 min. in the TIC LC-MS^2 chromatogram of the MS-trapped precursor ion of *m/z* 297.25 from reduced octadec-9-enoic acid hydroperoxides sample.

Rt: 32.19		
m/z	**Relative abundance**	**Composition**
279.23	100.00	$C_{18}H_{31}O_2$
157.09	48.31	$C_8H_{13}O_3$
169.12	24.19	$C_{10}H_{17}O_2$
206.10	7.27	$C_{12}H_{14}O_3$
183.01	3.77	$C_4H_7O_8$
206.09	2,74	$C_{12}H_{14}O_3$
190.33	2.54	$C_{11}H_{26}O_2$

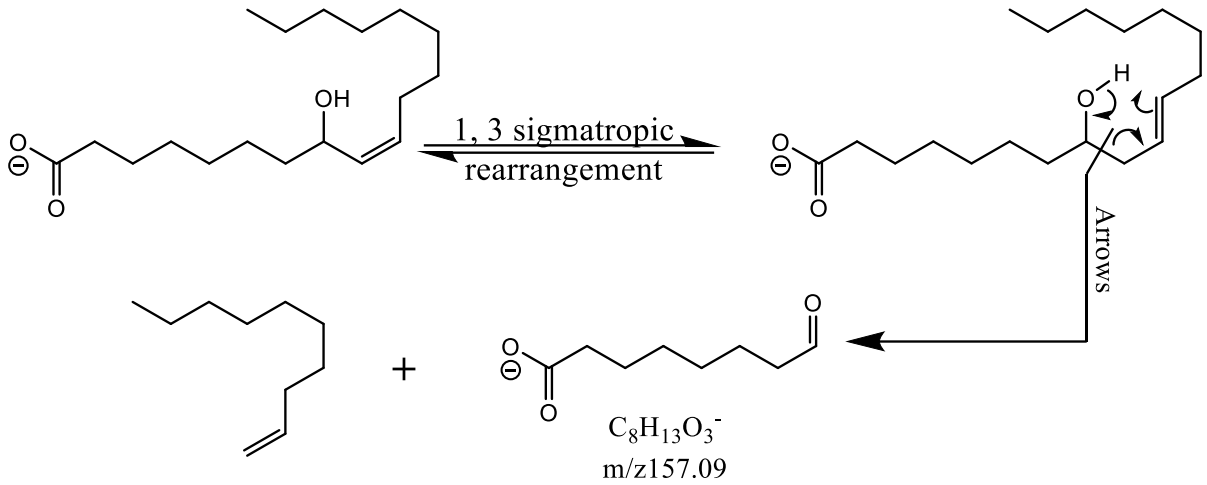

Scheme 3-24 Putative source of product ion *m/z* 157 from 8-HO9ME molecular ion in the MS^2 chromatographic peak at Rt 32.19 min.

The highly abundant product ion *m/z* 171 showed in the LC- MS^2 TIC chromatographic peak at Rt 32.62 min. that corresponds to precursor ion in the LC-MS chromatogram peak at Rt 32.61 min. (Figure 3-49) is proposed to be $[C_9H_{16}O_3–H^+]^-$. This acid-containing aldehyde product ion could be linked to 9-Hydroxy octadec-10-enoic (9-HO10ME) via the same charge remote allylic fragmentation pathway mentioned above to link product ion *m/z* 157 to the 8-HO9ME isomer with a cleavage in C9–C10 bond in this case (Scheme 3-25).

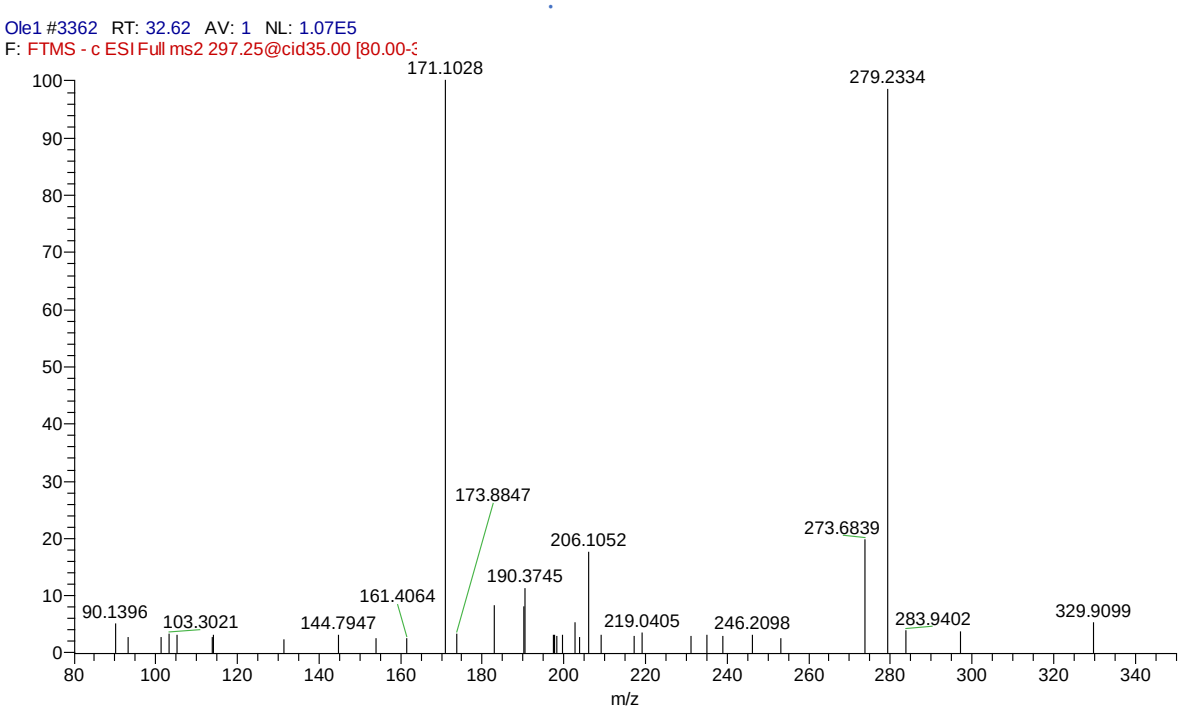

Figure 3-49 MS² spectrum of *m/z* 297.25 ion from octadec-9-enoic acid oxidation sample at Rt 32.62 min.

Table 3-11 The most abundant MS² spectrum ions at Rt 32.62 min. in the TIC LC-MS² chromatogram of the MS-trapped precursor ion of *m/z* 297.25 from reduced octadec-9-enoic acid hydroperoxides sample.

Rt: 32.62		
m/z	**Relative abundance**	**Composition**
171.10	100.00	$C_9 H_{15} O_3$
279.23	98.46	$C_{18} H_{31} O_2$
206.11	17.65	$C_{16} H_{14}$
183.01	8.23	$C_4 H_7 O_8$
90.14	5.12	$C_5 H_{14} O$

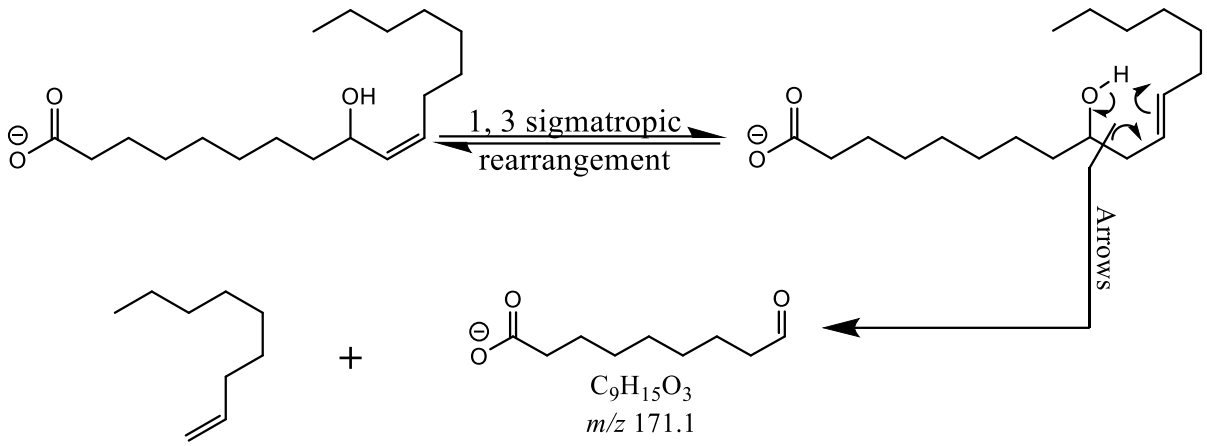

Scheme 3-25 Putative source of product ion *m/z* 171 from 9-HO10ME molecular ion in the MS^2 chromatographic peak at R 32.62 min.

The product ion at *m/z* 155 showed in LC- MS^2 TIC chromatographic peak at Rt 32.81 min. that corresponds to precursor ion LC-MS chromatogram peak at Rt 32.85 min. is proposed to be $[C_9H_{16}O_2 - H^+]^-$. The fragmentation mechanism suggested to link product ion *m/*z 169 to 11-Hydroxy octadec-9-enoic acid (11-HO9ME) can also be considered as pathway for the formation of *m/z* 155 from 10-Hydroxy octadec-8-enoic acid (10-HO8ME). This mechanism that facilitates cleavage in C9–C10 bond requires double bond shift to render the double bond homoallylic to the hydroxy group (Scheme 3-26).

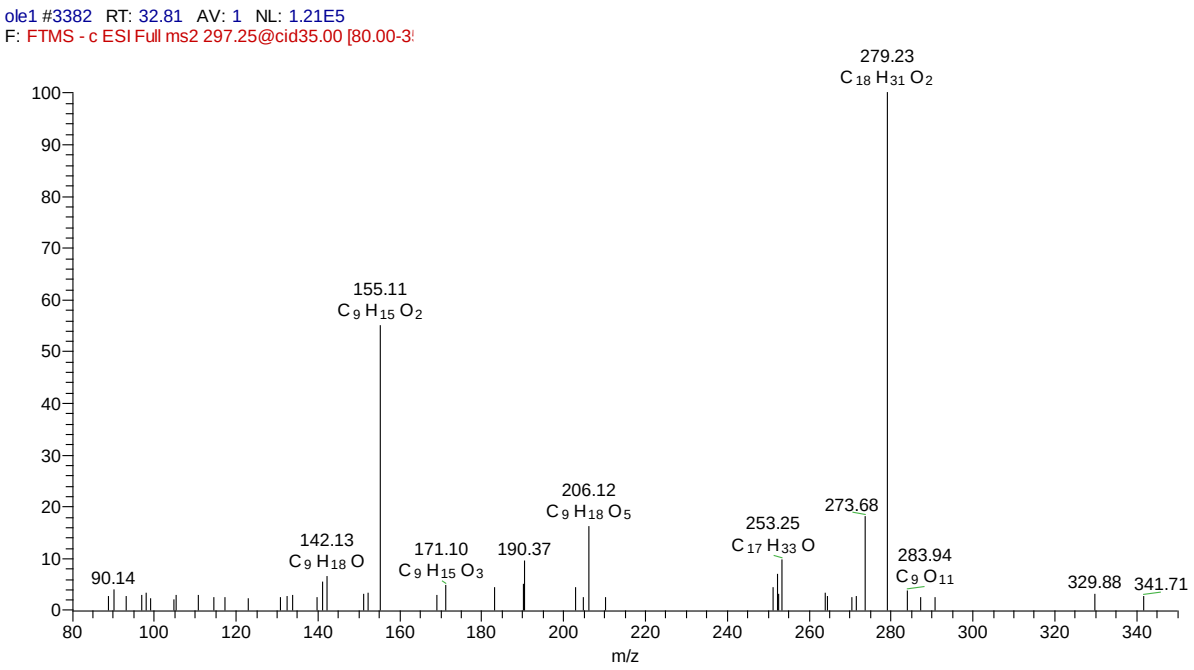

Figure 3-50 MS² spectrum of *m/z* 297.25 ion from octadec-9-enoic acid oxidation sample at Rt 32.81 min.

Table 3-12 The most abundant MS² spectrum ions at Rt 32.81 min. in the TIC LC-MS² chromatogram of the MS-trapped precursor ion of *m/z* 297.25 from reduced octadec-9-enoic acid hydroperoxides sample.

Rt: 32.81		
m/z	**Relative abundance**	**Composition**
279.23	100.00	$C_{18}H_{31}O_2$
155.11	54.94	$C_9H_{15}O_2$
206.12	16.16	$C_9H_{18}O_5$
253.25	9.77	$C_{17}H_{33}O$
252.24	6.96	$C_{17}H_{32}O$

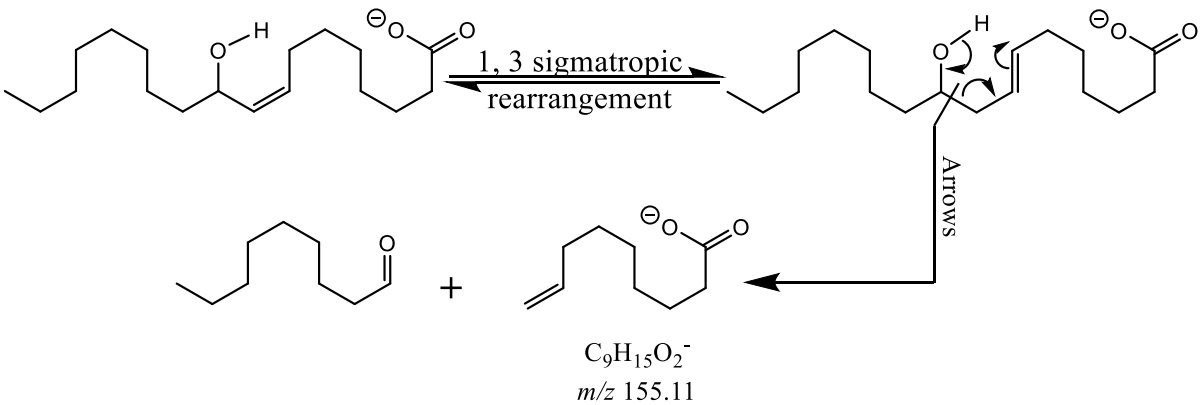

Scheme 3-26 Putative source of product ion *m/z* 155 from 10-HO8ME molecular ion in the MS² chromatographic peak at Rt 32.81 min.

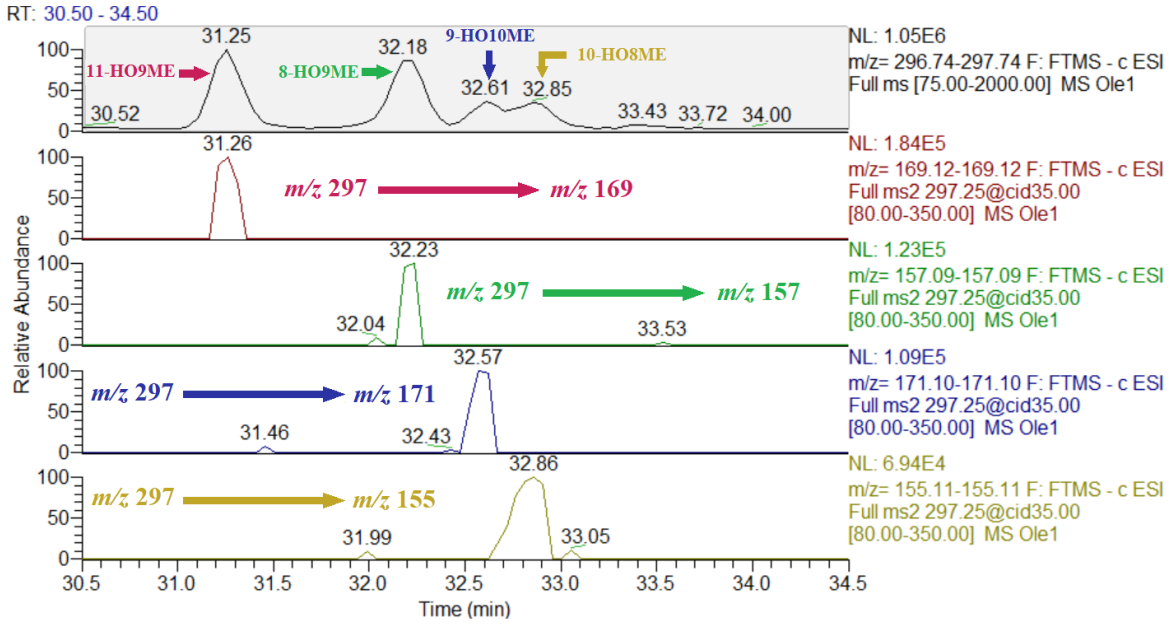

Figure 3-51 Mass range chromatogram of *m/z* 297 & mass spectra of precursor-product transitions *m/z* 297 to 169, 157, 171, and 155 specified for each hydroxy regioisomer in liquid chromatography- MS^2 spectrometry ($LC\text{-}MS^2$) analysis of reduced octadec-9-enoic acid hydroperoxides sample.

3.5.2 Analysis of Vaccenic acid hydroxides

3.5.2.1 Hydroxide formation

The application of hydroperoxides reduction by $NaBH_4$ on another positional isomer of octadecenoic acid such as vaccenic acid that has the single double bond on C11 of the acyl chain would result in the formation of different mixture hydroxides. The reduction process (Scheme 3-27) proceeds in the same mechanism reported in the case of oleic acid (Scheme 3-22).

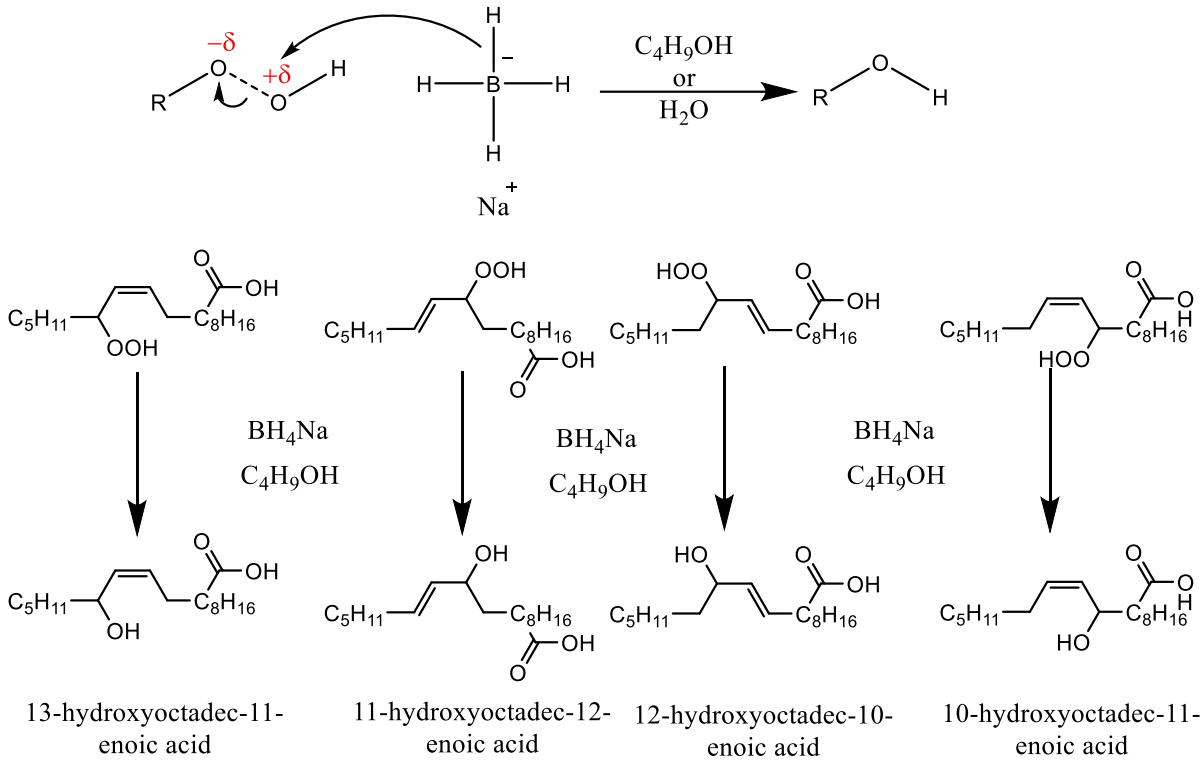

Scheme 3-27 purposed reaction scheme for reduction of Vaccenic acid hydroperoxides to hydroxides via NaBH4 nucleophilic attack

3.5.2.2 LC-MS analysis

Mass range chromatograms of hydroxyl derivatives octadec-11-enoic acid (Vaccenic acid, FA 18:1 (n−7)) generated by secondary decomposition of HpO11ME isomers showed only three isomer peaks instead of expected four isomer peaks resulting from previously determined hydroperoxide derivatives of octadec-11-enoic acid, which suggested the possibility of co-elution of two of the regioisomer peaks and there is some indication of partial resolution in the later eluting peak in the chromatogram (Figure 3-52). The absence of $[M - (H^+ + H_2O)]^-$ fragment ion in all spectra of hydroxides species in mass range chromatogram of $[M - H^+]^-$ was detected (Figure 3-52).

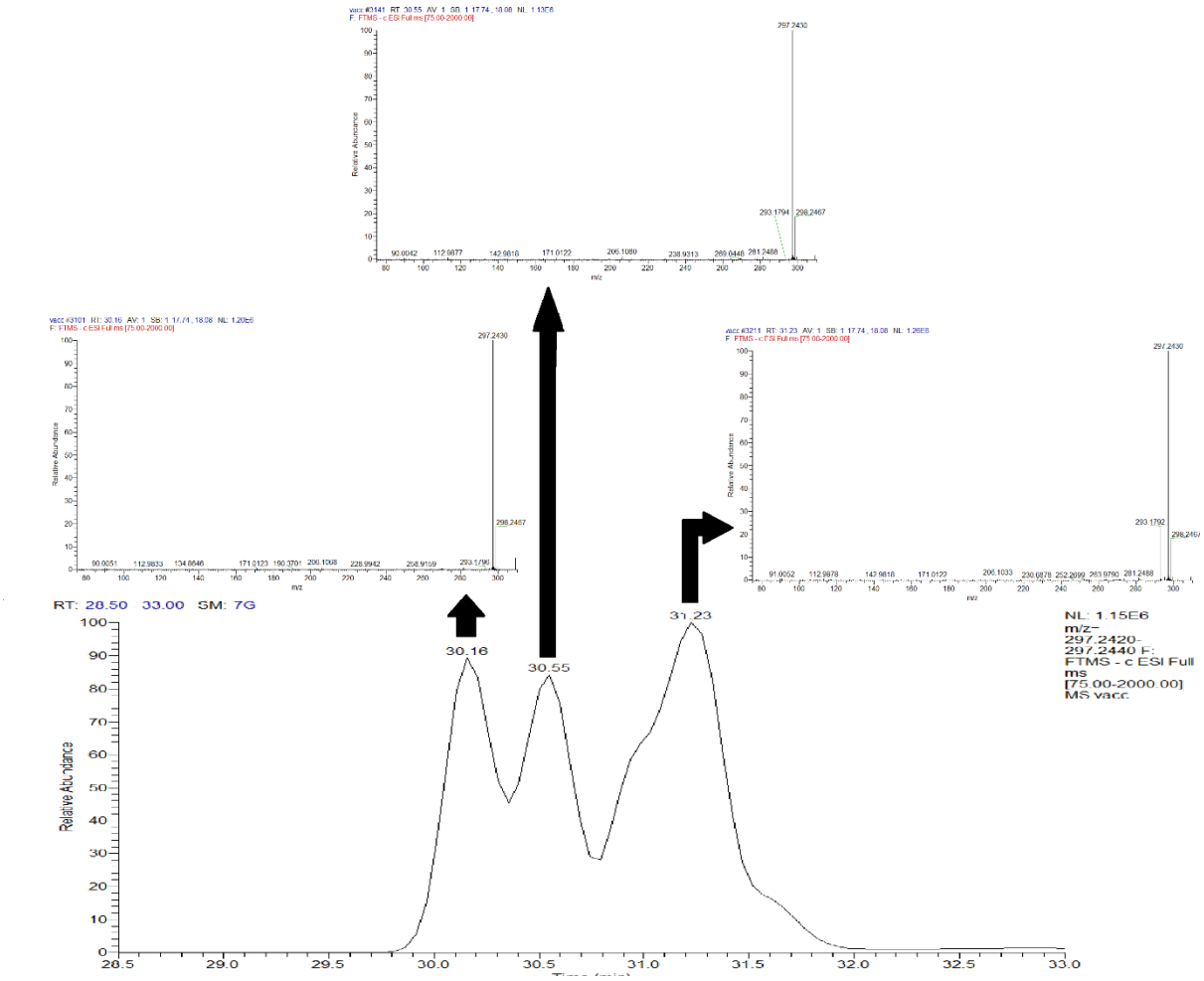

Figure 3-52 Mass range chromatogram & mass spectra of ions of m/z 297 in liquid chromatography-mass spectrometry (LC-MS) analysis of reduced octadec-11-enoic acid hydroperoxides sample.

More in-depth investigations using MS^2 spectrometry was required to elucidate the hydroxide isomers. Examination of the MS^2 spectra of the isomeric peaks showed four distinctive fragmentation patterns in agreement with the prospect of four isomers resulting from secondary decomposition of the HpO11ME regioisomers. Two of those distinctive MS^2 spectra were detected in LC- MS^2 TIC chromatographic peak at Rt 31.24 min. that corresponds to precursor ion LC-MS chromatogram peak at Rt 31.23 min. which asserted the probability of co-elution of two of the four anticipated regioisomers (Figure 3-53).

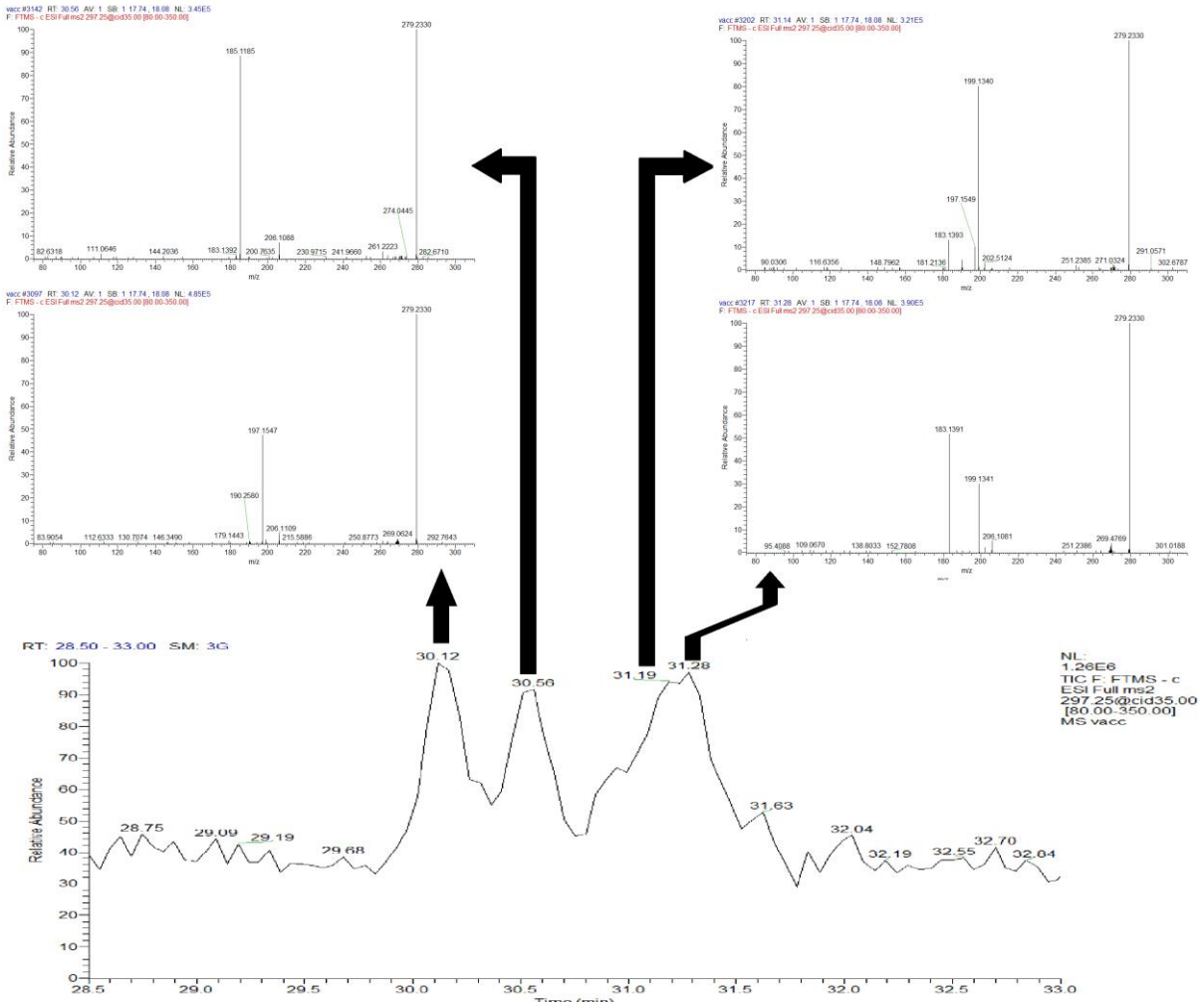

Figure 3-53 Total ion chromatogram & MS^2 spectrometry (LC- MS^2) following collision-induced decomposition of the molecular anion $[M - H^+]^-$ at *m/z* 297 of HO11ME.

The peak at Rt 30.12 min. in TIC LC- MS^2 chromatogram (Figure 3-53) that corresponds to precursor ion LC-MS chromatogram peak at Rt 30.16 min. (Figure 3-52) showed product ion *m/z* 197 which is proposed to be $[C_{12}H_{22}O_2 - H^+]^-$ and could be considered characteristic and linked to 13-Hydroxy octadec-11-enoic acid (13-HO11ME). This fragment ion is proposed to be formed by the same fragmentation mechanism as that of product ion *m/z* 169, which is proposed to be $[C_{10}H_{18}O_2 - H^+]^-$, in 11-HO9ME proposed fragmentation pathway, from oleic acid hydroxides, (Scheme 3-23). This charge remote allylic mechanism that involves retro-ene reaction and double bond migration towards the carboxyl end concludes with a cleavage in the

C11–C12 bond to form a negative product ion *m/z* 197 and leave an aldehyde (neutral species) (Scheme 3-28).

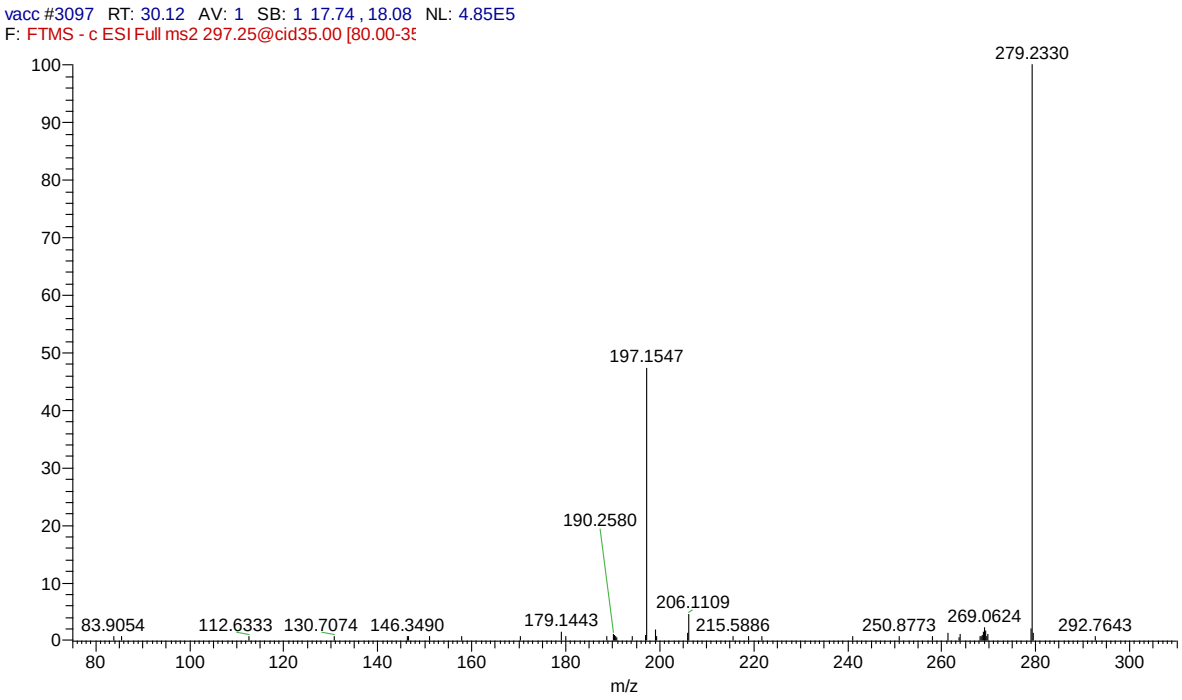

Figure 3-54 MS² spectrum of *m/z* 297.25 ion from octadec-11-enoic acid oxidation sample at Rt 30.12 min.

Table 3-13 The most abundant MS² spectrum ions at Rt 30.12 min. in the TIC LC-MS² chromatogram of the MS-trapped precursor ion of *m/z* 297.25 from reduced octadec-11-enoic acid hydroperoxides sample.

Rt: 30.12		
m/z	**Relative abundance**	**Composition**
279.23	100.00	$C_{18}H_{31}O_2$
197.15	47.25	$C_{12}H_{21}O_2$
206.11	5.94	$C_{16}H_{14}$
279.03	2.07	$C_{16}H_7O_5$
199.13	1.76	$C_{11}H_{19}O_3$

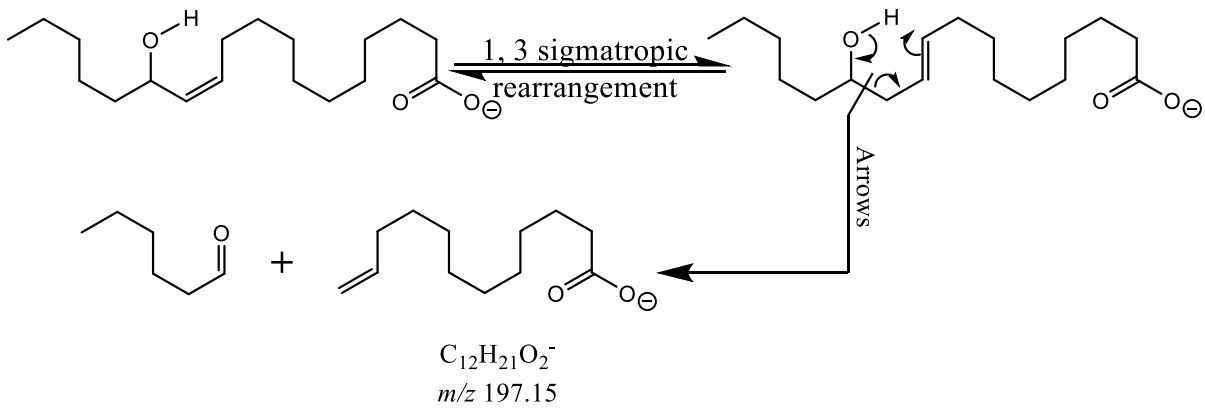

Scheme 3-28 Putative source of product ion *m/z* 197 from 13-HO11ME molecular ion in the MS^2 chromatographic peak at Rt 30.12 min.

The peak at Rt 30.56 min. (Figure 3-55) in TIC LC- MS^2 chromatogram that corresponds to precursor ion LC-MS chromatogram peak at Rt 30.55 min. showed product ion *m/z* 185 which is proposed to be $[C_{10}H_{18}O_3 - H^+]^-$ and could be linked to 10-Hydroxy octadec-11-enoic acid (10-HO11ME) via fragmentation process that matches that of product ion *m/z* 157, proposed to be $[C_{10}H_{18}O_2 - H^+]^-$, in fragmentation pathway 8-HO9ME, from oleic acid hydroxides, (Scheme 3-24). The double bond shift, 1,3 sigmatropic rearrangement, towards the methyl end preceded a retro-ene reaction that caused a cleavage in the C10–C11 bond. (Scheme 3-29).

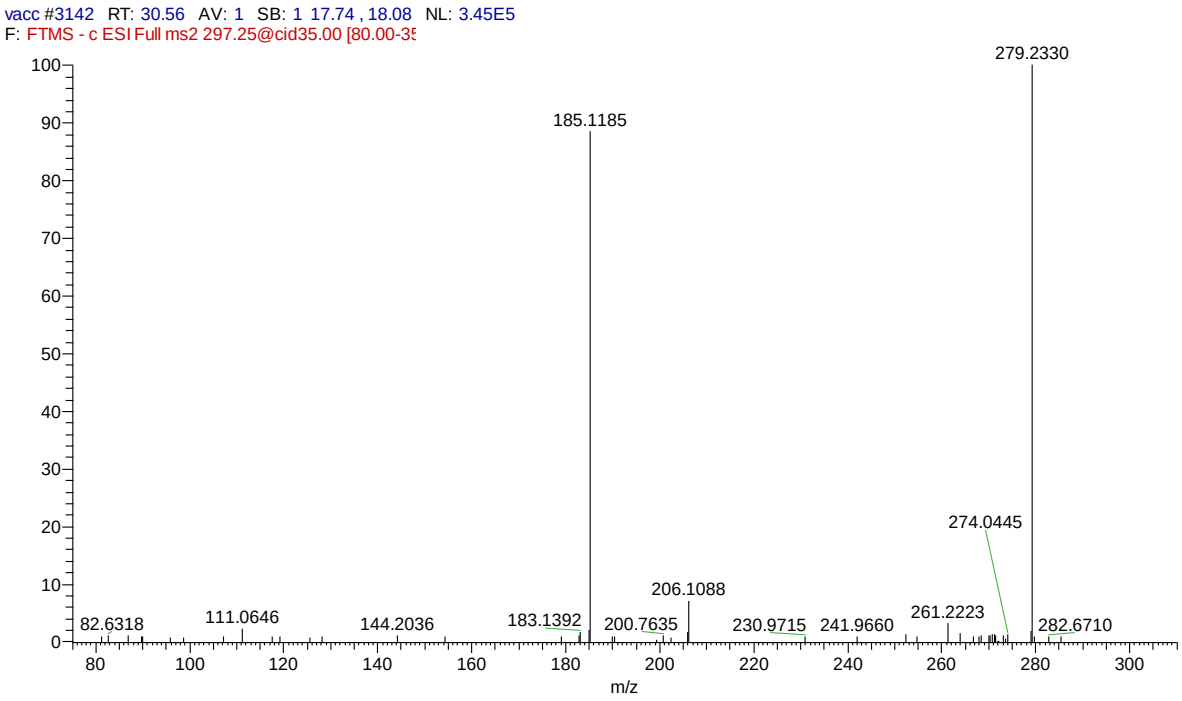

Figure 3-55 MS^2 spectrum of *m/z* 297.25 ion from octadec-11-enoic acid oxidation sample at Rt 30.56 min.

Table 3-14 The most abundant MS^2 spectrum ions at Rt 30.56 min. in the TIC LC-MS^2 chromatogram of the MS-trapped precursor ion of *m/z* 297.25 from reduced octadec-11-enoic acid hydroperoxides sample.

Rt: 30.56		
m/z	**Relative abundance**	**Composition**
279.23	100.00	$C_{18}H_{31}O_2$
185.12	86.93	$C_{10}H_{17}O_3$
206.11	8.95	$C_{16}H_{14}$
261.22	3.19	$C_{18}H_{29}O$
206.09	2.82	$C_{12}H_{14}O_3$

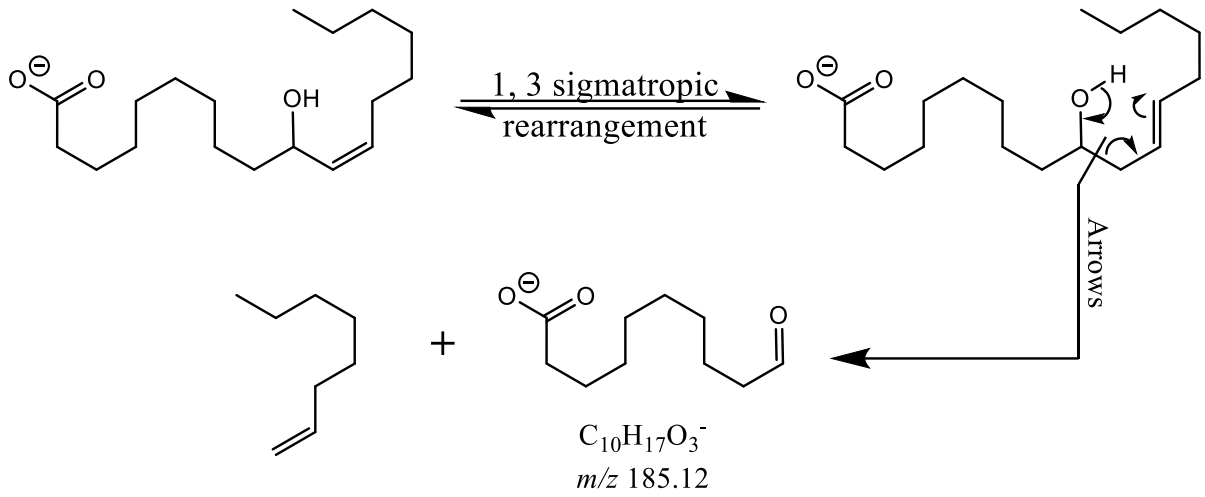

Scheme 3-29 Putative source of product ion *m/z* 185 from 10-HO11ME molecular ion in the MS^2 chromatographic peak at Rt 30.56 min.

The highly abundant product ion *m/z* 199 showed in LC- MS^2 TIC chromatographic peak at Rt 31.19 min. that corresponds to precursor ion LC-MS chromatogram peak at Rt 31.23 min. (Figure 3-56) is proposed to be $[C_{11}H_{20}O_3 - H^+]^-$. This acid-containing aldehyde product ion could be linked to 11-Hydroxy octadec-12-enoic via the charge remote allylic fragmentation pathway mentioned above in the analysis of oleic acid hydroxides to link *m/z* 171 to 9-Hydroxy octadec-10-enoic acid (9-HO10ME) (Scheme 3-25) to cause a cleavage in the C11–C12 bond in this case (Scheme 3-30).

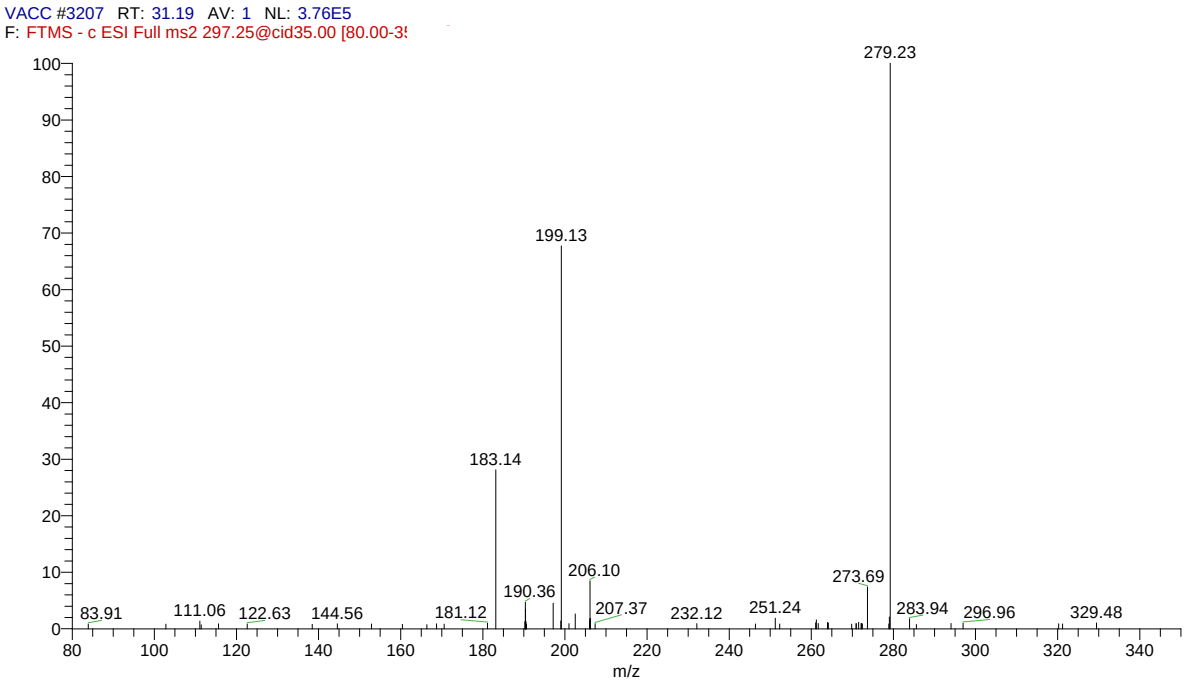

Figure 3-56 MS^2 spectrum of *m/z* 297.25 ion from octadec-11-enoic acid oxidation sample at Rt 31.19 min.

Table 3-15 The most abundant MS^2 spectrum ions at Rt 31.19 min. in the TIC LC-MS^2 chromatogram of the MS-trapped precursor ion of *m/z* 297.25 from reduced octadec-11-enoic acid hydroperoxides sample.

Rt: 31.19		
m/z	**Relative abundance**	**Composition**
279.23	100.00	$C_{18}H_{31}O_2$
199.13	67.71	$C_{11}H_{19}O_3$
183.14	28.09	$C_{11}H_{19}O_2$
206.10	8.47	$C_{12}H_{14}O_3$
197.15	4.50	$C_{12}H_{21}O_2$
279.03	2.07	$C_{16}H_7O_5$

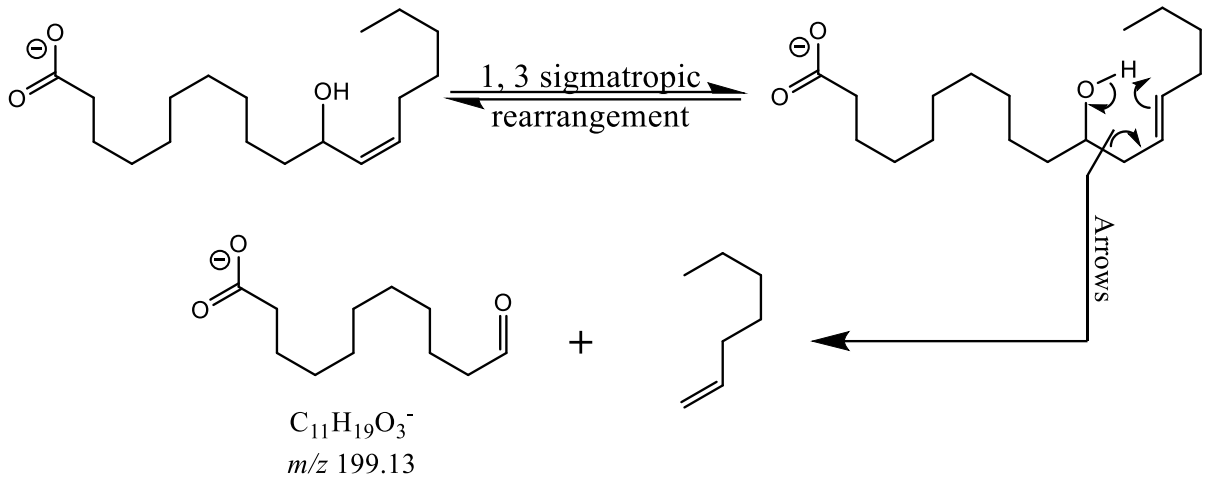

Scheme 3-30 Putative source of product ion *m/z* 199 from 11-HOD12E molecular ion in the MS^2 chromatographic peak at Rt 31.19 min.

Comparably, a cleavage in C9–C10 bond in the carbon chain of 12-Hydroxy octadec-10-enoic acid (12-HOD10E) would generate product ion *m/z* 183 shown in the LC-MS^2 TIC chromatographic peak at Rt 31.28 min. that corresponds to part of precursor ion LC-MS chromatogram peak at Rt 31.23 min. and proposed to be $[C_{11}H_{20}O_2 - H^+]^-$. Once again, the charge remote allylic fragmentation mechanism suggested above in the analysis of oleic acid hydroxides to link a product ion *m/z* 155 to 10-Hydroxy octadec-8-enoic acid (10-HO8ME) (Scheme 3-26) can also be considered to explain scission in the carbon bond vinylic to alcoholic moiety leaving a neutral aldehyde species on the other side of the cleavage (Scheme 3-31).

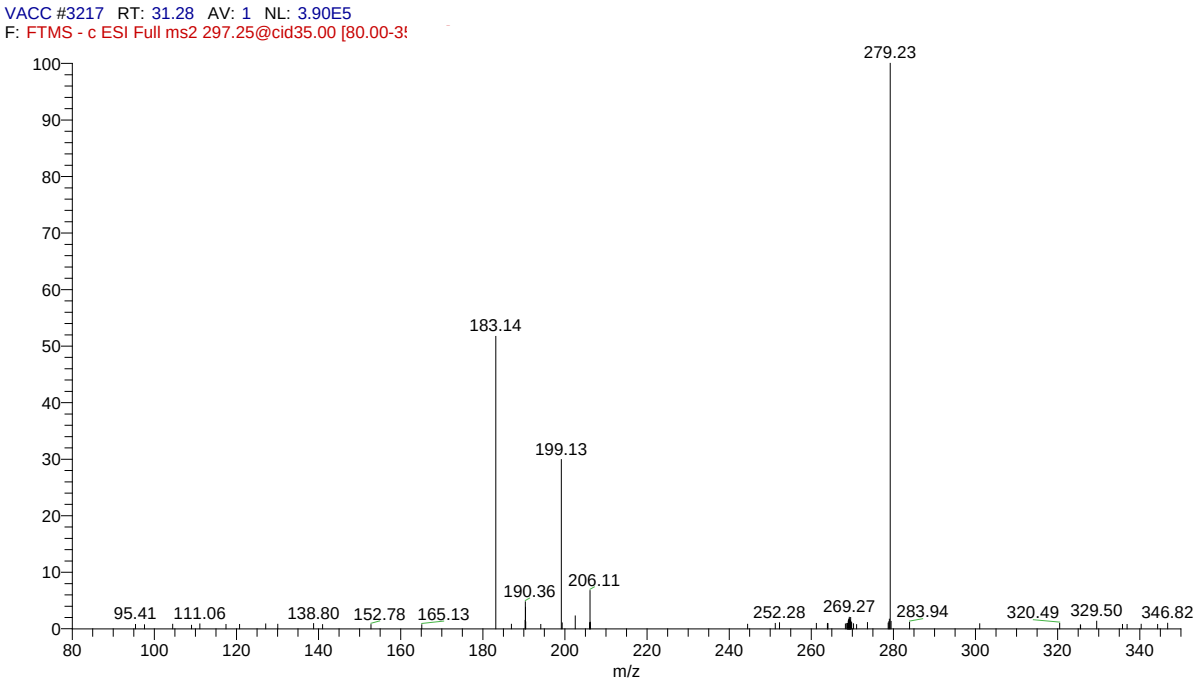

Figure 3-57 MS^2 spectrum of *m/z* 297.25 ion from octadec-11-enoic acid oxidation sample at Rt 31.28 min.

Table 3-16 The most abundant MS^2 spectrum ions at Rt 31.28 min. in the TIC LC-MS^2 chromatogram of the MS-trapped precursor ion of *m/z* 297.25 from reduced octadec-11-enoic acid hydroperoxides sample.

Rt: 31.28		
m/z	**Relative abundance**	**Composition**
279.23	100.00	$C_{18}H_{31}O_2$
183.14	51.71	$C_{11}H_{19}O_2$
199.13	29.93	$C_{11}H_{19}O_3$
206.11	6.75	$C_{16}H_{14}$
206.09	2.17	$C_{12}H_{14}O_3$
269.27	2.03	$C_{18}H_{37}O$

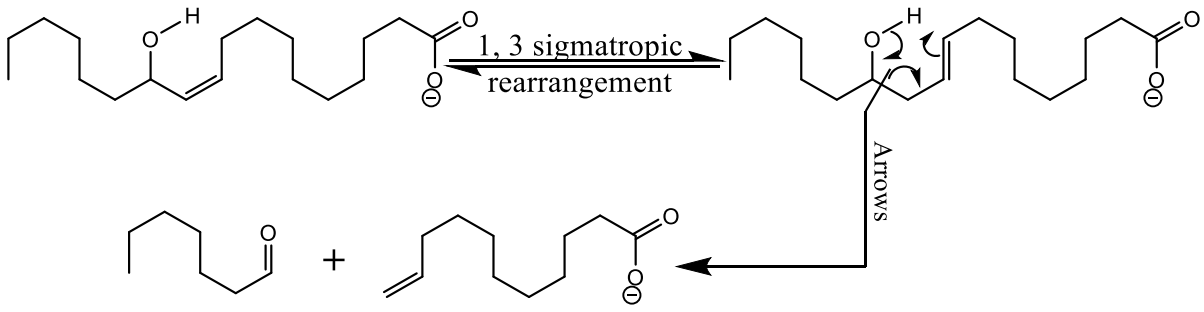

Scheme 3-31 Putative source of product ion *m/z* 183 from 12-HO10ME molecular ion in the MS^2 chromatographic peak at Rt 32.81 min.

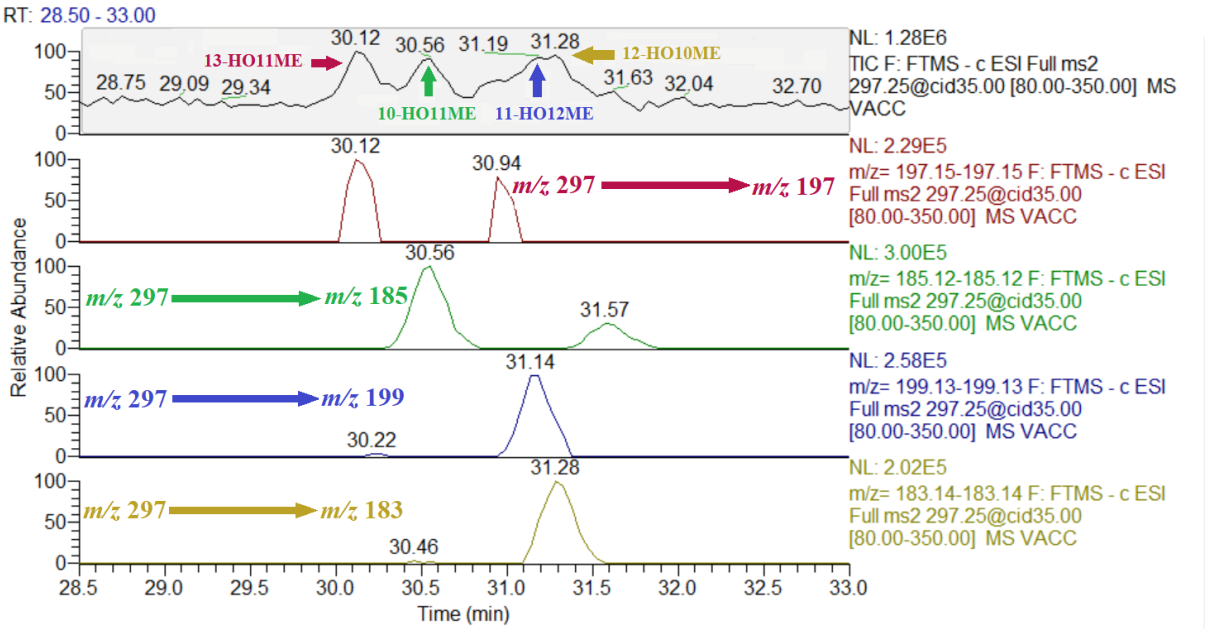

Figure 3-58 Mass range chromatogram of *m/z* 297 & mass spectra of precursor-product transitions *m/z* 297 to 197, 185, 199, and 183 specified for each hydroxy regioisomer in liquid chromatography- MS^2 spectrometry (LC-MS^2) analysis of reduced octadec-11-enoic acid hydroperoxides sample.

3.6 Discussion of hydroxy mono-unsaturated fatty acids analysis as a tool for double bond position determination

The CID of the hydroxides for oleic acid (*m/z* 297.2) produces four major fragments, one abundant ion for each positional isomer, via a fragmentation pathway that includes a single 1,3 sigmatropic rearrangement, double bond migration, that shifts the allylic double bond away from the hydroxy functional group to become in the homoallylic position relative to it and facilitates another rearrangement reaction, a retro-ene reaction, that involves the hydroxyl functional group and the double bond (Scheme 3-32). The characteristic fragment ions include ions at *m/z* 157.1, 171.1, 155.1, and 169.1 (Figure 3-51). All product ions carry a negative charge at the carboxyl group and are generated via fragmentation of each hydroxide regioisomer molecular ion in the same mechanism but with two different species of fragment ions (Schemes 3-23, 3-24, 3-25 and 3-26). For one fragmentation channel, an aldehyde group was generated at the distal end in ionised fragments as for ions at *m/z* 157.1 and 171.1, and in the other complementary fragmentation channel, an ethylene group was formed at the site of cleavage in the fragment ions via the same intramolecular hydrogen transfer as for the

ions at *m/z* 155.1, and 169.1. Therefore, four diagnostic fragment ions for each mono-unsaturated fatty acid can be detected and they can be used to accurately pinpoint the double bond location.

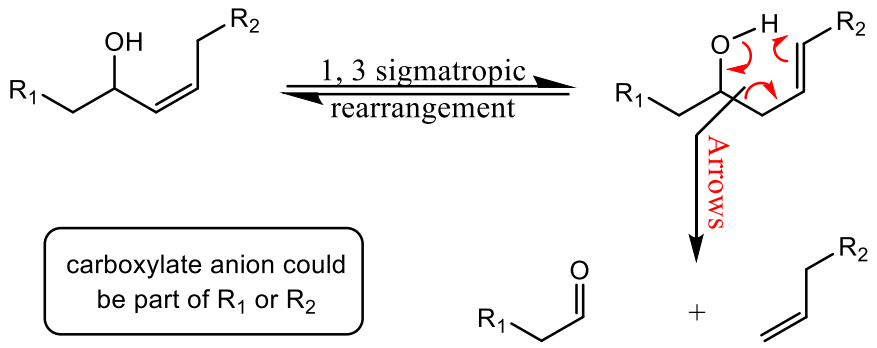

Scheme 3-32 Charge-remote allylic fragmentation in hydroxy MUFAs.

To assess the adaptability of the strategy of auto-oxidation combined with MS^2 spectrometry for double bond localisation toward other mono-unsaturated fatty acids, vaccenic acid (FA 18:1) was selected, and MS^2 analysis of the hydroxides yielded diagnostic ions similar to those observed for oleic acid. The behaviour of different monounsaturated hydroxy fatty acids (18:1 FA) in LC-MS was identical. Figures (3-46 and 1-53) show that collisional activation of the $[M - H^+]^-$ from monounsaturated hydroxy fatty acids led to neutral loss of H_2O as a fragment ion. Contrary to the case in hydroperoxy fatty acids, the dehydrated fragment ion was not observed in mass range chromatograms before collisional activation.

Vaccenic acid has the same chain length as oleic acid, and both contain one double bond, albeit at different locations. However, as the double bond in octadec-11-enoic acid (Vaccenic acid, FA 18:1 (n−7)) is two more carbons away from the carboxylic group than octadec-9-enoic acid (Oleic acid, FA 18:1 (n−9)), the diagnostic ions for the hydroxides of octadec-11-enoic acid were 28 Da higher in mass (*m/z* 185, 199, 183, and 197 vs 157, 171, 155, and 169) than those of octadec-9-enoic acid.

In contrast with the epoxidation of unsaturated lipid isomers, which can generate two characteristic ions only (Y. Zhao et al., 2017), autooxidation strategy can generate four characteristic ions at the same time. Therefore, the strategy reported in this work is more specific for the identification of MUFAs isomers. The other analytical advantages that should make this method accessible and attractive to many laboratories

include the easiness of interpretation of mass spectra, the simplicity of experimental setup for reactions, the absence of the necessity of mass spectrometry instrument modifications and the low costs as derivatising reagents (auto-oxidation initiator and reduction agent) are inexpensive.

3.7 Analysis of hydroxy Poly-unsaturated fatty acids

3.7.1 Analysis of Linoleic acid hydroxides

3.7.1.1 Hydroxide formation

Chemical reduction of the isomeric conjugated Linoleic acid hydroperoxides would result in the formation of mixture of two hydroxides that have their functional OH groups on the exact same carbons of the acyl chain (C9 and C13) as in their hydroperoxyl precursors (Scheme 3-33). The reduction process proceeds in the same mechanism reported in the case of MUFAs (Schemes 3-22 & 3-27). Accordingly, the ensuing isomers are:

9-hydroxyoctadeca-10, 12-dienoic acid (9-HO10,12DE)

13-hydroxyoctadeca-9, 11-dienoic acid (13-HO9,11DE)

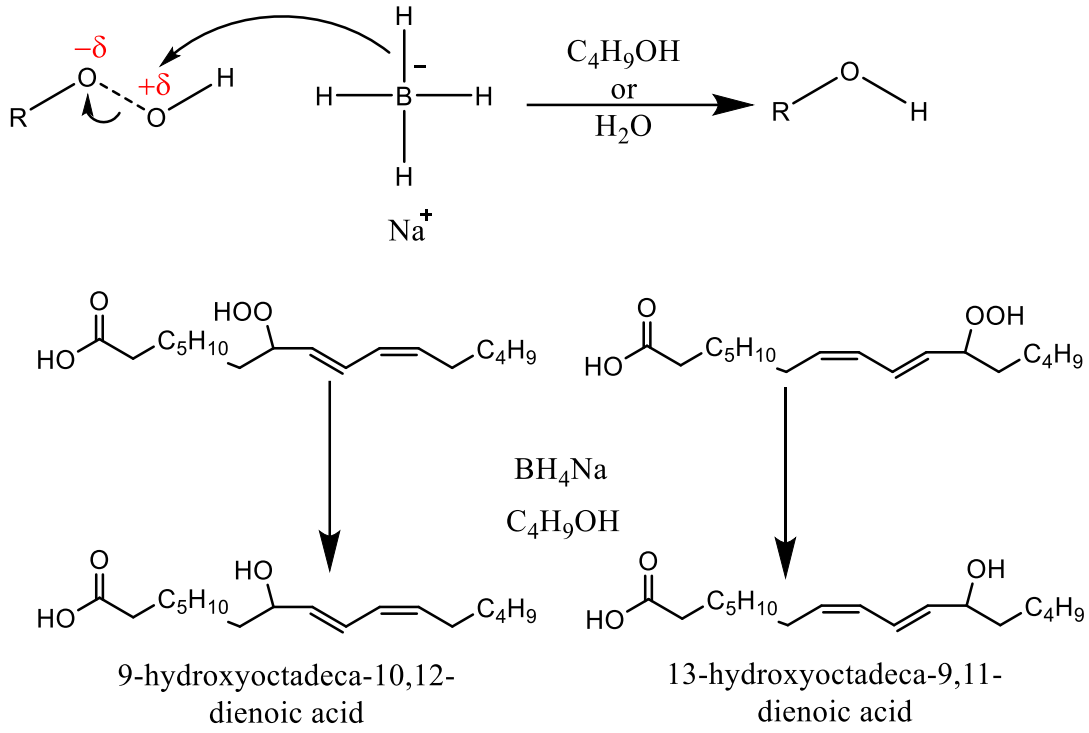

Scheme 3-33 purposed reaction scheme for reduction of Linoleic acid hydroperoxides to hydroxides via NaBH4 nucleophilic attack

3.7.1.2 LC-MS analysis of Linoleic acid hydroxides

Preliminary LC-MS analyses of chemically reduced octadeca-9,12-dienoic acid hydroxides (9-HO10,12DE and 13-HO9,11DE) showed two isomeric peaks in the parent ion Mass range chromatogram, corresponding to two expected regioisomeric hydroxide derivatives of linoleic acid. For both studied species, little or no characteristic fragmentation was observed. As was the case in the hydroxides of MUFAs, no peak for dehydrated fragment ion $[M - (H^+ + H_2O)]^-$ was observed in both spectra of hydroxides species obtained from mass range chromatogram of $[M - H^+]^-$ (Figure 3-59).

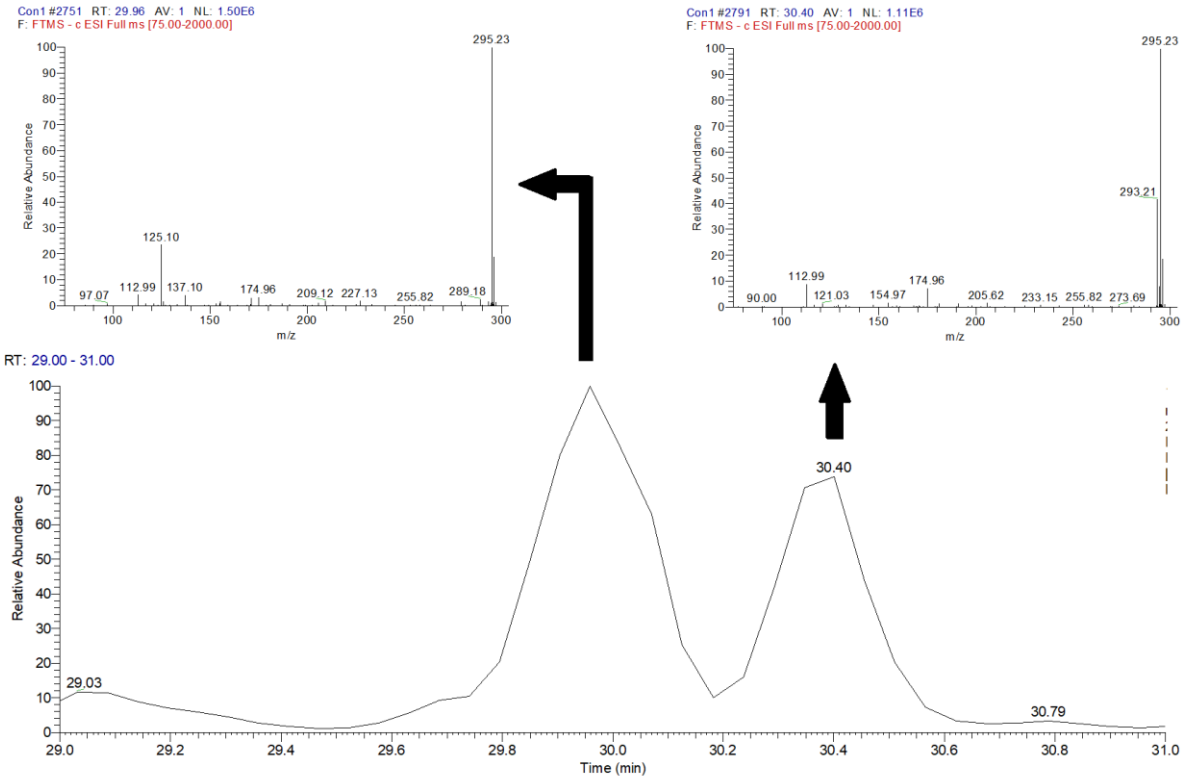

Figure 3-59 Mass range chromatogram & mass spectra of ions of *m/z* 311 in liquid chromatography- mass spectrometry (LC-MS) analysis of reduced octadeca-9,12-dienoic acid hydroperoxides sample.

Product ion spectra obtained of $[M - H^+]^-$ precursor ions derived from linoleic acid hydroxide isomers via further investigations using MS^2 spectrometry showed neutral loss of water, $[M - (H^+ + H_2O)]^-$ at *m/z* 277, to be the most abundant product ion peaks in both octadeca-9,12-dienoic acid hydroxyl isomers (HO9,12DEs) MS^2 spectra. Additionally, each isomeric peak showed a distinctive fragmentation pattern (Figure 3-60).

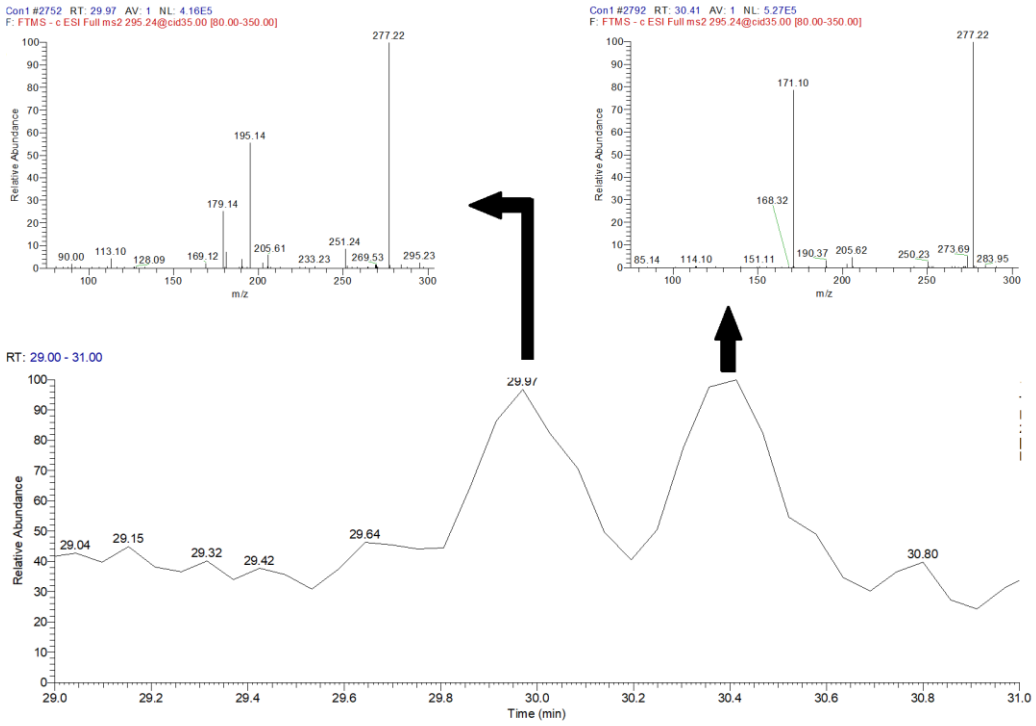

Figure 3-60 Total ion chromatogram & MS^2 spectrometry (LC- MS^2) following collision-induced decomposition of the molecular anion $[M - H]^-$ at *m/z* 295 derived from HOD9,12D.

The peak at Rt 29.97 min. in the TIC LC- MS^2 chromatogram that corresponds to precursor ion LC-MS chromatogram peak at Rt 29.96 min. (Figure 3-61) showed a highly abundant product ion, the most abundant aside from $[M - (H^+ + H_2O)]^-$, that can be considered characteristic and could be linked to 13-hydroxy-9, 11-octadecadienoic acid (13-HO9,11DE) having a mass of *m/z* 195 which is proposed to be $[C_{12}H_{20}O_2 - H^+]^-$ and to be formed by the charge remote allylic fragmentation mechanism suggested above as the pathway responsible for the generation of all characteristic product ions in all spectra of the regioisomer chromatographic peaks of MUFAs hydroxides. The fragmentation pathway necessitates a shift of the conjugated diene system, 1,5 sigmatropic proton rearrangement, to accommodate the nearest double bond into the homoallylic position, towards the carboxyl end in this case, facilitating a retro-ene reaction that cleaves carbon bond C10–C11 vinylic to hydroxy functional group and produces an aldehyde (neutral species) in the process (Scheme 3-34).

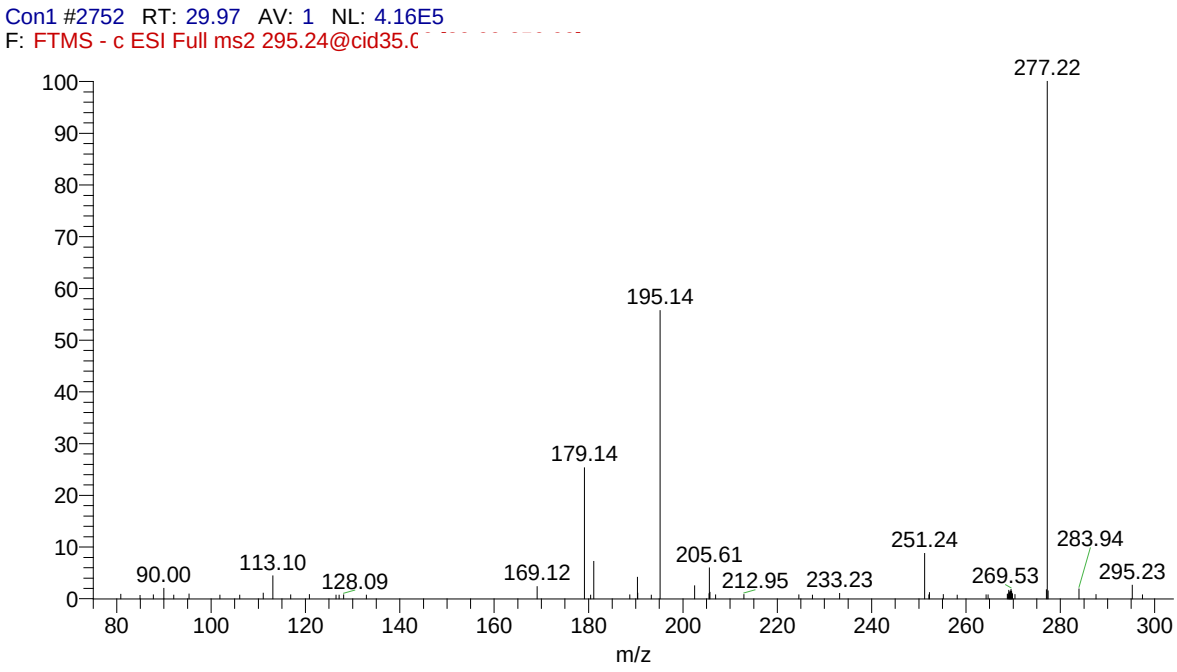

Figure 3-61 MS^2 spectrum of *m/z* 295.24 ion reduced octadeca-9,12-dienoic acid hydroperoxides sample at Rt 29.97 min.

Table 3-17 The most abundant MS^2 spectrum ions at Rt 29.97 min. in the TIC LC-MS^2 chromatogram of the MS-trapped precursor ion of *m/z* 295.23 from reduced octadeca-9,12-dienoic acid hydroperoxides sample.

Rt: 29.97		
m/z	**Relative abundance**	**Composition**
277.22	100.00	$C_{18}H_{29}O_2$
195.14	55.69	$C_{12}H_{19}O_2$
179.14	25.30	$C_{12}H_{19}O$
251.24	8.75	$C_{17}H_{31}O$
181.12	7.22	$C_{11}H_{17}O_2$
113.10	4.40	$C_7H_{13}O$

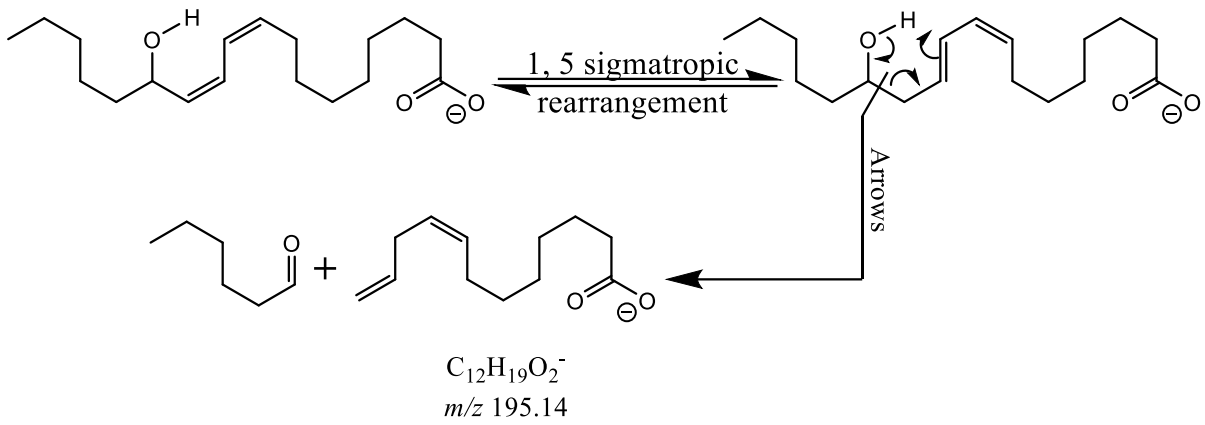

Scheme 3-34 Putative source of product ion *m/z* 195 from 13-HO9,11DE molecular ion in the MS^2 chromatographic peak at Rt 29.97 min.

The highly abundant product ion *m/z* 171 showed in LC- MS^2 TIC chromatographic peak at Rt 30.41 min. that corresponds to precursor ion LC-MS chromatogram peak at Rt 30.40 min. (Figure 3-62) is proposed to be acid-containing aldehyde product ion $[C_9H_{16}O_3- H^+]^-$. It could be considered characteristic to 9-hydroxy-10, 12-octadecadienoic acid (9-HO10,12DE) and can be generated via the charge remote allylic fragmentation pathway mentioned above to link *m/z* 195 to 13-hydroxy-9, 11-octadecadienoic acid 13-HO9,11DE, except that conjugated diene system would shift towards the Methyl end in this case to cause a cleavage in C9–C10 bond and the characteristic product ion would contain the resulting aldehyde group (Scheme 3-35).

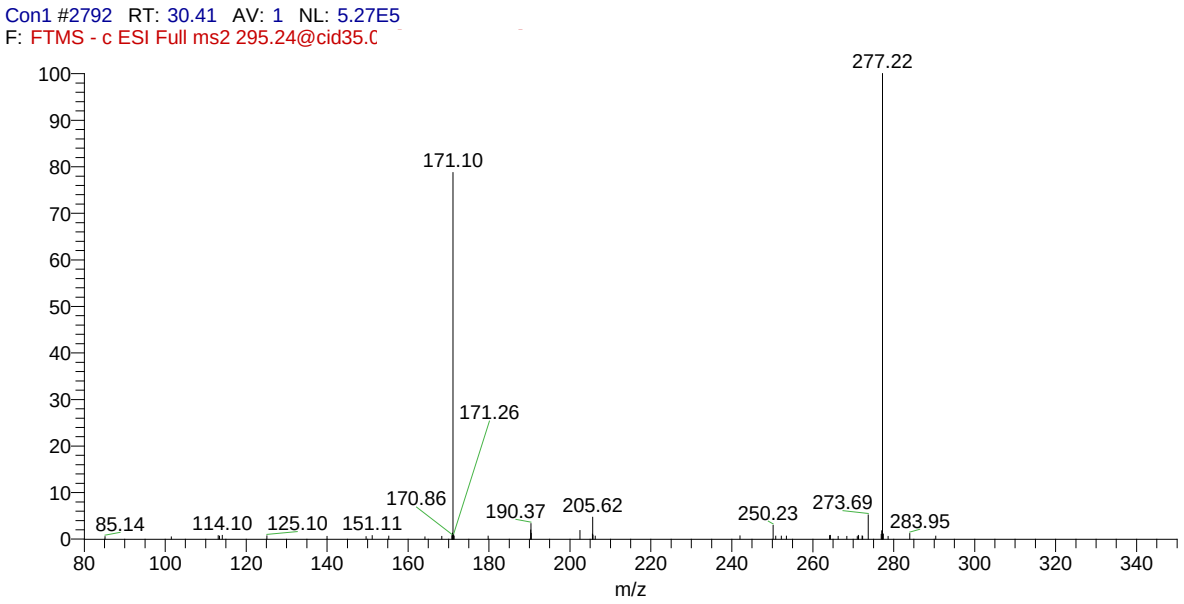

Figure 3-62 MS^2 spectrum of *m/z* 295.24 ion reduced octadeca-9,12-dienoic acid hydroperoxides sample at Rt 30.41 min.

Table 3-18 The most abundant MS^2 spectrum ions at Rt 30.41 min. in the TIC LC-MS^2 chromatogram of the MS-trapped precursor ion of *m/z* 295.23 from reduced octadeca-9,12-dienoic acid hydroperoxides sample.

Rt: 30.41		
m/z	**Relative abundance**	**Composition**
277.22	100.00	$C_{18}H_{29}O_2$
171.10	78.71	$C_9H_{15}O_3$
250.23	2.91	$C_{17}H_{30}O$
277.02	1.79	$C_{16}H_5O_5$
171.01	1.27	$C_{10}H_3O_3$

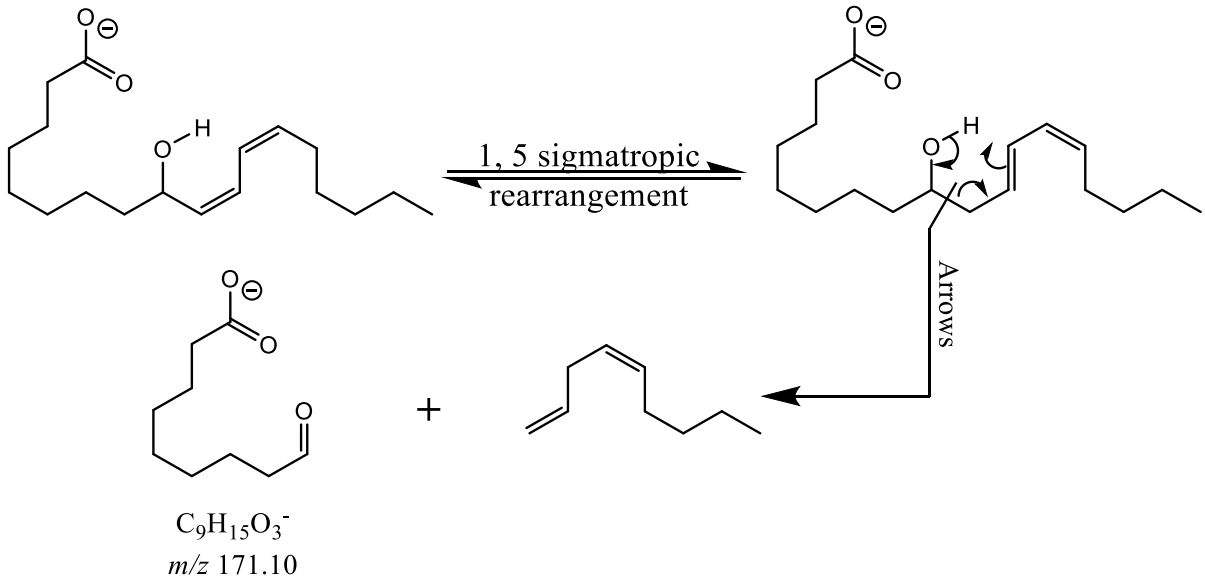

Scheme 3-35 Putative source of product ion *m/z* 171 from 9-HO10,12DE molecular ion in MS^2 chromatographic peak at Rt 30.41 min.

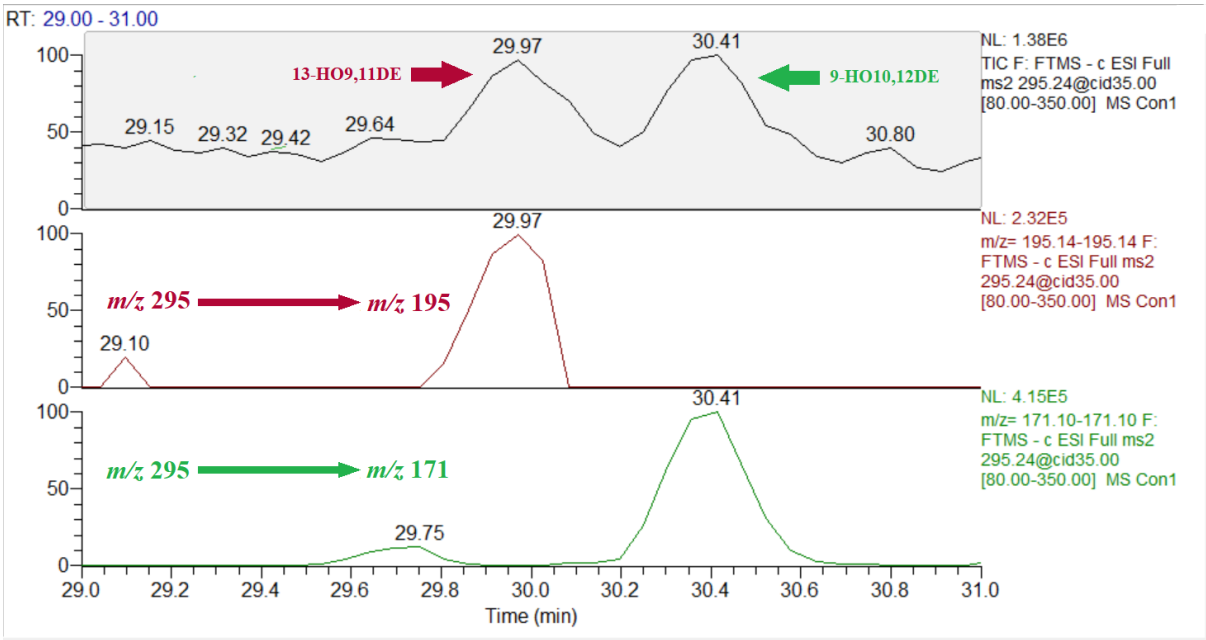

Figure 3-63 Mass range chromatogram of *m/z* 295 & mass spectra of precursor-product transitions *m/z* 295 to 195 and 171 specified for each hydroxy regioisomer in liquid chromatography- MS^2 spectrometry ($LC\text{-}MS^2$) analysis of reduced octadec-9,12-dienoic acid hydroperoxides sample.

3.7.2 Analysis of α-Linolenic acid hydroxides

3.7.2.1 Hydroxide formation

(Scheme 3-36) shows the chemical reduction of the hydroperoxyl derivatives of octadeca-9,12,15-trienoic acid (α-Linolenic acid, FA 18:3 (n-3)) into their consequent hydroxides with functional OH groups located on the exact same carbons on the acyl chain (C9, C12, C13 and C16) by the same mechanism reported in the case of MUFAs and octadeca-9,12-dienoic acid (Linoleic acid, FA 18:2 (n−6)). Thus, the following hydroxy isomers will be formed:

9-hydroxyoctadeca-10, 12, 15-trienoic acid (9-HO10,12,15TE)

12-hydroxyoctadeca-9, 13, 15-trienoic acid (12-HO9,13,15TE)

13-hydroxyoctadeca-9, 11, 15-trienoic acid (13-HO9,11,15TE)

16-hydroxyoctadeca-9, 12, 14-trienoic acid (16-HO9,12,14TE)

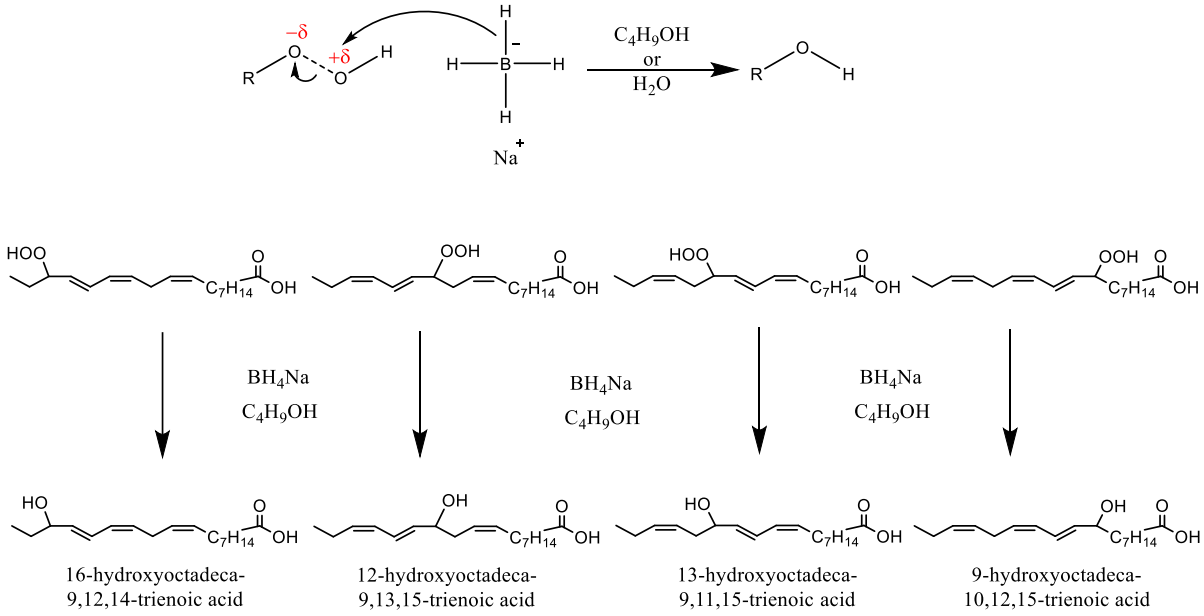

Scheme 3-36 purposed reaction scheme for reduction of Linolenic acid hydroperoxides to hydroxides via NaBH4 nucleophilic attack

3.7.2.2 LC-MS analysis of α-Linolenic acid hydroxides

Mass range chromatograms of hydroxyl derivatives of octadeca-9,12,15-trienoic acid (α-Linolenic acid, FA 18:3 (n-3)) samples (OD9,12,15TA) generated by secondary decomposition of HpO9,12,15TE isomers showed two peaks for the expected four isomers ensuing from previously determined hydroperoxide derivatives of octadeca-

9,12,15-trienoic acid which suggested the occurrence of co-elution within those peaks. The isomer peaks spectra did not contain any distinctive structural information that could be used for structure elucidation. The dehydration product ions $[M - (H^+ + H_2O)]^-$ *m/z* 275 showed low abundance in mass range chromatogram of $[M - H^+]^-$ (Figure 3-64).

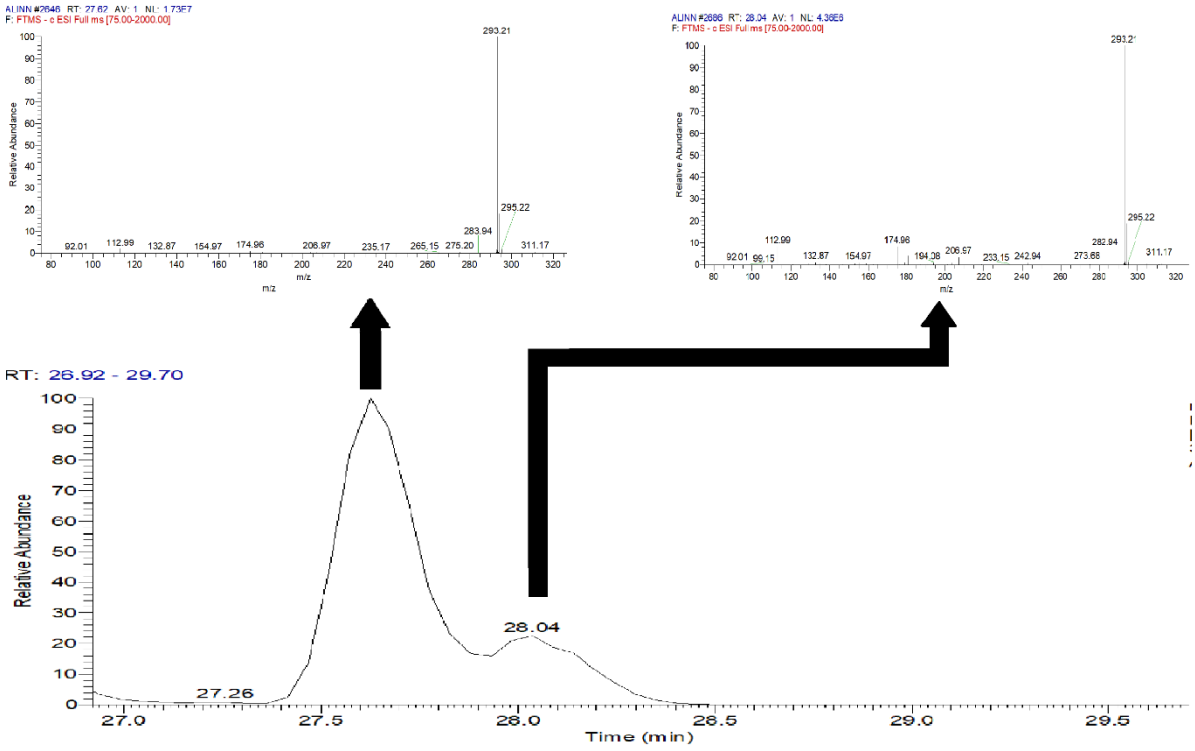

Figure 3-64 Mass range chromatogram & mass spectra of ions of *m/z* 293 in liquid chromatography- mass spectrometry (LC-MS) analysis of reduced octadeca-9,12,15-trienoic acid hydroperoxides sample.

MS^2 analysis was performed on hydroxy octadeca-9,12,15-trienoic acid molecular ions to reach better understanding of peaks in the mass range chromatogram of hydroxide isomers. As the resultant MS^2 spectra showed, four distinctive fragmentation patterns were recognised within observed chromatographic peaks which confirmed the coelution of two isomeric derivatives within each chromatographic peak. All fragmentation patterns showed neutral loss of water, $[M - (H^+ + H_2O)]^-$, with the dehydrated product ion *m/z* 275 as the highest abundance peak (Base peak) in all hydroxy octadeca-9,12,15-trienoic acid isomers (HO9,12,15TEs) MS^2 spectra (Figure 3-65).

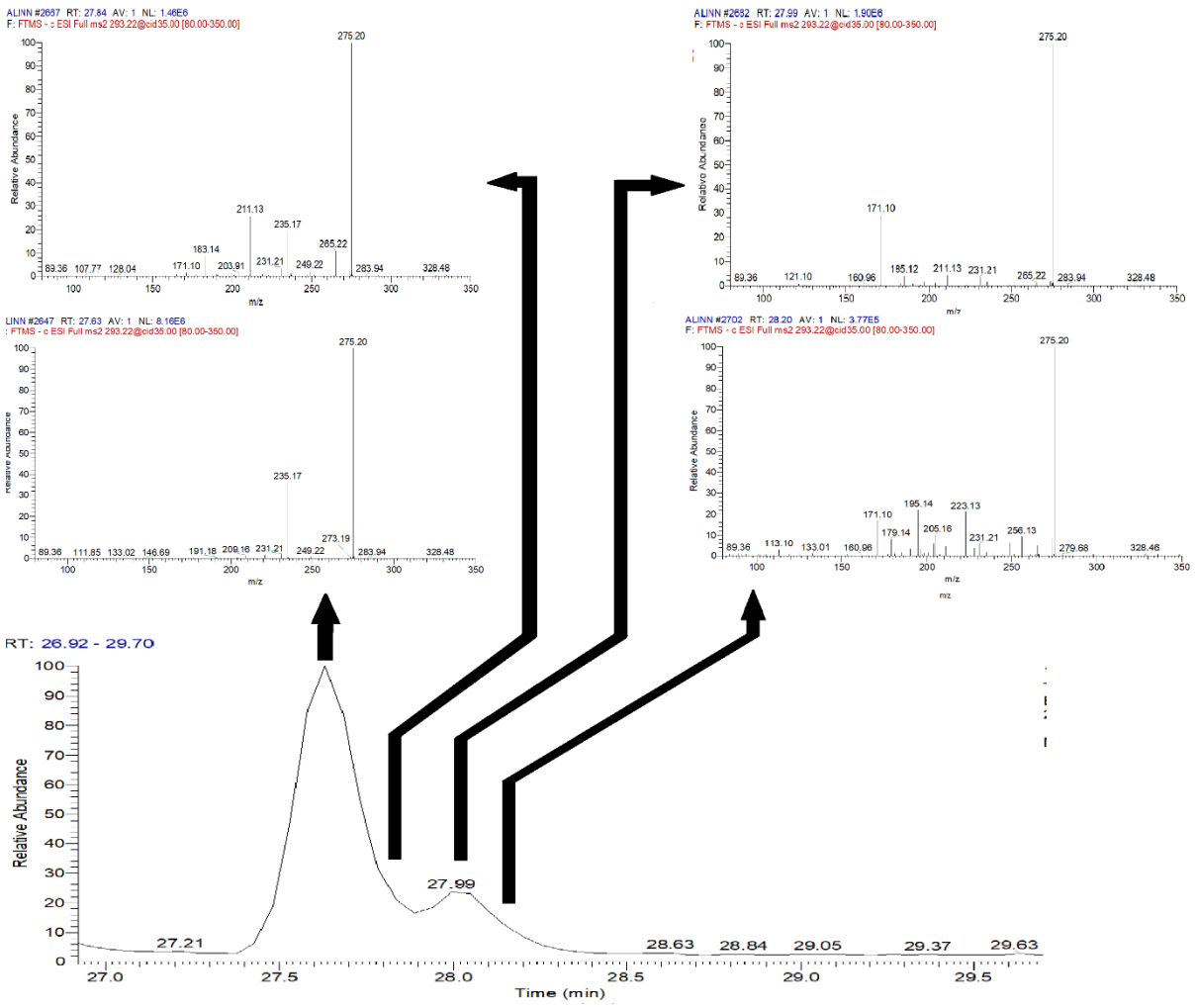

Figure 3-65 Total ion chromatogram & MS^2 spectrometry (LC-MS-MS) following collision-induced decomposition of the molecular anion [M – H+]- at *m/z* 293 of HO9,12,15TE.

The peak at Rt 27.63 min. in the TIC LC- MS^2 chromatogram that corresponds to precursor ion LC-MS chromatogram peak at Rt 27.62 min. (Figure 3-66) contained two characteristic fragments that could be linked to 16-hydroxyoctadeca-9, 12, 14-trienoic acid (16-HO9,12,14TE): one at *m/*z 219 and proposed to be $[C_{15}H_{24}O- H^+]^-$ and to be formed by dehydration of *m/*z 237, $[C_{15}H_{26}O_2- H^+]^-$, which in turn is a result of cleavage of C15–C16 bond adjacent to the hydroxide group after proton shift towards methyl end followed by keto-enol tautomerization and the other one at *m/z* 221 and proposed to be $[C_{14}H_{22}O_2- H^+]^-$ that would be a result of charge remote vinylic fragmentation preceded by migration of the two conjugated double bonds in a 1, 5-sigmatropic shift towards the carboxylic end as described in (Scheme 3-37).

The formation of the most abundant fragment ion, aside from the dehydrated molecular fragment ion, at *m/z* 235 which is proposed to be $[C_{15}H_{24}O_2 - H^+]^-$ can be a result of the charge remote allylic fragmentation mechanism suggested above as the pathway responsible for the generation of all characteristic product ions in all spectra of regioisomer chromatographic peaks of MUFAs hydroxides and linoleic acid hydroxides. The retro-ene reaction that cleaves carbon bond C15–C16 vinylic to hydroxy functional group and produces an aldehyde (neutral species) in the process is preceded by 1,5 sigmatropic proton rearrangement to shift conjugated diene system between C12 and C15 towards the carboxyl end into position between C11 and C14 rendering the nearest double bond into the homoallylic position relative to hydroxy functional group, C13-C14. Moreover, the fragment at *m/z* 209 which is proposed to be $[C_{13}H_{22}O_2 - H^+]^-$ might result from further cleavage at the C13-C14 bond of fragment ion *m/z* 235.

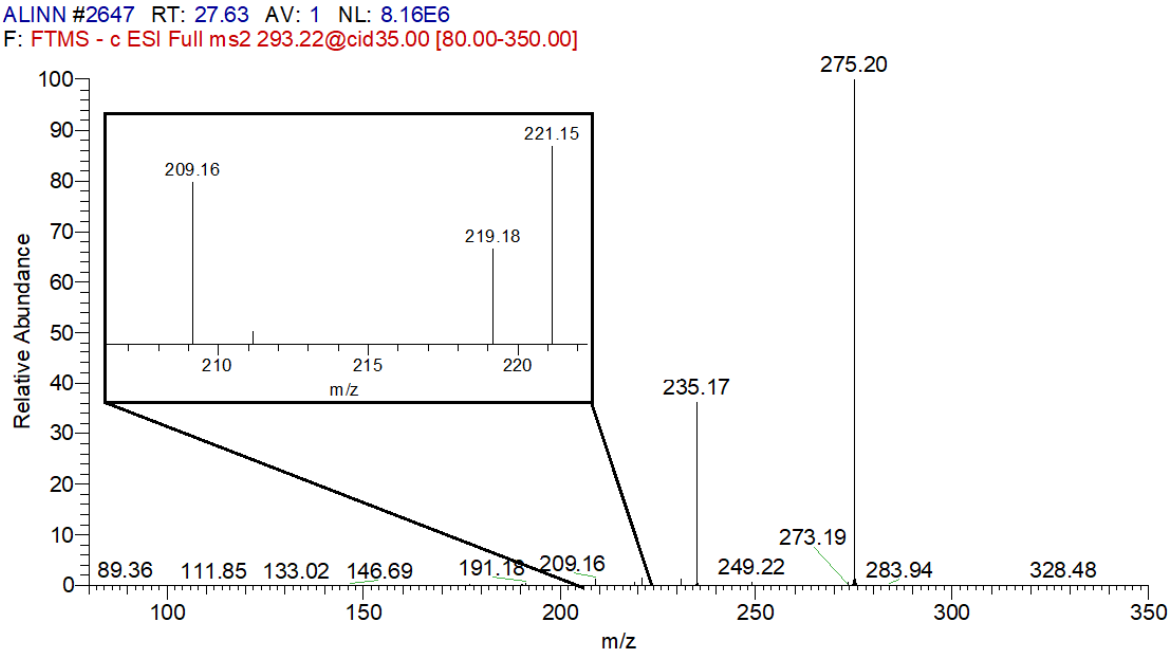

Figure 3-66 MS² spectrum of linolenic acid hydroxide molecular ion of *m/z* 293.22 from reduced linolenic acid hydroperoxides sample at Rt 27.63 min.

Table 3-19 The most abundant MS² spectrum ions at Rt 27.63 min. in the TIC LC-MS² chromatogram of the MS-trapped precursor ion of *m/z* 293.21 from reduced octadeca-9,12,15-trienoic acid hydroperoxides sample.

Rt: 27.63

m/z	Relative abundance	Composition
275.20	100.00	$C_{18}H_{27}O_2$
235.17	36.17	$C_{15}H_{23}O_2$
231.21	1.92	$C_{17}H_{27}$
221.15	1.63	$C_{14}H_{21}O_2$
209.16	1.34	$C_{13}H_{21}O_2$
219.18	0.78	$C_{15}H_{23}O$

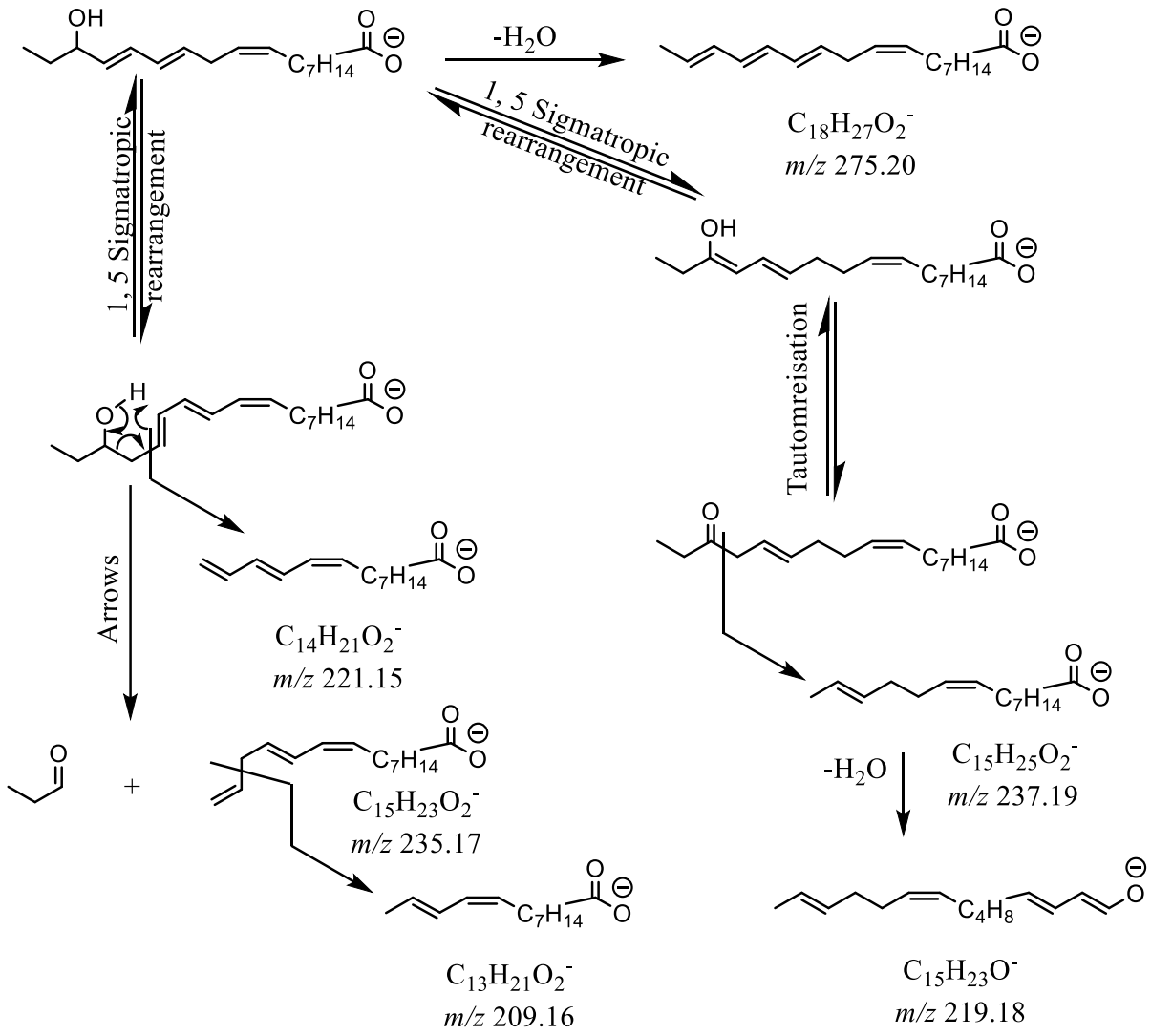

Scheme 3-37 Putative sources of product ions with characteristic significance from 16-HO9,12,14TE molecular ion in MS^2 chromatographic peak at Rt 27.63 min.

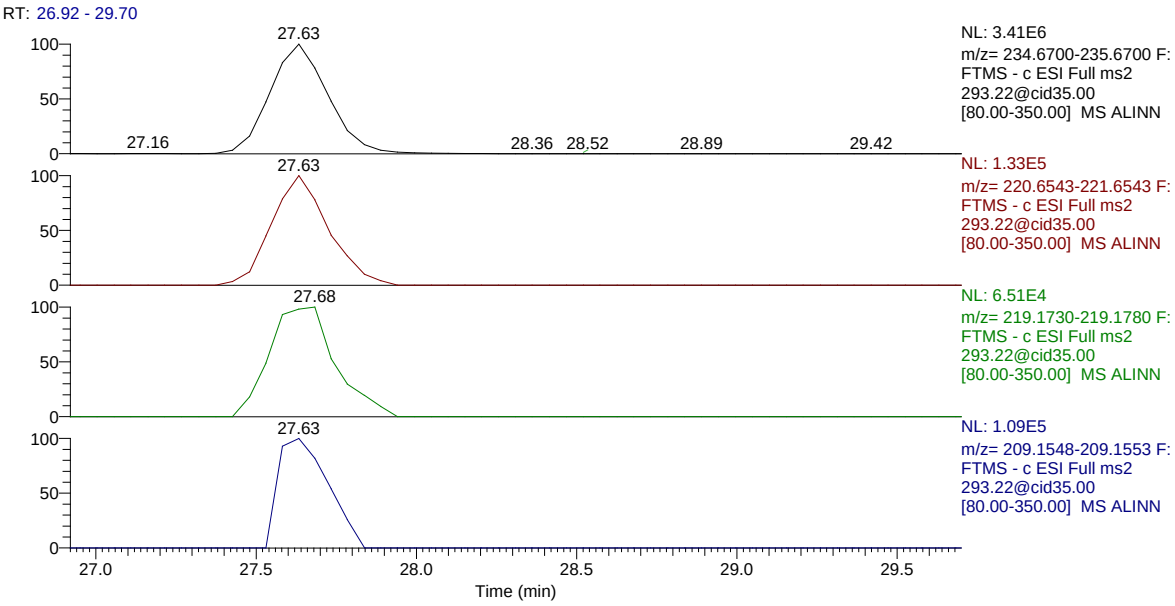

Figure 3-67 Selective mass range- chromatograms of characteristic MS^2 generated product ions (*m/z* 235, *m/z* 221, *m/z* 219 and *m/z* 209) linked to 16-HO9,12,14TE from reduced octadeca-9,12,15-trienoic acid hydroperoxides sample.

Fragment ions that can be considered characteristic for the 12-regioisomer were observed at Rt 27.84 min. in the TIC LC- MS^2 chromatogram (Figure 3-68) that does not correspond to any distinct peak in precursor ion LC-MS chromatogram peak which advocates the coelution with 16-regioisomer at Rt 27.62 min. The product ion at *m/z* 211 which is proposed to be $[C_{12}H_{20}O_3 - H^+]^-$ could be a result of the terminal aldehyde-forming a rearrangement that led to a charge remote allylic cleavage at the C12–C13 bond preceded by migration of both conjugated double bonds in a 1, 5-sigmatropic shift towards methyl end as described (Scheme 3-38). The other characteristic product ion, *m/z* 183 which is proposed to be $[C_{11}H_{20}O_2 - H^+]^-$, could be a result of the same charge remote allylic pathway that conduce to a scission in C11-C12 bond which is adjacent to the other side of alcoholic moiety and allylic to the isolated double bond in the carbon chain of 12-hydroperoxyoctadeca-9, 13, 15-trienoic acid. Except that, in this case, terminal aldehyde would be formed from ensuing neutral species (Scheme 3-38).

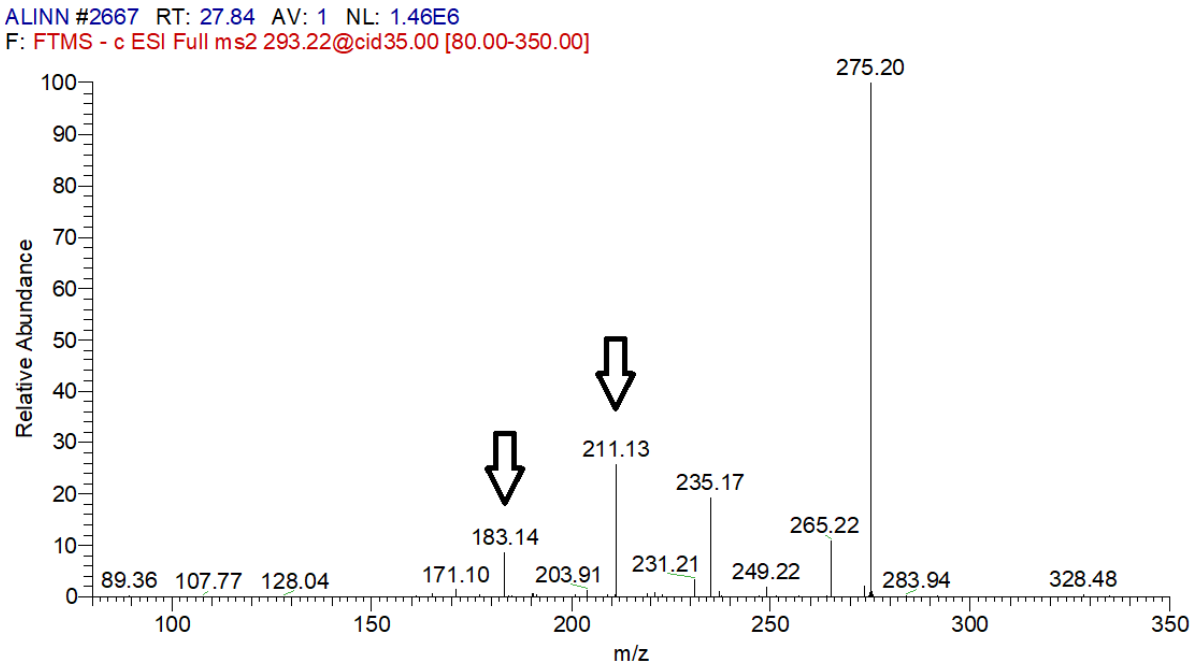

Figure 3-68 MS² spectrum of linolenic acid hydroxide molecular ion of *m/z* 293.22 from reduced linolenic acid hydroperoxides sample at Rt 27.84 min.

Table 3-20 The most abundant MS² spectrum ions at Rt 27.84 min. in the TIC LC-MS² chromatogram of the MS-trapped precursor ion of *m/z* 293.21 from reduced octadeca-9,12,15-trienoic acid hydroperoxides sample.

Rt: 27.84		
m/z	**Relative abundance**	**Composition**
275.20	100.00	$C_{18}H_{27}O_2$
211.13	25.72	$C_{12}H_{19}O_3$
235.17	19.30	$C_{15}H_{23}O_2$
265.22	11.01	$C_{17}H_{29}O_2$
183.14	8.82	$C_{11}H_{19}O_2$
231.21	3.45	$C_{17}H_{27}$

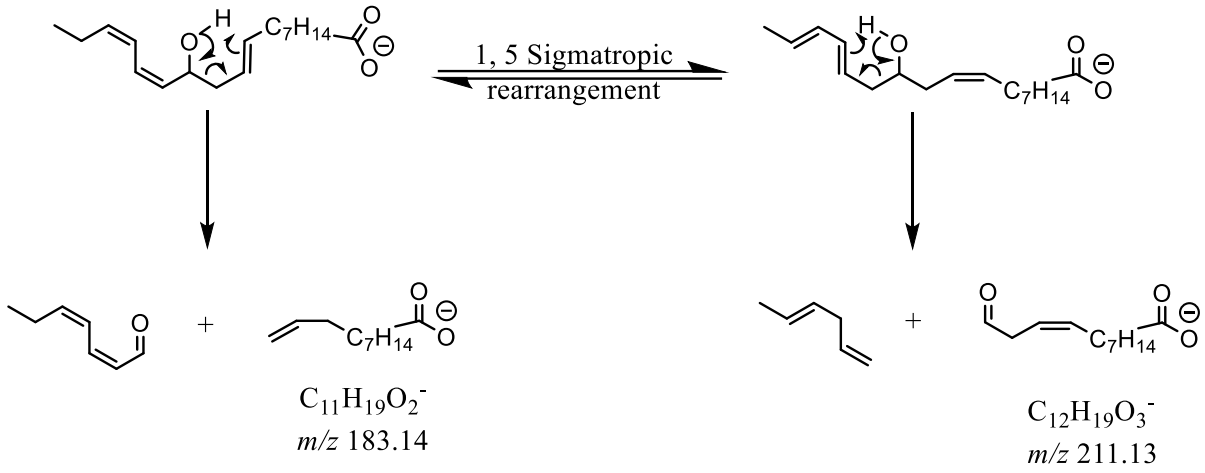

Scheme 3-38 Putative sources of product ions with characteristic significance from 12-HO9,13,15TE molecular ion in the MS^2 chromatographic peak at Rt 27.84 min.

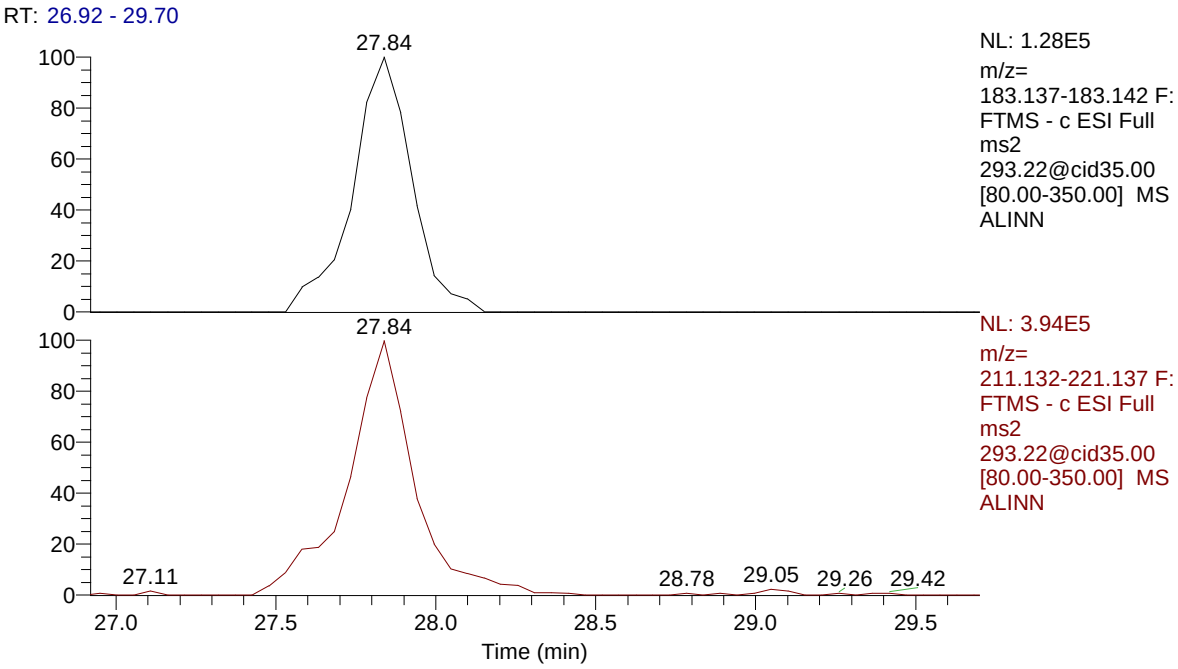

Figure 3-69 Selective mass range- chromatograms of characteristic MS^2-generated product ions (*m/z* 183 and *m/z* 211) linked to 12-HO9,13,15TE from reduced octadeca-9,12,15-trienoic acid hydroperoxide sample.

The most abundant product ion *m/z* 171 showed in LC- MS^2 TIC chromatographic peak at Rt 27.99 min. that corresponds to the precursor ion LC-MS chromatogram peak at Rt 28.04 min. (besides $[M - (H^+ + H_2O)]^-$) (Figure 3-70) is proposed to be $[C_9H_{16}O_3 - H^+]^-$. This acid-containing aldehyde product ion could be linked to 9-Hydroxyoctadeca-10, 12, 15-trienoic acid via the charge remote allylic fragmentation pathway that includes 1, 5 sigmatropic rearrangement shifting the diene system

towards the methyl end to render the nearest double bond homoallylic to alcohol functional group followed by rearrangement that is similar to that which produced the product ion at *m/z* 211 from the 12-regioisomer with a cleavage in the C9–C10 bond in this case (Scheme 3-39). In the case of shifting of the diene system in the opposite direction, towards the carboxylic end, that will render the nearest double bond adjacent to the alcohol functional group, keto-enol tautomerisation of the newly formed system might lead to a different fragmentation pathway that could be suggested to be source of the product ion at *m/z* 185 which is proposed to be $[C_{10}H_{18}O_3 - H^+]^-$ by a cleavage at C10-C11 position and product ion *m/z* 197 which is proposed to be $[C_{11}H_{18}O_3 - H^+]^-$ via scission at C11-C12 position preceded by double bond shift, 1, 3 sigmatropic rearrangement, towards the carboxylic end (Scheme 3-39).

Product ion *m/z* 121 which is proposed to be $[C_9H_{14} - H^+]^-$ can be linked to the fragmentation of 9-Hydroxyoctadecat-10, 12, 15-trienoic acid's molecular ion via an additional mechanism that involves charge driven events initiated by the abstraction of the proton of the alcohol functional group by the carboxylate anion, leaving an alkoxide anion at that position. This reactive charge localised species could undergo C9-C10 cleavage losing a neutral aldehyde species in the process and forming product carbon-centered anion that is stabilised by charge delocalisation caused by double bonds conjugation (Scheme 3-39).

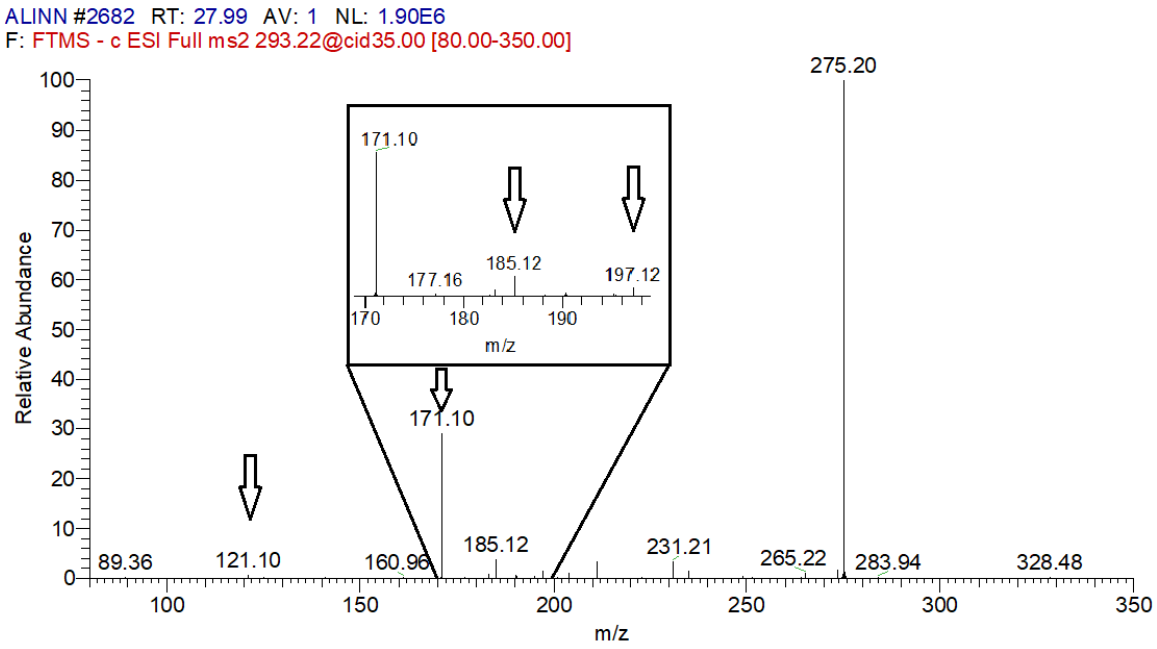

Figure 3-70 MS^2 spectrum of linolenic acid hydroxide molecular ion of *m/z* 293.22 from reduced linolenic acid hydroperoxides sample at Rt 27.99 min.

Table 3-21 The most abundant MS^2 spectrum ions at Rt 27.99 min. in the TIC LC-MS^2 chromatogram of the MS-trapped precursor ion of *m/z* 293.21 from reduced octadeca-9,12,15-trienoic acid hydroperoxides sample.

Rt: 27.99		
m/z	**Relative abundance**	**Composition**
275.20	100.00	$C_{18}H_{27}O_2$
171.10	29.12	$C_9H_{15}O_3$
211.13	4.06	$C_{12}H_{19}O_3$
185.12	3.93	$C_{10}H_{17}O_3$
231.21	3.45	$C_{17}H_{27}$
235.17	1.60	$C_{15}H_{23}O_2$
197.12	1.58	$C_{11}H_{17}O_3$

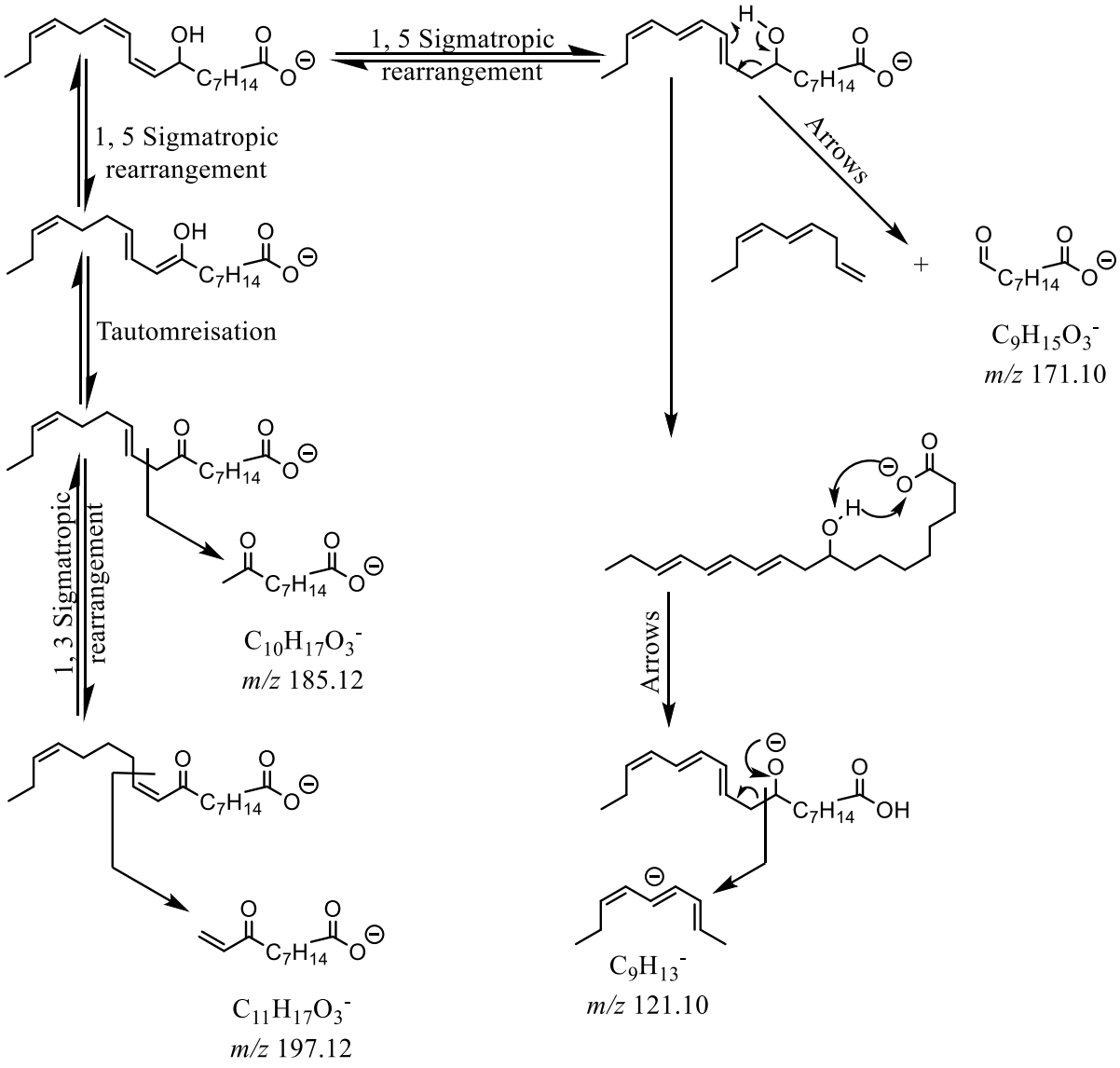

Scheme 3-39 Putative sources of product ions with characteristic significance from 9-HO10,12,15TE molecular ion in the MS^2 chromatographic peak at Rt 27.99 min.

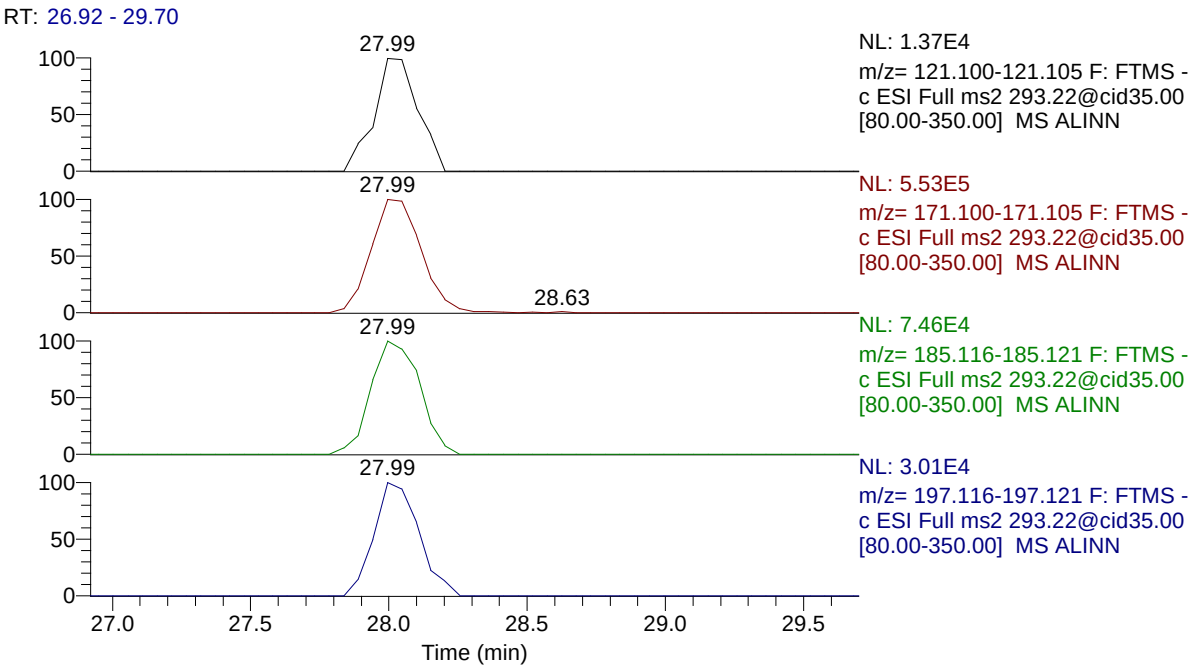

Figure 3-71 Selective mass range- chromatograms of characteristic MS^2-generated product ions (*m/z* 121 , *m/z* 171 , *m/z* 185 and *m/z* 197) linked to 9-HO10,12,15TE from reduced octadeca-9,12,15-trienoic acid hydroperoxides sample.

The chromatographic retention time window in the TIC LC- MS^2 chromatogram between Rt 28.15-28.20 min. does not correspond to any distinct peak in the precursor ion LC-MS chromatogram peak which advocates the coelution with peak at Rt 27.99 min. However. this retention time window showed fragment ions that can be considered characteristic for the 13-regioisomer (Figure 3-72) such as the product ion at *m/z* 195 which is proposed to be $[C_{12}H_{20}O_2 - H^+]^-$ that could be a result of the migration of both conjugated double bonds in a 1, 5-sigmatropic shift towards carboxylic end to facilitate the charge remote allylic rearrangement that cleaves the C12–C13 bond in an analogous reaction to the one that generated *m/z* 235 and *m/z* 183 from 16-HO9,12,14TE and 12-HO9,13,15TE, respectively (Scheme 3-40). The same rearrangement can occur between the alcohol group and the isolated double bond at C15-C16 which is already homoallylic to it to explain the generation of the product ion at *m/z* 223.13 which is proposed to be $[C_{13}H_{20}O_3 - H^+]^-$ via the terminal aldehyde-forming rearrangement that generated *m/z* 211 and *m/z* 171 from 12-HO9,13,15TE and 9-HO10,12,15TE, respectively.

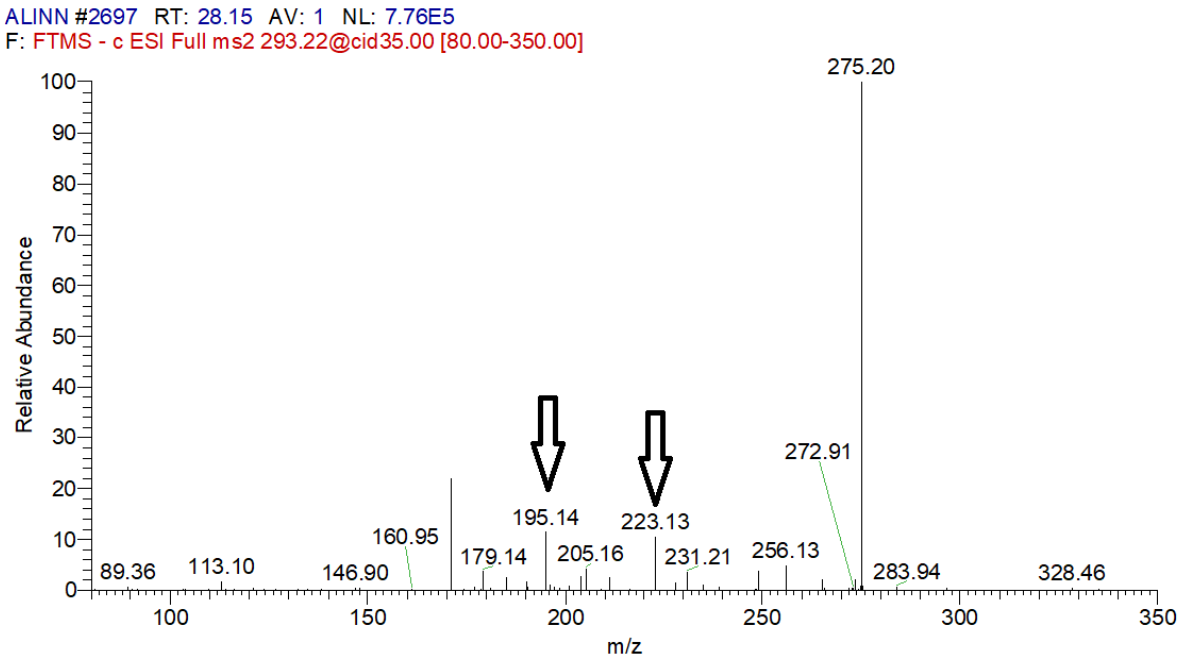

Figure 3-72 MS^2 spectrum of linolenic acid hydroxide molecular ion of *m/z* 293.22 from reduced linolenic acid hydroperoxides sample at Rt 28.15 min.

Table 3-22 The most abundant MS^2 spectrum ions at Rt 28.15 min. in the TIC LC-MS^2 chromatogram of the MS-trapped precursor ion of *m/z* 293.21 from reduced octadeca-9,12,15-trienoic acid hydroperoxides sample.

Rt: 28.15		
m/z	**Relative abundance**	**Composition**
275.20	100.00	$C_{18}H_{27}O_2$
171.10	22.02	$C_9H_{15}O_3$
195.14	11.51	$C_{12}H_{19}O_2$
223.13	10.50	$C_{13}H_{19}O_3$
256.13	4.91	$C_{13}H_{20}O_5$
205.16	4.34	$C_{14}H_{21}O$

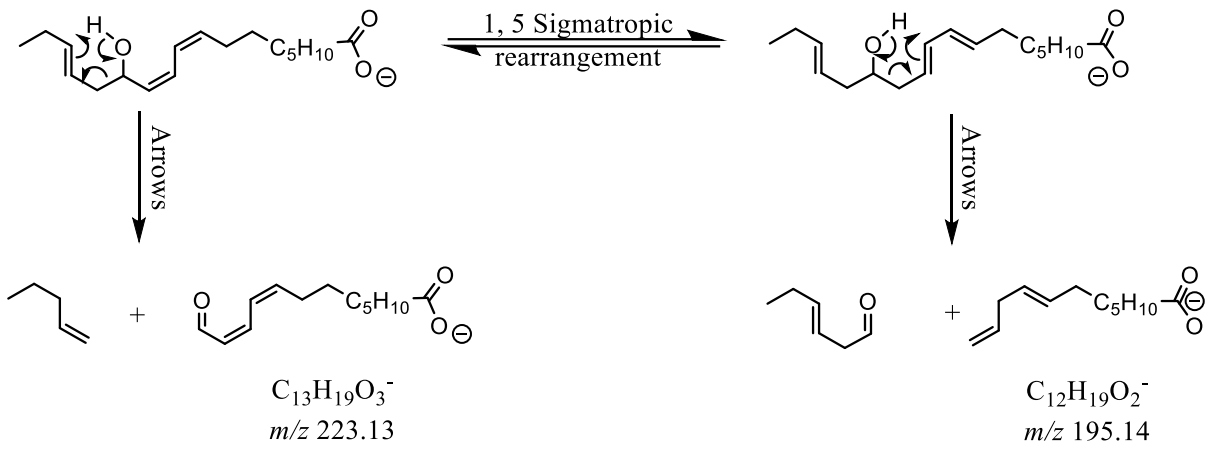

Scheme 3-40 Putative sources of product ions with characteristic significance from 13-HO9,11,15TE molecular ion in the MS^2 chromatographic peak at Rt 28.15 min.

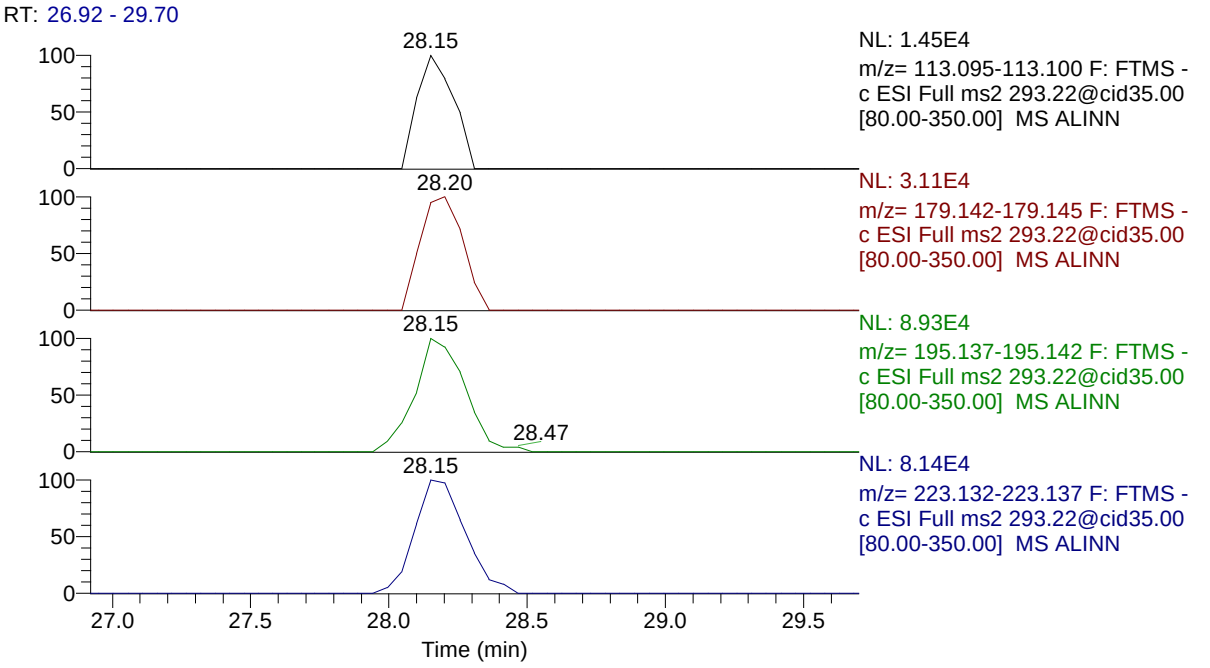

Figure 3-73 Selective mass range- chromatograms of characteristic MS^2-generated product ions (*m/z* 113 , *m/z* 179 , *m/z* 195 and *m/z* 223) linked to 13-HO9,11,15TE from reduced octadeca-9,12,15-trienoic acid hydroperoxides sample.

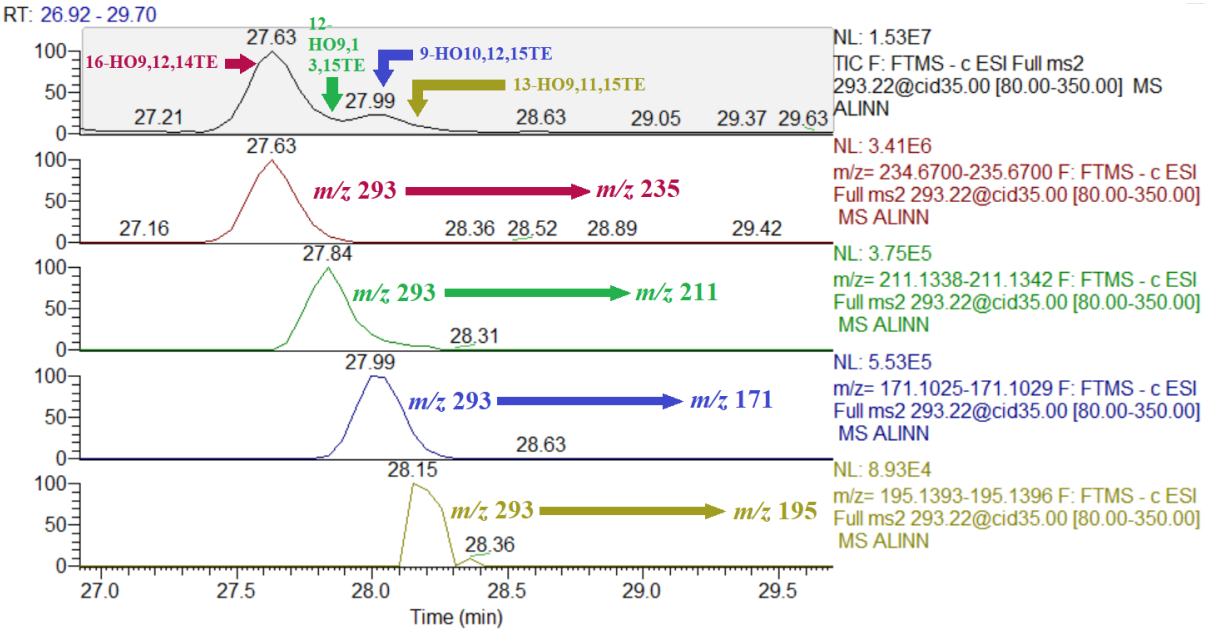

Figure 3-74 Mass range chromatogram of *m/z* 293 & mass spectra of precursor-product transitions *m/z* 293 to 235, 211, 171 and 195 specified for each hydroxy regioisomer in liquid chromatography- MS^2 spectrometry (LC-MS^2) analysis of reduced octadeca-9,12,15-trienoic acid hydroperoxides samples.

3.7.3 Analysis of γ-Linolenic acid hydroxides

3.7.3.1 Hydroxide formation

The method presented in this work additionally examined octadeca-6,9,12-trienoic acid (γ-linolenic acid, FA 18:3 (n−6)) samples, (OD6,9,12TE), which is a positional isomer of (α-Linolenic acid, FA 18:3 (n-3). Hydroperoxides formation and their secondary decomposition to form hydroxyl derivatives proceed via the same mechanism for other PUFAs. (Scheme 3-41) shows the mechanism of generating hydroxyl derivatives of octadeca-6,9,12-trienoic acid via reduction of their precursor chemically induced hydroperoxides. The resulting regioisomers would have functional OH groups located on carbons C6, C9, C10 and C13 on the fatty acyl chain. Thus, the following hydroxy isomers will be formed:

6-hydroxyoctadeca-7, 9, 12-trienoic acid (6-HO7,9,12TE)

9-hydroxyoctadeca-6, 10, 12-trienoic acid (9-HO6,10,12TE)

10-hydroxyoctadeca-6, 8, 12-trienoic acid (10-HO6,8,12TE)

13-hydroxyoctadeca-6, 9, 11-trienoic acid (13-HO6,9,11TE)

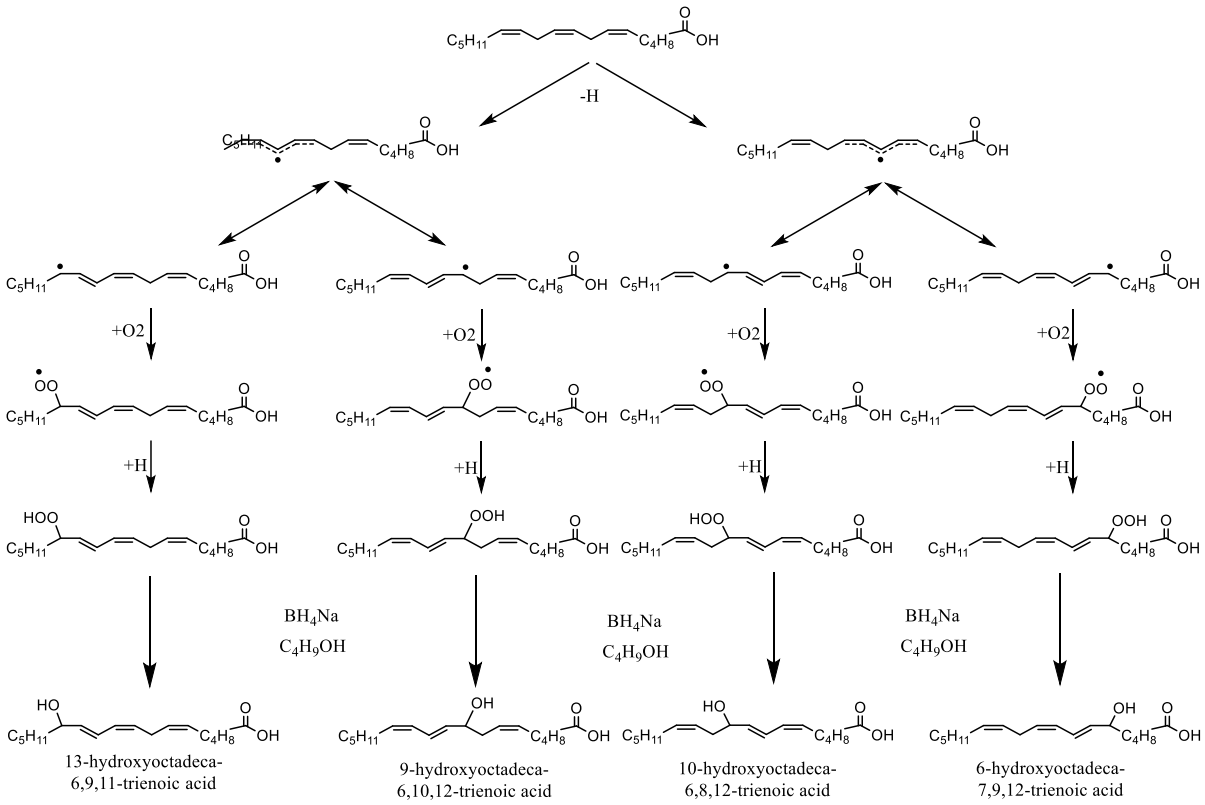

Scheme 3-41 Overall reaction scheme for linoleic acid hydroperoxides formation and a purposed scheme for their reduction to hydroxides via NaBH4 nucleophilic attack using version of the reaction scheme published by (Frankel, 1991) and data from (Wong, 2018). purposed reaction

3.7.3.2 LC-MS analysis of γ-Linolenic acid hydroxides

Four peaks for the anticipated four hydroxide isomers generated by secondary decomposition of hydroperoxide derivatives of octadeca-6,9,12-trienoic acid were observed in the mass range chromatograms for the reduced γ-linolenic acid hydroperoxides sample. The isomer peaks spectra did not contain any distinctive structural information that could be used for structure elucidation. The dehydration product ions $[M - (H^+ + H_2O)]^-$ *m/z* 275 showed low abundance in studied peaks in mass range chromatogram of $[M - H^+]^-$ (Figure 3-75).

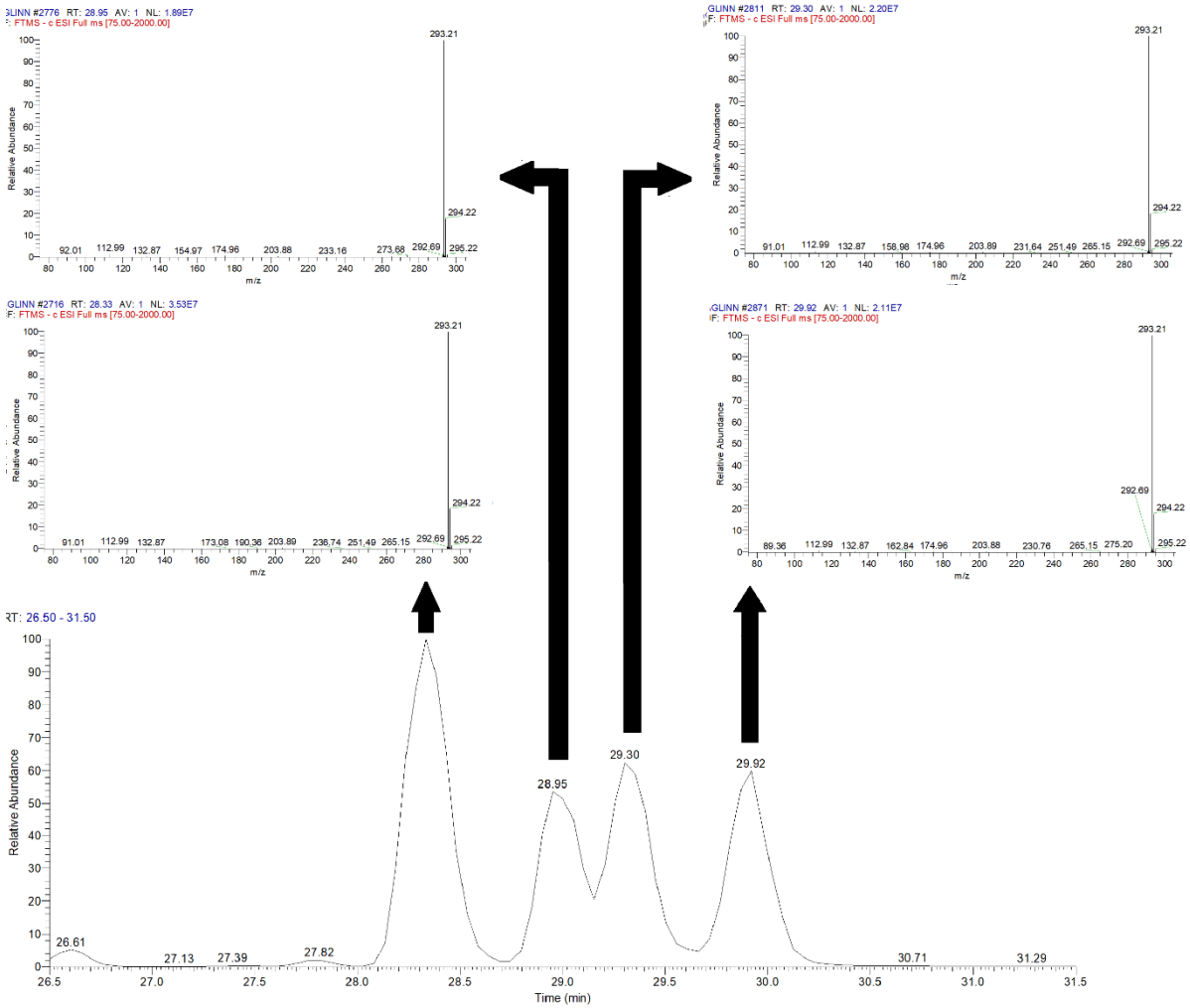

Figure 3-75 Mass range chromatogram & mass spectra of ions of *m/z* 293 in liquid chromatography- mass spectrometry (LC-MS) analysis of reduced octadeca-6,9,12-trienoic acid hydroperoxides sample.

The behaviour of hydroxy octadeca-9,12,15-trienoic acid molecular ions in MS^2 analysis was similar to those of the other PUFAs discussed above. The total ion chromatogram for CID of molecular ions showed four peaks that correspond to precursor ion LC-MS chromatographic peaks mentioned above. MS^2 spectra for each chromatographic peak offered a distinctive fragmentation pattern. Thus providing a better understanding of peaks in the mass range chromatogram of hydroxide isomers. All four fragmentation patterns showed neutral loss of water, $[M - (H^+ + H_2O)]^-$, with the dehydrated product ion *m/z* 275 observed in all hydroxy octadeca-6,9,12-trienoic acid isomers (HOD6,9,12Ts) MS^2 spectra (Figure 3-76).

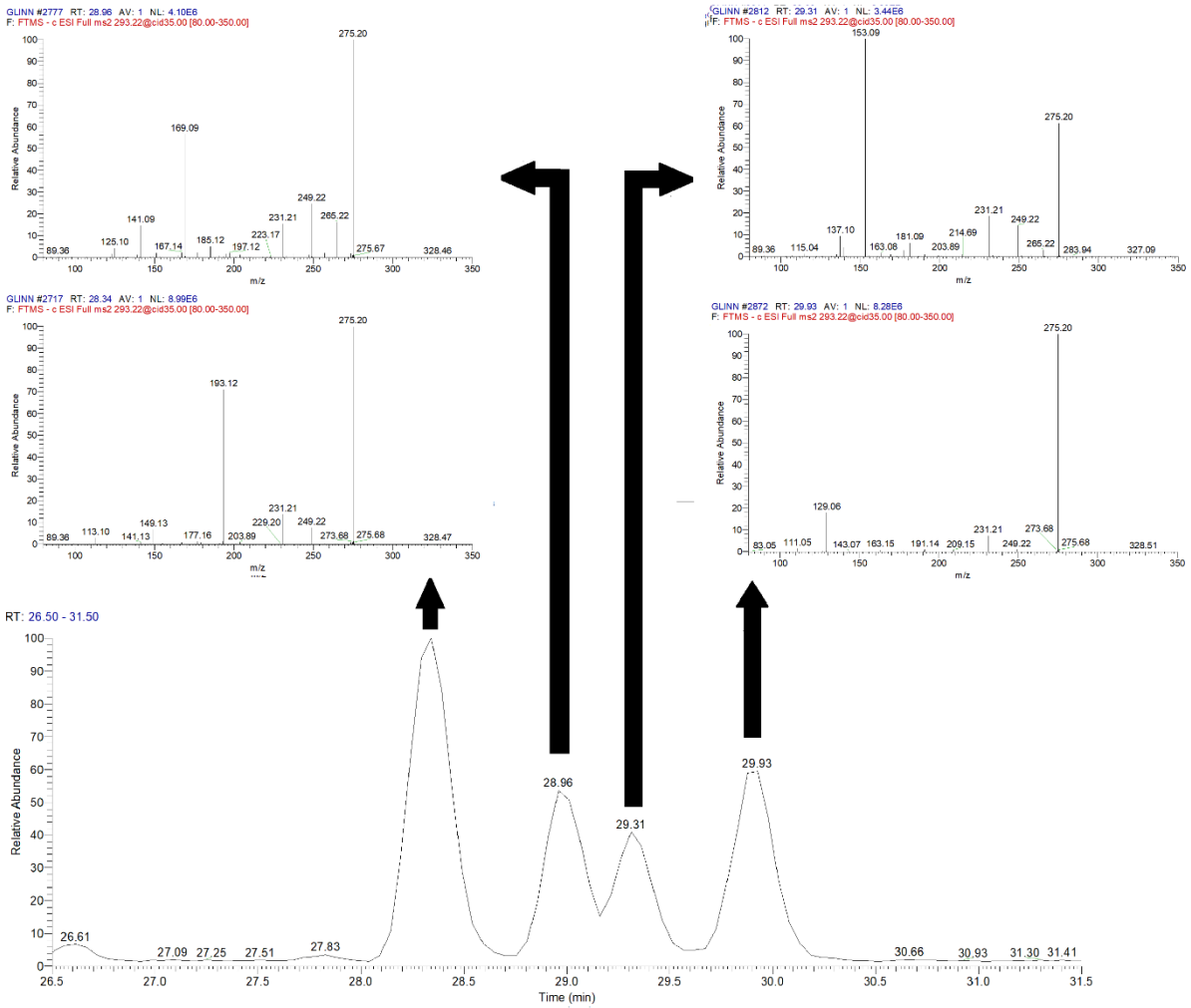

Figure 3-76 Total ion chromatogram & MS^2 spectrometry (LC- MS^2) following collision-induced decomposition of the molecular anion [M – H+]- at *m/z* 293 of HOD6,9,12T.

Peak at Rt 28.34 min. in the TIC LC- MS^2 chromatogram that corresponds to precursor ion LC-MS chromatogram peak at Rt 28.33 min. (Figure 3-77) contained two characteristic fragments that could be linked to 13-hydroxyoctadeca-6, 9, 11-trienoic acid (13-HO6,9,11TE): one at *m/*z 193 and proposed to be $[C_{12}H_{18}O_2 - H^+]^-$ and to be formed by the charge remote allylic fragmentation mechanism suggested previously as the pathway responsible for the generation of fragment ion *m/z* 235 which is proposed to be $[C_{15}H_{24}O_2 - H^+]^-$ from 16-hydroxy α-linolenic acid (16-HO6,9,11TE) and the other at *m/z* 149 and proposed to be $[C_{11}H_{18} - H^+]^-$ that would be originated from the first one by neutral loss of CO_2.

(Scheme 3-42) demonstrates the retro-ene reaction that cleaves carbon bond C12–C13 vinylic to hydroxy functional group and produces an aldehyde (neutral species) in the

process and the preceding 1,5 sigmatropic proton rearrangement that shifts conjugated diene system between C9 and C12 towards the carboxyl end into position between C8 and C11 to render the nearest double bond into homoallylic position relative to the hydroxy functional group, C10-C11.

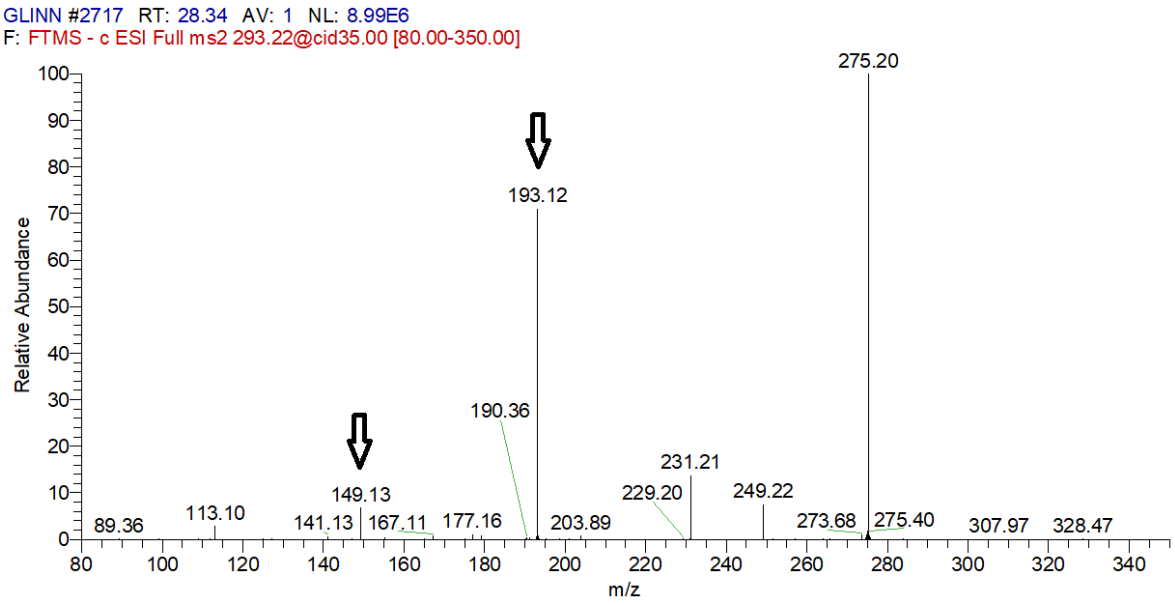

Figure 3-77 MS^2 spectrum of γ-linolenic acid hydroxide molecular ion of *m/z* 293.22 from reduced γ-linolenic acid hydroperoxides sample at Rt 28.34 min.

Table 3-23 The most abundant MS^2 spectrum ions at Rt 28.34 min. in the TIC LC-MS^2 chromatogram of the MS-trapped precursor ion of *m/z* 293.21 from reduced octadeca-6,9,12-trienoic acid hydroperoxides sample.

Rt: 28.34		
m/z	**Relative abundance**	**Composition**
275.20	100.00	$C_{18}H_{27}O_2$
193.12	71.12	$C_{12}H_{17}O_2$
231.21	13.79	$C_{17}H_{27}$
249.22	7.57	$C_{17}H_{29}O$
149.13	6.83	$C_{11}H_{17}$

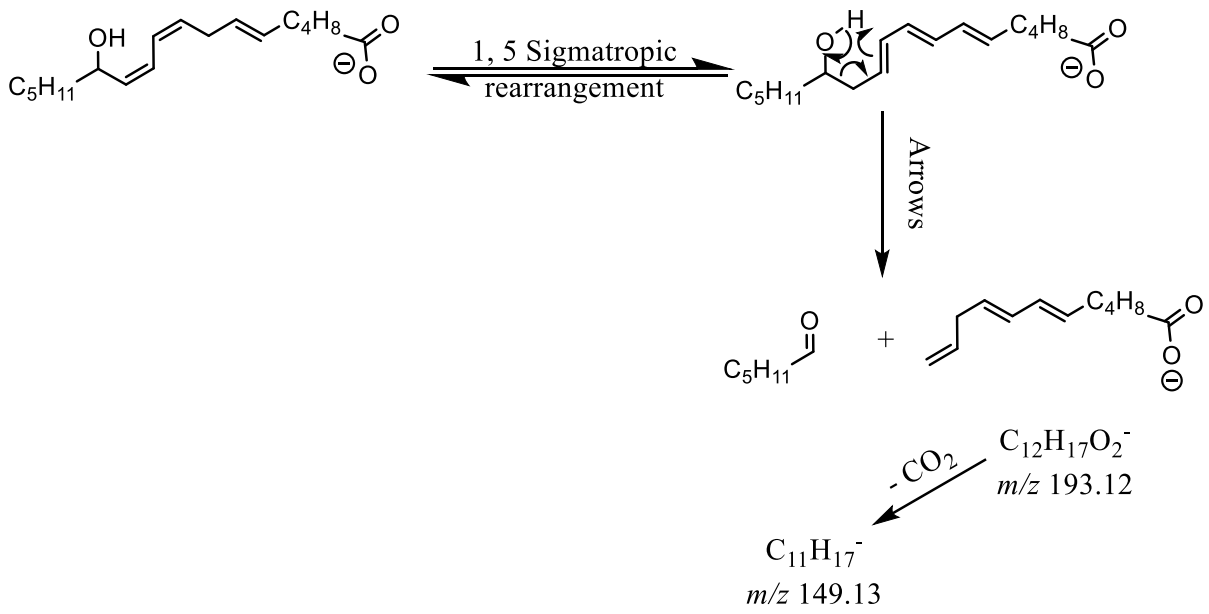

Scheme 3-42 Putative sources of product ions with characteristic significance from 13-HO6,9,11TE molecular ion in the MS^2 chromatographic peak at Rt 28.34 min.

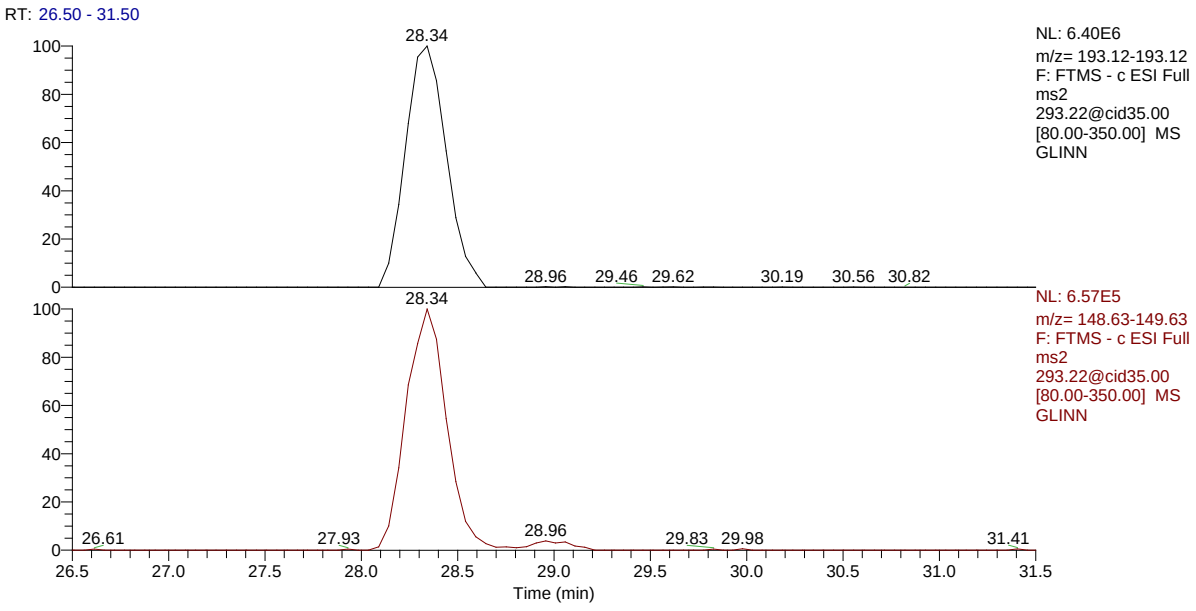

Figure 3-78 Selective mass range- chromatograms of characteristic MS^2-generated product ions (*m/z* 193 and *m/z* 149) linked to 13-HO6,9,11TE from reduced octadeca-6.9,12-trienoic acid hydroperoxides sample.

Fragment ions that can be considered characteristic for 9-HO6,10,12TE were observed for the peak at Rt 28.96 min. in the TIC LC- MS^2 chromatogram that corresponds to precursor ion LC-MS chromatogram peak at Rt 28.95 min. (Figure 3-79). The product ion at *m/z* 141 which is proposed to be $[C_8H_{14}O_2 - H^+]^-$ could be a result of the terminal aldehyde-forming rearrangement that led to a charge remote allylic cleavage at C8-C9 bond which is adjacent to the alcoholic moiety and allylic to the isolated double bond in the carbon chain of 9-hydroperoxyoctadeca-6, 10, 12-trienoic acid, while terminal aldehyde would be formed on the ensuing neutral species (Scheme 3-43). The other more abundant characteristic product ion, *m/z* 169 which is proposed to be $[C_9H_{14}O_3 - H^+]^-$, could be a result of a comparable charge remote allylic pathway that results a scission in the C9–C12 bond that is adjacent to the other side of hydroxyl group. Except that, in this case, it would be preceded by migration of both conjugated double bonds in a 1, 5-sigmatropic shift towards the methyl end as described (Scheme 3-43).

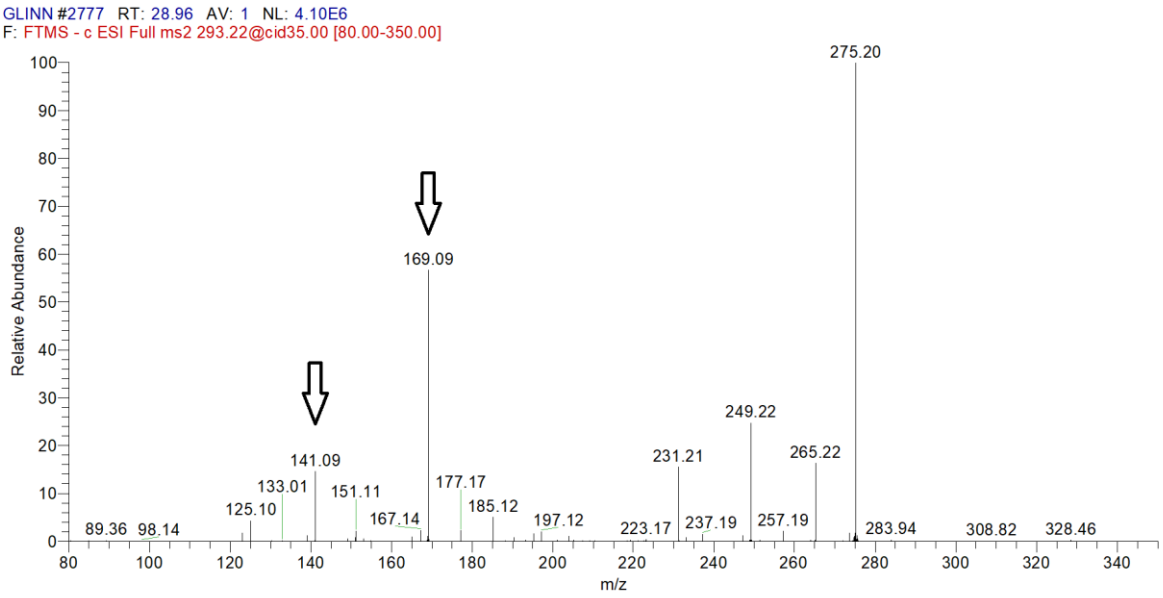

Figure 3-79 MS^2 spectrum of γ-linolenic acid hydroxide molecular ion of *m/z* 293.22 from reduced γ-linolenic acid hydroperoxides sample at Rt 28.96 min.

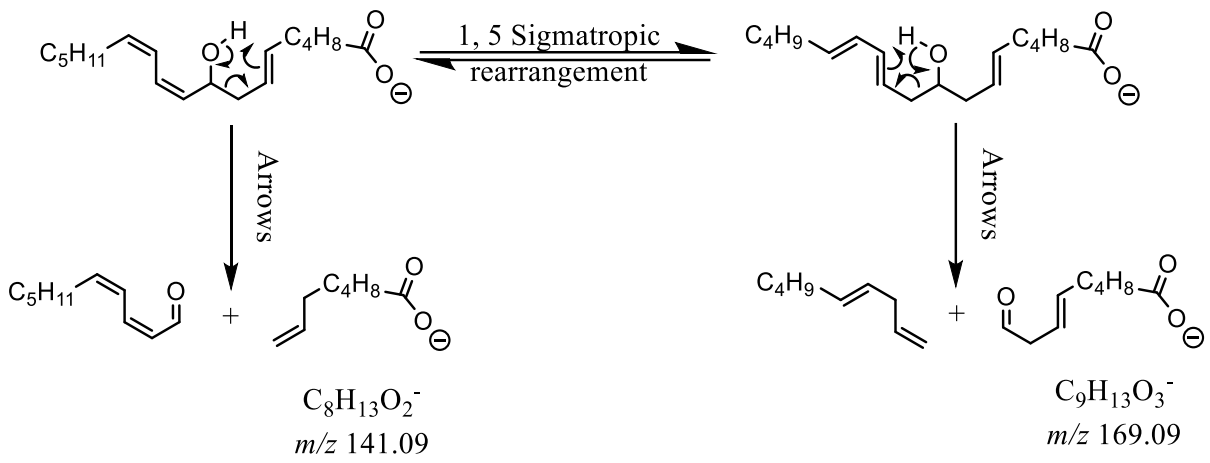

Scheme 3-43 Putative sources of product ions with characteristic significance from 9-HO6,10,12TE molecular ion in the MS^2 chromatographic peak at Rt 28.96 min.

Table 3-24 The most abundant MS^2 spectrum ions at Rt 28.96 min. in the TIC LC-MS^2 chromatogram of the MS-trapped precursor ion of *m/z* 293.21 from reduced octadeca-6,9,12-trienoic acid hydroperoxides sample.

Rt: 28.96		
m/z	**Relative abundance**	**Composition**
275.20	100.00	$C_{18}H_{27}O_2$
169.09	56.69	$C_9H_{13}O_3$
249.22	24.81	$C_{17}H_{29}O$
265.22	16.35	$C_{17}H_{29}O_2$
231.21	15.60	$C_{17}H_{27}$
141.09	14.67	$C_8H_{13}O_2$

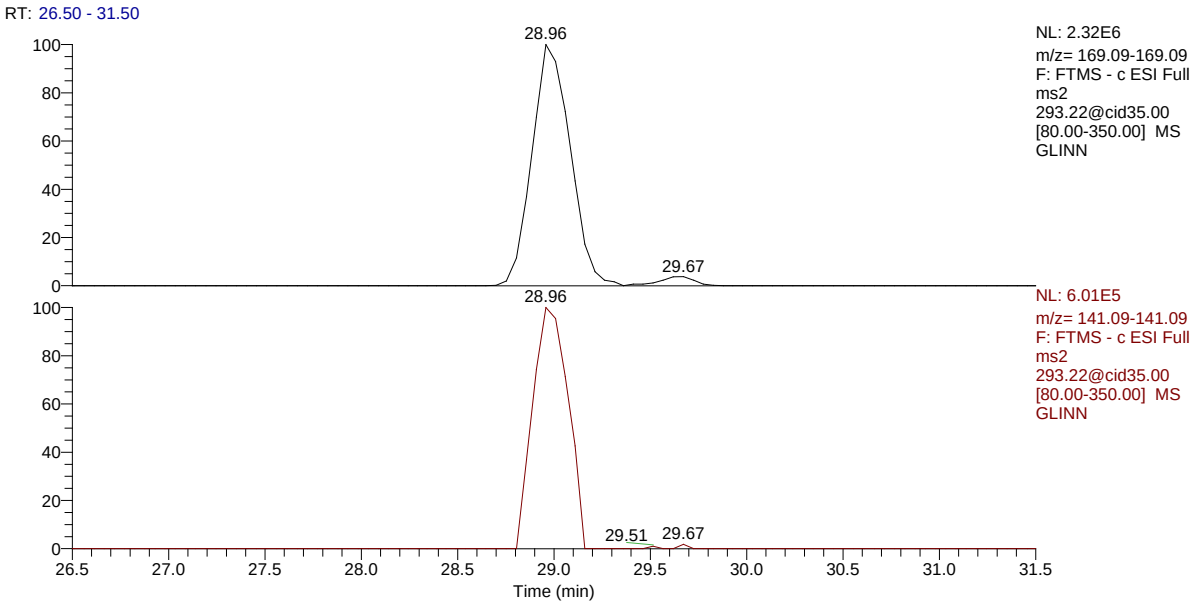

Figure 3-80 Selective mass range- chromatograms of characteristic MS^2-generated product ions (*m/z* 141 and *m/z* 169) linked to 9-HO6,10,12TE from reduced octadeca-6,9,12-trienoic acid hydroperoxide sample

The most abundant product ion *m/z* 153 showed in LC- MS^2 TIC chromatographic peak at Rt 29.31 min. that corresponds to precursor ion LC-MS chromatogram peak at Rt 29.30 min. (Figure 3-81) is proposed to be $[C_9H_{14}O_2 - H^+]^-$. This fragment ion can be considered characteristic for the 10-regioisomer and could be a result of the migration of both conjugated double bonds in a 1, 5-sigmatropic shift towards carboxylic end to facilitate the charge remote allylic rearrangement that cleaves the C9–C10 bond in an analogous reaction to the one that generated *m/z* 195 from 13-hydroxy α-linolenic acid (13-HOD9,11,15T). The same rearrangement can occur between the alcohol group and the isolated double bond at C12-C13 which is already homoallylic to it to explain the generation of product ion at *m/z* 181 which is proposed to be $[C_{10}H_{14}O_3 - H^+]^-$ via the exact terminal aldehyde-forming rearrangement that generated *m/z* 223 from 13-hydroxy α-linolenic acid (13-HOD9,11,15T). Fragment ions *m/z* 163 and *m/z* 137 are proposed to be $[C_{10}H_{12}O_2 - H^+]^-$ and $[C_9H_{14}O - H^+]^-$ and to be originated from product ion *m/z* 181 by neutral loss of H_2O and CO2, respectively (Scheme 3-44).

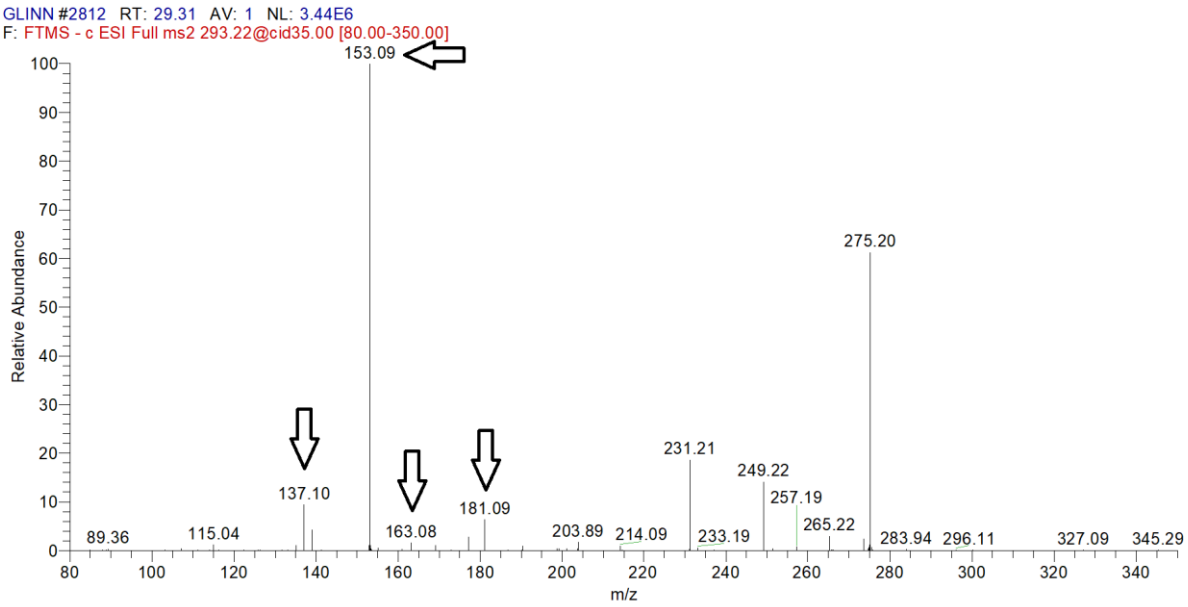

Figure 3-81 MS^2 spectrum of γ-linolenic acid hydroxide molecular ion of *m/z* 293.22 from reduced γ-linolenic acid hydroperoxides sample at Rt 29.31 min.

Table 3-25 The most abundant MS^2 spectrum ions at Rt 29.31 min. in the TIC LC-MS^2 chromatogram of the MS-trapped precursor ion of *m/z* 293.21 from reduced octadeca-6,9,12-trienoic acid hydroperoxides sample.

Rt: 29.31		
m/z	**Relative abundance**	**Composition**
153.09	100.00	$C_9 H_{13} O_2$
275.20	61.34	$C_{18} H_{27} O_2$
231.21	18.71	$C_{17} H_{27}$
249.22	14.22	$C_{17} H_{29} O$
265.22	16.35	$C_{17} H_{29} O_2$
137.10	9.47	$C_9 H_{13} O$
181.09	6.41	$C_{10} H_{13} O_3$

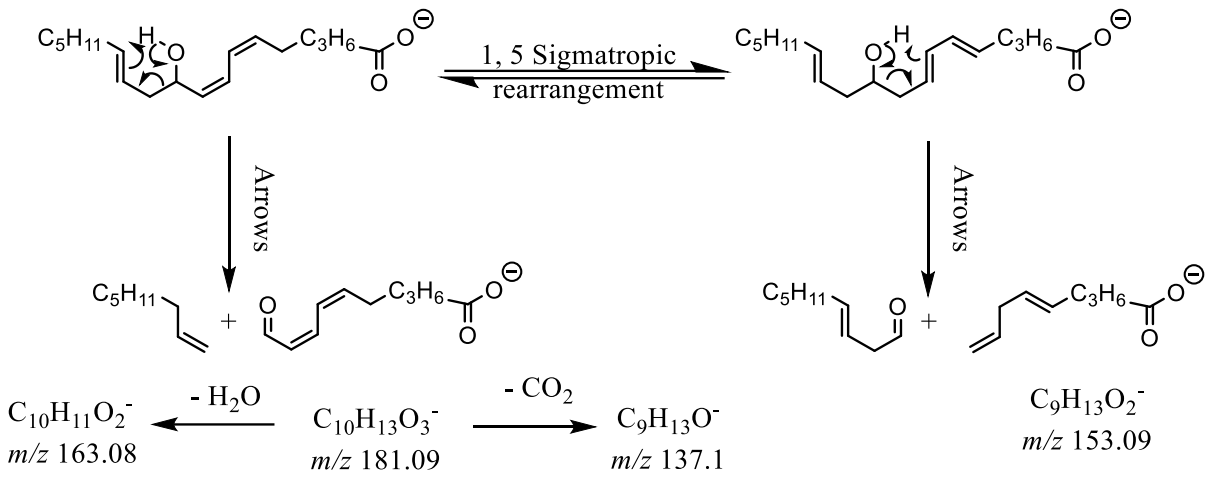

Scheme 3-44 Putative sources of product ions with characteristic significance from 10-HO6,8,12TE molecular ion in the MS^2 chromatographic peak at Rt 29.31 min.

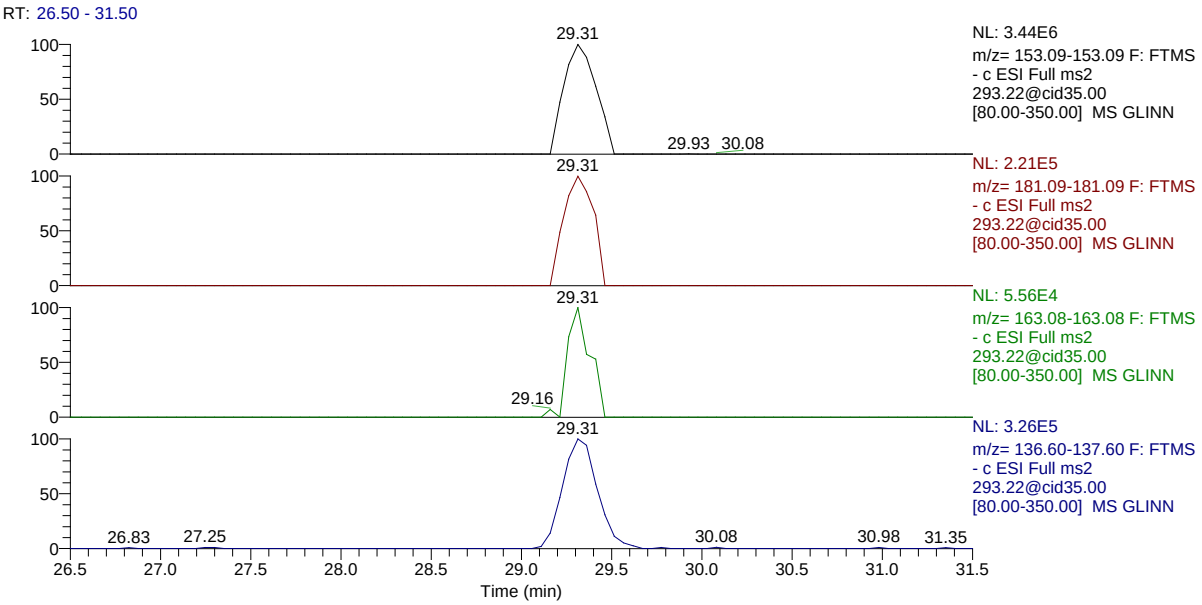

Figure 3-82 Selective mass range- chromatograms of characteristic MS^2-generated product ions (*m/z* 137, *m/z* 153, *m/z* 163 and *m/z* 181) linked to 10-HO6,8,12TE from reduced octadeca-6,9,12-trienoic acid hydroperoxides sample.

The product ion at *m/z* 129 showed in LC- MS^2 TIC chromatographic peak at Rt 29.93 min. that corresponds to the precursor ion LC-MS chromatogram peak at Rt 29.92 min. (Figure 3-83) is proposed to be $[C_6H_{10}O_3 - H^+]^-$. This acid-containing aldehyde product ion could be linked to 6-Hydroxy octadeca-7, 9, 12-trienoic acid via the charge remote allylic fragmentation pathway that includes a 1, 5 sigmatropic rearrangement shifting the diene system towards the methyl end to render the nearest double bond homoallylic

to alcohol functional group followed by rearrangement that is similar to that which produced the product ion at *m/z* 171 from 9-hydroxy α-linolenic acid (9-HOD10,12,15T) (Scheme 3-45). Fragment ion *m/z* 111 is proposed to be $[C_6H_8O_2 - H^+]^-$ and could be linked to the 6-regioisomer as it could be originated from *m/z* 129 by neutral loss of water.

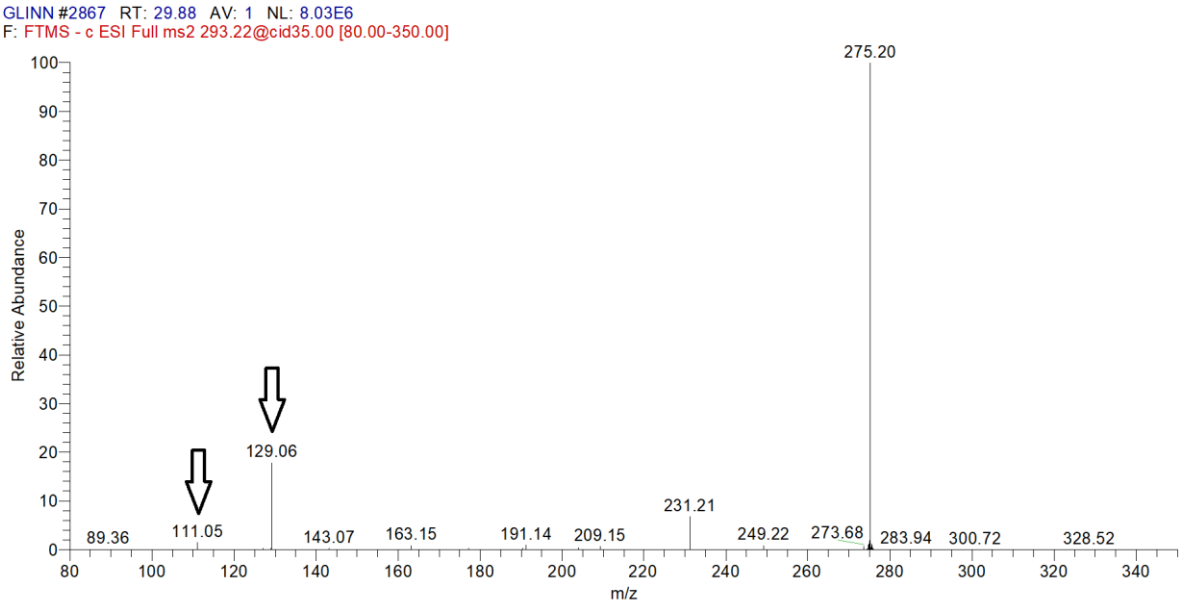

Figure 3-83 MS^2 spectrum of γ-linolenic acid hydroxide molecular ion of *m/z* 293.22 from reduced γ-linolenic acid hydroperoxides sample at Rt 29.93 min.

Table 3-26 The most abundant MS^2 spectrum ions at Rt 29.93 min. in the TIC LC-MS^2 chromatogram of the MS-trapped precursor ion of *m/z* 293.21 from reduced octadeca-6,9,12-trienoic acid hydroperoxides sample.

Rt: 29.93		
m/z	**Relative abundance**	**Composition**
275.20	100.00	$C_{18}H_{27}O_2$
129.06	17.93	$C_6H_9O_3$
231.21	6.84	$C_{17}H_{27}$
275.00	1.95	$C_9H_7O_{10}$
111.05	1.48	$C_6H_7O_2$

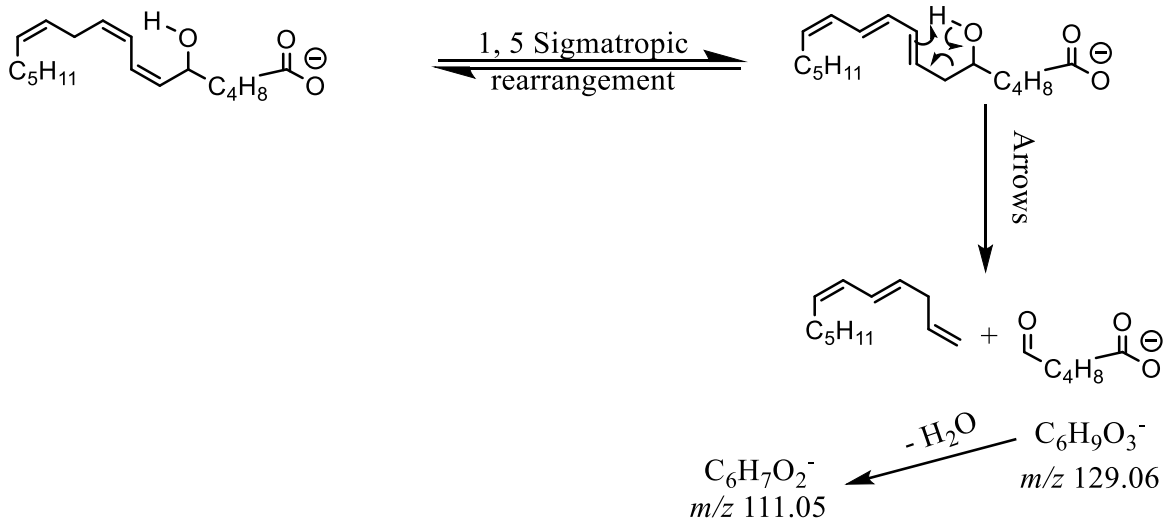

Scheme 3-45 Putative sources of product ions with characteristic significance from 6-HO7,9,12TE molecular ion in the MS^2 chromatographic peak at Rt 29.93 min.

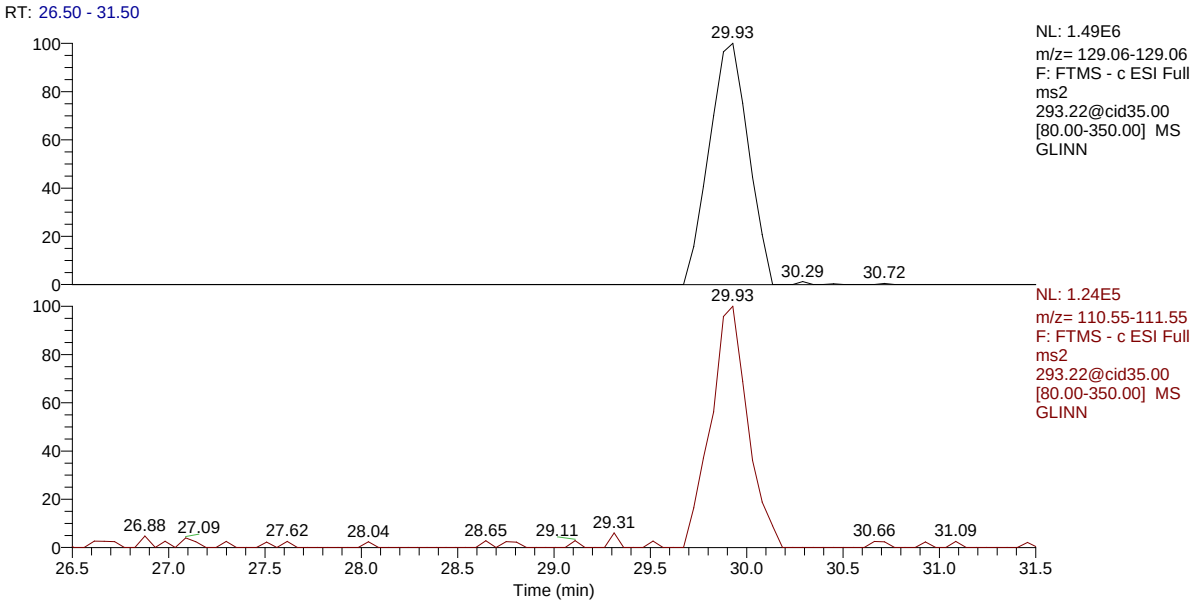

Figure 3-84 Selective mass range- chromatograms of characteristic MS^2-generated product ions (*m/z* 111 and *m/z* 129) linked to 6-HO7,9,12TE from reduced octadeca-6,9,12-trienoic acid hydroperoxides sample.

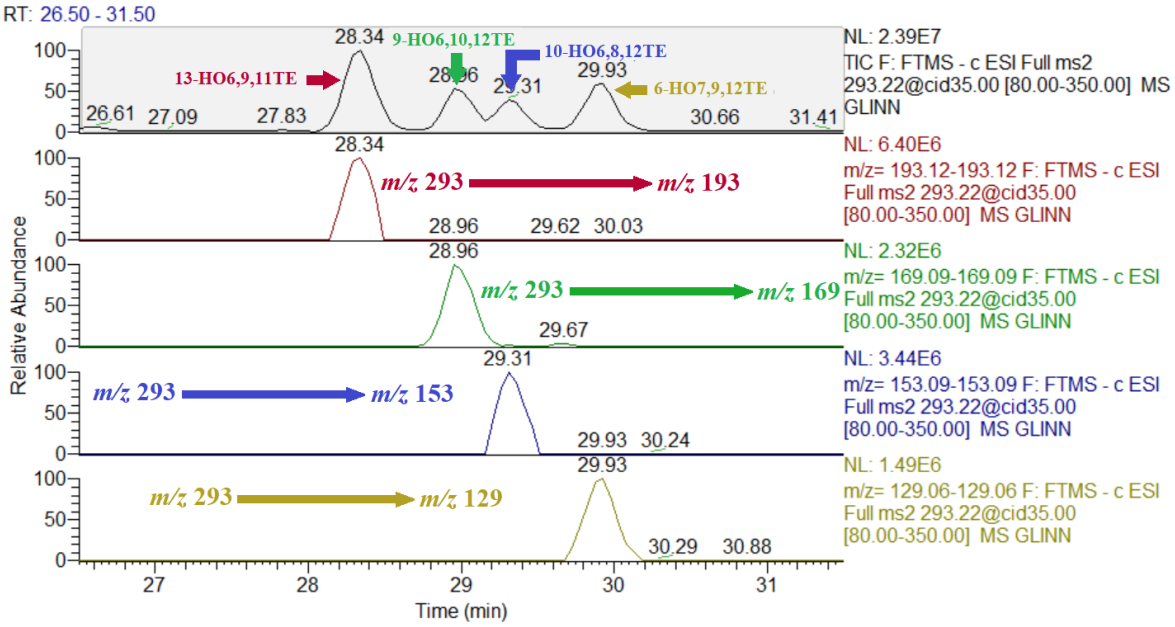

Figure 3-85 Mass range chromatogram of *m/z* 293 & mass spectra of precursor-product transitions *m/z* 293 to 193, 169, 153 and 129 specified for each hydroxy regioisomer in liquid chromatography- MS^2 spectrometry (LC-MS^2) analysis of reduced octadeca-6,9,12-trienoic acid hydroperoxides samples.

3.8 Discussion of hydroxy poly-unsaturated fatty acids analysis as a tool for double bond position determination

When an unsaturated fatty acid has more than one double bond, free radical oxidation reaction, which products have been analysed in this work, proceeds through the classical mechanism that involves the abstraction of hydrogen and that not only relies on number of double bonds and their locations but also on their relative positions to each other. Taking linoleic acid as an example, the active bis-allylic methylene group on carbon-11 between two double bonds that produces a hybrid pentadienyl radical when it suffers a hydrogen atom represents the main factor that dictates the formation of oxidation products including the secondarily produced hydroxides. This phenomenon is very useful in identifying the locations of multiple double bonds in a PUFA as monitoring the hydroxide isomers is enough to reveal all the double bond locations in a PUFA. This fact was verified through the analysis of linoleic acid (FA 18:2) and linolenic acid

(FA 18:3). As linoleic acid and linolenic acid contain two and three double bonds. When subjected to collisional induced dissociation in LC-MS^2 analysis, the molecular ions of the resulting hydroxides of Linoleic acid (*m/z* 295.2) produces two major fragments at *m/z* 195.1 and 171.1, one abundant ion for each positional isomer. The fragmentation pathway that produces these diagnostic ions is almost the same one reported for the hydroxy MUFAs fragmentations. The only difference is that in the case of the linoleic acid hydroxides, the process of relocating double bond out of allylic position to hydroxyl function group comprises a single 1,5 sigmatropic rearrangement instead of 1,3 sigmatropic rearrangement to shift the conjugated diene system away from the hydroxy functional group. Subsequently, diagnostic ions at *m/z* 171.1 and at *m/z* 195.1 would be generated after C9−C10 bond and C12−C13 bond cleavages, respectively, that are caused by the rearrangement reactions that involve the hydroxyl function group and the nearest double bond (Scheme 3-46), retro-ene reaction.

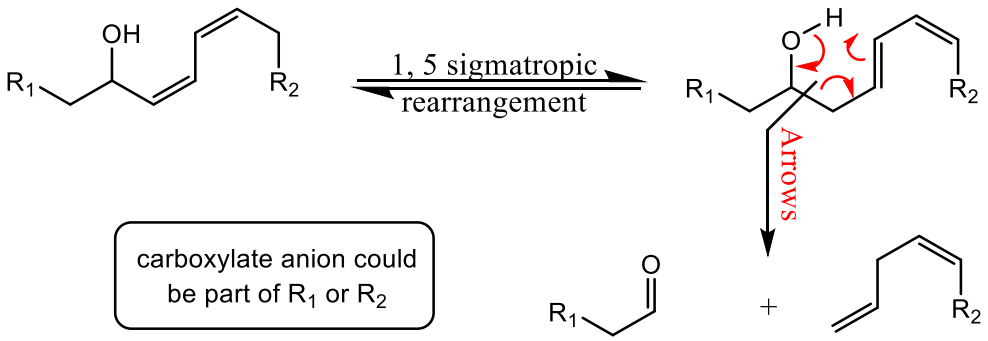

Scheme 3-46 Charge-remote allylic fragmentation in hydroxy PUFAs

As it was the case for hydroxy MUFAs, two different types of fragment ion species were generated. One comprises a generated aldehyde group at the distal end in ionised fragment (*m/z* 171.1), and the other has an ethylene group formed at the site of cleavage in the fragment ion (*m/z* 195.1). Similar results were observed for α-linolenic acid (FA 18:3 (n-3)), except that its hydroxides included four regioisomers that released four abundant diagnostic ions after CID (*m/z* 235.1, *m/z* 211.1, *m/z* 195.1 and *m/z* 171.1) (Figure 3-74) via same fragmentation pathways reported for the linoleic acid

hydroxides. Moreover, these hydroxides contain a conjugated diene system with a third isolated double bond and in two of them, 12- and 13-regioisomers, the hydroxyl group is located between the conjugated diene system and the isolated double bond. Located on a homoallylic position to hydroxy group, isolated double bonds on 12- and 13- positional isomers would go through same cleaving rearrangement to produce two extra characteristic fragment ions (*m/z* 223.1 and *m/z* 183.1) (Scheme 3-47).

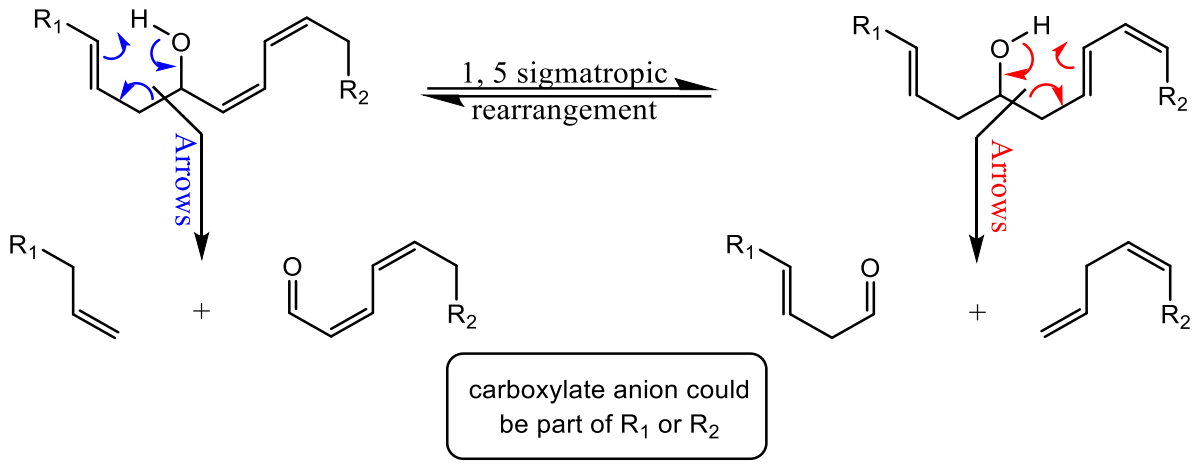

Scheme 3-47 Fragmentation mechanism of hydroxy PUFAs isomers where -OH is in between double bonds

For further evaluation of the versatility of the strategy of auto-oxidation combined with MS^2 spectrometry for double bond localisation toward other poly-unsaturated fatty acids, γ-linolenic acid (FA 18:3 (n-3)) was selected, and MS^2 analysis of the hydroxides yielded diagnostic ions similar to those observed for α-linolenic acid.

γ-linolenic acid and α-linolenic acid have the same chain length, and both of them contain three double bonds, although at different locations (6, 9, and 12 vs 9, 12 and 15). However, as double bonds in octadeca-6,9,12-trienoic acid (γ-linolenic acid, FA 18:3 (n−6)) are three more carbons closer to the carboxylic group than octadeca-9,12,15-trienoic acid (α-Linolenic acid, FA 18:3 (n-3)), the diagnostic ions of octadeca-6,9,12-trienoic acid were 42 Da lower in mass (*m/z* 193, 181, 169, 153, 141 and 129 vs *m/z* 235, 223, 211, 195, 183 and 171) than those of octadeca-9,12,15-trienoic acid (Figures 3-74 & 3-85).

(Wheelan et al., 1993) reported the remarkable change in CID of fatty acids' carboxylate anions when a double bond is adjacent to a hydroxy group as typically encountered for oxygenated PUFAs. In their isotope labelling supported work using low-energy collision induced dissociation (CID) of the carboxylate anions generated by fast atom bombardment ionisation, (Wheelan et al., 1993) suggested that the mechanism of formation of the most abundant product ions when the hydroxyl substituent was allylic to a double bond involved a charge-remote allylic fragmentation. Overall, the reported characteristic fragment ions of some hydroxides derived from oleic, linoleic and linolenic acids in (Wheelan et al., 1993) work are in accordance with our findings. Moreover, they concluded that CID spectra of unknown compounds could be used to establish the hydroxyl substituent position in relationship to certain sites of unsaturation, thus locating the adjacent double bond but would not be indicative of all double bond locations.

(Masoodi et al., 2008) described MRM method to quantify many fatty acid hydroxides including those of linoleic, arachidonic, eicosapentaenoic, and docosahexaenoic acids. The same MRM transitions suggested in this work for identification of 9-HODE (295→171) and 13-HODE (295→195) were used in the (LC/ESI-MS/MS) assay method adopted by (Masoodi et al., 2008). In a similar approach, linoleic acid hydroxides generated by the same method of hydroperoxides reduction used in this work were analysed and quantified using selected reaction monitoring in the method developed by (Reverberi et al., 2010). Characteristic ionised fragments monitored for linoleic acid hydroxides in (Reverberi et al., 2010) work match those observed in this work.

The method introduced here suggests that combining LC-MS^2 and MRM for several hydroxide isomers of a specific fatty with the well-established knowledge of chemically induced free radical oxidation that leads to the formation of these isomers would conquers the shortcoming highlighted by (Wheelan et al., 1993) and would help pinpointing all double bond positions.

3.9 Identification of fatty acids isomers in natural oils.

Fatty acids content in natural oils was used to test the application of the developed oxidation-based method toward real-world applications.

Triacylglycerols (TAGs), are formed of a glycerol skeleton which is esterified with three FAs and compose the basic component of natural fixed oils. The regioisomer composition of esterified FAs and the positional distribution of them in TAGs play the main role in dictating TAGs biosynthesis and metabolism and affect the biological and nutritional properties of natural oils (Dubois et al., 2007). Investigations on the physiological and nutritional effects of fats have been hindered by uncertainties in aspects of their molecular structure (Mitchell et al., 2009).

The differentiation of regioisomers of MUFAs and PUFAs in a group of natural oils using secondary hydroxylation combined with LC- MS^2 discussed shown below.

3.9.1 Detection and identification of fatty acids in Almond oil

Almond (Prunus dulcis) is one of the most common commercially produced nuts. Therefore, chemical composition and fatty acid profile of almond oils has been the subject of extensive research. Almond oil is considered as an unsaturated oil since it is mainly composed of mono and di-unsaturated fatty acids (Orsavova et al., 2015; Ouzir et al., 2021). Variations in almond oil fatty acid profile have been attributed to various factors including almond harvest origin and the extraction method of the oil (Ouzir et al., 2021). However, regarding abundance, the main unsaturated fatty acids that appear in almond oil are oleic (FA 18:1) (43–82%). In most reports, no regeoisomer differentiation is normally made, albeit vaccenic acid presence was reported in the work of Zhu et al (Zhu et al., 2015). Linoleic acids (FA 18:2) varies between (6–37%), while linolenic acids (FA 18:3) appears to be hard to detect (Fernandes et al., 2017; Orsavova et al., 2015; Ouzir et al., 2021), although some harvests have been reported to have percentages higher than 11% in (Askin et al., 2007).

Figure 3-86 shows that our method for identifying the isomers of unsaturated fatty acids by oxidation was able to differentiate between isomeric oleic acids (octadec-9-enoic acid, FA 18:1 (n−9), octadec-11-enoic acid, FA 18:1 (n−7)) in almond oil. Chromatographic peaks of the hydroxides of vaccenic acid were distinctly isolated

from the total hydroxides of oleic acids (FA 18:1) and enabled the detection of vaccenic acid in the tested sample of Almond oil.

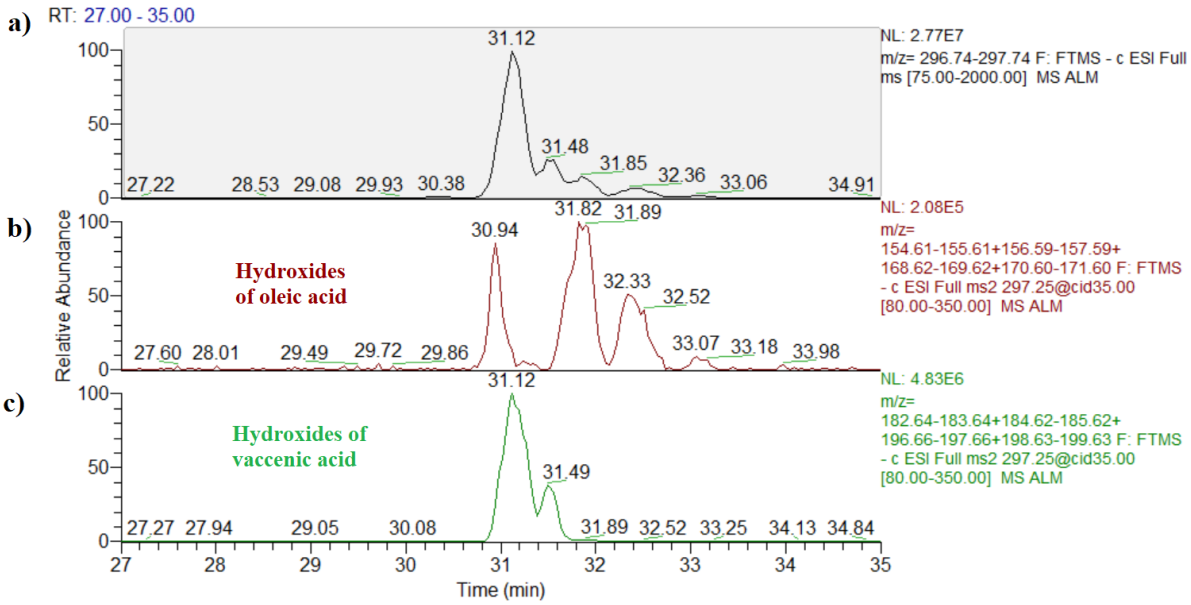

Figure 3-86 a) Mass range chromatogram of *m/z* 297 in oxidised Almond oil sample. b) Reconstructed chromatogram of precursor-product MS^2 transitions *m/z* 297 to 169, 157, 171, and 155 that are characteristic for hydroxy octadec-9-enoic acid in LC-MS^2 analysis of oxidised Almond oil sample. c) Reconstructed chromatogram of precursor-product MS^2 transitions *m/z* 297 to 197, 185, 199, and 183 that are characteristic for hydroxy octadec-11-enoic acid in LC-MS^2 analysis of oxidised Almond oil sample.

The application of our method to almond oil sample to detect and differentiate positional isomers of linolenic acids (FA C18:3) (α- and γ-linolenic acids) was not able to determine the presence of the hydroxides of linolenic acids. These findings are consistent with what has been reported in letirature (Orsavova et al., 2015; Ouzir et

al., 2021) that reports the scarcity of linolenic acids (FA C18:3) in Almond oil harvests (Figure 3-87).

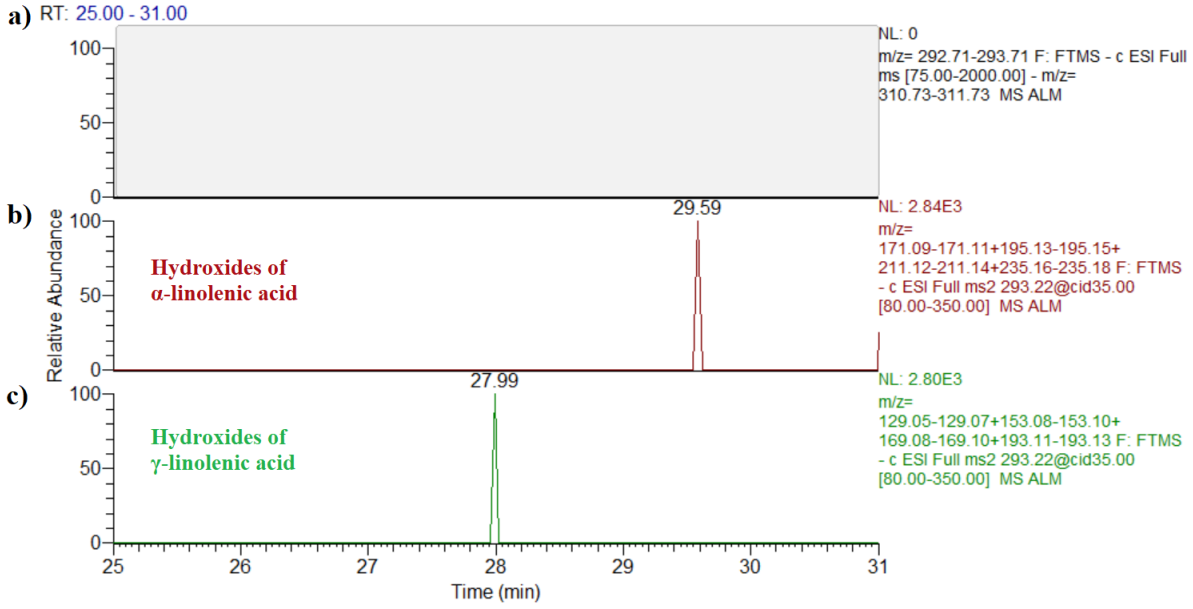

Figure 3-87 a) Mass range chromatogram of *m/z* 293 in oxidised Almond oil sample. b) Reconstructed chromatogram of precursor-product MS^2 transitions *m/z* 293 to 171, 195, 211, and 235 that are characteristic for hydroxy octadeca-9,12,15-trienoic acid in LC-MS^2 analysis of oxidised Almond oil sample. c) Reconstructed chromatogram of precursor-product MS^2 transitions *m/z* 293 to 129, 153, 169, and 193 that are characteristic for hydroxy octadeca-6,9,12-trienoic acid in LC-MS^2 analysis of oxidised Almond oil sample.

3.9.2 Detection and identification of fatty acids in Avocado oil

The fatty acid composition of avocado oil has been reported in several studies. It has essential similarities with that of almond oil namely the significantly high content of mono and di-unsaturated fatty acids, especially oleic (C18:1) and linolenic (C18:2) acids, (41-74%) and (8-21%) respectively, and a paucity of linolenic acids (C18:3) (0-2%) (Flores et al., 2019; Nasri et al., 2021). This fatty acid profile is commonly used as a part of purity parameters to determine if an oil is adulterated (Green & Wang, 2020). In figure 3-88, our oxidation-based method demonstrated the ability to identify and detect isomeric oleic acids (FA 18:1 (n−9) and FA 18:1 (n−7)) besides detecting and identifying the hydroxides of α-linolenic acid in figure 3-89.

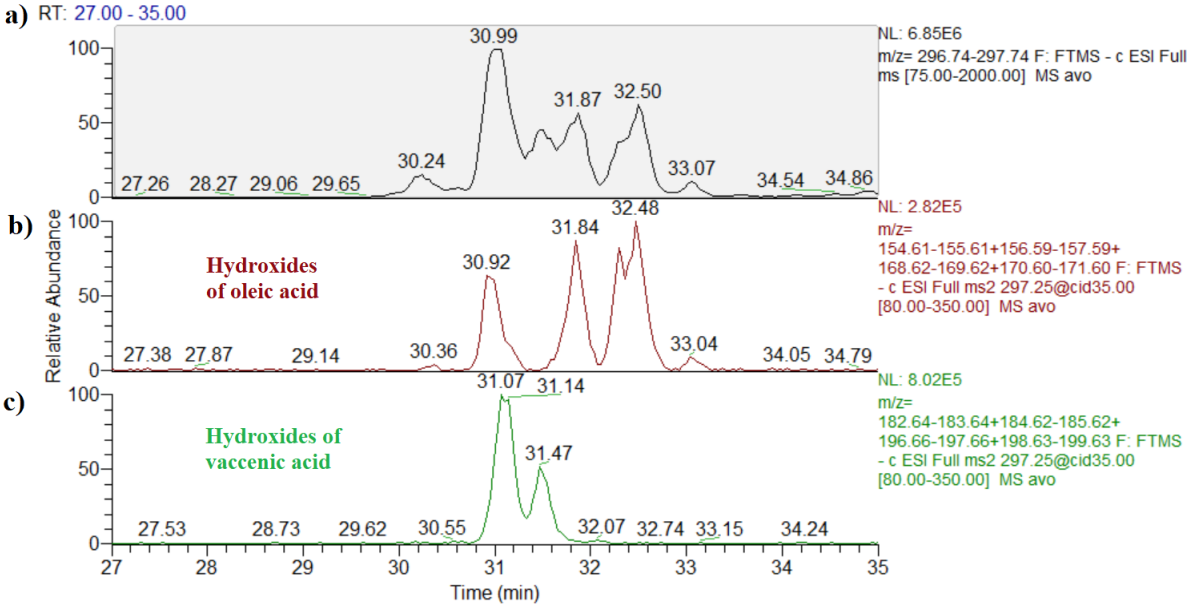

Figure 3-88 a) Mass range chromatogram of *m/z* 297 in oxidised Avocado oil sample. b) Reconstructed chromatogram of precursor-product MS^2 transitions *m/z* 297 to 169, 157, 171, and 155 that are characteristic for hydroxy octadec-9-enoic acid in LC-MS^2 analysis of oxidised Avocado oil sample. c) Reconstructed chromatogram of precursor-product MS^2 transitions *m/z* 297 to 197, 185, 199, and 183 that are characteristic for hydroxy octadec-11-enoic acid in LC-MS^2 analysis of oxidised Avocado oil sample.

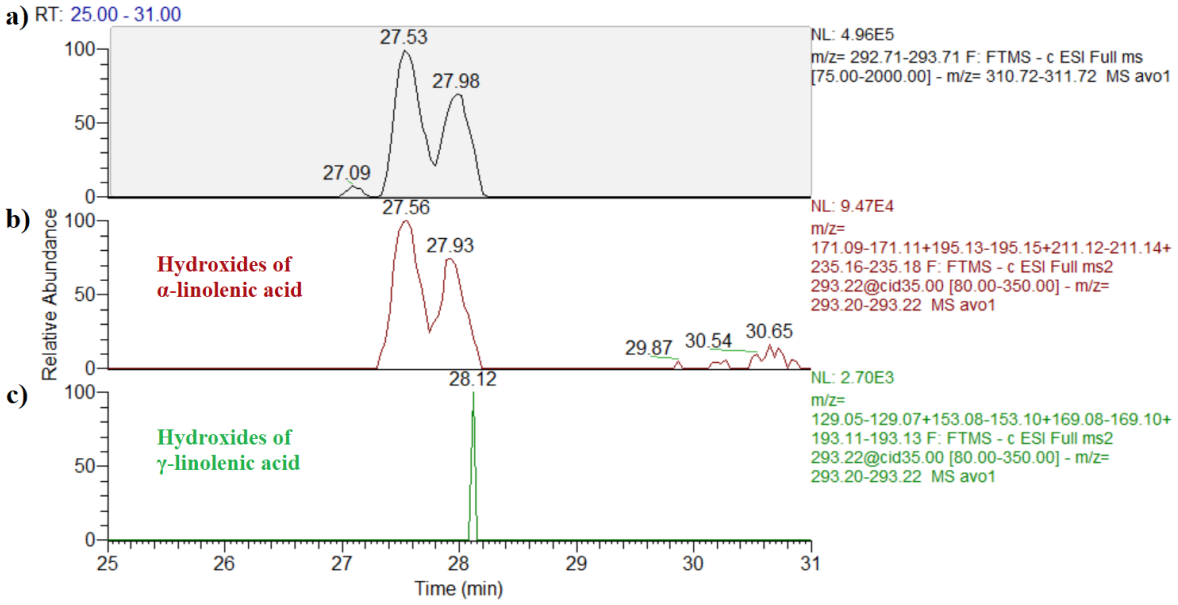

Figure 3-89 a) Mass range chromatogram of *m/z* 293 in oxidised Avocado oil sample. b) Reconstructed chromatogram of precursor-product MS^2 transitions *m/z* 293 to 171, 195, 211, and 235 that are characteristic for hydroxy octadeca-9,12,15-trienoic acid in LC-MS^2 analysis of oxidised Avocado oil sample. c) Reconstructed chromatogram of precursor-product MS^2 transitions *m/z* 293 to 129, 153, 169, and 193 that are characteristic for hydroxy octadeca-6,9,12-trienoic acid in LC-MS^2 analysis of oxidised Avocado oil sample.

3.9.3 Detection and identification of fatty acids in Borage seed oil

Borage is cultivated around the world because its seeds are considered to be the best natural source of γ-linolenic acid (octadeca-6,9,12-trienoic acid) (FA 18:3 n- 6) (Al-

Okbi et al., 2018; Molero Gómez & Martínez de la Ossa, 2002; Scrimgeour & Clough, 2014).

The oil yield of borage seeds is considerably high 30–40 % by weight with a γ-linolenic acid content of 17–30 % of total fatty acids of the oil and very low, generally undetectable levels of α-linolenic acid (octadeca-9,12,15-trienoic acid) (FA 18:3 n- 3) (Asadi-Samani et al., 2014; Borowy & Kapłan, 2020; Molero Gómez & Martínez de la Ossa, 2002; Tasset-Cuevas et al., 2013).

For MUFAs content in borage seed oil, the literature reports that they are mainly oleic (FA 18:1) (16–21% of total fatty acids) with little efforts being made towards regeoisomer differentiation or the detection of vaccenic acid (FA 18:1 n-7) (Al-Okbi et al., 2018; Asadi-Samani et al., 2014; Borowy & Kapłan, 2020; Molero Gómez & Martínez de la Ossa, 2002; Tasset-Cuevas et al., 2013). Notwithstanding that the work of (Scrimgeour & Clough, 2014) reported the incidence of vaccenic acid.

For these reasons, borage seed oil represents a useful candidate for testing the ability of our oxidation-based method to pinpoint double bond positions in unsaturated fatty acids, especially in the regioisomers of PUFAs.

Figure 3-90 shows the distinction of isomeric oleic acids (octadec-9-enoic acid, FA 18:1 (n−9), octadec-11-enoic acid, FA 18:1 (n−7)) in borage seed oil using our method as chromatographic peaks of the hydroxides of each regioisomer of octadecenoic acid were clearly isolated from the total hydroxides of oleic acids (FA 18:1) and the detection of vaccenic acid in the tested sample of borage seed oil was possible.

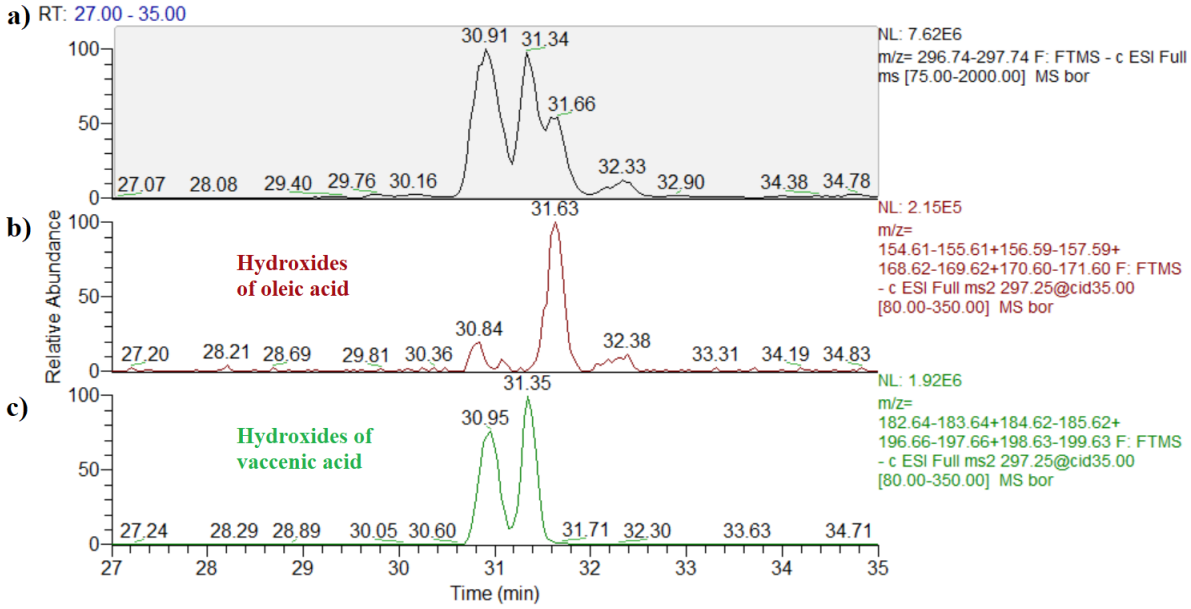

Figure 3-90 a) Mass range chromatogram of *m/z* 297 in oxidised Borage seed oil sample. b) Reconstructed chromatogram of precursor-product MS^2 transitions *m/z* 297 to 169, 157, 171, and 155 that are characteristic for hydroxy octadec-9-enoic acid in LC-MS^2 analysis of oxidised Borage seed oil sample. c) Reconstructed chromatogram of precursor-product MS^2 transitions *m/z* 297 to 197, 185, 199, and 183 that are characteristic for hydroxy octadec-11-enoic acid in LC-MS^2 analysis of oxidised Borage seed oil sample.

The application of our method on borage seed oil sample to detect positional isomers of linolenic acids (FA C18:3) (α- and γ-linolenic acids) was successfully tested and the hydroxides of γ-linolenic acid were detected and isolated from the total hydroxides of linolenic acids (FA 18:3) while signals for the hydroxides of α-linolenic acid were not intense enough to be detected (Figure 3-91).

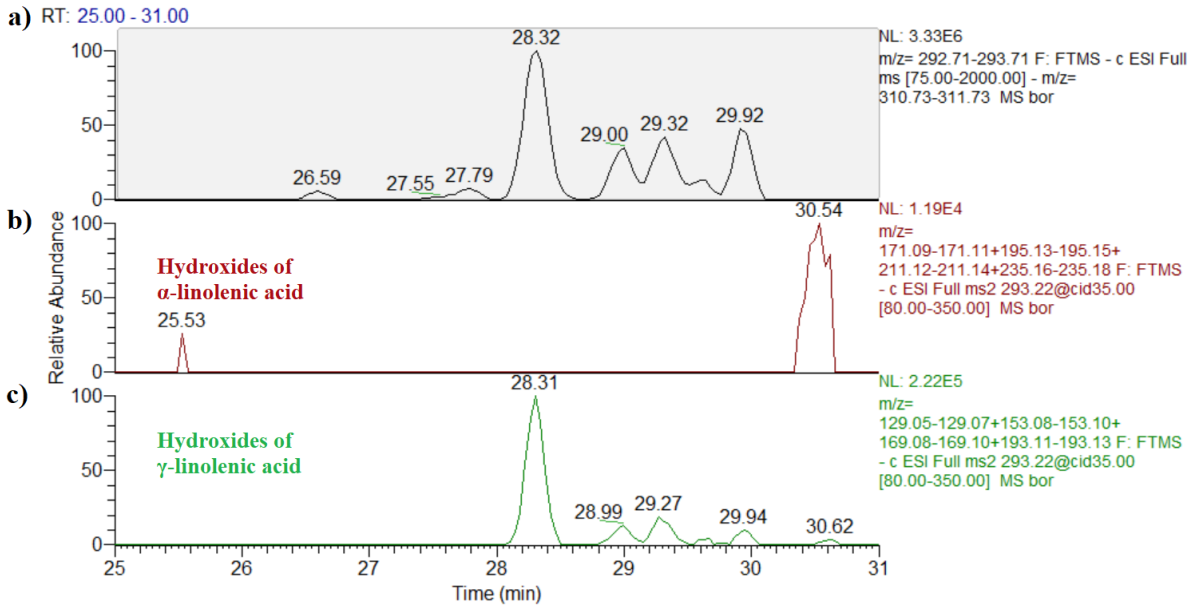

Figure 3-91 a) Mass range chromatogram of *m/z* 293 in oxidised Borage seed oil sample. b) Reconstructed chromatogram of precursor-product MS^2 transitions *m/z* 293 to 171, 195, 211, and 235 that are characteristic for hydroxy octadeca-9,12,15-trienoic acid in LC-MS^2 analysis of oxidised Borage seed oil sample. c) Reconstructed chromatogram of precursor-product MS^2 transitions *m/z* 293 to 129, 153, 169, and 193 that are characteristic for hydroxy octadeca-6,9,12-trienoic acid in LC-MS^2 analysis of oxidised Borage seed oil sample.

3.9.4 Detection and identification of fatty acids in Grape seed oil

The variable environmental factors besides maturation degree of the seeds cause alterations in the composition of grape seed oil, including fatty acids profile. Nonetheless, grape seed oil from all harvests has a high content of PUFA that has an estimated range of 85%–90% of total fatty acids (Garavaglia et al., 2016). The most abundant FA in grape seed oils is linoleic acid (62.8- 75.3%) followed by oleic acid (13.9-21.9), however, these percentages included all isomers of octadecenoic acid (FA 18:1).

(Dabetic et al., 2020) reported the presence of low amounts of vaccenic acid (octadec-11-enoic) in grapeseed oil (<1%) while linolenic acid showed concentrations in the same range (<1%) with no assessment of differential contribution of regioisomers. Low concentrations of linolenic acids has been a common observation in the literature (0.15-1.14%) (Dabetic et al., 2020; Garavaglia et al., 2016; Lutterodt et al., 2011).

The fatty acid profile reported in the literature explains our results shown in figures 3-92 & 3-93. The identification of octadec-11-enoic acid (FA 18:1 n−7) in our samples

of grapeseed oil and the separation of the chromatographic peaks of the hydroxides of vaccenic acid from those of the hydroxides of all octadecenoic acids (FA 18:1) are demonstrated in figure 3-92 whereas lack of isomers of linolenic acid (FA C18:3) (α- and γ-linolenic acids) can be noted in figure 3-93.

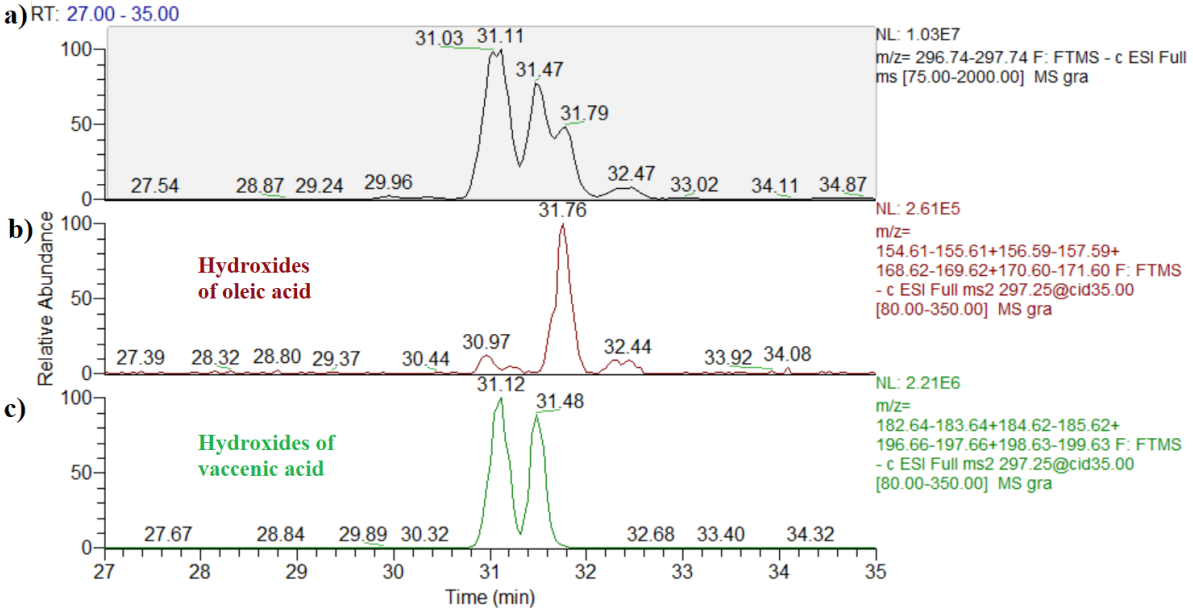

Figure 3-92 a) Mass range chromatogram of *m/z* 297 in oxidised Grape seed oil sample. b) Reconstructed chromatogram of precursor-product MS^2 transitions *m/z* 297 to 169, 157, 171, and 155 that are characteristic for hydroxy octadec-9-enoic acid in LC-MS^2 analysis of oxidised Grape seed oil sample. c) Reconstructed chromatogram of precursor-product MS^2 transitions *m/z* 297 to 197, 185, 199, and 183 that are characteristic for hydroxy octadec-11-enoic acid in LC-MS^2 analysis of oxidised Grape seed oil sample.

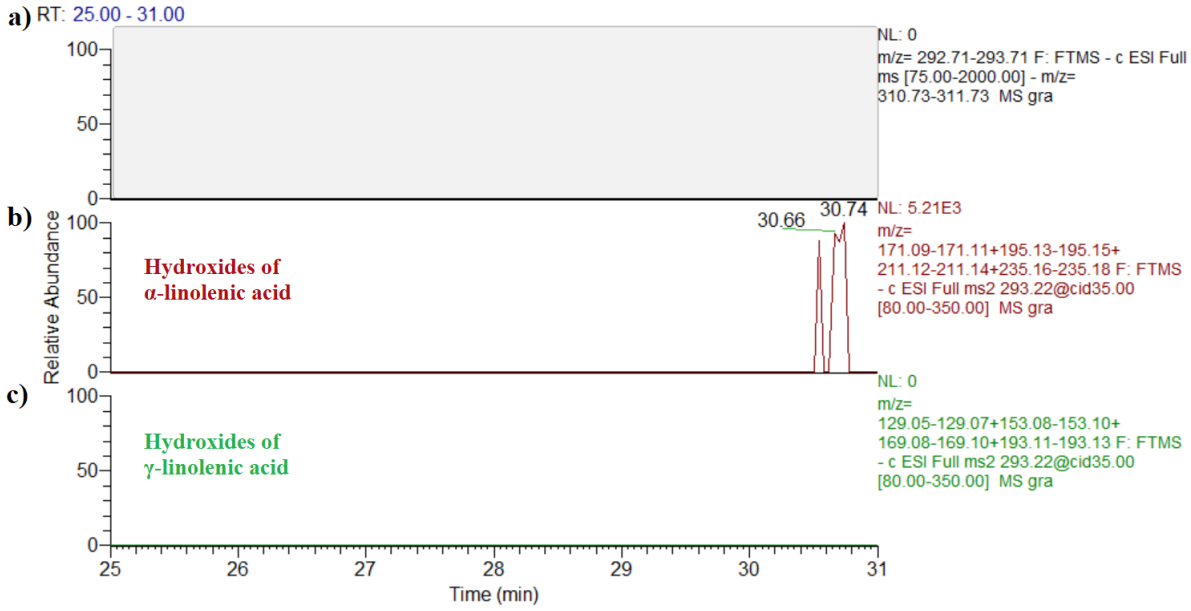

Figure 3-93 a) Mass range chromatogram of *m/z* 293 in oxidised Grape seed oil sample. b) Reconstructed chromatogram of precursor-product MS^2 transitions *m/z* 293 to 171, 195, 211, and 235 that are characteristic for hydroxy octadeca-9,12,15-trienoic acid in LC-MS^2 analysis of oxidised Grape seed oil sample. c) Reconstructed chromatogram of precursor-product MS^2 transitions *m/z* 293 to 129, 153, 169, and 193 that are characteristic for hydroxy octadeca-6,9,12-trienoic acid in LC-MS^2 analysis of oxidised Grape seed oil sample.

3.9.5 Detection and identification of fatty acids in Hazelnut oil

Diverse origins of hazelnut varieties besides different harvesting seasons and growing conditions have important impact on fatty acid composition (Vujević et al., 2014). Oleic acid (FA 18:1 n-9) is, by far, the dominant fatty acid among the identified fatty acids in natural hazelnut oils (76.30 to 86.91%), which caused it to be frequently compared to olive oil due to their similar compositions, followed by linoleic acid (FA 18:2 n-6) (6.5 to 15.6%), while the remaining fatty acids, including α-linolenic acid (FA 18:3 n-3), were present in less than 1% of the total fatty acids present (Altuntas et al., 2018; Bacchetta et al., 2013; Cui et al., 2020; Fernandes et al., 2017; Kesen et al., 2018). Presence of γ-linolenic acids (FA 18:3 n-6) has not been reported in hazelnut oil while vaccenic acid (FA 18:1 n-7) was detected by (Vujević et al., 2014).

Our results, although on qualitative level only, correlate with the findings reported in literature mentioned above. Positional isomers of oleic acids (octadec-9-enoic acid, FA 18:1 (n−9) and octadec-11-enoic acid, FA 18:1 (n−7)) in hazelnut oil could be identified by the chromatographic peaks of their hydroxides in figure 3-94 while only

traces of the hydroxides of α-linolenic acid could be detected and defferentiated in the tested sample of hazelnut oil as shown in figure 3-95.

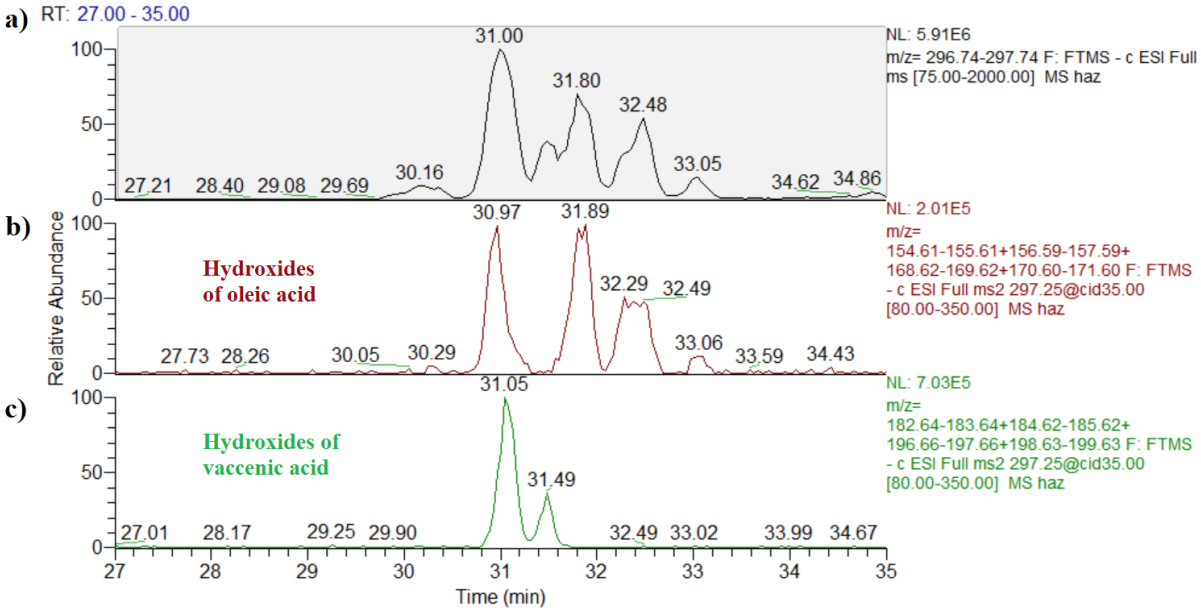

Figure 3-94 a) Mass range chromatogram of *m/z* 297 in oxidised Hazelnut oil sample. b) Reconstructed chromatogram of precursor-product MS^2 transitions *m/z* 297 to 169, 157, 171, and 155 that are characteristic for hydroxy octadec-9-enoic acid in LC-MS^2 analysis of oxidised Hazelnut oil sample. c) Reconstructed chromatogram of precursor-product MS^2 transitions *m/z* 297 to 197, 185, 199, and 183 that are characteristic for hydroxy octadec-11-enoic acid in LC-MS^2 analysis of oxidised Hazelnut oil sample.

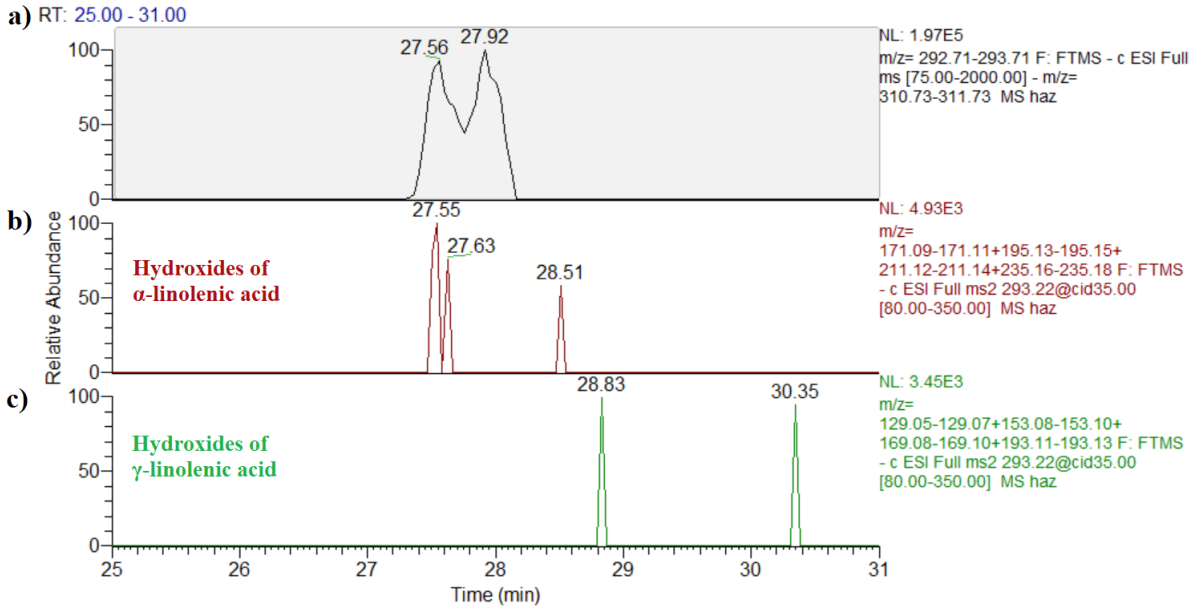

Figure 3-95 a) Mass range chromatogram of *m/z* 293 in oxidised Hazelnut oil sample. b) Reconstructed chromatogram of precursor-product MS^2 transitions *m/z* 293 to 171, 195, 211, and 235 that are characteristic for hydroxy octadeca-9,12,15-trienoic acid in LC-MS^2 analysis of oxidised Hazelnut oil sample. c) Reconstructed chromatogram of precursor-product MS^2 transitions *m/z* 293 to 129, 153, 169,

and 193 that are characteristic for hydroxy octadeca-6,9,12-trienoic acid in LC-MS^2 analysis of oxidised Hazelnut oil sample.

3.9.6 Detection and identification of fatty acids in Macadamia oil

The non-volatile fats extracted from the flesh of macadamia nut compose Macadamia oil that makes up 69-78% of nut's weight (Aquino-Bolaños et al., 2017; W. Hu et al., 2019). Almost 80% of fatty acids (FAs) present in macadamia oil are MUFAs, with oleic acid and its isomer (vaccenic acid) contributing the most to that percentage (40-70% of total fatty acid content), while PUFAs content is relatively very low (<10%), with linoleic acid being the highest and α-linolenic acid showing low traces (0.1-0.3% that reached 3% via using specific extraction method), which gives the oil a comparatively long shelf life (Aquino-Bolaños et al., 2017; W. Hu et al., 2019; Kochhar & Henry, 2009; Ribeiro et al., 2020).

The hydroxides of the anticipated highly abundant oleic acid (FA 18:1) in the tested samples of macadamia oil can be shown in figure 3-96 where our method was able to identify and differentiate between isomeric oleic acids (octadec-9-enoic acid, FA 18:1 (n−9) and octadec-11-enoic acid, FA 18:1 (n−7)). Chromatographic peaks of the hydroxides of positional isomers were distinctly isolated from the total hydroxides of oleic acids (FA 18:1) and enabled the detection of each of them.

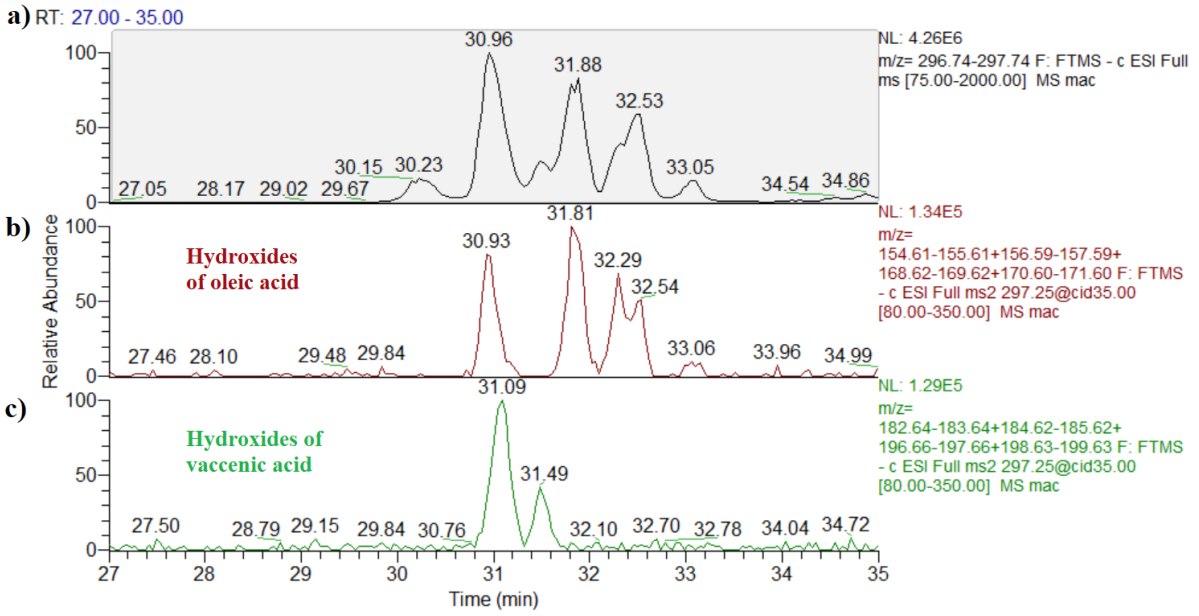

Figure 3-96 Mass range chromatogram of *m/z* 297 in oxidised Macadamia oil sample. b) Reconstructed chromatogram of precursor-product MS^2 transitions *m/z* 297 to 169, 157, 171, and 155 that are characteristic for hydroxy octadec-9-enoic acid in LC-MS^2 analysis of oxidised Macadamia oil sample. c) Reconstructed chromatogram of precursor-product MS^2 transitions *m/z* 297 to 197, 185, 199, and 183 that are characteristic for hydroxy octadec-11-enoic acid in LC-MS^2 analysis of oxidised Macadamia oil sample.

The reported scarcity of linolenic acids (FA C18:3) in the literature may explain lack of detection of the hydroxides of positional isomers of linolenic acids (FA C18:3) (α- and γ-linolenic acids) as can be noted in (Figure 3-97).

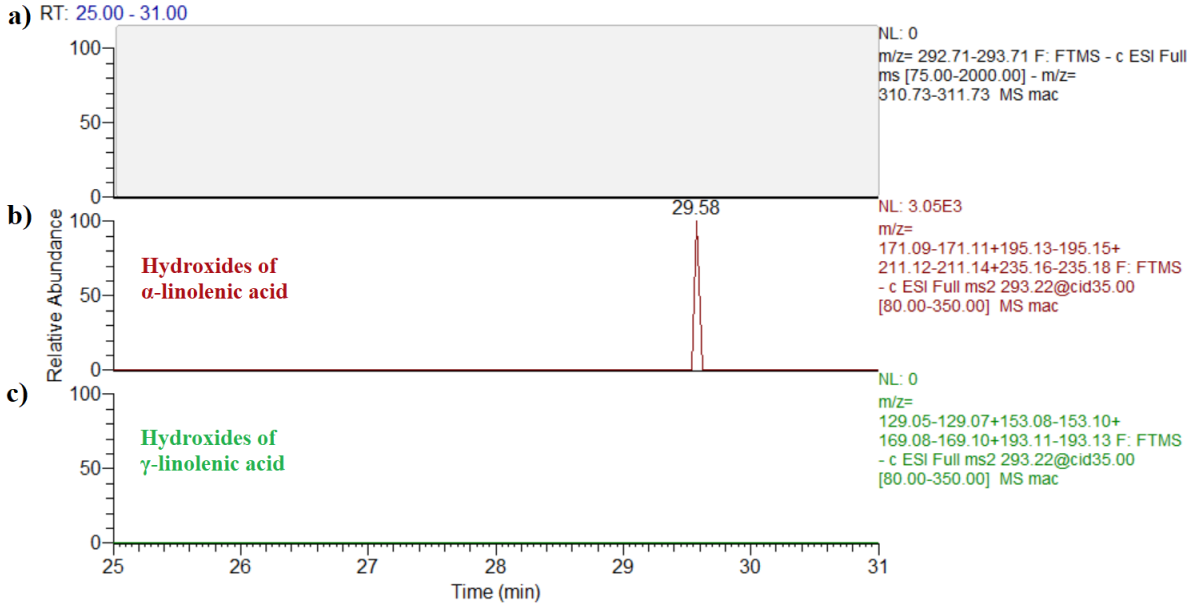

Figure 3-97 a) Mass range chromatogram of *m/z* 293 in oxidised Macadamia nut oil sample. b) Reconstructed chromatogram of precursor-product MS^2 transitions *m/z* 293 to 171, 195, 211, and 235 that

are characteristic for hydroxy octadeca-9,12,15-trienoic acid in LC-MS^2 analysis of oxidised Macadamia nut oil sample. c) Reconstructed chromatogram of precursor-product MS^2 transitions *m/z* 293 to 129, 153, 169, and 193 that are characteristic for hydroxy octadeca-6,9,12-trienoic acid in LC-MS^2 analysis of oxidised Macadamia nut oil sample.

3.9.7 Detection and identification of fatty acids in Wheat germ oil

Wheat germ oil is the non-volatile fats extracted from wheat germ using different techniques. Wheat germ itself is a by-product of wheat milling whose oil contains essential polyunsaturated fatty acids that cannot be synthesised by mammals and must be obtained from food which gives it significant nutritional and biological value (Ghafoor et al., 2016; Harrabi et al., 2021).

The most abundant fatty acid in wheat germ oil is linoleic acid (FA 18:2 n-6) which composes 49- 60% of total fatty acids. Oleic acids (FA 18:1) are reported to make up 14-25% of the total fatty acids, specified vaccenic acid content was reported by (Crăciun, 2018). Moreover, a relatively high concentrations of α-linolenic 2-10% have been registered in the literature (Crăciun, 2018; Ghafoor et al., 2016; Harrabi et al., 2021; Rehman et al., 2021).

Presence of both explored regioisomers of oleic acid (octadec-9-enoic acid, FA 18:1 (n−9) and octadec-11-enoic acid, FA 18:1 (n−7)) in tested samples of wheat germ oil was successfully demonstrated using our oxidation-based method and chromatographic peaks of the hydroxides of these positional isomers were distinctly isolated from the total hydroxides of oleic acids (FA 18:1) (Figure 3-98).

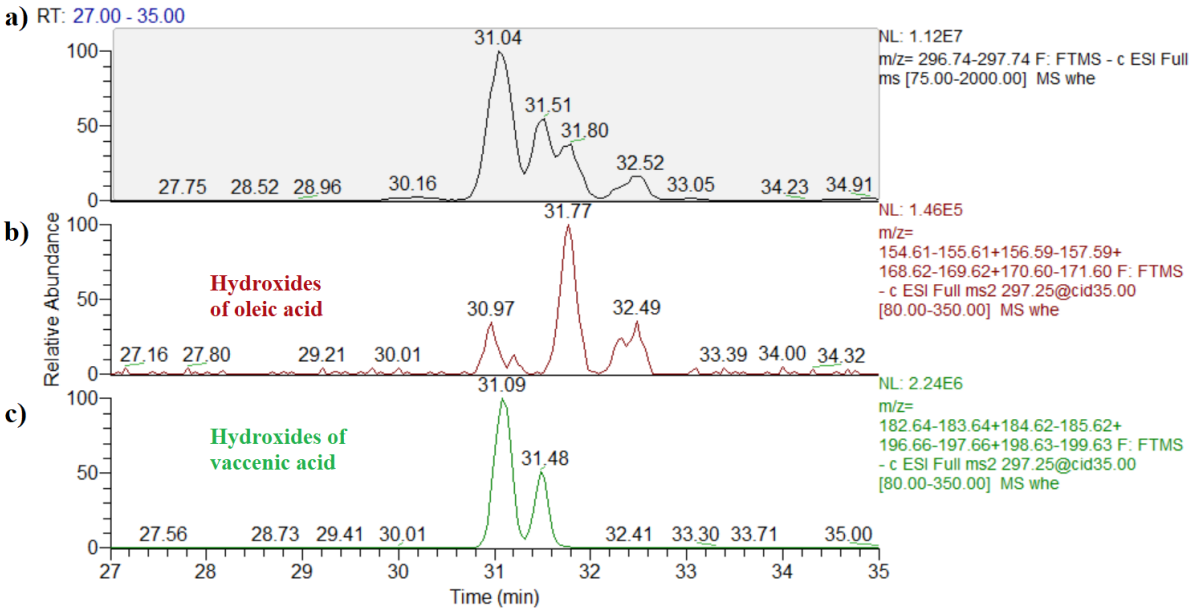

Figure 3-98 Mass range chromatogram of *m/z* 297 in oxidised Wheat germ oil sample. b) Reconstructed chromatogram of precursor-product MS^2 transitions *m/z* 297 to 169, 157, 171, and 155 that are characteristic for hydroxy octadec-9-enoic acid in LC-MS^2 analysis of oxidised Wheat germ oil sample. c) Reconstructed chromatogram of precursor-product MS^2 transitions *m/z* 297 to 197, 185, 199, and 183 that are characteristic for hydroxy octadec-11-enoic acid in LC-MS^2 analysis of oxidised Wheat germ oil sample.

The application of our method on wheat germ oil samples to detect positional isomers of linolenic acids (FA C18:3) (α- and γ-linolenic acids) was additionally fruitful to determine the double bond locations and the hydroxides of α-linolenic acid were detected and isolated from the total hydroxides of linolenic acids (FA 18:3) while no signal for the hydroxides of γ-linolenic acid was intense enough to be detected (Figure 3-99).

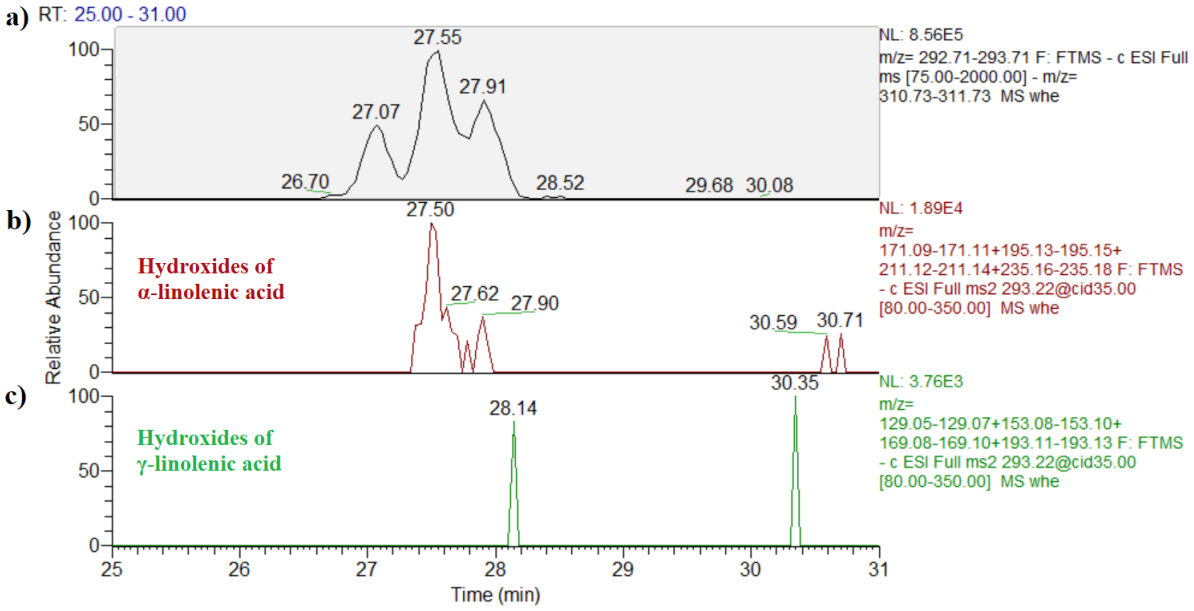

Figure 3-99 a) Mass range chromatogram of *m/z* 293 in oxidised Wheat germ oil sample. b) Reconstructed chromatogram of precursor-product MS^2 transitions *m/z* 293 to 171, 195, 211, and 235 that are characteristic for hydroxy octadeca-9,12,15-trienoic acid in LC-MS^2 analysis of oxidised Wheat germ oil. c) Reconstructed chromatogram of precursor-product MS^2 transitions *m/z* 293 to 129, 153, 169, and 193 that are characteristic for hydroxy octadeca-6,9,12-trienoic acid in LC-MS^2 analysis of oxidised Wheat germ oil.

3.9.8 Detection and identification of linoleic acid in natural oils

Linoleic acid (FA 18:2 n-6; octadeca-9,12-dienoic acid) is the most abundant PUFA found in the human diet (Raatz et al., 2018). It is regarded as the precursor compound for the family of ω6 PUFAs, elongation and desaturation of linoleic acid can lead to generating other bioactive ω6 PUFAs, such as γ-linolenic acid (FA 18:3 n-6) and arachidonic acid (FA 20:4 n-6). Eicosanoids are various bioactive compounds that include prostaglandins and leukotrienes and are products of the conversion of arachidonic acid that, in turn, cannot be produced without the intake of linoleic acid and other ω6 PUFAs (Taha, 2020).

It is well acknowledged that vegetable oils comprise a major dietary source of linoleic acid besides nuts, seeds, meats, and eggs. Furthermore, even foods with very low fat-content (vegetables, fruits, and grains) are mainly rich in linoleic acid compared to other PUFAs (Yunping Zhou et al., 2016).

According to previously mentioned literature, the content of linoleic acid in the selected vegetable oils in this work varies according to type of oil as some of them can

be considered high linoleic acid oils such as borage seed, grapeseed, and wheat germ oils while others are considered more as high oleic acid-based oils such as almond, avocado, hazelnut, and macadamia oils. Despite this variability in content, linoleic acid has been reported to be present in all these oils and it was detected using our oxidation-based method and chromatographic peaks generated by its hydroxides were identified. Hence, double bonds positions were unequivocally pinpointed (Figure 3-100).

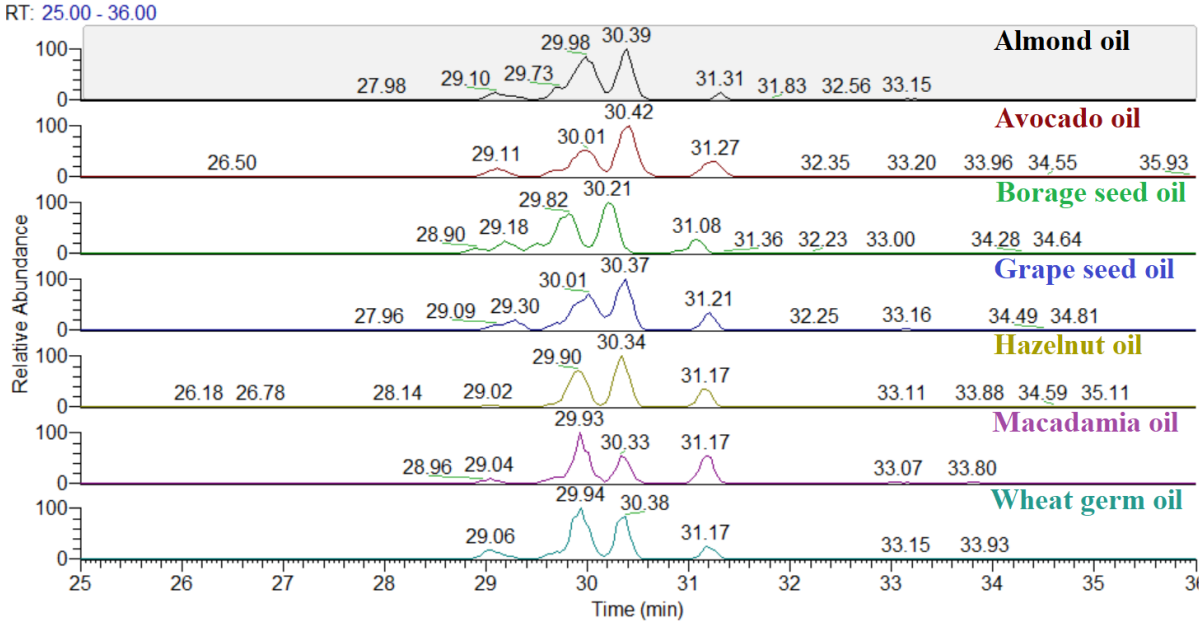

Figure 3-100 Reconstructed chromatogram of precursor-product MS^2 transitions *m/z* 295 to 171 and 195 that are characteristic for hydroxy octadeca-9,12-dienoic acid in LC-MS^2 analysis of oxidised vegetable oil samples.

3.10 Conclusion and future work

The purpose of the assay suggested in this work was to locate double bond position in unsaturated lipids and hence in the containing lipids. In future this method could be built upon to develop a validated, selective, and sensitive method for the determination of trace levels of oxidised fatty acid in complex samples like biological or food samples. A method like that would require special procedures to establish standard solutions for calibration. NMR can be used for establishing the structure of stable isomeric hydroxides prepared by oxidising a quantity of the fatty acids of interest. The amounts of each hydroxy isomer in the mixture can be established by using quantitative NMR. Once standards of established purity are attained, method calibration can proceed in the usual way. From that

point on, method validation could be carried out according to the FDA guidelines on the validation of bioanalytical methods to examine precision, accuracy, recovery, and matrix effects.

The use of MS/MS in the suggested method as a means of analyte detection in combination with an optimised liquid chromatographic assay permits the achievement of relatively low levels of both detection and quantification, given that the technique is very selective and sensitive.

The limit of detection (LoD) specifies the least amount of analyte in a sample that the developed method is capable of detecting without being able to quantify it. This means that at the LoD value an analyte must produce a signal that is at least reliably distinguishable from background noise associated with the analytical method, while the limit of quantification (LoQ), which is also known as the lower limit of quantification (LLoQ), is taken to mean the least concentration of analyte in a sample that a developed method can accurately quantify with enough precision. The LoQ is expectedly higher than the LoD value by approximately a factor of 3.

The LoD and LoQ values can be computed using regression lines that will be obtained from a set of calibration standards of the stable isomeric hydroxides prepared near the concentration range of the LoD value. The standard deviation of the measurements of these samples can be used to calculate LoD and LoQ according to the following equations:

Equation 14

$$LoD = 3.3\left(\frac{\delta}{s}\right)$$

Equation 15

$$LoQ = 10\left(\frac{\delta}{s}\right)$$

Where.

δ is the standard deviation of the response (blank responses, or residual standard deviation of the regression line, or standard deviation of the intercept of the regression line, or standard error of the estimate sy/x).

s is the slope of the calibration curve.

The standard deviation parameters of any regression can conveniently be computed using the LINEST function for plots made in Microsoft Excel®. Normally the calibration plot should be prepared from at least a 6-point calibration series.

Chapter Two:
Application of *N,N*-Dimethyl-P-phenylenediamine, *N,N*-Dimethyl-*N'*-ethylethylenediamine, 1-methylpiperazine and 1-ethyl-3-(3-dimethylaminopropyl) carbodiimide hydrochloride as tagging agents in the Analysis of fatty acids by LCMS

4 Chapter two introduction

4.1 Derivatisation in bioanalysis

Qualitative and quantitative determination of natural species or xenobiotics of various origins, that can vary from small molecular species to macromolecular biopharmaceuticals, such as proteins and peptides, constructs the main research objective for bioanalysis. This includes drugs and their metabolites, markers, toxins, environmental pollutants and contaminants, etc. (Z. Chen et al., 2020; Kightlinger et al., 2020). The bioanalytical process incorporates a wide range of complicated procedures. However, these procedures usually are focused on two distinct directions, first one is sample preparation and the other one is the analytical technique itself. Sample preparation serves many purposes but improving the sample compliance to the core analytical technique is its main task. Additionally, sample preparation can play a critical role in the optimisation of the bioanalytical method via enhancing analytical performances (precision, accuracy, detection limit, stability, chromatographic retention, selectivity, and others (He & Concheiro-Guisan, 2019; Hill, 2011; Moldoveanu & David, 2014).

The various separation and detection mechanisms coupled with High-performance liquid chromatography (HPLC) represents an important span of the analytical techniques used in quantitative and qualitative bioanalysis (Ahmad Dar et al., 2020). A vast range of possibilities for determination of the analytes or their derivatives is offered by the array of detection techniques used in HPLC such as UV–vis absorption, fluorescence, chemiluminescence, refractive index, different types of electrochemical detection, evaporative light-scattering, etc.

Chemical derivatisation is a chemical modification introduced to the target compound(s) usually as part of sample preparation to cause changes in physio-chemical properties with the aim of enhancing specific aspects of analytical performance of different classes of analytes e.g., the performance of HPLC separation, the UV absorbance and fluorescence, chemical stability of analytes and the ionisation (Deng et al., 2012; Santa, 2013). Chemical derivatisation is achieved by the means of chemical reaction and/or supporting physical factors (i.e., heating, irradiation, or electric field) (Higashi et al., 2010; Higashi & Ogawa, 2016; Santa, 2011).

Derivatisation process can be comprised of simple reactions between analyte and reagent, when a reactive derivatisation reagent causes a substitution or a condensation of a functional group in the analyte structure, or can include complex routes, when parts of small molecules are eliminated, and new moieties are formed during the process as a result of many successive reactions that involve more than one functional group. It should be noted that the common aim of derivatisations is to introduce particular moieties to the molecular structure of the analyte such as chromophores, fluorophores or groups for enhancing the MS detectability (Moldoveanu & David, 2015a).

The purpose of analysis and the intended detection technique direct the selection of the derivatisation method. This selection depends on several parameters concerning the sample and the analyte, such as: functional groups(s) from the target compounds, their concentration in the sample matrix and the complexity of the sample matrix, and other parameters concerning the analytical method such as the detection mode and the number of derivatisation artifacts produced (Moldoveanu & David, 2015a; Qi et al., 2014).

4.2 Derivatisation in LC-ESI-MS

Highly desired analytical advantages regarding selectivity and sensitivity of the challenging analysis of trace small-molecule compounds in complex samples were brought by coupling liquid chromatography with high resolution mass spectrometry by virtue of the strong separation capability of HPLC and UPLC and high selectivity and sensitivity of HRMS (Borden et al., 2020; Leendert et al., 2015; Spaggiari et al., 2014). Moreover, good universality of ESI source has rendered liquid chromatography-electrospray ionization-mass spectrometry (LC-ESI-MS) to be the most prominent analytical platform for small-molecule compounds analysis (Banerjee & Mazumdar, 2012).

The attractiveness of ESI comes from the generation of intact protonated or other adduct ions (or deprotonated) species of neutral molecules, which produce abundant signals in the mass spectrometer since that the weak covalent bonds in the molecule within the resulting gas-phase ion are preserved in this soft ionisation technique (Banerjee & Mazumdar, 2012; Leendert et al., 2015). Moreover, these ions can be used

to assign molecular structure by getting mass selection followed by dissociation experiments such as collision-induced dissociation or photodissociation, to get the informative fragment ion peaks. The constant developments of ESI-MS are speeding up advances in the field of lipidomics research with the ever-increasing sensitivity, higher resolution, speed and dynamic range of detection of analytes (Christie & Han, 2012a).

Nevertheless, LC-ESI-MS use in direct analysis of small molecule compounds still holds some issues caused by poor ionisation yield in the ionisation chamber of some compounds that lack efficiently ionisable functional groups on their structures or by poor structural stability of some compounds that can lead to easy decomposition during chromatographic separation or to dissociation in the ESI source. Furthermore, ionisation efficiency of analytes in ESI can fluctuate as a result of matrix effects that often occur in LC-ESI-MS analysis and are caused by co-eluting components (T. Y. Zhang et al., 2019). Moreover, spatial distribution within droplets can cause variation in ESI-MS response as some of highly hydrophilic compounds are more likely to be distributed in the droplet interior and their ions do not enter the gas phase as readily as those distributed in the droplets surface, hence exhibiting lower ESI-MS response (Santa, 2011).

Chemical derivatisation strategies have been demonstrated to represent an effective approach to enhance the performance of LC-ESI-MS in the analysis of compounds with small-molecular weights from complex samples. The main aspects of LC-ESI-MS analysis impacted by the implementation of an appropriate derivatisation method include improvement of detection sensitivity and selectivity and achieving higher resolution in LC separation and better quantitation accuracy in the absence of stable isotope internal standards (Moldoveanu & David, 2015b).

Enhancement of the ionisation efficiency of the analyte in ESI and its fragment ions upon getting subjected to CID leads to improvement of detection sensitivity. Therefore, derivatisation strategies that incorporate introducing a permanent positively charged group or easily protonated group as a moiety of derivatisation reagent into analytes that usually are negatively ionised have been implemented to enhance the MS detection sensitivity because ionisation efficiency in the ESI positive ion mode is

generally higher than that of the ESI negative ion mode (Moldoveanu & David, 2015b; Santa, 2013). Moreover, chemical derivatisation can be helpful to improve the MS detection selectivity since the derivatisation reaction may be highly selective for a given functional group under a certain reaction condition, eliminating possible interferences owing to coelution with the target analyte of components that do not react with the derivatisation reagent. Detection sensitivity and selectivity can benefit as well from shifting the derivatised analyte signals to a higher *m/z* range as it could reduce the interference of matrix ions usually showing in the low-mass range of the spectra and possibly avoid isobaric overlap of analyte ions with matrix signals. Additionally, some false positive interferences in CID can be reduced and thus the selectivity of LC-MS analytical methods can be improved further when derivatisation products possess characteristic fragmentation pathways (Eggink et al., 2008; Quirke et al., 1994; Z. Wu et al., 2004).

Higher resolution in LC separation can be improved through derivatisation. The retention time of analyte in a chromatographic method is determined by the chromatographic method parameters and the physical and chemical properties of the molecular structure of the analyte itself. The modification of analytes with derivatisation reagents can adjust their hydrophobicity and regulate their retention behaviours, illustrated by increasing retention times of hydrophilic compounds on reverse-phase columns or decreasing them on normal-phase and HILIC columns thereby shortening the chromatographic separation time via introducing hydrophobic groups on the structures of analytes. Equally, the introduction of appropriate hydrophilic group to highly hydrophobic compounds can diminish their retention on reverse-phase columns or delay their elution from normal-phase columns (Alothaim et al., 2017; Bawazeer et al., 2017; Rebane et al., 2012). An additional example of LC separation enhancement by chemical labelling is the conversion of enantiomers to diastereomers by chiral derivatisation reagents which leads to enabling the separation of enantiomers on common LC columns (Jin et al., 2021; Pandey et al., 2021).

Some categories of analytes in biological samples have very high reactivity and poor stability during the standard steps of sample preparation and analysis. The stability of analytes can be improved via a chemical derivatisation strategy that ensures the modification of the unstable moiety of analytes. For example, in thiol-containing

metabolites, the sulfhydryl group is very readily oxidised to form disulphide or sulfonate compounds and can have interactions with other types of molecules and can get involved in different enzymatic activities during sample preparation or LC separation (Comini, 2016; Vichi et al., 2013). These spontaneous redox reactions in the biological system adversely affect the accurate quantification of primary thiol-containing analytes, including cysteine, homocysteine, glutathione, etc., The stability and the ESI–MS response of thiol compounds could be significantly enhanced by tagging the thiol group with isotopic pair of derivatisation reagents that react selectively with thiols (Y. Q. Huang et al., 2011). A recent detailed evaluation of additional two thiol-protecting reagents for thiol group derivatisation in LC-MS analysis has been performed (Russo et al., 2020).

Derivatisation can improve another aspect of the stability of ions by reducing the confusion in the detection of metabolites arising from in-source fragmentation of metabolite ions. This confusion can be caused by wrongly considering the fragment ions produced in ESI source to be the molecular ions of other metabolites. Derivatisation can reduce the chances of forming fragment ions during the ion transport from the ionisation source to the mass analyser by improving the stability of ions. For instance, it is not easy for dansyl-labelled amines to fragment in the source region (Zheng & Li, 2012).

In most cases, the improved ionisation efficiency of analytes in ESI source by chemical tagging enhances the accuracy of quantitative analysis and reduces the detection limits for analyte profiling and accurate quantification. Furthermore, to overcome the variation of MS

response of analyte between different runs of a same sample, target analyte quantification, profiling and validation can make use of isotope dilution method. In this method, the analytes to be detected can be derivatised by the incorporation of heavy ^{2}H, ^{13}C, ^{15}N and/or ^{18}O isotopes into their structure, thereby providing stable isotopically labelled analogues that are used as internal standards to guarantee the quantitation accuracy in LC-MS analysis. Different types of isotopically labelled internal standards for analytes can be prepared by labelling the standards with an isotope-coded reagent, containing heavy isotopes; this approach is referred to as

isotope coded derivatisation. A balance between attaining comparable chromatographic behaviour to non-isotope-labelled analytes in samples and minimising interference from natural occurring isotope peaks is a preferable quality that is generally achieved by keeping the number of coding atoms on isotope-coded reagents between 3-5 (Zaikin & Borisov, 2021; T. Y. Zhang et al., 2019).

4.3 Chemical derivatisation of fatty acids

Free fatty acids and their oxylipins, such as eicosanoids, docosanoids, octadecanoids, hydroxy fatty acids, and so forth compose the main share of lipids that contain a carboxyl functional group. They play crucial roles in various physiological processes ranging from cellular signalling transduction to energy homeostasis (Wang et al., 2019). Any insights into the roles of carboxyl-containing lipids in health and diseases essentially requires qualitative profiling that provides broad coverage and accurate quantification of these compounds. While GC-MS has been widely considered as the standard commonly used platform for detection of FAs, the limited sensitivity and time-consuming sample preparation procedures shifted attention towards LC-HRMS with its high sensitivity character as it increasingly becomes a powerful alternative tool in the analysis of FAs, especially for FAs of trace abundance (Al-Dirbashi et al., 2008; X. Li & Franke, 2011). Direct detection of carboxyl-containing lipids including FAs by ESI-MS in the negative ion mode is possible and is commonly used carried out, but with low sensitivity (Brose et al., 2013; Hellmuth et al., 2012). Even with the advanced analytical instruments, the qualitative and quantitative determination of fatty acids is withstanding great complications due to the poor ionisation efficiency brought by carboxyl-containing species, high structural similarity, and low abundance. Moreover, acidified mobile phases used in reverse phase separation to promote retention of carboxylic acids are not compatible with high sensitivity negative ion mode ESI-MS (Xia & Wan, 2021).

Chemical modification of FAs is an efficient methodology to overcome these issues. Several derivatisation studies over the recent decades have used LC-MS to detect FAs (Halket & Zaikin, 2005). In general, the derivatisation strategies are designed to target the carboxyl group and increase the ionisation efficiency by introducing a chemical moiety with high ionisation capability in positive ion mode can enhance the ionisation efficiency of FAs, leading to the improved MS sensitivity (X. E. Zhao et al., 2020).

This method is also known as charge reversal chemical derivatisation. In addition to the enhancement of MS sensitivity, the introduction of a moiety or tag that is hydrophobic or capable of blocking the polar carboxyl group would lead to increasing the hydrophobicity of the derivatised analytes (David et al., 2021). Consequently, higher quality chromatographic parameters, such as better peak shape and retention on the reverse phase column might be obtained. Furthermore, one-to-one internal standards that can help achieving an accurate and reliable quantitative analysis can be provided by introducing isotopic elements (^{2}H, ^{13}C) to the derivatising reagent (Y. Q. Huang et al., 2014). In the past two decades, derivatisation strategy of targeting carboxyl group has been extensively used for the untargeted profiling and absolute quantitation of FAs in biological samples and it has involved various chemical reagent classes, including amines, hydrazines, active halogens, acylchlorides, nucleophilic addition reagents and diazos (Xiang et al., 2020; T. Y. Zhang et al., 2019). Among them, amine reagents are the most commonly utilised as the carboxyl group can react with primary or secondary amines to form the amido bond through amide formation. The amide-forming derivatising reactions take place in the presence of an initiator such as carbodiimides, in particular EDC, N-(3-dimethylaminopropyl)-N-ethylcarbodiimide, and can be used for highly sensitive determination of FAs and other carboxyl-containing compounds in lipidomics (Alothaim et al., 2017; Jiang et al., 2017; Ogawa et al., 2016; Y. Wang et al., 2018; Wei et al., 2020).

4.4 Amide formation

Amide bond formation represents one of the most significant chemical reactions that play a key role in the elaboration and composition of biological systems. The ubiquitous occurrence of amide bonds can be seen in nature and life as they represent the main chemical bonds that link amino acid building blocks together to give proteins, peptides and many amide-bond containing biomolecules that play a vital role in virtually all biological processes. Biological systems are not the exclusive media where amide bonds have high prevalence as they present in a vast range of synthetic compounds with diverse applications as synthetic polymers or pharmaceutically active compounds, including some of the most important drugs in the market such as, Atorvastatin. Lisinopril, Valsartan and Diltiazem (Valeur & Bradley, 2009). As a matter of fact, an in-depth examination carried out by Ghose et al., 1999 revealed that

the carboxamide group appears in more than quarter of identified drugs in the Comprehensive Medicinal Chemistry database at that time. Additionally, an analysis of chemical reactions employed by the Process Chemistry R&D departments in three leading pharmaceutical companies for the synthesis of drug candidates demonstrated that acylation of nitrogen into amide was by far the most dominant acylation reaction (66% of acylation reactions applied) (Carey et al., 2006), while a similar study that included drug candidates in the same pharmaceutical companies run by Roughley & Jordan, 2011 confirmed that fact with amide formation being accounted for more than 71% of acylation reactions applied and almost 16% of the total reactions in the dataset. This is sensible, since carboxamides are of great interest in organic chemistry due to their high stability, neutral nature, conformational diversity and possession of both hydrogen-bond accepting and donating properties (Pattabiraman & Bode, 2011).

The formation of amides by the reaction of a carboxylic acid and an amine (*N*-acylation) that is conventionally often used in medicinal chemistry for drug synthesis and the formation of peptides has recently become one of the most used reactions within the field of analytical chemistry for the derivatisation of carboxyl functional group (S. Y. Han & Kim, 2004; W. C. Yang et al., 2008).

Synthetic condensation of carboxylic acids and amines to form amide bonds does not occur spontaneously at ambient temperature. Owing to the unfavourable thermodynamics of the amide-forming reaction, when they are mixed, the carboxylic acid and the amine simply form a carboxylate-ammonium salt, rather than an amide product. In order to achieve the direct condensation with the necessary elimination of water, high temperature of ~ 200℃ should be applied, which is usually quite incompatible with preserving the integrity of the substrates. For that reason, it is typically necessary to initially convert the carboxylic acid into an activated form. This activation can usually be accomplished by replacing the OH of the carboxyl group with a good leaving group prior to treatment with the amine. Therefore, the use of a so-called coupling reagent, condensation agent or cross-linker that can attach a leaving group to the acyl carbon of the acid is critical (Leiro et al., 2018; Valeur & Bradley, 2009).

The activation of the carboxyl functional group can be attained via a wide range of methods and strategies that have been developed and reported in the fields of the synthetic, medicinal, analytical, or pharmaceutical chemistry. The activated forms of carboxylic acids included acyl halides, acyl azides, acylimidazoles, anhydrides, and esters besides *O*-Acylisourea derivatives that could be obtained using carbodiimides as coupling reagents (Montalbetti & Falque, 2005).

4.5 The use of carbodiimides for amide formation

The use of carbodiimides to mediate the formation of amide bonds between carboxylates and amines or phosphoramidate bonds between phosphates and amines is well recognised as the most traditional approach in use for so-called zero-length crosslinking to form peptide bonds in proteomics (Sinz, 2003). Zero-length cross-linkers are the smallest available reagent systems for bioconjugation. This is because, as the name implies, these compounds mediate the conjugation of two molecules by forming a covalent bond that attach one atom of a molecule to an atom of a second molecule with no intervening linker or spacer. This comes with great significance for method specificity in the field of proteomics as only amino acid residues whose side chains are within salt bridge distance can interact (Rivera-Santiago et al., 2015).

Due to their efficiency in forming conjugates between two amino acid residues, between amino acid residue and a surface, particle, or small molecule or between two small molecules that hold the functional groups mentioned above, the use of carbodiimides is one of the most common synthetic procedures (Chan & Cox, 2007; Leiro et al., 2018; Montalbetti & Falque, 2005; Rivera-Santiago et al., 2015). They react with the carboxylic acid to replace OH of the carboxyl group giving the corresponding labile *O*-acylisourea. This reactive *O*-acylisourea intermediate can then directly react with the amine to yield the desired amide and a urea by-product. Different water-solubility designates carbodiimides into two basic types: water-soluble and water insoluble. The water-soluble ones are the most common choice for biochemical conjugations since it allows the in-situ reaction to be carried out in aqueous medium and most macromolecules of biological origin are soluble in aqueous buffer solutions. Not only is the carbodiimide itself able to dissolve in the reaction medium, but the corresponding active intermediate *O*-acylisourea and the isourea by-

product of the reaction, is also water soluble, facilitating easy purification. Other carbodiimides that have poor aqueous solubility, by contrast, are used frequently in peptide synthesis and other conjugations involving molecules soluble only in organic solvents. Both the organic-soluble carbodiimides, their corresponding active intermediate *O*-acylisourea and their isourea by-products are insoluble in water (Cao et al., 2020; El-Faham & Albericio, 2011; Leiro et al., 2018; Valeur & Bradley, 2009).

4.6 EDC

For the purpose of conjugating biological substances that contain carboxylates and amines, the most frequently used carbodiimide is EDC (or EDAC; 1-ethyl-3-(3-dimethylaminopropyl) carbodiimide hydrochloride). In fact, the widespread utilisation of it in combination with NHS (*N*-hydroxy sulfosuccinimide) or sulfo-NHS in the field of peptides crosslinking can designate it as the most frequently used crosslinking method of all. EDC is water soluble, which eliminate the need for dissolution in organic solvent prior to its addition to a reaction. Both the reagent itself and the corresponding by-product isourea of the reaction are water soluble and may be used for amide formation without the need for the isolation of the intermediate before reacting with amines (Dunetz et al., 2016; El-Faham & Albericio, 2011; Pottorf et al., 2017; J. Sheehan et al., 1961; J. C. Sheehan et al., 1965).

EDC can be used to catalyse formation of amide bond in a variety of chemical conjugates for different objectives, as long as one of the molecules contains a carboxylate group and the other an amine (Alothaim et al., 2017; Dunetz et al., 2016; Noche et al., 2011; Wei et al., 2020; Yamada et al., 1981; Young et al., 2004). Formation of highly reactive *O*-acylisourea intermediate is the main step in EDC-mediated amide formation (Schemes 4-1 & 4-2). The reaction of this active species with a nucleophile like a primary amine forms an amide bond. Additionally, the active *O*-acylisourea is also susceptible to attack by other nucleophiles such as sulfhydryl groups to form thiol ester linkages, although these are not as stable as the amide bond. However, nucleophile attack by oxygen atoms in water molecules that causes hydrolysis is the major competing reaction, which results in breakdown of the activated ester intermediate, formation of an isourea, and regeneration the carboxylate group (Gilles et al., 1990; Williams & Ibrahim, 1981) (Scheme 4-1).

EDC used to be considered to be potentially genotoxic as it showed to be mutagenic in the Ames test; however, later studies determined that EDC is not an *in vivo* mutagen. This was attributed to the rapid hydrolysis of EDC to the corresponding urea form which is known to be non-mutagenic in the Ames test (Bercu et al., 2018).

The investigations of the reactions of EDC amide bond formation carried out by (Chan & Cox, 2007; Nakajima & Ikada, 1995) indicate that EDC hydrolysis occurs maximally at acidic pH values with increasing stability of the carbodiimide in alkaline solutions at or above pH 6.5. Nevertheless, carboxylate activation of EDC occurs most efficiently between pH 4.5 and 7.5. Beyond this pH range, however, the coupling reaction keeps taking place but more slowly and with lower yields.

Hydrolysis is one of several potential side reactions that can occur in EDC-mediated amide formation in aqueous solution besides the desired derivatisation product and it can take place at two stages in the reaction sequence to obstruct the desired product formation. One of these stages follows the first step that facilitates the desired reaction route which is the protonation of one of the nitrogens on the imide group of EDC, which results in the formation of an intermediate carbocation on the central carbon atom. At this stage, this carbocation modified carbodiimide can either proceed with the desired reaction route by reacting with an available ionised carboxylate group to create the required *O*-acylisourea reactive ester intermediate or go through hydrolysis to form an inactive isourea that no longer can participate in the reaction process (Scheme 4-1). Hydrolysis, the formation of the same undesired isourea derivative that inactivates the compound, can also happen to the *O*-acylisourea reactive ester intermediate after its acceptance of another proton to form a second carbocation on the central carbon atom (Scheme 4-1). This form of the reactive ester, if does not suffer hydrolysis, is that can go on to react with the amine-containing compound to create the intended tagged carboxylic group (Chan & Cox, 2007; Dunetz et al., 2016; Nakajima & Ikada, 1995) (Scheme 4-2).

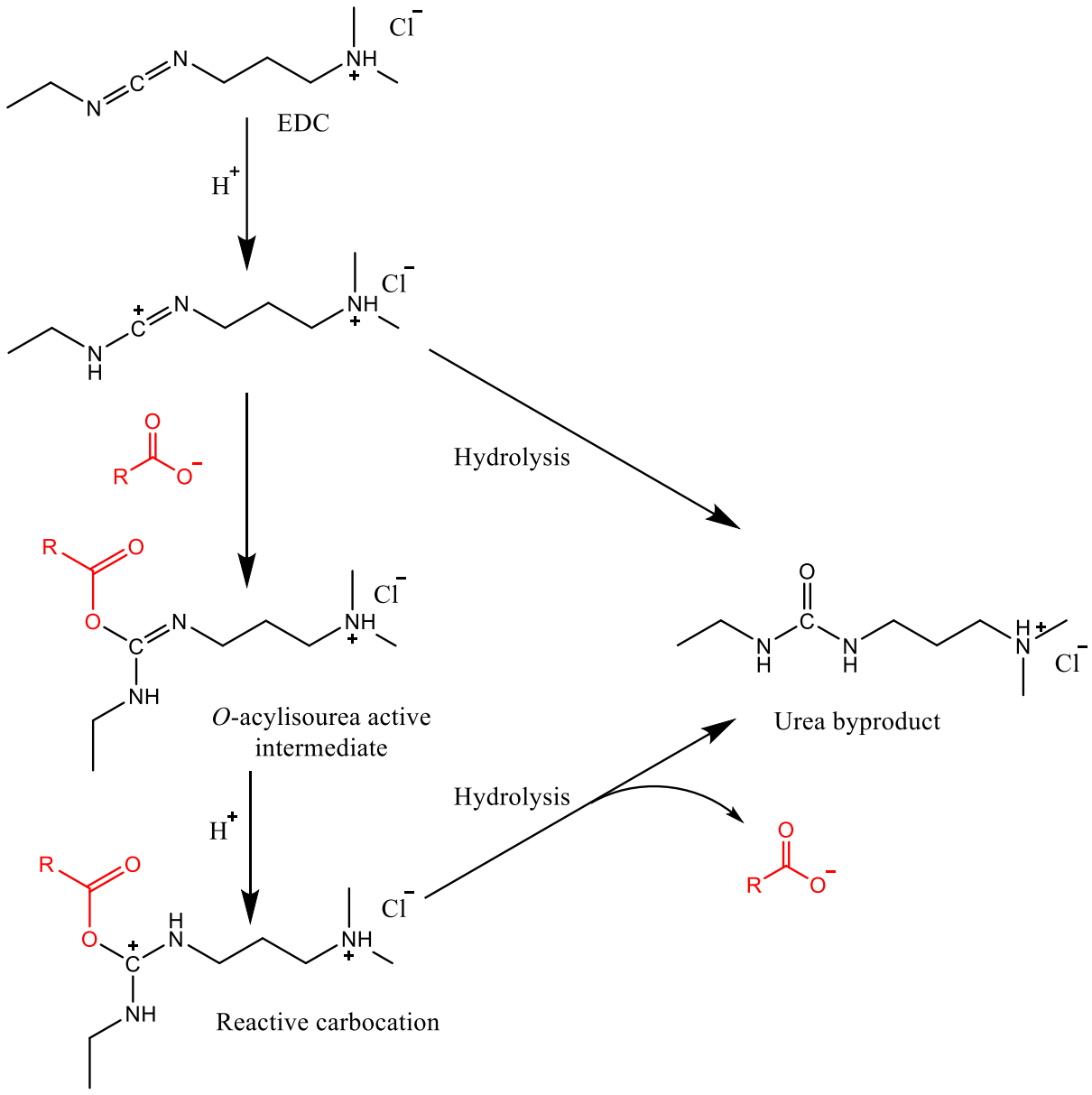

Scheme 4-1 Pathways of the hydrolysis of EDC; 1-ethyl-3-(3-dimethylaminopropyl) carbodiimide hydrochloride in the presence of carboxylic acid in aqueous solution

If hydrolysis does not occur, there are at least two subsequent reactions that can happen, in addition to the desired amide bond formation. The reaction process can proceed through formation of an anhydride intermediate with a neighbouring carboxylate group if it is in close proximity to the doubly protonated *O*-acylisourea ester. This particularly can take place in the case of excess carboxylic acid or in polymers containing repeating carboxylate groups, such as in polymethacrylate, where the primary intermediate reactive group formed from EDC may be anhydrides (Dunetz et al., 2016; C. Wang et al., 2011). The positive aspect about this side reaction is the

fact that the symmetrical anhydride is also a good acylating agent that can react with amine groups to form the desired amide bond with at least one of the two carboxylates making up the anhydride (Scheme 4-2). In fact, in certain cases, higher yields of amide bond formation may be a result of anhydride formation (Dunetz et al., 2016; Nakajima & Ikada, 1995). Another reaction that is attributed to the prolonged existence of the doubly protonated intermediate that can lead to intramolecular rearrangement of this ester by acyl transfer as a result of the reaction with the neighbouring secondary amines in the carbodiimide and thus form an *N*-acylisourea derivative (Scheme 4-2). This can occur if EDC is in large excess over the amount of carboxylates present and the resulting *N*-acylisourea derivative is inactive and permanently produces the EDC derivative of the carboxylate compound (Dunetz et al., 2016; Nakajima & Ikada, 1995).

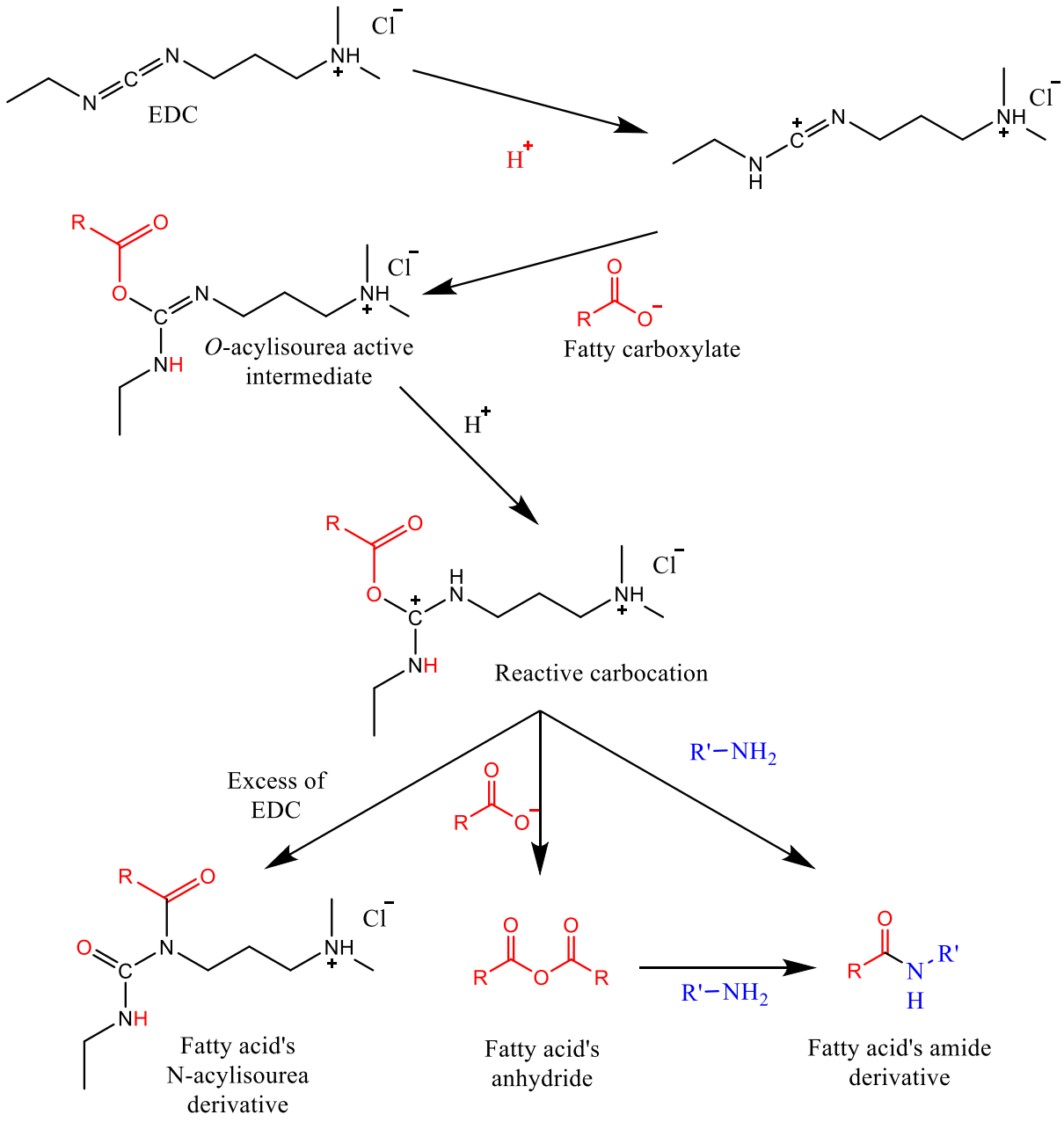

Scheme 4-2 Pathways of the reaction process of fatty acids derivatisation by amide formation in the presence of EDC in aqueous solution

4.7 Aim

The aim of this study was to investigate the suitability of three tagging agents, N,N-Dimethyl-P-phenylenediamine, N,N-Dimethyl-N'-ethylethylenediamine and 1-methylpiperazine in the presence of 1-ethyl-3-(3-dimethylaminopropyl) carbodiimide hydrochloride (EDC) as an activating agent, for the analysis of fatty acids to evaluate their suitability for application to analytical methods. Moreover, to carry out a primary assessment of the possibility of applying 1-ethyl-3-(3-dimethylaminopropyl)

carbodiimide hydrochloride (EDC) itself as a derivatising agent for the same purpose of improving sensitivity of LC-MS analysis of FAs. The labelling agents were used in the first instance to derivatise the fatty acids: oleic acid, linoleic acid and α-linolenic acid before analysis of the resulting derivatives by ESI-LCMS on an Orbitrap mass spectrometer.

5 Chapter two materials and methods

5.1 Chemicals and Materials

Where possible, FAs are annotated using the recommended shorthand notation. Oleic acid, linoleic acid, α-linolenic acid and Asolectin and the derivatization reagents DPD, DMEE, 1MP and EDC were obtained from Sigma-Aldrich (Dorset, U.K.); All solvents, reagents, and additives for sample preparation and LC-MS including tetrahydrofuran (THF), formic acid, acetonitrile and methanol were HPLC-grade and were obtained from Fisher Scientific (Leicestershire, UK). HPLC grade water was prepared in house using a Whatman Milli Q system.

5.2 Derivatisation with amines in the presence of EDC

First, standard stock solutions of EDC, DPD, DMEE, and 1MP were prepared as described below. A solution of 1 M EDC was prepared by weighing 1.92 g of EDC into a vial and dissolving it in a mixture of THF:water (1:1) to make 10 ml of solution. Similarly, 10 ml of a 0.01 M solutions of tagging agents were prepared by weighing out 13.6 mg of DPD, 11.6 mg of DMEE and 10 mg of 1MP before dissolving in THF:water (1:1). Finally, 25 µl of 1M EDC and 50 µl of 0.01 M of each tagging agent were added to vials containing 25 µl of fatty acid standard solutions (0.01 M) and the mixture was heated in a heating block at 60 degrees for 45 min. 600 µl of water was then added and solution transferred into HPLC vials for LCMS analysis. These derivatisation conditions were arrived at after undertaking different method development experiments that included varying amount of reagent, temperature and length of derivatisation.

5.3 Derivatisation with EDC

In addition to the standard stock solution of EDC described above, another standard stock solution with lower concentration (0.1 M) was prepared as an attempt to improve chromatographic peaks shape. The 0.1 M solution of EDC was prepared by weighing 192 mg of EDC into a vial and dissolving it in a mixture of THF:water (1:1) to make 10 ml of solution. Initially, 25 µl aliquots of 1M EDC were added to vials containing 25 µl of fatty acid standard solutions (0.01 M) while the attenuated EDC solution was added to 25 µl of fatty acid standard solutions (0.001 M) the resultant mixtures were ultrasonicated for 45 min at 60 degrees. 600 µl of water was then added and solution transferred into HPLC vials for LCMS analysis.

5.4 Asolectin sample Preparation

Firstly, the fatty acids were liberated from the phospholipids in asolectin via hydrolysis. A stock solution of 0.5 M KOH in ethanol was prepared to achieve fatty acids saponification. Samples of 200 mg of the asolectin were taken and dissolved in 2ml of ethanolic potassium hydroxide and heated in a sealed tube at 60°C for 30 minutes. The generated potassium fatty acids salts were hydrolysed by addition of 2 ml of 1 M HCl to liberate fatty acids before they were extracted with 4 ml of hexane. The hexane layer was removed and blown to dryness. An estimate of 80 mg of the fatty acids would be obtained which was then put through the EDC derivatisation process described above.

5.5 LC-MS Analysis

Preliminary identification of the chemical structure of the derivatisation products was performed by using a Dionex HPLC instrument connected to an Exactive Orbitrap (Thermo Fisher Scientific, UK). The HPLC was fitted with an ACE 5 C18-AR column (5 µm, 150mm x 4.6mm, HiChrom, Reading UK). The mobile phases consisted of 0.1% formic acid in water (A) and 0.1% formic acid in acetonitrile (B) and the flow rate of the mobile phase was 0.3 ml/min. Two different gradient systems were used; the first one was 10% B, (0 min.); 90% B, (20-34 min.); 10% B, (35-40 min.) while the second one was 60% B, (0 min.); 90% B, (20-34 min.); 60% B, (35-40 min.). The gradients used are illustrated in in the table below (Table 5-1)

Table 5-1 Illustration of mobile phase gradient programs used in LC-MS analysis.

Time	Original gradient		Modified gradient		Flow Rate (µL/min)
	A%	B%	A%	B%	
0	90	10	40	60	300
20	10	90	10	90	300
34	10	90	10	90	300
35	90	10	40	60	300
40	90	10	40	60	300

The ESI interface was operated in dual positive/negative switching mode, with a spray voltage was 4.5 kV for positive mode and 4.0 kV for negative mode. The temperature of the ion transfer capillary was 275 °C and sheath and auxiliary gas were set at 50 and 17 arbitrary units respectively. The full scan range was 75 to 1200 *m/z* for both positive and negative modes with the settings for the Automatic Gain Control (AGC) target and resolution set as Balanced and High (1E6 and 50,000) respectively. The data was recorded using the Xcalibur 2.1.2 soft-ware package (ThermoFisher Scientific, Bremen, Germany). Mass calibration was performed for both ESI polarities prior to the analysis using the standard ThermoCalmix solution with additional compounds to cover the low mass range and the signals of 83.0604 *m/z* (2 **x** ACN + H) and 91.0037 *m/z* (2 **x** formate - H) were selected as lock masses for positive and negative mode respectively during each analytical run.

6 Chapter two results

6.1 Derivatisation with *N,N*-Dimethyl-P-phenylenediamine (DPD)

The derivatisation of FAs occurs via reaction with the carbodiimide, EDC, that achieves deprotonation and activation of the fatty acid resulting in the formation of an

O-acylisourea active intermediate. This intermediate then reacts with the amine, DPD, to form a final stable amide and a urea by-product (Scheme 6-1).

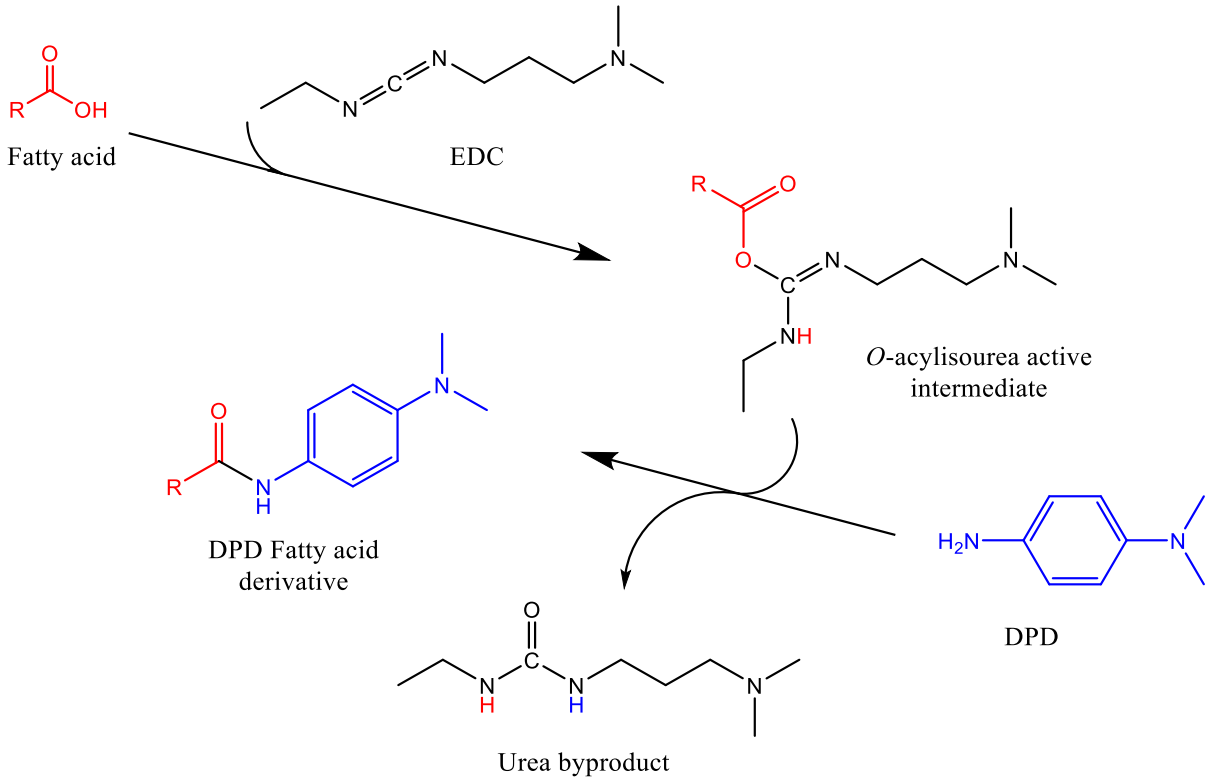

Scheme 6-1 Derivatisation of fatty acids (FAs) with EDC and DPD. The EDC deprotonates and activates the fatty acid leading to the formation of an O-acylisourea, an intermediate which then reacts with DPD to form the final stable amide derivative.

As a result of the reaction outlined above, (Scheme 6-1), it is evident that the final consequence of the derivatisation is a loss of a hydroxyl group (OH 17 Da) from the FA and a single proton (1 Da) loss from DPD. These losses cause transformation of EDC into the urea by-product. Therefore, the calculated mass of the protonated DPD derivative molecular ion in positive mode ESI-MS can be expressed by the following formula:

Mass of DPD derivative cation = (mass of FA) + (mass of DPD) - 17

Thus, the masses of the derivatives for the tested FAs can be determined, following the reaction, as shown in the table below (for DPD, Formula = $C_8H_{12}N_2$, MW = 136.19) (Table 6-1).

Table 6-1 Formulae and MW of the tested FA derivatives after reaction with EDC and DPD.

Name	Underivatised		Derivatised	
	Formula	Molecular weight	Formula	Molecular weight
Oleic acid	$C_{18}H_{34}O_2$	282.47	$C_{26}H_{44}N_2O$	400.65
Linoleic acid	$C_{18}H_{32}O_2$	280.45	$C_{26}H_{42}N_2O$	398.64
α-Linolenic acid	$C_{18}H_{30}O_2$	278.44	$C_{26}H_{40}N_2O$	396.62

It should be noted that the FA derivatives will only ionise in the positive mode following the reaction illustrated above (Scheme 6-1). Since the carboxylate group of the FAs, which is ordinarily ionised in the usually preferred negative ESI mode, has been converted into an amide, the FA derivatives formed no longer ionise in the negative ESI mode. At this point, the tertiary amino group on the DPD reagent *para* to the site of derivatisation with the FA is the favoured ionisation site. This entails that *m/z* values for DPD-FA derivatives would be one atomic mass unit higher than the calculated MW of the individual derivatives as they would have gained an additional proton via ionisation.

The figures below (Figures 6-1 to 6-3) show the mass spectra and elemental compositions of the derivatives of oleic acid, linoleic acid and α-linolenic acid as obtained after derivatisation with DPD in presence of EDC.

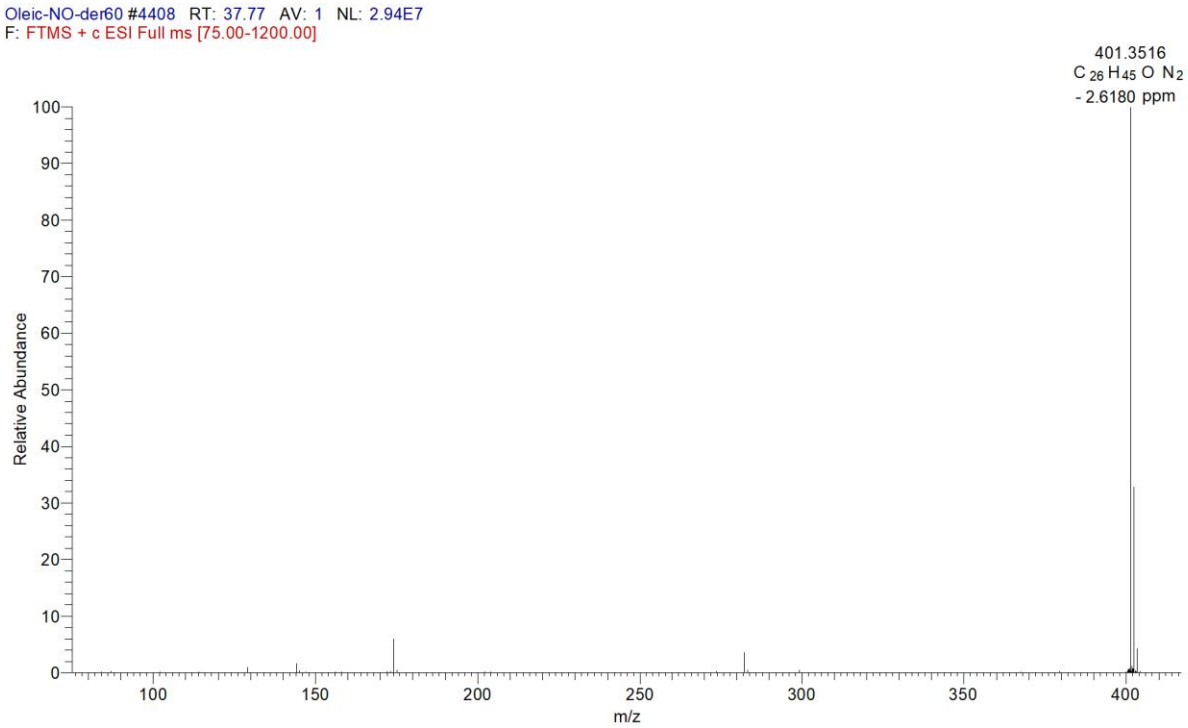

Figure 6-1 Mass spectrum of the positively charged DPD-derivative of oleic acid showing the expected accurate mass of 401.3516.

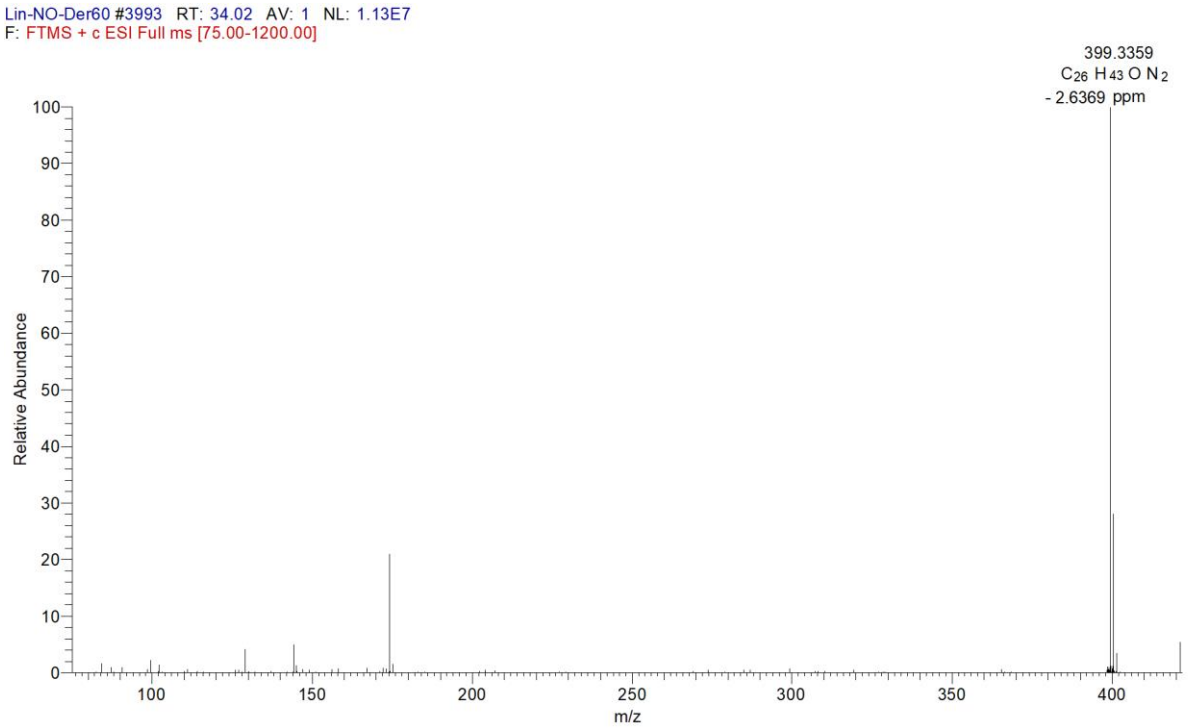

Figure 6-2 Mass spectrum of the positively charged DPD-derivative of linoleic acid showing the expected accurate mass of 399.3359.

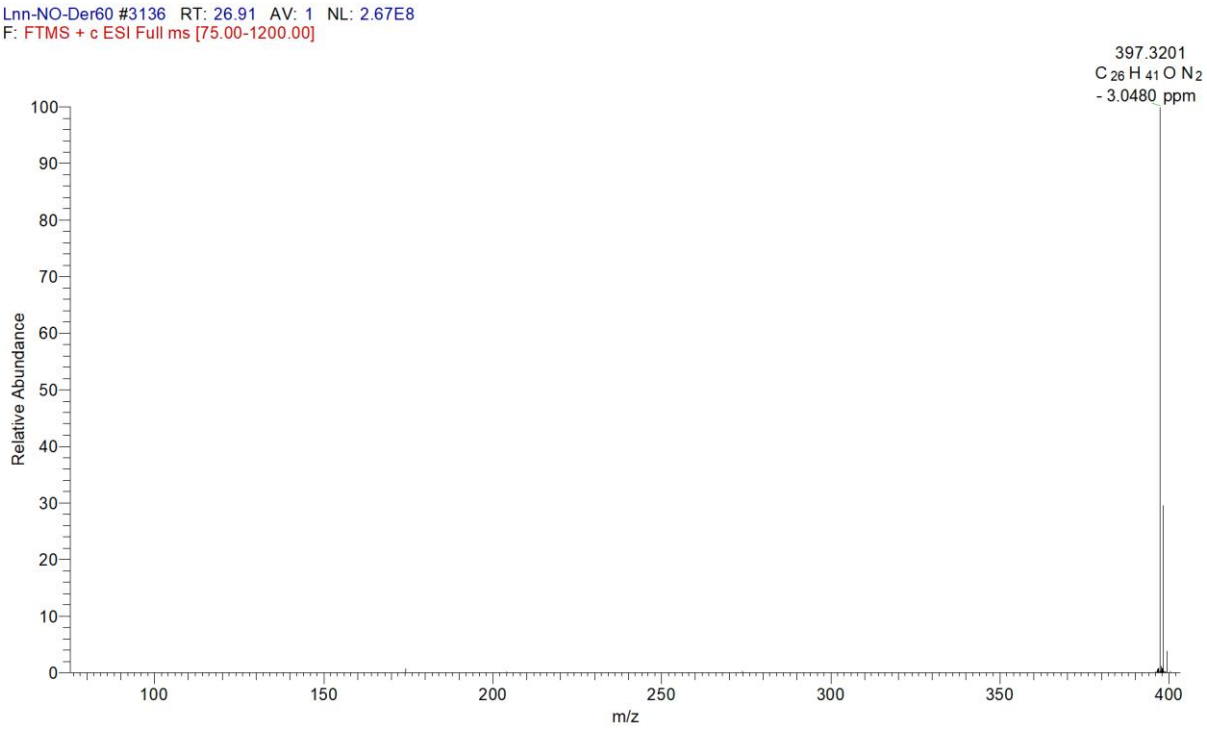

Figure 6-3 Mass spectrum of the positively charged DPD-derivative of α-linolenic acid showing the expected accurate mass of 397.3201.

Figure 6-4 shows the chromatograms obtained from the derivatisation reaction of oleic acid, linoleic acid, and α-linolenic acid with DPD in presence of EDC.

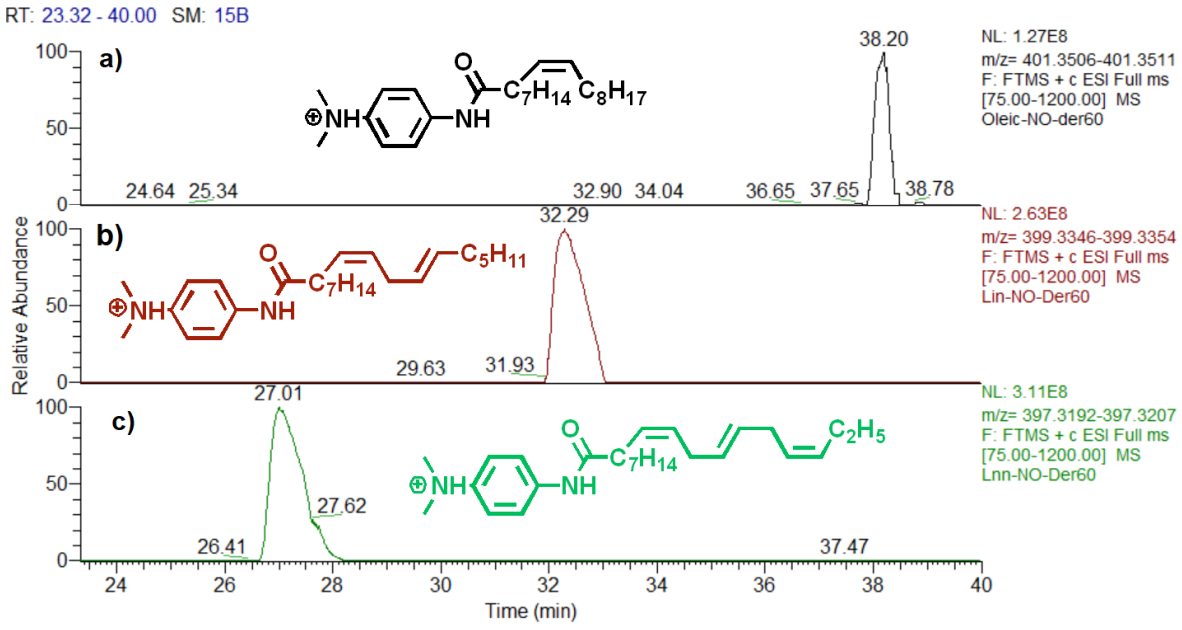

Figure 6-4 The chromatograms of the three fatty acids derivatised with DPD in presence of EDC; oleic acid (a), linoleic acid (b) and α-linolenic acid (c).

The mass spectra of the derivatized FAs showed the expected molecular ions at *m/z* 401.3516, *m/z* 399.3359 and *m/z* 397.3201 for oleic acid, linoleic acid and α-linolenic acid, respectively, which are correct for these fatty acids elemental compositions (Figures 6-1, 6-2 and 6-3). The tagged FAs had extremely strong retention on the reverse phase column, especially the derivative of oleic acid that did not elute under the original gradient conditions (Figure 6-5a) while the other FAs had retention times of Rt 39.14 and 35.32 minutes for linoleic acid and α-linolenic acid, respectively. Adjustment of the mobile phase gradient conditions into a gradient with higher initial organic content gave shorter elution times for the derivatives without compromising the resolution between the tagged FAs (Figure 6-5b). The retention times of the tagged FAs under the modified chromatographic method showed that the derivative of α-linolenic acid was still the least retained (Rt 27.01 minutes), while the derivative of oleic acid was the most retained of all three tested FAs (Rt 38.20 minutes), and there was good separation between the three FA derivatives eluted between 27.01 and 38.20 minutes (Table 6-2). Moreover, their peak shapes were approximately symmetrical, which is indicative of good chromatography.

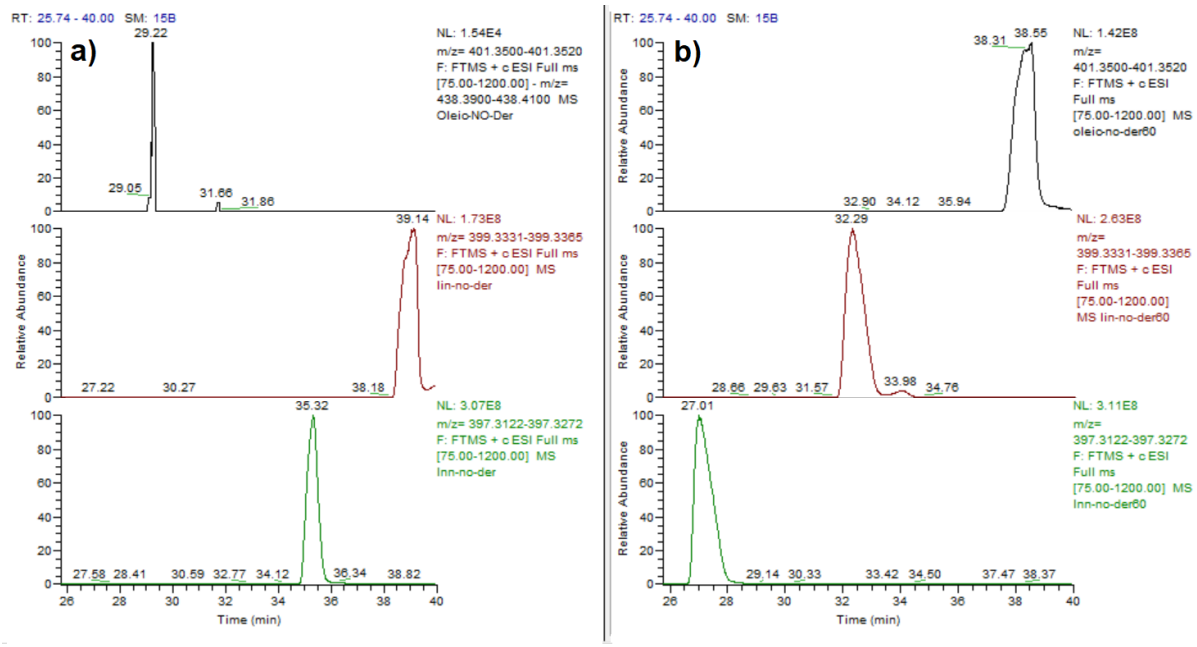

Figure 6-5 Comparison of the chromatographic retention times of the three fatty acids derivatised with DPD in presence of EDC between original gradient condition (a), gradient with higher initial organic content (b).

Table 6-2 Summary of the results obtained from the analysis of FA derivatised with DPD in presence of EDC.

Tagged fatty acid	Elemental composition	*m/z*	Rt (min) at different initial %B for 40 min	
			10	60
Oleic acid	$C_{26}H_{45}N_2O$	401.35	N/A	38.55
Linoleic acid	$C_{26}H_{43}N_2O$	399.34	39.14	32.29
α-Linolenic acid	$C_{26}H_{41}N_2O$	397.32	35.32	27.01

6.2 Derivatisation with *N,N*-Dimethyl-N'-ethylethylenediamine (DMEE)

The derivatisation method with DMEE occurs through the same reaction mechanism of the amidation of FAs in the presence of the carbodiimide, EDC, and it proceeds via deprotonation and activation of EDC to form the *O*-acylisourea active intermediate that reacts with the amine, DMEE, in the same pathway of the reaction with DPD, to form the amide bond eventually (Scheme 6-2).

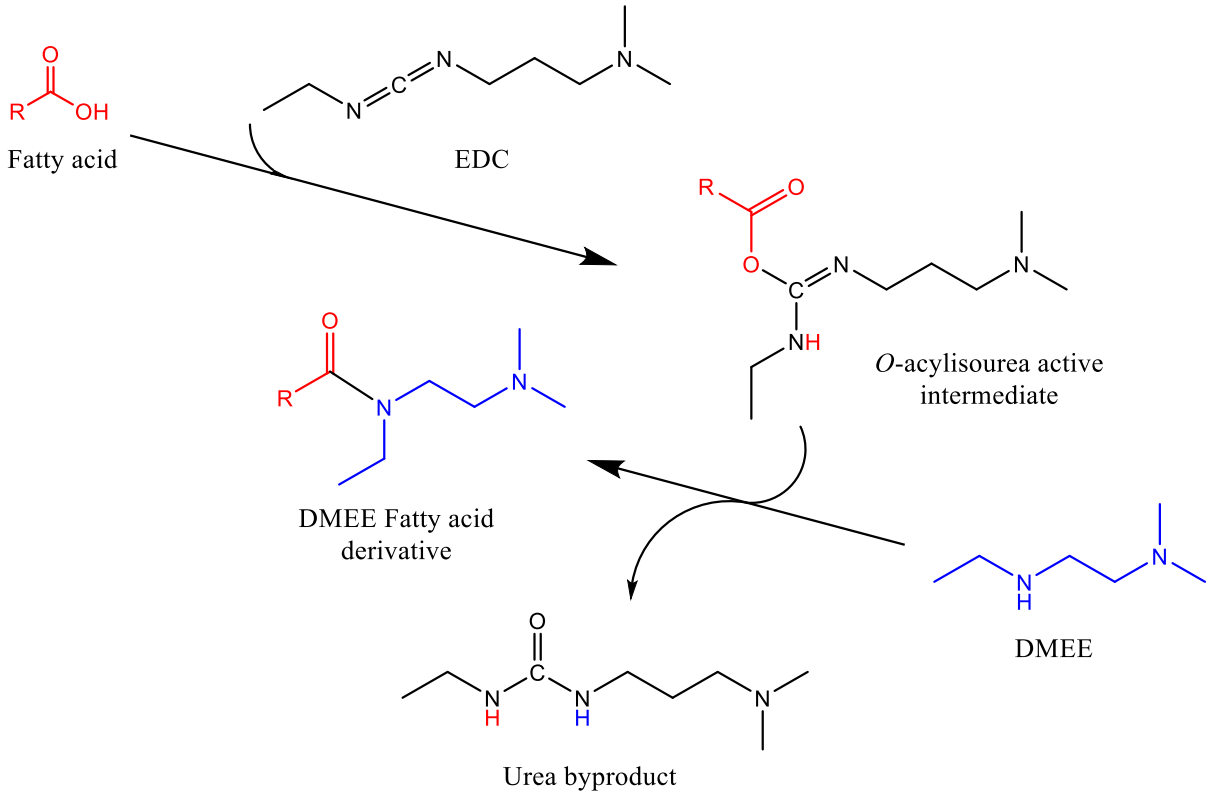

Scheme 6-2 Derivatisation of fatty acids (FAs) with EDC and DMEE. The EDC deprotonates and activates the fatty acid leading to the formation of an O-acylisourea, an intermediate which then reacts with DMEE to form the final stable amide derivative.

As it is the case with DPD derivatisation, besides the transformation of EDC into the urea by-product, the final outcome of the derivatisation reaction outlined above includes a loss of a hydroxyl group (OH 17 Da) from the FA and a single proton (1 Da) loss from the amine, DMEE (Scheme 6-2). Therefore, the calculated mass of the protonated DMEE derivative molecular ion in positive mode ESI-MS can be expressed by the following formula:

Mass of DMEE derivative cation = (mass of FA) + (mass of DMEE) - 17

Thus, the masses of the derivatives for the tested FAs can be determined, following the reaction, as shown in the table below (for DMEE, Formula = $C_6H_{16}N_2$, MW = 116.13) (Table 6-3).

Table 6-3 Formulae and MW of the tested FA derivatives after reaction with EDC and DMEE.

Name	Underivatised		Derivatised	
	Formula	Molecular weight	Formula	Molecular weight
Oleic acid	$C_{18}H_{34}O_2$	282.47	$C_{24}H_{48}N_2O$	380.66
Linoleic acid	$C_{18}H_{32}O_2$	280.45	$C_{24}H_{46}N_2O$	378.65

The charge-reversal in the FA derivatives should be achieved in the case of completion of the reaction illustrated above (Scheme 6-2) and only ionisation in the positive mode should be observed as the carboxylate group of the FAs, which is ordinarily ionised in the usually preferred negative ESI mode, has been converted into an amide. At this point, the tertiary amino group on the DMEE reagent is the favoured ionisation site. This implies that *m/z* values for DMEE-FA derivatives would be one atomic mass unit higher than the calculated MW of the individual derivatives as they would have gained an additional proton via ionisation.

the mass spectra and elemental compositions of the DMEE-derivatives of oleic acid and linoleic acid that were formed in presence of EDC are shown in the figures below (Figures 6-6 & 6-7).

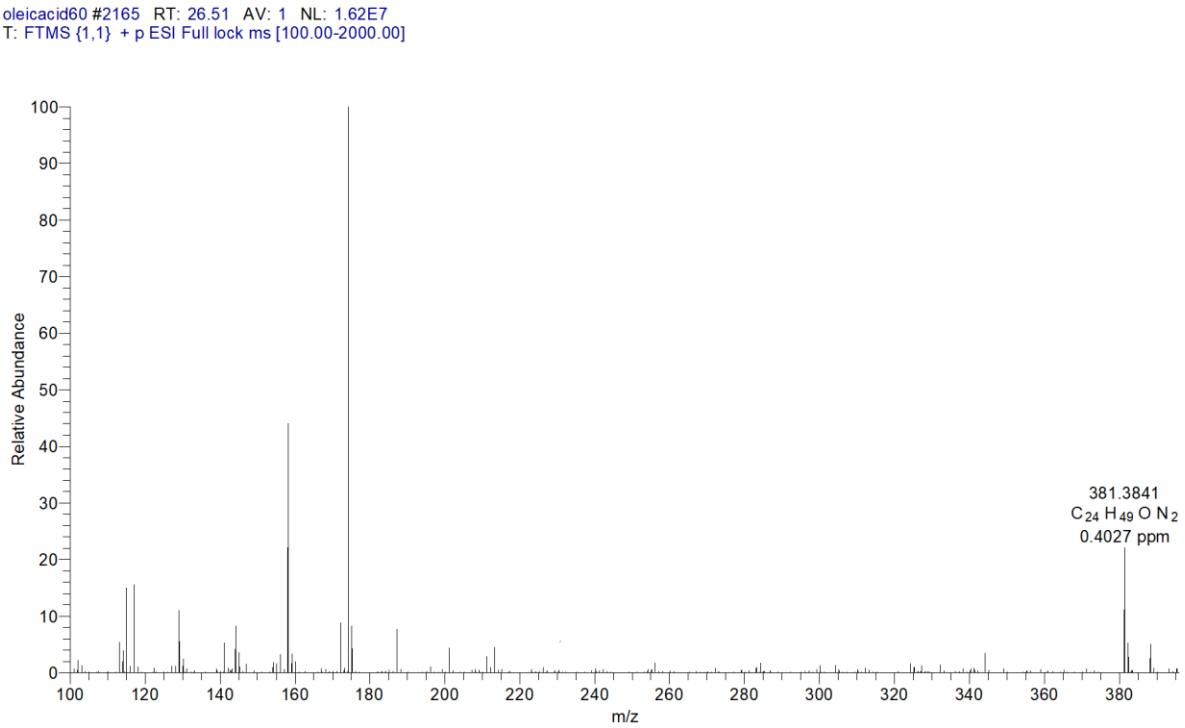

Figure 6-6 Mass spectrum of the positively charged DMEE-derivative of oleic acid showing the expected accurate mass of 381.3841.

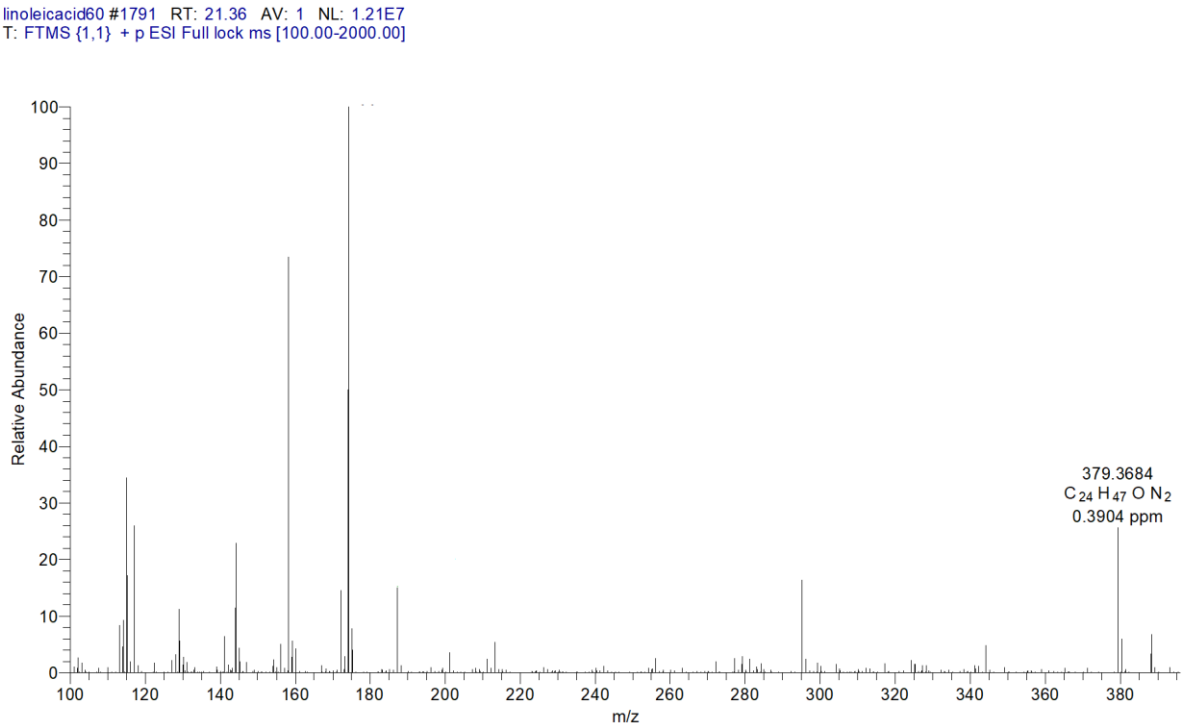

Figure 6-7 Mass spectrum of the positively charged DMEE-derivative of linoleic acid showing the expected accurate mass of 379.3684.

The chromatograms obtained from the derivatisation reactions of oleic acid and linoleic acid with DMEE in presence of EDC can be seen in figure 6-8.

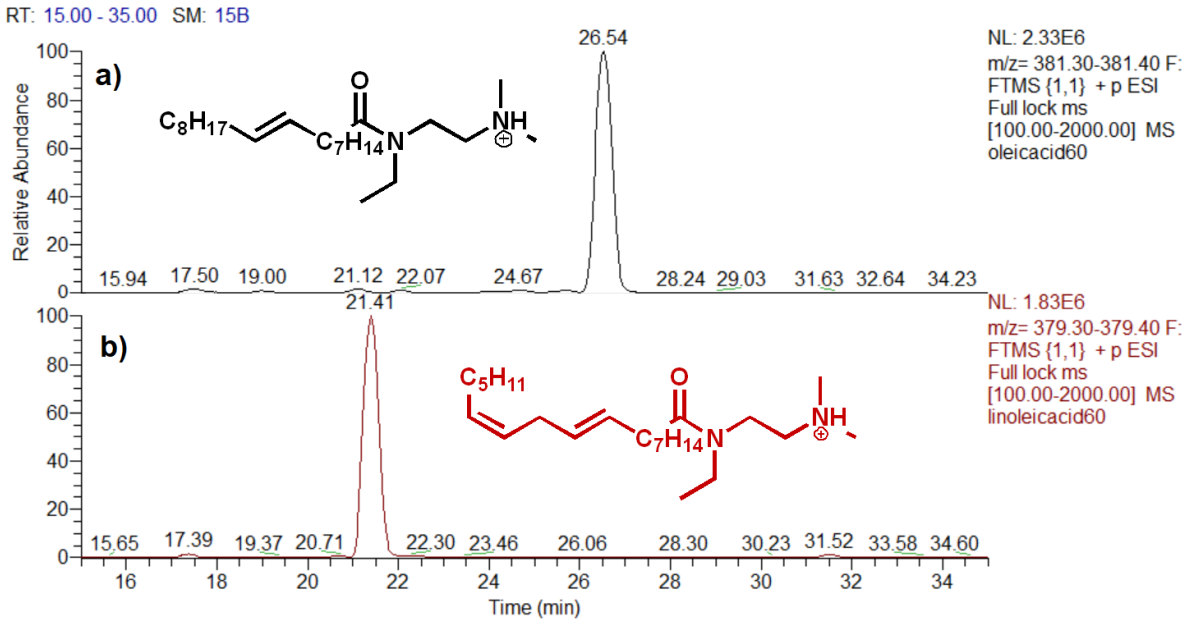

Figure 6-8 The chromatograms of the fatty acids derivatised with DMEE in presence of EDC; oleic acid (a), and linoleic acid (b).

The mass spectra of the DMEE derivatised FAs showed the expected molecular ions $[M+H]^+$ at *m/z* 381.3841 and *m/z* 379.3684 for oleic acid and linoleic acid , respectively, which are correct for the calculated elemental compositions (Table 6-3). The retention times of the tagged FAs on the reverse phase column showed that derivatised oleic acid was the most retained (Figure 6-8). Oleic and linoleic acids were well separated with retention times of Rt 26.54 and 21.41 minutes, respectively. The peak shapes for the FA derivatives were approximately symmetrical, characteristic of good chromatography.

6.3 Derivatisation with 1-methylpiperazine (1MP)

The amide-formation reaction of FAs with 1MP in the presence of the carbodiimide, EDC, proceeds via the same pathway discussed above with the other tested amines, where the *O*-acylisourea intermediate formed as a result of deprotonation and activation of EDC by the fatty acid reacts with the amine, 1MP (Scheme 6-3).

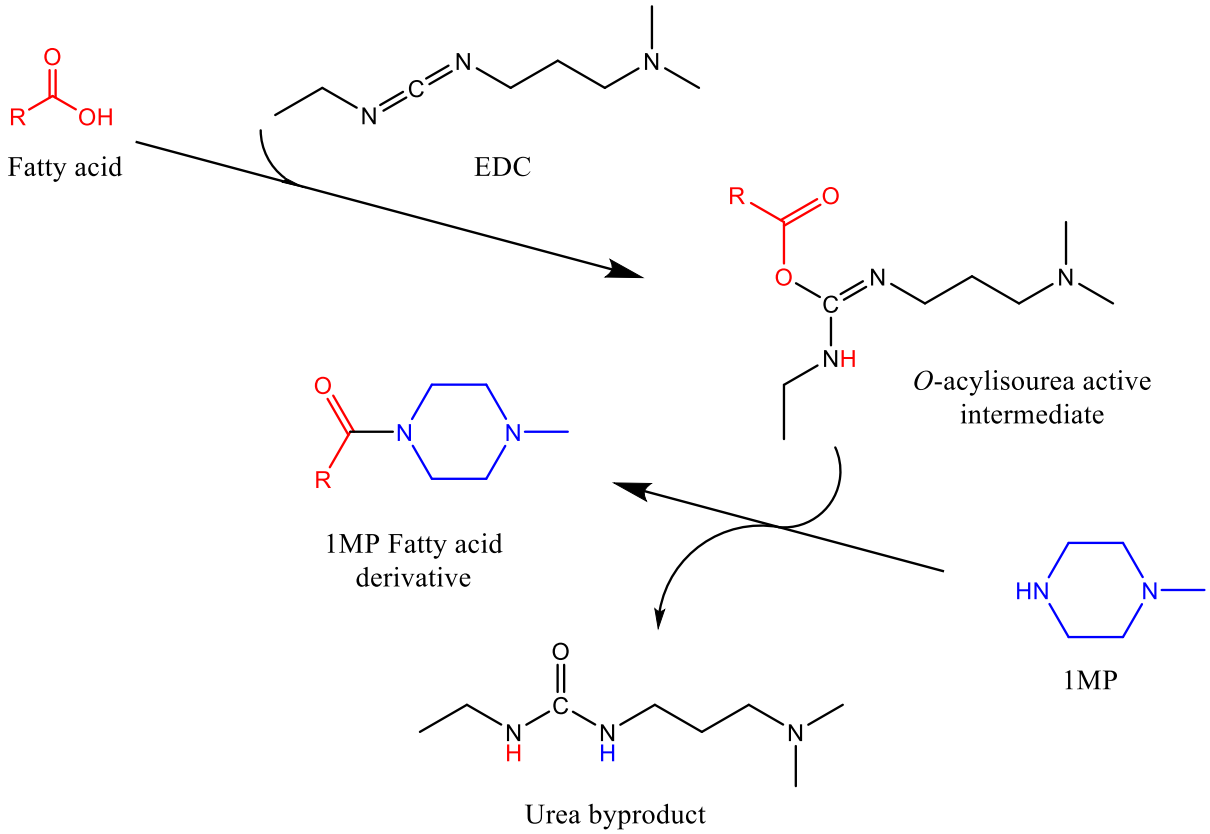

Scheme 6-3 Derivatisation of fatty acids (FAs) with EDC and 1MP. The EDC deprotonates and activates the fatty acid leading to the formation of an O-acylisourea, an intermediate which then reacts with 1MP to form the final stable amide derivative.

As it has the same mechanism as the earlier discussed amide formation reactions, the 1MP tagging of FAs has the same losses in the reacting molecules that include a loss of a hydroxyl group (OH 17 Da) from the FA and a loss of a single proton (1 Da) from the tagging agent, 1MP. Consequently, a similar formula can be used to calculate mass of the protonated 1MP derivative molecular ion in positive mode ESI-MS:

Mass of 1MP derivative cation = (mass of FA) + (mass of 1MP) - 17

Thus, the masses of the derivatives for the tested FAs can be determined, following the reaction, as shown in the table below (for 1MP, Formula = $C_5H_{12}N_2$, MW = 100.17) (Table 6-4).

Table 6-4 Formulae and MW of the tested FA derivatives after reaction with EDC and DMEE.

Name	Underivatised	Derivatised

	Formula	Molecular weight	Formula	Molecular weight
Oleic acid	$C_{18}H_{34}O_2$	282.47	$C_{23}H_{44}N_2O$	364.62
Linoleic acid	$C_{18}H_{32}O_2$	280.45	$C_{23}H_{42}N_2O$	362.60

The tagged FA derivatives should preferably ionise in the positive ESI-mode in the case of completion of the reaction illustrated above (Scheme 6-3) and not in the negative ESI-mode that is usually preferred for the carboxylate group of the FAs. The amide formation would mask the carboxylic group while the favoured ionisation site would become the other amino group that is fully substituted as it gains an additional proton via ionisation. Hence, the ionised 1MP-tagged FAs would have *m/z* values of one atomic mass unit higher than the calculated MW of the individual derivatives.

the mass spectra and elemental compositions of the 1MP-derivatives of oleic acid and linoleic acid that were formed in presence of EDC are shown in the figures below (Figures 6-9 & 6-10).

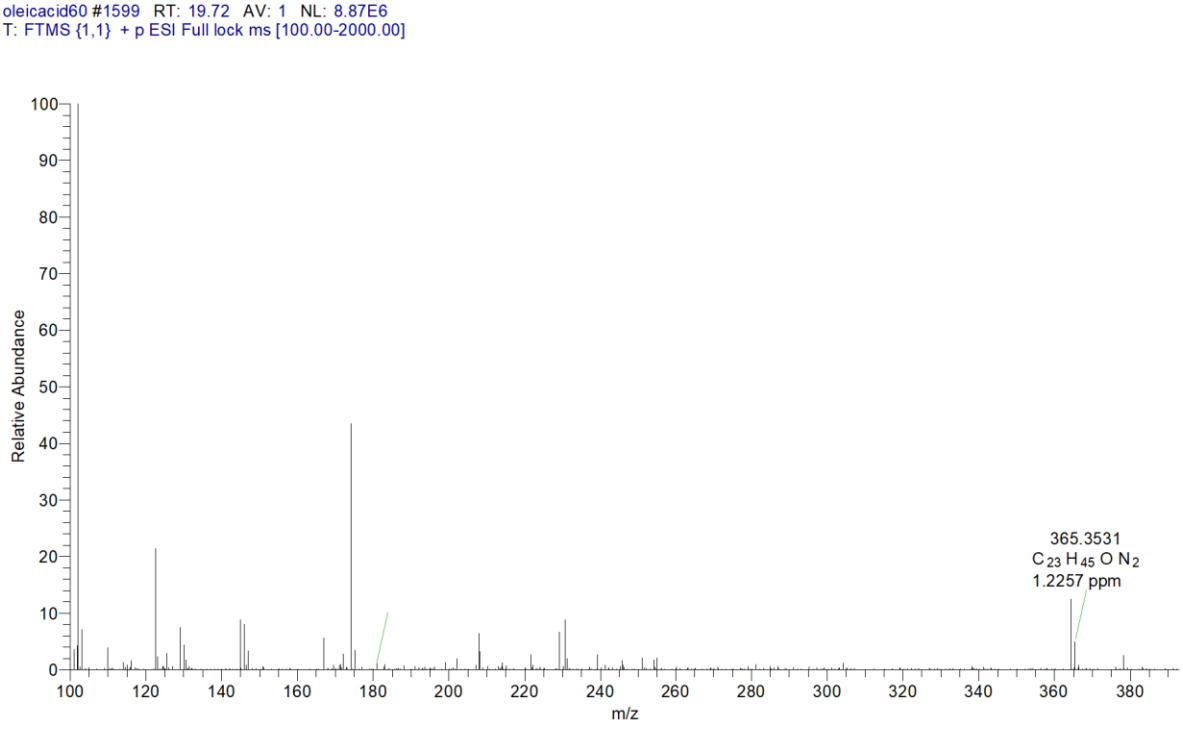

Figure 6-9 Mass spectrum of the positively charged 1MP-derivative of oleic acid showing the expected accurate mass of 365.3531.

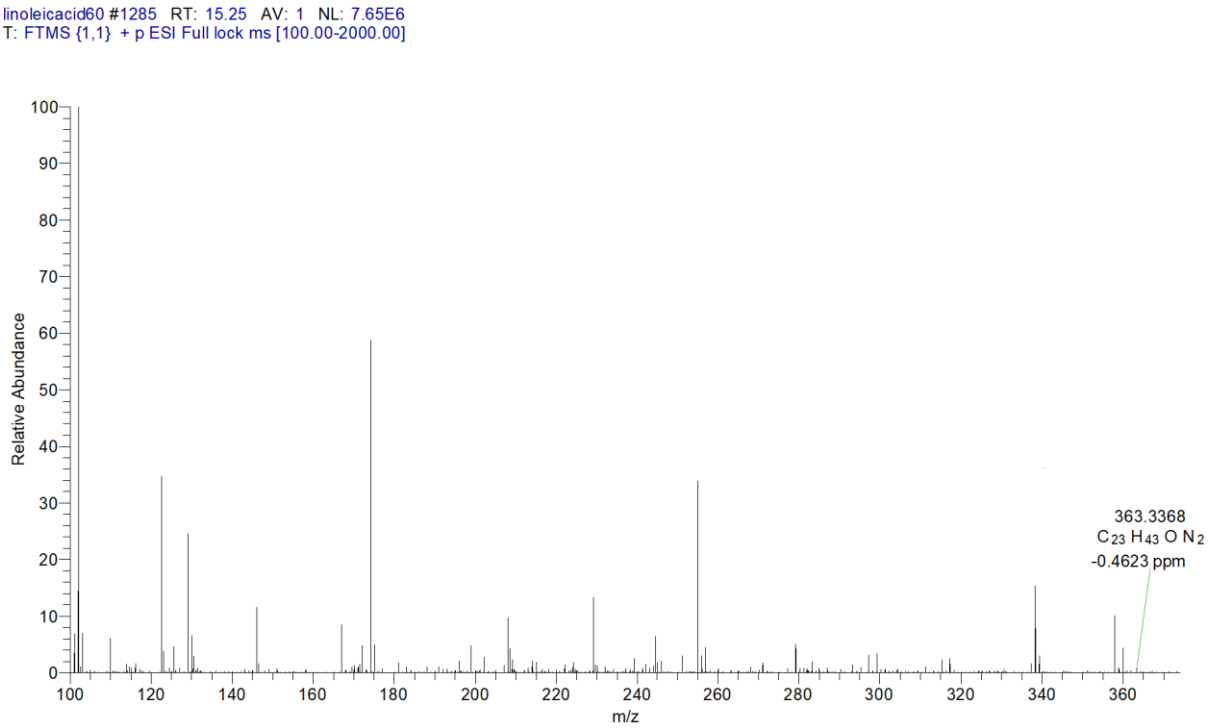

Figure 6-10 Mass spectrum of the positively charged 1MP-derivative of linoleic acid showing the expected accurate mass of 363.3368.

The chromatograms obtained from the derivatisation reactions of oleic acid and linoleic acid with 1MP in presence of EDC can be seen in figure 6-11.

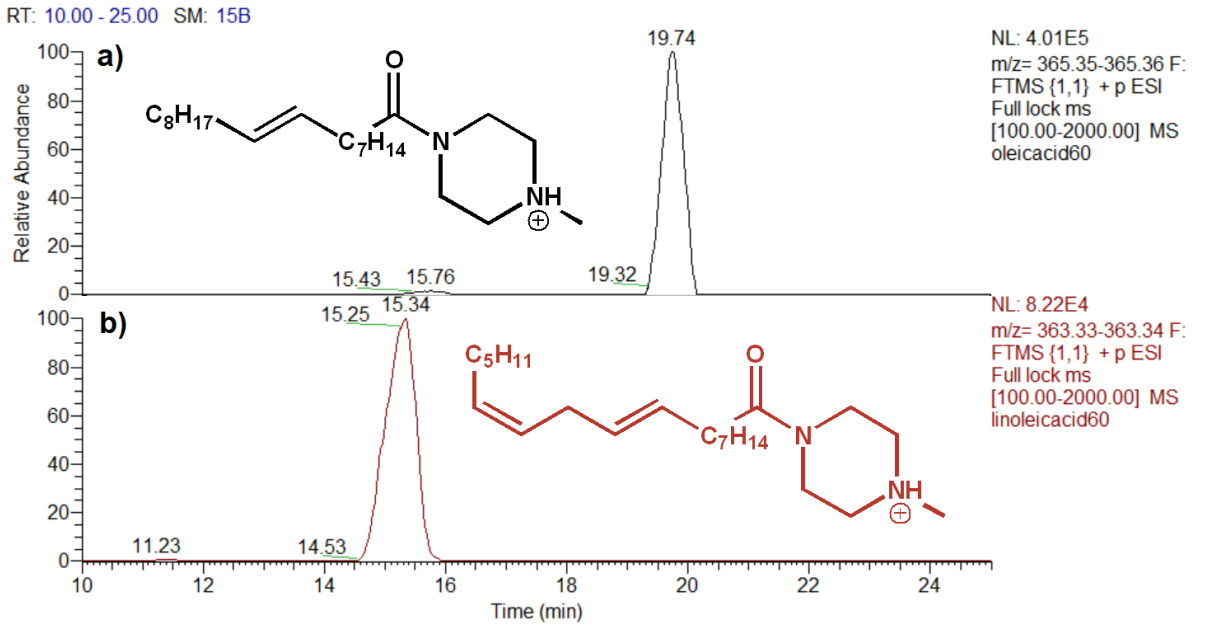

Figure 6-11 The chromatograms of the fatty acids derivatised with 1MP in presence of EDC; oleic acid (a), and linoleic acid (b).

The mass spectra of the 1 MP FA derivatives showed the expected molecular ions $[M+H]^+$ at *m/z* 365.3531 and *m/z* 363.3368 for oleic acid and linoleic acid , respectively, which are correct for the calculated elemental compositions (Table 6-4). The retention times of the tagged FAs on the reverse phase column showed that derivatised oleic acid was the most retained (Figure 6-11), as it was the case when tagged with other tested amines. Oleic and linoleic acids were well separated with retention times of Rt 19.74 and 15.34 minutes, respectively. The peak shapes for the FA derivatives were approximately symmetrical, characteristic of good chromatography.

6.4 Discussion of derivatisation with tested amine tagging agents

Fatty acids are difficult to analyse and detect by LCMS due to their poor ionisation efficiency caused by carboxyl functional group, high structural similarity, and their low abundance (Brose et al., 2013; Hellmuth et al., 2012). In addition to the drawbacks in applying negative ion mode MS while using acidified mobile phases for better separation on reverse phase (Xia & Wan, 2021). Tagging such analytes has been demonstrated to be of great value in overcoming these challenges (Moldoveanu & David, 2015b).

This work was therefore focused on the investigation of the application of N,N-Dimethyl-P-phenylenediamine (DPD), N,N-Dimethyl-N'-ethylethylenediamine (DMEE) and 1-methylpiperazine (1MP) as tagging agents in order to evaluate their ability to aid the analysis of FAs. The use of both DPD and for less extent DMEE tags significantly increased the degree of ionisation which aided their detection in positive mode by LCMS (Figures 6-4 & 6-8). However, the ionisation enhancement obtained with 1MP was not satisfactory in spite of the observed good peak shapes (Figure 6-11). It is envisioned that derivatisation using either DPD or DMEE in the presence of EDC can offer fairly quick and inexpensive methods that would be suitable for use in the analysis of fatty acids in food and biological samples. It is also anticipated that superior degree of ionisation produced by DPD as a tagging agent for long chain fatty acids and stronger retention of the derivative can be of greater benefit for trace detection in complex samples. These observations are consistent with what DPD derivatisation method had shown with short chain fatty acids (Alothaim et al., 2017).

6.5 Derivatisation with 1-ethyl-3-(3-dimethylaminopropyl) carbodiimide hydrochloride (EDC)

The potential application of EDC as a derivatising agent originates theoretically from one side pathway of the reaction process of amide formation in the presence of EDC which is outlined in scheme 4-2. In theory, the prolonged occurrence of the doubly protonated *O*-acylisourea intermediate during the amide formation reaction can lead to intramolecular rearrangement of this ester via migration of acyl group from the oxygen attached to the central carbon in the carbodiimide structure to the neighbouring secondary amines and thus formation of a stable and inactive *N*-acylisourea derivative of the FA and discontinuation of the reaction with amine tagging agent (Dunetz et al., 2016; Nakajima & Ikada, 1995). This one-step reaction associated with intramolecular rearrangement (Scheme 6-4) can be proposed to be the main derivatisation mechanism that eliminate the need of additional amines to achieve the intended objectives of derivatisation, since the fact that EDC would be playing the role of the derivatising agent besides its role as activating reagent.

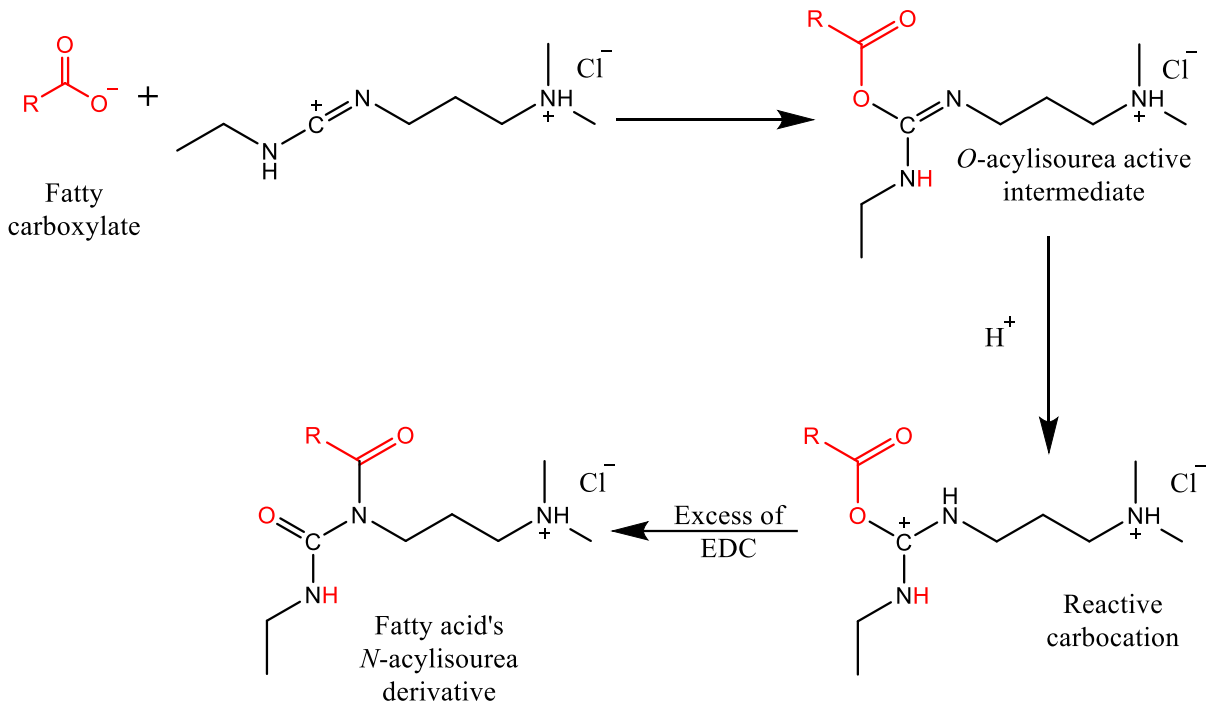

Scheme 6-4 Derivatisation of fatty acids (FAs) with EDC as tagging agent. The EDC deprotonates and activates the fatty acid leading to the formation of an *O*-acylisourea, an intermediate which then goes through intramolecular rearrangement to form stable and inactive *N*-acylisourea derivative.

Since the suggested mechanism of the derivatisation reaction outlined above (Scheme 6-4) does not include the transformation of EDC into the corresponding urea by-product and since the amide bond formed within the structure of the *N*-acylisourea derivative occur as a result of intramolecular rearrangement, it is obvious that no loss in mass from the FA nor from the tagging agent, EDC, is proposed to take place in the final derivatisation product. Therefore, the calculated mass of the protonated EDC *N*-acylisourea derivative molecular ion in positive mode ESI-MS can be expressed by the following formula:

Mass of N-acylisourea derivative cation = (mass of FA) + (mass of EDC) + 1

Thus, the masses of the derivatives for the tested FAs can be determined, following the reaction, as shown in the table below (for EDC, Formula = $C_8H_{17}N_3$, MW = 155.25) (Table 6-5).

Table 6-5 Formulae and MW of the tested FA derivatives after reaction with EDC.

Name	Underivatised		Derivatised	
	Formula	Molecular weight	Formula	Molecular weight
Oleic acid	$C_{18}H_{34}O_2$	282.47	$C_{26}H_{51}N_3O_2$	437.71
Linoleic acid	$C_{18}H_{32}O_2$	280.45	$C_{26}H_{49}N_3O_2$	435.70
α-Linolenic acid	$C_{18}H_{30}O_2$	278.44	$C_{26}H_{47}N_3O_2$	433.68

The favoured site of ionisation in the *N*-acylisourea derivatives would be the tertiary amino group on the EDC structure. Therefore, the FA derivatives will only ionise in the positive mode following the reaction illustrated above (Scheme 6-4) and will no longer ionise in the negative ESI mode since the carboxylate group of the FAs, which is ordinarily ionised in the usually preferred negative ESI mode, has been converted into an amide. This means that *m/z* values for EDC-FA derivatives would be one atomic mass unit higher than the calculated MW of the individual derivatives as they would have gained an additional proton via ionisation.

The figures below (Figures 6-12 to 6-14) show the mass spectra and elemental compositions of the derivatives of oleic acid, linoleic acid and α-linolenic acid as obtained after derivatisation with EDC.

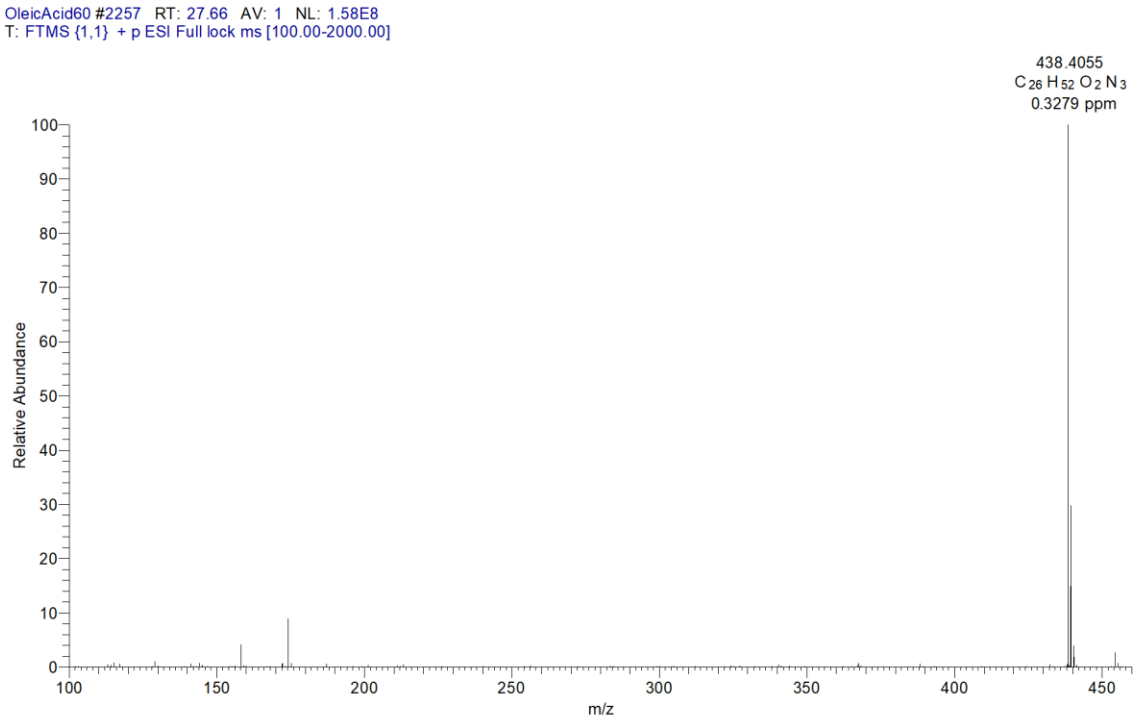

Figure 6-12 Mass spectrum of the positively charged EDC *N*-acylisourea derivative of oleic acid showing the expected accurate mass of 438.4055.

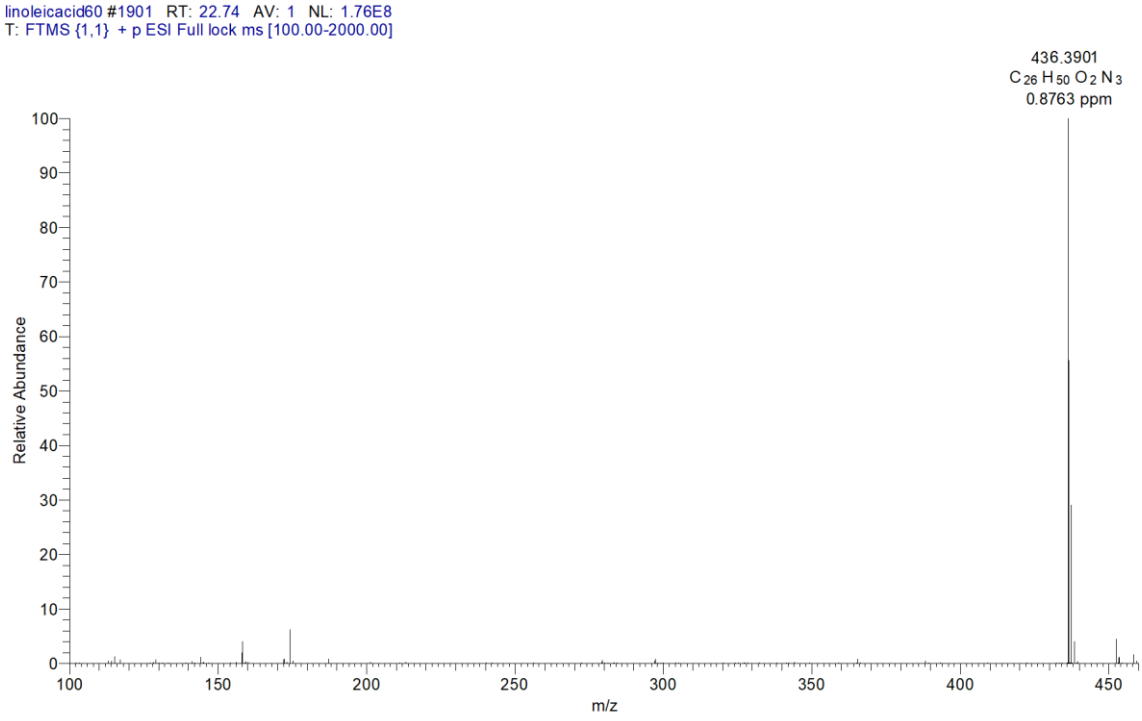

Figure 6-13 Mass spectrum of the positively charged EDC *N*-acylisourea derivative of linoleic acid showing the expected accurate mass of 436.3901.

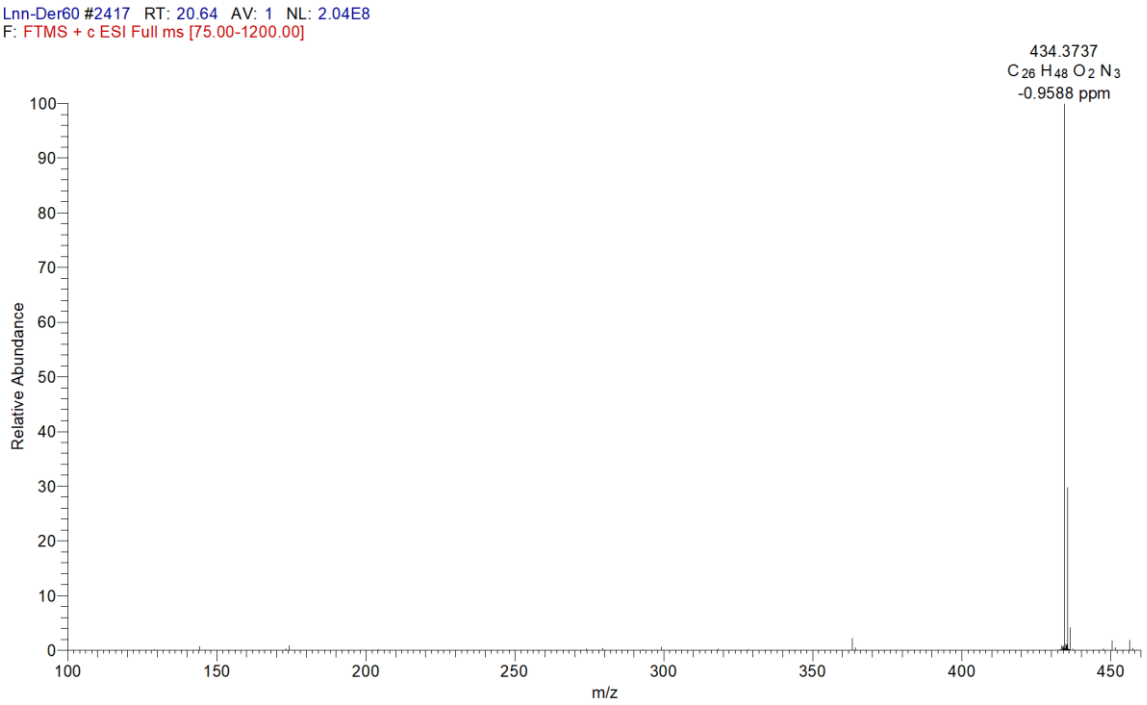

Figure 6-14 Mass spectrum of the positively charged EDC *N*-acylisourea derivative of α-linolenic acid showing the expected accurate mass of 434.3737.

Figure 6-15 shows the chromatograms obtained from the derivatisation reaction of oleic acid, linoleic acid, and α-linolenic acid with EDC.

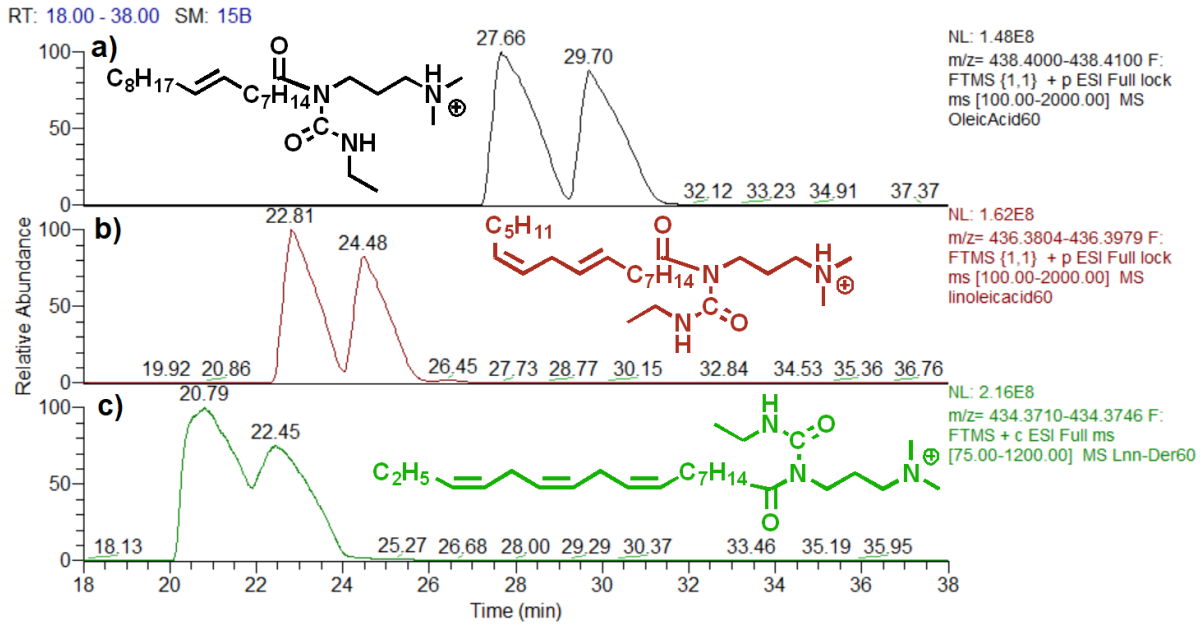

Figure 6-15 The chromatograms of the three fatty acids derivatised with EDC; oleic acid (a), linoleic acid (b) and α-linolenic acid (c).

The mass spectra of the derivatized FAs showed two peaks for each expected molecular ion at *m/z* 438.4055, *m/z* 436.3901 and *m/z* 434.3737 for oleic acid, linoleic acid and α-linolenic acid, respectively, which are correct for these fatty acids elemental compositions (Figures 6-12, 6-13 and 6-14). The reason of observing two isobaric peaks for each fatty acid derivative could be the possible formation of two structural isomers as a result of two intramolecular rearrangements where the acyl in the doubly protonated *O*-acylisourea ester is transferred to react with one of the two neighbouring secondary amines in the carbodiimide and thus to form two *N*-acylisourea isomeric derivatives (Scheme 6-5).

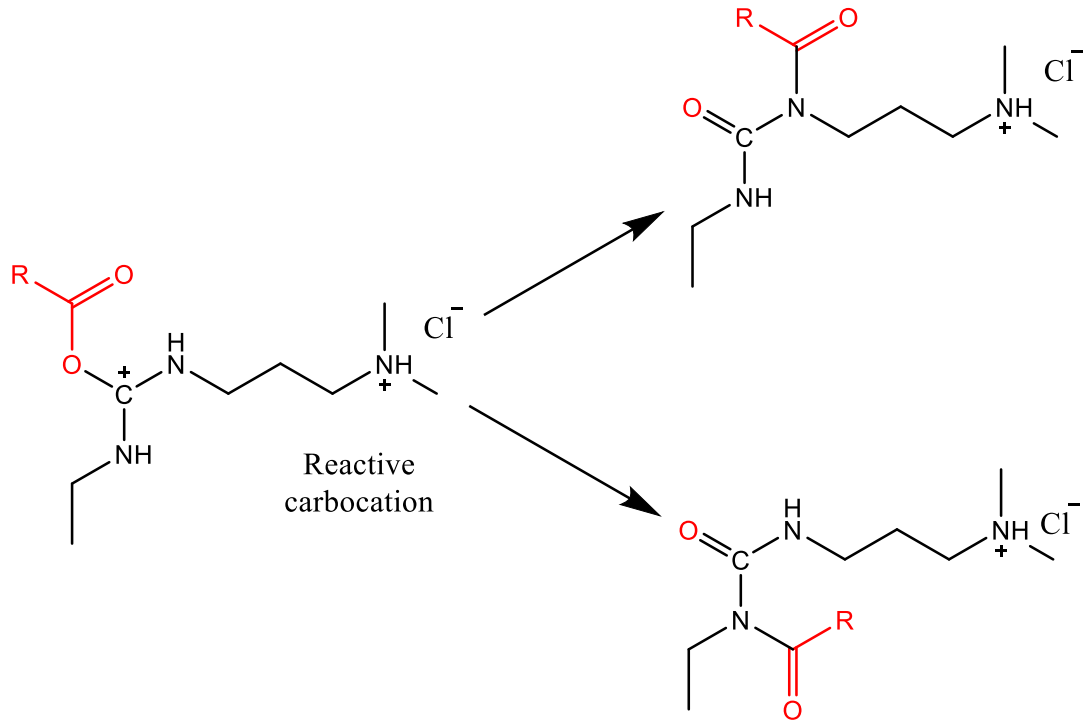

Scheme 6-5 Proposed mechanism of the formation of two structurally isomeric derivatives of FA.

The retention times of the tagged FAs under chromatographic method showed that the derivatives of α-linolenic acid were the least retained (Rt 20.79 and 22.45 minutes), while the derivatives of oleic acid were the most retained of all three tested FAs (Rt 27.66 and 29.70 minutes), and the derivatives of the three FA eluted between 20.79 and 29.70 minutes with the derivatives of linolenic acid eluting at Rt 22.81 and 24.48 minutes (Figure 6-15). The derivatives of α-linolenic acid and linolenic acid however did not show any appreciable separation between them. This implies that although all the long chain fatty acids analysed could all be successfully tagged with EDC as a

derivatising reagent; the tagged α-linolenic acid and linolenic acid were not sufficiently different to result in appreciable separation between them under the conditions of the method. This is however not a problem when using the Orbitrap as the derivatives have distinct masses and can therefore be accurately integrated even in a mixture. Nevertheless, peak tailing was obvious for the derivatives of all three FAs which could be caused by column overloading as FAs and EDC were used in relatively high concentrations to ensure thourough derivatisation reaction. Figures 6-16 & 6-17 show how the use of reduced amounts of reactants resulted in improved peak shapes that were approximately symmetrical with base line resolution, which are indicatives of good chromatography.

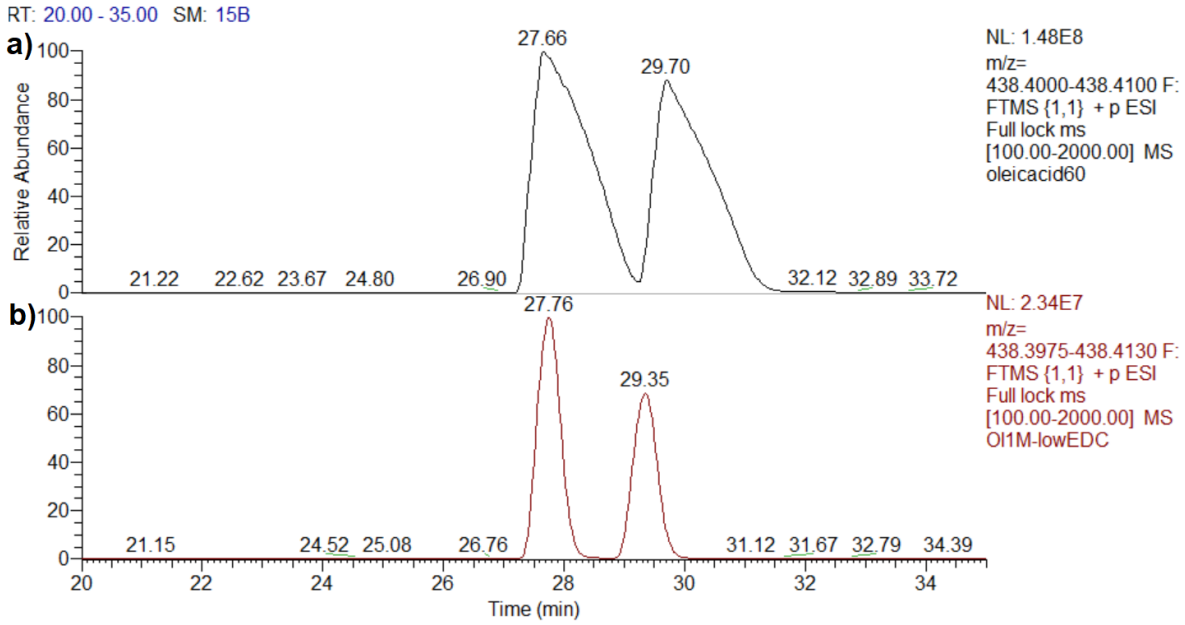

Figure 6-16 Comparison between the extracted ion chromatograms of the EDC *N*-acylisourea derivatives of oleic acid using initial reactants concentrations (a) and reduced reactants concentrations (b).

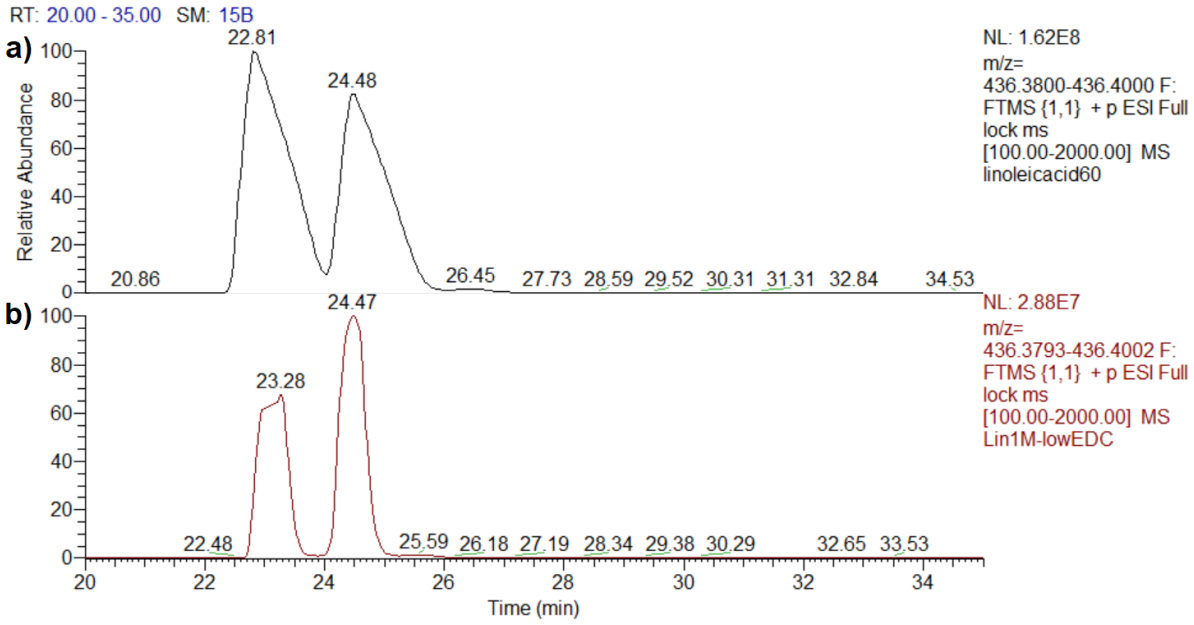

Figure 6-17 Comparison between the extracted ion chromatograms of the *EDC N*-acylisourea derivatives of oleic acid using initial reactants concentrations (a) and reduced reactants concentrations (b).

6.6 Profiling of fatty acids in azolectin

In order to evaluate the efficacy of this method in real-world analytical applications, the derivatisation procedure was used in the analysis of mixture of the FAs isolated from asolectin. The extracted ion traces for the FA derivatives found is shown in (Table 6-6) along with extracted ion chromatograms. Linoleic acid and oleic acid derivatives were found to be abundant in the mixture of tagged FAs extracted from azolectin with small amounts of α-linolenic acid derivatives also present. There were also traces of many fatty acids and their hydroxides that were derivatised and could be primarily profiled using their elemental composition that were generated within mass error of <1PPM.

Table 6-6 Elemental composition and extracted ion chromatograms of EDC-tagged FAs extracted from azolectin.

Elemental composition of the derivative	*m/z*	Elemental composition of the FA	Mass error in PPM	Extracted Chromatogram
$C_{22}H_{46}N_3O_2$	384.3586	$C_{14}H_{29}O_2$	0.483	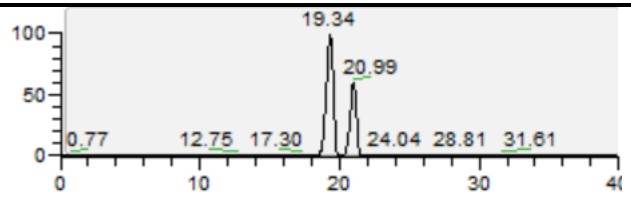
$C_{23}H_{48}N_3O_2$	398.3742	$C_{15}H_{31}O_2$	0.190	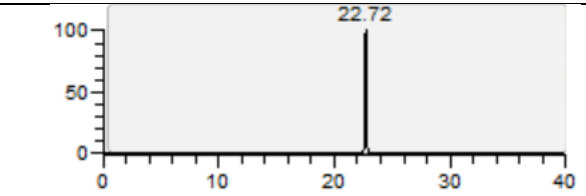
$C_{22}H_{46}N_3O_3$	400.3536	$C_{14}H_{29}O_3$	0.528	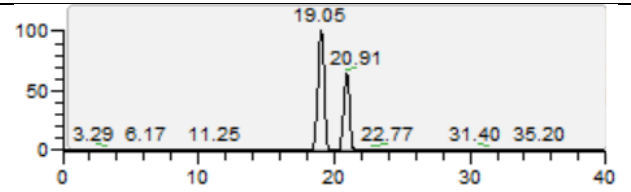
$C_{23}H_{50}N_3O_2$	400.3897	$C_{15}H_{33}O_2$	0.111	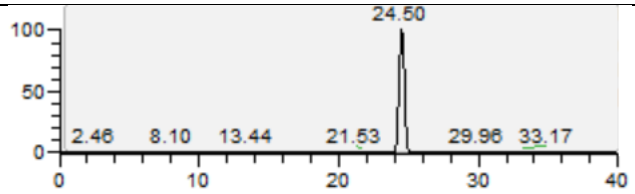

Elemental composition of the derivative	*m/z*	Elemental composition of the FA	Mass error in PPM	Extracted Chromatogram
$C_{24}H_{48}N_3O_2$	410.3741	$C_{16}H_{31}O_2$	-0.059	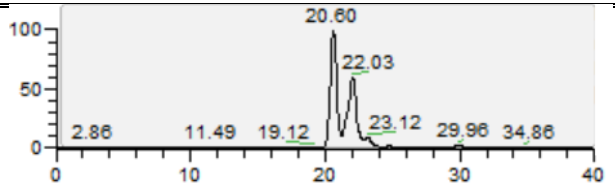
$C_{24}H_{50}N_3O_2$	412.3897	$C_{16}H_{33}O_2$	-0.107	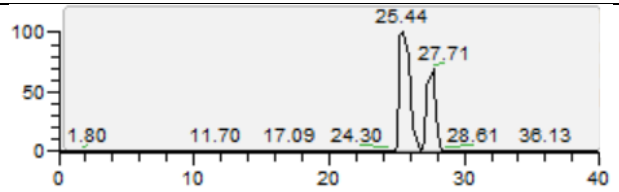
$C_{24}H_{48}N_3O_3$	426.3691	$C_{16}H_{31}O_3$	0.284	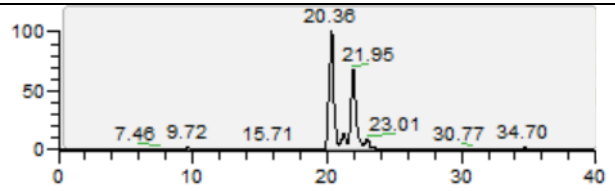
$C_{25}H_{52}N_3O_2$	426.4056	$C_{17}H_{35}O_2$	0.412	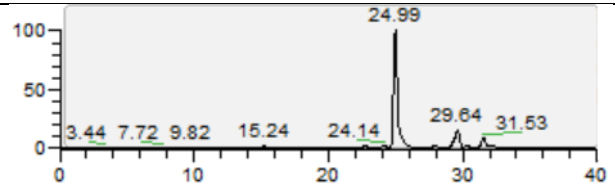

Elemental composition of the derivative	*m/z*	Elemental composition of the FA	Mass error in PPM	Extracted Chromatogram
$C_{24}H_{50}N_3O_3$	428.3846	$C_{16}H_{33}O_2$	-0.208	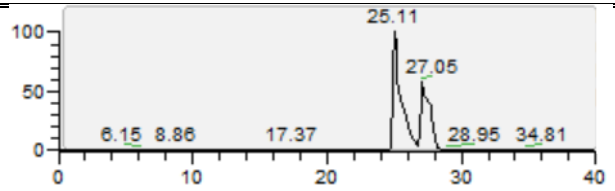
$C_{26}H_{48}N_3O_2$	434.3745	$C_{18}H_{31}O_2$	0.796	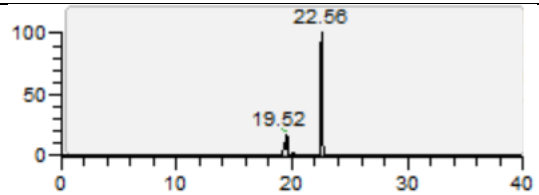
$C_{26}H_{50}N_3O_2$	436.3898	$C_{18}H_{33}O_2$	0.036	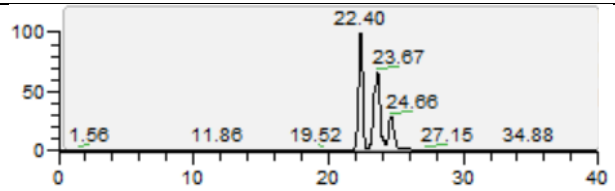
$C_{26}H_{52}N_3O_2$	438.4055	$C_{18}H_{35}O_2$	0.195	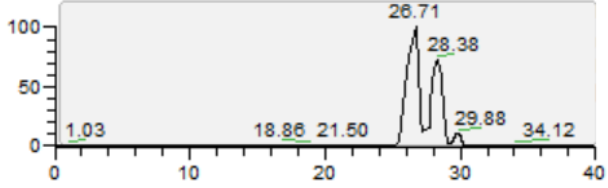

Elemental composition of the derivative	*m/z*	Elemental composition of the FA	Mass error in PPM	Extracted Chromatogram
$C_{26}H_{54}N_3O_2$	440.4209	$C_{18}H_{37}O_2$	-0.283	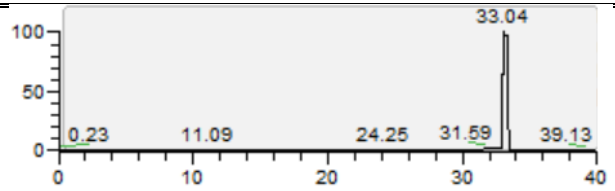
$C_{27}H_{50}N_3O_2$	448.3897	$C_{19}H_{33}O_2$	-0.032	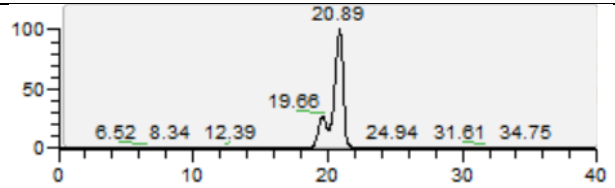
$C_{26}H_{50}N_3O_3$	452.3847	$C_{18}H_{33}O_3$	0.069	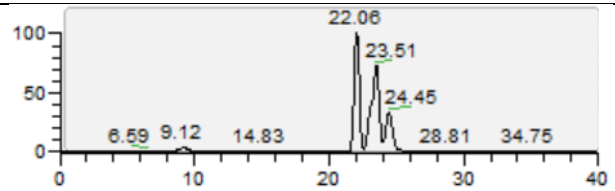
$C_{27}H_{54}N_3O_2$	452.4210	$C_{19}H_{37}O_2$	-0.076	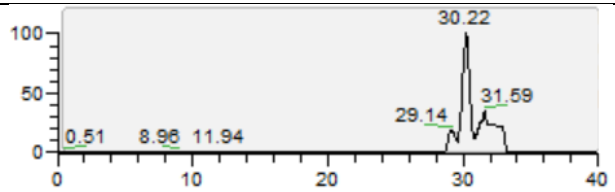

Elemental composition of the derivative	*m/z*	Elemental composition of the FA	Mass error in PPM	Extracted Chromatogram
$C_{26}H_{52}N_3O_3$	454.4002	$C_{18}H_{35}O_3$	-0.174	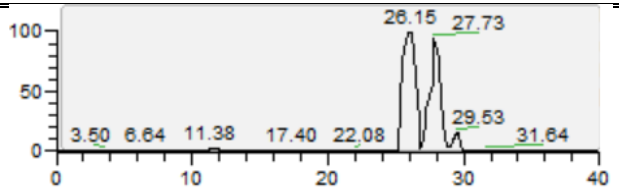
$C_{28}H_{46}N_3O_2$	456.3586	$C_{20}H_{29}O_2$	0.144	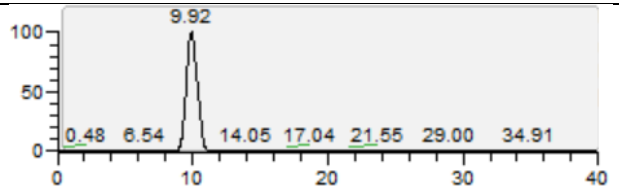
$C_{26}H_{54}N_3O_3$	456.4162	$C_{18}H_{37}O_3$	0.440	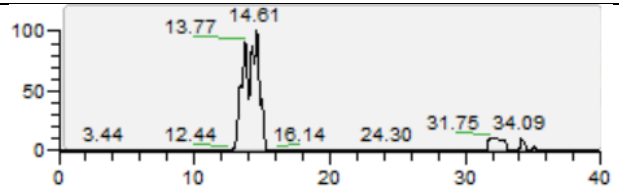
$C_{28}H_{50}N_3O_2$	460.3897	$C_{20}H_{33}O_2$	-0.031	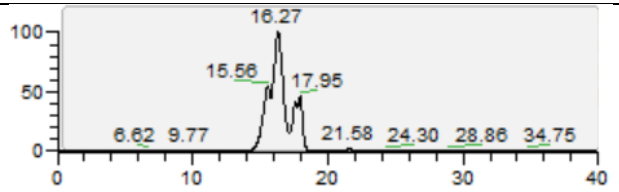

Elemental composition of the derivative	*m/z*	Elemental composition of the FA	Mass error in PPM	Extracted Chromatogram
$C_{28}H_{52}N_3O_2$	462.4054	$C_{20}H_{35}O_2$	0.055	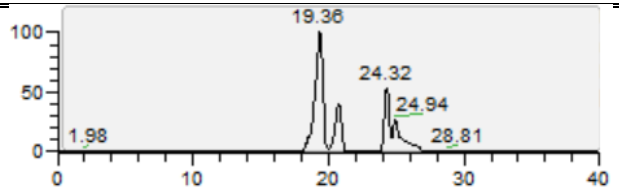
$C_{28}H_{56}N_3O_2$	466.4367	$C_{20}H_{39}O_2$	-0.052	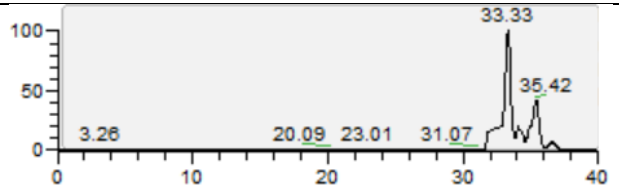
$C_{28}H_{46}N_3O_3$	472.3534	$C_{20}H_{29}O_3$	0.045	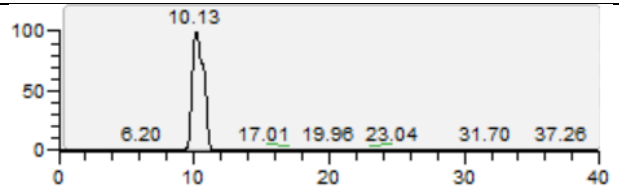
$C_{26}H_{54}N_3O_4$	472.4108	$C_{18}H_{37}O_4$	-0.241	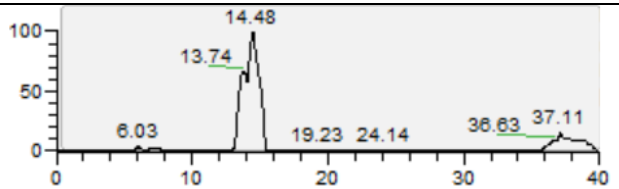

Elemental composition of the derivative	*m/z*	Elemental composition of the FA	Mass error in PPM	Extracted Chromatogram
$C_{28}H_{48}N_3O_3$	474.3689	$C_{20}H_{31}O_3$	-0.251	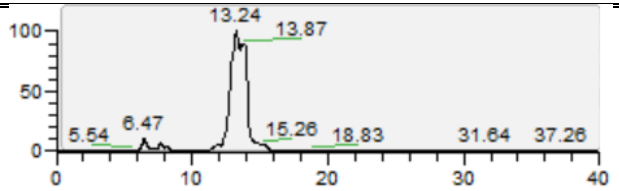
$C_{28}H_{50}N_3O_3$	476.3844	$C_{20}H_{33}O_3$	-0.564	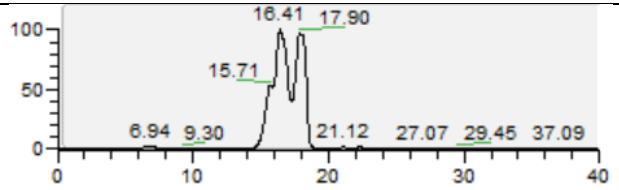
$C_{30}H_{52}N_3O_2$	486.4054	$C_{22}H_{35}O_2$	-0.009	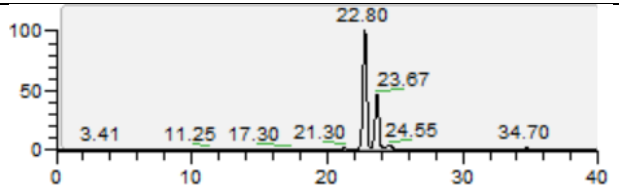

6.7 Conclusion and Future work

The aim of this study was to investigate the suitability of three tagging agents, DPD, DMEE and 1MP in the presence of EDC as an activating agent, in addition to assess the possibility of applying EDC itself as a derivatising agent for the analysis of fatty acids to evaluate their suitability for improving sensitivity of LC-MS analysis of FAs as a step towards developing validated, selective, and significantly more sensitive methods for the determination of trace levels of fatty acid in complex samples like biological or food samples. Such methods would need further development mainly by improving the chromatographic conditions through carrying out investigations of the effects of pH/ different solvent and different columns in addition to column oven temperature. Further optimisation could be carried out using experimental design software. Validation of these methods could be carried out according to the FDA guidelines on the validation of bioanalytical methods to examine precision, accuracy, recovery, and matrix effects using internal standards that could be isomers or a labelled versions of the fatty acids .

7 General conclusion

The results of the studies confirm that derivatisation of FAs can greatly improve their detection identification and quantification by reverse phase LC-MS. The ionisation efficiency for all the FAs in our experiments was improved apart from when 1MP was used as a derivatising agent. The masses expected for the derivatised FAs were observed in all cases. The retention times were generally acceptable and good separation of the various FAs was achieved using all of our tagging agents. There is probably room for optimisation of the derivatisation of FAs using 1MP in the presence of EDC which gave much smaller peaks than were obtained with the other tagging agents. This is probably because of the competition with the reaction that causes formation of EDC *N*-acylisourea derivative. This however demonstrates that the concept works and that better tagging agents can be developed which will meet the initial aims of the study. DPD or DMEE in the presence of EDC remain potentially useful tagging agents for use in the analysis of fatty acids in complex samples.

The results of the study on EDC as a tagging agent confirms that this derivatisation method of FAs can greatly improve their detection identification and quantification by LCMS. The ionisation FAs in positive mode in our experiments was significantly improved following derivatisation with EDC and the masses expected for the derivatised FAs were observed in all cases. The method offers a one-step derivatisation strategy, moreover, it is highly sensitive and thus very useful, but more work is required to eliminate background contamination. This conclusion is consistent with previous work on EDC as a tagging agent for carboxyl containing compounds (D. Li et al., 2016, 2017; Woudneh et al., 2013). Synthesis of stable-isotope-labelled EDC (Cao et al., 2020) could offer more options for this method to be applied in quantitative analysis. The analysis of azolectin using EDC as a derivatising agent revealed the presence of minor amounts of hydroxy fatty acids. Thus, EDC shows potential for the sensitive analysis of bioactive oxidised fatty acids which are found in trace amounts in biological systems.

References

Ahima, R. S., & Flier, J. S. (2000). Leptin. *Annu. Rev. Physiol.*, *62*, 413–37.

Ahmad Dar, A., Sangwan, P. L., & Kumar, A. (2020). Chromatography: An important tool for drug discovery. *Journal of Separation Science*, *43*(1), 105–119. https://doi.org/10.1002/jssc.201900656

Akash, M. S. H., & Rehman, K. (2019). Essentials of pharmaceutical analysis. In *Essentials of Pharmaceutical Analysis*. https://doi.org/10.1007/978-981-15-1547-7

Al-Dirbashi, O. Y., Santa, T., Rashed, M. S., Al-Hassnan, Z., Shimozawa, N., Chedrawi, A., Jacob, M., & Al-Mokhadab, M. (2008). Rapid UPLC-MS/MS method for routine analysis of plasma pristanic, phytanic, and very long chain fatty acid markers of peroxisomal disorders. *Journal of Lipid Research*, *49*(8), 1855–1862. https://doi.org/10.1194/jlr.D800019-JLR200

Al-Okbi, S. Y., El-Qousy, S. M., El-Ghlban, S., & Moawad, H. F. (2018). Role of borage seed oil and fish oil with or without turmeric and alpha-tocopherol in prevention of cardiovascular disease and fatty liver in rats. *Journal of Oleo Science*, *67*(12), 1551–1562. https://doi.org/10.5650/jos.ess18064

Alothaim, I., Gaya, D. R., & Watson, D. G. (2017). Development of a Sensitive Liquid Chromatography Mass Spectrometry Method for the Analysis of Short Chain Fatty Acids in Urine from Patients with Ulcerative Colitis. *Current Metabolomics*, *6*(2), 124–130. https://doi.org/10.2174/2213235x05666170424163105

Alpert, A. J. (1990). Hydrophilic-interaction chromatography for the separation of peptides, nucleic acids and other polar compounds. *Journal of Chromatography A*, *499*(C), 177–196. https://doi.org/10.1016/S0021-9673(00)96972-3

Altuntas, A. H., Ketenoglu, O., Cetinbas, S., Erdogdu, F., & Tekin, A. (2018). Deacidification of Crude Hazelnut Oil Using Molecular Distillation – Multiobjective Optimization for Free Fatty Acids and Tocopherol. *European Journal of Lipid Science and Technology*, *120*(4), 1–7. https://doi.org/10.1002/ejlt.201700369

Alvarez-Rivera, G., Ballesteros-Vivas, D., Parada-Alfonso, F., Ibañez, E., & Cifuentes, A. (2019). Recent applications of high resolution mass spectrometry for the characterization of plant natural products. *TrAC - Trends in Analytical Chemistry*, *112*, 87–101. https://doi.org/10.1016/j.trac.2019.01.002

Alvarez-Segura, T., Cabo-Calvet, E., Baeza-Baeza, J. J., & García-Alvarez-Coque, M. C. (2019). Study of the column efficiency using gradient elution based on Van Deemter plots. *Journal of Chromatography A*, *1584*, 126–134. https://doi.org/10.1016/j.chroma.2018.11.042

Antonny, B., Vanni, S., Shindou, H., & Ferreira, T. (2015). From zero to six double bonds: Phospholipid unsaturation and organelle function. *Trends in Cell Biology*, *25*(7), 427–436. https://doi.org/10.1016/j.tcb.2015.03.004

Aquino-Bolaños, E. N., Mapel-Velazco, L., Martín-del-Campo, S. T., Chávez-Servia, J. L., Martínez, A. J., & Verdalet-Guzmán, I. (2017). Fatty acids profile of oil from nine varieties of Macadamia nut. *International Journal of Food Properties*, *20*(6), 1262–1269. https://doi.org/10.1080/10942912.2016.1206125

Asadi-Samani, M., Bahmani, M., & Rafieian-Kopaei, M. (2014). The chemical composition, botanical characteristic and biological activities of Borago officinalis: A review. *Asian Pacific Journal of Tropical Medicine*, *7*(S1), S22–S28. https://doi.org/10.1016/S1995-7645(14)60199-1

Askin, M. A., Balta, M. F., Tekintas, F. E., Kazankaya, A., & Balta, F. (2007). Fatty acid composition affected by kernel weight in almond [Prunus dulcis (Mill.) D.A. Webb.] genetic resources. *Journal of Food Composition and Analysis*, *20*(1), 7–12. https://doi.org/10.1016/j.jfca.2006.06.005

Awad, H., Khamis, M. M., & El-Aneed, A. (2015). Mass spectrometry, review of the basics: Ionization. *Applied Spectroscopy Reviews*, *50*(2), 158–175. https://doi.org/10.1080/05704928.2014.954046

Ayala, A., Muñoz, M. F., & Argüelles, S. (2014). Lipid Peroxidation: Production, Metabolism, and Signaling Mechanisms of Malondialdehyde and 4-Hydroxy-2-Nonenal Antonio. *Oxidative Medicine and Cellular Longevity*, *2014*, 1–31. http://dx.doi.org/10.1155/2014/360438%0AReview

Baba, T., Campbell, J. L., Blanc, J. C. Y. Le, & Baker, P. R. S. (2016). *In-depth sphingomyelin characterization using electron impact excitation of ions from organics and mass spectrometry*. *57*. https://doi.org/10.1194/jlr.M067199

Baba, T., Campbell, J. L., Blanc, J. C. Y. Le, Hager, J. W., & Thomson, B. A. (2015). *Electron Capture Dissociation in a Branched Radio-Frequency Ion Trap*. https://doi.org/10.1021/ac503773y

Baba, T., Campbell, J. L., Le Blanc, J. C. Y., & Baker, P. R. S. (2016). Structural identification of triacylglycerol isomers using electron impact excitation of ions from organics (EIEIO). *Journal of Lipid Research*, *57*(11), 2015–2027. https://doi.org/10.1194/jlr.M070177

Bacchetta, L., Aramini, M., Zini, A., Di Giammatteo, V., Spera, D., Drogoudi, P., Rovira, M., Silva, A. P., Solar, A., & Botta, R. (2013). Fatty acids and alpha-tocopherol composition in hazelnut (Corylus avellana L.): A chemometric approach to emphasize the quality of European germplasm. *Euphytica*, *191*(1), 57–73. https://doi.org/10.1007/s10681-013-0861-y

Baker, E. J., Miles, E. A., Burdge, G. C., Yaqoob, P., & Calder, P. C. (2016). Metabolism and functional effects of plant-derived omega-3 fatty acids in humans. *Progress in Lipid Research*, *64*, 30–56. https://doi.org/10.1016/j.plipres.2016.07.002

Bamba, T., Lee, J. W., Matsubara, A., & Fukusaki, E. (2012). Metabolic profiling of lipids by supercritical fluid chromatography/mass spectrometry. *Journal of Chromatography A*, *1250*, 212–219. https://doi.org/10.1016/j.chroma.2012.05.068

Banerjee, S., & Mazumdar, S. (2012). Electrospray Ionization Mass Spectrometry: A Technique to Access the Information beyond the Molecular Weight of the Analyte. *International Journal of Analytical Chemistry*, *2012*, 1–40. https://doi.org/10.1155/2012/282574

Bawazeer, S., Muhsen Ali, A., Alhawiti, A., Khalaf, A., Gibson, C., Tusiimire, J., & Watson, D. G. (2017). A method for the analysis of sugars in biological systems using reductive amination in combination with hydrophilic interaction chromatography and high resolution mass spectrometry. *Talanta*, *166*(January), 75–80.

https://doi.org/10.1016/j.talanta.2017.01.038

Becker, J. S. (2008). *Inorganic Mass Spectrometry Principles and Applications*.

Belov, M. E., Rakov, V. S., Nikolaev, E. N., Goshe, M. B., Anderson, G. A., & Smith, R. D. (2003). Initial implementation of external accumulation liquid chromatography/electrospray ionization fourier transform ion cyclotron resonance with automated gain control. *Rapid Communications in Mass Spectrometry*, *17*(7), 627–636. https://doi.org/10.1002/rcm.955

Bercu, J. P., Galloway, S. M., Parris, P., Teasdale, A., Masuda-Herrera, M., Dobo, K., Heard, P., Kenyon, M., Nicolette, J., Vock, E., Ku, W., Harvey, J., White, A., Glowienke, S., Martin, E. A., Custer, L., Jolly, R. A., & Thybaud, V. (2018). Potential impurities in drug substances: Compound-specific toxicology limits for 20 synthetic reagents and by-products, and a class-specific toxicology limit for alkyl bromides. *Regulatory Toxicology and Pharmacology*, *94*(February), 172–182. https://doi.org/10.1016/j.yrtph.2018.02.001

Bollinger, J. G., Thompson, W., Lai, Y., Oslund, R. C., Hallstrand, T. S., Sadilek, M., Turecek, F., & Gelb, M. H. (2010). Improved sensitivity mass spectrometric detection of eicosanoids by charge reversal derivatization. *Analytical Chemistry*, *82*(16), 6790–6796. https://doi.org/10.1021/ac100720p

Borden, S. A., Palaty, J., Termopoli, V., Famiglini, G., Cappiello, A., Gill, C. G., & Palma, P. (2020). Mass Spectrometry Analysis of Drugs of Abuse: Challenges and Emerging Strategies. *Mass Spectrometry Reviews*, *39*(5–6), 703–744. https://doi.org/10.1002/mas.21624

Borowy, A., & Kapłan, M. (2020). Chemical composition and antioxidant activity of borage (Borago officinalis L.) seeds. *Acta Scientiarum Polonorum, Hortorum Cultus*, *19*(6), 79–90. https://doi.org/10.24326/ASPHC.2020.6.7

Brose, S. A., Baker, A. G., & Golovko, M. Y. (2013). A fast one-step extraction and UPLC-MS/MS analysis for E2/D 2 series prostaglandins and isoprostanes. *Lipids*, *48*(4), 411–419. https://doi.org/10.1007/s11745-013-3767-5

Brouwer, I. A., Wanders, A. J., & Katan, M. B. (2013). Trans fatty acids and cardiovascular health: Research completed? *European Journal of Clinical Nutrition*, *67*(5), 541–547. https://doi.org/10.1038/ejcn.2013.43

Brown, S. H. J., Mitchell, T. W., & Blanksby, S. J. (2011). Analysis of unsaturated lipids by ozone-induced dissociation. *Biochimica et Biophysica Acta - Molecular and Cell Biology of Lipids*, *1811*(11), 807–817. https://doi.org/10.1016/j.bbalip.2011.04.015

Bryant, D. K., Orlando, R. C., Fenselau, C., Sowder, R. C., & Henderson, L. E. (1991). Four-Sector Tandem Mass Spectrometric Analysis of Complex Mixtures of Phosphatidylcholines Present in a Human Immunodeficiency Virus Preparation. *Analytical Chemistry*, *63*(11), 1110–1114. https://doi.org/10.1021/ac00011a010

Cammack, R., Attwood, T. K., Campbell, P. N., Parish, J. H., Smith, A. D., Stirling, J. L., & Vella, F. (Eds.). (2006). *OXFORD DICTIONARY OF Biochemistry and Molecular Biology* (2 nd renis). Oxford University Press Inc.

Campbell, J. L., & Baba, T. (2015). *Near-Complete Structural Characterization of*

Phosphatidylcholines Using Electron Impact Excitation of Ions from Organics. https://doi.org/10.1021/acs.analchem.5b01460

Cao, K., Brailsford, J. A., & Bonacorsi, S. J. (2020). Synthesis of stable-isotope-labeled N-(3-dimethylaminopropyl)-N'-ethylcarbodiimide and N-(3-dimethylaminopropyl)-N'-ethylurea. *Journal of Labelled Compounds and Radiopharmaceuticals*, *63*(13), 526–530. https://doi.org/10.1002/jlcr.3877

Carey, J. S., Laffan, D., Thomson, C., & Williams, M. T. (2006). Analysis of the reactions used for the preparation of drug candidate molecules. *Organic and Biomolecular Chemistry*, *4*(12), 2337–2347. https://doi.org/10.1039/b602413k

Castro-Perez, J., Roddy, T. P., Nibbering, N. M. M., Shah, V., McLaren, D. G., Previs, S., Attygalle, A. B., Herath, K., Chen, Z., Wang, S. P., Mitnaul, L., Hubbard, B. K., Vreeken, R. J., Johns, D. G., & Hankemeier, T. (2011). Erratum: Localization of fatty acyl and double bond positions in phosphatidylcholines using a dual stage CID fragmentation coupled with ion mobility mass spectrometry (Journal of The American Society for Mass Spectrometry DOI: 10.1007/s13361-011-0172-2). *Journal of the American Society for Mass Spectrometry*, *22*(9), 1568–1569. https://doi.org/10.1007/s13361-011-0199-4

Chan, L. C., & Cox, B. G. (2007). Kinetics of amide formation through carbodiimide/N-hydroxybenzotriazole (HOBt) couplings. *Journal of Organic Chemistry*, *72*(23), 8863–8869. https://doi.org/10.1021/jo701558y

Chen, J., & Liu, H. (2020). Nutritional indices for assessing fatty acids: A mini-review. *International Journal of Molecular Sciences*, *21*(16), 1–24. https://doi.org/10.3390/ijms21165695

Chen, Z., Gao, Y., & Zhong, D. (2020). Technologies to improve the sensitivity of existing chromatographic methods used for bioanalytical studies. *Biomedical Chromatography*, *34*(3). https://doi.org/10.1002/bmc.4798

Christie, W. W. (1998). Gas chromatography-mass spectrometry methods for structural analysis of fatty acids. *Lipids*, *33*(4), 343–353. https://doi.org/10.1007/s11745-998-0214-x

Christie, W. W., & Han, X. (2012a). Characterization of lipids by electrospray ionization mass spectrometry. *Lipid Analysis*, 305–338. https://doi.org/10.1533/9780857097866.305

Christie, W. W., & Han, X. (2012b). Lipids: their structures and occurrence. *Lipid Analysis*, 3–19. https://doi.org/10.1533/9780857097866.3

CHRISTIE, W. W., & HAN, X. (2010). *Lipid analysis ISOLATION, SEPARATION, IDENTIFICATION AND LIPIDOMIC ANALYSIS* (4th ed.).

Comini, M. A. (2016). Measurement and meaning of cellular thiol: Disufhide redox status. *Free Radical Research*, *50*(2), 246–271. https://doi.org/10.3109/10715762.2015.1110241

Cosgrove, J., Church, D., & Pryor, W. (1987). The kinetics of the autoxidation of polyunsaturated fatty acids. *Lipids*, *22*(5), 299–304. https://doi.org/10.1007/BF02533996

Crăciun, I. (2018). Comparative Study of Liposoluble Vitamins and Fatty Acids from Sea

Buckthorn Oil, Wheat Germ Oil and Fish Oil. *Acta Universitatis Cibiniensis. Series E: Food Technology*, *22*(2), 85–90. https://doi.org/10.2478/aucft-2018-0016

Criegee, R. (1975). Mechanism of Ozonolysis. *Angewandte Chemie International Edition in English*, *14*(11), 745–752. https://doi.org/10.1002/anie.197507451

Cui, N., Wang, G., Ma, Q., Zhao, T., Li, R., & Liang, L. (2020). Effect of cold-pressed on fatty acid profile, bioactive compounds and oil oxidation of hazelnut during oxidation process. *Lwt*, *129*(May), 109552. https://doi.org/10.1016/j.lwt.2020.109552

Dabetic, N. M., Todorovic, V. M., Djuricic, I. D., Antic Stankovic, J. A., Basic, Z. N., Vujovic, D. S., & Sobajic, S. S. (2020). Grape Seed Oil Characterization: A Novel Approach for Oil Quality Assessment. *European Journal of Lipid Science and Technology*, *122*(6), 1–10. https://doi.org/10.1002/ejlt.201900447

Dacks, J. B., & Field, M. C. (2007). Evolution of the eukaryotic membrane-trafficking system: Origins, tempo and mode. *Journal of Cell Science*, *120*(17), 2977–2985. https://doi.org/10.1242/jcs.013250

Danne-Rasche, N., Coman, C., & Ahrends, R. (2018). Nano-LC/NSI MS Refines Lipidomics by Enhancing Lipid Coverage, Measurement Sensitivity, and Linear Dynamic Range. *Analytical Chemistry*, *90*(13), 8093–8101. https://doi.org/10.1021/acs.analchem.8b01275

David, V., Moldoveanu, S. C., & Galaon, T. (2021). Derivatization procedures and their analytical performances for HPLC determination in bioanalysis. *Biomedical Chromatography*, *35*(1). https://doi.org/10.1002/bmc.5008

Davis, H., Magistrali, A., Butler, G., & Stergiadis, S. (2022). Nutritional Benefits from Fatty Acids in Organic and Grass-Fed Beef. *Foods*, *11*(5), 1–19. https://doi.org/10.3390/foods11050646

de Hoffmann, E., & Stroobant, V. (2007). Mass Spectrometry Principles and Applications. In *Methods in Molecular Biology* (Third Edit, Vol. 1796). John Wiley & Sons Ltd. https://doi.org/10.1007/978-1-4939-7877-9_17

De Souza, R. J., Mente, A., Maroleanu, A., Cozma, A. I., Ha, V., Kishibe, T., Uleryk, E., Budylowski, P., Schünemann, H., Beyene, J., & Anand, S. S. (2015). Intake of saturated and trans unsaturated fatty acids and risk of all cause mortality, cardiovascular disease, and type 2 diabetes: Systematic review and meta-analysis of observational studies. *BMJ (Online)*, *351*, 1–16. https://doi.org/10.1136/bmj.h3978

Deng, P., Zhan, Y., Chen, X., & Zhong, D. (2012). Derivatization methods for quantitative bioanalysis by LC-MS/MS. *Bioanalysis*, *4*(1), 49–69. https://doi.org/10.4155/bio.11.298

Deng, P., Zhong, D., Wang, X., Dai, Y., Zhou, L., Leng, Y., & Chen, X. (2016). Analysis of diacylglycerols by ultra performance liquid chromatography-quadrupole time-of-flight mass spectrometry: Double bond location and isomers separation. *Analytica Chimica Acta*, *925*, 23–33. https://doi.org/10.1016/j.aca.2016.04.051

Derogis, P. B. M. C., Chaves-Fillho, A. B., & Miyamoto, S. (2019). Characterization of hydroxy and hydroperoxy polyunsaturated fatty acids by mass spectrometry. *Advances in Experimental Medicine and Biology*, *1127*, 21–35. https://doi.org/10.1007/978-3-030-11488-6_2

Dolan, J. W. (2013). Making the most of a gradient scouting run. *LCGC North America*, *31*(1), 30–35.

Dubois, V., Breton, S., Linder, M., Fanni, J., & Parmentier, M. (2007). Fatty acid profiles of 80 vegetable oils with regard to their nutritional potential. *European Journal of Lipid Science and Technology*, *109*(7), 710–732. https://doi.org/10.1002/ejlt.200700040

Dunetz, J. R., Magano, J., & Weisenburger, G. A. (2016). Large-Scale Applications of Amide Coupling Reagents for the Synthesis of Pharmaceuticals. *Organic Process Research and Development*, *20*(2), 140–177. https://doi.org/10.1021/op500305s

Dunkelblum, E., Tan, S. H., & Silk, P. J. (1985). Double-bond location in monounsaturated fatty acids by dimethyl disulfide derivatization and mass spectrometry: Application to analysis of fatty acids in pheromone glands of four lepidoptera. *Journal of Chemical Ecology*, *11*(3), 265–277. https://doi.org/10.1007/BF01411414

Eggink, M., Wijtmans, M., Ekkebus, R., Lingeman, H., De Esch, I. J. P., Kool, J., Niessen, W. M. A., & Irth, H. (2008). Development of a selective ESI-MS derivatization reagent: Synthesis and optimization for the analysis of aldehydes in biological mixtures. *Analytical Chemistry*, *80*(23), 9042–9051. https://doi.org/10.1021/ac801429w

El-Faham, A., & Albericio, F. (2011). Peptide coupling reagents, more than a letter soup. *Chemical Reviews*, *111*(11), 6557–6602. https://doi.org/10.1021/cr100048w

Eliuk, S., & Makarov, A. (2015). Evolution of Orbitrap Mass Spectrometry Instrumentation. *Annual Review of Analytical Chemistry*, *8*, 61–80. https://doi.org/10.1146/annurev-anchem-071114-040325

Ellis, S. R., Hughes, J. R., Mitchell, T. W., Panhuis, M. in Het, & Blanksby, S. J. (2012). Using ambient ozone for assignment of double bond position in unsaturated lipids. *The Analyst*, *137*(5), 1100. https://doi.org/10.1039/c1an15864c

Esterbauer, H. (1993). Cytotoxicity and genotoxicity of lipid-oxidation. *Am. J. Clin. Nutr.*, *57*(Suppl.), 779S-786S.

Fahy, E., Cotter, D., Sud, M., & Subramaniam, S. (2012). Lipid classification, structures and tools. *Biochim Biophys Acta*, *29*(11), 997–1003. https://doi.org/10.1016/j.biotechadv.2011.08.021.Secreted

Fahy, E., Subramaniam, S., Murphy, R. C., Nishijima, M., Raetz, C. R. H., Shimizu, T., Spener, F., Van Meer, G., Wakelam, M. J. O., & Dennis, E. A. (2009). Update of the LIPID MAPS comprehensive classification system for lipids. *Journal of Lipid Research*, *50*(SUPPL.), 9–14. https://doi.org/10.1194/jlr.R800095-JLR200

Fauland, A., Köfeler, H., Trötzmüller, M., Knopf, A., Hartler, J., Eberl, A., Chitraju, C., Lankmayr, E., & Spener, F. (2011). A comprehensive method for lipid profiling by liquid chromatography-ion cyclotron resonance mass spectrometry. *Journal of Lipid Research*, *52*(12), 2314–2322. https://doi.org/10.1194/jlr.D016550

Fenn, J. B., Mann, M., Meng, C. K. A. I., Wong, S. F., & Whitehouse, C. M. (1989). Electrospray Ionization for Mass Spectrometry of Large Biomolecules. *Science*, *246*(6).

Fernandes, G. D., Gómez-Coca, R. B., Pérez-Camino, M. D. C., Moreda, W., & Barrera-Arellano, D. (2017). Chemical Characterization of Major and Minor Compounds of Nut Oils: Almond, Hazelnut, and Pecan Nut. *Journal of Chemistry*, *2017*, 5–7.

https://doi.org/10.1155/2017/2609549

Flores, M., Saravia, C., Vergara, C. E., Avila, F., Valdés, H., & Ortiz-Viedma, J. (2019). Avocado oil: Characteristics, properties, and applications. *Molecules*, *24*(11), 1–21. https://doi.org/10.3390/molecules24112172

Frankel, E. N. (1991). Review. Recent advances in lipid oxidation. *Journal of the Science of Food and Agriculture*, *54*(4), 495–511. https://doi.org/10.1002/jsfa.2740540402

Frankel, E. N., Garwood, R. F., Khambay, B. P. S., Moss, G. P., & Weedon, B. C. L. (1984). Stereochemistry of olefin and fatty acid oxidation. Part 3. The allylic hydroperoxides from the autoxidation of methyl oleate. *Journal of the Chemical Society, Perkin Transactions 1*, *3*(8), 2233–2240.

Gao, F., Zhang, Z., Fu, X., Li, W., Wang, T., & Liu, H. (2007). Analysis of phospholipids by NACE with on-line ESI-MS. *Electrophoresis*, *28*(9), 1418–1425. https://doi.org/10.1002/elps.200600533

Gao, P., Hirano, T., Chen, Z., Yasuhara, T., Nakata, Y., & Sugimoto, A. (2012). Isolation and identification of C-19 fatty acids with anti-tumor activity from the spores of Ganoderma lucidum (reishi mushroom). *Fitoterapia*, *83*(3), 490–499. https://doi.org/10.1016/j.fitote.2011.12.014

Garavaglia, J., Markoski, M. M., Oliveira, A., & Marcadenti, A. (2016). Grape seed oil compounds: Biological and chemical actions for health. *Nutrition and Metabolic Insights*, *9*, 59–64. https://doi.org/10.4137/NMI.S32910

Garscha, U., Nilsson, T., & Oliw, E. H. (2008). Enantiomeric separation and analysis of unsaturated hydroperoxy fatty acids by chiral column chromatography-mass spectrometry. *Journal of Chromatography. B, Analytical Technologies in the Biomedical and Life Sciences*, *872*(1–2), 90–98. https://doi.org/10.1016/j.jchromb.2008.07.013

Ghafoor, K., Özcan, Mehmet Musa AL-Juhaımı, F., Elfadıl, E. B., Sarker, Z. I., & Ahmed, Isam A.Mohamed Ahmed, M. A. (2016). Nutritional Compotition, Ekstraction and Utilization of Wheat Germ Oil. *European Journal of Lipid Science and Technology*, 1–22.

Ghose, A. K., Viswanadhan, V. N., & Wendoloski, J. J. (1999). A knowledge-based approach in designing combinatorial or medicinal chemistry libraries for drug discovery. 1. A qualitative and quantitative characterization of known drug databases. *Journal of Combinatorial Chemistry*, *1*(1), 55–68. https://doi.org/10.1021/cc9800071

Gidez, L. I. (1984). The lore of lipids. *Journal of Lipid Research*, *25*, 1430–1436.

Gilchrist, T. L. (1991). Reduction of N=N, N-N, N-O and 0-0 Bonds. In B. M. Trost & I. Fleming (Eds.), *Comprehensive Organic Synthesis: Selectivity, Strategy, and Efficiency in Modern Organic Chemistry* (illustrate, pp. 381–402). Elsevier Science. https://books.google.co.uk/books?id=vrITBZ-%5C_jwEC

Gilles, M. A., Hudson, A. Q., & Borders, C. L. (1990). Stability of water-soluble carbodiimides in aqueous solution. *Analytical Biochemistry*, *184*(2), 244–248. https://doi.org/10.1016/0003-2697(90)90675-Y

Goñi, F. M. (2014). The basic structure and dynamics of cell membranes: An update of the Singer-Nicolson model. *Biochimica et Biophysica Acta - Biomembranes*, *1838*(6), 1467–

1476. https://doi.org/10.1016/j.bbamem.2014.01.006

Green, H. S., & Wang, S. C. (2020). First report on quality and purity evaluations of avocado oil sold in the US. *Food Control*, *116*(February), 107328. https://doi.org/10.1016/j.foodcont.2020.107328

Griesinger, H., Fuchs, B., Süß, R., Matheis, K., Schulz, M., & Schiller, J. (2014). Stationary phase thickness determines the quality of thin-layer chromatography/matrix-assisted laser desorption and ionization mass spectra of lipids. *Analytical Biochemistry*, *451*(1), 45–47. https://doi.org/10.1016/j.ab.2014.02.002

Grinfeld, D., Stewart, H., Skoblin, M., Denisov, E., Monastyrsky, M., & Makarov, A. (2019). Space-charge dynamics in Orbitrap mass spectrometers. *International Journal of Modern Physics A*, *34*(36). https://doi.org/10.1142/S0217751X19420077

Gross, R. W., Jenkins, C. M., Yang, J., Mancuso, D. J., & Han, X. (2005). Functional lipidomics: the roles of specialized lipids and lipid-protein interactions in modulating neuronal function. *Prostaglandins & Other Lipid Mediators*, *77*(1–4), 52–64. https://doi.org/10.1016/j.prostaglandins.2004.09.005

Gurr, M. I., Harwood, J. L., Frayn, K. N., Murphy, D. J., & Michell, R. H. (2016). *Lipids: Biochemistry, Biotechnology and Health* (6th ed.). Wiley-Blackwell.

Haefliger, O. P., & Sulzer, J. W. (2007). Rapid LC-UV-ESI-MS method to investigate the industrial preparation of polyunsaturated fatty acid hydroperoxides in real-time. *Chromatographia*, *65*(7–8), 435–442. https://doi.org/10.1365/s10337-007-0178-x

Haidar Ahmad, I. A. (2017). Necessary Analytical Skills and Knowledge for Identifying, Understanding, and Performing HPLC Troubleshooting. *Chromatographia*, *80*(5), 705–730. https://doi.org/10.1007/s10337-016-3225-7

Halket, J. M., & Zaikin, V. G. (2005). Derivatization in mass spectrometry - 5. Specific derivatization of monofunctional compounds. *European Journal of Mass Spectrometry*, *11*(1), 127–160. https://doi.org/10.1255/ejms.712

Hamberg, M., Su, C., & Oliw, E. (1998). Manganese lipoxygenase. Discovery of a bis-allylic hydroperoxide as product and intermediate in a lipoxygenase reaction. *Journal of Biological Chemistry*, *273*(21), 13080–13088. https://doi.org/10.1074/jbc.273.21.13080

Han, S. Y., & Kim, Y. A. (2004). Recent development of peptide coupling reagents in organic synthesis. *Tetrahedron*, *60*(11), 2447–2467. https://doi.org/10.1016/j.tet.2004.01.020

Han, X., & Gross, R. W. (2003). Global analyses of cellular lipidomes directly from crude extracts of biological samples by ESI mass spectrometry: A bridge to lipidomics. *Journal of Lipid Research*, *44*(6), 1071–1079. https://doi.org/10.1194/jlr.R300004-JLR200

Han, X., & Gross, R. W. (2005). Shotgun lipidomics: Electrospray ionization mass spectrometric analysis and quantitation of cellular lipidomes directly from crude extracts of biological samples. *Mass Spectrometry Reviews*, *24*(3), 367–412. https://doi.org/10.1002/mas.20023

Han, X., Yang, K., & Gross, R. W. (2012). Multi-dimensional mass spectrometry-based shotgun lipidomics and novel strategies for lipidomic analyses. *Mass Spectrometry*

Reviews, *31*(1), 134–178. https://doi.org/10.1002/mas.20342

Hannah Sunshine and M. Luisa Iruela-Arisp. (2017). Membrane Lipids and Cell Signaling Hannah. *Curr Opin Lipidol.*, *28*(5), 408–413. https://doi.org/10.1016/j.physbeh.2017.03.040

Hannun, Y. A., & Bell, R. M. (1989). Regulation of protein kinase C by sphingosine and lysosphingolipids. *Clinica Chimica Acta*, *185*(3), 333–345. https://doi.org/10.1016/0009-8981(89)90224-6

Harrabi, S., Ferchichi, A., Fellah, H., Feki, M., & Hosseinian, F. (2021). Chemical composition and in vitro anti-inflammatory activity of wheat germ oil depending on the extraction procedure. *Journal of Oleo Science*, *70*(8), 1051–1058. https://doi.org/10.5650/jos.ess20317

Harris, D C, & Lucy, C. A. (2020). *Quantitative Chemical Analysis* (10th ed.). Macmillan Learning. https://books.google.co.uk/books?id=iijAywEACAAJ

Harris, Daniel C., & Lucy, C. A. (2016). *Quantitative Chemical Analysis* (Ninth). https://doi.org/10.1007/978-1-4939-2565-0_6

Harrison, K. a, & Murphy, R. C. (1996). Direct mass spectrometric analysis of ozonides: application to unsaturated glycerophosphocholine lipids. *Analytical Chemistry*, *68*(18), 3224–3230.

He, Y., & Concheiro-Guisan, M. (2019). Microextraction sample preparation techniques in forensic analytical toxicology. *Biomedical Chromatography*, *33*(1), 1–12. https://doi.org/10.1002/bmc.4444

Hellmuth, C., Weber, M., Koletzko, B., & Peissner, W. (2012). Nonesterified fatty acid determination for functional lipidomics: Comprehensive ultrahigh performance liquid chromatography-tandem mass spectrometry quantitation, qualification, and parameter prediction. *Analytical Chemistry*, *84*(3), 1483–1490. https://doi.org/10.1021/ac202602u

Henne, W. M., Reese, M. L., & Goodman, J. M. (2019). The assembly of lipid droplets and their roles in challenged cells. *The EMBO Journal*, *38*(9). https://doi.org/10.15252/embj.2019101816

Higashi, T., Ichikawa, T., Inagaki, S., Min, J. Z., Fukushima, T., & Toyo'oka, T. (2010). Simple and practical derivatization procedure for enhanced detection of carboxylic acids in liquid chromatography-electrospray ionization-tandem mass spectrometry. *Journal of Pharmaceutical and Biomedical Analysis*, *52*(5), 809–818. https://doi.org/10.1016/j.jpba.2010.03.001

Higashi, T., & Ogawa, S. (2016). Isotope-coded ESI-enhancing derivatization reagents for differential analysis, quantification and profiling of metabolites in biological samples by LC/MS: A review. *Journal of Pharmaceutical and Biomedical Analysis*, *130*, 181–193. https://doi.org/10.1016/j.jpba.2016.04.033

Hill, H. (2011). Bioanalysis in drug discovery. *Bioanalysis*, *3*(19), 2155–2158. https://doi.org/10.4155/bio.11.218

Hofferek, V., Su, H., & Reid, G. E. (2021). Chemical Derivatization-Aided High Resolution Mass Spectrometry for Shotgun Lipidome Analysis. In F. Hsu (Ed.), *Mass Spectrometry-*

Based Lipidomics Methods and Protocols (pp. 1–313).

Horwitz, W. (1982). Pearson's Chemical Analysis of Foods, 8th Edition. *Journal of Association of Official Analytical Chemists*, *65*(4), 1037. https://doi.org/10.1093/jaoac/65.4.1037

Hsu, F.-F., & Turk, J. (1999). Structural characterization of triacylglycerols as lithiated adducts by electrospray ionization mass spectrometry using low-energy collisionally activated dissociation on a triple stage quadrupole instrument. *Journal of the American Society for Mass Spectrometry*, *10*(7), 587–599. https://doi.org/10.1016/S1044-0305(99)00035-5

Hsu, F.-F., & Turk, J. (2008). Structural characterization of unsaturated glycerophospholipids by multiple-stage linear ion-trap mass spectrometry with electrospray ionization. *Journal of the American Society for Mass Spectrometry*, *19*(11), 1681–1691. https://doi.org/10.1016/j.jasms.2008.07.023

Hsu, F.-F., & Turk, J. (2010). Electrospray ionization multiple-stage linear ion-trap mass spectrometry for structural elucidation of triacylglycerols: assignment of fatty acyl groups on the glycerol backbone and location of double bonds. *Journal of the American Society for Mass Spectrometry*, *21*(4), 657–669. https://doi.org/10.1016/j.jasms.2010.01.007

Hu, B., & Yao, Z. P. (2022). Electrospray ionization mass spectrometry with wooden tips: A review. *Analytica Chimica Acta*, *1209*, 339136. https://doi.org/10.1016/j.aca.2021.339136

Hu, Q., Noll, R. J., Li, H., Makarov, A., Hardman, M., & Cooks, R. G. (2005). The Orbitrap: A new mass spectrometer. *Journal of Mass Spectrometry*, *40*(4), 430–443. https://doi.org/10.1002/jms.856

Hu, W., Fitzgerald, M., Topp, B., Alam, M., & O'Hare, T. J. (2019). A review of biological functions, health benefits, and possible de novo biosynthetic pathway of palmitoleic acid in macadamia nuts. *Journal of Functional Foods*, *62*(August), 103520. https://doi.org/10.1016/j.jff.2019.103520

Huang, C., Li, L. S., & Wang, G. (1997). Effects of various cis double bonds in the sn-2 acyl chain of phosphatidylethanolamine on the bilayer's gel-to-liquid crystalline phase transition. *FASEB Journal*, *11*(9), 21917–21926.

Huang, Y. Q., Ruan, G. D., Liu, J. Q., Gao, Q., & Feng, Y. Q. (2011). Use of isotope differential derivatization for simultaneous determination of thiols and oxidized thiols by liquid chromatography tandem mass spectrometry. *Analytical Biochemistry*, *416*(2), 159–166. https://doi.org/10.1016/j.ab.2011.05.020

Huang, Y. Q., Wang, Q. Y., Liu, J. Q., Hao, Y. H., Yuan, B. F., & Feng, Y. Q. (2014). Isotope labelling – paired homologous double neutral loss scan-mass spectrometry for profiling of metabolites with a carboxyl group. *Analyst*, *139*(13), 3446–3454. https://doi.org/10.1039/c4an00312h

Hurley, J. H., Boura, E., Carlson, L. A., & Róycki, B. (2010). Membrane budding. *Cell*, *143*(6), 875–887. https://doi.org/10.1016/j.cell.2010.11.030

Jarc, E., & Petan, T. (2019). Lipid Droplets and the Management of Cellular Stress. *The Yale*

Journal of Biology and Medicine, *92*(3), 435–452.

Jiang, R., Jiao, Y., Zhang, P., Liu, Y., Wang, X., Huang, Y., Zhang, Z., & Xu, F. (2017). Twin Derivatization Strategy for High-Coverage Quantification of Free Fatty Acids by Liquid Chromatography-Tandem Mass Spectrometry. *Analytical Chemistry*, *89*(22), 12223–12230. https://doi.org/10.1021/acs.analchem.7b03020

Jin, Y., Pan, Y., Jin, B., Jin, D., & Zhang, C. (2021). (S)-1-(5-(4-Methylpiperazin-1-yl)-2,4-dinitrophenyl)pyrrolidine-2-carboxylic acid as a derivatization reagent for ultrasensitive detection of amine enantiomers by HPLC-MS/MS and its application to the chiral metabolite analysis of (R)-1-aminoindan in sali. *Journal of Pharmaceutical and Biomedical Analysis*, *194*, 113815. https://doi.org/10.1016/j.jpba.2020.113815

Jones, J. W., Thompson, C. J., Carter, C. L., & Kane, M. A. (2015). Electron-induced dissociation (EID) for structure characterization of glycerophosphatidylcholine: determination of double-bond positions and localization of acyl chains. *Journal of Mass Spectrometry*, *50*(12), ii–ii. https://doi.org/10.1002/jms.3499

Kania, E., Roest, G., Vervliet, T., Parys, J. B., & Bultynck, G. (2017). IP3 receptor-mediated calcium signaling and its role in autophagy in cancer. *Frontiers in Oncology*, *7*(JUL), 1–15. https://doi.org/10.3389/fonc.2017.00140

Kesen, S., Amanpour, A., & Selli, S. (2018). Comparative Evaluation of the Fatty Acids and Aroma Compounds in Selected Iranian Nut Oils. *European Journal of Lipid Science and Technology*, *120*(10), 1–9. https://doi.org/10.1002/ejlt.201800152

Kightlinger, W., Warfel, K. F., Delisa, M. P., & Jewett, M. C. (2020). Synthetic Glycobiology: Parts, Systems, and Applications. *ACS Synthetic Biology*, *9*(7), 1534–1562. https://doi.org/10.1021/acssynbio.0c00210

Kochhar, S. P., & Henry, C. J. K. (2009). Oxidative stability and shelf-life evaluation of selected culinary oils. *International Journal of Food Sciences and Nutrition*, *60*(SUPPL. 7), 289–296. https://doi.org/10.1080/09637480903103774

Kundu, M., Mahata, B., Banerjee, A., Chakraborty, S., Debnath, S., Ray, S. S., Ghosh, Z., & Biswas, K. (2016). Ganglioside GM2 mediates migration of tumor cells by interacting with integrin and modulating the downstream signaling pathway. *Biochimica et Biophysica Acta - Molecular Cell Research*, *1863*(7), 1472–1489. https://doi.org/10.1016/j.bbamcr.2016.04.004

Kwon, Y., Lee, S., Oh, D. C., & Kim, S. (2011). Simple determination of double-bond positions in long-chain olefins by cross-metathesis. *Angewandte Chemie - International Edition*, *50*(36), 8275–8278. https://doi.org/10.1002/anie.201102634

Lange, M., Ni, Z., Criscuolo, A., & Fedorova, M. (2019). Liquid Chromatography Techniques in Lipidomics Research. *Chromatographia*, *82*(1), 77–100. https://doi.org/10.1007/s10337-018-3656-4

Lawrence, P., & Brenna, J. T. (2006). Acetonitrile covalent adduct chemical ionization mass spectrometry for double bond localization in non-methylene-interrupted polyene fatty acid methyl esters. *Analytical Chemistry*, *78*(4), 1312–1317. https://doi.org/10.1021/ac0516584

Leendert, V., Van Langenhove, H., & Demeestere, K. (2015). Trends in liquid

chromatography coupled to high-resolution mass spectrometry for multi-residue analysis of organic micropollutants in aquatic environments. *TrAC - Trends in Analytical Chemistry*, *67*, 192–208. https://doi.org/10.1016/j.trac.2015.01.010

Leiro, V., Parreira, P., Freitas, S. C., Martins, M. C. L., & Pêgo, A. P. (2018). Conjugation Chemistry Principles and Surface Functionalization of Nanomaterials. In *Biomedical Applications of Functionalized Nanomaterials: Concepts, Development and Clinical Translation*. Elsevier Inc. https://doi.org/10.1016/B978-0-323-50878-0.00002-1

Li, D., Guo, Z., & Chen, Y. (2016). Direct Derivatization and Quantitation of Ultra-trace Gibberellins in Sub-milligram Fresh Plant Organs. *Molecular Plant*, *9*(1), 175–177. https://doi.org/10.1016/j.molp.2015.07.001

Li, D., Guo, Z., Liu, C., Li, J., Xu, W., & Chen, Y. (2017). Quantification of near-attomole gibberellins in floral organs dissected from a single Arabidopsis thaliana flower. *Plant Journal*, *91*(3), 547–557. https://doi.org/10.1111/tpj.13580

Li, L., Han, J., Wang, Z., Liu, J., Wei, J., Xiong, S., & Zhao, Z. (2014). Mass spectrometry methodology in lipid analysis. *International Journal of Molecular Sciences*, *15*(6), 10492–10507. https://doi.org/10.3390/ijms150610492

Li, M., Yang, L., Bai, Y., & Liu, H. (2014). Analytical methods in lipidomics and their applications. *Analytical Chemistry*, *86*(1), 161–175. https://doi.org/10.1021/ac403554h

Li, X., & Franke, A. A. (2011). Improved LC-MS method for the determination of fatty acids in red blood cells by LC-orbitrap MS. *Analytical Chemistry*, *83*(8), 3192–3198. https://doi.org/10.1021/ac103093w

Li, Z. L., & Buck, M. (2017). Computational Modeling Reveals that Signaling Lipids Modulate the Orientation of K-Ras4A at the Membrane Reflecting Protein Topology. *Structure*, *25*(4), 679-689.e2. https://doi.org/10.1016/j.str.2017.02.007

Ling, Y. S., Liang, H. J., Lin, M. H., Tang, C. H., Wu, K. Y., Kuo, M. L., & Lin, C. Y. (2014). Two-dimensional LC-MS/MS to enhance ceramide and phosphatidylcholine species profiling in mouse liver. *Biomedical Chromatography*, *28*(9), 1284–1293. https://doi.org/10.1002/bmc.3162

López-Yerena, A., Domínguez-López, I., Vallverdú-Queralt, A., Pérez, M., Jáuregui, O., Escribano-Ferrer, E., & Lamuela-Raventós, R. M. (2021). Metabolomics technologies for the identification and quantification of dietary phenolic compound metabolites: An overview. *Antioxidants*, *10*(6), 1–25. https://doi.org/10.3390/antiox10060846

Lutterodt, H., Slavin, M., Whent, M., Turner, E., & Yu, L. (2011). Fatty acid composition, oxidative stability, antioxidant and antiproliferative properties of selected cold-pressed grape seed oils and flours. *Food Chemistry*, *128*(2), 391–399. https://doi.org/10.1016/j.foodchem.2011.03.040

Ma, X., Chong, L., Tian, R., Shi, R., Hu, T. Y., Ouyang, Z., & Xia, Y. (2016). Identification and quantitation of lipid C=C location isomers: A shotgun lipidomics approach enabled by photochemical reaction. *Proceedings of the National Academy of Sciences of the United States of America*, *113*(10), 2573–2578. https://doi.org/10.1073/pnas.1523356113

Ma, X., & Xia, Y. (2014). Pinpointing double bonds in lipids by paternò-büchi reactions and mass spectrometry. *Angewandte Chemie (International Ed. in English)*, *53*(10), 2592–2596. https://doi.org/10.1002/anie.201310699

Macmillan, D. K., & Murphy, R. C. (1995). *Denise K. MacMillan*. *0305*(95).

Mahata, B., Banerjee, A., Kundu, M., Bandyopadhyay, U., & Biswas, K. (2015). TALEN mediated targeted editing of GM2/GD2-synthase gene modulates anchorage independent growth by reducing anoikis resistance in mouse tumor cells. *Scientific Reports*, *5*, 1–12. https://doi.org/10.1038/srep09048

Makarov, A., Denisov, E., & Lange, O. (2009). Performance Evaluation of a High-field Orbitrap Mass Analyzer. *Journal of the American Society for Mass Spectrometry*, *20*(8), 1391–1396. https://doi.org/10.1016/j.jasms.2009.01.005

Makarov, A., & Scigelova, M. (2010). Coupling liquid chromatography to Orbitrap mass spectrometry. *Journal of Chromatography A*, *1217*(25), 3938–3945. https://doi.org/10.1016/j.chroma.2010.02.022

Mann, J. P., & Savage, D. B. (2019). What lipodystrophies teach us about the metabolic syndrome. *Journal of Clinical Investigation*, *129*(10), 4009–4021. https://doi.org/10.1172/JCI129190

Marsh, D. (1999). Thermodynamic analysis of chain-melting transition temperatures for monounsaturated phospholipid membranes: Dependence on cis-monoenoic double bond position. *Biophysical Journal*, *77*(2), 953–963. https://doi.org/10.1016/S0006-3495(99)76946-8

Martinez-Seara, H., Róg, T., Pasenkiewicz-Gierula, M., Vattulainen, I., Karttunen, M., & Reigada, R. (2007). Effect of double bond position on lipid bilayer properties: Insight through atomistic simulations. *Journal of Physical Chemistry B*, *111*(38), 11162–11168. https://doi.org/10.1021/jp071894d

Martinez-Seara, H., Róg, T., Pasenkiewicz-Gierula, M., Vattulainen, I., Karttunen, M., & Reigada, R. (2008). Interplay of unsaturated phospholipids and cholesterol in membranes: effect of the double-bond position. *Biophysical Journal*, *95*(7), 3295–3305. https://doi.org/10.1529/biophysj.108.138123

Masoodi, M., Mir, A. A., Petasis, N. A., Serhan, C. N., & Nicolaou, A. (2008). Simultaneous lipidomic analysis of three families of bioactive lipid mediators leukotrienes, resolvins, protectins and related hydroxy-fatty acids by liquid chromatography/electrospray ionisation tandem mass spectrometry. *Rapid Communications in Mass Spectrometry*, *22*(2), 75–83. https://doi.org/10.1002/rcm.3331

McCloskey, J. A., & McClell, M. J. (1965). Mass Spectra of O-Isopropylidene Derivatives of Unsaturated Fatty Esters. *Journal of the American Chemical Society*, *87*(22), 5090–5093. https://doi.org/10.1021/ja00950a019

McMahon, H. T., & Boucrot, E. (2015). Membrane curvature at a glance. *Journal of Cell Science*, *128*(6), 1065–1070. https://doi.org/10.1242/jcs.114454

Mérida, I., Arranz-Nicolás, J., Rodríguez-Rodríguez, C., & Ávila-Flores, A. (2019). Diacylglycerol kinase control of protein kinase C. *Biochemical Journal*, *476*(8), 1205–1219. https://doi.org/10.1042/BCJ20180620

Meyer, V. R. (2010). *Practical high-performance liquid chromatography*. John Wiley & Sons.

Michaud, A. L., Diau, G. Y., Abril, R., & Brenna, J. T. (2002). Double bond localization in minor homoallylic fatty acid methyl esters using acetonitrile chemical ionization tandem mass spectrometry. *Analytical Biochemistry*, *307*(2), 348–360. https://doi.org/10.1016/S0003-2697(02)00037-4

Michaud, A. L., Yurawecz, M. P., Delmonte, P., Corl, B. A., Bauman, D. E., & Brenna, J. T. (2003). Identification and characterization of conjugated fatty acid methyl esters of mixed double bond geometry by acetonitrile chemical ionization tandem mass spectrometry. *Analytical Chemistry*, *75*(18), 4925–4930. https://doi.org/10.1021/ac034221+

Mitchell, T. W., Pham, H., Thomas, M. C., & Blanksby, S. J. (2009). Identification of double bond position in lipids: From GC to OzID. *Journal of Chromatography B: Analytical Technologies in the Biomedical and Life Sciences*, *877*(26), 2722–2735. https://doi.org/10.1016/j.jchromb.2009.01.017

Moe, M. K., Anderssen, T., Strøm, M. B., & Jensen, E. (2004). Vicinal hydroxylation of unsaturated fatty acids for structural characterization of intact neutral phospholipids by negative electrospray ionization tandem quadrupole mass spectrometry. *Rapid Communications in Mass Spectrometry*, *18*(18), 2121–2130. https://doi.org/10.1002/rcm.1601

Moe, M. K., Anderssen, T., Strøm, M. B., & Jensen, E. (2005). Total structure characterization of unsaturated acidic phospholipids provided by vicinal di-hydroxylation of fatty acid double bonds and negative electrospray ionization mass spectrometry. *Journal of the American Society for Mass Spectrometry*, *16*(1), 46–59. https://doi.org/10.1016/j.jasms.2004.09.014

Moe, M. K., & Jensen, E. (2004). Structure elucidation of unsaturated fatty acids after vicinal hydroxylation of the double bonds by negative-ion electrospray ionisation low-energy tandem mass spectrometry. *European Journal of Mass Spectrometry*, *10*(1), 47–55. https://doi.org/10.1255/ejms.587

Moldoveanu, S., & David, V. (2014). Modern Sample Preparation for Chromatography. In *Modern Sample Preparation for Chromatography*. https://doi.org/10.1016/C2011-0-00093-5

Moldoveanu, S., & David, V. (2015a). Chemical Reactions Used in Derivatizations. In *Modern Sample Preparation for Chromatography*. https://doi.org/10.1016/b978-0-444-54319-6.00010-4

Moldoveanu, S., & David, V. (2015b). The Role of Derivatization in Chromatography. In *Modern Sample Preparation for Chromatography* (pp. 307–331). https://doi.org/10.1016/b978-0-444-54319-6.00009-8

Molero Gómez, A., & Martínez de la Ossa, E. (2002). Quality of borage seed oil extracted by liquid and supercritical carbon dioxide. *Chemical Engineering Journal*, *88*(1–3), 103–109. https://doi.org/10.1016/S1385-8947(01)00260-1

Mondal, M., Mesmin, B., Mukherjee, S., & R. Maxfield, F. (2009). Sterols Are Mainly in the Cytoplasmic Leaflet of the Plasma Membrane and the Endocytic Recycling Compartment in CHO Cells. *Molecular Biology of the Cell*, *20*(2), 581–188.

https://www.molbiolcell.org/doi/full/10.1091/mbc.e08-07-0785

Montalbetti, C. A. G. N., & Falque, V. (2005). Amide bond formation and peptide coupling. *Tetrahedron*, *61*(46), 10827–10852. https://doi.org/10.1016/j.tet.2005.08.031

Mulya, A., & Kirwan, J. P. (2016). Brown and Beige Adipose Tissue. *Endocrinology and Metabolism Clinics of North America*, *45*(3), 605–621. https://doi.org/10.1016/j.ecl.2016.04.010

Murphy, R. C., Fiedler, J., Hevko, J., & Ceramides, A. (2001). Analysis of Nonvolatile Lipids by Mass Spectrometry. *Chemical Reviews*, *101*, 479–526.

Nakajima, N., & Ikada, Y. (1995). Mechanism of Amide Formation by Carbodiimide for Bioconjugation in Aqueous Media. *Bioconjugate Chemistry*, *6*(1), 123–130. https://doi.org/10.1021/bc00031a015

Nasri, C., Halabi, Y., Harhar, H., Mohammed, F., Bellaouchou, A., Guenbour, A., & Tabyaoui, M. (2021). Chemical characterization of oil from four Avocado varieties cultivated in Morocco. *OCL - Oilseeds and Fats, Crops and Lipids*, *28*. https://doi.org/10.1051/ocl/2021008

Nelson, D. L., & Cox, M. M. (2021). Lehninger Principles of Biochemistry. In *Nucl. Phys.* (Vol. 13, Issue 1).

Niki, E. (1990). Free radical initiators as source of water- or lipid-soluble peroxyl radicals. *Methods in Enzymology*, *186*(C), 100–108. https://doi.org/10.1016/0076-6879(90)86095-D

Noche, G. G., Laespada, M. E. F., Pavón, J. L. P., Cordero, B. M., & Lorenzo, S. M. (2011). In situ aqueous derivatization and determination of non-steroidal anti-inflammatory drugs by salting-out-assisted liquid-liquid extraction and gas chromatography-mass spectrometry. *Journal of Chromatography A*, *1218*(37), 6240–6247. https://doi.org/10.1016/j.chroma.2011.06.112

Nolting, D., Malek, R., & Makarov, A. (2019). Ion traps in modern mass spectrometry. *Mass Spectrometry Reviews*, *38*(2), 150–168. https://doi.org/10.1002/mas.21549

Ogawa, S., Tomaru, K., Matsumoto, N., Watanabe, S., & Higashi, T. (2016). LC/ESI-MS/MS method for determination of salivary eicosapentaenoic acid concentration to arachidonic acid concentration ratio. *Biomedical Chromatography*, *30*(1), 29–34. https://doi.org/10.1002/bmc.3421

Oliw, E. H., Garscha, U., Nilsson, T., & Cristea, M. (2006). Payne rearrangement during analysis of epoxyalcohols of linoleic and α-linolenic acids by normal phase liquid chromatography with tandem mass spectrometry. *Analytical Biochemistry*, *354*(1), 111–126. https://doi.org/10.1016/j.ab.2006.04.010

Olsen, J. V., Macek, B., Lange, O., Makarov, A., Horning, S., & Mann, M. (2007). Higher-energy C-trap dissociation for peptide modification analysis. *Nature Methods*, *4*(9), 709–712. https://doi.org/10.1038/nmeth1060

Onal, G., Kutlu, O., Gozuacik, D., & Dokmeci Emre, S. (2017). Lipid Droplets in Health and Disease. *Lipids in Health and Disease*, *16*(1), 1–15. https://doi.org/10.1186/s12944-017-0521-7

Orsavova, J., Misurcova, L., Vavra Ambrozova, J., Vicha, R., & Mlcek, J. (2015). Fatty acids composition of vegetable oils and its contribution to dietary energy intake and dependence of cardiovascular mortality on dietary intake of fatty acids. *International Journal of Molecular Sciences*, *16*(6), 12871–12890. https://doi.org/10.3390/ijms160612871

Orsburn, B. C. (2021). Proteome discoverer-a community enhanced data processing suite for protein informatics. *Proteomes*, *9*(1). https://doi.org/10.3390/proteomes9010015

Ouzir, M., Bernoussi, S. El, Tabyaoui, M., & Taghzouti, K. (2021). Almond oil: A comprehensive review of chemical composition, extraction methods, preservation conditions, potential health benefits, and safety. *Comprehensive Reviews in Food Science and Food Safety*, *20*(4), 3344–3387. https://doi.org/10.1111/1541-4337.12752

Paglia, G., & Astarita, G. (2017). Metabolomics and lipidomics using traveling-wave ion mobility mass spectrometry. *Nature Protocols*, *12*(4), 797–813. https://doi.org/10.1038/nprot.2017.013

Paglia, G., Kliman, M., Claude, E., Geromanos, S., & Astarita, G. (2015). Applications of ion-mobility mass spectrometry for lipid analysis. *Analytical and Bioanalytical Chemistry*, *407*(17), 4995–5007. https://doi.org/10.1007/s00216-015-8664-8

Pandey, R., Collins, M., Lu, X., Sweeney, S. R., Chiou, J., Lodi, A., & Tiziani, S. (2021). Novel Strategy for Untargeted Chiral Metabolomics using Liquid Chromatography-High Resolution Tandem Mass Spectrometry. *Analytical Chemistry*, *93*(14), 5805–5814. https://doi.org/10.1021/acs.analchem.0c05325

Park, M. J., Sheng, R., Silkov, A., Jung, D. J., Wang, Z. G., Xin, Y., Kim, H., Thiagarajan-Rosenkranz, P., Song, S., Yoon, Y., Nam, W., Kim, I., Kim, E., Lee, D. G., Chen, Y., Singaram, I., Wang, L., Jang, M. H., Hwang, C. S., … Cho, W. (2016). SH2 Domains Serve as Lipid-Binding Modules for pTyr-Signaling Proteins. *Molecular Cell*, *62*(1), 7–20. https://doi.org/10.1016/j.molcel.2016.01.027

Pattabiraman, V. R., & Bode, J. W. (2011). Rethinking amide bond synthesis. *Nature*, *480*(7378), 471–479. https://doi.org/10.1038/nature10702

Perillo, V. L., Fernández-Nievas, G. A., Vallés, A. S., Barrantes, F. J., & Antollini, S. S. (2012). The position of the double bond in monounsaturated free fatty acids is essential for the inhibition of the nicotinic acetylcholine receptor. *Biochimica et Biophysica Acta - Biomembranes*, *1818*(11), 2511–2520. https://doi.org/10.1016/j.bbamem.2012.06.001

Pol, A., Gross, S. P., & Parton, R. G. (2014). Biogenesis of the multifunctional lipid droplet: Lipids, proteins, and sites. *Journal of Cell Biology*, *204*(5), 635–646. https://doi.org/10.1083/jcb.201311051

Porter, N. A., Caldwell, S. E., & Mills, K. A. (1995). Mechanisms of free radical oxidation of unsaturated lipids. *Lipids*, *30*(4), 277–290. https://doi.org/10.1007/BF02536034

Pottorf, R. S., Szeto, P., & Srinivasarao, M. (2017). 1-Ethyl-3-(3'-dimethylaminopropyl)carbodiimide Hydrochloride. In *Encyclopedia of Reagents for Organic Synthesis* (pp. 1–5). https://doi.org/https://doi.org/10.1002/047084289X.re062.pub2

Pratt, D. A., Tallman, K. A., & Porter, N. E. D. A. (2011). *Free Radical Oxidation of Polyunsaturated Lipids : New Mechanistic Insights and the Development of Peroxyl Radical Clocks*. *44*(6).

PRIVETT, O. S. ., Blank, L., & ROMANUS, O. (1963). *Isolation analysis*. *4*(3).

Qi, B. L., Liu, P., Wang, Q. Y., Cai, W. J., Yuan, B. F., & Feng, Y. Q. (2014). Derivatization for liquid chromatography-mass spectrometry. *TrAC - Trends in Analytical Chemistry*, *59*, 121–132. https://doi.org/10.1016/j.trac.2014.03.013

Quirke, J. M. E., Adams, C. L., & Van Berkel, G. J. (1994). Chemical Derivatization for Electrospray Ionization Mass Spectrometry. 2. Aromatic and Highly Conjugated Molecules. *Analytical Chemistry*, *66*(13), 2096–2102. https://doi.org/10.1021/ac00085a027

Raatz, S. K., Conrad, Z., & Jahns, L. (2018). Trends in linoleic acid intake in the United States adult population: NHANES 1999–2014. *Prostaglandins Leukotrienes and Essential Fatty Acids*, *133*(April), 23–28. https://doi.org/10.1016/j.plefa.2018.04.006

Rebane, R., Oldekop, M. L., & Herodes, K. (2012). Comparison of amino acid derivatization reagents for LC-ESI-MS analysis. Introducing a novel phosphazene-based derivatization reagent. *Journal of Chromatography B: Analytical Technologies in the Biomedical and Life Sciences*, *904*, 99–106. https://doi.org/10.1016/j.jchromb.2012.07.029

Rehman, H. U., Farooq, U., Akram, K., Hayat, Z., Shafi, A., Sarfarz, F., Sidhu, A., & Hakim, A. (2021). Fatty acid profile and bio-efficacy of wheat germ oil in hyperlipidemic rabbits. *Pakistan Journal of Agricultural Sciences*, *58*(2), 621–625. https://doi.org/10.21162/PAKJAS/21.1430

Reverberi, M., Punelli, F., Scarpari, M., Camera, E., Zjalic, S., Ricelli, A., Fanelli, C., & Fabbri, A. A. (2010). Lipoperoxidation affects ochratoxin A biosynthesis in Aspergillus ochraceus and its interaction with wheat seeds. *Applied Microbiology and Biotechnology*, *85*(6), 1935–1946. https://doi.org/10.1007/s00253-009-2220-4

Ribeiro, A. P. L., Haddad, F. F., Tavares, T. de S., Magalhães, K. T., Pimenta, C. J., & Nunes, C. A. (2020). Characterization of macadamia oil (macadamia integrifolia) obtained under different extraction conditions. *Emirates Journal of Food and Agriculture*, *32*(4), 295–302. https://doi.org/10.9755/ejfa.2020.v32.i4.2095

Rioux, V., Choque, B., Ezanno, H., Duby, C., Catheline, D., & Legrand, P. (2015). Influence of the cis-9, cis-12 and cis-15 double bond position in octadecenoic acid (18:1) isomers on the rat FADS2-catalyzed Δ6-desaturation. *Chemistry and Physics of Lipids*, *187*, 10–19. https://doi.org/10.1016/j.chemphyslip.2015.02.001

Rivera-Santiago, R. F., Sriswasdi, S., Harper, S. L., & Speicher, D. W. (2015). Probing structures of large protein complexes using zero-length cross-linking. *Methods*, *89*, 99–111. https://doi.org/10.1016/j.ymeth.2015.04.031

Robbins, A. L., & Savage, D. B. (2015). The genetics of lipid storage and human lipodystrophies. In *Trends in Molecular Medicine* (Vol. 21, Issue 7, pp. 433–438). Elsevier Ltd. https://doi.org/10.1016/j.molmed.2015.04.004

Romero-González, R., & Frenich, A. G. (2017). *Applications in High Resolution Mass Spectrometry: Food Safety and Pesticide Residue Analysis*. Elsevier Science.

https://books.google.co.uk/books?id=u5ypDQAAQBAJ

Roughley, S. D., & Jordan, A. M. (2011). The medicinal chemist's toolbox: An analysis of reactions used in the pursuit of drug candidates. *Journal of Medicinal Chemistry*, *54*(10), 3451–3479. https://doi.org/10.1021/jm200187y

Russo, M. S. T., Napylov, A., Paquet, A., & Vuckovic, D. (2020). Comparison of N-ethyl maleimide and N-(1-phenylethyl) maleimide for derivatization of biological thiols using liquid chromatography-mass spectrometry. *Analytical and Bioanalytical Chemistry*, *412*(7), 1639–1652. https://doi.org/10.1007/s00216-020-02398-x

Rustam, Y. H., & Reid, G. E. (2018). Analytical Challenges and Recent Advances in Mass Spectrometry Based Lipidomics. *Analytical Chemistry*, *90*(1), 374–397. https://doi.org/10.1021/acs.analchem.7b04836

Santa, T. (2011). Derivatization reagents in liquid chromatography/electrospray ionization tandem mass spectrometry. *Biomedical Chromatography*, *25*(1), 1–10. https://doi.org/10.1002/bmc.1548

Santa, T. (2013). Derivatization in Liquid Chromatography for Mass Spectrometric Detection. *Drug Discoveries & Therapeutics*, *7*(1), 9–17. https://doi.org/10.5582/ddt.2013.v7.1.9

Santrock, J., Gorski, R. A., & O'Gara, J. F. (1992). Products and Mechanism of the Reaction of Ozone with Phospholipids in Unilamellar Phospholipid Vesicles. *Chemical Research in Toxicology*, *5*(1), 134–141. https://doi.org/10.1021/tx00025a023

Schneider, C., Schreier, P., & Herderich, M. (1997). *Analysis of Lipoxygenase-Derived Fatty Acid Hydroperoxides by Electrospray Ionization Tandem Mass Spectrometry*. *32*(3), 331–336.

Schoeniger, A., Fuhrmann, H., & Schumann, J. (2016). LPS- or Pseudomonas aeruginosa-mediated activation of the macrophage TLR4 signaling cascade depends on membrane lipid composition. *PeerJ*, *2016*(2), 1–17. https://doi.org/10.7717/peerj.1663

Schuberth, J. (2000). ANALYTICAL TECHNIQUES/Mass spwctrometry. In J. Siegel, G. Knupfer, & P. Saukko (Eds.), *MEncyclopedia of Forensic Sciencesethods* (Issue c, pp. 155–161). Oxford: Elsevier.

Scigelova, M., Hornshaw, M., Giannakopulos, A., & Makarov, A. (2011). Fourier transform mass spectrometry. *Molecular and Cellular Proteomics*, *10*(7), M111.009431. https://doi.org/10.1074/mcp.M111.009431

Scrimgeour, C., & Clough, P. (2014). Authentication of borage oil. *Lipid Technology*, *26*(10), 230–233. https://doi.org/10.1002/lite.201400059

Sheehan, J. C., Preston, J., & Cruickshank, P. A. (1965). A Rapid Synthesis of Oligopeptide Derivatives without Isolation of Intermediates. *Journal of the American Chemical Society*, *87*(11), 2492–2493. https://doi.org/10.1021/ja01089a034

Sheehan, J., Cruickshank, P., & Boshart, G. (1961). Notes- A Convenient Synthesis of Water-Soluble Carbodiimides. *The Journal of Organic Chemistry*, *26*(7), 2525–2528. https://doi.org/10.1021/jo01351a600

Shimizu, T. (2009). Lipid mediators in health and disease: Enzymes and receptors as

therapeutic targets for the regulation of immunity and inflammation. *Annual Review of Pharmacology and Toxicology*, *49*, 123–150. https://doi.org/10.1146/annurev.pharmtox.011008.145616

Silver, J. (2019). Overview of Analytical-to-Preparative Liquid Chromatography Method Development. *ACS Combinatorial Science*, *21*(9), 609–613. https://doi.org/10.1021/acscombsci.8b00187

Sinz, A. (2003). Chemical cross-linking and mass spectrometry for mapping three-dimensional structures of proteins and protein complexes. *Journal of Mass Spectrometry*, *38*(12), 1225–1237. https://doi.org/10.1002/jms.559

Snyder, L. R., Kirkland, J. J., & Dolan, J. W. (2010). *Introduction to Modern Liquid Chromatography, Third Edition* (Third). John Wiley & Sons, Inc. https://doi.org/10.1007/s13361-010-0021-8

Son, H. H., Moon, J. Y., Seo, H. S., Kim, H. H., Chung, B. C., & Choi, M. H. (2014). High-temperature GC-MS-based serum cholesterol signatures may reveal sex differences in vasospastic angina. *Journal of Lipid Research*, *55*(1), 155–162. https://doi.org/10.1194/jlr.D040790

Spaggiari, D., Geiser, L., & Rudaz, S. (2014). Coupling ultra-high-pressure liquid chromatography with mass spectrometry for in-vitro drug-metabolism studies. *TrAC - Trends in Analytical Chemistry*, *63*, 129–139. https://doi.org/10.1016/j.trac.2014.06.021

Spitzer, V. (1996). Structure analysis of fatty acids by gas chromatography - Low resolution electron impact mass spectrometry of their 4,4-dimethyloxazoline derivatives - A review. *Progress in Lipid Research*, *35*(4), 387–408. https://doi.org/10.1016/S0163-7827(96)00011-2

Stubbs, C. D., Kouyama, T., Kinosita, K., & Ikegami, A. (1981). Effect of Double Bonds on the Dynamic Properties of the Hydrocarbon Region of Lecithin Bilayers. *Biochemistry*, *20*(15), 4257–4262. https://doi.org/10.1021/bi00518a004

T.S. Work and E. Work. (1972). *Laboratory Techniques in Biochemistry and Molecular Biology: Determination of sequences in RNA* (Vol. 3). North-Holland Publishing Company. https://doi.org/10.1016/S0075-7535(08)70359-0

Taha, A. Y. (2020). Linoleic acid–good or bad for the brain? *Npj Science of Food*, *4*(1). https://doi.org/10.1038/s41538-019-0061-9

Tasset-Cuevas, I., Fernández-Bedmar, Z., Lozano-Baena, M. D., Campos-Sánchez, J., de Haro-Bailón, A., Muñoz-Serrano, A., & Alonso-Moraga, Á. (2013). Protective Effect of Borage Seed Oil and Gamma Linolenic Acid on DNA: In Vivo and In Vitro Studies. *PLoS ONE*, *8*(2). https://doi.org/10.1371/journal.pone.0056986

Thomas, M. C., Mitchell, T. W., & Blanksby, S. J. (2006). Ozonolysis of phospholipid double bonds during electrospray ionization: A new tool for structure determination. *Journal of the American Chemical Society*, *128*(1), 58–59. https://doi.org/10.1021/ja056797h

Thomas, M. C., Mitchell, T. W., Harman, D. G., Deeley, J. M., Murphy, R. C., & Blanksby, S. J. (2007). Elucidation of double bond position in unsaturated lipids by ozone electrospray ionization mass spectrometry. *Analytical Chemistry*, *79*(13), 5013–5022.

https://doi.org/10.1021/ac0702185

Thomas, M. C., Mitchell, T. W., Harman, D. G., Deeley, J. M., Nealon, J. R., & Blanksby, S. J. (2008). Ozone-induced dissociation: Elucidation of double bond position within mass-selected lipid ions. *Analytical Chemistry*, *80*(1), 303–311. https://doi.org/10.1021/ac7017684

Tomer, K. B., Crow, F. W., & Gross, M. L. (1983). Location of Double Bond Position in Unsaturated Fatty Acids by Negative Ion MS/MS. *Journal of the American Chemical Society*, *105*(16), 5487–5488. https://doi.org/10.1021/ja00354a055

Trades, L., & Chem, L. (1947). *Holman & Elmer 1947*. *6*, 127–129.

Tu, J., Zhou, Z., Li, T., & Zhu, Z. J. (2019). The emerging role of ion mobility-mass spectrometry in lipidomics to facilitate lipid separation and identification. *TrAC - Trends in Analytical Chemistry*, *116*, 332–339. https://doi.org/10.1016/j.trac.2019.03.017

Tvrzicka, E., Kremmyda, L. S., Stankova, B., & Zak, A. (2011). Fatty acids as biocompounds: Their role in human metabolism, health and disease - a review. part 1: Classification, dietary sources and biological functions. *Biomedical Papers*, *155*(2), 117–130. https://doi.org/10.5507/bp.2011.038

Ueno, K., Nagano, M., Shimizu, S., Toshima, J. Y., & Toshima, J. (2016). Lipid droplet proteins, Lds1p, Lds2p, and Rrt8p, are implicated in membrane protein transport associated with ergosterol. *Biochemical and Biophysical Research Communications*, *475*(4), 315–321. https://doi.org/10.1016/j.bbrc.2016.05.099

Valeur, E., & Bradley, M. (2009). Amide bond formation: Beyond the myth of coupling reagents. *Chemical Society Reviews*, *38*(2), 606–631. https://doi.org/10.1039/b701677h

Van Pelt, C. K., & Brenna, J. T. (1999). Acetonitrile chemical ionization tandem mass spectrometry to locate double bonds in polyunsaturated fatty acid methyl esters. *Analytical Chemistry*, *71*(10), 1981–1989. https://doi.org/10.1021/ac981387f

Vance, J. E., & Vance, D. E. (2002). Biochemistry Of Lipids, Lipoproteins And Membranes. In *Biochemistry of Lipids, Lipoproteins and Membranes*. https://doi.org/10.1016/B978-0-444-53219-0.X5001-6

Vichi, S., Cortés-Francisco, N., & Caixach, J. (2013). Determination of volatile thiols in lipid matrix by simultaneous derivatization/extraction and liquid chromatography-high resolution mass spectrometric analysis. Application to virgin olive oil. *Journal of Chromatography A*, *1318*, 180–188. https://doi.org/10.1016/j.chroma.2013.10.015

Visioli, F., & Poli, A. (2020). Fatty Acids and Cardiovascular Risk. Evidence, Lack of Evidence , and Diligence. *Nutrients*, *12*(12), 1–19.

Voet, D., Voet, J. G., & Pratt, C. W. (2016). *Fundamentals of biochemistry life at the molecular level* (5th ed.).

Vogeser, M., & Seger, C. (2010). Pitfalls associated with the use of liquid chromatography-tandem mass spectrometry in the clinical laboratory. *Clinical Chemistry*, *56*(8), 1234–1244. https://doi.org/10.1373/clinchem.2009.138602

Vrkoslav, V., & Cvaˇ, J. (2012). *Identification of the double-bond position in fatty acid methyl esters by liquid chromatography / atmospheric pressure chemical ionisation mass spectrometry*. *1259*, 244–250. https://doi.org/10.1016/j.chroma.2012.04.055

Vrkoslav, V., Háková, M., Pecková, K., Urbanová, K., & Cvačka, J. (2011). Localization of double bonds in wax esters by high-performance liquid chromatography/atmospheric pressure chemical ionization mass spectrometry utilizing the fragmentation of acetonitrile-related adducts. *Analytical Chemistry*, *83*(8), 2978–2986. https://doi.org/10.1021/ac1030682

Vujević, P., Petrović, M., Vahčić, N., Milinović, B., & Čmelik, Z. (2014). Lipids and minerals of the most represented hazelnut varieties cultivated in Croatia. *Italian Journal of Food Science*, *26*(1), 24–30.

Wang, C., Yan, Q., Liu, H. B., Zhou, X. H., & Xiao, S. J. (2011). Different EDC/NHS activation mechanisms between PAA and PMAA brushes and the following amidation reactions. *Langmuir*, *27*(19), 12058–12068. https://doi.org/10.1021/la202267p

Wang, M., Ma, L. J., Yang, Y., Xiao, Z., & Wan, J. B. (2019). n-3 Polyunsaturated fatty acids for the management of alcoholic liver disease: A critical review. *Critical Reviews in Food Science and Nutrition*, *59*(S1), S116–S129. https://doi.org/10.1080/10408398.2018.1544542

Wang, S., Zhou, L., Wang, Z., Shi, X., & Xu, G. (2017). Simultaneous metabolomics and lipidomics analysis based on novel heart-cutting two-dimensional liquid chromatography-mass spectrometry. *Analytica Chimica Acta*, *966*, 34–40. https://doi.org/10.1016/j.aca.2017.03.004

Wang, W., & Seale, P. (2016). Control of brown and beige fat development. *Nature Reviews Molecular Cell Biology*, *17*(11), 691–702. https://doi.org/10.1038/nrm.2016.96

Wang, Y., Luan, G., Zhou, W., You, J., Hu, N., & Suo, Y. (2018). 2-(4-Amino)-Phenyl-1-Hydrogen-Phenanthrene [9,10-d] Imidazole as a Novel Fluorescent Labeling Reagent for Determination of Fatty Acids in Raspberry. *Food Analytical Methods*, *11*(2), 451–465. https://doi.org/10.1007/s12161-017-1016-x

Watson, D. G. (2012). Pharmaceutical Analysis: A textbook for pharmacy students and pharmaceutical chemists. In *Pharmaceutical Analysis: A textbook for pharmacy students and pharmaceutical chemists* (THIRD EDIT). Churchil Livingstone Elsevier. https://pharmabookbank.files.wordpress.com/2019/03/2.3.david_g_watson_pharmaceutical_analysis-1.pdf

Wei, J., Xiang, L., Li, X., Song, Y., Yang, C., Ji, F., Chung, A. C. K., Li, K., Lin, Z., & Cai, Z. (2020). Derivatization strategy combined with parallel reaction monitoring for the characterization of short-chain fatty acids and their hydroxylated derivatives in mouse. *Analytica Chimica Acta*, *1100*, 66–74. https://doi.org/10.1016/j.aca.2019.11.009

Werber, J., Wang, Y. J., Milligan, M., Li, X., & Ji, J. A. (2011). Analysis of 2,2'-Azobis (2-amidinopropane) dihydrochloride degradation and hydrolysis in aqueous solutions. *Journal of Pharmaceutical Sciences*, *100*(8), 3307–3315. https://doi.org/10.1002/jps.22578

Wheelan, P., Zirrolli, J. A., & Murphy, R. C. (1993). Low-energy fast atom bombardment

tandem mass spectrometry of monohydroxy substituted unsaturated fatty acids. *Biological Mass Spectrometry*, *22*(8), 465–473. https://doi.org/10.1002/bms.1200220808

Williams, A., & Ibrahim, I. T. (1981). Carbodiimide Chemistry: Recent Advances. *Chemical Reviews*, *81*(6), 589–636. https://doi.org/10.1021/cr00046a004

Wong, D. (2018). *Mechanism and Theory in Food Chemistry, Second Edition*. https://doi.org/10.1007/978-3-319-50766-8

Woudneh, M. B., Coreen Hamilton, M., Benskin, J. P., Wang, G., McEachern, P., & Cosgrove, J. R. (2013). A novel derivatization-based liquid chromatography tandem mass spectrometry method for quantitative characterization of naphthenic acid isomer profiles in environmental waters. *Journal of Chromatography A*, *1293*, 36–43. https://doi.org/10.1016/j.chroma.2013.03.040

Wu, M., Church, D. F., Mahier, T. J., Barker, S. A., & Pryor, W. A. (1992). Separation and spectral data of the six isomeric ozonides from methyl oleate. *Lipids*, *27*(2), 129–135. https://doi.org/10.1007/BF02535812

Wu, Z., Gao, W., Phelps, M. A., Wu, D., Miller, D. D., & Dalton, J. T. (2004). Favorable Effects of Weak Acids on Negative-Ion Electrospray Ionization Mass Spectrometry. *Analytical Chemistry*, *76*(3), 839–847. https://doi.org/10.1021/ac0351670

Xia, F., & Wan, J. B. (2021). Chemical derivatization strategy for mass spectrometry-based lipidomics. *Mass Spectrometry Reviews*, *2021*(July), 1–21. https://doi.org/10.1002/mas.21729

Xiang, L., Zhu, L., Huang, Y., & Cai, Z. (2020). Application of Derivatization in Fatty Acids and Fatty Acyls Detection: Mass Spectrometry-Based Targeted Lipidomics. *Small Methods*, *4*(8), 1–19. https://doi.org/10.1002/smtd.202000160

Xie, X., & Xia, Y. (2019). Analysis of Conjugated Fatty Acid Isomers by the Paternò-Büchi Reaction and Trapped Ion Mobility Mass Spectrometry. *Analytical Chemistry*, *91*(11), 7173–7180. https://doi.org/10.1021/acs.analchem.9b00374

Xu, Y., & Brenna, J. T. (2007). Atmospheric pressure covalent adduct chemical ionization tandem mass spectrometry for double bond localization in monoene- and diene-containing triacylglycerols. *Analytical Chemistry*, *79*(6), 2525–2536. https://doi.org/10.1021/ac062055a

Yamada, H., Imoto, T., Fujita, K., Okazaki, K., & Motomura, M. (1981). Selective Modification of Aspartic Acid-101 in Lysozyme by Carbodiimide Reaction. *Biochemistry*, *20*(17), 4836–4842. https://doi.org/10.1021/bi00520a005

Yang, K., Dilthey, B. G., & Gross, R. W. (2013). Identification and quantitation of fatty acid double bond positional isomers: A shotgun lipidomics approach using charge-switch derivatization. *Analytical Chemistry*, *85*(20), 9742–9750. https://doi.org/10.1021/ac402104u

Yang, K., & Han, X. (2011). Accurate quantification of lipid species by electrospray ionization mass spectrometry - Meets a key challenge in lipidomics. *Metabolites*, *1*(1), 21–40. https://doi.org/10.3390/metabo1010021

Yang, K., & Han, X. (2016). Lipidomics: Techniques, Applications, and Outcomes Related to

Biomedical Sciences. *Trends in Biochemical Sciences*, *41*(11), 954–969. https://doi.org/10.1016/j.tibs.2016.08.010

Yang, L., Nie, H., Zhao, F., Song, S., Meng, Y., Bai, Y., & Liu, H. (2020). A novel online two-dimensional supercritical fluid chromatography/reversed phase liquid chromatography–mass spectrometry method for lipid profiling. *Analytical and Bioanalytical Chemistry*, *412*(10), 2225–2235. https://doi.org/10.1007/s00216-019-02242-x

Yang, W. C., Regnier, F. E., & Adamec, J. (2008). Comparative metabolite profiling of carboxylic acids in rat urine by CE-ESI MS/MS through positively pre-charged and 2H-coded derivatization. *Electrophoresis*, *29*(22), 4549–4560. https://doi.org/10.1002/elps.200800156

Yin, H., Brooks, J. D., Gao, L., Porter, N. A., & Morrow, J. D. (2007). Identification of novel autoxidation products of the ω-3 fatty acid eicosapentaenoic acid in vitro and in vivo. *Journal of Biological Chemistry*, *282*(41), 29890–29901. https://doi.org/10.1074/jbc.M703108200

Young, J. J., Cheng, K. M., Tsou, T. L., Liu, H. W., & Wang, H. J. (2004). Preparation of cross-linked hyaluronic acid film using 2-chloro-1-methylpyridinium iodide or water-soluble 1-ethyl-(3,3-dimethylaminopropyl)carbodiimide. *Journal of Biomaterials Science, Polymer Edition*, *15*(6), 767–780. https://doi.org/10.1163/156856204774196153

Zaikin, V. G., & Borisov, R. S. (2021). Options of the Main Derivatization Approaches for Analytical ESI and MALDI Mass Spectrometry. *Critical Reviews in Analytical Chemistry*, *0*(0), 1–81. https://doi.org/10.1080/10408347.2021.1873100

Zanfini, A., Dreassi, E., Berardi, A., Piomboni, P., Costantino-Ceccarini, E., & Luddi, A. (2014). GC-EI-MS analysis of fatty acid composition in brain and serum of twitcher mouse. *Lipids*, *49*(11), 1115–1125. https://doi.org/10.1007/s11745-014-3945-0

Zárate, R., Jaber-Vazdekis, N., Tejera, N., Pérez, J. A., & Rodríguez, C. (2017). Significance of long chain polyunsaturated fatty acids in human health. *Clinical and Translational Medicine*, *6*(1). https://doi.org/10.1186/s40169-017-0153-6

Zhang, J. I., Tao, W. A., & Cooks, R. G. (2011). Facile Determination of Double Bond Position in Unsaturated Fatty Acids and Esters by Low Temperature Plasma. *Analytical Chemistry*, *83*, 4738–4744. https://doi.org/10.1021/ac1030946

Zhang, T. Y., Li, S., Zhu, Q. F., Wang, Q., Hussain, D., & Feng, Y. Q. (2019). Derivatization for liquid chromatography-electrospray ionization-mass spectrometry analysis of small-molecular weight compounds. *TrAC - Trends in Analytical Chemistry*, *119*, 115608. https://doi.org/10.1016/j.trac.2019.07.019

Zhang, X., Quinn, K., Cruickshank-Quinn, C., Reisdorph, R., & Reisdorph, N. (2018). The application of ion mobility mass spectrometry to metabolomics. *Current Opinion in Chemical Biology*, *42*, 60–66. https://doi.org/10.1016/j.cbpa.2017.11.001

Zhao, X. E., Zhu, S., & Liu, H. (2020). Recent progresses of derivatization approaches in the targeted lipidomics analysis by mass spectrometry. *Journal of Separation Science*, *43*(9–10), 1838–1846. https://doi.org/10.1002/jssc.201901346

Zhao, Y., Zhao, H., Zhao, X., Jia, J., Ma, Q., Zhang, S., Zhang, X., Chiba, H., Hui, S. P., & Ma, X.

(2017). Identification and Quantitation of C=C Location Isomers of Unsaturated Fatty Acids by Epoxidation Reaction and Tandem Mass Spectrometry. *Analytical Chemistry*, *89*(19), 10270–10278. https://doi.org/10.1021/acs.analchem.7b01870

Zheng, J., & Li, L. (2012). Fragmentation of protonated dansyl-labeled amines for structural analysis of amine-containing metabolites. *International Journal of Mass Spectrometry*, *316–318*, 292–299. https://doi.org/10.1016/j.ijms.2012.02.019

Zhou, Ying, Park, H., Kim, P., Jiang, Y., & Costello, C. E. (2014). Surface oxidation under ambient air--not only a fast and economical method to identify double bond positions in unsaturated lipids but also a reminder of proper lipid processing. *Analytical Chemistry*, *86*(12), 5697–5705. https://doi.org/10.1021/ac404214a

Zhou, Yunping, Wang, T., Zhai, S., Li, W., & Meng, Q. (2016). Linoleic acid and breast cancer risk: A meta-analysis. *Public Health Nutrition*, *19*(8), 1457–1463. https://doi.org/10.1017/S136898001500289X

Zhu, Y., Taylor, C., Sommer, K., Wilkinson, K., & Wirthensohn, M. (2015). Influence of deficit irrigation strategies on fatty acid and tocopherol concentration of almond (Prunus dulcis). *Food Chemistry*, *173*, 821–826. https://doi.org/10.1016/j.foodchem.2014.10.108

Zubarev, R. A., & Makarov, A. (2013). Orbitrap mass spectrometry. *Analytical Chemistry*, *85*(11), 5288–5296. https://doi.org/10.1021/ac4001223

Züllig, T., & Köfeler, H. C. (2021). High Resolution Mass Spectrometry in Lipidomics. *Mass Spectrometry Reviews*, *40*(3), 162–176. https://doi.org/10.1002/mas.21627